UNCLASSIFIED

AD NUMBER

AD907110

NEW LIMITATION CHANGE

TO

Approved for public release, distribution unlimited

FROM

Distribution authorized to U.S. Gov't. agencies only; Administrative/Operational Use; DEC 1972. Other requests shall be referred to Federal Aviation Administration, Annt: ss, Washington, DC.

AUTHORITY

FAA ltr, 26 Apr 1977

THIS PAGE IS UNCLASSIFIED

THIS REPORT HAS BEEN DELIMITED
AND CLEARED FOR PUBLIC RELEASE
UNDER DOD DIRECTIVE 5200.20 AND
NO RESTRICTIONS ARE IMPOSED UPON
ITS USE AND DISCLOSURE.

DISTRIBUTION STATEMENT A

APPROVED FOR PUBLIC RELEASE;
DISTRIBUTION UNLIMITED.

AD907110

Report No. FAA-SS-72-42

SUPERSONIC TRANSPORT NOISE REDUCTION TECHNOLOGY SUMMARY

PHASE I

SUMMARY OF GE4/SST ACOUSTIC SUPPRESSION RESEARCH

VOLUME 2

J.F. Brausch
V.L. Doyle

Group Engineering Division
Aircraft Engine Group
General Electric Company
Cincinnati, Ohio 45215



D D C
RECEIVED
FEB 8 1973
E

December 1972

FINAL REPORT

Approved for U.S. Government only. Transmittal of this document outside the U.S. Government must have prior approval of the Supersonic Transport Office.

Prepared for

DEPARTMENT OF TRANSPORTATION
FEDERAL AVIATION ADMINISTRATION
Supersonic Transport Office
Washington, D.C. 20590

The contents of this report reflect the views of the General Electric Company, which is responsible for the facts and the accuracy of the data presented herein. The contents do not necessarily reflect the official views or policy of the Department of Transportation. This report does not constitute a standard, specification, or regulation.

1. Report No.	2. Government Accession No.	3. Recipient's Catalog No.
FAA-SS-72-42 Vol.II of II		

4. Title and Subtitle	5. Report Date
SUMMARY OF GE4/SST ACOUSTIC SUPPRESSION RESEARCH	DECEMBER 1972
	6. Performing Organization Code

7. Author(s)	8. Performing Organization Report No.
J. F. BRAUSCH and V. L. DOYLE	R72-AEG-342 Vol.II of II
	10. Work Unit No.

9. Performing Organization Name and Address	11. Contract or Grant No.
Group Engineering Division Aircraft Engine Group General Electric Company Cincinnati, Ohio 45215	FA-SS-71-13
	13. Type of Report and Period Covered
	FINAL

12. Sponsoring Agency Name and Address	14. Sponsoring Agency Code
Department of Transportation Federal Aviation Administration Supersonic Transport Office, Washington, D.C. 20590	

15. Supplementary Notes

16. Abstract

A development program for a commercial supersonic aircraft and engines was sponsored by the Federal Aviation Administration during a five-year period from 1966 through 1971. The unique propulsion system, an afterburning turbojet, required acoustic suppression techniques to reduce its noise levels to those federally regulated for subsonic aircraft. An acoustic suppression research program was conducted by the General Electric Company to develop technology applicable to prototype and commercial supersonic engines. Primary emphasis was on jet noise suppressor development through model and engine testing. Various systems were studied including ejector pumping, simple mechanical primary and secondary suppressors, fluid injectants, multi-element tube nozzles, acoustically treated ejectors, highly segmented annular plug nozzles, etc. A research study on fundamental jet noise generation and reduction mechanisms was conducted at the General Electric Corporate Research and Development Center. In addition, investigatory tests were conducted for identification of total system noise. Application of a choked inlet and an open Ag exhaust cycle were studied for noise reduction. Source turbomachinery noise generation and suppression through treatment application were investigated. This report summarizes the acoustic and aerodynamic technology with emphasis toward development of guidelines for future applications.

17. Key Words (Suggested by Author(s))		18. Distribution Statement
Supersonic Transport Jet Noise Suppressors Supersonic Jet Noise Fundamental Jet Mechanisms Two-Stage Ejector Nozzles Simple Mechanical Suppressors	Multi-Tube Suppressors Acoustic Ejectors Segmented Jet Plug Nozzles Engine System Noise Turbomachinery Noise	Approved for U. S. Government only. Transmittal of this document outside the U. S. Government must have prior approval of the Supersonic Transport Office.

19. Security Classif. (of this report)	20. Security Classif. (of this page)	21. No. of Pages	22. Price
Unclassified	Unclassified	486	

"PRECEDING PAGE BLANK-NOT FILMED."

TABLE OF CONTENTS

Section		Page
	VOLUME II	
V.	JET NOISE SUPPRESSOR CONFIGURATIONS AND PARAMETRIC STUDIES (Concluded)	1
	V.G ACOUSTIC EJECTORS ON TUBE AND CONICAL NOZZLES	7
	V.H ANNULAR PLUG NOZZLE SUPPRESSOR MODEL STUDIES	69
	V.H.1 RODS, TUBES, CHUTES, C.D.B. AND PRIMARY FLAPS ON ANNULAR PLUG NOZZLES	73
	V.H.2 MULTI-ELEMENT SPOKE/CHUTE MODEL SUPPRESSOR PARAMETRIC INVESTIGATIONS ON ANNULAR PLUG NOZZLES	131
VI.	SYSTEM STUDIES	221
	VI.A CHOKED INLET - GE4 ENGINE	223
	VI.B EXHAUST NOZZLE OPEN AREA SCHEDULE - GE4 ENGINE	259
	VI.C TURBOMACHINERY NOISE ON GE4 ENGINE	267
	VI.C.1 COMPRESSOR SOURCE NOISE IDENTIFICATION WITH ACOUSTIC PROBES	271
	VI.C.2 COMPRESSOR TIP SHROUD TREATMENT STUDY	285
	VI.C.3 NOISE SOURCE IDENTIFICATION WITH DIRECTIONAL MICROPHONE ARRAY	299
	VI.C.4 J79 TURBOMACHINERY NOISE TEST	307
	VI.C.5 GE4 ENGINE 435-007 NEAR AND FAR FIELD ACOUSTIC MEASUREMENTS	321
VII.	GENERAL ELECTRIC CORPORATE RESEARCH AND DEVELOPMENT CENTER'S FUNDAMENTAL JET NOISE WORK	345
	VII.A SUPERSONIC JET NOISE SUPPRESSION RESULTS AND PREDICTION METHODS	349
	VII.A.1 INTRODUCTION	351
	VII.A.2 CHARACTERISTICS OF SUBSONIC AND SUPERSONIC JETS	353

TABLE OF CONTENTS (Concluded)

Section		Page
	VOLUME II (Concluded)	
VII.A.3	ACOUSTICS OF SHOCK WAVES IN SUPERSONIC JETS	358
VII.A.4	PARALLEL FLOW AND CONVERGENT NOZZLES WITH RODS, SHROUD, AND INDUCED FLOW	367
VII.A.5	REVERSE SLOTTED CONE SUPPRESSORS	380
VII.A.6	MULTITUBES AND MULTISHROUDS SUPPRESSORS	384
VII.A.7	SUPERSONIC JET NOISE SUPPRESSOR MODEL	396
VII.A.8	CONCLUSIONS	405
APPENDIX A	NOMENCLATURE	484

LIST OF TABLES

Table		Page
V.A-1	Jet Suppressor Categories	4
V.G-1	Test Summary of Acoustic Ejectors on Multi-Tube Conical Nozzles	20
V.H.1-1	Summary of Annular Plug Nozzle Test Configurations	80
V.H.1-2	Test Summary (Model 0-3)	83
V.H.1-3	Test Summary (Model V-1)	85
V.H.1-4	Test Summary (Model V-1-1)	88
V.H.1-5	Test Summary (Model V-1-2)	90
V.H.1-6	Test Summary (Model V-1-2-1)	92
V.H.1-7	Test Summary (Model V-1-2-2)	94
V.H.1-8	Test Summary (Model V-1-2-7)	96
V.H.1-9	Test Summary (Model V-1-2-4)	98
V.H.1-10	Test Summary (Model V-1-2-6)	100
V.H.1-11	Test Summary (Model V-1-2-5)	102
V.H.1-12	Test Summary (Model V-2)	104
V.H.1-13	Test Summary (Model V-5)	106
V.H.1-14	Test Summary (Model V-5-1)	108
V.H.1-15	Test Summary (Model V-5-2)	110
V.H.1-16	Test Summary (Model V-8-1)	112
V.H.1-17	Test Summary (Model V-1-2-3)	114
V.H.1-18	Test Summary (Model V-1-3-1)	116
V.H.1-19	Test Summary (Model V-1-3)	118
V.H.1-20	Test Summary (Model V-1-3-3)	120

LIST OF TABLES (Continued)

Table		Page
V.H.1-21	Test Summary (Model V-1-3-2)	122
V.H.1-22	Test Summary (Model V-1-3-4)	124
V.H.1-23	Test Summary (Model V-16)	126
V.H.2-1	Summary of Acoustic and Aerodynamic Model Spoke/Chute and Unsuppressed Configurations	144
V.H.2-2	Test Summary (Model 5.7" Cone)	146
V.H.2-3	Test Summary (Model 1)	151
V.H.2-4	Test Summary (Model 2)	154
V.H.2-5	Test Summary (Model 3)	157
V.H.2-6	Test Summary (Model 4)	160
V.H.2-7	Test Summary (Model 5)	163
V.H.2-8	Test Summary (Model 6)	166
V.H.2-9	Test Summary (Model 7)	169
V.H.2-10	Test Summary (Model 8)	172
V.H.2-11	Test Summary (Model 9)	175
V.H.2-12	Test Summary (Model 10)	178
V.H.2-13	Test Summary (Model 11)	181
V.H.2-14	Test Summary (Model 12)	184
V.H.2-15	Summary of Aerodynamic Test Results on Scale Model Nozzles	217
VI.A-1	Choked Inlet-GE4 Engine 435-002 - Test Summary	232
VII.A-1	Flow and Acoustic Conditions for Parallel Flow Nozzle with Shrouds, $P_r = 3.7$, $M_j = 1.5$	412
VII.A-2	Flow and Acoustic Conditions for Convergent Nozzle with Shroud and Rods, $P_r = 3.7$, $M_j = 1.5$	413

LIST OF TABLES (Concluded)

Table		Page
VII.A-3	Comparison of Acoustic Properites of a M_j = 1.5 Convergent and Parallel Flow Nozzle With and Without Suppressors	414
VII.A-4	Acoustic Power Levels for Convergent Nozzle, M_j = 1.4, with Reverse Slotted Cones and Shrouds	415
VII.A-5	Acoustic Power Levels for Convergent Nozzle, 191 Tubes, 191 Shrouds and Single Shroud	416
VII.A-6	Acoustic Power Levels for Convergent Nozzle and 50 Tubes with Shrouds, M_j = 1.4	417

"PRECEDING PAGE BLANK-NOT FILMED."

LIST OF ILLUSTRATIONS

Figure		Page
V.G-1	Schematic of 37 Tube Greatrex Nozzle with Fiberglass Lined Ejector.	22
V.G-2	37 Tube Greatrex Primary Nozzle Hardware.	23
V.G-3	Schematic of 4.148" I.D. Cone Plus Fiberglass Lined Ejector.	24
V.G-4A-C	Suppression Effects of Fiberglass Liner on 37 Tube Greatrex and 4.1 Conic Nozzles.	25-27
V.G-5A-C	Suppression Effects of Fiberglass Liner on 37 Tube Greatrex Nozzle.	28-30
V.G-6	37 Tube Greatrex Nozzle Hardware with Rigimesh Treated Ejector.	31
V.G-7	Schematic of 37 Tube Greatrex Nozzle with Rigimesh Lined Ejector.	32
V.G-8A,B	Suppression Effects of Short and Long Rigimesh Liners on 37 Tube Greatrex Nozzle.	33,34
V.G-9	97 Tube Nozzle Hardware with Hardwall Ejector.	35
V.G-10	Schematic of 97 Tube Nozzle Plus Ejector with Interchangeable Acoustic Liners.	36
V.G-11A,B	Schematic of 97 Hole Nozzle Plus Ejector with Interchangeable Acoustic Liners.	37-38
V.G-12A,B	Suppression Effect of 7.5% Open Soft Liner on 97 Tube and 97 Hole Nozzles.	39,40
V.G-13A,B	Suppression Effect of 4% Open Soft Liner on 97 Hole Nozzle.	41,42
V.G-14A,B	Suppression Effect of 15% Open Soft Liner on 97 Hole Nozzle.	43,44
V.G-15A-C	Suppression Effect of 22.5% Open, Cerafelt Packed Liner on 97 Hole Nozzle.	45-47
V.G-16A-C	Comparison of Suppression Effect of Soft Liners on 97 Hole Nozzle.	48-50
V.G-17A,B	Comparison of Suppression Effect of Soft Liners on 97 Hole Nozzle at Various Jet Velocities.	51,52

"PRECEDING PAGE BLANK-NOT FILMED."

LIST OF ILLUSTRATIONS

Figure		Page
V.G-1	Schematic of 37 Tube Greatrex Nozzle with Fiberglass Lined Ejector.	22
V.G-2	37 Tube Greatrex Primary Nozzle Hardware.	23
V.G-3	Schematic of 4.148" I.D. Cone Plus Fiberglass Lined Ejector.	24
V.G-4A-C	Suppression Effects of Fiberglass Liner on 37 Tube Greatrex and 4.1 Conic Nozzles.	25-27
V.G-5A-C	Suppression Effects of Fiberglass Liner on 37 Tube Greatrex Nozzle.	28-30
V.G-6	37 Tube Greatrex Nozzle Hardware with Rigimesh Treated Ejector.	31
V.G-7	Schematic of 37 Tube Greatrex Nozzle with Rigimesh Lined Ejector.	32
V.G-8A,B	Suppression Effects of Short and Long Rigimesh Liners on 37 Tube Greatrex Nozzle.	33,34
V.G-9	97 Tube Nozzle Hardware with Hardwall Ejector.	35
V.G-10	Schematic of 97 Tube Nozzle Plus Ejector with Interchangeable Acoustic Liners.	36
V.G-11A,B	Schematic of 97 Hole Nozzle Plus Ejector with Interchangeable Acoustic Liners.	37-38
V.G-12A,B	Suppression Effect of 7.5% Open Soft Liner on 97 Tube and 97 Hole Nozzles.	39,40
V.G-13A,B	Suppression Effect of 4% Open Soft Liner on 97 Hole Nozzle.	41,42
V.G-14A,B	Suppression Effect of 15% Open Soft Liner on 97 Hole Nozzle.	43,44
V.G-15A-C	Suppression Effect of 22.5% Open, Corafelt Packed Liner on 97 Hole Nozzle.	45-47
V.G-16A-C	Comparison of Suppression Effect of Soft Liners on 97 Hole Nozzle.	48-50
V.G-17A,B	Comparison of Suppression Effect of Soft Liners on 97 Hole Nozzle at Various Jet Velocities.	51,52

LIST OF ILLUSTRATIONS (Continued)

Figure		Page
V.G-18	Schematic of 37 Tube Greatrex Nozzle with Perforated Sheet Metal/Cerafelt Packed Ejector.	53
V.G-19	300 Ft Sideline Jet Noise and PNL Suppression Levels for 37 Greatrex Tube Primary Nozzle with Treated and Hardwall Ejectors.	54
V.G-20	1500 Ft Sideline Jet Noise and PNL Suppression Levels for 37 Greatrex Tube Primary Nozzle with Treated and Hardwall Ejector.	55
V.G-21A,B	Suppression Effect of 22.5% Open, Cerafelt Packed Liner on 37 Greatrex Tube Nozzle.	56,57
V.G-22A-F	300 Ft Sideline Spectra and Directivity for 37 Greatrex Tube Nozzle with Treated and Hardwall Ejectors.	58-63
V.G-23	Suppression Effect of Treated Ejector on 37 Greatrex Tube Nozzle at Various Jet Velocities.	64
V.G-24A,B	Spectral Comparison of 97 Hole Nozzle Plus Hardwall Ejector to 37 Greatrex Tube Nozzle Plus Hardwall Ejector.	65,66
V.G-25	Secondary Ejector Skin Temperature Distribution	67
V.H.1-1	Schematic and 320 Ft. Arc Average Jet Noise Level for Model 0-3, 4" I.D. Conical Nozzle Average Baseline.	82
V.H.1-2	Schematic, 320 Ft. Arc Jet Noise Level and Aerodynamic Test Results for Model V-1	84
V.H.1-3	Schematic, 320 Ft. Arc Jet Noise Level and Aerodynamic Test Results for Model V-1-1.	87
V.H.1-4	Schematic and 320 Ft. Arc Jet Noise Level for Model V-1-2.	89
V.H.1-5	Schematic and 320 Ft. Arc Jet Noise Level for Model V-1-2-1.	91
V.H.1-6	Schematic and 320 Ft. Arc Jet Noise Level for Model V-1-2-2.	93

LIST OF ILLUSTRATIONS (Continued)

Figure		Page
V.H.1-7	Schematic and 320 Ft. Arc Jet Noise Level for Model V-1-2-7.	95
V.H.1-8	Schematic, 320 Ft. Arc Jet Noise Level and Aerodynamic Test Results for Model V-1-2-4.	97
V.H.1-9	Schematic and 320 Ft. Arc Jet Noise Level for Model V-1-2-6.	99
V.H.1-10	Schematic and 320 Ft. Arc Jet Noise Level for Model V-1-2-5.	101
V.H.1-11	Schematic, 320 Ft. Arc Jet Noise Level and Aerodynamic Test Results for Model V-2.	103
V.H.1-12	Schematic and 320 Ft. Arc Jet Noise Level for Model V-5.	105
V.H.1-13	Schematic and 320 Ft. Arc Jet Noise Level for Model V-5-1.	107
V.H.1-14	Schematic and 320 Ft. Arc Jet Noise Level for Model V-5-2.	109
V.H.1-15	Schematic and 320 Ft. Arc Jet Noise Level for Model V-8-1.	111
V.H.1-16	Schematic and 320 Ft. Arc Jet Noise Level for Model V-1-2-3.	113
V.H.1-17	Schematic and 320 Ft. Arc Jet Noise Level for Model V-1-3-1.	115
V.H.1-18	Schematic and 320 Ft. Arc Jet Noise Level for Model V-1-3.	117
V.H.1-19	Schematic and 320 Ft. Arc Jet Noise Level for Model V-1-3-3.	119
V.H.1-20	Schematic and 320 Ft. Arc Jet Noise Level for Model V-1-3-2.	121
V.H.1-21	Schematic, 320 Ft. Arc Jet Noise Level Aerodynamic Test Results for Model V-1-3-[illegible].	123
V.H.1-22	Hardware, Schematic and 320 Ft. Arc Jet Noise Level for Model V-16.	125

LIST OF ILLUSTRATIONS (Continued)

Figure		Page
V.H.1-23A,B	Representative Configurations of Annular Plug Suppressor Hardware.	128,129
V.H.2-1	Baseline Conical Nozzle Schematic and Test Summary.	146
V.H.2-2	Conical Test Summary and Baseline 320 Ft. Arc Jet Noise Levels.	147
V.H.2-3	Baseline 300 Ft. Sideline Jet Noise Levels From 1971 and 1969 Tests.	148
V.H.2-4	Baseline 1500 Ft. Sideline Jet Noise Levels From 1971 and 1969 Tests.	149
V.H.2-5	Baseline 1500 Ft. Sideline PNL Directivity From 1971 Tests.	150
V.H.2-6	Hardware and Test Summary for Model 1.	151
V.H.2-7	320 Ft. Arc and 300 Ft. Sideline Jet Noise Levels for Model 1.	152
V.H.2-8	1500 Ft. Sideline Jet Noise Levels and PNL Directivity for Model 1.	153
V.H.2-9	Hardware and Test Summary for Model 2.	154
V.H.2-10	320 Ft. Arc and 300 Ft. Sideline Jet Noise Levels for Model 2.	155
V.H.2-11	1500 Ft. Sideline Jet Noise Levels and PNL Directivity for Model 2.	156
V.H.2-12	Hardware and Test Summary for Model 3.	157
V.H.2-13	320 Ft. Arc and 300 Ft. Sideline Jet Noise Levels for Model 3.	158
V.H.2-14	1500 Ft. Sideline Jet Noise Levels and PNL Directivity for Model 3.	159
V.H.2-15	Hardware and Test Summary for Model 4.	160
V.H.2-16	320 Ft. Arc and 300 Ft. Sideline Jet Noise Levels for Model 4.	161
V.H.2-17	1500 Ft. Sideline Jet Noise Levels and PNL Directivity for Model 4.	162

LIST OF ILLUSTRATIONS (Continued)

Figure		Page
V.H.2-18	Hardware and Test Summary for Model 5.	163
V.H.2-19	320 Ft. Arc and 300 Ft. Sideline Jet Noise Levels for Model 5.	164
V.H.2-20	1500 Ft. Sideline Jet Noise Levels and PNL Directivity for Model 5.	165
V.H.2-21	Hardware and Test Summary for Model 6.	166
V.H.2-22	320 Ft. Arc and 300 Ft Sideline Jet Noise Levels for Model 6.	167
V.H.2-23	1500 Ft. Sideline Jet Noise Levels and Directivity for Model 6.	168
V.H.2-24	Hardware and Test Summary for Model 7.	169
V.H.2-25	320 Ft. Arc and 300 Ft. Sideline Jet Noise Levels for Model 7.	170
V.H.2-26	1500 Ft. Sideline Jet Noise Levels and PNL Directivity for Model 7.	171
V.H.2-27	Hardware and Test Summary for Model 8.	172
V.H.2-28	320 Ft. Arc and 300 Ft. Sideline Jet Noise Levels for Model 8.	173
V.H.2-29	1500 Ft. Sideline Jet Noise Levels and PNL Directivity for Model 8.	174
V.H.2-30	Hardware and Test Summary for Model 9.	175
V.H.2-31	320 Ft. Arc and 300 Ft. Sideline Jet Noise Levels for Model 9.	176
V.H.2-32	1500 Ft. Sideline Jet Noise Levels and PNL Directivity for Model 9.	177
V.H.2-33	Hardware and Test Summary for Model 10.	178
V.H.2-34	320 Ft. Arc and 300 Ft. Sideline Jet Noise Levels for Model 10.	179
V.H.2-35	1500 Ft. Sideline Jet Noise Levels and PNL Directivity for Model 10.	180

LIST OF ILLUSTRATIONS (Continued)

Figure		Page
V.H.2-36	Hardware and Test Summary for Model 11.	181
V.H.2-37	320 Ft. Arc and 300 Ft. Sideline Jet Noise Levels for Model 11.	182
V.H.2-38	1500 Ft. Sideline Jet Noise Levels and PNL Directivity for Model 11.	183
V.H.2-39	Hardware and Test Summary for Model 12.	184
V.H.2-40	320 Ft. Arc and 300 Ft. Sideline Jet Noise Levels for Model 12.	185
V.H.2-41	1500 Ft. Sideline Jet Noise Levels and PNL Directivity for Model 12.	186
V.H.2-42	Gross Thrust Coefficient Variation for Baseline Unsuppressed Plub Nozzles.	187
V.H.2-43	Hardware used for Parametric Investigation of Area Ratio; Aerodynamic Test Results.	188
V.H.2-44	Effect of Area Ratio on 300 Ft. and 1500 Ft Sideline PNL Suppression for Plug Nozzle Configurations.	189
V.H.2-45A-C	Effect of Area Ratio on 1500 Ft. Sideline Spectra.	190-192
V.H.2-46	Hardware used for Parametric Investigation of Spoke Number; Aerodynamic Test Results.	193
V.H.2-47	Effect of Spoke Number on 300 Ft. and 1500 Ft. Sideline PNL Suppression for Plug Nozzle Configurations.	194
V.H.2-48A-C	Effect of Spoke Number on 1500 Ft. Sideline Spectra.	195-197
V.H.2-49	Hardware used for Parametric Investigation of Spoke Angle-of-Attack; Aerodynamic Test Results.	198
V.H.2-50	Effect of Spoke Angle-of-Attack on 300 Ft. and 1500 Ft. Sideline PNL Suppression for Plug Nozzle Configurations.	199

LIST OF ILLUSTRATIONS (Continued)

Figure		Page
V.H.2-51A-C	Effect of Spoke Angle-of-Attack on 1500 Ft. Sideline Spectra.	200-202
V.H.2-52	Hardware used for Parametric Investigation of Spoke Planform, Aerodynamic Test Results.	203
V.H.2-53	Effect of Spoke Planform on 300 Ft. and 1500 Ft. Sideline PNL Suppression for Plug Nozzle Configurations.	204
V.H.2-54A-C	Effect of Spoke Planform on 1500 Ft. Sideline Spectra.	205-207
V.H.2-55	Hardware used for Parametric Investigation of Chutes Versus Spokes; Aerodynamic Test Results.	208
V.H.2-56	Effect of Chutes Versus Spokes on 300 Ft. and 1500 Ft. Sideline PNL Suppression for Plug Nozzle Configurations.	209
V.H.2-57A-C	Effect of Chutes Versus Spokes on 1500 Ft Sideline Spectra.	210-212
V.H.2-58	Suppressed Model Hardware and Aerodynamic Results.	213
V.H.2-59	Unsuppressed Plug Nozzle Hardware Showing Flight Mode Configurations.	214
V.H.2-60	Flight Mode Test Results on Unsuppressed Plug Nozzles.	215
V.H.2-61	Simulated Full Scale Shroud Length Variation Effects.	216
VI.A-1	GE4 Engine 435-002 With Boeing Inlet - Sharp Edged Lip - Peebles Site 4D.	230
VI.A-2	Schematic of Boeing Inlet for GE4 Engine Test.	231
VI.A-3	Effect of Choked Inlet on 300 Ft. Sideline PNL Directivity at 4000 RPM.	233
VI.A-4	Effect of Choked Inlet on 300 Ft. Sideline PNL Directivity at 4500 RPM.	234

LIST OF ILLUSTRATIONS (Continued)

Figure		Page
VI.A-5	Effect of Choked Inlet on 300 Ft. Sideline PNL Directivity at 4500 RPM.	235
VI.A-6	Effect of Choked Inlet on 300 Ft. Sideline Peak PNL.	236
VI.A-7	Effect of Choked Inlet on 250 Ft. Arc Spectra at 30° to the Inlet.	237
VI.A-8	Effect of Choked Inlet on 250 Ft. Arc Spectra at 110° to the Inlet.	238
VI.A-9A-L	Narrowband Analysis of GE4 Choked Inlet Acoustic Test.	239-250
VI.A-10	Effect of Choked Inlet on 300 Ft. Sideline Spectra at 110° and 4000 RPM.	251
VI.A-11	Effect of Choked Inlet on 300 Ft. Sideline Spectra at 110° and 4500 RPM.	252
VI.A-12	Effect of Choked Inlet on 300 Ft. Sideline Spectra at 110° and 4700 RPM.	253
VI.A-13	GE4 Engine 435-003 with Boeing Inlet - Bellmouth - Peebles Site 4D.	254
VI.A-14	Effect of Main Inlet Mach Number on Compressor First Stage Fundamental Tone.	255
VI.A-15	Effect of Variable Inlet Door Opening on Far Field Spectra at 30° and 110° to Inlet.	256
VI.A-16	Effect of Variable Inlet Door Opening on Far Field PNL Directivity.	257
VI.B-1	Effect of Exhaust Nozzle Open Area Schedule on GE4 Engine 435-002 Noise Levels.	263
VI.B-2	Effect of Open Area Schedule on GE4 Peak PNL.	264
VI.B-3	Effect of A_8 on GE4 Noise Spectra at Constant Thrust.	265
VI.B-4	Normalized GE4 Noise Levels as a Function of Jet Velocity.	266

LIST OF ILLUSTRATIONS (Continued)

Figure		Page
VI.C.1-1	Schematic of FTS Compressor Test Vehicle.	275
VI.C.1-2	GE4 Compressor Geometry.	276
VI.C.1-3	Schematic of GE4 Engine 435-007 with Inlet Acoustic Probe.	277
VI.C.1-4	FTS Compressor Tank Test - Acoustic Narrowband Plot.	278
VI.C.1-5	FTS Compressor Tank Test - Acoustic Narrowband Plot.	279
VI.C.1-6	GE4 FTS Compressor Tank Test - Acoustic Narrowband Plot.	280
VI.C.1-7	GE4 FTS Compressor Tank Test - Forward and Aft Propagated Fundamental Tone Power Levels.	281
VI.C.1-8	GE4 Block II and FTS Compressor Tests - First Stage Fundamental Tone Power Levels.	282
VI.C.1-9	GE4 FTS Compressor Noise Levels - Peebles Engine Test.	283
VI.C.2-1	GE4 Compressor Tip Shroud Treatment.	290
VI.C.2-2	Schematic of 15" Compressor and Tip Treatment Variations.	291
VI.C.2-3	Tip Shroud Treatment Effectiveness - 3 Blade Chord Widths - with IGV's.	292
VI.C.2-4	Tip Shroud Treatment Effectiveness - Single Blade Chord Widths - with IGV's.	293
VI.C.2-5	Tip Shroud Treatment Effectiveness - 3 Blade Chord Widths - without IGV's.	294
VI.C.2-6	Tip Shroud Treatment Effectiveness - SDOF Over Blade Row Only.	295
VI.C.2-7	Tip Shroud Treatment Effectiveness - Narrowband Analysis and 1/3 Octave Band Suppression.	296
VI.C.2-8	Estimated GE4 Tip Shroud Suppression.	297

LIST OF ILLUSTRATIONS (Continued)

Figure		Page
VI.C.3-1	Directional Microphone Array System.	303
VI.C.3-2	Beam Patterns of Directional Acoustic Array.	304
VI.C.3-3	GE4 First Stage Compressor Tone Source Locations.	305
VI.C.4-1	Schematic of J79 Turbomachinery Noise Test Vehicle.	312
VI.C.4-2	J79-15 Near/Far Field Turbomachinery Noise Test.	313
VI.C.4-3	Comparison of Measured and Predicted J79 Perceived Noise Levels.	314
VI.C.4-4	J79 Turbomachinery Noise Suppressor Performance - Far Field and Duct Sound Power Level Reductions.	315
VI.C.4-5	J79 Turbomachinery Noise Suppressor Performance - Narrowband Analysis.	316
VI.C.4-6	Comparison of J79 Casing Strain Gage and Microphone Spectra.	317
VI.C.4-7	Near Field Array Noise Contours of Tone from Radial Bevel Gear.	318
VI.C.4-8	Near Field Array Noise Contours of Tone from 15th and 17th Compressor Stages.	319
VI.C.5-1	GE4 Acoustic Microphone Array.	326
VI.C.5-2	GE4 FTS Engine Far Field Noise Levels.	327
VI.C.5-3	Comparison of GE4 Block I and FTS Engine Far Field Noise Levels.	328
VI.C.5-4	GE4 Block I and FTS Directivity Comparison at High Jet Velocity.	329
VI.C.5-5	GE4 Block I and FTS Spectra Comparison at High Jet Velocity.	330
VI.C.5-6	GE4 Block I and FTS Directivity at High Jet Velocity.	331
VI.C.5-7	GE4 Block I and FTS Spectra Comparison at High Jet Velocity.	332

LIST OF ILLUSTRATIONS (Continued)

Figure		Page
VI.C.5-8	GE4 Block I and FTS Directivity Comparison at Low Jet Velocity.	333
VI.C.5-9	GE4 Block I and FTS Spectra Comparison at Low Jet Velocity.	334
VI.C.5-10	GE4 Noise Data-Narrowband Spectra at Several Engine Speeds on Normal A_8 Schedule.	335
VI.C.5-11	GE4 Noise Data-Narrowband Spectra Variation with Normal and Loiter A_8 Schedule.	336
VI.C.5-12	GE4 Near Field Noise Contours - Stage 9 Compressor Fundamental Pure Tone.	337
VI.C.5-13	GE4 Near Field Contours - Stage 2 Turbine Fundamental Pure Tone.	338
VI.C.5-14	GE4 Near Field CAsing Microphone Noise Levels.	339
VI.C.5-15	GE4 Near Field Noise Reduction by Engine Cowling.	340
VI.C.5-16	GE4 Near/Far Field Overall Sound Pressure Levels at Maximum Speed.	341
VI.C.5-17	GE4 Near/Far Field Overall Sound Pressure Levels at Maximum Speed.	342
VI.C.5-18	GE4 Near/Far Field Overall Sound Pressure Levels at Maximum Dry.	343
VI.C.5-19	GE4 Near/Far Field Overall Sound Pressure Levels at Part Reheat.	344
VII.A-1	Shadowgraph Photographs of Flow from a Convergent Nozzle at Mach Numbers of 1.0 and 1.4.	418
VII.A-2A	Variation of Flow Mach Number along the Jet Axis with Distance for Convergent Nozzle.	419
VII.A-2B	Velocity Ratio on Jet Axis for Two Inch Diameter Convergent Nozzle.	420
VII.A-3	Variation of Impact Pressure Fluctuations on Jet Axis with Distance from Jet Axis for Two Inch Diameter Convergent Nozzle.	421

LIST OF ILLUSTRATIONS (Continued)

Figure		Page
VII.A-4	Jet Core Length, and Supersonic Length, as a Function of Jet Mach Number.	422
VII.A-5	Overall Sound Pressure Level as a Function of Angular Position from Jet Axis for Different Jet Mach Numbers.	423
VII.A-6	Comparison of Sound Power Spectra for Plain Convergent Jet at Various Mach Numbers.	424
VII.A-7	Near Field Overall Sound Pressure Level as a Function of Jet Mach Number and Axial Distance at 2 Diameters from Nozzle Exit.	425
VII.A-8	Acoustic Power Per Unit of Length of Jet Obtained With Microphone Traverse Parallel to Jet Axis at Two Nozzle Diameters from Nozzle Periphery.	426
VII.A-9	Axial Mach Number Profile With Plain Nozzle.	427
VII.A-10	Comparison of Directivities for M=1.5 Parallel Flow and Convergent Nozzles.	428
VII.A-11	Comparison of Power Level Spectra for M=1.5 Parallel Flow and Convergent Nozzles.	429
VII.A-12A	Comparison of Axial Mach Number Variation of Jet With and Without Rods, Convergent Nozzle, P_r=3.2, M_j=1.4.	430
VII.A-12B	Overall Sound Pressure Level as a Function of Angular Position from the Jet Axis With and Without Rods, Convergent Nozzle, P_r=3.2, M_j=1.4.	431
VII.A-12C	Sound Power Level Spectra of the Jet With and Without Rods, Convergent Nozzle, P_r=3.2, M_j=1.4.	432
VII.A-13A	Overall Sound Pressure Level as a Function of Angular Position from the Jet Axis With Rods, Convergent Nozzle, P_r=3.7, M_j=1.5.	433
VII.A-13B	Sound Power Level Spectra With Rods, Convergent Nozzle, P_r=3.7, M_j=1.5.	434
VII.A-14A	Sketch of Convergent Nozzle, Shroud, and Rods.	435

LIST OF ILLUSTRATIONS (Continued)

Figure		Page
VII.A-14B	Shroud Pressure Distribution With Rods and Shroud Closed, Convergent Nozzle, P_r=3.7, M_j=1.5.	436
VII.A-14C	Radial Mach Number Profiles at Jet Exhaust Exit With Rods and Shroud, Convergent Nozzle, P_r=3.7, M_j=1.5.	437
VII.A-14D	Axial Mach Number Profile With Rods and Shroud, Convergent Nozzle, P_r=3.7, M_j=1.5.	438
VII.A-14E	Overall Sound Pressure Level as a Function of Angular Position from the Jet Axis With Rods and Shroud Closed, Convergent Nozzle, P_r=3.7, M_j=1.5.	439
VII.A-14F	Sound Power Level Spectra With Rods and Shroud Closed, Convergent Nozzle, P_r=3.7, M_j=1.5.	440
VII.A-15A	Sketch of Nozzle and Shrouds.	441
VII.A-15B	Shroud Pressure Distribution With 4 and 6 Inch Shrouds for Parallel Flow Nozzle, P_r=3.7, M_j=1.5.	442
VII.A-15C	Radial Mach Number Profile at Jet Exhaust Exit With Shrouds for Parallel Flow Nozzle.	443
VII.A-15D	Mixed Jet Velocity as a Function of Induced Flow With Single and Double Shrouds for Parallel Flow Nozzle.	444
VII.A-15E	Overall Sound Pressure Level as a Function of Angular Position from Jet Axis With 4 or 6 Inch Shroud for Parallel Flow Nozzle.	445
VII.A-15F	Sound Power Level Spectra With 4 or 6 Inch Shrouds for Parallel Flow Nozzle, P_r=3.7, M_j=1.5.	446
VII.A-15G	Acoustic Power Reduction as a Function of Induced Flow for Parallel Flow Nozzle With 4 or 6 Inch Shrouds, P_r=3.7, M_j=1.5.	447
VII.A-16A	Shroud Pressure Distribution With Rods and Shroud Open, Convergent Nozzle, P_r=3.7, M_j=1.5.	448
VII.A-16B	Axial Pressure Fluctuations for Convergent Nozzle and Suppressors, P_r=3.7, M_j=1.5.	449

LIST OF ILLUSTRATIONS (Continued)

Figure		Page
VII.A-16C	Overall Sound Pressure Level as a Function of Angular Position from the Jet Axis With Rods and Shroud Open for Convergent Nozzle, P_r=3.7, M_j=1.5.	450
VII.A-16D	Sound Power Level Spectra With Rods and Shroud Open for Convergent Nozzle, P_r=3.7, M_j=1.5.	451
VII.A-17A	Comparison of Directivities for M=1.5 Parallel Flow and Convergent Nozzles With and Without Suppressors.	452
VII.A-17B	Comparison of Power Level Spectra for M=1.5 Parallel Flow and Convergent Nozzles With and Without Suppressors.	453
VII.A-17C	Variation in Overall Sound Power Level With Rods and Shroud as a Function of Induced Mass Flow for M_j=1.5.	454
VII.A-18A	Photograph of 60° Reverse Slotted Cone With 28 Slots.	455
VII.A-18B	Sketch of 60° Reverse Slotted Cone and Shroud.	456
VII.A-18C	Mach Number Profile Across the Jet at One Inch Downstream of Apex of the Reverse Slotted Cones, P_r=3.2, M_j=1.4.	457
VII.A-18D	Axial Mach Number Variations for Reverse Slotted Cones and Plain Jet, P_r=3.2, M_j=1.4.	458
VII.A-18E	Axial Distance from Apex of Reverse Slotted Cone-Inches, Axial Impact Pressure Fluctuations for Reverse Slotted Cones, P_r=3.2, M_j=1.4.	459
VII.A-18F	Base Pressure on the Solid Portion of the Reverse Slotted Cones, P_r=3.2, M_j=1.4.	460
VII.A-18G	Overall Sound Pressure Level as a Function of Angular Position from Jet Axis for Reverse Slotted Cones With and Without Shrouds, P_r=3.2, M_j=1.4.	461
VII.A-18H	Sound Power Level Spectra for Reverse Slotted Cones With and Without Shrouds, P_r=3.2, M_j=1.4.	462
VII.A-19A	Photograph of Multitube and Multishroud Suppressor.	463
VII.A-19B	Sketch of Multitube Suppressor and Shrouds.	464

LIST OF ILLUSTRATIONS (Continued)

Figure		Page
VII.A-19C	Mach Number Profile Across Exits of Multitubes and Multishroud.	465
VII.A-19D	Axial Mach Number Variation for Multitubes With and Without Shrouds.	466
VII.A-19E	Axial Impact Pressure Fluctuations for Multitubes With and Without Shrouds.	467
VII.A-19F	Base Pressure Distribution for Various Multishroud Configurations.	468
VII.A-19G	Overall Sound Pressure Level as a Function of Angular Position from Jet Axis for Multitubes With and Without Shrouds.	469
VII.A-19H	Sound Power Level Spectra for Multitubes With and Without Shrouds.	470
VII.A-19I	Variation of Overall Sound Power Level Reduction and Percentage Thrust Loss for 191 Tubes With 191-Shroud Length.	471
VII.A-20A	Photograph of 50 Tube Suppressors and Shrouds.	472
VII.A-20B	Sketch of 50 Tube Suppressors and Shrouds.	473
VII.A-20C	Mach Number Profile Across Exits of 50 Tube Nozzles 1/32" Downstream of Tube Exit, P_c=3.2, M_j=1.4.	474
VII.A-20D	Mach Number Profile Across Exits of Shrouds, L=2", L/D=8.	475
VII.A-20E	Axial Mach Number Distribution for 50 Tube Nozzle, With and Without Shrouds, L=2", L/D=8.	476
VII.A-20F	Axial Impact Pressure Fluctuations for 50 Multitube Nozzle With and Without Shrouds, L/D=8.	477
VII.A-20G	Base Pressure Distribution for Various Multitube Lengths and Shroud Arrangements.	478
VII.A-20H	Overall Sound Pressure Level as a Function of Angular Position from the Jet Axis for 50 Tube Nozzle With and Without Shrouds, L/D=8.	479

LIST OF ILLUSTRATIONS (Continued)

Figure		Page
VII.A-19C	Mach Number Profile Across Exits of Multitubes and Multishroud.	465
VII.A-19D	Axial Mach Number Variation for Multitubes With and Without Shrouds.	466
VII.A-19E	Axial Impact Pressure Fluctuations for Multitubes With and Without Shrouds.	467
VII.A-19F	Base Pressure Distribution for Various Multishroud Configurations.	468
VII.A-19G	Overall Sound Pressure Level as a Function of Angular Position from Jet Axis for Multitubes With and Without Shrouds.	469
VII.A-19H	Sound Power Level Spectra for Multitubes With and Without Shrouds.	470
VII.A-19I	Variation of Overall Sound Power Level Reduction and Percentage Thrust Loss for 191 Tubes With 191-Shroud Length.	471
VII.A-20A	Photograph of 50 Tube Suppressors and Shrouds.	472
VII.A-20B	Sketch of 50 Tube Suppressors and Shrouds.	473
VII.A-20C	Mach Number Profile Across Exits of 50 Tube Nozzle-1/32" Downstream of Tube Exit, P_r=1.2, M_j=1.4.	474
VII.A-20D	Mach Number Profile Across Exits of Shrouds, L=3", L/D=8.	475
VII.A-20E	Axial Mach Number Distribution for 50 Tube Jet, with and Without Shrouds, L=2", L/D=8.	476
VII.A-20F	Axial Impact Pressure Fluctuations for 50 Multitube Nozzle With and Without Shrouds, L/D=8	477
VII.A-20G	Base Pressure Distribution for Various Multitube Lengths and Shroud Arrangements.	478
VII.A-20H	Overall Sound Pressure Level as a Function of Angular Position from the Jet Axis for 50 Tube Nozzle With and Without Shrouds, L/D=8.	479

LIST OF ILLUSTRATIONS (Concluded)

Figure		Page
VII.A-20I	Sound Power Spectra for 50 Tube Nozzle With and Without Shrouds, L/D=8.	480
VII.A-20J	Variation of Overall Sound Power Level Reduction and Percentage Thrust Loss With Tube Length for 50 Tube Suppressors With and Without Shrouds.	481
VII.A-21	Variations of Coalesced Mach Number and Distance for Jets to Coalesce as a Function of Tube Spacing, P_r=3.2.	482
VII.A-22	Overall Sound Power Level Reduction as a Function of Coalesced Mach Number for Multiholes, Multitubes, and Multishrouds, P_r=3.2 and M_j=1.4.	483

V. JET NOISE SUPPRESSOR CONFIGURATIONS AND PARAMETRIC STUDIES (Concluded)

"PRECEDING PAGE BLANK-NOT FILMED."

V. JET NOISE SUPPRESSOR CONFIGURATIONS AND PARAMETRIC STUDIES (Concluded)

The jet noise suppressor configurations and parametric studies of Section V, reported on in Volume I of this summary document, are concluded in Volume II. Table V.A-1 in Section V.A, which summarizes the model and engine jet suppressors reported on in Section V, is again included for reference. In Volume I major Sections I through IV plus suppressor categories of Sections V.B through V.F.10 were documented. This volume contains the remainder of Section V (i.e., Sections V.G, V.H.1 and V.H.2), as well as the last two major sections of the report, Sections VI and VII.

TABLE V.A-1 JET SUPPRESSOR CATEGORIES.

Section	Jet Suppressor Category	Figures	Tables
	Volume I		
V.B.	Two Stage Ejector Nozzle Tests on Suppressor Models and Full Scale Engines	V.B-1 through V.B-23	V.B-1 through V.B-10
V.C.1	Primary Radial Rods Within TSEN-3	V.C.1-1 through V.C.1-16	V.C.1-1 through V.C.1-9
V.C.2	Primary Thrust Reverser Tab Variations for Model and Engine Tests	V.C.2-1 through V.C.2-22	V.C.2-1 through V.C.2-14
V.C.3	Primary Vented Chute Suppressors	V.C.3-1 through V.C.3-6	V.C.3-1 and V.C.3-2
V.D.1	Hollow Radial Spokes with Ambient Pumping and Axial Injecting Simulated Compressor Discharge Bleed	V.D.1-1 through V.D.1-11	None
V.D.2	Hollow Radial Spokes with Radial and Axial Air and Water Injection	V.D.2-1 through V.D.2-5	None
V.D.3	Air and Water Injection Over Primary Thrust Reverser Tabs	V.D.3-1 through V.D.3-3	None
V.E.	Secondary Reverser - Suppressor Flaps	V.E-1 through V.E.-11	None
V.F.1	Comparison of Tube Length, Area Ratio, Secondary Ejector and Secondary Ejector Airflow Effects on 72 Tube/Hole Nozzles	V.F.1-1 through V.F.1-12	V.F.1-1 and V.F.1-2
V.F.2	Baseplate and Tube Exit Plane Stagger Angle Variations on 72 Tube Model Suppressors	V.F.2-1 through V.F.2-24	V.F.2-1 through V.F.2-7
V.F.3	Variations of a 37 Tube Nozzle	V.F.3-1 through V.F.3-24	V.F.3-1 through V.F.3-5

TABLE V.A-1 JET SUPPRESSOR CATEGORIES (Concluded)

Section	Jet Suppressor Category	Figures	Tables
	Volume I (Concluded)		
V.F.4	Tube End Variations on 37 Straight, Convergent, Greatrex and Canted End Tubes	V.F.4-1 through V.F.4-30	V.F.4-1 through V.F.4-8
V.F.5	Tube Internal and External Length To Diameter Studies on an 85 Tube Nozzle	V.F.5-1 through V.F.4-25	V.F.5-1 through V.F.5-8
V.F.6	Hole Shape, Equal and Unequal Hole Size and Spacing Studies on 97 Hole Plates	V.F.6-1 through V.F.6-18	V.F.6-1 through V.F.6-5
V.F.7	Variations of 97 Tube Primary Nozzle with Large and Small Center Hole; Comparisons with Hardwall and 7.5% Open Lined Ejectors	V.F.7-1 through V.F.7-17	V.F.7-1 through V.F.7-4
V.F.8	Geometric Variations of Center Hole Shape on 97 Hole Nozzle; Hardwall and Acoustically Lined Ejector Comparisons; D_S/D_{Td} Variations	V.F.8-1 through V.F.8-35	V.F.8-1 through V.F.8-10
V.F.9	Multi-Hole Nozzle Parametric Variations of Area Ratio, Hole Number, Shroud D_S/D_{Td}, and Shroud Axial Spacing, X_S	V.F.9-1 through V.F.9-67	V.F.9-1 through V.F.9-16
V.F.10	Multi-Tube Preliminary Design Number 3 (PD-3)	V.F.10-1 through V.F.10-27	V.F.10-1 through V.F.10-4
	Volume II		
V.G.	Acoustic Ejectors on Tube and Conical Nozzles	V.G-1 through V.G-25	V.G-1
V.H.1	Rods, Tubes, Chutes, C.D.B and Primary Flaps on Annular Plug Nozzles	V.H.1-1 through V.H.1-23	V.H.1-1 through V.H.1-23
V.H.2	Multi-Element Spoke/Chute Model Suppressor Parametric Investigations on Annular Plug Nozzles	V.H.2-1 through V.H.2-61	V.H.2-1 through V.H.2-15

"PRECEDING PAGE BLANK-NOT FILMED."

V.G ACOUSTIC EJECTORS ON TUBE AND CONICAL NOZZLES

"PRECEDING PAGE BLANK-NOT FILMED."

V.G ACOUSTIC EJECTORS ON MULTI-TUBE AND CONICAL NOZZLES

Objectives of Test Series

Acoustic treatment addition to an ejector of a jet noise suppressor system has shown to attain noise suppression gain over hardwall ejectors. With the emphasis in 1968 and 1969 on multi-element primary suppressors, which move the primary jet noise generation region closer to the nozzle exit plane than a non-suppressed or simply suppressed primary nozzle, acoustic ejector studies were initiated. A series of tests were run at the GE Evendale JENOTS acoustic facility in six phases from 8/68 through 6/69 in sequential steps to develop treated ejector technology. Table V.G - 1 is a listing of the acoustic tests for the six phases giving model numbers, test dates, model descriptions and general purpose of each test phase. For the Greatrex tube models, test conditions over an engine operating line ranged from nozzle pressure ratios of 1.4 to 3.0, exhaust gas temperature of 1100 to 1960° R and ideal jet velocities of 1150 to 2500 ft/sec. These tubes were not of high-temperature resistent material, therefore the test velocity range was somewhat limited. For the 97 tube and 97 hole nozzles the test conditions over an engine operating line ranged from pressure ratios of 1.4 to 3.4, temperatures from 1200 to 2330°R, and ideal jet velocities of 1150 to 2930 ft/sec. Acoustic measurements were taken on a 40 ft. arc and scaled by frequency and size to full scale application using a scale factor of 8:1. All data presented are therefore of simulated engine size and engine frequency range.

The six study phases are summarized as follows:

o Phase I

This was an initial test of a bulk fiberglass lined ejector on a non-suppressed conical nozzle and on a 37 Greatrex tube nozzle to determine if treatment could gain additional jet suppression in the far field and to determine how strong an influence the jet noise source location is in relation to the shrouding ejector and treatment (see Figures V.G-1, -2 & -3). A bulk fiberglass ejector is not practical in engine hardware but, since it is a good broadband suppressor, it would show magnitude of suppression achievable by treatment and would set a goal to which effectiveness of practical treatment could be referenced.

Results of this phase are shown in Figures V.G-4A through -4C and -5A through -5C. This phase showed the bulk liner to have very good suppression characteristics for far field measurements from the 500 Hz band and up and to influence a 5 PNdB suppression gain over an unlined ejector when used with the multi-tube primary suppressor. Minor suppression gain was seen when the bulk liner was used with the conical primary since the noise spectra, upon which the treatment is effective, was generated external to the ejector. Thus, if a practical treatment could be developed to the equivalent effectiveness of the bulk absorber, a lined ejector would be quite beneficial in conjunction with a multi-element primary jet suppressor.

o Phase II

This was a first cut practical approach to ejector treatment using available tube nozzle hardware (the 37 Greatrex tube nozzle system on loan from The Boeing Company, Figures V.G-6 and -7). A cylindrical ejector, lined with Rigimesh acoustic treatment, was built in two sections to determine a) Rigimesh effectiveness as an acoustic treatment, and b) the effect of treated ejector length on achievable suppression. Ejector length to diameter ratios, L_S/D_S of .625 and 1.25, resulted from use of one, then a combination of both ejector sections. The Rigimesh proved effective when compared to a hardwall ejector of the same geometry, especially in the 1K, 2K and 4K Hz bands, suppression increasing substantially with the added ejector length. PNL suppression gain was near constant for a wide range of jet velocity at about 2.5 PNdB for the L_S/D_S = .625 ejector and at 4.5 PNdB for the longer ejector. Therefore, an ejector for practical engine application of L_S/D_S = 1.0, when designed similar to the Rigimesh ejector, would anticipate about 3.5 PNdB suppression gain due to the treatment.

o Phase III

Tube nozzle technology developed to a level where a viable suppression system could be designed for engine application. This took the form, in model hardware, of a 97 tube nozzle (see Figures V.G-9 & -10). A series of tests were planned to evaluate ejector liner porosity effect within practical physical dimension limitations while using the 97 tube primary jet suppressor. Several configurations were tested including a 7.5% open lined ejector and a

hardwall ejector before the primary tube nozzle failed in test. A new primary nozzle of slightly different design was built to replace the 97 tube nozzle in the test series.

o Phase IV

The new nozzle, a 97 hole configuration (see Figure V.G-11A and 11B), was identical to the 97 tube nozzle in hole size and spacing, internal tube length, and tube exit plane stagger; but was a thick baseplate design with no external tube length. In addition, a lobed (Greatrex) center replaced the large center hole of the 97 tube nozzle design. Perforated sheet metal ejectors of 4%, 7.5%, and 15% porosity plus a 22.5% porous liner with Cerafelt packing were tested with the new nozzle. The cavity depth behind the porous plates was increased to .22" from the .10" of the Rigimesh liner of Phase II to lower the peak frequency attenuated.

A study of the results of the 97 tube and 97 hole nozzle treated ejector tests showed results to be much poorer than anticipated. The 4%, 7.5% and 15% liners gave very low suppression. The best PNL suppression gain was about 4 PNdB with the 22.5% packed Cerafelt liner, but then only in the very low jet velocity range and decreasing to no suppression gain at higher velocity. Suppression gain was essentially the same with the 7.5% liner at about 2 PNdB at intermediate V_J when used with either 97 tube or hole primary nozzles.

o Phase V

With the results of the 97 tube/hole treated ejector study, primary concern was why the perforated sheet metal liners - in particular the 22.5% porous liner with Cerafelt packing - performed so poorly when compared to their anticipated suppression levels. It was believed that the Cerafelt packed liner would exhibit suppression gain of the magnitude experienced with the Rigimesh liners of the 37 Greatrex tube nozzles, namely, to have reasonable PNL suppression across the V_J test range. Since the perforated liners were expected to perform much better, it was reasoned that the primary nozzle spectral noise content, on which the lining was to work, differed sufficiently to cause the change in far field noise suppression levels. To substantiate this reasoning, either a Rigimesh liner could be built to match the physical parameters of the perforated sheet metal liners and tested on the 97 hole nozzle, or a perforated

metal liner could be built to the specifics of the original Rigimesh liner and tested on the 37 Greatrex tube nozzle. The latter was judged to be a more practical treatment application, so the best anticipated suppression model of 22.5 % porous liner with Cerafelt packing was built and tested (see Figure V.G-18).

Test data showed the suppression gain to hold between 3.5 to 5 PNdB across the tested jet velocity range with the lesser suppression at high velocity. These good suppression results thus indirectly supported the prior reasoning, proving the ineffectiveness of the liner designs on the 97 tube nozzles was due to the spectra content within the ejector length on which the treatment had to work. The test also proved that a practical design with perforated sheet metal liners and acoustic packing can achieve a reasonable level of additional suppression over a hardwall ejector.

o Phase VI

To further refine a treatment design it became obvious that the acoustic environment at the walls of the ejector must be known. If the acoustic signature was known, the treatment could be tuned to suppress most efficiently within the bands requiring the most suppression for beneficial far field results. The 97 tube/hole configuration was still in contention as a viable engine suppressor; therefore, plans were made to determine the thermal environment at the secondary ejector walls so that dynamic instrumentation could be chosen to measure the acoustic environment. The ejector for the 97 hole nozzle was thermocouple instrumented and subjected to the normal engine cycle test conditions. A nozzle sketch and resulting measured thermal environment are shown in Figure V.G-25. Effort applied to acoustic treatment development for application to multi-element suppressors was terminated after this test.

Test Configurations and Specific Results

o Phase I

For model hardware definition see Figures V.G-1, -2, and -3. The broadband fiberglass ejector was tested with both the 37 Greatrex tube nozzle at area ratio of 4.0 and a non-suppressed primary conical nozzle. A hardwall ejector was tested with the 37 tube nozzle but not with the conical nozzle. The purpose

of hardwall tests throughout the study were to separate the effects due to acoustic treatment from those due to the addition of an ejector. Figures V.G-4A through -4C show the 300 ft. sideline octave band spectra and PNL suppression gain of both the fiberglass lining and ejector relative to the tube and primary nozzles alone. Figures V.G-5A through -5C show the 300 ft. sideline octave band spectral and PNL suppression gain due solely to the fiberglass lining when used with the tube nozzle referenced to the primary plus hardwall ejector configuration.

o Phase I Conclusions

a) The bulk liner had very good suppression characteristics from the 500 Hz octave band on up in frequency and showed 5 PNdB suppression over an unlined ejector when used with the tube primary (see Figures V.G-5C).

b) The bulk liner's effect on conical nozzle noise suppression was much less due to the much larger shroud-to-primary nozzle diameter ratio and a radical difference in spectra content generated by tube and conical nozzles, upon which the liner had to work. The major portion of the conical nozzle jet stream noise, upon which the treatment could be effective, was generated aft of the ejector exit plane. The tube nozzles break the jet stream into many elements, moving the noise generating region closer to the exit plane and partially within the effective region of the treated ejector.

o Phase II

For model hardware definition, see photograph and schematic on Figures V.G-6 and -7. Four configurations were acoustically tested namely, the primary 37 Greatrex tube nozzle of area ratio = 4.0 with hardwall and Rigimesh lined ejectors, each at ejector lengths of L_S = 6.5" and 13", resulting in length to diameter ratios L_S/D_S, of .625 and 1.25. Thus the effect of Rigimesh lining plus treated ejector lengths could be gauged against equal length hardwall ejectors. The tube cover (see Figure V.G-7) over the primary nozzle was used for this and subsequent tests with the 37 tube nozzle to simulate a practical external tube length for an engine/suppressor system. The 37 Greatrex tube nozzle was temperture limited; therefore, testing was restrained to a maximum jet velocity of about 2550 ft/sec.

Figures V.G-8A and -8B show the 300 ft. sideline octave band spectra and PNL suppressions as a function of jet velocity and ejector length, each referenced to same length hardwall ejectors.

o Phase II Conclusions

a) Octave band and PNL suppression of Figures V.G-8A and -8B show effectiveness primarily in the 1K, 2K, and 4KHz bands with magnitude of suppression increasing rapidly as the shroud was lengthened.

b) PNL suppression gain due solely to the Rigimesh treatment is near constant across the V_J range of 1250 to 2550 ft/sec at 2.5 PNdB for the short ejector, L_S/D_S = .625, and at 4.5 PNdB for the long ejector, L_S/D_S = 1.25.

o Phase III

The 97 tube nozzle/ejector hardware of this phase is detailed in Figures V.G-9 and -10. The tube bundle, at an area ratio of 2.0, was designed to be actuated into the engine jet stream on 16 equal size flaps. The nozzle had unequal tube sizes and lengths, and had a fairly large center hole remaining after the simulated flaps were deployed. The hardware more closely simulated a viable engine suppressor system than did the previous tube configurations and had practical ejector diameter and length ratios of D_S/D_{T_q} = 1.185 and L_S/D_S = 1.03. The 7.5% porous liner and an equivalent hardwall ejector were acoustically tested before the primary nozzle failed in test. Results of these tests are coupled with those of Phase IV.

o Phase IV

The 97 tube nozzle was replaced with the 97 hole nozzle of Figures V.G-11A and -11B. The nozzles were identical, with the exception of external tube length and Greatrex versus round center hole, as mentioned previously. Five configurations were acoustically tested, shown in Table V.G-1 and Figure V.G-11A, including the hardwall ejector and lined ejectors, of 4%, 7.5%, 15% and 22.5% with Cerafelt packing. The following figures show the individual octave band spectra and PNL suppression as a function of jet velocity.

- Figures V.G-12A and -12B — 7.5% Porous Liner on 97 tube & 97 Hole Nozzles
- Figures V.G-13A and -13B — 4% Porous Liner on 97 Hole Nozzle
- Figures V.G-14A and -14B — 15% Porous Liner on 97 Hole Nozzle
- Figures V.G-15A,-15B and -15C — 22.5% Porous Liner Plus Cerafelt on 97 Hole Nozzle

The 7.5% porous liner data are from both the 97 tube configurations of Phase III and the 97 hole configurations of this phase. Each set is referenced to the hardwall ejector so that suppressions shown are due solely to the treatment. Composite plots of the mean suppression lines of the above figures are included as Figures V.G-16A, -16B, and -16C so that direct comparisons for porosity effect can be made. To show suppression change as a function of frequency and porosity at a given jet velocity, Figures V.G-17A and -17B were plotted at V_J = 1000, 1500,2000,2500 and 3000 ft/sec.

o Phase III and IV Conclusions

a) Suppression results are much lower than anticipated with little or no suppression attributable to the treatment at most jet velocities and frequencies (see Figures V.G-16A, -16B and -16C).

b) The 4% liner was only slightly effective and then only at low V_J and in the lower octave bands.

c) Suppression gain with the 7.5% liner was essentially the same with either the 97 tube or 97 hole primary but still only showed 1 to 2 PNdB.

d) The 15% porous liner performed almost as poorly as the 4% liner with only slight PNL suppression at low jet velocity.

e) Maximum PNL suppression gain was about 4 PNdB with the 22.5% porous Cerafelt packed liner, but then only in the very low jet velocity range and decreasing to no suppression gain at high velocity.

f) Indications were that the major cause for lack of suppression by all four treatment designs is the original noise content of the primary nozzle jet stream within the region of the ejector shroud where the

liner material can be effective. Generations of the primary noise which is transmitted to the far field is probably aft of the ejector plane due primarily to the small area ratio and to the unequal tube/hole size, non-uniform spacing, non-coplanar exit plane and the large central flow area. Therefore, the same treatment designs could be expected to perform more efficiently if a more uniform noise source such as the 37 Greatrex tube nozzle with equal tube size, uniform spacing, and coplanar exit plane was used, providing its principal offending noise source was internal to the ejector.

g) A further test should be planned to prove the above conclusion.

o Phase V

Hardware chosen for this phase (for reasons discussed previously under "Objectives of Test Series - Phase V" and "Phase IV - Conclusions") is shown schematically in Figure V.G-.8. The hardware consists of the same 37 Greatrex tube primary nozzle used in Phase II but with a 22.5% open perforated sheet metal liner and a .22" deep cavity behind the porous face plate packed with Cerafelt CR-400, identical to the treatment design of Phase IV. Two configurations, hardwall and treated, were tested as shown in Table V.G-1 and Figure V.G.-18. Figures V.G.-19 and -20 show the 300 and 1500 ft. sideline normalized peak PNL for the hardwall and treated ejector configurations plus the PNL suppression referenced to the hardwall configuration. Magnitude of suppression in each octave band and PNL suppression as a function of jet velocity are shown at the 300 ft. sideline in Figures V.G-21A and -21B. The plotted data are at 80° from the jet exhaust since sideline noise was consistently peak at this location with the treated ejector. The PNL suppression curve will, therefore, not exactly match the peak PNL suppression curve of Figure V.G-19. Octave band spectra and PNdB directivity at the 300 ft. sideline are compared between the treated and hardwall ejectors in Figures V.G-22A through V.G-22F. The data sets are in order of increasing jet velocity from 1145 to 2540 ft/sec. The spectra are again at 80° to the jet, the peak PNL angle for both configurations. To gauge liner effectiveness as a function of frequency at a given jet velocity, Figure V.G-23 presents octave band suppression versus frequency at 1000, 1500, 2000 and 2500 ft/sec.

- Phase V Conclusions

a) Suppression gain with treatment holds between 5 PNdB at low V_j to 3 to 4 PNdB at high V_j (see Figure V.G-19 and -20), indirectly supporting the conclusion of Phase IV that ineffectiveness of the liners designed for the 97 tube/hole nozzles was due to the spectra content within the ejector length on which the treatment had to work. The good suppression results are therefore in line with those of the fiberglass ejector of Phase I and the Rigimesh liner of Phase II.

b) High frequency is greatly reduced with much less effect on low frequency noise content. (See Figure V.G-23 and the spectra comparisons of Figures V.G-22A through -22F.) This was expected since high frequencies are generated primarily from the individual tube flows just aft of the tube exits within the confines of the treated ejector. The low frequency content of the spectra is generated from the coalesced flow and primarily after the flow exits the ejector. The trend is for intermediate and high frequency suppression over the complete V_j range of tests as seen from Figure V.G-23.

c) The PNL directivity plots of Figures V.G-22A through -22F show fairly uniform suppression from 50° through 90° from the jet exhaust but with lesser effect for angles closer to the jet. The spectra at the closer angles are more low frequency dominated than the higher angle spectra and since spectra suppression of the low frequencies was less, the PNL levels were affected less.

d) The test proved that a practical treatment design of perforated sheet metal backed with acoustic packing can achieve a reasonable level of additional suppression over a hardwall ejector as long as the primary jet noise source is controlled.

e) Returning to the purpose of Phase V testing, i.e., to prove that poor suppression in the Phase III and IV series with the perforated sheet metal liners was due to the spectra on which the liner had to work, an attempt to substantiate the reasoning with measured data is done in Figures V.G-24A and -24B. These are 300 ft. sideline

spectra plots comparing the 97 hole nozzle and 37 Greatrex tube nozzle, both with hardwall ejectors, at various jet velocities. The spectra show no radical change between models in the frequency range of greatest treatment effectiveness (500 Hz through 2 KH with the exception of the inherently lower spectra of the 37 [illegible] tube nozzle. The comparison offers no apparent explanat[illegible] why the acoustic treatment (22.5% porous plate plus Ceraf[illegible] pressed the 37 Greatrex tube spectra but not that of the [illegible]. However, it must be realized that the spectra are for field [illegible]ta and not necessarily indicative of the noise content along the inner flow-path of the ejector in the area of acoustic treatment application. This suggests a possible explanation. The 97 hole nozzle was of area ratio = 2.0, had unequal hole sizes, non-uniform hole spacing, staggered exit plane, and a relatively large center hole. The 37 Greatrex tube was of area ratio = 4.0, had equal size and uniformly spaced tubes, and had a coplanar exit plane. The most influencing design difference was area ratio. The more compact spacing of the 97 hole nozzle, due to its lower area ratio, caused earlier coalescence of the individual tube flows to a single mixed flow system similar to a conical nozzle. The noise was produced by this coalesced jet occurred primarily after exiting the treated ejector. The area ratio of 4.0 Greatrex tube bundle would not coalesce to a merged jet as soon and, therefore, would produce its high frequency noise within the shroud where the lining is effective. This reasoning is enforced by examining the 97 hole nozzle plus lined ejector PNL suppression curve of Figure V.G-16C at low pressure ratio/jet velocity where coalescence is not as rapid as at high pressure ratio/jet velocity. In this region the 22.5% liner plus Cerafelt treatment had good suppression up to 5 PNdB but then it quickly disappeared as pressure ratio/jet velocity increased.

f) The acoustic signature within a hardwall ejector on a segmented jet suppressor nozzle must therefore be determined before design of the treatment. Identification of the acoustic signature will establish whether the frequency range of interest is generated within the bounds of the treatment application and therefore allow for tuning the treatment design for maximum acoustic efficiency.

o Phase VI

To determine the acoustic environment inside a hardwall ejector, it was first necessary to determine the thermal environment under hot jet test conditions so that dynamic instrumentation could be selected. Figure V.G-25 shows the hardware setup, thermocouple locations, primary gas stream test conditions and resulting ejector skin temperature for the 97 hole plus ejector system.

o Phase VI Conclusions

a) For the nozzle/ejector system under test the ejector skin temperature reached a maximum temperature of slightly over 900° R for the highest test condition of P_{T8}/P_o = 3.41, T_{T8} = 2692° R.

TABLE V.G-1 TEST SUMMARY OF ACOUSTIC EJECTORS ON MULTI-TUBE CONICAL NOZZLES

Phase	Purpose	Model No.	Test Date	Model Description	Ref. Figure
I.	o Determine Suppression of Bulk Treatment on Cone & 37 Greatrex Tube Primary + Ejector Systems	4.1T37-1	8-5-68	37 Tube Greatrex Primary	V.G-2
		4.1T37-10CS	8-6-68	37 Tube Greatrex + Fiberglass Ejector	V.G-1
		4.1T37-10CS-1	8-6-68	37 Tube Greatrex Hardwall Ejector	V.G-1
		4.1	8-15-68	4.1" Conical Primary	V.G-3
		4.1-10.0CSL	8-15-68	4.1" Cone + Fiberglass Ejector	V.G-3
II.	o Determine Suppression of Rigimesh on 37 Greatrex Tube Primary + Ejector	4.1T37-10.8CSL	8-9-68	37 Tube Greatrex + 6.5" Long Rigimesh Ejector	V.G-7
		4.1T37-10.8CS	8-9-68	37 Tube Greatrex + 6.5" Long Hardwall Ejector	V.G-7
	o Effect of Length of Treated Ejector	4.1T37-10.8CSEL	8-12-68	37 Tube Greatrex + 13" Long Rigimesh Ejector	V.G-7
		4.1T37-10.8CSE	8-12-68	37 Tube Greatrex + 13" Long Hardwall Ejector	V.G-7
III.	o Determine Suppression of 7.5% Open Liner on 97 Tube Primary + Ejector	4.2T97-7.7CS-1	9-23-68	97 Tube + 7.5% Open Lined Ejector	V.G-10
		4.2T97-7.7CS	9-20-68	97 Tube + Hardwall Ejector	V.G-10

TABLE V.G-1 (Continued) TEST SUMMARY OF ACOUSTIC EJECTORS ON MULTI-TUBE CONICAL NOZZLES

Phase	Purpose	Model No.	Test Date	Model Description	Ref. Figure
IV.	o Determine Suppression of 4%, 7.5%, 15% Open Liners & 22½% Open Liner with Cerafelt on 97 Hole Primary + Ejector	4.2H97N-CS-4	1-14-69	97 Hole + 4% Open Lined Ejector	V.G-11
		4.2H97N-CS-1	11-22-68	97 Hole + 7.5% Open Lined Ejector	V.G-11
		4.2H97N-CS-5	1-20-69	97 Hole + 15% Open Lined Ejector	V.G-11
		4.2H97N-CS-6	2-13-69	97 Hole + 22% Open with Cerafelt Lined Ejector	V.G-11
		4.2H97N-CS	11-29-68	97 Hole + Hardwall Ejector	V.G-11
V.	o Prove Suppression Dependency on Source Noise Internal to Ejector	4.1T37-10.4CS	6-6-69	37 Tube Greatrex + 22½% Open with Cerafelt Ejector	V.G-18
		4.1T37-10.8CSE	6-6-69	37 Tube Greatrex + Hardwall Ejector	V.G-18
VI.	o Determine Thermal Environment on Ejector Wall	4.2H97N-CS	-	97 Hole Hardwall Ejector	V.G-25

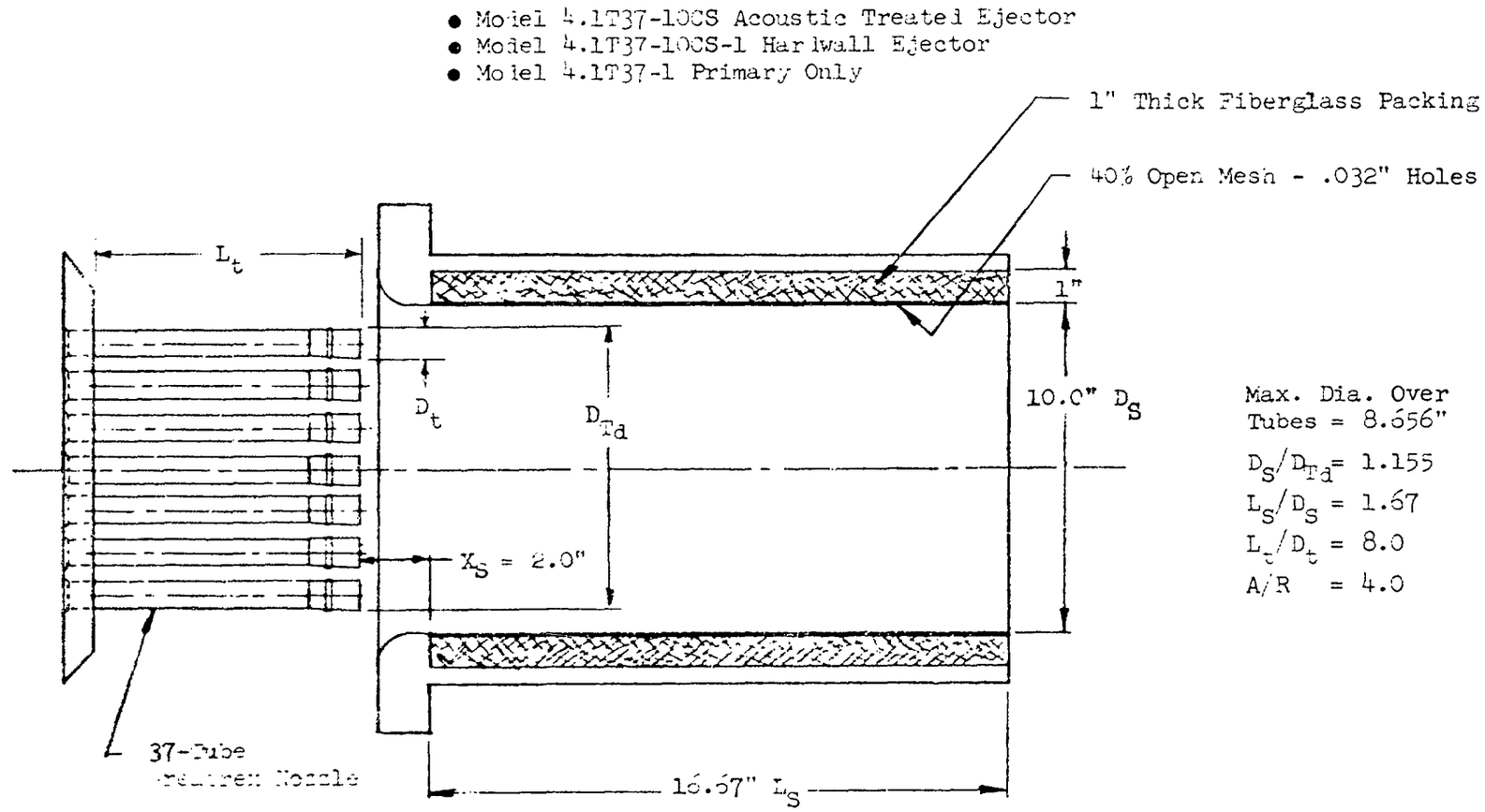


FIGURE V.C-1 SCHEMATIC OF 37 TUBE GREATREX NOZZLE WITH FIBERGLASS LINED EJECTOR

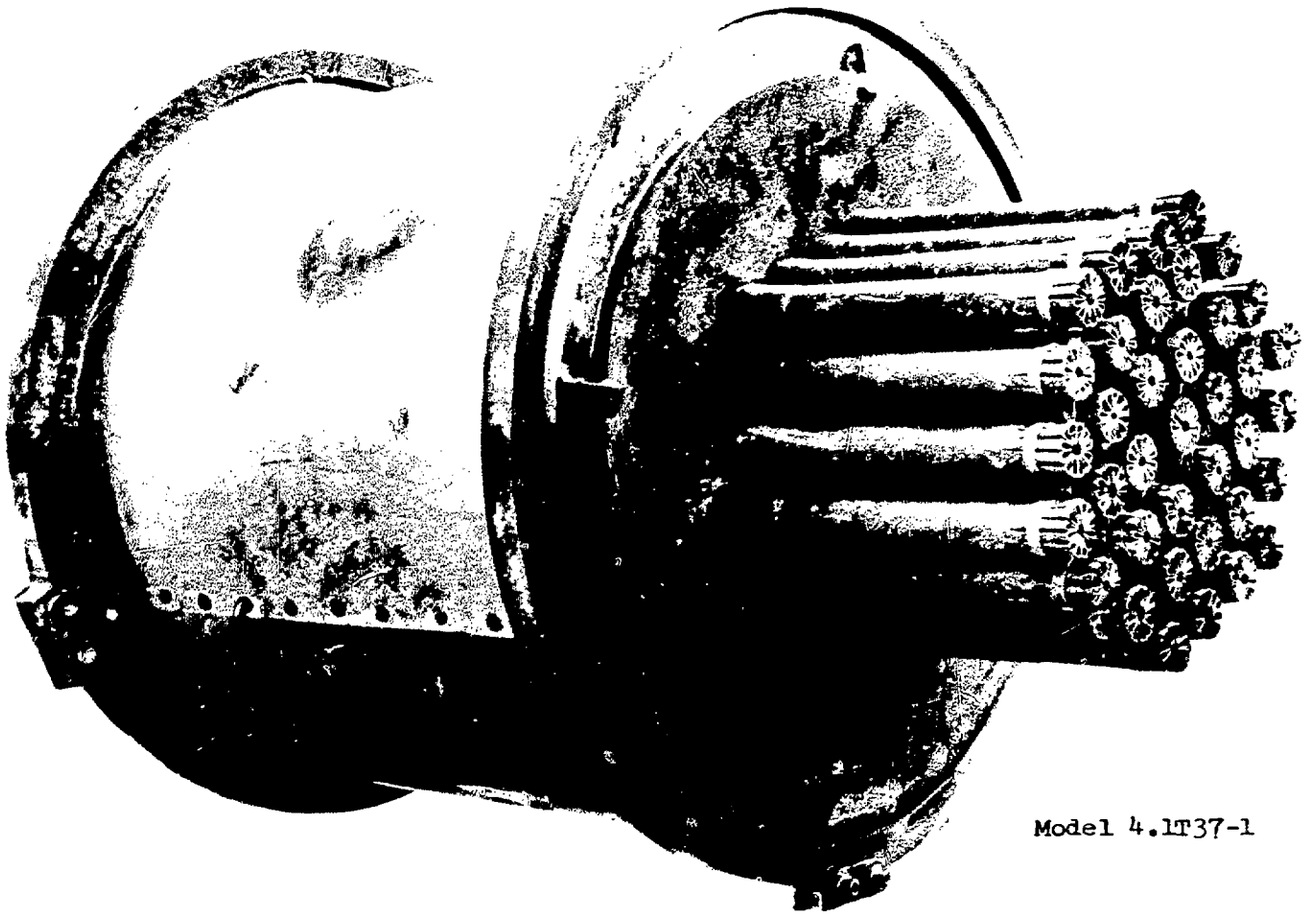


FIGURE V.G-2 37 TUBE GREATREX PRIMARY NOZZLE HARDWARE

- Model 4.1-10.0-DSL-Acoustic Treated Ejector
- Model 4.1 - Primary Only

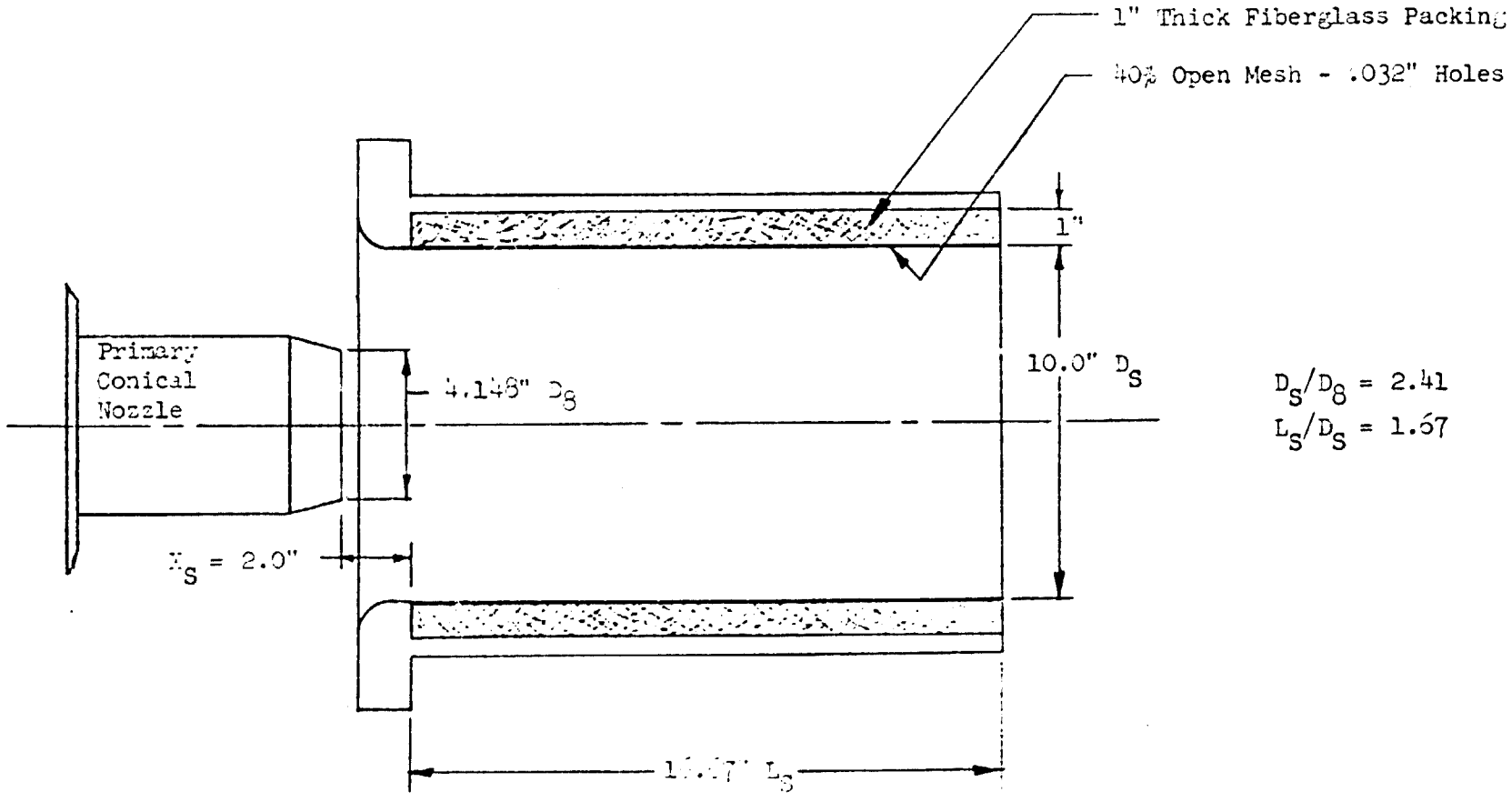


FIGURE V.C-3 SCHEMATIC OF 4.148" I.D. CONE PLUS FIBERGLASS LINED EJECTOR

- o Suppression Relative to 37 GREATREX Tubes or 4.148" Cone W/O Ejector
- o 300 Ft. Sideline
- o Ejector = 10" I.D. X 16.62" Long, 40% Open, 1" Fiberglass Packed

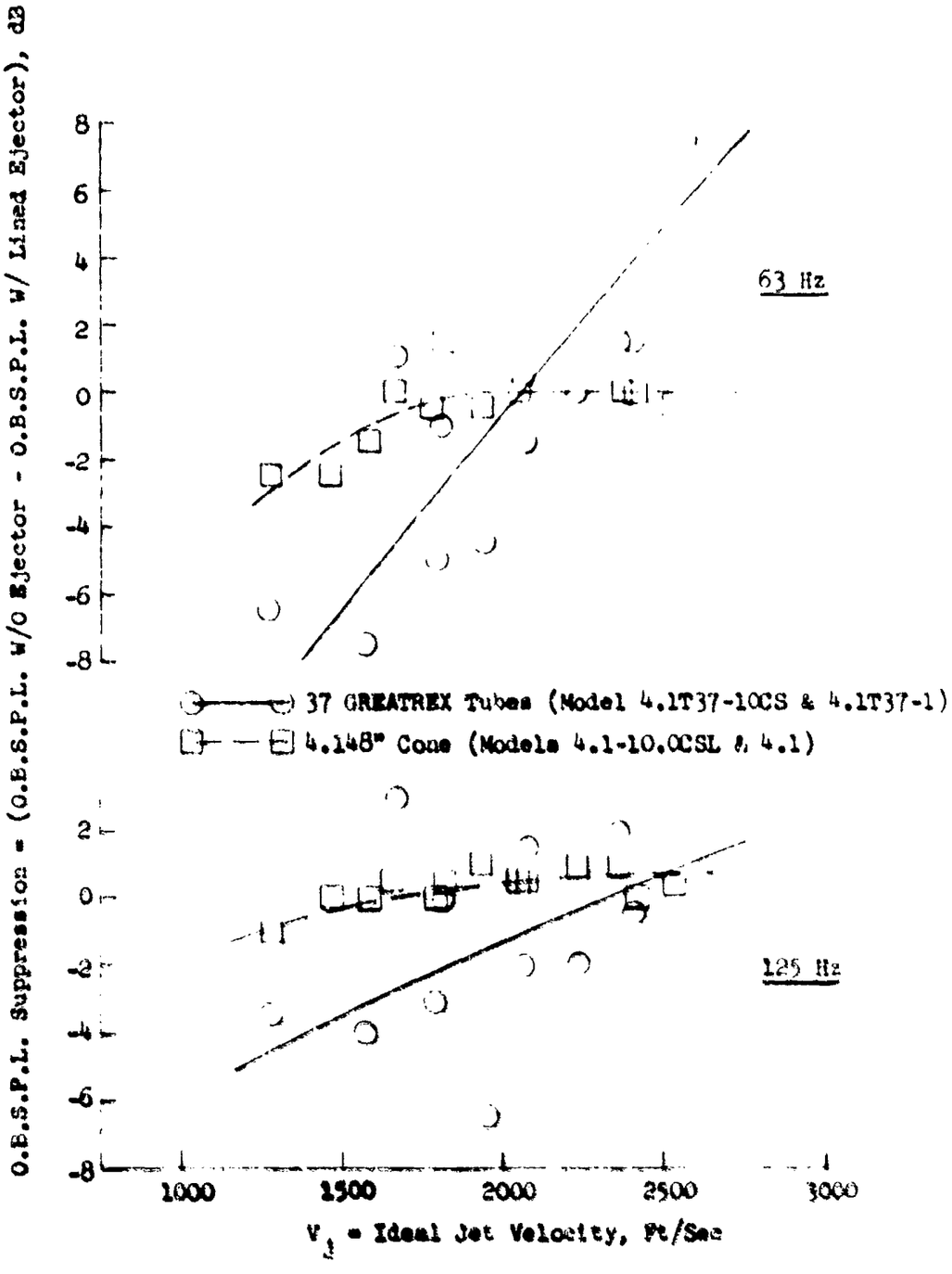


FIGURE V.G-4A SUPPRESSION EFFECTS OF FIBERGLASS LINER ON 37 TUBE GREATREX AND 4.1 CONIC NOZZLES

o Suppression Relative to 37 Tube GREATREX or 4.148" Cone W/O Ejector

o 300 Ft. Sideline

o Ejector = 10" I.D. X 16.62" Long, 40% Open, 1" Fiberglass Packed

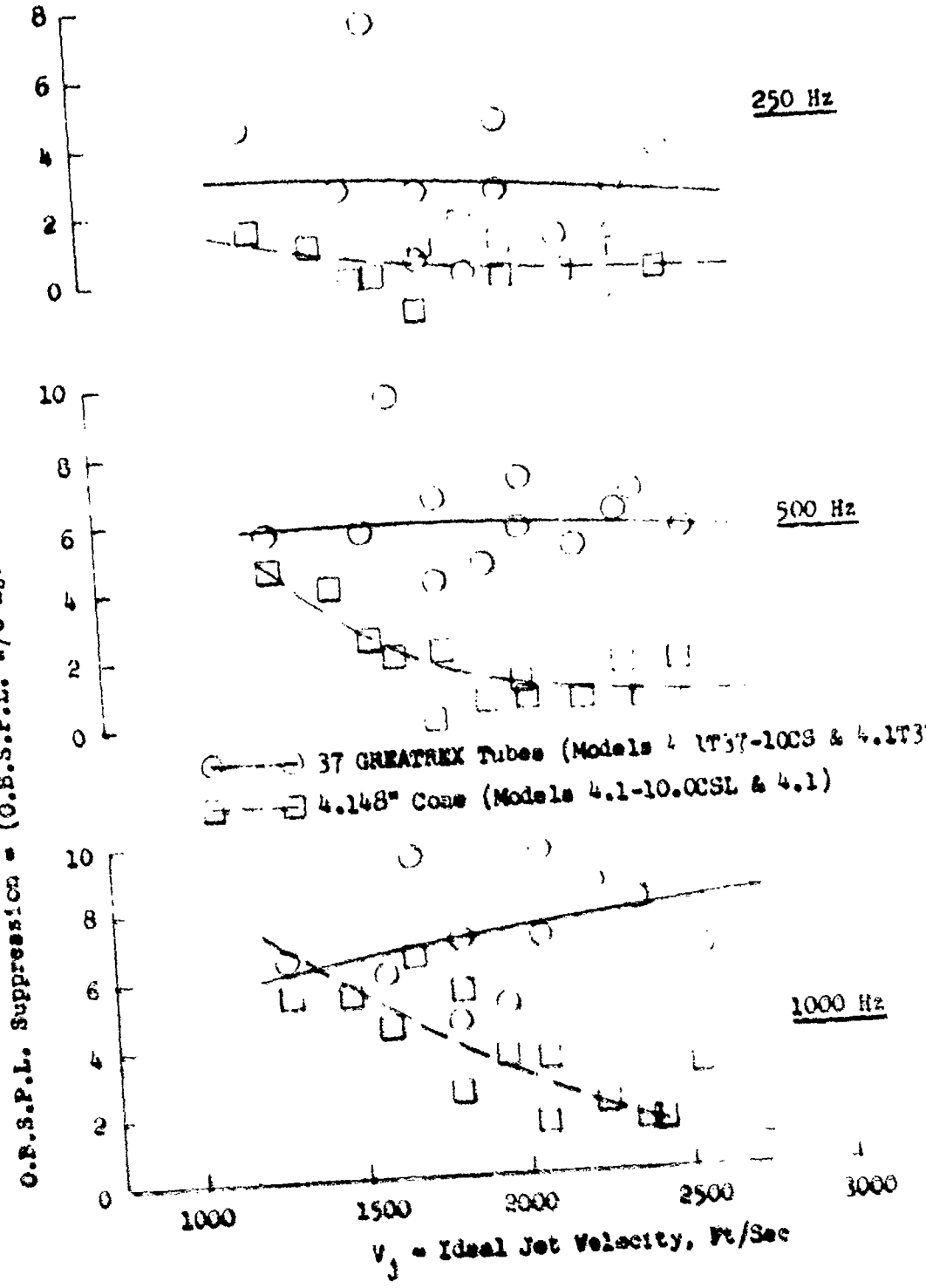


FIGURE V.G-4B SUPPRESSION EFFECTS OF FIBERGLASS LINER ON 37 TUBE GREATREX AND 4.1 CONIC NOZZLES

o Suppression Relative to 37 Tube GREATREX or 4.148" Cone W/O Ejector

o 300 Ft. Sideline

o Ejector = 10" I.D. X 16.62" Long, 40% Open, 1" Fiberglass Packed

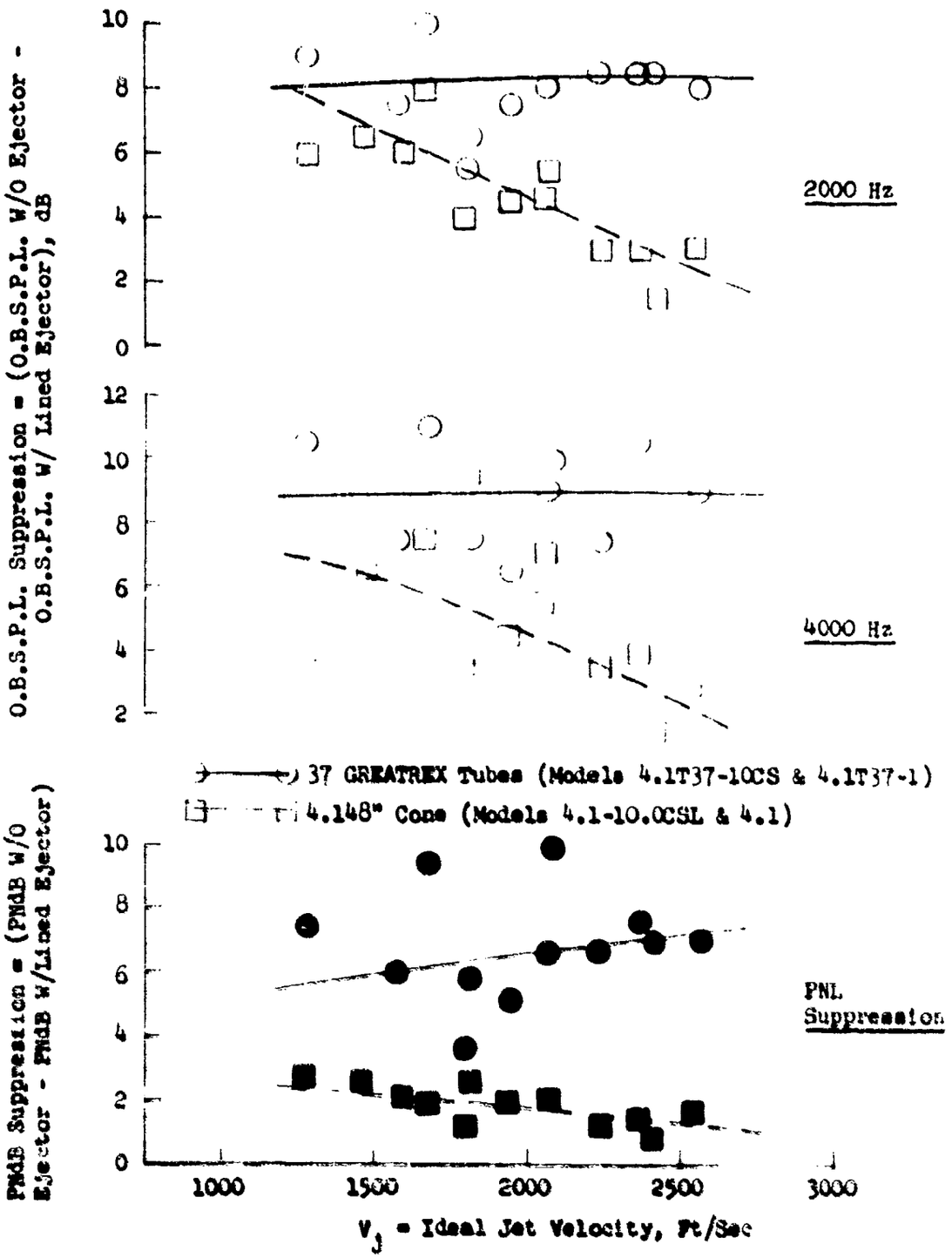


FIGURE V.G-4C SUPPRESSION EFFECTS OF FIBERGLASS LINER ON 37 TUBE GREATREX AND 4.1 CONIC NOZZLES

- o Suppression Relative to 37 GREATREX Tubes W/ Hard Ejector
- o 300 Ft. Sideline
- o Soft Liner 10" I.D. X 16.62" Long, 40% Open, 1" Fiberglass Packed
- o Hard Liner 10" I.D. X 16.62" Long

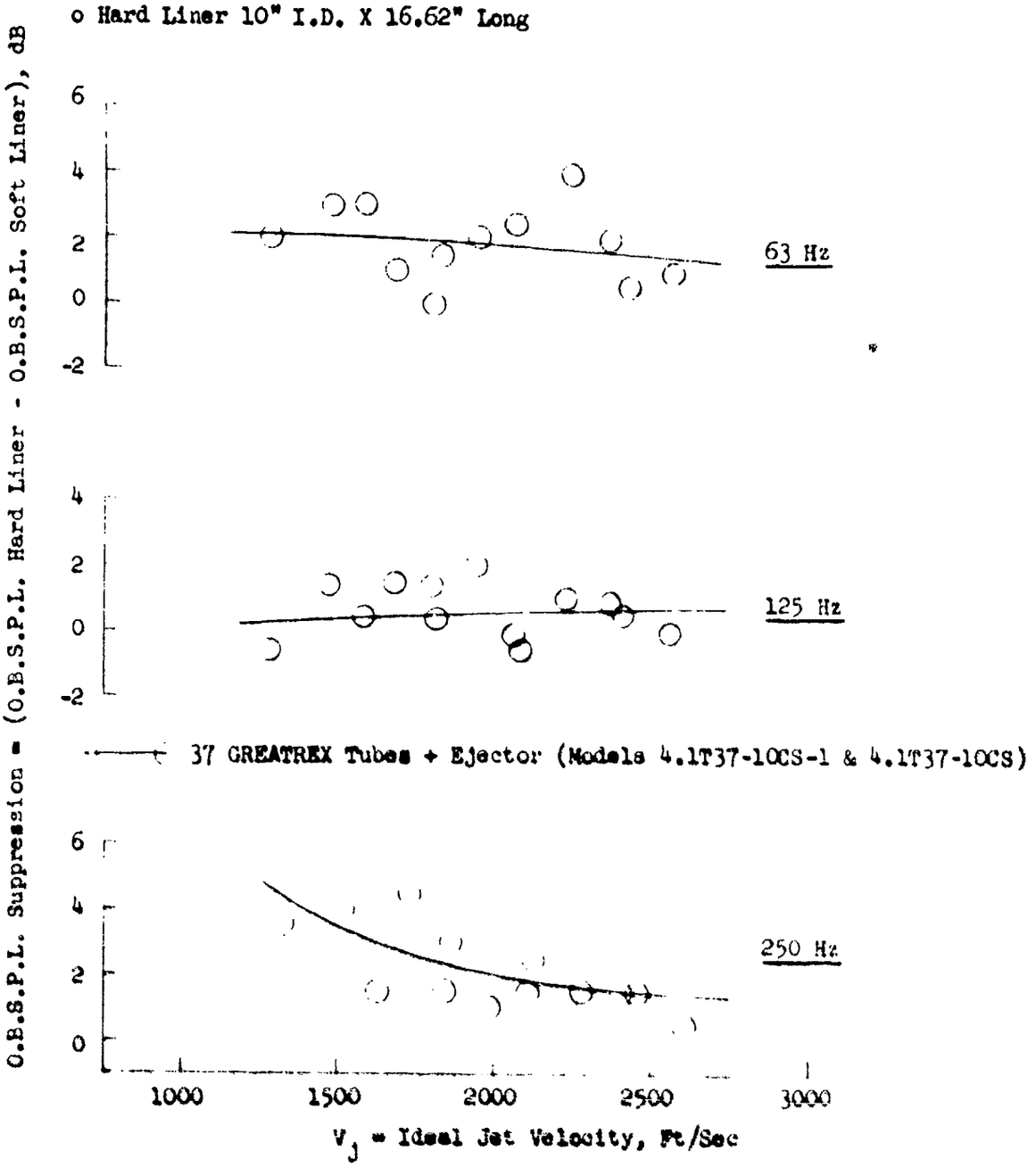


FIGURE V.C-5A SUPPRESSION EFFECTS OF FIBERGLASS LINER ON 37 TUBE GREATREX NOZZLE

o Suppression Relative to 37 Tube GREATREX W/ Hard Ejector

o 300 Ft. Sideline

o Soft Liner 10" I.D. X 16.62" Long, 40% Open, 1" Fiberglass Packed

o Hard Liner 10" I.D. X 16.62" Long

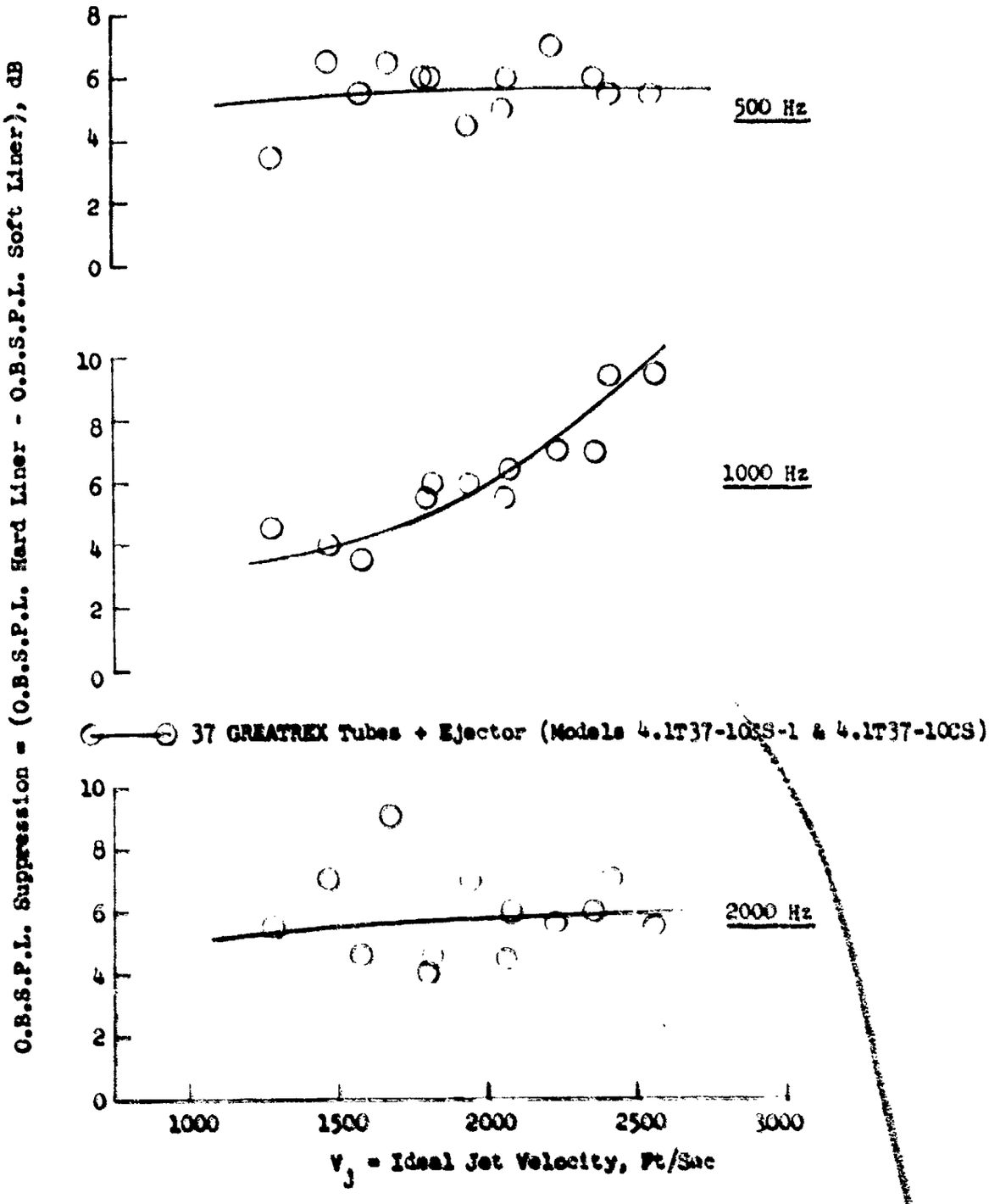
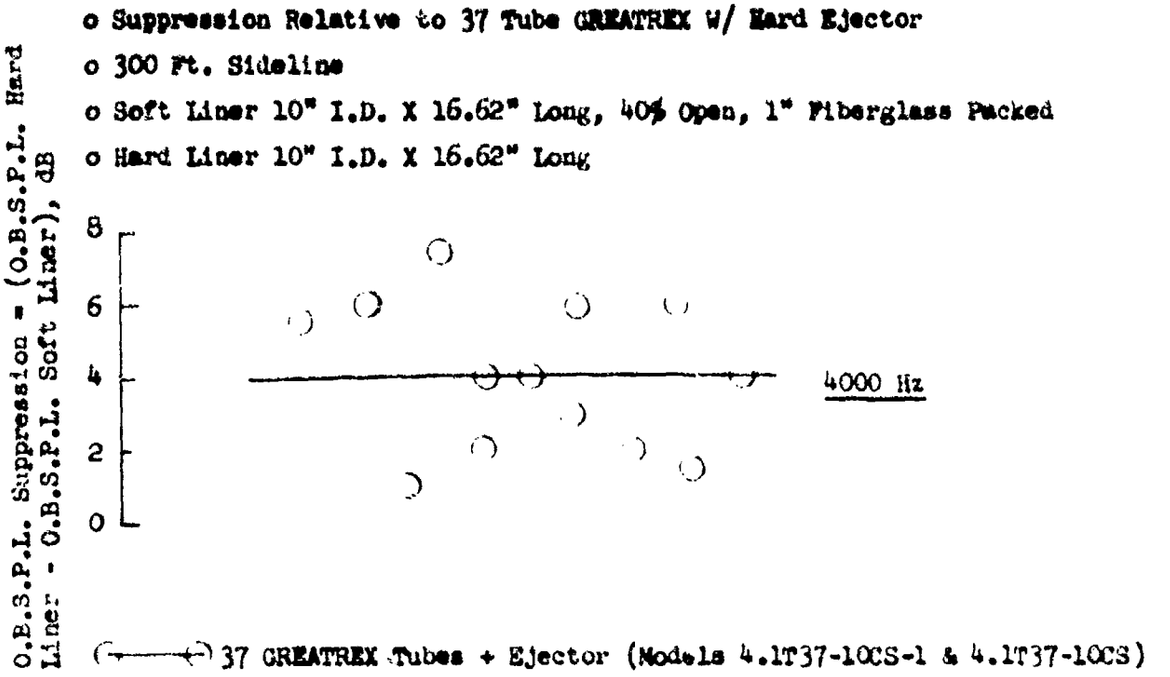


FIGURE V.G-5B SUPPRESSION EFFECTS OF FIBERGLASS LINER ON 37 TUBE GREATREX NOZZLE



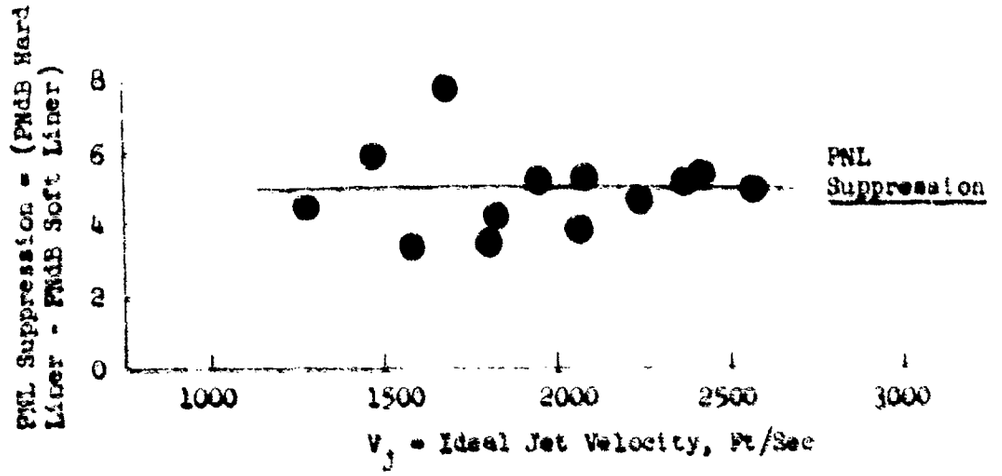
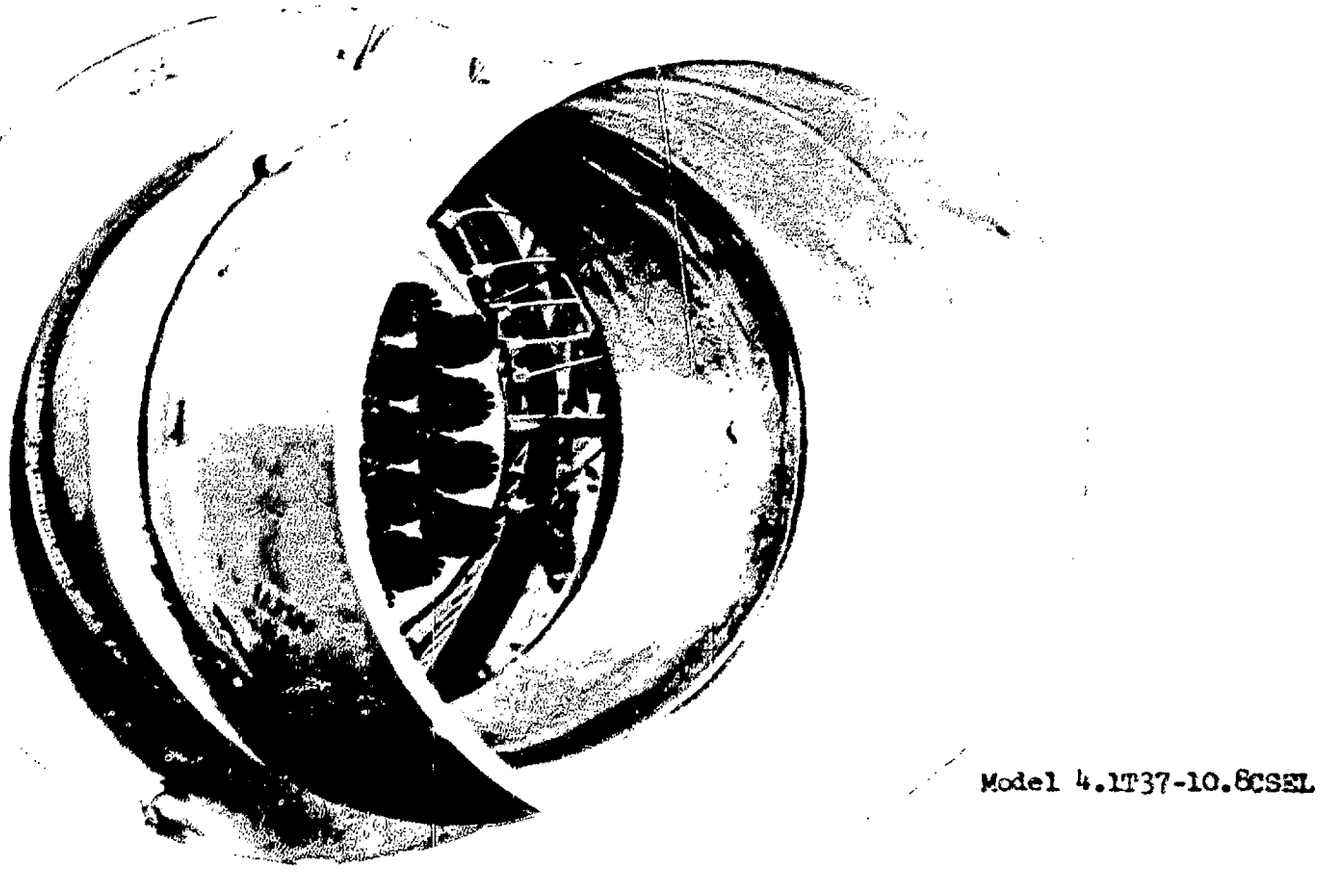


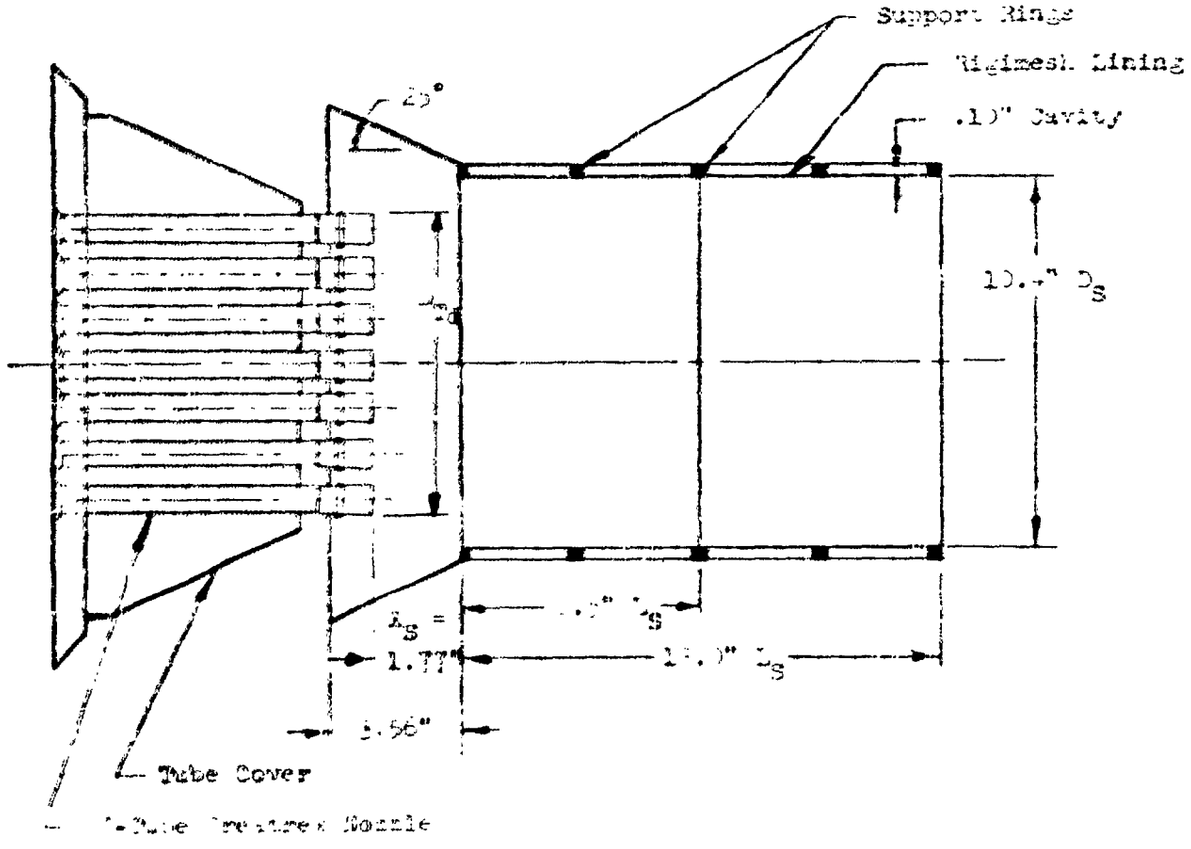
FIGURE V.G-5C SUPPRESSION EFFECTS OF FIBERGLASS LINER ON 37 TUBE GREATREX NOZZLE



Model 4.1T37-10.8CSEL

FIGURE V.G-6 37 TUBE GREATREX NOZZLE HARDWARE WITH RIGIMESH TREATED EJECTOR

- Model 4.1T37-10.5 CSEL - 13" L_S Rigimesh Ejector
- Model 4.1T37-10.5 CSE - 13" L_S Hardwall Ejector
- Model 4.1T37-10.5 CSL - 6.5" L_S Rigimesh Ejector
- Model 4.1T37-10.5 CS - 6.5" L_S Hardwall Ejector



D_{Td} = Max. Dia.
Over Tubes = 8.656"

D_S/D_{Td} = 1.20
L_c/D_t = 1.5
A/R = 4.0

FIGURE V.G-7 SCHEMATIC OF 37 TUBE GREATREX NOZZLE WITH RIGIMESH LINED EJECTOR

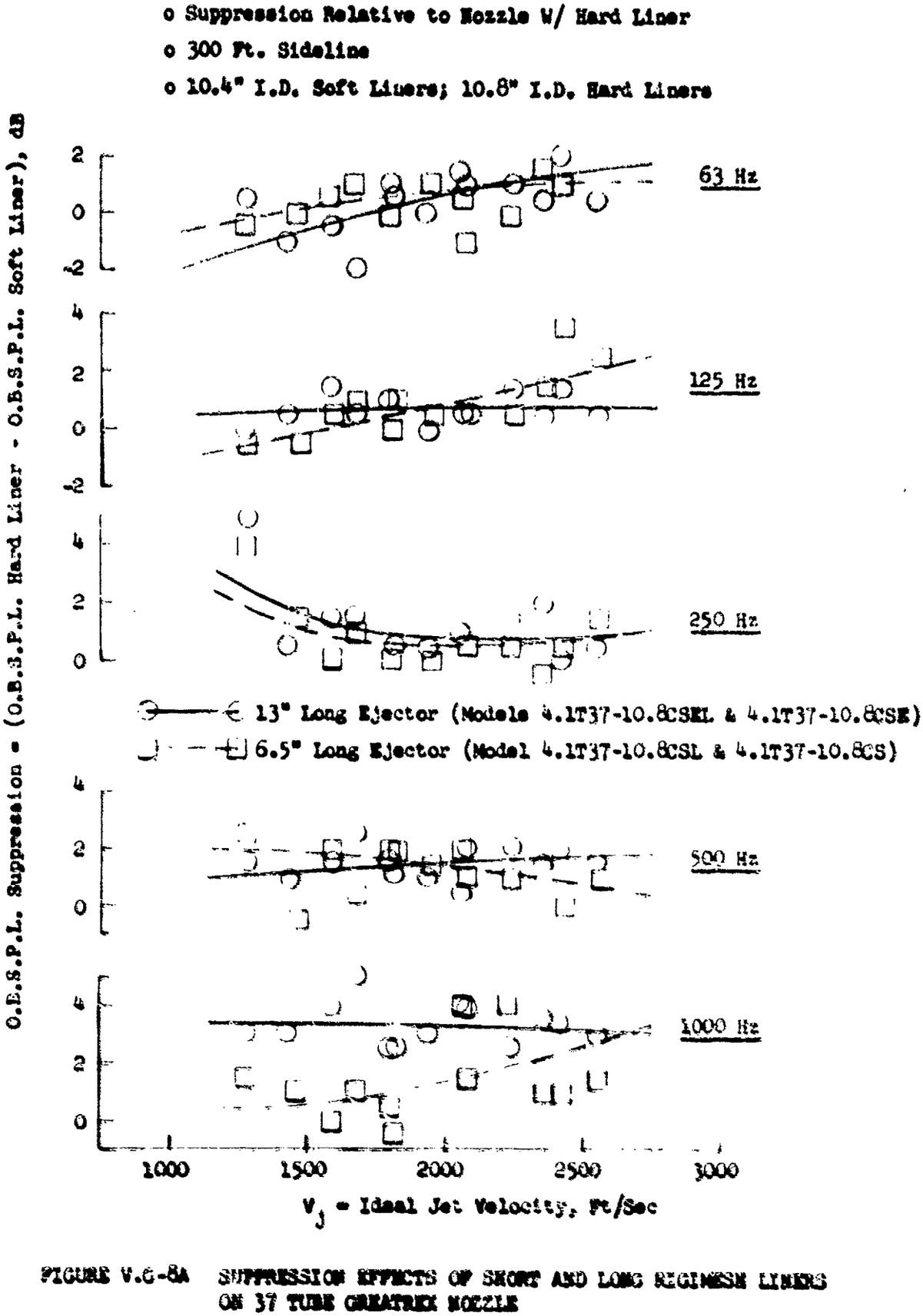
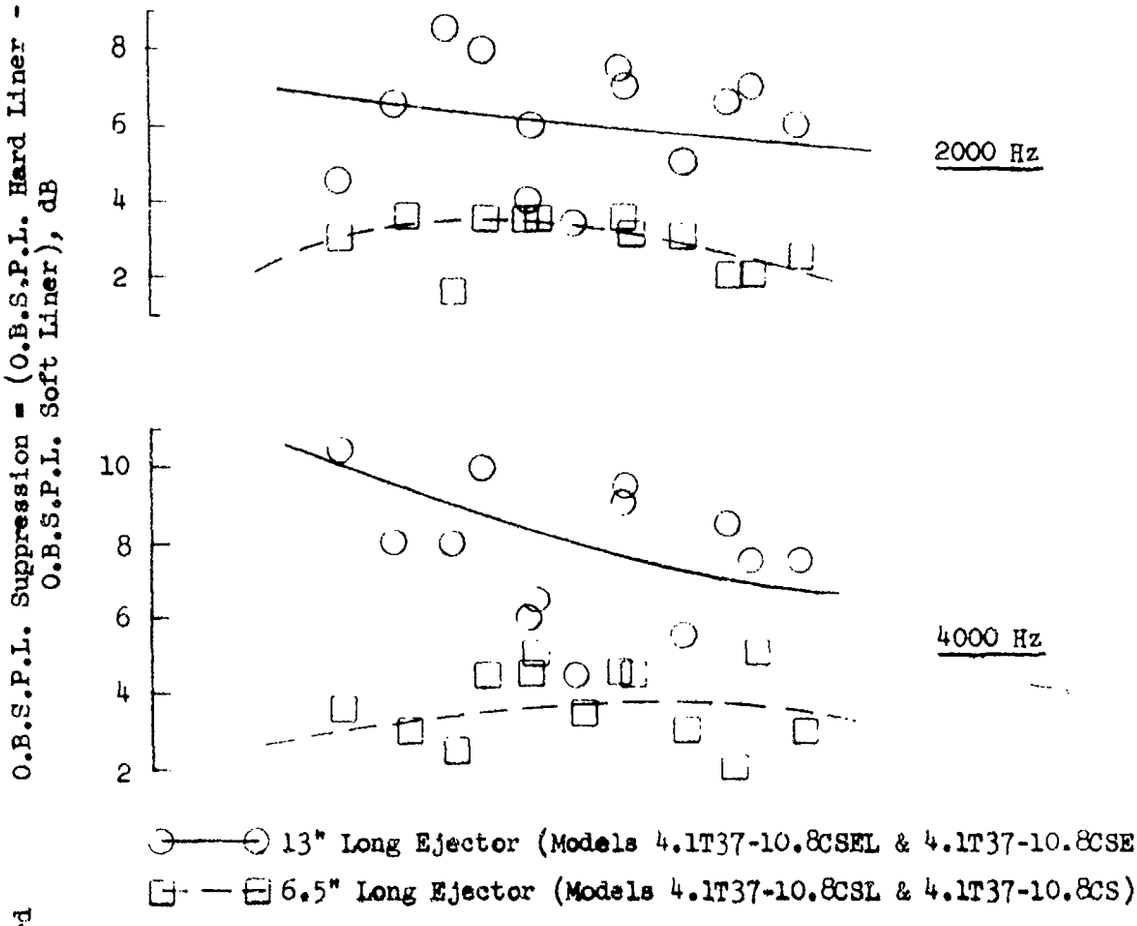


FIGURE V.C-8A SUPPRESSION EFFECTS OF SHORT AND LONG REGIMESH LINERS ON 37 TUBE CHEATRIX NOZZLE

o Suppression Relative to Nozzle W/ Hard Liner

o 300 Ft. Sideline

o 10.4" I.D. Soft Liners; 10.8" I.D. Hard Liners



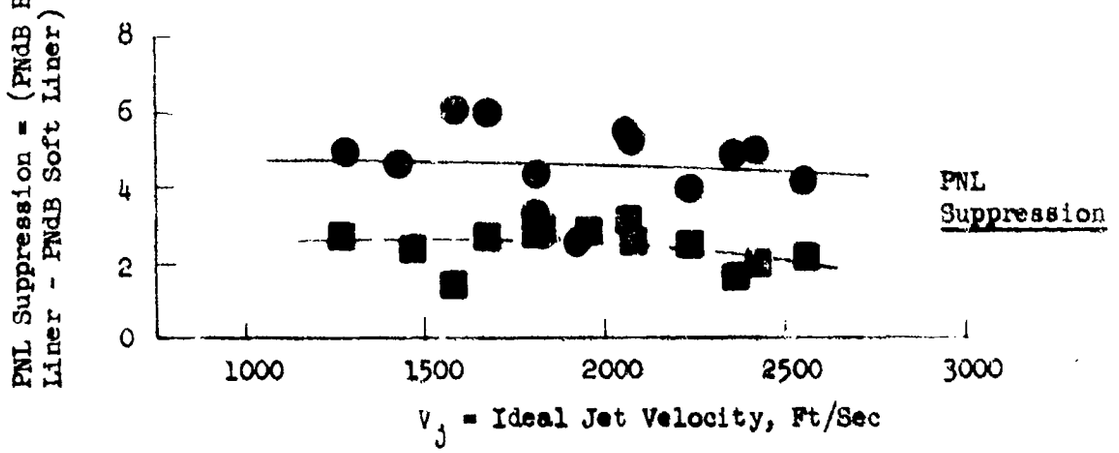


FIGURE V.G-8B SUPPRESSION EFFECTS OF SHORT AND LONG RIGIMESH LINERS ON 37 TUBE GREATREX NOZZLE

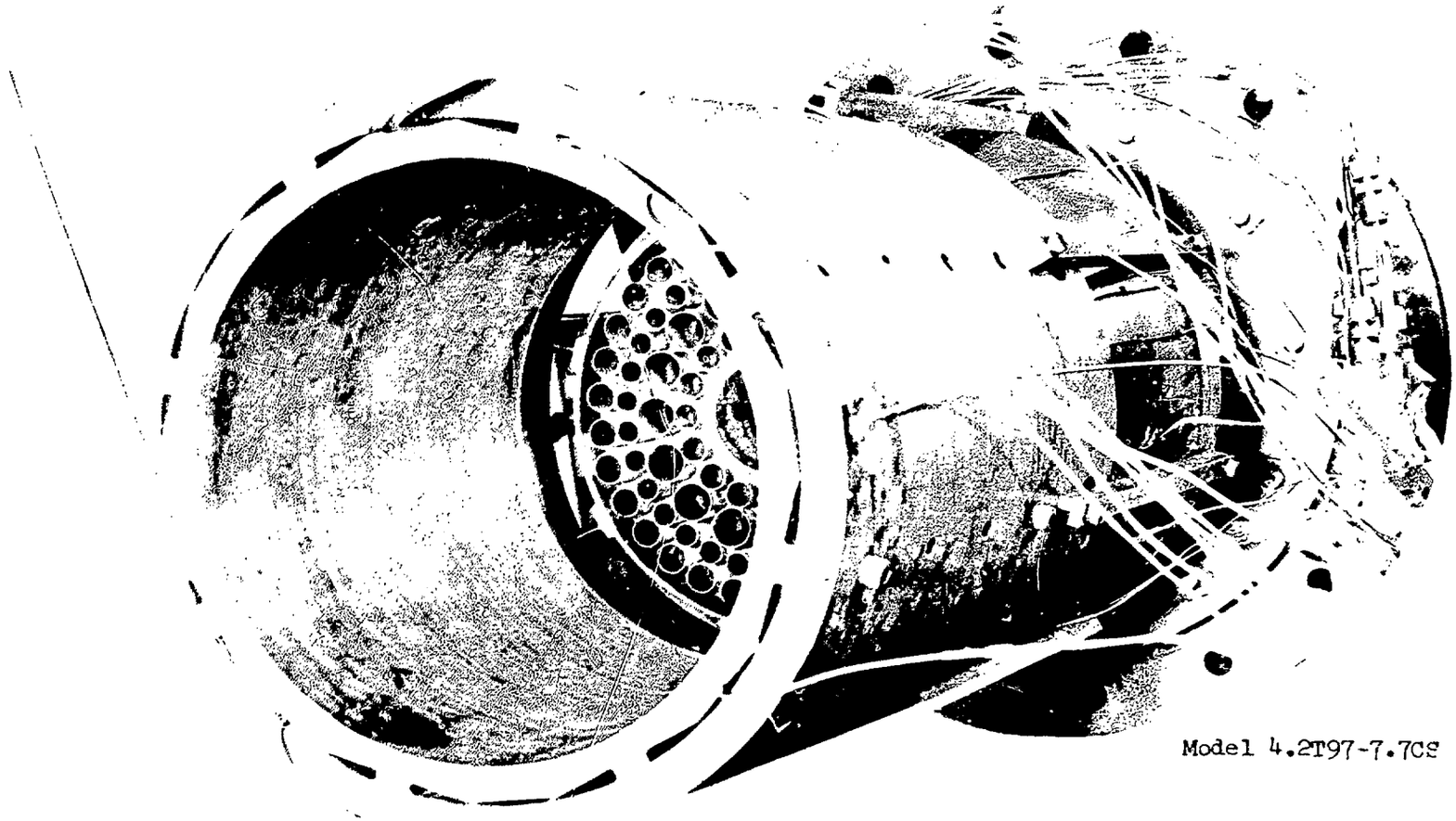


FIGURE V.G-9 97 TUBE PRIMARY NOZZLE AND HARDWALL EJECTOR HARDWARE

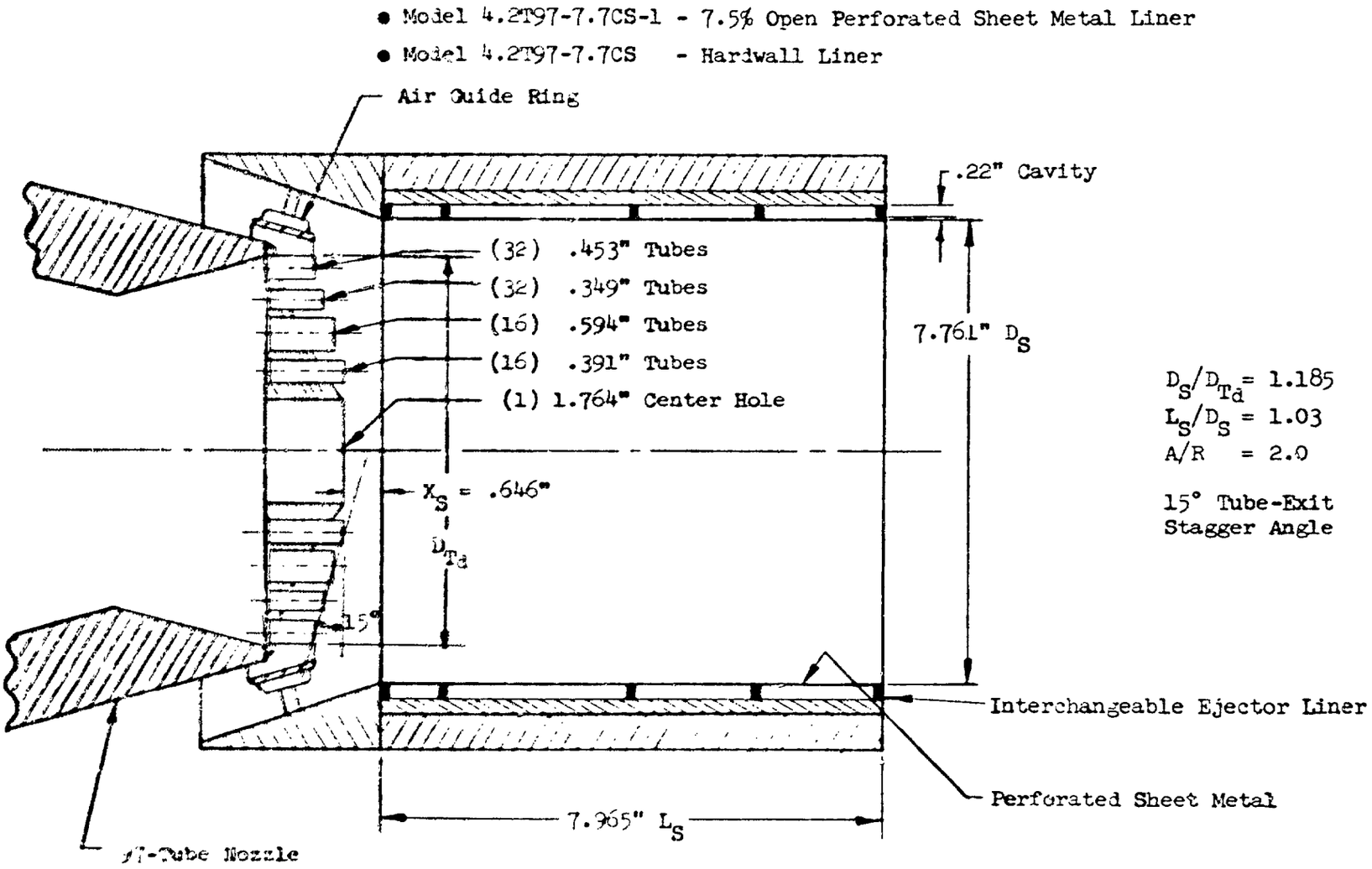


FIGURE V.C-10 SCHEMATIC OF 97 TUBE NOZZLE PLUS EJECTOR WITH INTERCHANGEABLE ACOUSTIC LINERS

- Model 4.2H97N-CS-4
  4% Open Perforated Sheet Metal Liner
- Model 4.2H97N-CS-1
  7.5% Open Perforated Sheet Metal Liner
- Model 4.2H97N-CS-5
  15% Open Perforated Sheet Metal Liner
- Model 4.2H97N-CS-6
  22.5% Open Perforated Sheet Metal Liner
  and Cavity Packed With Cerafelt
- Model 4.2H97N-CS
  Hardwall Liner

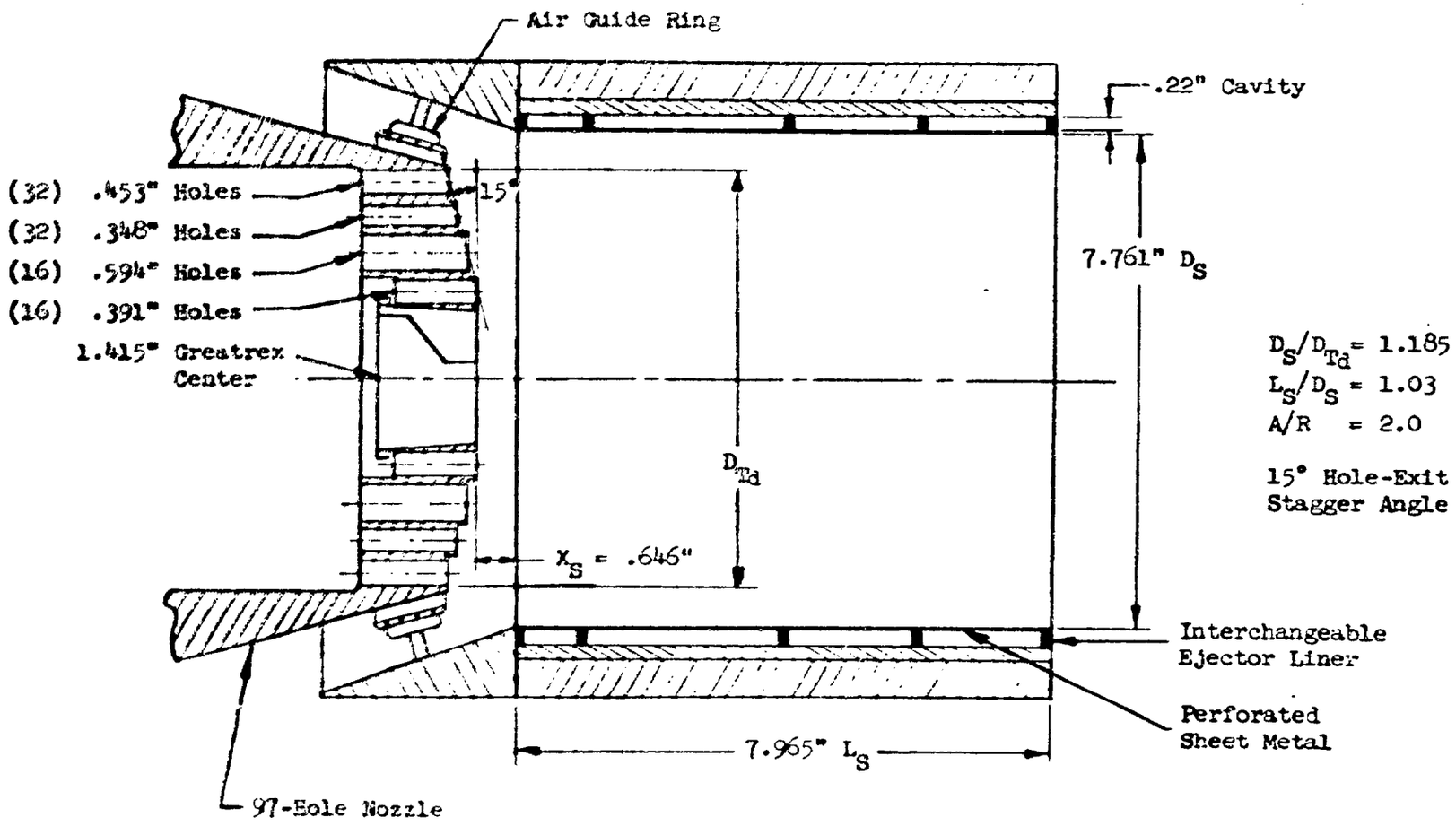


FIGURE V.G-11A SCHEMATIC OF 97 HOLE NOZZLE PLUS EJECTOR WITH INTERCHANGEABLE ACOUSTIC LINERS

• View of Primary Nozzle Hole Pattern
With 8-Lobed Greatrex Center

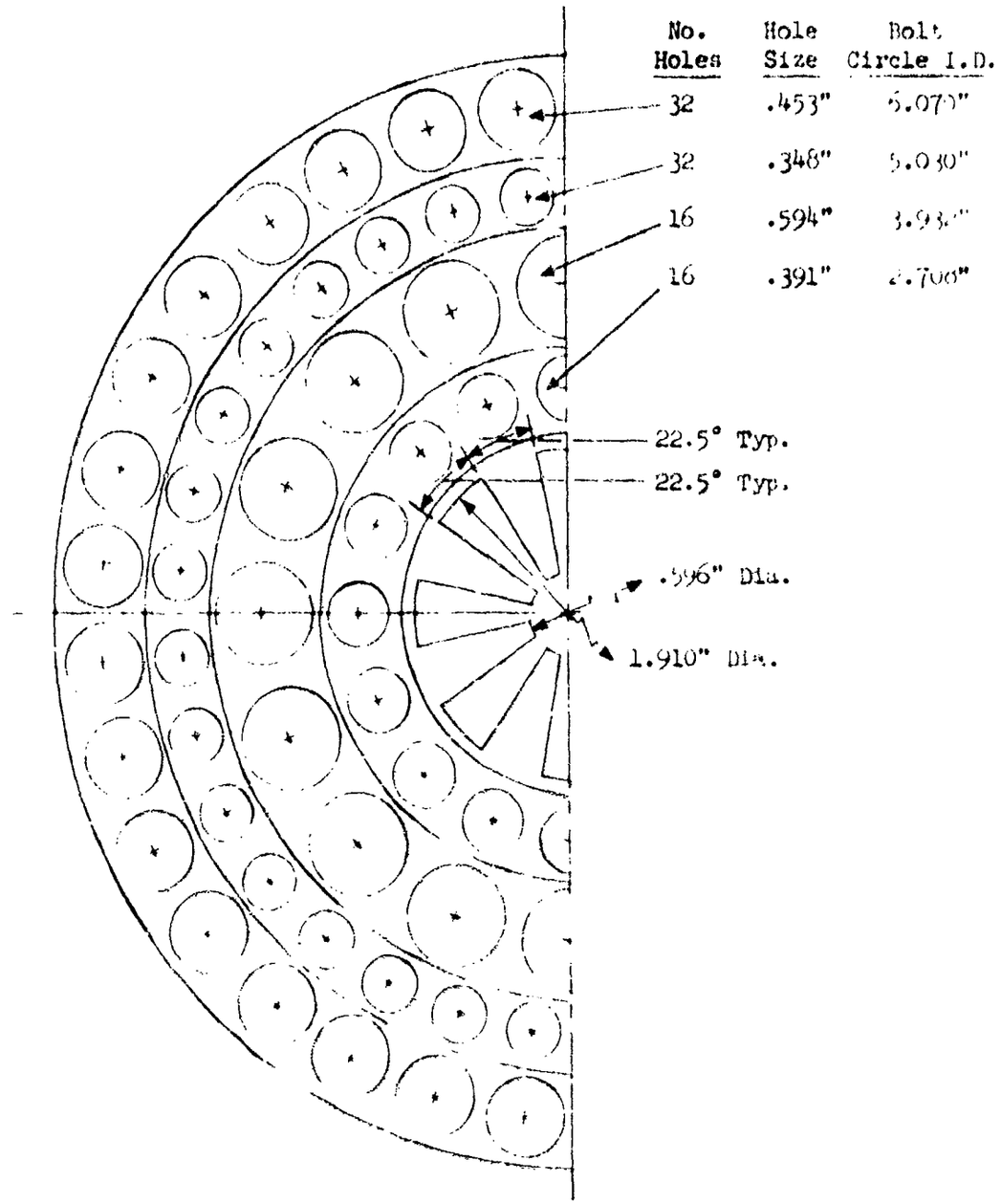


FIGURE V.C-11B SCHEMATIC OF 97 HOLE NOZZLE PLUS EJECTOR WITH INTERCHANGEABLE ACOUSTIC LINERS

o Suppression Relative to Hard Liner of Same Dimensions

o 300 Ft. Sideline

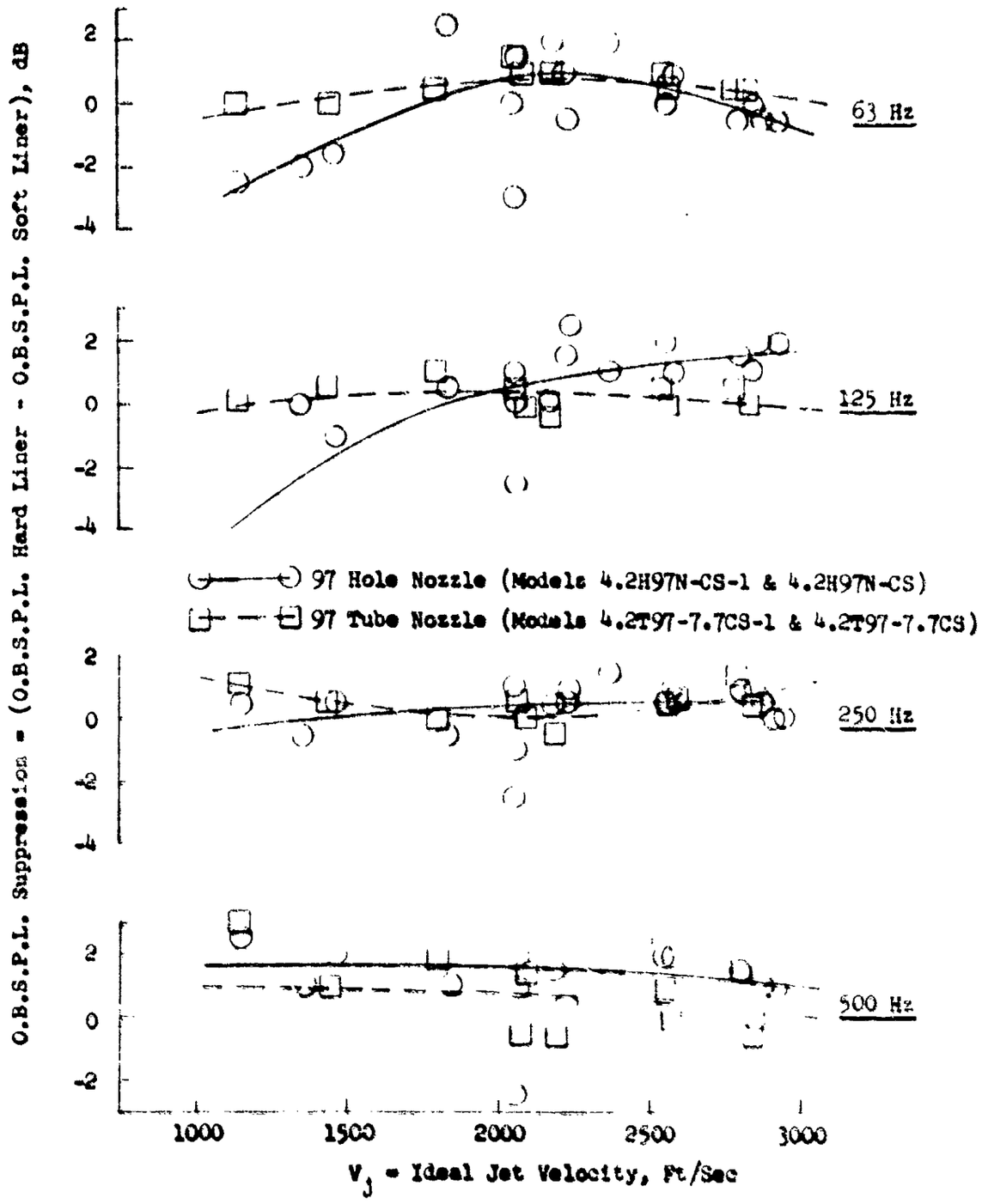


FIGURE V.C-12A SUPPRESSION EFFECT OF 7.5% OPEN SOFT LINER ON 97 TUBE AND 97 HOLE NOZZLES

o Suppression Relative to Hard Liner of Same Dimensions

o 300 Ft. Sideline

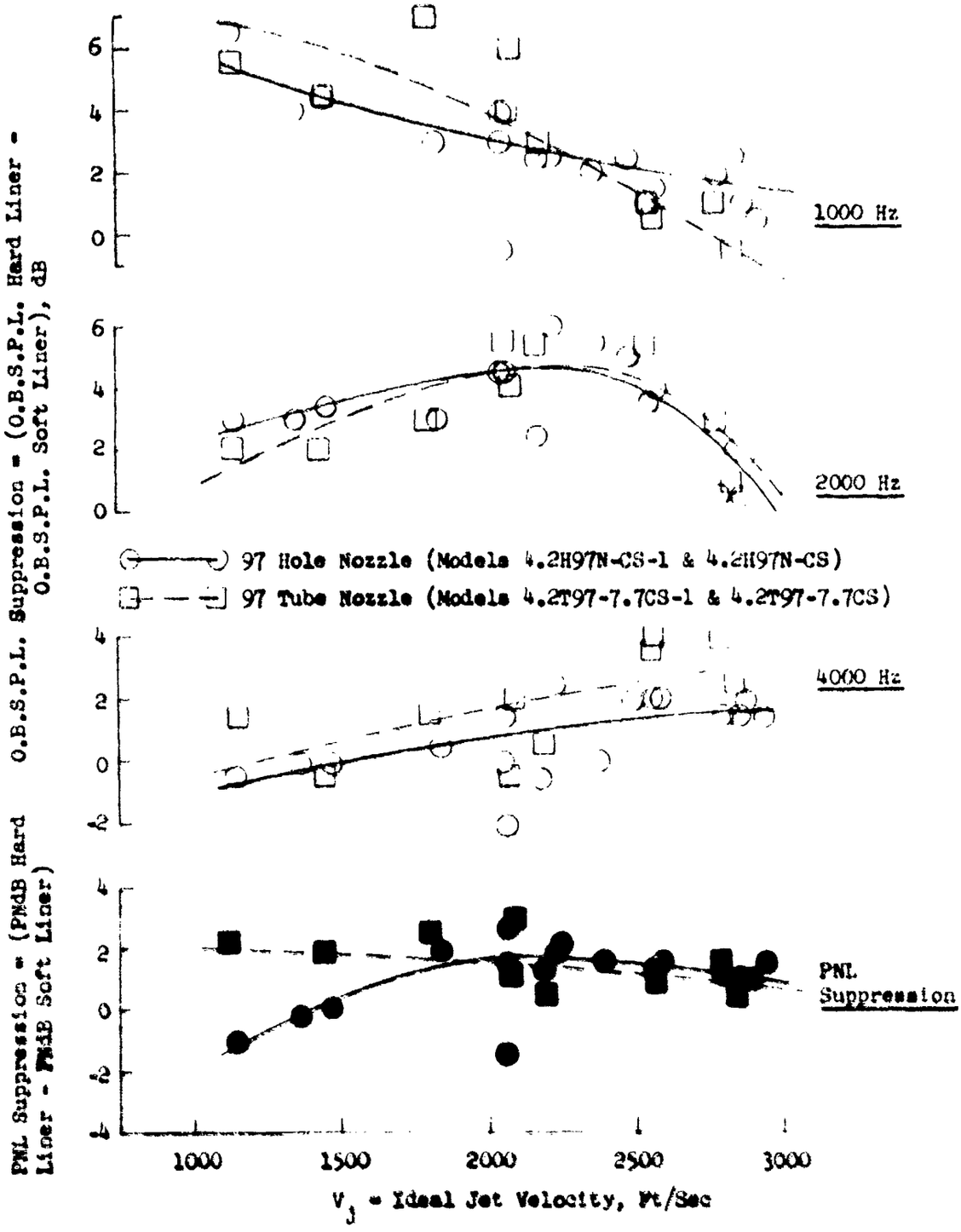


FIGURE V.G-12B SUPPRESSION EFFECT OF 7.5% OPEN SOFT LINER ON 97 TUBE AND 97 HOLE NOZZLES

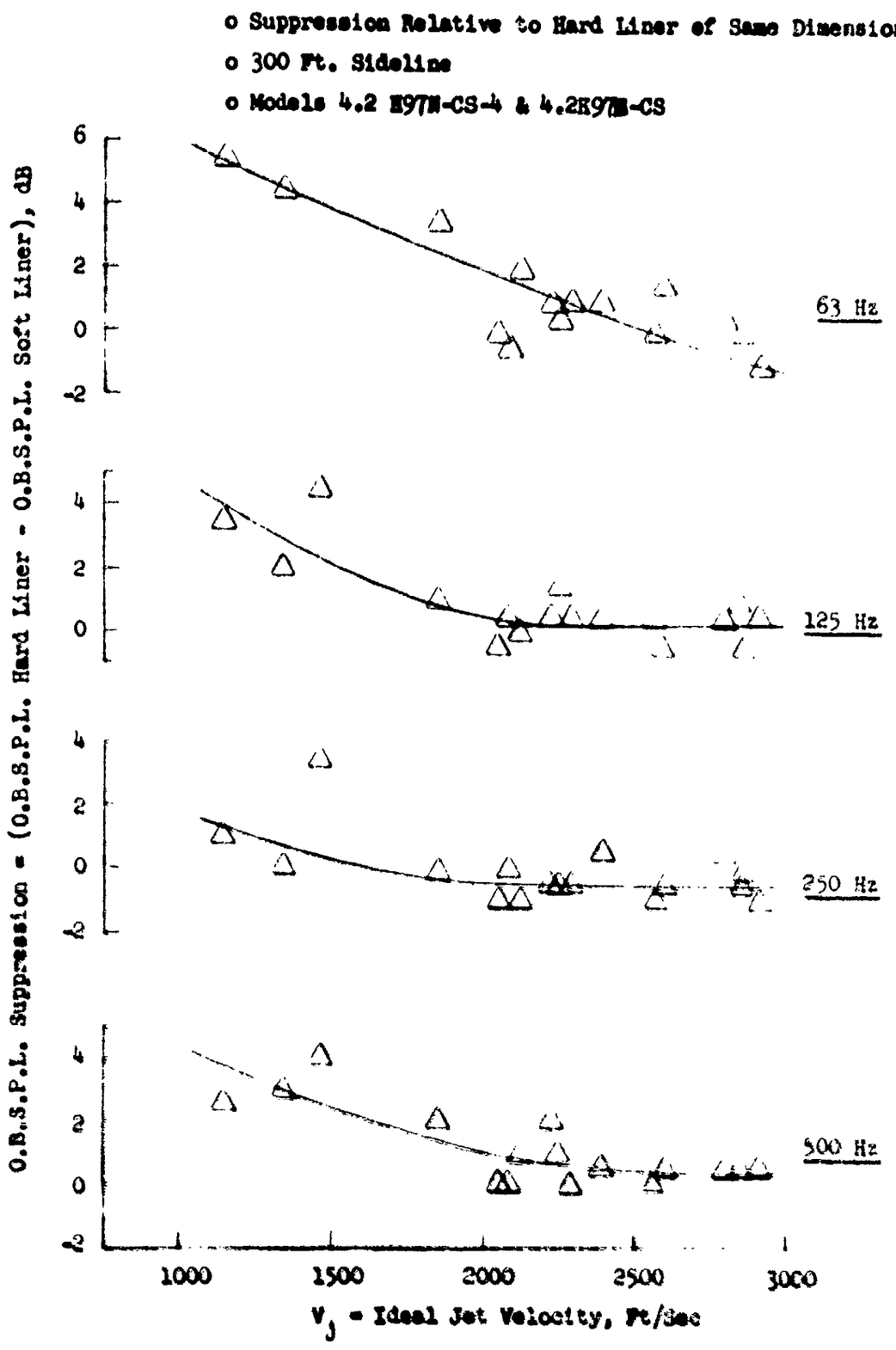


FIGURE V.C-13A SUPPRESSION EFFECT OF 4% OPEN SOFT LINER ON 97 HOLE NOZZLE

- o Suppression Relative to Hard Liner of Same Dimensions
- o 300 Ft. Sideline
- o Models 4.2E97N-CS-4 & 4.2E97N-CS

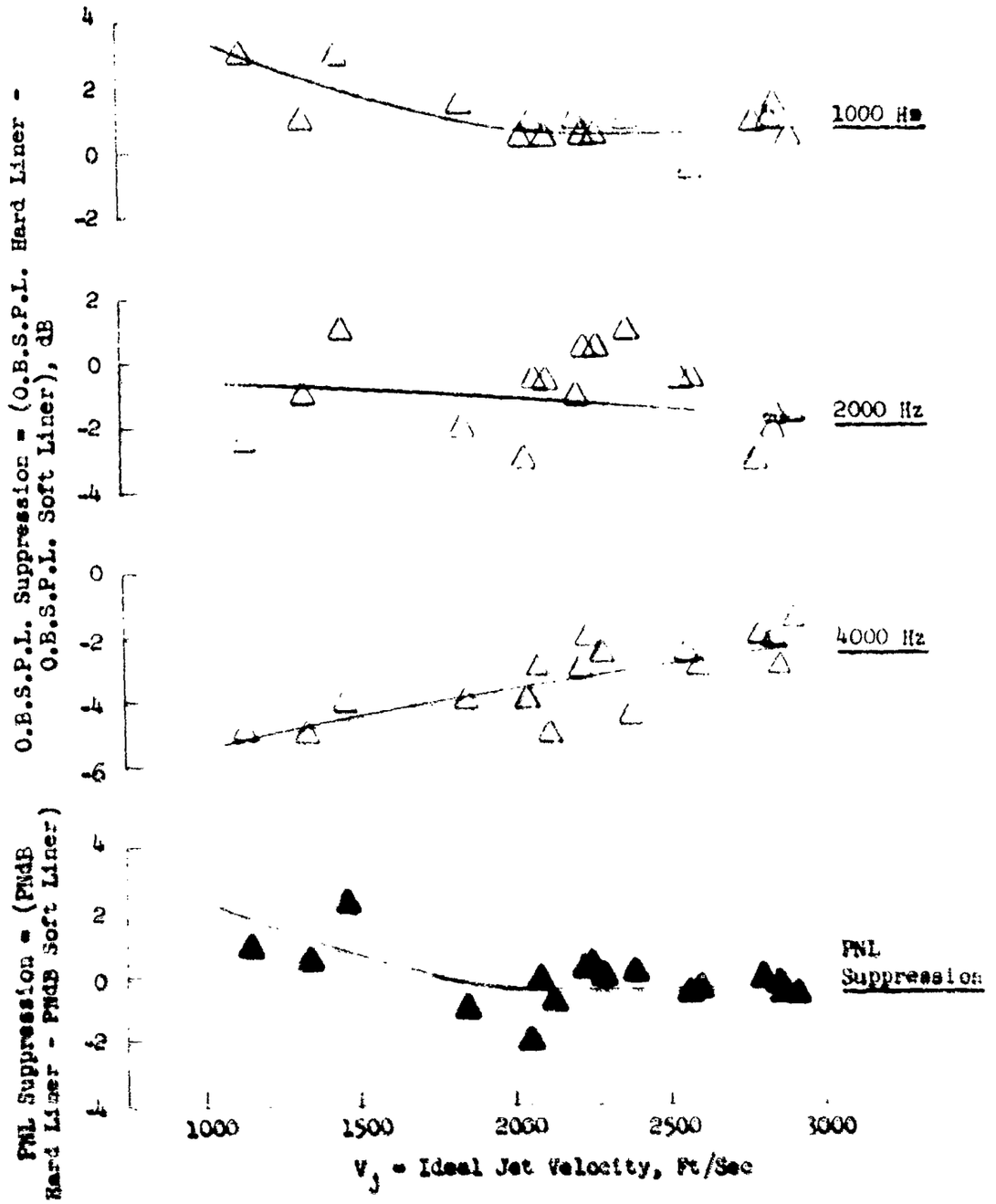


FIGURE V.C-13B SUPPRESSION EFFECT OF 4% OPEN SOFT LINER ON 97 HOLE NOZZLE

o Suppression Relative to Hard Liner of Same Dimensions

o 300 Ft. Sideline

o Models 4.2H97N-CS-5 & 4.2H97N-CS

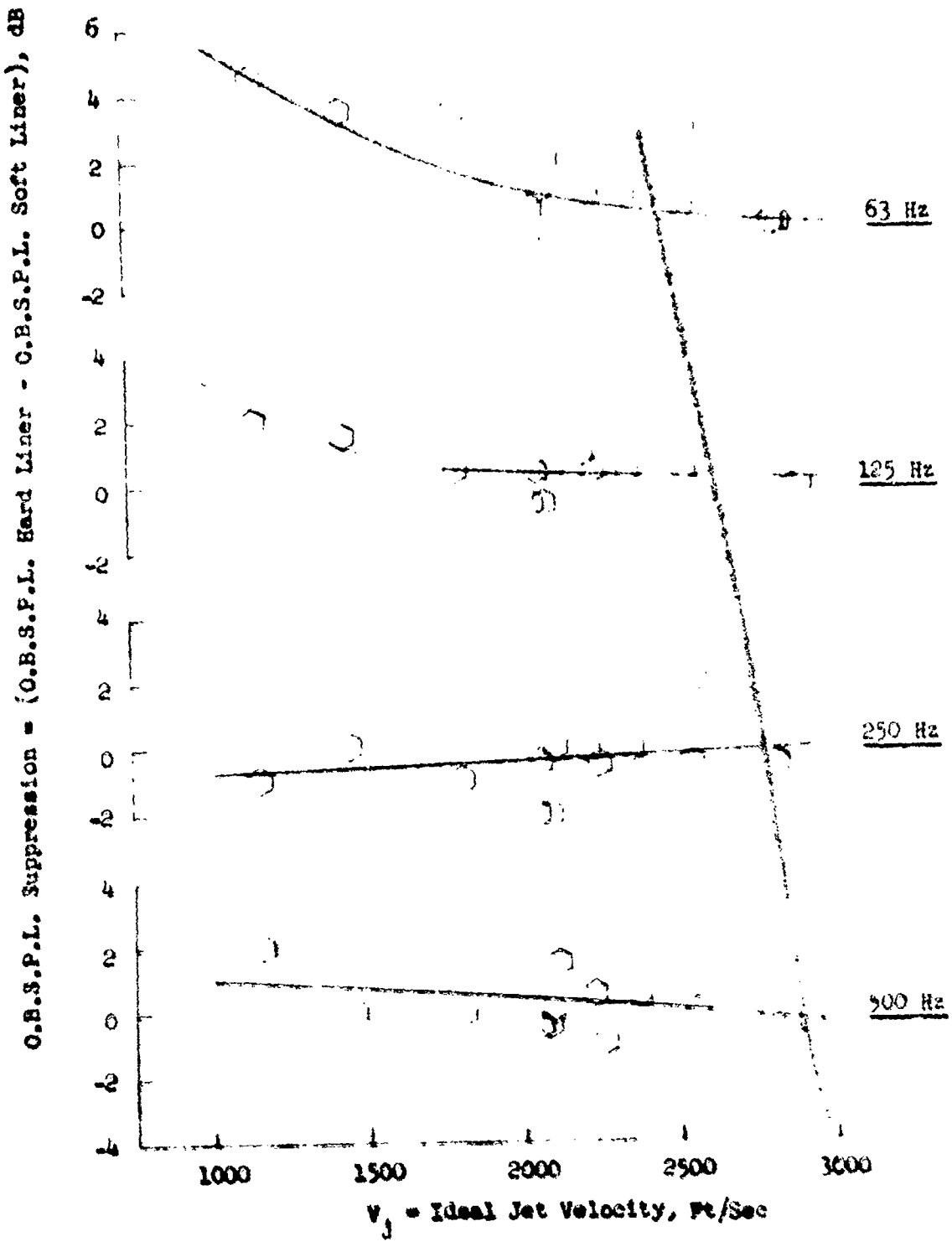


FIGURE V.C-14A SUPPRESSION EFFECT OF 15% OPEN SOFT LINER ON 97 HOLE NOZZLE

- o Suppression Relative to Hard Liner of Same Dimensions
- o 300 Ft. Sideline
- o Models 4.2H97N-CS-5 & 4.2H97N-CS

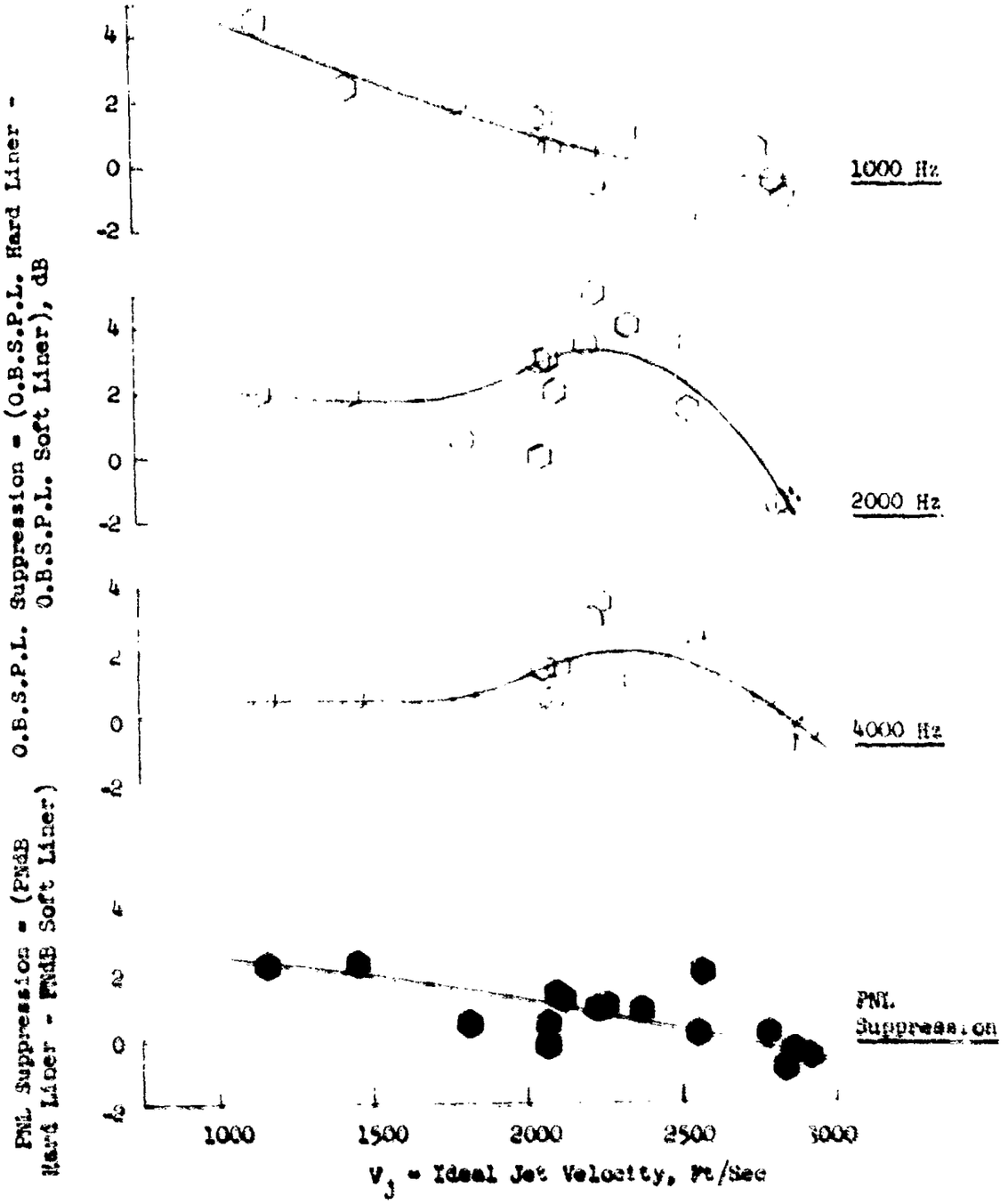


FIGURE V.C-14B SUPPRESSION EFFECT OF 15% OPEN SOFT LINER ON 97 HOLE NOZZLE

- Suppression Relative to Hard Liner of Same Dimensions
- 300 Ft. Sideline
- Models 4.2H97N-CS-6 & 4.2H97N-CS

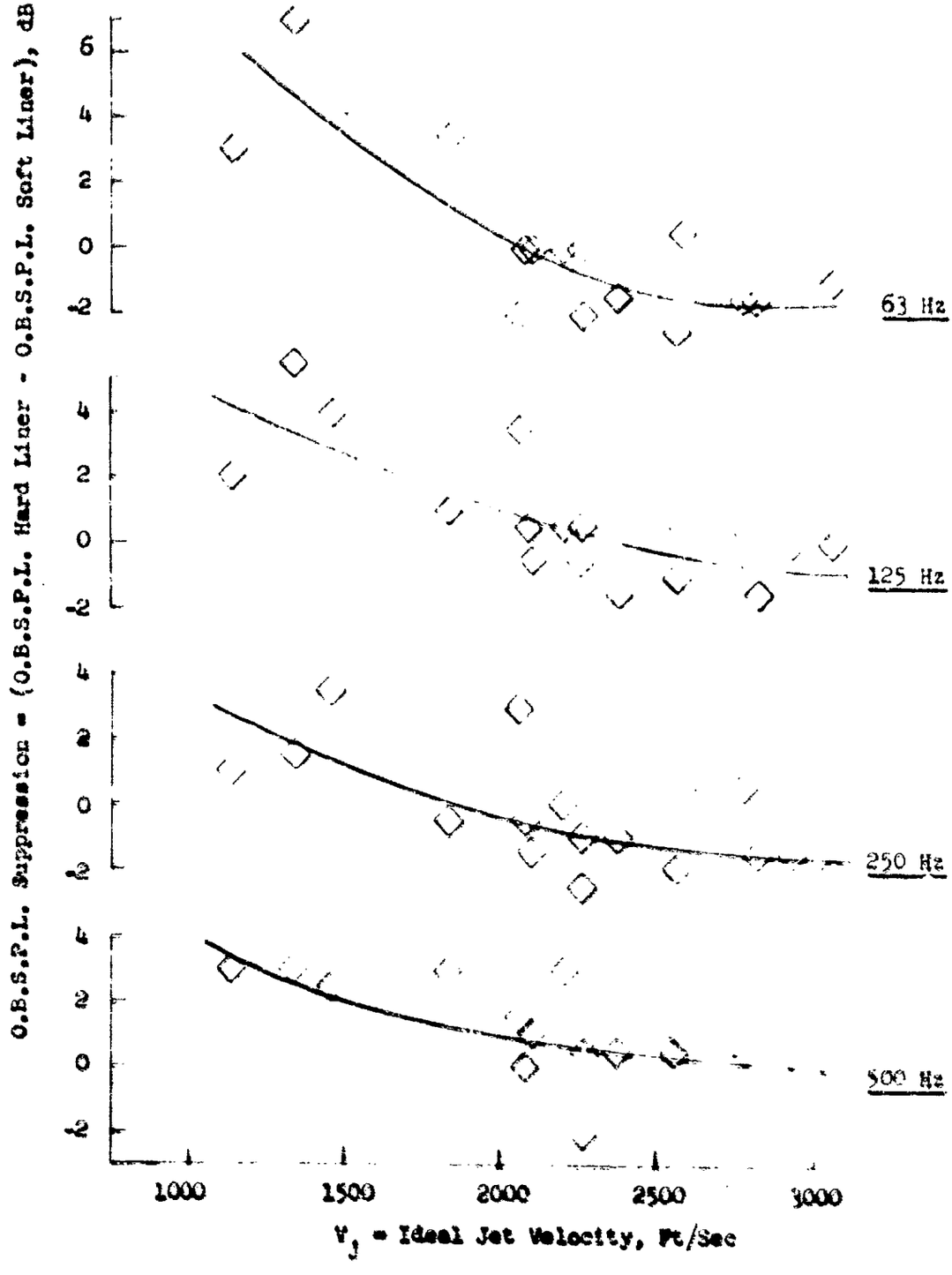


FIGURE V.6-15A SUPPRESSION EFFECT OF 22.5% OPEN, CERAFELT PACKED LINER ON 97 MOLE NOZZLE

- o Suppression Relative to Hard Liner of Same Dimensions
- o 300 Ft. Sideline
- o Models 4.2H97M-CS-6 & 4.2H97M-CS

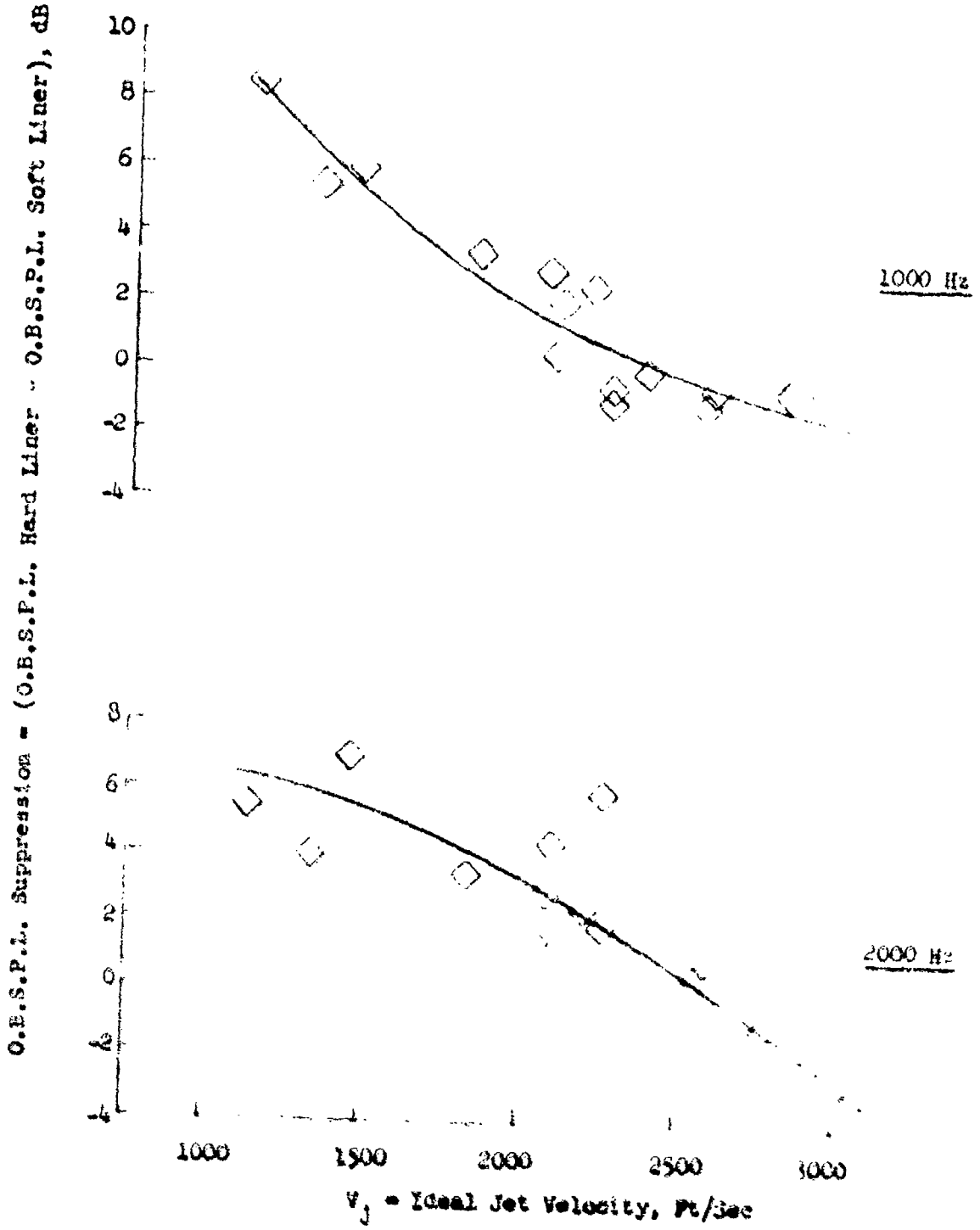


FIGURE V.C-158 SUPPRESSION EFFECT OF 22.5% OPEN, CERAFELT PACKED LINER ON 97 HOLE NOZZLE

- Suppression Relative to Hard Liner of Same Dimensions
- 300 Ft. Sideline
- Models 4.2H97H-CS-6 & 4.2H97H-CS

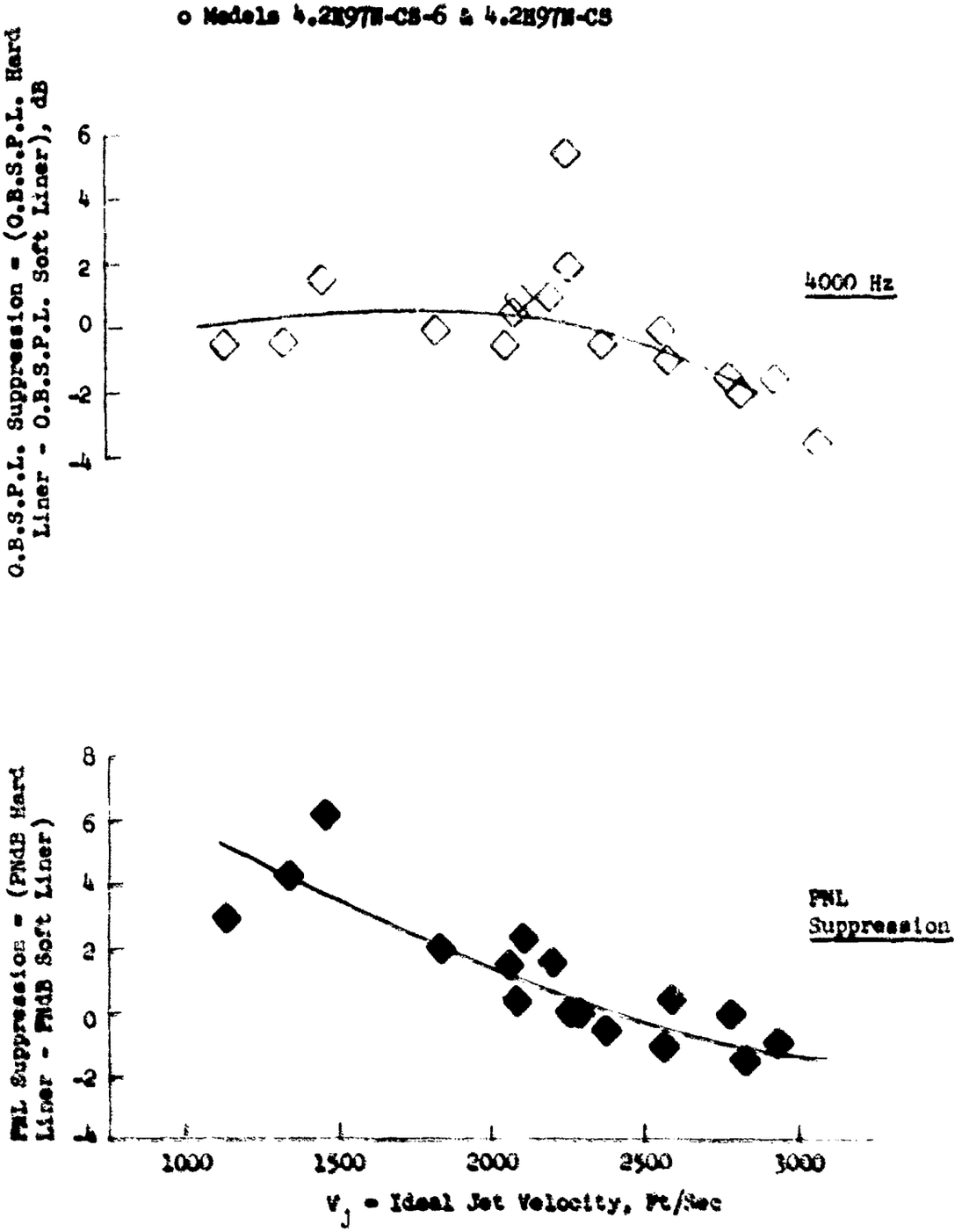


FIGURE V.C-15C SUPPRESSION EFFECT OF 22.5% OPEN, CERAFELT PACKED LINER ON 97 HOLE NOZZLE

o Suppression Relative to Hard Liner of Same Dimensions

o 300 Ft. Sideline

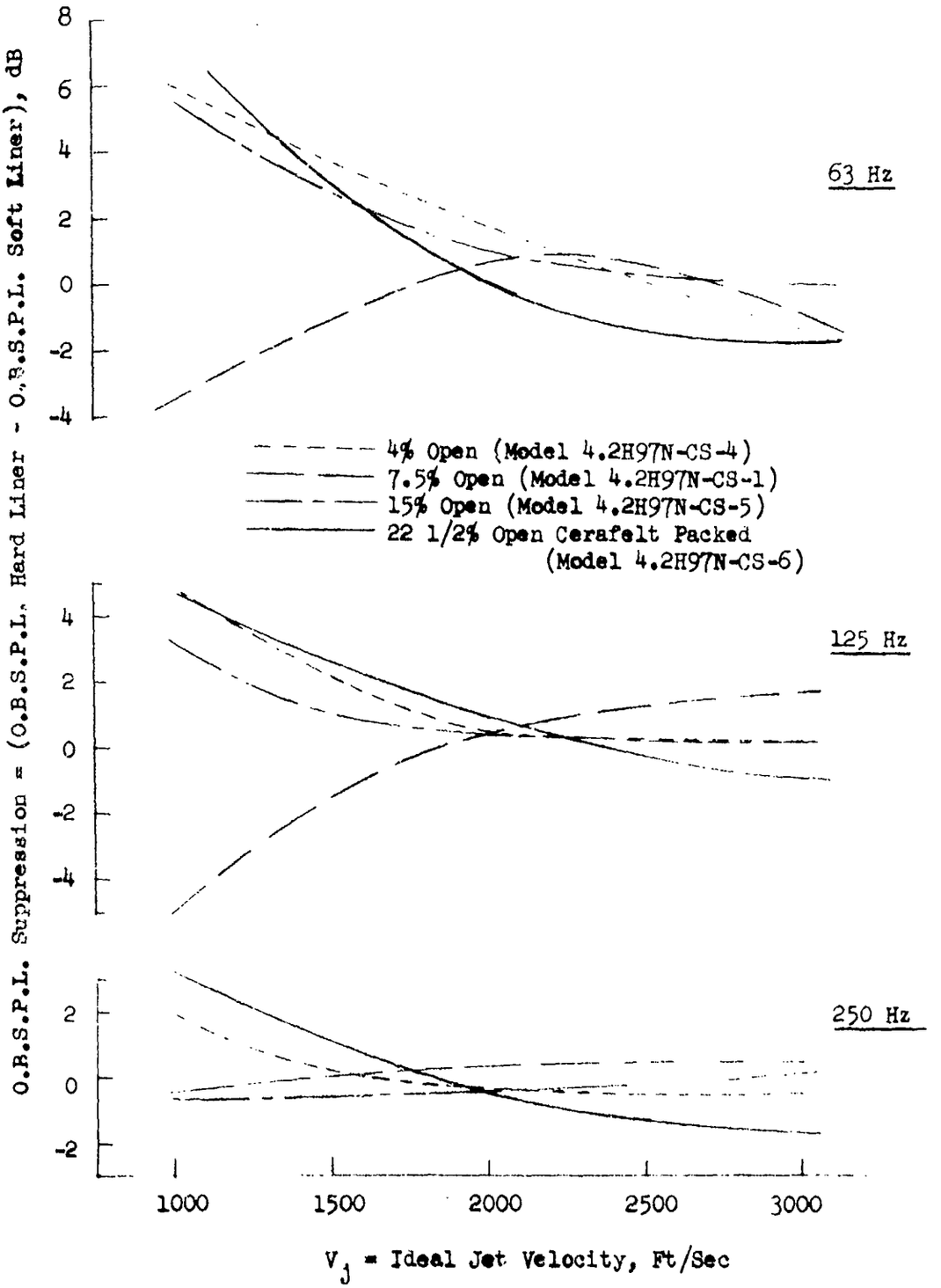


FIGURE V.G-16A COMPARISON OF SUPPRESSION EFFECT OF SOFT LINERS ON 97 HOLE NOZZLE

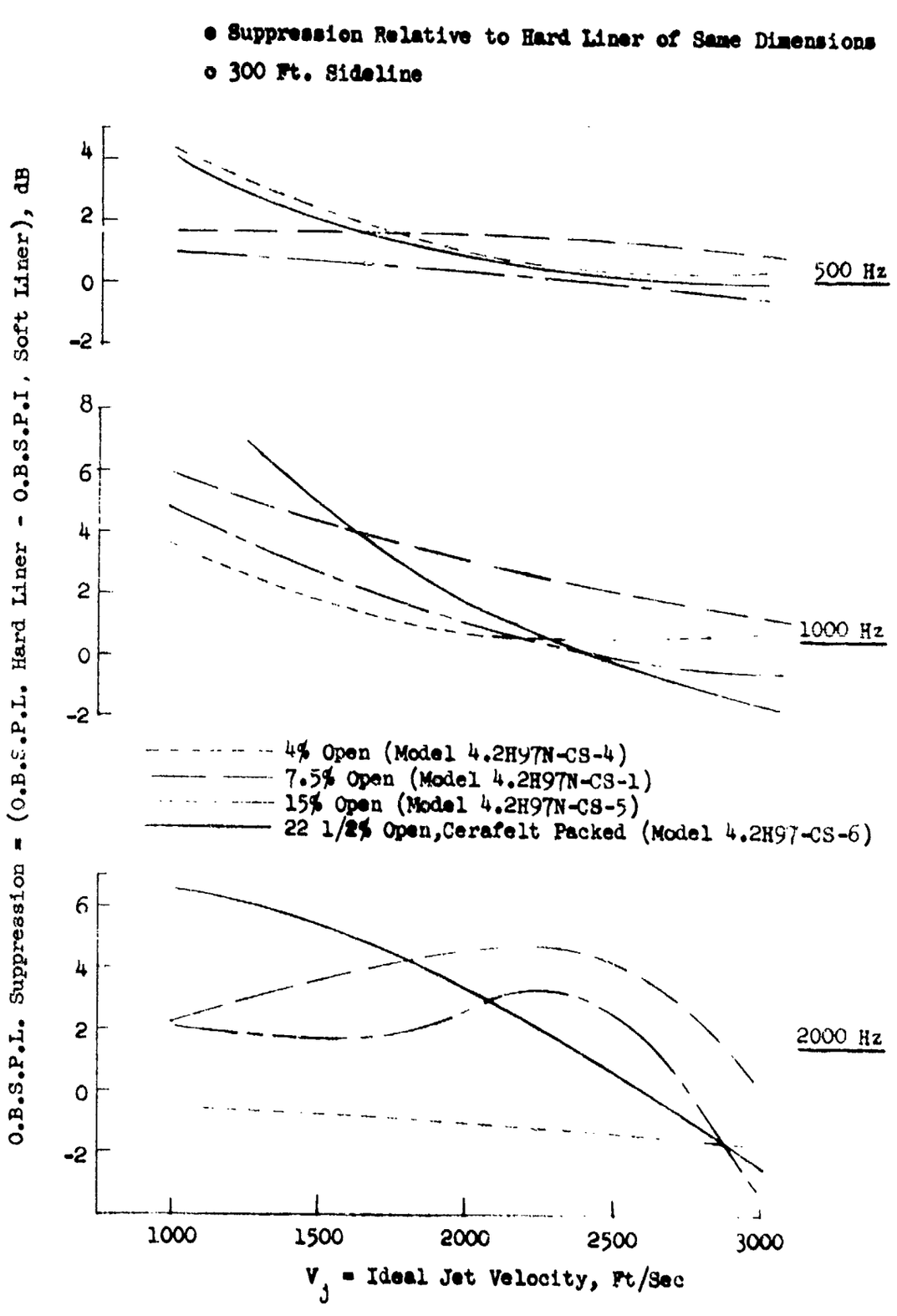


FIGURE V.G-16B COMPARISON OF SUPPRESSION EFFECT OF SOFT LINERS ON 97 HOLE NOZZLE

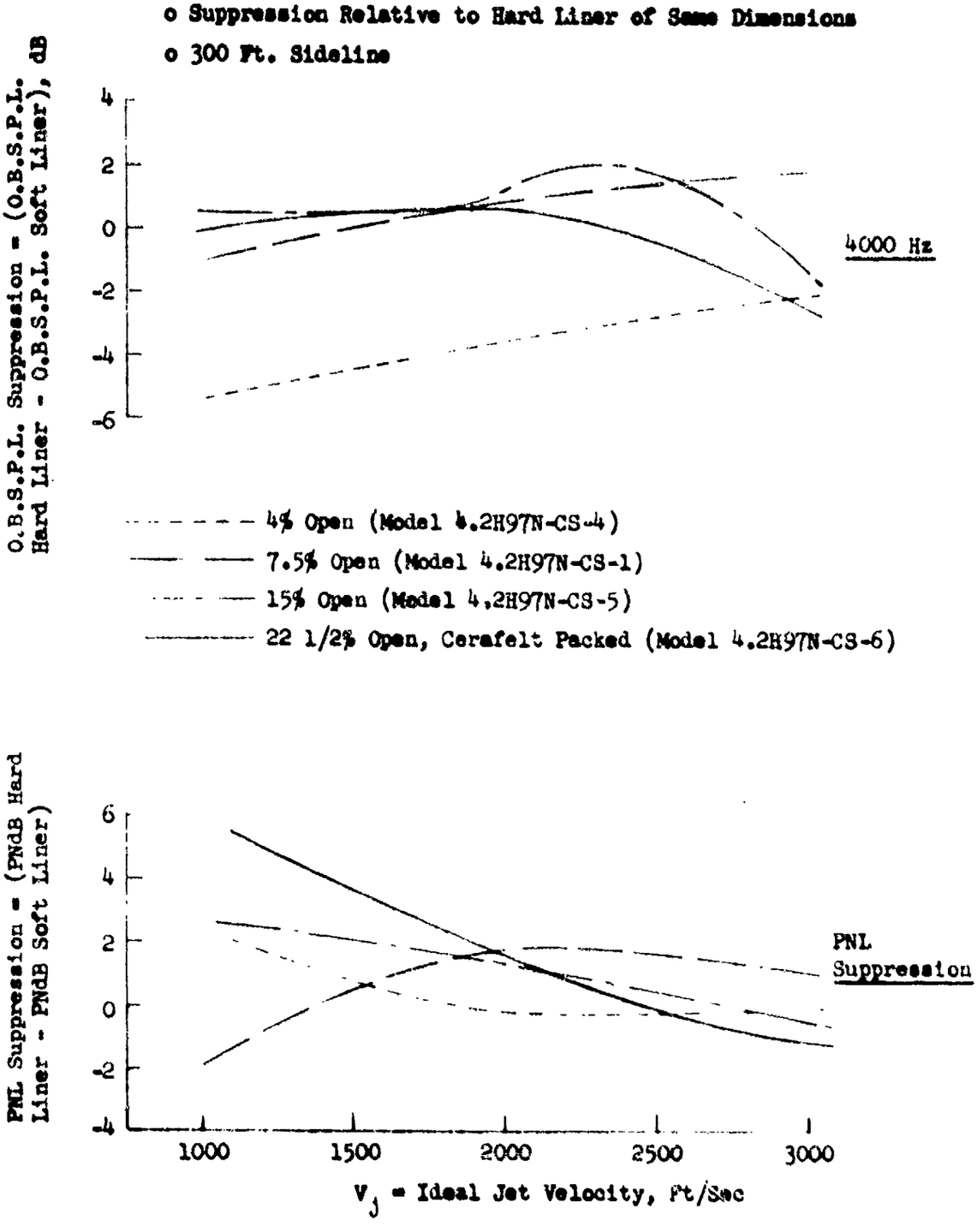


FIGURE V.G-16C COMPARISON OF SUPPRESSION EFFECT OF SOFT LINERS ON 97 HOLE NOZZLE

o Suppression Relative to Hard Liner of Same Dimensions

o 300 Ft. Sideline

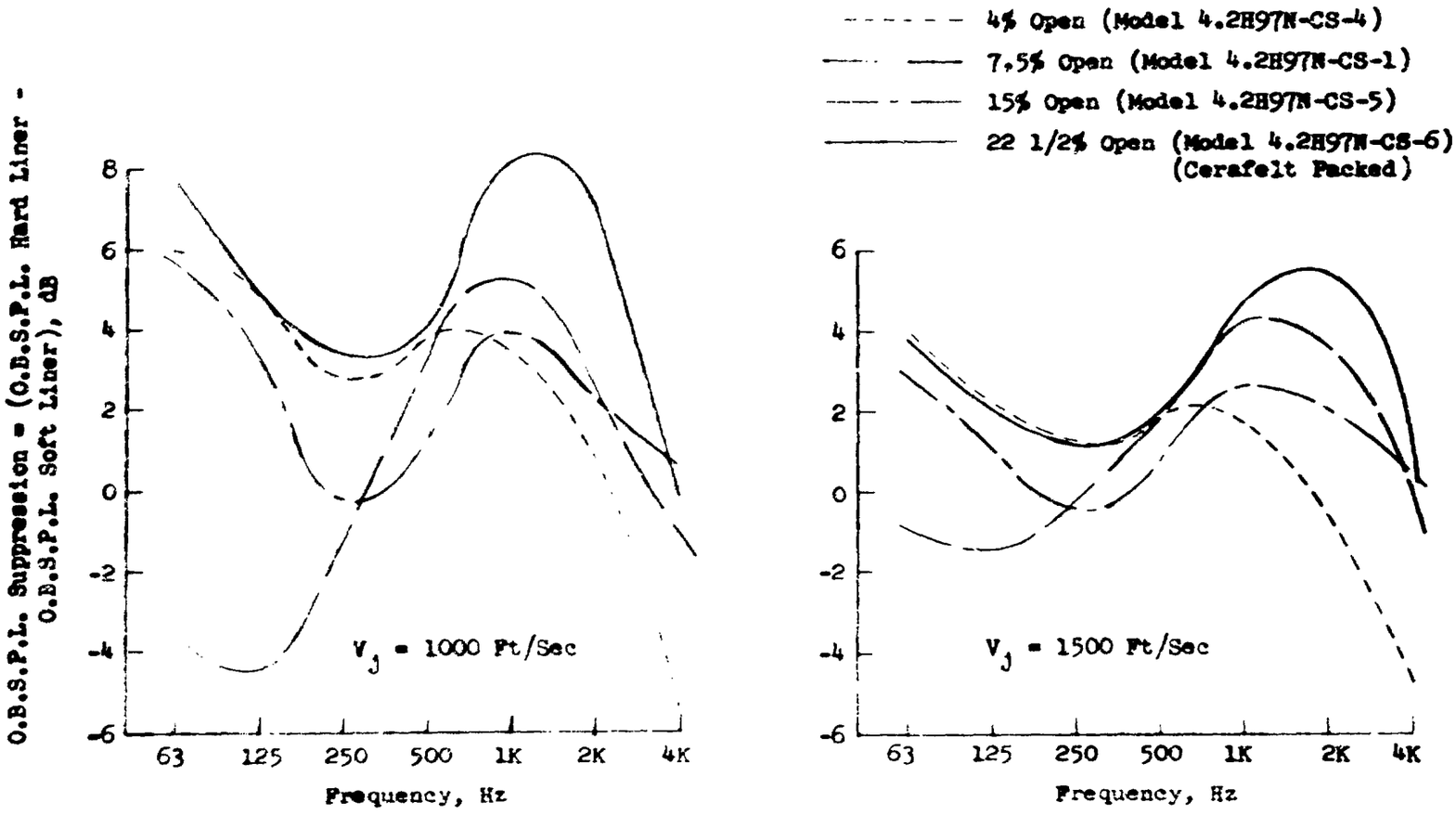


FIGURE V.G-17A COMPARISON OF SUPPRESSION EFFECT OF SOFT LINERS ON 97 HOLE NOZZLE AT VARIOUS JET VELOCITIES

o Suppression Relative to Hard Liner of Same Dimensions

o 300 Ft. Sideline

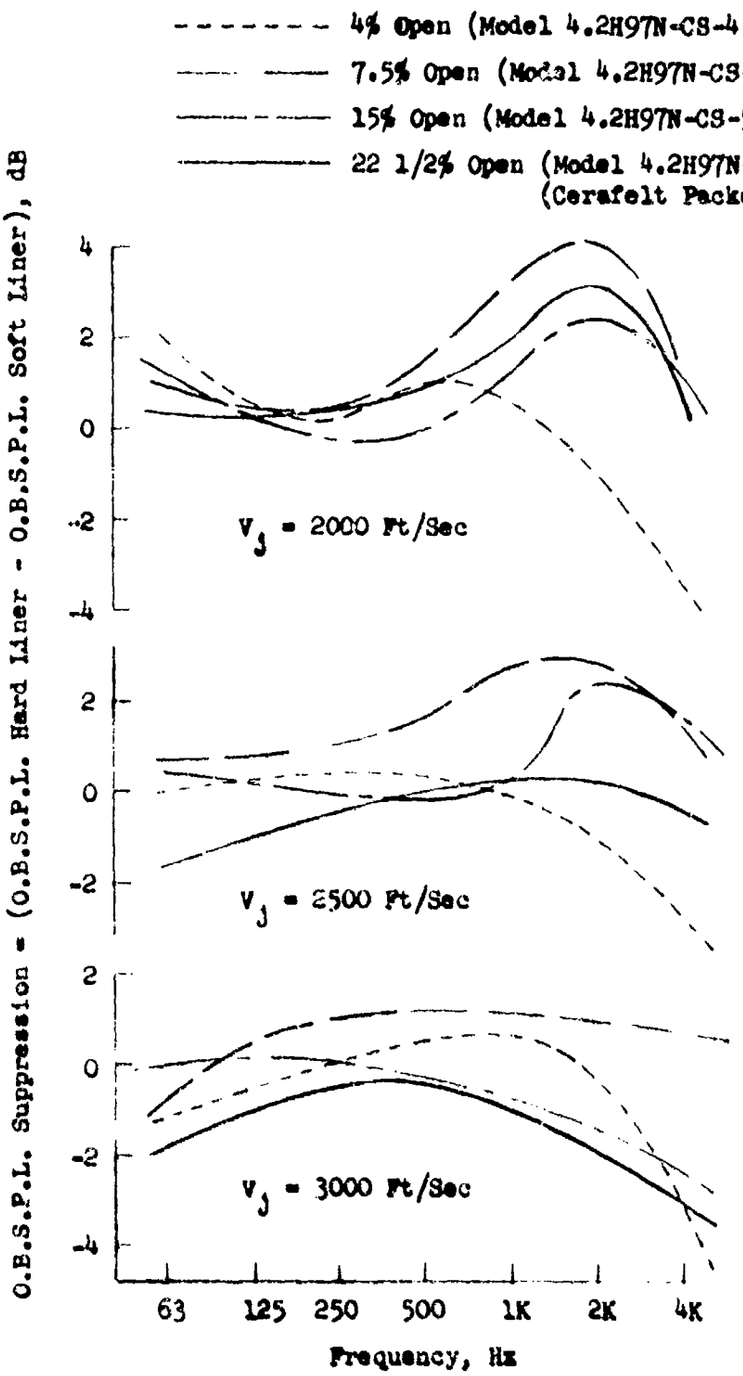


FIGURE V.G-17B COMPARISON OF SUPPRESSION EFFECT OF SOFT LINERS ON 97 HOLE NOZZLE AT VARIOUS JET VELOCITIES

- Model 4.1T37-10.4-CS - 22.5% Open Sheet Metal and Cerafelt
- Model 4.1T37-10.8-CSE - Hardwall Ejector

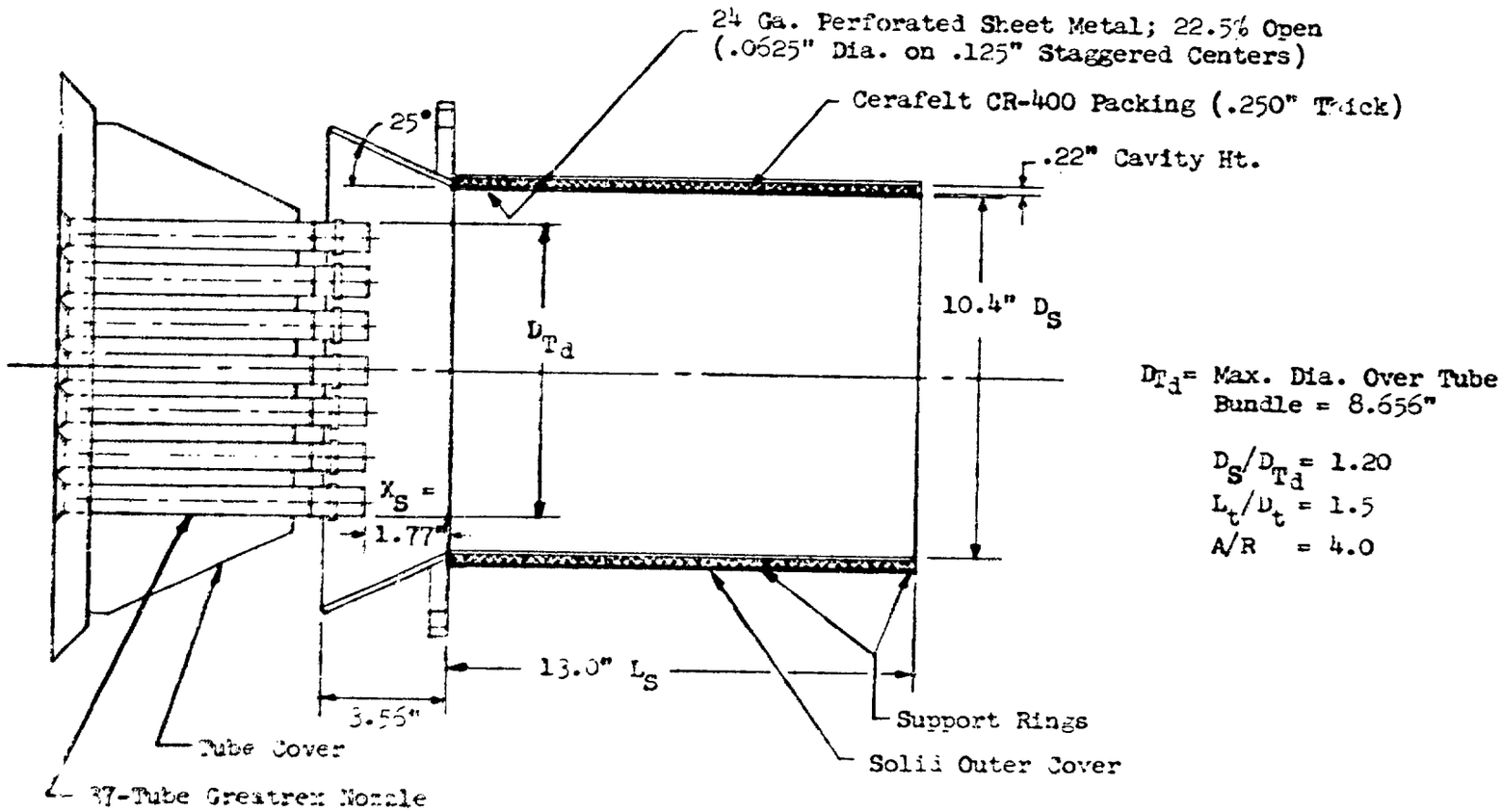


FIGURE V.G-18 SCHEMATIC OF 37 TUBE GREATREX NOZZLE WITH PERFORATED SHEET METAL/CERAFELT PACKED EJECTOR

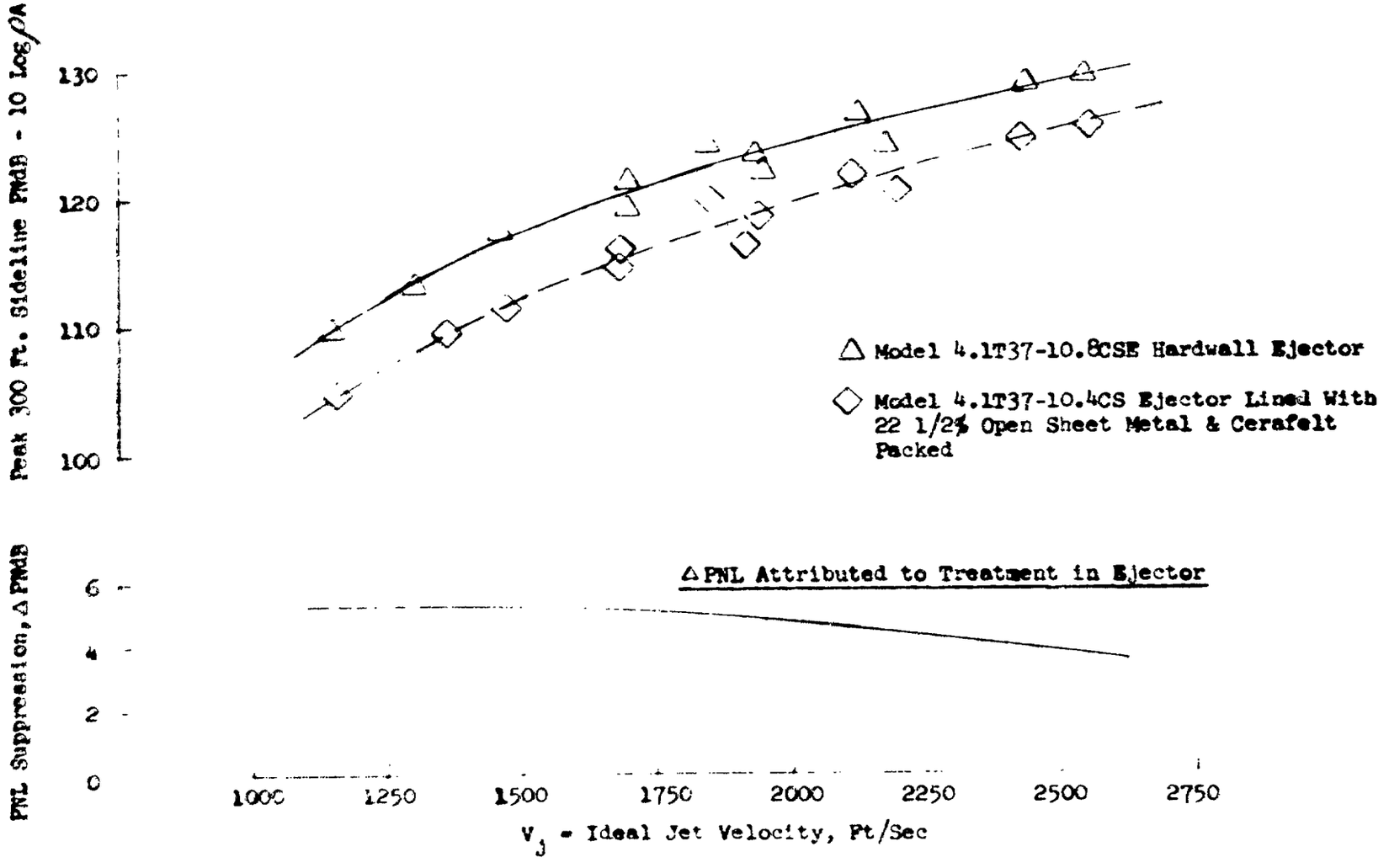


FIGURE V.G-19 300 FT SIDELINE JET NOISE AND PNL SUPPRESSION LEVELS FOR 37 GREATREX TUBE PRIMARY NOZZLE WITH TREATED AND HARDWALL EJECTORS

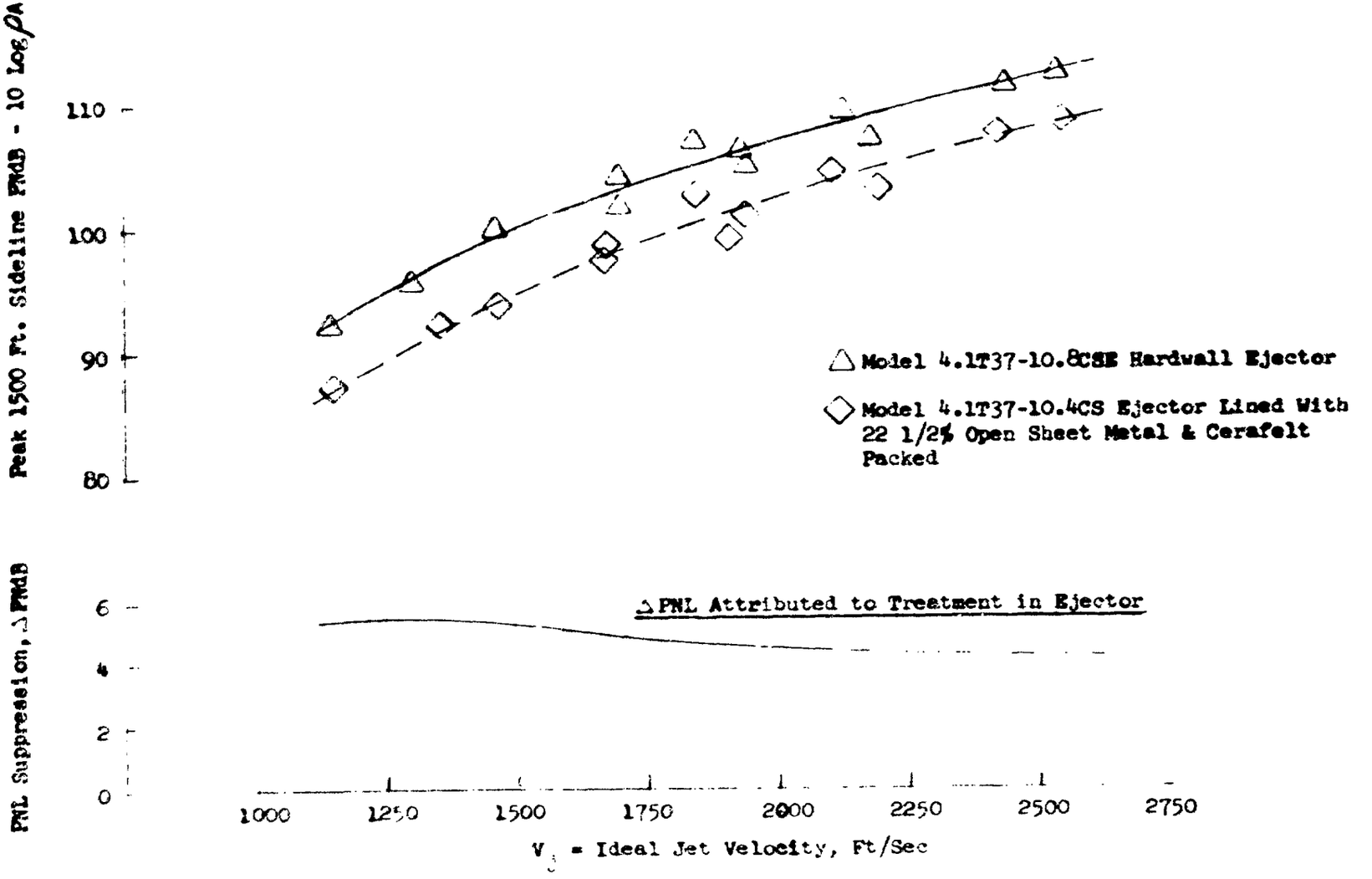


FIGURE V.G-20 1500 FT SIDELINE JET NOISE AND PNL SUPPRESSION LEVELS FOR 37 GREATREX TUBE PRIMARY NOZZLE WITH TREATED AND HARDWALL EJECTORS

- Suppression Relative to Hard Liner of Same Dimensions
- 300 Ft. Sideline - 80° From Jet Exhaust
- Models 4.1T37-10.8CSE & 4.1T37-10.4CS

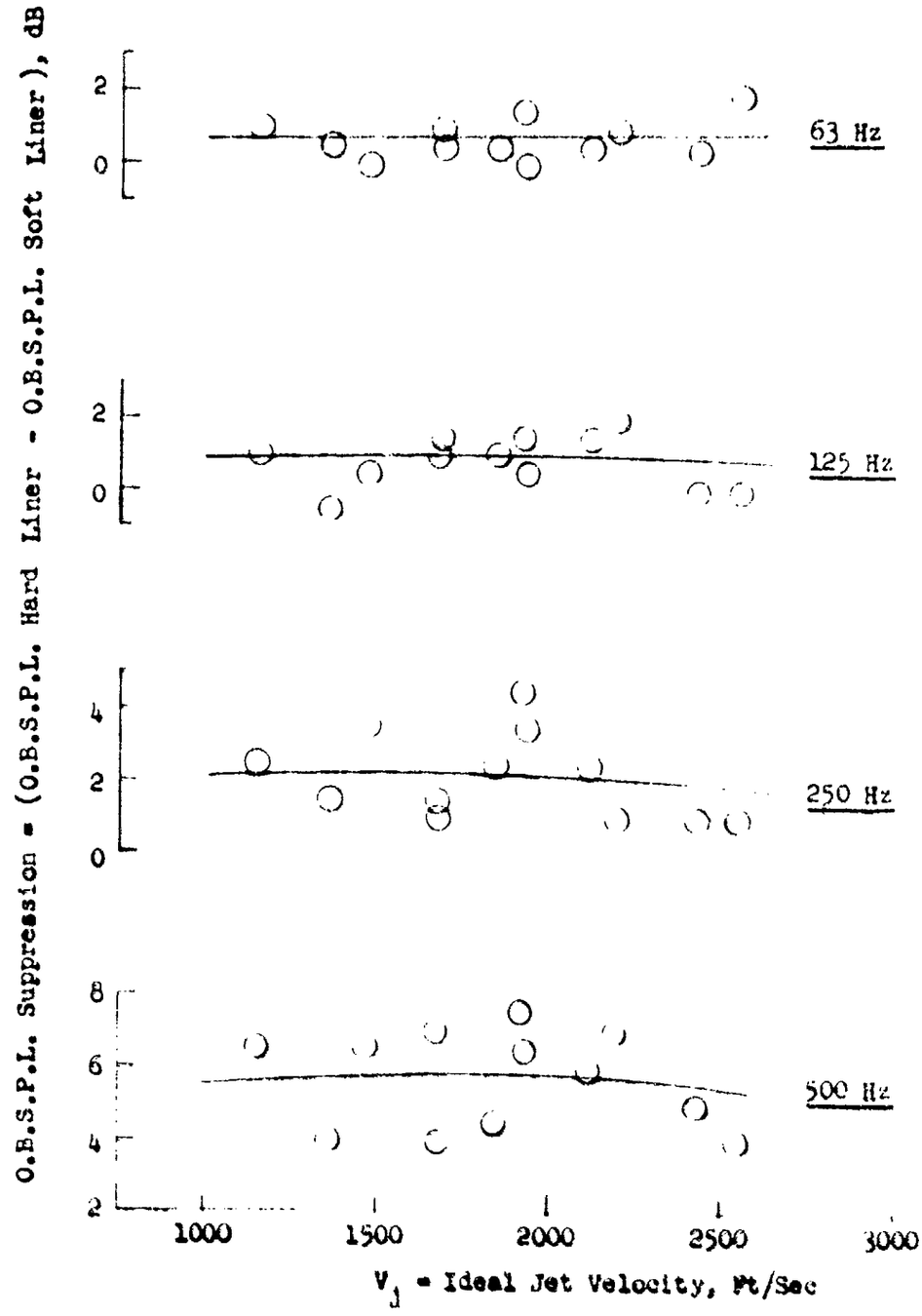


FIGURE V.G-21A SUPPRESSION EFFECT OF 22.5% OPEN, CERAFELT PACKED LINER ON 37 GREATREX TUBE NOZZLE

- o Suppression Relative to Hard Liner of Same Dimensions
- o 300 Ft. Sideline - 80° From Jet Exhaust
- o Models 4.1T37-10.8CSE & 4.1T37-10.4CS

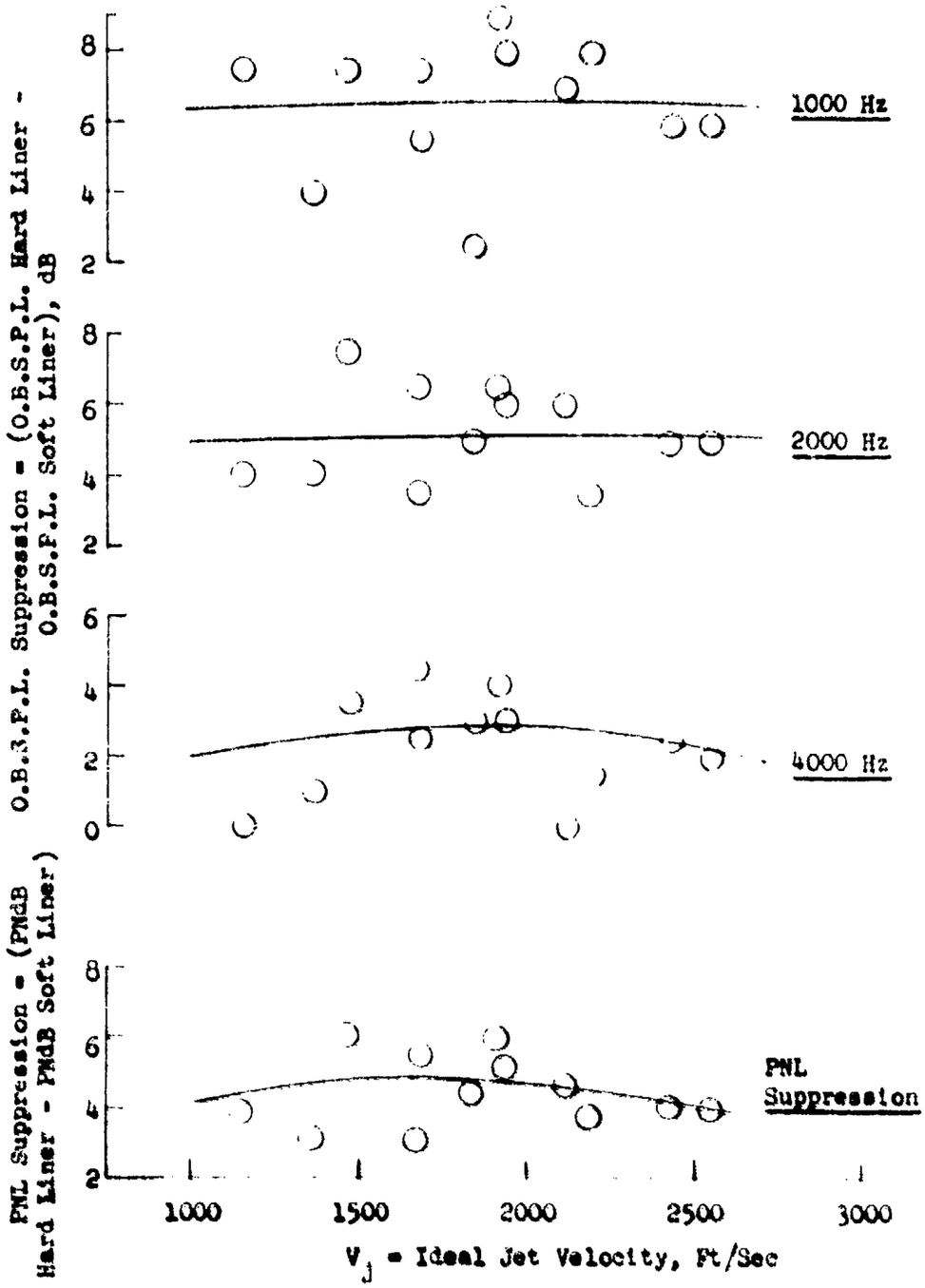
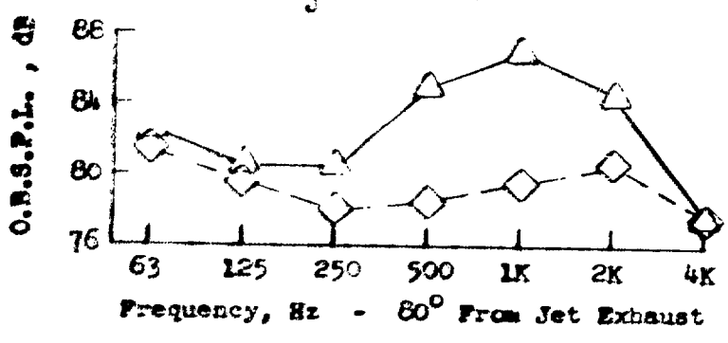


FIGURE V.G-21B SUPPRESSION EFFECT OF 22.5% OPEN, CERAFELT PACKED LINER ON 37 GREATREX TUBE NOZZLE

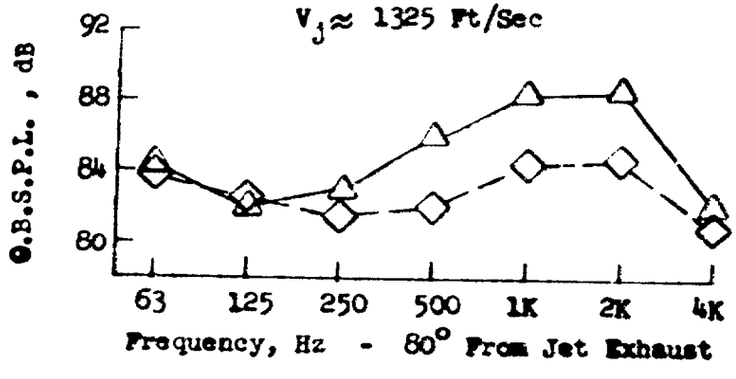
△ Hard Ejector (Model 4.1T37-10.8CSE)

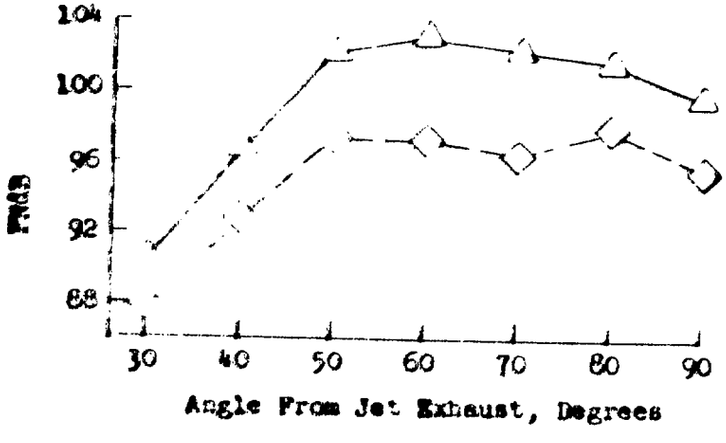
◇ Treated Ejector (Model 4.1T37-10.4CS)

$P_{T8}/P_0 \approx 1.41$
$T_{T8} \approx 1160°R$
$V_j \approx 1145$ Ft/Sec



$P_{T8}/P_0 \approx 1.40$
$T_{T8} \approx 1530°R$
$V_j \approx 1325$ Ft/Sec





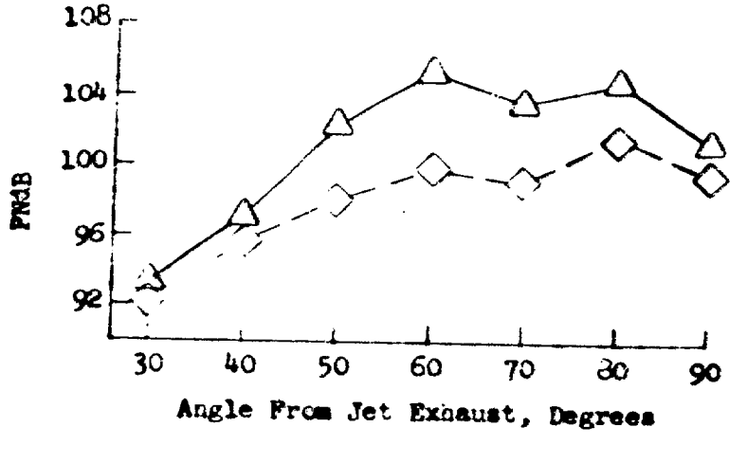


FIGURE V.G-22A 300 FT SIDELINE SPECTRA AND DIRECTIVITY FOR 37 GREATREX TUBE NOZZLE WITH TREATED AND HARDWALL EJECTORS

△ Hard Ejector (Model 4.1T37-10.8CSE)

◇ Treated Ejector (Model 4.1T37-10.4CS)

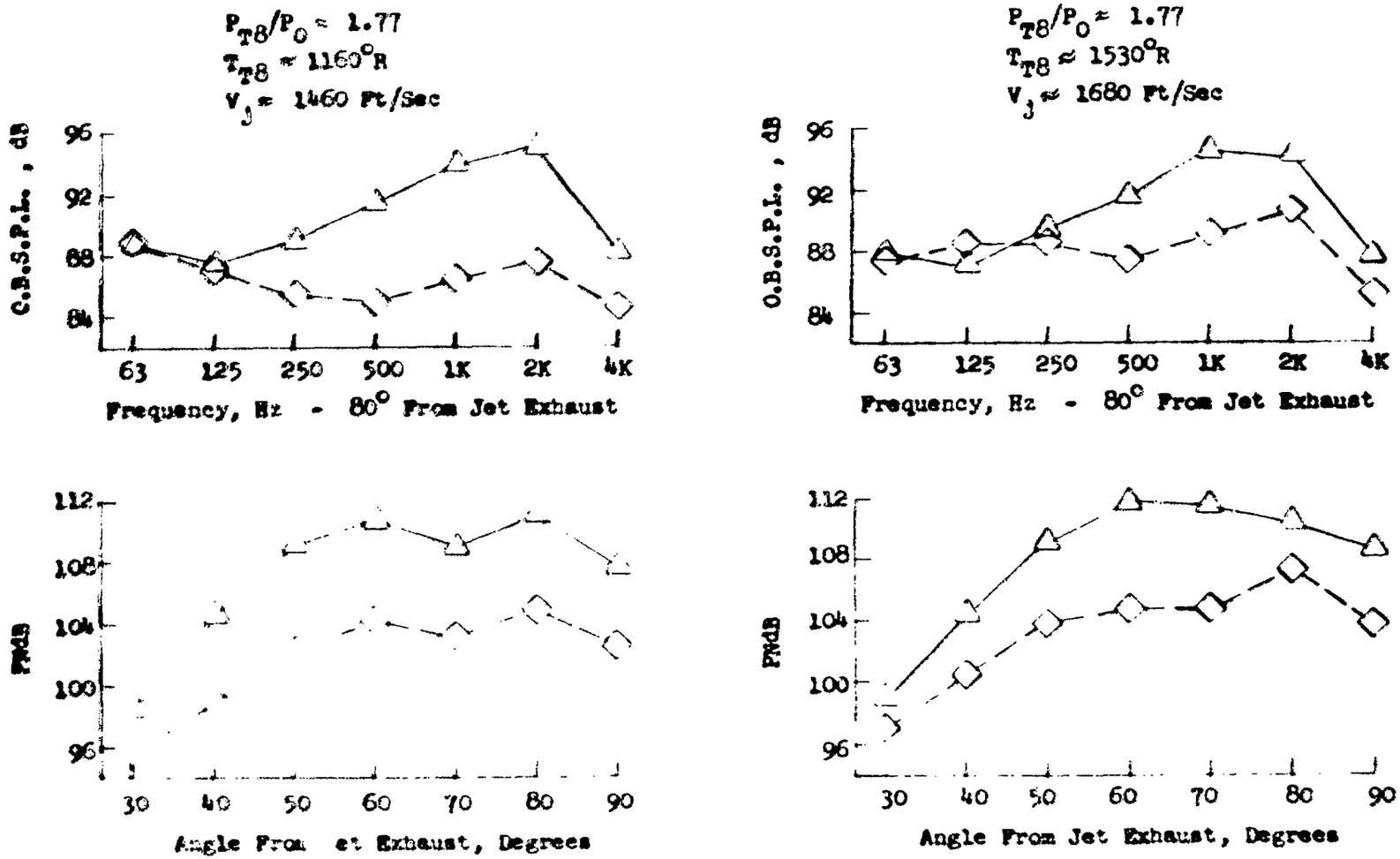
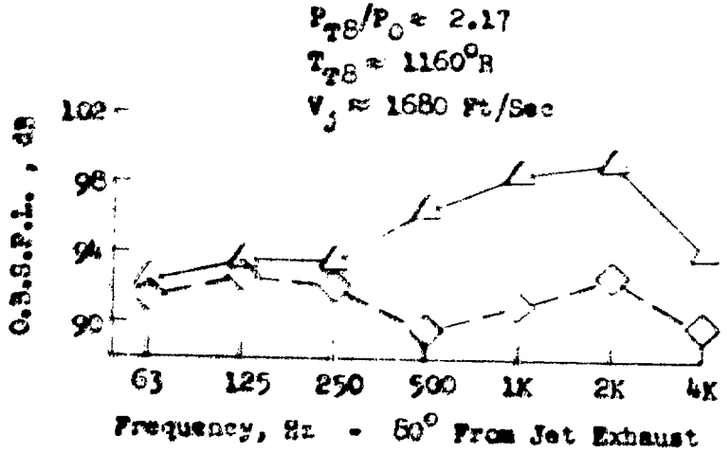
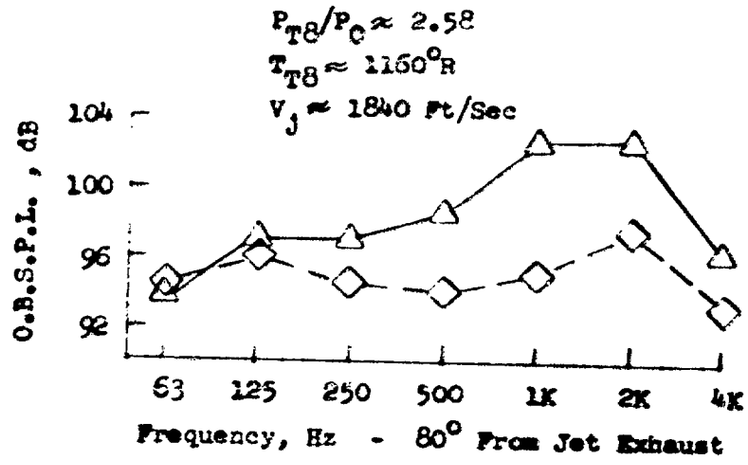


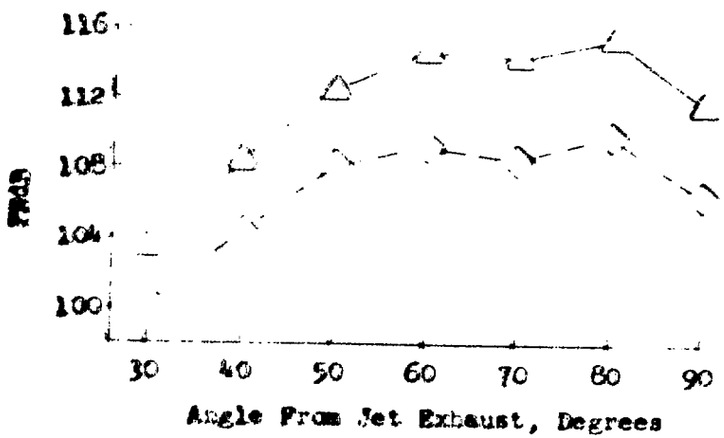
FIGURE V.C-22B 30C FT SIDELINE SPECTRA AND DIRECTIVITY FOR 37 GREATREX TUBE NOZZLE WITH TREATED AND HARDWALL EJECTORS

△ Hard Ejector (Model 4.1T37-10.8CSE)

◇ Treated Ejector (Model 4.1T37-10.4CS)







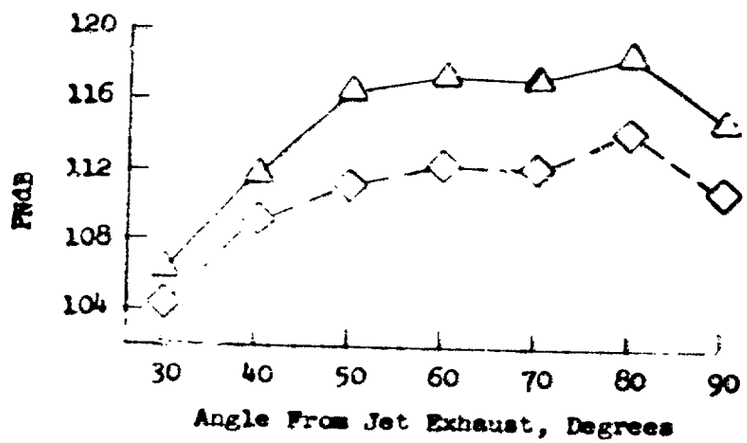
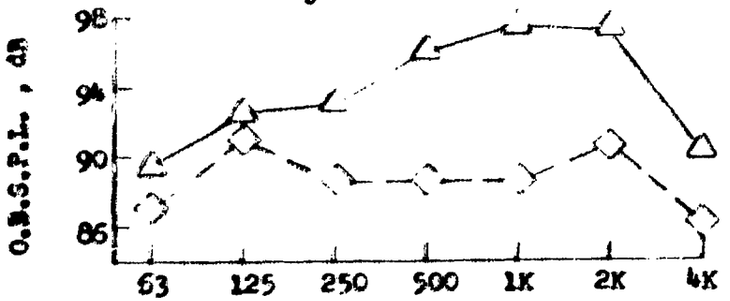


FIGURE V.C-22C 300 FT SIDELINE SPECTRA AND DIRECTIVITY FOR 37 GREATREX TUBE NOZZLE WITH TREATED AND HARDWALL EJECTORS

△ Hard Ejector (Model 4.1T37-10.8CSE)

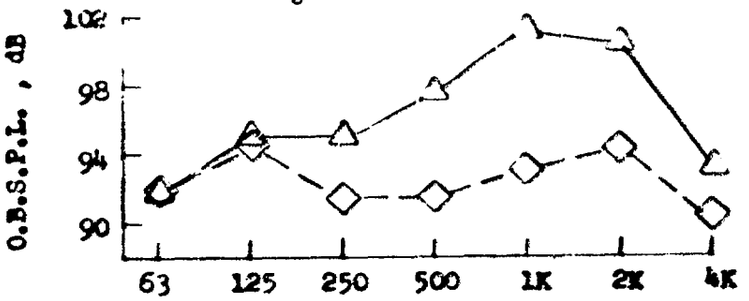
◇ Treated Ejector (Model 4.1T37-10.4CS)

$P_{T8}/P_0 \approx 1.60$
$T_{T8} \approx 1975^\circ R$
$V_j \approx 1920$ Ft/Sec

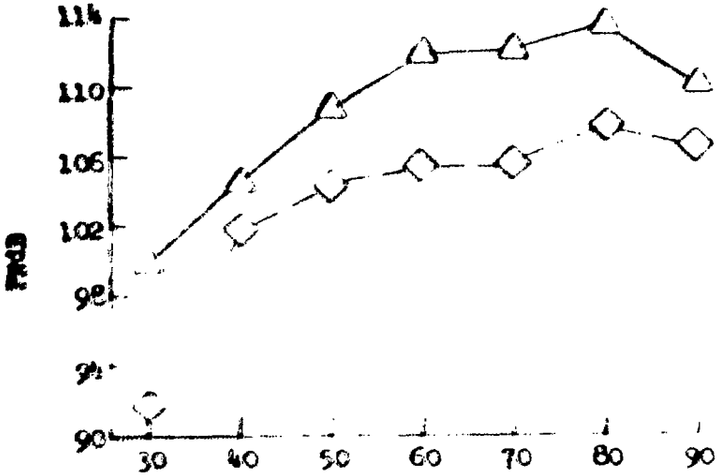


Frequency, Hz - 90° From Jet Exhaust

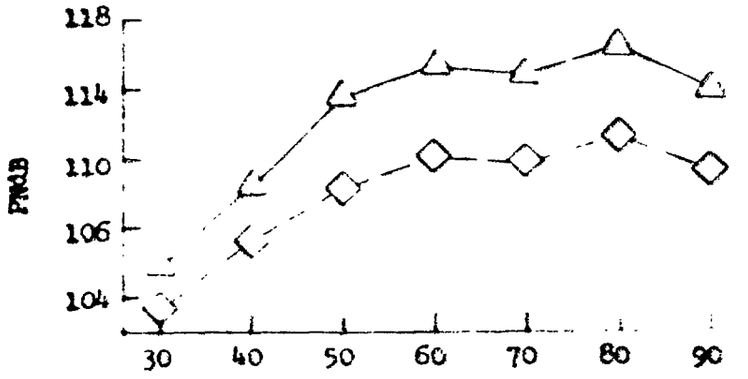
$P_{T8}/P_0 \approx 2.15$
$T_{T8} \approx 1522^\circ R$
$V_j \approx 1930$ Ft/Sec



Frequency, Hz - 80° From Jet Exhaust



Angle From Jet Exhaust, Degrees



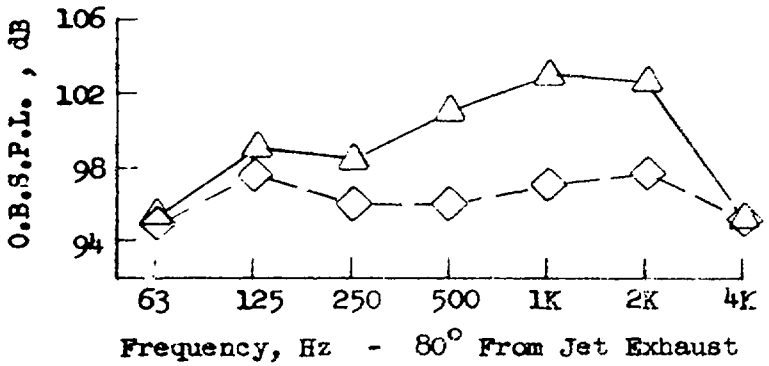
Angle From Jet Exhaust, Degrees

FIGURE V.C-22D 300 FT SIDELINE SPECTRA AND DIRECTIVITY FOR 37 GREATREX TUBE NOZZLE WITH TREATED AND HARD WALL EJECTORS

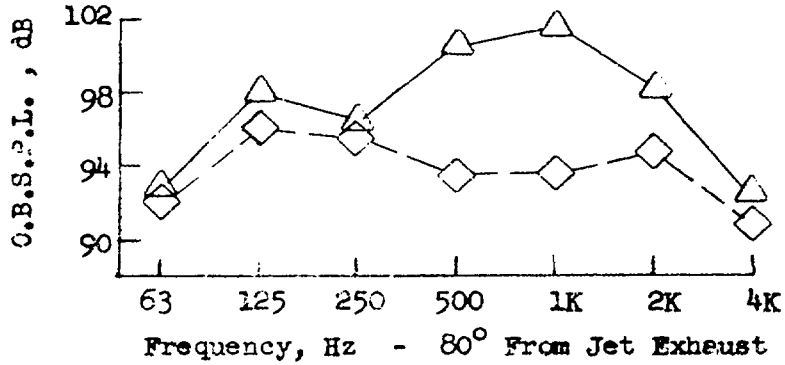
△ Hard Ejector (Model 4.1T37-10.8CSE)

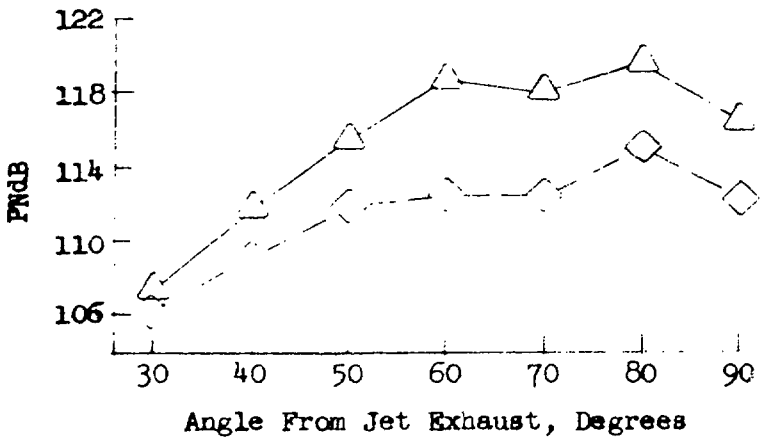
◇ Treated Ejector (Model 4.1T37-10.4CS)

$P_{T8}/P_0 \approx 2.58$
$T_{T8} \approx 1530^{\circ}R$
$V_j \approx 2120$ Ft/Sec



$P_{T8}/P_0 \approx 2.16$
$T_{T8} \approx 1965^{\circ}R$
$V_j \approx 2180$ Ft/Sec





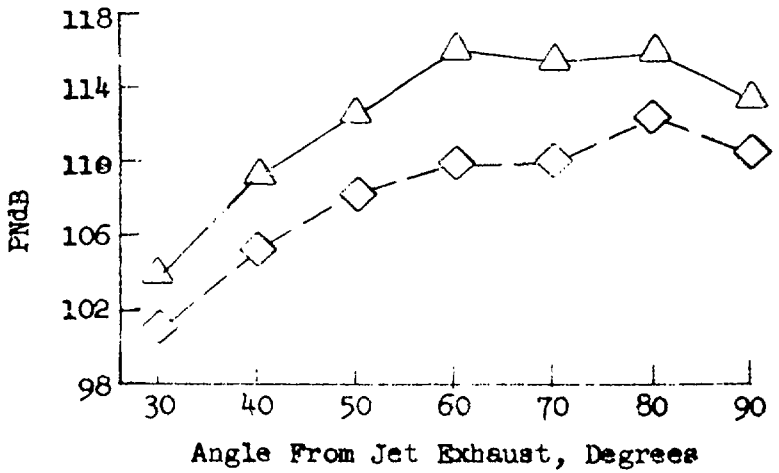
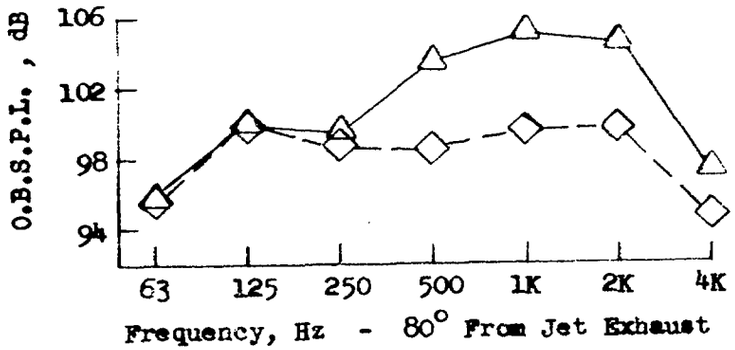


FIGURE V.G-22E 300 FT SIDELINE SPECTRA AND DIRECTIVITY FOR 37 GREATREX TUBE NOZZLE WITH TREATED AND HARDWALL EJECTORS

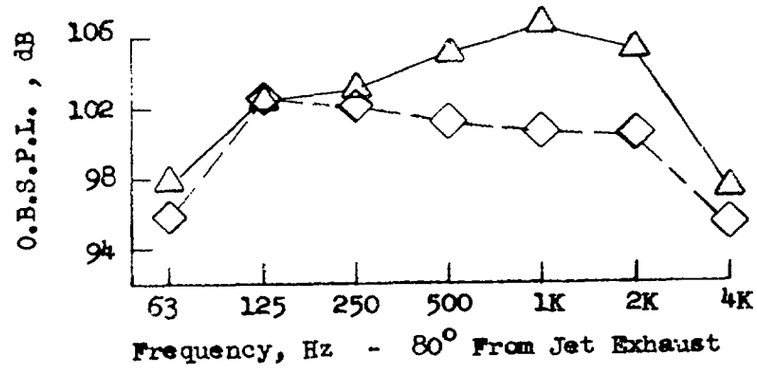
△ Hard Ejector (Model 4.1T37-10.8CSE)

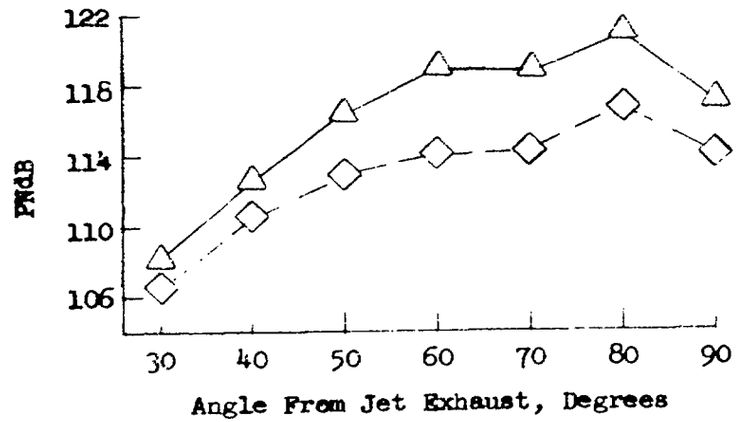
◇ Treated Ejector (Model 4.1T37-10.4CS)

$P_{T8}/P_0 \approx 2.61$
$T_{T8} \approx 1995°R$
$V_j \approx 2430$ Ft/Sec



$P_{T8}/P_0 \approx 2.89$
$T_{T8} \approx 2000°R$
$V_j \approx 2540$ Ft/Sec





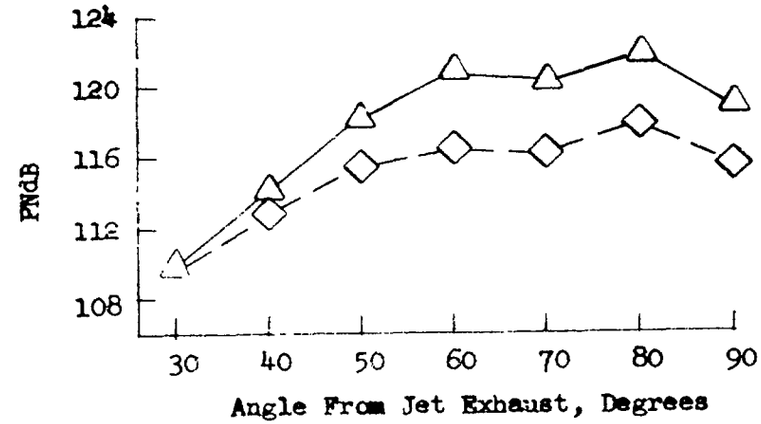


FIGURE V.G-22F 300 FT SIDELINE SPECTRA AND DIRECTIVITY FOR 37 GREATREX TUBE NOZZLE WITH TREATED AND HARDWALL EJECTORS

- o Suppression Relative to Hard Liner of Same Dimensions
- o 22 1/2% Open Sheet Metal Liner With Cerafelt Packing
- o 300 Ft. Sideline

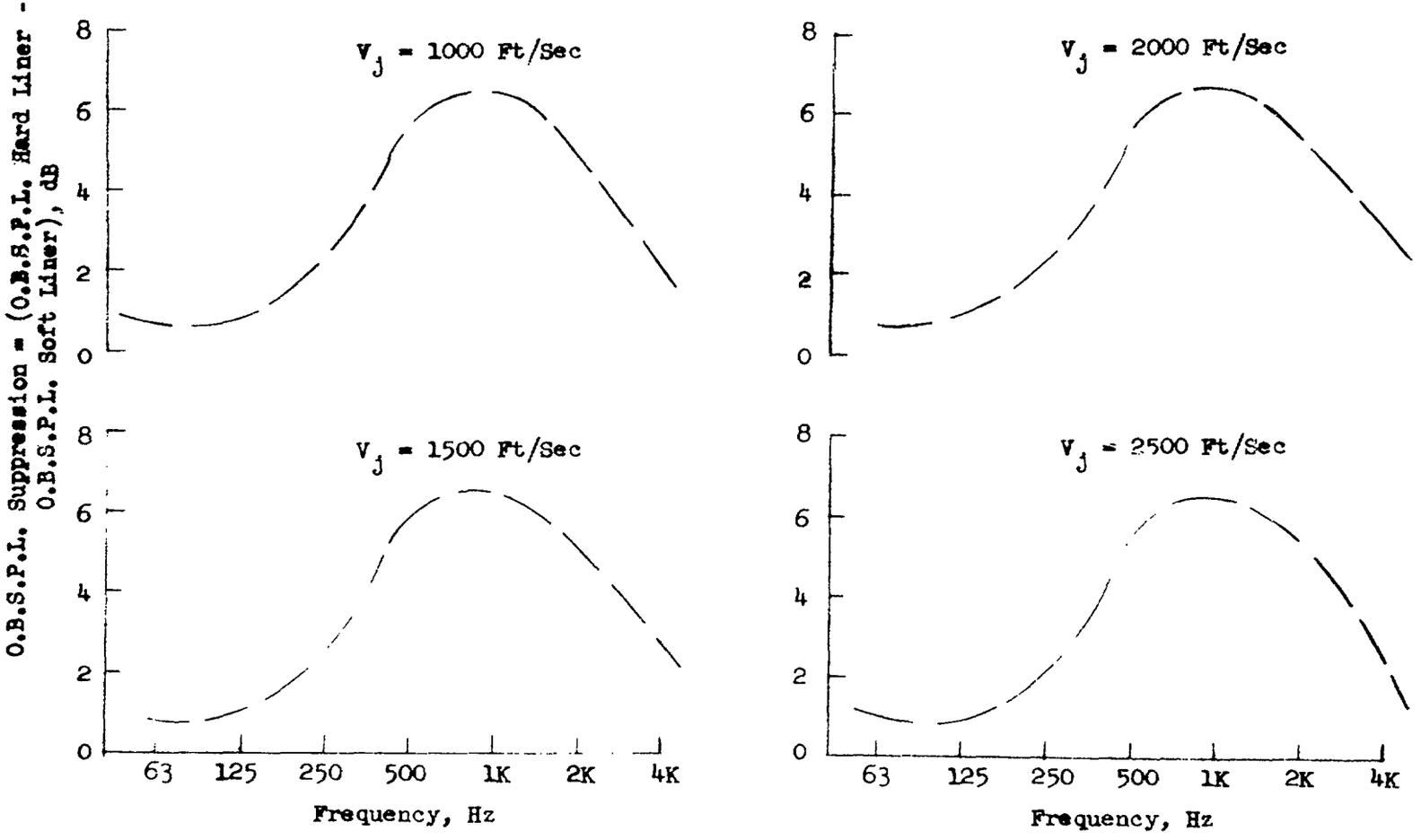
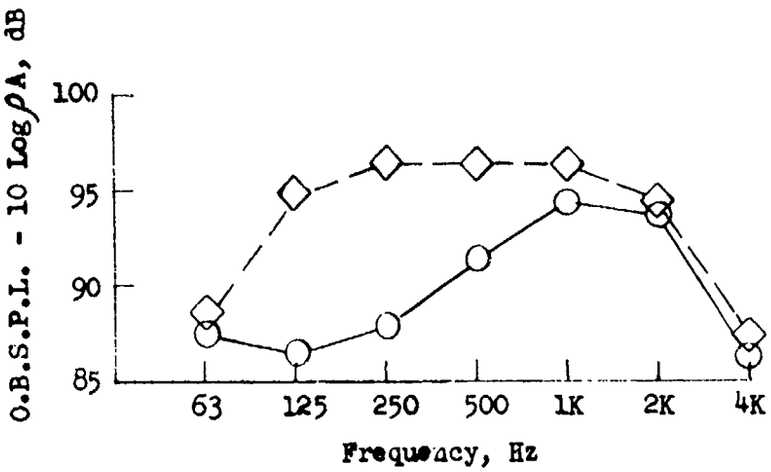


FIGURE V.G-23 SUPPRESSION EFFECT OF TREATED EJECTOR ON 37 GREATREX TUBE NOZZLE AT VARIOUS JET VELOCITIES

o 300 Ft. Sideline

o Angle of Peak PNdB

	P_{T8}/P_0	$T_{T8}(^{\circ}R)$	V_j(Ft/Sec)
◇ 97 Hole (Model 4.2H97N-CS)	1.40	1235	1173
○ 37 GR. Tube (Model 4.1T37-10.8CSE)	1.41	1161	1141



Data Includes Ground Reflection Interference

	P_{T8}/P_0	$T_{T8}(^{\circ}R)$	V_j(Ft/Sec)
◇ 97 Hole (Model 4.2H97N-CS)	1.54	1293	1349
○ 37 GR. Tube (Model 4.1T37-10.8CSE)	1.39	1535	1291

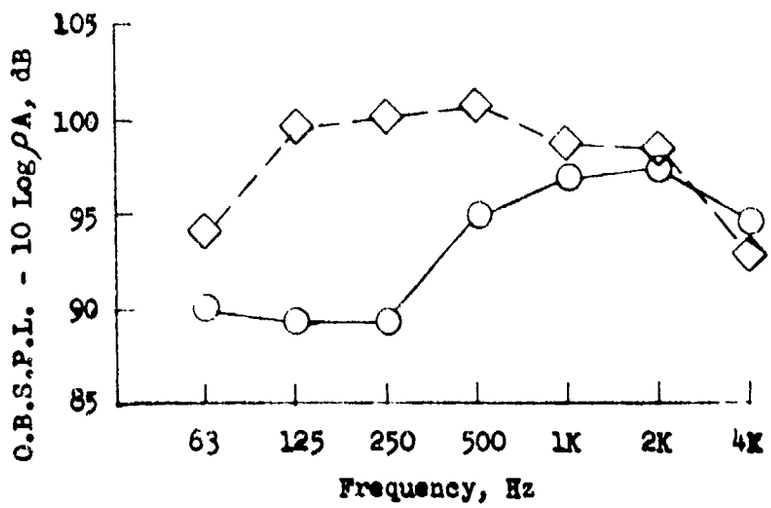
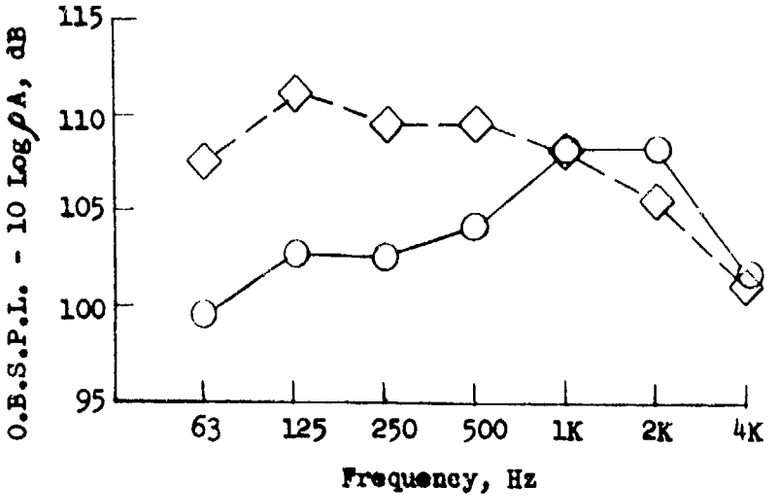


FIGURE V.G-24A SPECTRAL COMPARISON OF 97 HOLE NOZZLE PLUS HARDWALL EJECTOR TO 37 GREATREX TUBE NOZZLE PLUS HARDWALL EJECTOR

○ 300 Ft. Sideline

● Angle of Peak PNdB

	P_{T8}/P_0	$T_{T8}(^\circ R)$	V_j(Ft/Sec)
◇ 97 Hole (Model 4.2H97N-CS)	2.01	1525	1834
○ 37 GR. Tube (Model 4.1T37-10.8CSE)	2.58	1158	1839



Data Includes Ground Reflection Interference

	P_{T8}/P_0	$T_{T8}(^\circ R)$	V_j(Ft/Sec)
◇ 97 Hole (Model 4.2H97N-CS)	2.22	1622	2013
○ 37 GR. Tube (Model 4.1T37-10.8CSE)	1.80	1996	1938

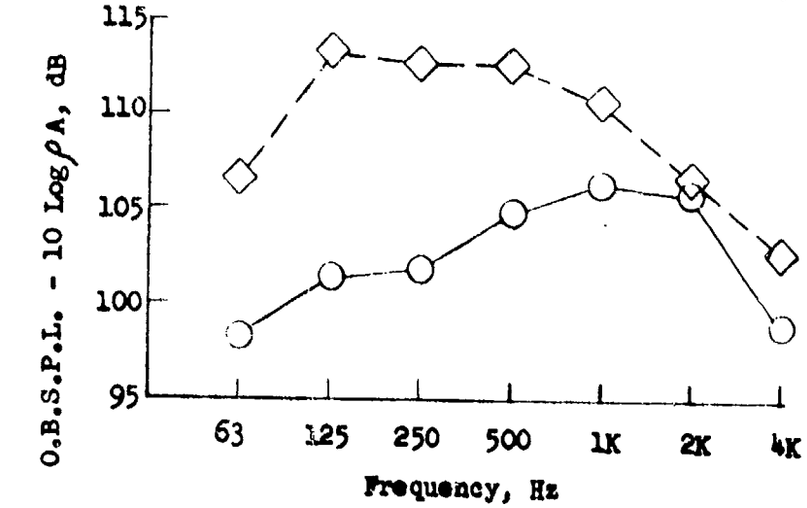


FIGURE V.G-24B SPECTRAL COMPARISON OF 97 HOLE NOZZLE PLUS HARDWALL EJECTOR TO 37 GREATREX TUBE NOZZLE PLUS HARDWALL EJECTOR

- D_S/D_t = 1.185; L_S/D_S = 1.03
- AR_d = 2.0; Hard Liner in Ejector
- 97 Hole Nozzle With GREATREX Center
- X=Location of C/A Thermocouples

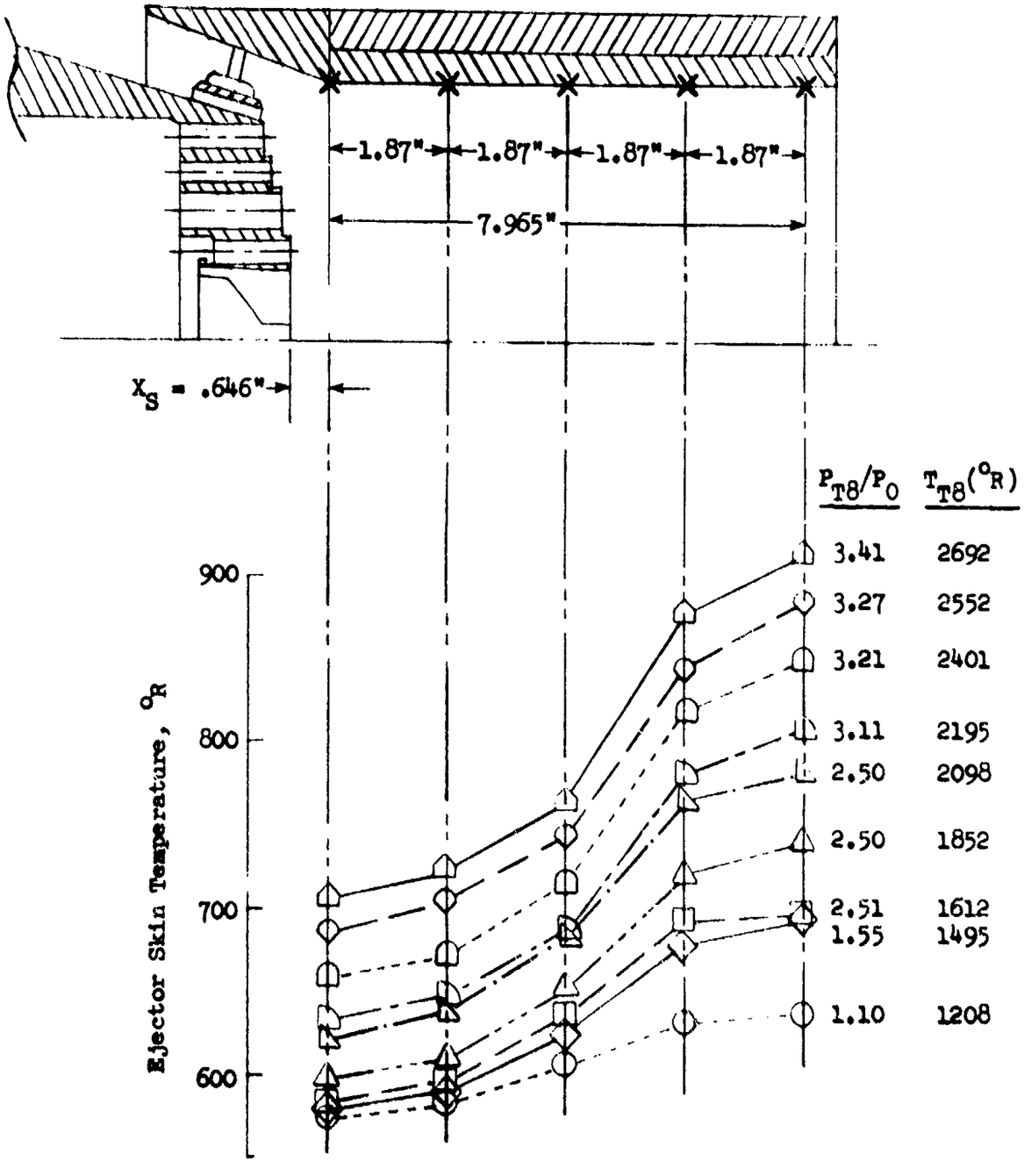


FIGURE V.G-25 SECONDARY EJECTOR SKIN TEMPERATURE DISTRIBUTION

"PRECEDING PAGE BLANK-NOT FILMED."

V.H ANNULAR PLUG NOZZLE SUPPRESSOR MODEL STUDIES

"PRECEDING PAGE BLANK-NOT FILMED."

V.H. ANNULAR PLUG NOZZLE SUPPRESSOR MODEL STUDIES

Sections V.H.1 and V.H.2 document the annular plug nozzle suppressor model studies. A 1967 series of suppressor configurations used rods, tubes, C.D.B., and flap mechanical blockers. These suppressor mechanisms were tested on annular plug nozzles, with and without secondary ejectors, and are presented in Section V.H.1.

Section V.H.2 documents the multi-element spoke/chute model suppressor parametric studies on annular plug nozzles. This was a 1970 to 1971 effort to develop that suppressor concept for application to the high-airflow, low exhaust velocity cycle of the GE4J6H2 engine. The parallel acoustic and aerodynamic static and wind-on test series resulted in development of design guidelines for future refinement of the multi-element annular plug suppressor concept.

"PRECEDING PAGE BLANK-NOT FILMED."

V.H.1 RODS, TUBES, CHUTES, C.D.B. AND PRIMARY FLAPS ON ANNULAR PLUG NOZZLES

"PRECEDING PAGE BLANK-NOT FILMED."

V.H.1 RODS, TUBES, CHUTES, C.D.B., AND PRIMARY FLAPS ON ANNULAR PLUG NOZZLES

Objectives of Test Series

This 1967 jet noise program was a preliminary design study to define the most promising suppressor configurations for the GE4/JX series of dry turbojet engines proposed for the supersonic transport.

Due to the limited time period available, test models were designed around existing hardware. The full scale design was based upon a 20° included angle plug primary nozzle. No similar angled model plug was available, so acoustic testing was performed on a 30° plug nozzle, for which a two stage ejector nozzle system was manufactured. The final model was designed essentially to have similar area ratios and expansion rates to the full scale engine.

Test Conditions

At liftoff, the nozzle conditions for the proposed dry engine were approximately T_{T8} = 2300° R and P_{T8}/P_o = 3.0. A range of test conditions covering these values was used for each model.

At an exhaust gas temperature, T_{T8} of 2300° R, nozzle pressure ratios, P_{T8}/P_o, of 2.0, 2.5, 3.0, 3.2, and 3.5 were set.

The T_{T8} = 2300° R, P_{T8}/P_o = 3.2 condition was performed twice - once at the beginning, and once at the end of the test series - to assess the repeatability of data.

Test Configurations

Twenty two configurations were tested within this study, separated into categories of: a) baseline nozzles, b) primary suppressors, c) secondary suppressors and d) tube suppressor. Table V.H.1-1 categorizes the models, gives a brief description of each and indexes the summary tables, hardware schematics and results plots.

The proposed full scale nozzle consisted of a 20° included angle conical plug surrounded by a convergent primary shroud. The secondary shroud was formed by a two stage ejector nozzle. No existing 20° included angle plain plug hardware was available, so the tests were conducted around a 30° basic plug nozzle.

Model V-1, shown in Figure V.H.1-2. A two stage ejector nozzle system was designed for this nozzle which, as closely as possible, resembled the full scale configuration. A baseline 4" I.D. conical nozzle, Figure V.H.1-1, was tested at the beginning and end of the test series. The data from the two test days established an average unsuppressed nozzle baseline to which all suppressor nozzles were referenced for suppression.

Acoustic tests were performed on the GE, Evendale, Jet Engine Noise Outdoor Test Stand (JENOTS), with data recorded on an arc of 40 ft. radius from the nozzle exit at angles of 20, 30, 40, 50, 60 and 70 degrees from the jet exhaust axis. Data were recorded directly in octave bands using a B&K spectrometer/level recorder unit. PNdB levels were calculated from the recorded data after the frequencies had been scaled by 8:1 to simulate full scale single engine levels at a 320 ft. radius. The peak PNdB level for each model was compared with the baseline conical nozzle value at the same jet temperature and total pressure. Thrust tests were only performed on the conical and basic plug configurations, plus the most promising suppressor models. Comparisions were made relative to the conical nozzle.

Presentation of Test Results

o Baseline Nozzles

In addition to the baseline conical nozzle, Model 0-3 of Figure V.H.1-1, two unsuppressed plug configurations were acoustically tested. They were the plain 30° plug, Model V-1 of Figure V.H.1-2, and the 30° plug with a secondary shroud, Model V-1-1 of Figure V.H.1-3. Both plug configurations produced peak PNL levels equivalent to the unsuppressed baseline conical nozzle. Thrust data shows these models to have a 2 to 2.5% decrement in C_{fg} relative to the basic cone. A photo of Model V-1 is included in Figure V.H.1-23A.

o Primary Suppressors

Radial rods (or tubes) with 100% penetration of the annulus were initially used to obtain suppression. On the full scale engine, these suppressor elements would have been retractable into the plug. Initially, eight solid radial rod elements were employed (Model V-1-2 of Figure V.H.1-4). The rods were later replaced by eight hollow tubes (Model V-1-2-1 of Figure V.H.1-5) through which

simulated compressor discharge bleed (C.D.B) air was ejected, axially aft, at a rate 4.5% of the primary flow rate. The cold air injection increased PNL suppression by 2 PNdB over the initial 5 PNdB suppression of the solid tube model at the design point pressure ratio of 3.0. Use of radial C.D.B. injection at plane 8 through the six tubes of Model V-1-2-2 in Figure V.H.1-6 lowered the total suppression to 2.5 PNL at design point due to the removal of the mechanical blockage, retaining only the suppression level attributable to the C.D.B. of the eight tube model.

The eight circular rods/tubes of Models V-1-2 and V-1-2-1 were replaced by 16 elliptical tubes of cross section so as to maintain the primary blockage at 23% while at 100% penetration of the annulus. Variations were tested with the 16 tubes, including: a) Model V-1-2-7, Figure V.H.1-7, 16 tubes with ends open to ambient, no secondary shroud, b) Model V-1-2-4, Figure V.H.1-8, addition of secondary shroud to Model V-1-2-7, c) Model V-1-2-6, Figure V.H.1-9, addition of blow-in-door shroud to Model V-1-2-4, and d) Model V-1-2-5, Figure V.H.1-10, same as Model V-1-2-6 but with the ends closed on the elliptical tubes so as to block any ambient air pumping through the tubes.

Use of the 16 tubes with a secondary shroud, Model V-1-2-4, increased suppression at a pressure ratio of 3.0 by 1.5 PNdB above the eight rod model. Adding the blow-in-door shroud to Models V-1-2-6 and V-1-2-5 set up a flow reversal pattern between the blow-in-door shroud and primary shroud, and also gave reduced suppression. This reverse flow invalidated the data of these models for direct comparison to other models. Without the blow-in-door shroud, Model V-1-2-4, thrust loss relative to the conical nozzle was about 8%.

Four other primary suppressor configurations were tested on the 30° plug, all four segmenting the primary shroud to form either deep or shallow penetrating chutes into the primary flow. Model V-2 (Figure V.H.1-11 and photograph in Figure V.H.1-23A) segmented the primary shroud into 36 sectors, 18 sectors forming full penetration chutes into the plug resulting in 55% blockage of the annulus. No blow-in-door or secondary shrouds were used. The nozzle gave 8.5 PNL suppression at design of P_{T8}/P_o = 3.0 and held good suppression across the tested velocity range. Also it was the only suppressor to attenuate the low to mid-frequencies, instead of the mid to high. Thrust decrement of about

6% C_{fg} relative to the conical nozzle was measured. Models V-5, Figure V.H.1-12, Model V-5-1, Figure V.H.1-13 and Model V-5-2, Figure V.H.1-14, are termed primary flip-flap designs. The primary shroud is segmented in 16 sectors, eight retaining the original primary shroud contour and eight partially penetrating the primary stream. A photograph of Model V-5 is included in Figure V.H.1-23A. The eight segments penetrating the annulus had semi-sidewalls to partially retain the primary flow. Model V-5, without a secondary shroud, gave about 5.5 PNL suppression at design pressure ratio = 3.0. Models V-5-1 and V-5-2 used a secondary shroud at two axial locations; however, reverse flow through the secondary inlet resulted and reduced the suppression attained at higher nozzle pressure ratios.

The last primary suppressor, Model V-8-1, Figure V.H.1-15, used a 20° fluted plug and a 36 segment primary shroud. The plug was relieved in eight equally spaced locations as shown in the picture of Figure V.H.1-23B. The segmented primary shroud had 18 sectors fully penetrating the annulus to the plug, the other 18 retaining the original shroud contour. This model gave near 5 PNL suppression at P/R = 3.0.

o Secondary Suppressors

Secondary suppressors consisted of two basic systems. The first, Model V-1-2-3 of Figure V.H.1-16, had 8 radial rods at the D_s which simulated blockers that could be retracted into the plug. It gave about 4 PNdB suppression at design P/R = 3. The second system, with a series of five models, used 8 equally spaced chutes within the secondary shroud. In the initial tests of this system at 50% chute penetration (Model V-1-3-1 of Figure V.H.1-17) and at 85% penetration (Model V-1-3 of Figure V.H.1-18 and Model V-1-3-3 of Figure V.H.1-19) the models were set up such that primary air could flow down the backs of the chutes, and limited suppression was attained. Addition of the blow-in-door shroud in Model V-1-3-3 increased suppression slightly over Model V-1-3. A photograph of Model V-1-3 is in Figure V.H.1-23B.

The secondary chute positioning scheme was changed to that of Models V-1-3-2 in Figure V.H.1-20 and V-1-3-4 in Figure V.H.1-21 so that flow of primary air down the back of the chutes was eliminated. Penetration of these two models was 95% of the annulus, Model V-1-3-4 being identical to Model

V-1-3-2 but with addition of the blow-in-door annulus. The models gave 6.5 and 5.5 PNL suppression, without and with the blow-in-door shroud, respectively, but had a thrust loss of about 17% at P/R = 3.0. A photograph of Model V-1-3-4 is shown in Figure V.H.1-23E.

o Tube Suppressor

A multi-tube/annular plug configuration, Model V-16 of Figure V.H.1-22, was tested. It had 72 tubes of .444" I.D. on a 30° included angle plug, with the tubes exhausting around and down the plug. The model was tested over a wider range of test conditions than the previous models and the plot of Figure V.H.1-22 shows varying suppression to about 10 PNdB maximum near 2000 to 2100 ft/sec jet velocity.

Conclusions

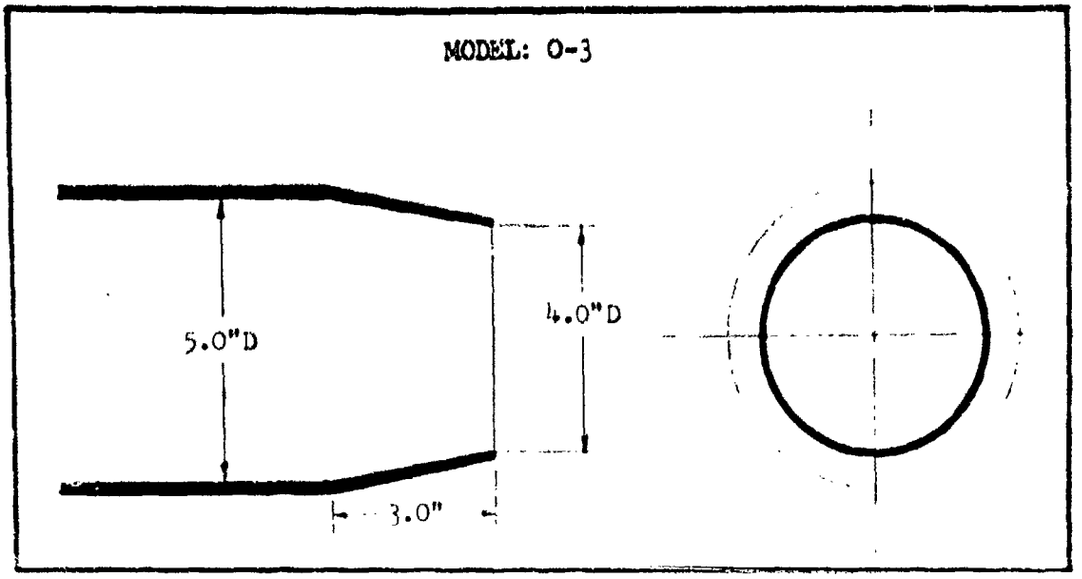
- The basic 30° plug nozzle configuration had no inherent suppression relative to a conical nozzle, but a thrust loss of 2 to 2.5% C_{fg}.
- Primary suppressor configurations which gave the best ratio of suppression/thrust loss were 16 radial U-chutes and 18 swept chutes. The measured PNdB/ΔC_{fg} ratios for these models were 0.75 and 1.6, respectively.
- The 20° fluted plug primary suppressor was no more effective than similar suppressors tested with the 30° plug.
- The 95% penetration secondary chute model gave a suppression of 6.5 PNdB, but had a high thrust loss of 17%. Further work is required to define a configuration of this type with a higher ΔPNdB/ΔC_{fg} ratio.
- The tube nozzle configuration gave a high suppression level of near 10 PNdB at 2000 to 2100 ft/sec jet velocities.
- Basically similar magnitudes of suppression (6.5 to 8.5 dB) were obtained from all three types of suppressors at design P/R = 3.0. However, primary suppressor thrust losses were, in general, considerably less than those produced by the secondary chute type in the ratio of 2:1 or greater. To obtain an effective secondary chute suppressor, chutes with inherently lower thrust losses must be designed.

TABLE V.H.1-1 SUMMARY OF ANNULAR PLUG NOZZLE TEST CONFIGURATIONS

NOZZLE CATEGORY	MODEL NO.	DESCRIPTION	SUMMARY TABLE	SCHEMATIC & RESULTS
BASELINE NOZZLES	0-3	4" I.D. Conical Nozzle	V.H.1-2	V.H.1-1
	V-1	30° Plug	V.H.1-3	V.H.1-2
	V-1-1	30° Plug + Secondary Shroud	V.H.1-4	V.H.1-3
PRIMARY SUPPRESSORS	V-1-2	30° Plug + Secondary Shroud + 8 Rods @ 100% Penet.	V.H.1-5	V.H.1-4
	V-1-2-1	30° Plug + Secondary Shroud + 8 CDB Tubes @ 100% Penet. With Axial Injection	V.H.1-6	V.H.1-5
	V-1-2-2	30° Plug + Secondary Shroud + 6 CDB Tubes @ 0% Penet. With Radial Injection	V.H.1-7	V.H.1-6
	V-1-2-3	30° Plug + 16 Tubes @ 100% Penet. - Open to Ambient	V.H.1-8	V.H.1-7
	V-1-2-4	30° Plug + Secondary Shroud + 16 Tubes @ 100% Penet. - Open to Ambient	V.H.1-9	V.H.1-8
	V-1-2-6	30° Plug + B.I.D. & Secondary Shrouds + 16 Tubes @ 100% Penet. - Open to Ambient	V.H.1-10	V.H.1-9
	V-1-2-5	30° Plug + B.I.D. & Secondary Shrouds + 16 Tubes @ 100% Penet. - Closed to Ambient	V.H.1-11	V.H.1-10
	V-2	30° Plug + 16 Chutes @ 100% Penet.	V.H.1-12	V.H.1-11
	V-5	30° Plug + 16 Segmented Primary Shroud With Semi-Sidewalls	V.H.1-13	V.H.1-12
	V-5-1	30° Plug + 16 Segmented Primary Shroud With Semi-Sidewalls + Secondary Shroud @ 1.31"	V.H.1-14	V.H.1-13
	V-5-2	30° Plug + 16 Segmented Primary Shroud With Semi-Sidewalls + Secondary Shroud @ 1.06"	V.H.1-15	V.H.1-14
	V-8-1	20° Fluted Plug + 36 Segmented Shroud - 18 In, 18 Out	V.H.1-16	V.H.1-15

TABLE V.H.1-1 (Continued) SUMMARY OF ANNULAR PLUG NOZZLE TEST CONFIGURATIONS

NOZZLE CATEGORY	MODEL NO.	DESCRIPTION	SUMMARY TABLE	SCHEMATIC & RESULTS
SECONDARY SUPPRESSORS	V-1-2-3	30° Plug + Secondary Shroud + 8 Rods @ D_S & 100% Penet.	V.H.1-17	V.H.1-16
	V-1-3-1	30° Plug + Secondary Shroud + 8 Chutes @ 50% Penet.	V.H.1-18	V.H.1-17
	V-1-3	30° Plug + Secondary Shroud + 8 Chutes @ 85% Penet.	V.H.1-19	V.H.1-18
	V-1-3-3	30° Plug + B.I.D. & Secondary Shrouds + 8 Chutes @ 85% Penet.	V.H.1-20	V.H.1-19
	V-1-3-2	30° Plug + Secondary Shroud + 8 Chutes @ 95% Penet.	V.H.1-21	V.H.1-20
	V-1-3-4	30° Plug + B.I.D. & Secondary Shrouds + 8 Chutes @ 95% Penet.	V.H.1-22	V.H.1-21
TUBE SUPPRESSOR	V-14	30° Plug + 72 Tubes Around Annulus	V.H.1-23	V.H.1-22



DESCRIPTION

Model O-3 was a 4" I.D. conical nozzle used for baseline comparisons in this series of annular plug nozzle tests.
Exit area, A_8 = .0840 ft^2.
Material: 321 s.s. Full scale A_8 = 5.3760 Ft^2; Scale factor = 8:1.

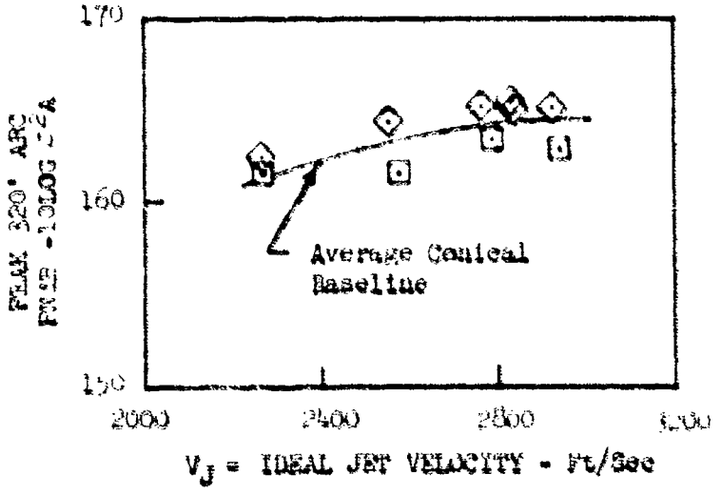


FIGURE V.H.1-1 SCHEMATIC AND 320 FT. ARC AVERAGE JET NOISE LEVEL FOR MODEL O-3, 4" I.D. CONICAL NOZZLE AVERAGE BASELINE

TABLE V.H.1-2 TEST SUMMARY

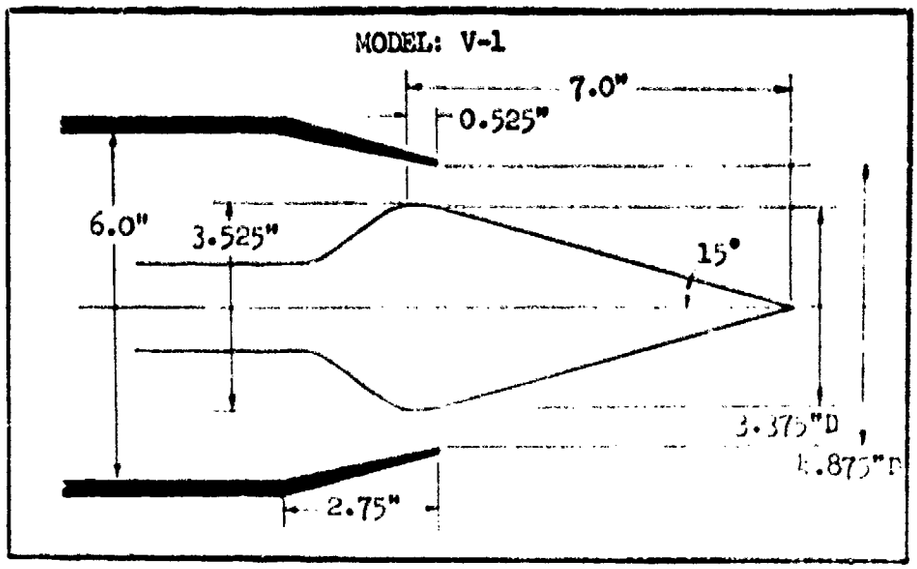
MODEL NO. O-3

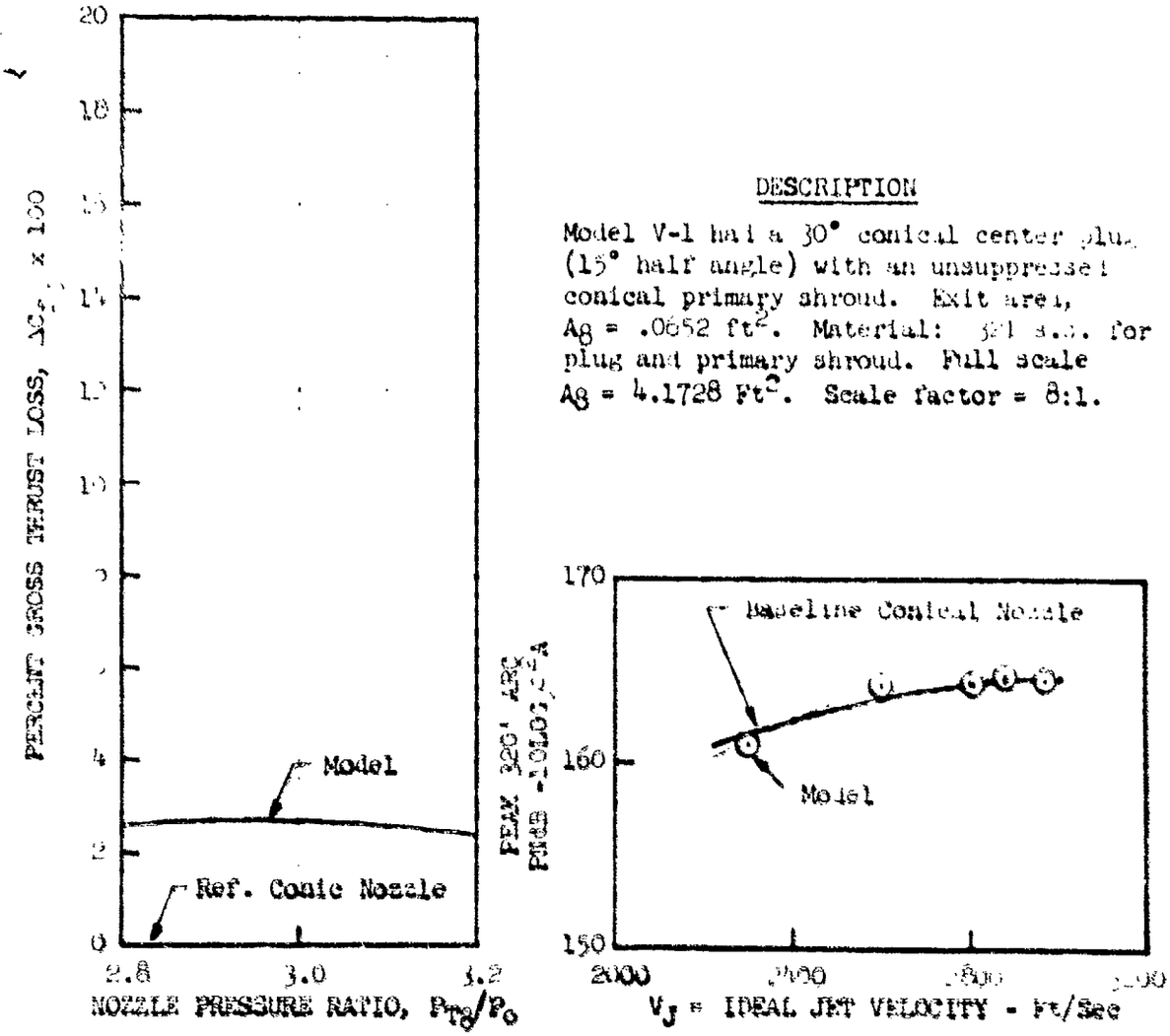
DESCRIPTION 4" I.D. BASELINE CONICAL NOZZLE

MODEL A_8 = .0840 FT.^{2}; FULL SCALE A_8 = 5.3760 FT.^{2}; SCALE FACTOR = 8:1

	TEST CONDITIONS					ACOUSTIC TEST RESULTS *							
EDI NO.	V_8 (F/S)	P_{T8}/P_o	T_{T8} °R	IDEAL V_J FT/SEC	% BLEED $W_B/W_8 \times 10^2$	PEAK PNdB OR 320° ARC	ANGLE OF MAX PNdB (DEG.)	$10\log\beta^2_A$	PEAK PNdB $-10\log\beta^2_A$	FWL DIRECTIVITY ON 320° ARC MEASURED FROM NOZZLE EXIT					
										20°	30°	40°	50°	60°	70°
1	5.79	3.22	2298	2840		140.0	60	-25.0	165.0	128.8	132.5	137.0	140.0	140.0	135.4
2	6.30	3.51	2295	2927		140.4	60	-24.7	165.1	128.5	132.6	136.3	140.0	140.4	136.4
3	5.34	3.00	2302	2766		139.8	50	-25.3	165.1	127.7	132.5	136.6	139.8	139.2	134.9
4	4.45	2.51	2305	2556		138.3	60	-25.9	164.2	126.6	131.7	134.8	138.0	138.3	132.3
5	3.46	2.01	2328	2267		135.7	50	-26.6	162.3	124.2	129.6	133.3	135.7	133.4	129.4
6	5.76	3.21	2294	2834		140.1	60	-25.0	165.4	128.1	133.1	136.9	139.9	140.4	135.4
10	6.80	3.54	2307	2945		138.4	60	-24.5	162.9	129.0	132.2	135.5	138.1	138.4	134.4
15	5.56	3.05	2310	2788		138.3	60	-25.1	163.4	127.2	131.0	133.2	136.9	138.3	133.1
21	4.55	2.54	2312	2576		135.9	50	-25.7	161.6	125.8	129.2	133.0	135.9	135.6	131.9
30	3.53	2.03	2315	2274		135.3	50	-26.4	162.7	124.4	128.3	132.2	135.3	132.4	127.5

*Data Includes Ground Reflection Interference





DESCRIPTION

Model V-1 had a 30° conical center plug (15° half angle) with an unsuppressed conical primary shroud. Exit area, A_8 = .0652 ft^2. Material: 321 s.s. for plug and primary shroud. Full scale A_8 = 4.1728 Ft^2. Scale factor = 8:1.

FIGURE V.H.1-2 SCHEMATIC, 320 FT. ARC JET NOISE LEVEL AND AERODYNAMIC TEST RESULTS FOR MODEL V-1

TABLE V.M.1-3 TEST SUMMARY

MODEL NO. V-1

DESCRIPTION 30° CONICAL PLUG WITH CONICAL PRIMARY SHROUD

MODEL A_8 = .0652 FT.^{2}; FULL SCALE A_8 = 4.1728 FT.^{2}; SCALE FACTOR = 8:1

	TEST CONDITIONS					ACOUSTIC TEST RESULTS*								
										PNL DIRECTIVITY ON 320° ARC MEASURED FROM NOZZLE EXIT					
RUN NO.	W_8 (PPS)	P_{T8}/P_∞	T_{T8} °R	IDEAL V_j FT/SEC	% BLEED W_B/W_8 * 100	PEAK PNLS ON 320° ARC	ANGLE OF MAX PNLS (DEG.)	$10\log\beta^2 A$	PEAK PNLS $-10\log\beta^2 A$	20°	30°	40°	50°	60°	70°
1	4.15	2.041	998	1499		123.7	20	-20.3	144.0	123.7	123.7	122.2	119.6	118.0	115.2
2	5.24	2.547	997	1694		130.9	30	-19.7	150.6	129.3	130.9	128.7	125.3	122.7	120.9
3	6.23	3.058	996	1833		134.6	40	-19.0	153.6	132.2	134.0	134.6	129.9	127.4	124.9
4	6.68	3.268	996	1890		135.5	40	-18.8	154.3	132.8	135.4	135.5	132.5	129.8	126.6
5	7.26	3.559	995	1937		137.2	40	-18.4	155.6	133.5	136.2	137.2	133.3	131.0	129.3
6	6.44	3.562	1244	2166		139.4	40	-20.4	159.8	134.0	137.4	139.4	137.1	132.8	130.8
7	5.83	3.266	1244	2106		137.4	40	-20.7	158.1	132.0	136.3	137.4	136.0	131.8	129.4
8	5.34	3.053	1245	2048		135.9	40	-21.0	156.9	130.2	133.4	135.9	134.3	129.6	127.4
9	4.49	2.549	1245	1894		133.9	40	-21.6	155.5	129.2	131.7	133.9	130.8	126.9	123.9
10	3.54	2.037	1246	1675		128.0	30	-22.6	150.6	127.2	128.0	127.4	123.8	121.4	118.8
11	2.70	2.039	2365	2307		133.2	50	-27.8	161.0	127.7	130.4	132.6	133.2	129.1	125.0
12	3.31	2.55	2355	2606		137.0	50	-27.1	164.1	128.4	132.0	134.4	137.0	133.1	129.2
13	4.06	3.058	2345	2813		137.8	50	-26.5	164.3	129.4	132.2	135.3	137.8	136.4	130.8
14	4.35	3.267	2338	2880		138.6	50	-26.2	164.8	129.3	133.1	136.0	138.6	137.8	131.9
15	4.71	3.562	2334	2967		138.7	50	-25.9	164.6	130.3	133.2	136.0	138.7	138.1	132.3
16	5.00	3.562	2035	2770		138.6	50	-24.7	163.3	130.4	133.3	137.0	138.6	135.3	132.2
17	4.60	3.261	2037	2681		138.4	50	-25.0	163.4	129.5	133.2	135.8	138.4	136.0	131.6
18	4.31	3.055	2038	2622		137.9	50	-25.2	163.1	130.0	132.9	135.7	137.9	134.8	131.0
19	3.54	2.552	2041	2427		137.6	50	-25.9	163.5	129.2	131.5	134.5	137.6	132.8	128.8

*Data Includes Ground Reflection Interference

TABLE V.H.1-3 (Cont.) TEST SUMMARY

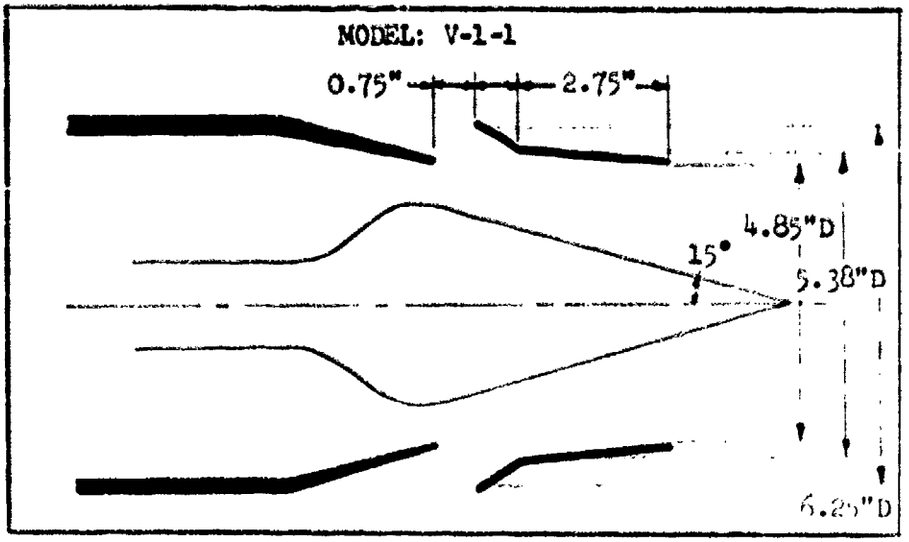
MODEL NO. V-1

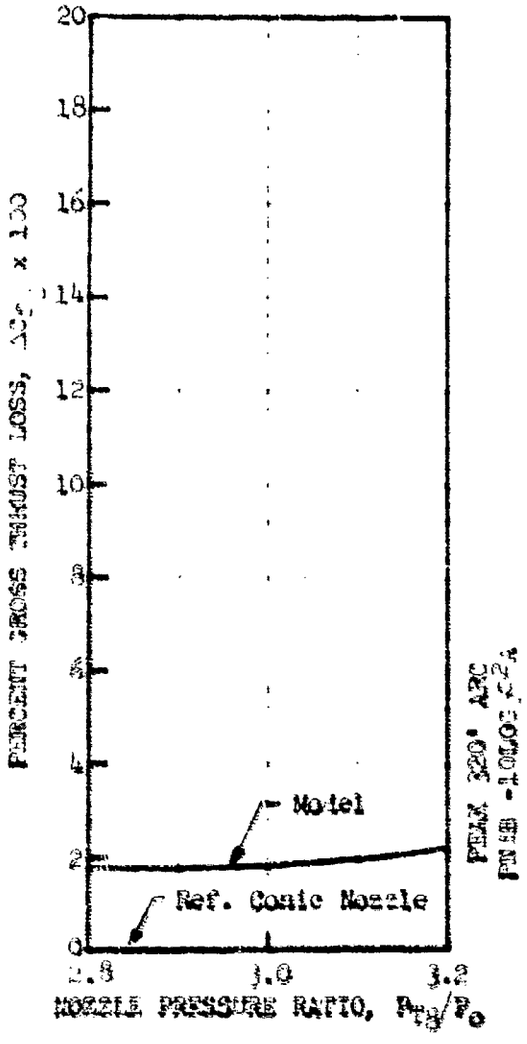
DESCRIPTION 30° CONICAL PLUG WITH CONICAL PRIMARY SHROUD

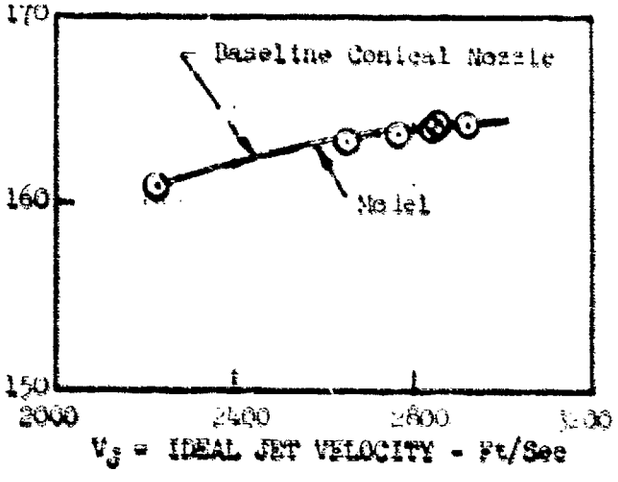
MODEL A_8 = .0652 FT.^{2}; FULL SCALE A_8 = 4.1728 FT.^{2}; SCALE FACTOR = 8:1

	TEST CONDITIONS					ACOUSTIC TEST RESULTS *								
										PNL DIRECTIVITY ON 320° ARC MEASURED FROM NOZZLE EXIT				
RUN NO.	W_8 (PPS)	P_{T8}/P_o	T_{T8} °R	IDEAL V_j FT/SEC	% BLEED W_B/W_8 x 100	PEAK PNLB ON 320° ARC	ANGLE OF MAX PNLB (DEG.)	$10\log\beta^2_A$	PEAK PNLB $-10\log\beta^2_A$	20°	30°	40°	50°	60°	70°
20	2.68	2.037	2050	2146		132.4	40	-26.6	159.0	127.7	130.2	132.4	131.7	127.0	124.2
21	3.08	2.037	1765	1991		131.6	40	-25.3	156.9	127.6	129.9	131.6	129.9	125.4	122.3
22	3.69	2.548	1760	2252		134.9	50	-24.6	159.5	129.0	132.3	134.8	134.9	129.8	127.0
23	4.71	3.056	1758	2435		137.2	50	-24.0	161.2	129.9	132.8	135.8	137.2	133.2	129.7
24	5.15	3.264	1756	2495		138.2	50	-23.7	161.9	130.5	133.8	136.4	138.2	134.1	130.7
25	5.45	3.562	1756	2573		139.3	50	-23.4	162.7	131.2	134.9	138.2	139.3	135.6	132.7
26	5.92	3.562	1511	2387		139.9	40	-22.1	162.0	133.8	136.5	139.9	138.7	134.2	131.9
27	5.56	3.264	1512	2315		138.8	40	-22.4	161.2	133.8	136.9	138.8	137.4	132.6	130.4
28	5.10	3.056	1513	2259		136.0	40	-22.7	158.7	131.1	133.5	136.0	135.6	130.9	127.9
29	4.29	2.550	1514	2089		134.7	40	-23.3	158.0	130.1	132.8	134.7	133.4	129.0	125.6
30	3.41	2.037	1516	1846		130.1	40	-24.0	154.1	127.7	129.5	130.1	126.7	123.9	121.1
31	4.15	2.037	998	1497		124.2	30	-20.3	142.5	123.6	124.2	122.2	120.8	119.0	116.1
32	4.20	2.037	998	1497		124.5	30	-20.3	142.8	123.1	124.5	121.7	120.8	118.4	116.5

* Data Includes Ground Reflection Interference







DESCRIPTION

Model V-1-1 had a conical secondary shroud in addition to the conical primary shroud and 30° plug. Primary-to-secondary shroud gap was set at 1.5". Exit area, A_8 = .0677 ft^2.
Material: 321 a.s. for plug, primary and secondary shrouds. Full scale A_8 = 4.3328 Ft^2. Scale factor = 8:1.

FIGURE V.H.1-3 SCHEMATIC. 320 FT. ARC JET NOISE LEVEL AND AERODYNAMIC TEST RESULTS FOR MODEL V-1-1

TABLE V.M.1-4 TEST SUMMARY

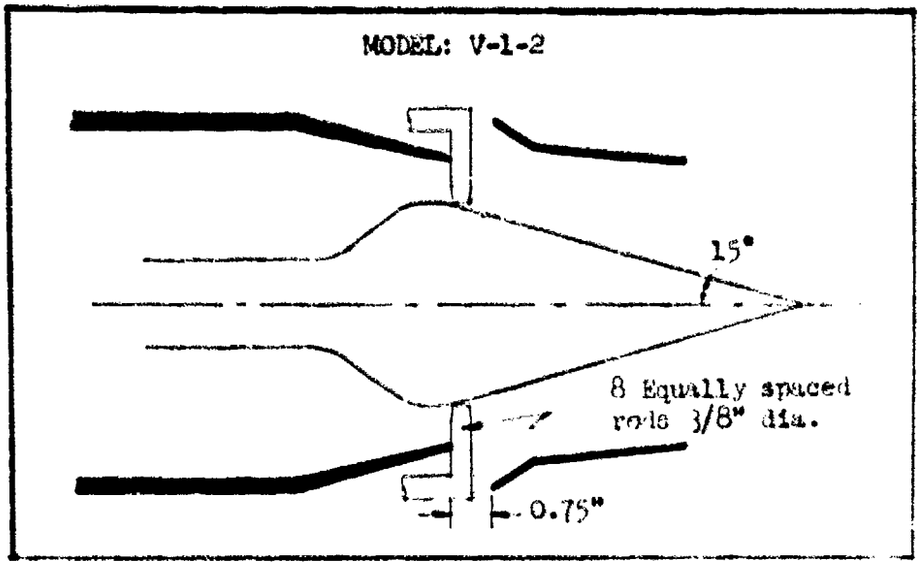
MODEL NO. V-1-1

DESCRIPTION 30° CONICAL PLUG, CONICAL PRIMARY AND SECONDARY SHROUD

MODEL A_8 = .0677 FT.^{2}; FULL SCALE A_8 = 4.3328 FT.^{2}; SCALE FACTOR = 8:1

	TEST CONDITIONS					ACOUSTIC TEST RESULTS *								
RUN NO.	W_8 (PPS)	P_{T8}/P_o	T_{T8} °R	IDEAL V_j FT/SEC	% BLEED W_B/W_8 x 100	PEAK PNdB ON 320° ARC	ANGLE OF MAX PNdB (DEG.)	$10\log\beta^2_A$	PEAK PNdB $-10\log\beta^2_A$	PNL DIRECTIVITY ON 320° ARC MEASURED FROM NOZZLE EXIT					
										20°	30°	40°	50°	60°	70°
1	4.30	3.193	2315	2842		138.0	60	-26.0	164.0	126.3	131.5	135.7	137.9	138.0	133.5
2	4.75	3.474	2304	2922		138.5	60	-25.7	164.2	126.2	132.8	136.2	138.5	138.5	134.8
3	4.00	2.990	2307	2765		137.6	50	-26.2	163.8	127.9	131.8	134.6	137.6	137.3	132.0
4	3.35	2.463	2314	2550		136.4	50	-26.9	163.3	127.5	130.3	133.4	136.4	134.5	129.9
5	2.66	2.010	2299	2253		133.5	50	-27.4	160.9	125.4	128.4	131.3	133.5	130.5	125.6
6	4.28	3.191	2322	2845		138.2	60	-26.1	164.3	127.8	132.4	135.4	138.1	138.2	134.0

* Data Includes Ground Reflection Interference



DESCRIPTION

Model V-1-2 used both conical primary and secondary shrouds and the 30° plug. Shroud gap was 1.5". Suppressor elements were 8 equally spaced .375" O.D. radial rods with 100% penetration to plug. Exit area, A_8 = .0518 ft^2. Material: 321 s.s., plug, shrouds and rods. Full scale A_8 = 3.3152 Ft^2. Scale factor = 8:1.

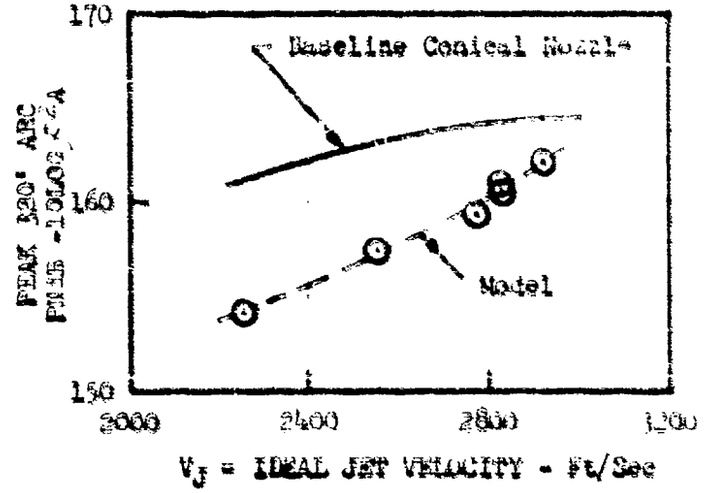


FIGURE V.H.1-4 SCHEMATIC AND 320 FT. ARC JET NOISE LEVEL FOR MODEL V-1-2

TABLE V.H.1-5 TEST SUMMARY

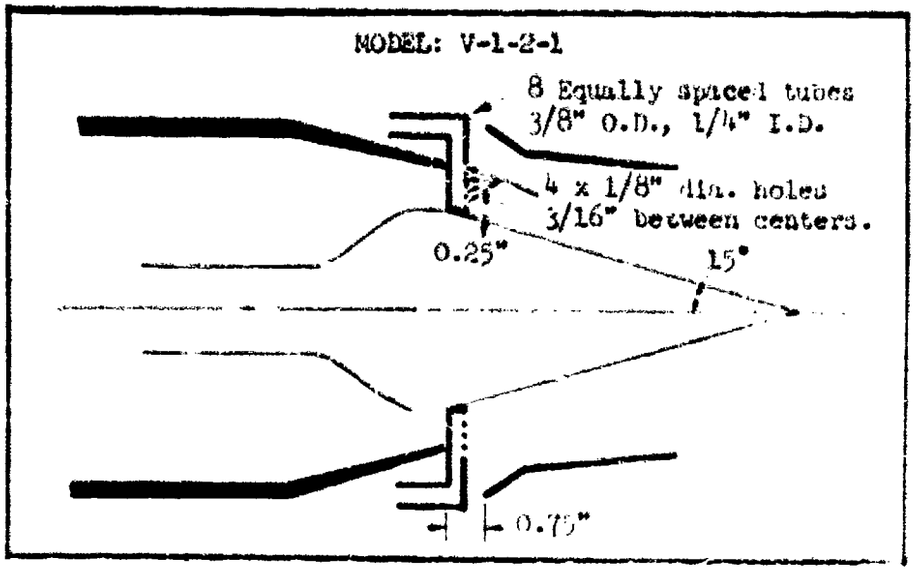
MODEL NO. V-1-2

DESCRIPTION 30° PLUG, CONICAL PRIMARY AND SECONDARY SHROUDS, 8 EQUALLY SPACED RADIAL RODS, .375"OD

MODEL A_8 = .0518 FT.^{2}; FULL SCALE A_8 = 3.3152 FT.^{2}; SCALE FACTOR = 8:1

	TEST CONDITIONS					ACOUSTIC TEST RESULTS*								
RUN NO.	W_8 (PPS)	P_{T8}/P_{∞}	T_{T8} °R	IDEAL V_j FT/SEC	% BLEED W_B/W_8 x 100	PEAK PNdB OVER 320° ARC	ANGLE OF MAX PNdB (DEG.)	$10\log\beta^2 A$	PEAK PNdB $-10\log\beta^2 A$	PNL DIRECTIVITY OVER 320° ARC MEASURED FROM NOZZLE EXIT					
										20°	30°	40°	50°	60°	70°
1	3.67	3.186	2307	2834		133.8	50	-27.3	161.1	127.9	131.5	133.2	133.8	132.8	129.4
2	4.05	3.488	2305	2927		135.2	50	-26.9	162.1	128.9	132.3	134.3	135.2	134.2	129.6
3	3.47	2.954	2328	2776		132.2	40	-27.3	159.5	128.8	130.9	132.2	132.1	130.8	128.2
4	2.88	2.486	2313	2551		129.3	60	-28.1	157.4	126.1	127.9	128.5	129.0	129.3	126.4
5	2.29	2.003	2316	2256		125.4	50	-28.8	154.2	121.5	123.1	124.8	125.4	124.8	123.1
6	3.67	3.189	2307	2835		133.5	50	-27.2	160.7	128.1	131.7	133.1	133.5	131.3	129.8

* Data Includes Ground Reflection Interference



DESCRIPTION

Model V-1-2-1 employed conical primary and secondary shrouds and the 30° plug. Shroud gap was 1.5". A total of 8 equally spaced CDB tubes, .375" O.D./.25" I.D., with 100% penetration to plug surface were used. Each tube had 4 holes, .125" I.D., through which compressor discharge bleed air was blown axially aft. Exit area, A_8 = .0518 ft^2. Material: 321 s.s. for plug, shrouds, and tubes. Full scale A_8 = 3.3152 Ft^2. Scale factor = 8:1.

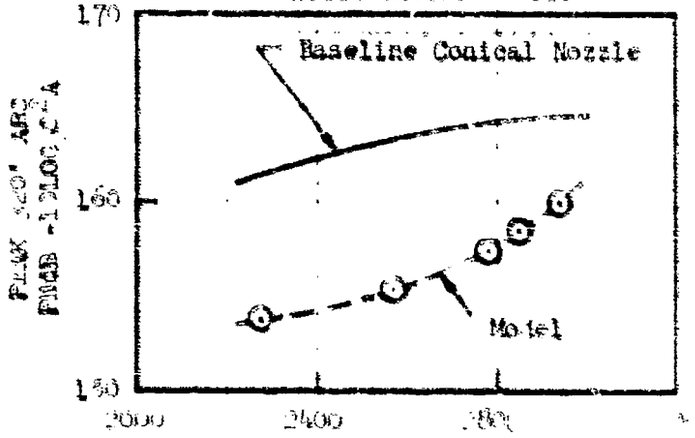


FIGURE V.B.1-5 SCHEMATIC AND 320 FT. ARC JET NOISE LEVEL FOR MODEL V-1-2-1

TABLE V.H.1-6 TEST SUMMARY

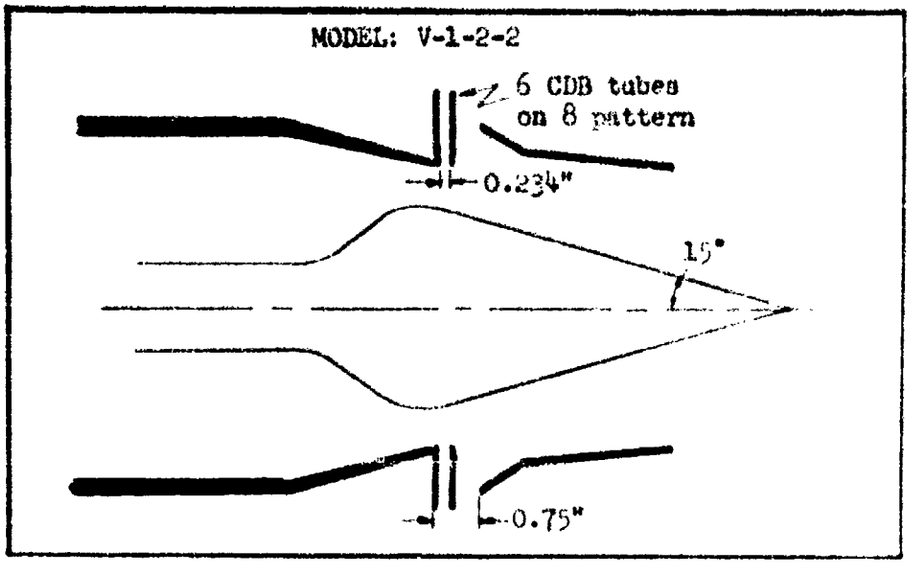
MODEL NO. V-1-2-1

DESCRIPTION 30° PLUG, PRIMARY AND SECONDARY SHROUDS; 8 EQUALLY SPACED CDB TUBES WITH 4 HOLES (.125" ID) IN EACH TUBE BLOWING AXIALLY AFT

MODEL A_8 = .0518 FT.^{2}; FULL SCALE A_8 = 3.3152 FT.^{2}; SCALE FACTOR = 8:1

	TEST CONDITIONS					ACOUSTIC TEST RESULTS*								
										FNL DIRECTIVITY ON 320° ARC MEASURED FROM NOZZLE EXIT				
RUN NO.	W_8 (PPS)	P_{T8}/P_o	T_{T8} °R	IDEAL V_j FT/SEC	% BLEED W_B/W_8 x 100	PEAK PNLR ON 320° ARC	ANGLE OF MAX PNLR (DEG.)	$10LOG\beta^2_A$	PEAK PNLR $-10LOG\beta^2_A$	20°	30°	40°	50°	60°	70°
1	3.64	3.24	2309	2853	4.35	131.6	50	-27.1	158.7	127.0	129.9	131.4	131.6	131.5	128.8
2	3.88	3.52	2308	2938	4.66	133.2	50	-26.8	160.0	127.2	131.0	133.0	133.2	132.8	129.3
3	3.41	3.03	2310	2782	4.31	130.0	50	-27.4	157.4	124.8	129.5	129.9	130.0	129.9	127.6
4	2.81	2.52	2313	2566	4.02	127.3	60	-28.0	155.3	123.2	126.1	127.1	127.2	127.3	125.7
5	2.19	2.03	2316	2276	4.34	125.1	50	-28.6	153.7	119.4	122.2	124.5	125.1	124.4	123.6
6	3.49	3.24	2311	2855	4.73	131.4	50	-27.1	158.5	126.5	130.2	130.6	131.4	130.6	128.6

*Data Includes Ground Reflection Interference



DESCRIPTION

Model V-1-2-2 had 6 radial CDB tubes set on an 8-tube pattern, flush mounted to shroud I.D. Shroud gap was 1.5". Exit area, A_8 = .0677 ft^2. Material: 321 s.s. for plug, shrouds and tubes. Full scale A_8 = 4.3328 Ft^2. Scale factor = 8:1.

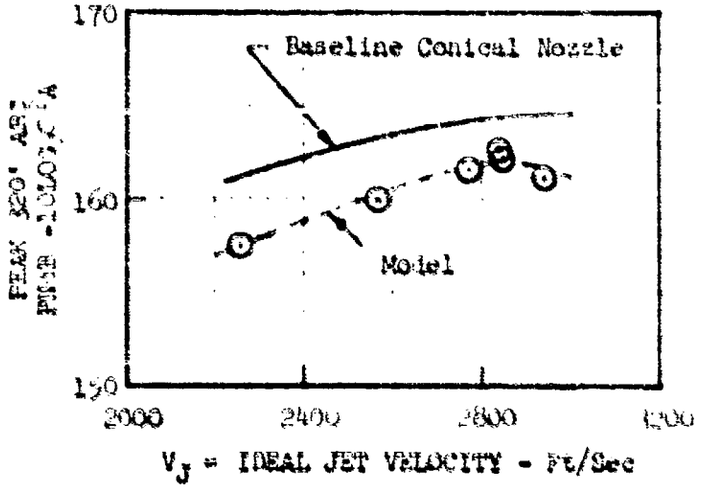


FIGURE V.H.1-6 SCHEMATIC AND 320 FT. ARC JET NOISE LEVEL FOR MODEL V-1-2-2

TABLE V.N.1-7 TEST SUMMARY

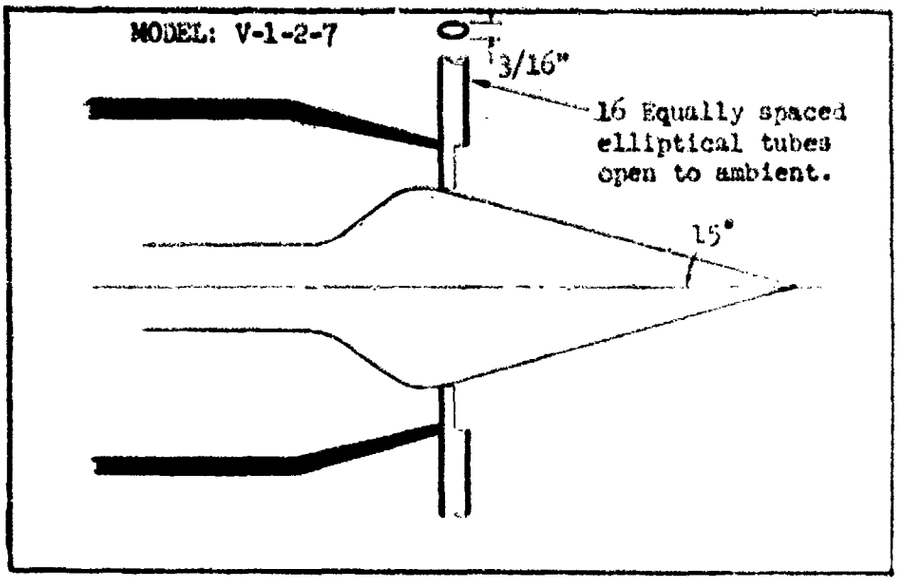
MODEL NO. V-1-2-2

DESCRIPTION 30° PLUG, PRIMARY AND SECONDARY SHROUDS; 6 CDB TUBES ON 8-TUBE PATTERN

MODEL A_8 = .0677 FT.^{2}; FULL SCALE A_8 = 4.3328 FT.^{2}; SCALE FACTOR = 8:1

	TEST CONDITIONS					ACOUSTIC TEST RESULTS *									
										PWL DIRECTIVITY ON 320° ARC MEASURED FROM NOZZLE EXIT					
RUN NO.	V_E (FPS)	P_{T9}/P_0	T_{T9} °R	IDEAL V_J FT/SEC	% BLEED $W_B/W_8 \times 100$	PEAK PWLB ON 320° ARC	ANGLE OF MAX PWLS (DEG.)	$10\log\beta^2_A$	PEAK PWLB $-10\log\beta^2_A$	20°	30°	40°	50°	60°	70°
1	4.29	3.24	2306	2852	4.66	136.2	50	-25.9	162.1	129.8	132.6	134.3	136.2	135.1	131.0
2	4.63	3.54	2305	2942	4.70	135.5	60	-25.6	161.1	130.6	133.4	135.0	134.8	135.5	132.1
3	4.00	3.03	2289	2769	4.68	135.6	50	-26.1	161.7	130.0	133.1	134.5	135.6	134.2	129.8
4	3.20	2.53	2313	2573	5.15	133.2	50	-26.8	160.0	126.1	130.4	130.8	133.2	131.7	128.3
5	2.62	2.03	2296	2266	4.50	130.1	50	-27.4	157.5	123.5	128.3	129.2	130.1	127.1	125.3
6	4.26	3.24	2290	2842	4.58	136.9	50	-25.9	162.8	130.2	133.5	135.3	136.9	135.4	131.0

*Data Includes Ground Reflection Interference



DESCRIPTION

Model V-1-2-7 used the 16 elliptical tubes, 3/16" wide, equally spaced around the annulus, with 100% tube penetration to plug surface. Tube ends were open to ambient. No blow-in-door or secondary shroud were used. Exit area, A_8 = .0518 ft^2. Material: 321 s.s. Full scale A_8 = 3.3152 Ft^2. Scale factor = 8:1.

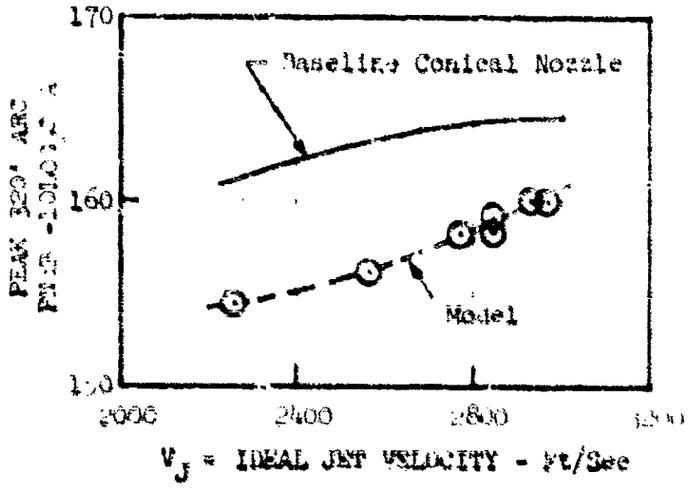


FIGURE V.H.1-7 SCHEMATIC AND 320 FT. ARC JET NOISE LEVEL FOR MODEL V-1-2-7

TABLE V.H.1-8 TEST SUMMARY

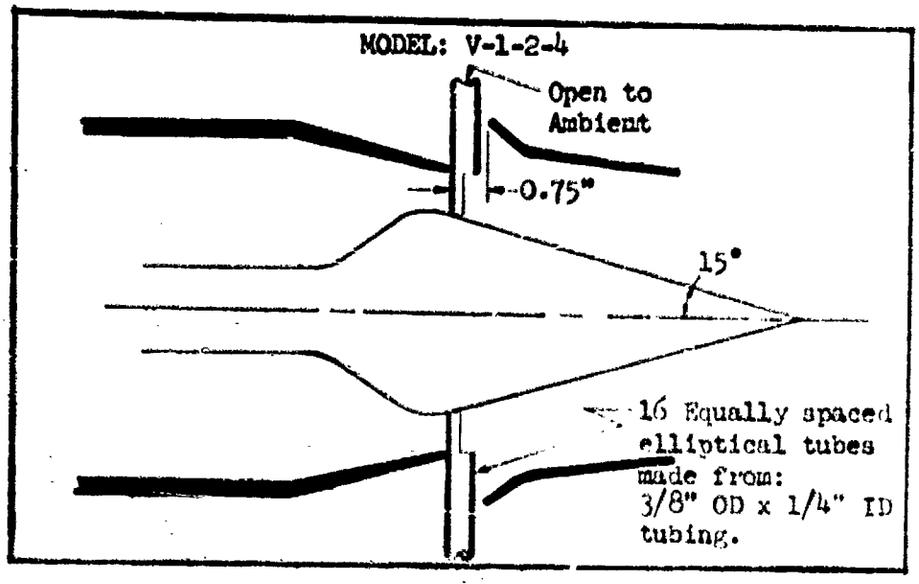
MODEL NO. V-1-2-7

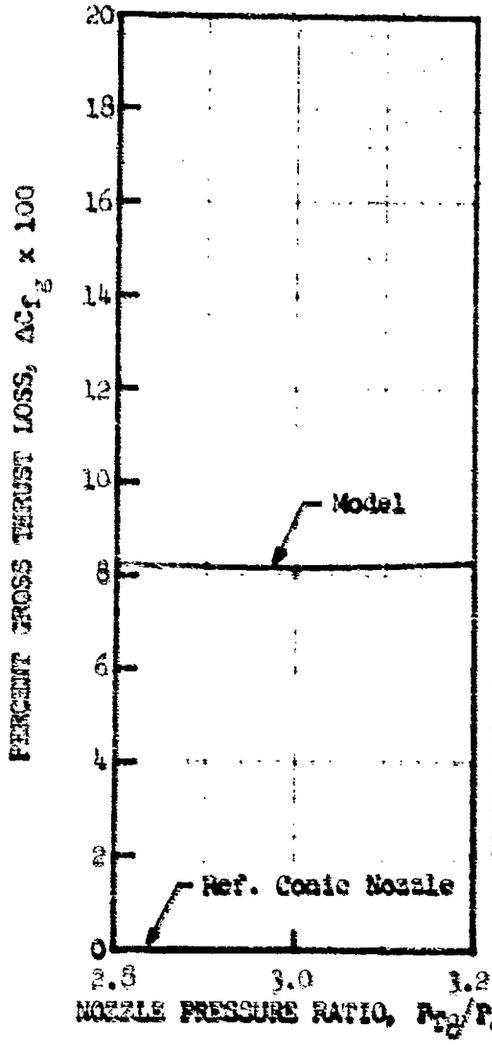
DESCRIPTION 30° PLUG, PRIMARY SHROUD ONLY; 16 ELLIPTICAL TUBES, OPEN ENDS

MODEL A_8 = .0518 FT.^{2}; FULL SCALE A_8 = 3.3152 FT.^{2}; SCALE FACTOR = 8:1

	TEST CONDITIONS					ACOUSTIC TEST RESULTS *								
										PNL DIRECTIVITY ON 320° ARC MEASURED FROM NOZZLE EXIT					
RUN NO.	V_8 (FPS)	P_{T8}/P_0	T_{T8} °R	IDEAL V_J FT/SEC	% BLEED $W_B/W_8 \times 100$	PEAK PNLB ON 320° ARC	ANGLE OF MAX PNLB (DEG.)	$10\log\beta^2_A$	PEAK PNLB $-10\log\beta^2_A$	20°	30°	40°	50°	60°	70°
1	3.33	3.22	2311	2848		131.9	50	-27.2	159.1	127.4	129.9	131.5	131.9	130.0	129.0
2	3.44	3.49	2306	2928		133.3	50	-26.8	160.1	128.0	130.3	132.4	133.2	131.9	129.8
3	2.75	2.98	2674	2973		131.3	50	-28.7	160.0	126.1	128.7	130.6	131.3	129.7	128.6
4	3.06	2.99	2310	2767		130.8	40	-27.4	158.2	126.5	128.6	130.8	130.3	128.7	127.1
5	2.64	2.51	2314	2563		128.2	40	-28.0	156.2	124.9	127.3	128.2	127.9	127.1	125.3
6	2.07	2.01	2314	2260		125.8	40	-28.7	154.5	122.6	124.9	125.8	125.4	123.4	122.3
7	3.20	3.21	2310	2844		131.2	50	-27.2	158.4	126.8	129.3	130.8	131.2	129.4	128.1

*Data Includes Ground Reflection Interference





DESCRIPTION

Model V-1-2-4 had 16 elliptical tubes, 3/16" wide, equally spaced around the annulus, with 100% penetration to plug surface. Tube ends were open to ambient. Shroud gap was 1.5". Exit area, A_8 = .0518 ft^2. Material: 321 s.s. for plug, shrouds and tubes. Full scale A_8 = 3.3152 Ft^2. Scale factor = 8:1.

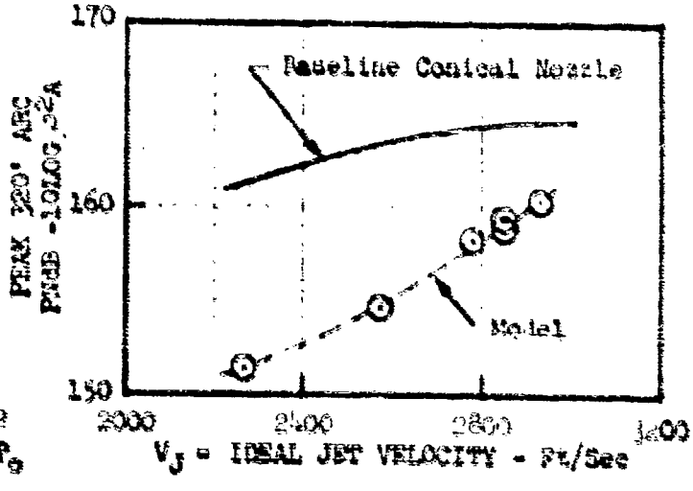


FIGURE V.H.1-8 SCHEMATIC, 320 FT. ARC JET NOISE LEVEL AND AERODYNAMIC TEST RESULTS FOR MODEL V-1-2-4

TABLE V.H.1-9 TEST SUMMARY

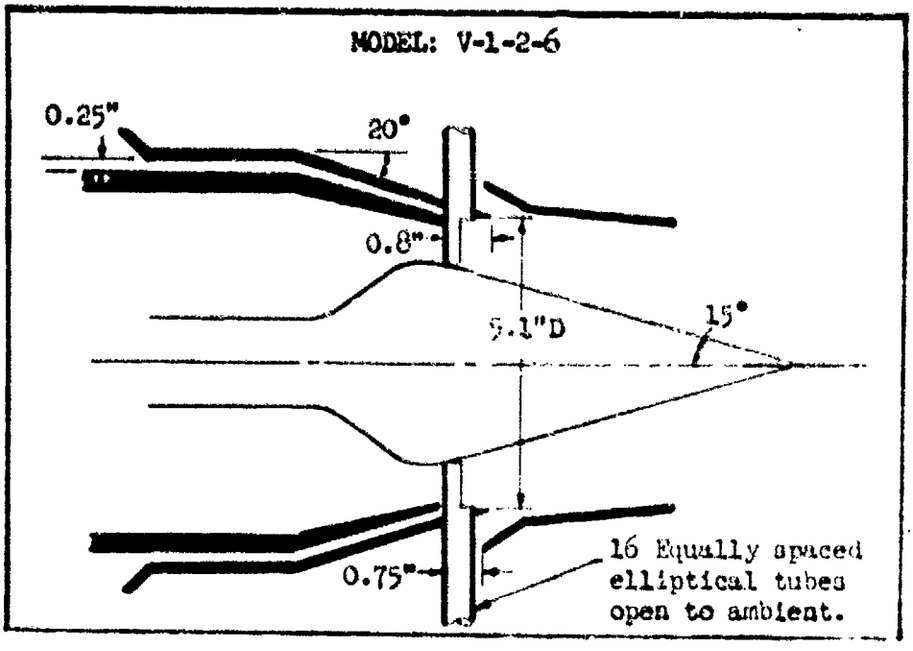
MODEL NO. V-1-2-4

DESCRIPTION 30° PLUG, PRIMARY AND SECONDARY SHROUDS; 16 ELLIPTICAL TUBES, OPEN ENDS

MODEL A_8 = .0518 FT.^{2}; FULL SCALE A_8 = 3.3152 FT.^{2}; SCALE FACTOR = 8:1

	TEST CONDITIONS					ACOUSTIC TEST RESULTS *								
RUN NO.	V_8 (FPS)	P_{T8}/P_o	T_{T8} °R	IDEAL V_j FT/SEC	% BLEED W_B/W_8 x 100	PEAK PNLB ON 320° ARC	ANGLE OF MAX PNLB (DEG.)	$10\log\beta^2 A$	PEAK PNLB $-10\log\beta^2 A$	PNL DIRECTIVITY ON 320° ARC MEASURED FROM NOZZLE EXIT				
										20°	30°	40°	50°	60°	70°
1	3.54	3.22	2308	2846		131.6	40	-27.1	158.7	127.6	129.9	131.6	131.5	129.6	126.6
2	3.74	3.51	2307	2935		133.5	40	-26.8	160.3	129.1	131.3	133.5	133.3	131.6	129.0
3	3.09	3.01	2317	2779		130.8	40	-27.4	158.2	126.9	129.2	130.8	130.7	128.6	127.0
4	2.67	2.51	2325	2569		126.6	50	-28.1	154.7	123.9	126.1	126.5	126.6	124.7	124.5
5	2.02	2.01	2330	2269		122.6	70	-28.7	151.3	119.6	120.4	120.9	121.4	121.7	122.6
6	3.33	3.22	2310	2847		132.3	40	-27.1	159.4	127.6	130.5	132.3	131.7	130.3	127.3

* Data Includes Ground Reflection Interference



DESCRIPTION

Model V-1-2-6 used the blow-in-door shroud arrangement open to ambient air. Equally spaced around the annulus were 16 elliptical tubes, 3/16" wide, with ends open to ambient. Tube penetration was 100% to plug surface. Primary-to-secondary shroud gap was 1.5". Exit area, A_8 = .0518 ft^2. Material: 321 s.s. for plug, shrouds, blow-in-door and tubes. Full scale A_8 = 3.3152 Ft^2.

Scale factor = 8:1.

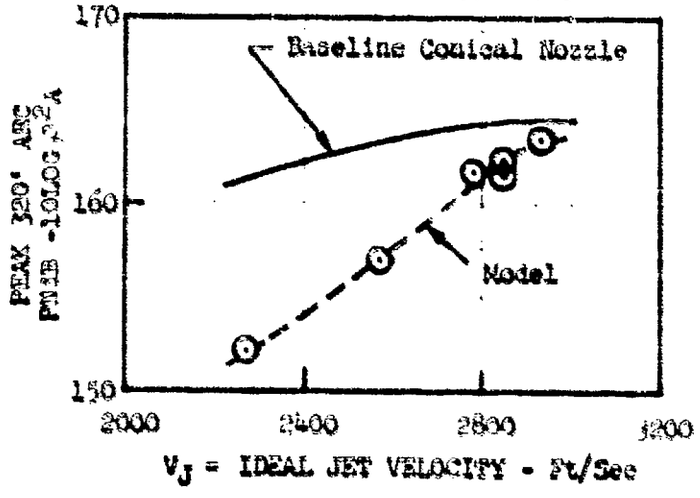


FIGURE V.H.1-9 SCHEMATIC AND 320 FT. ARC JET NOISE LEVEL FOR MODEL V-1-2-6

TABLE V.H.1-10 TEST SUMMARY

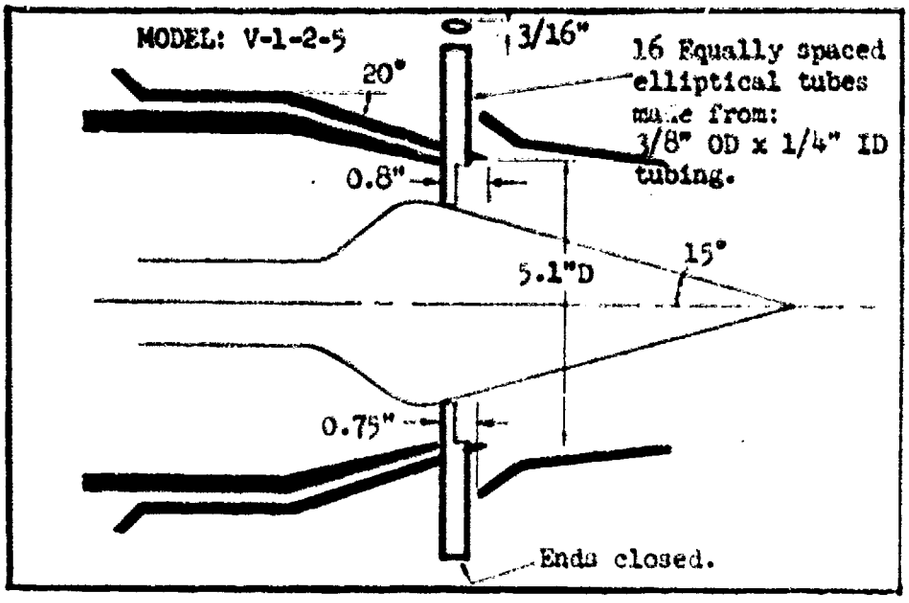
MODEL NO. V-1-2-6

DESCRIPTION 30° PLUG, PRIMARY AND SECONDARY SHROUDS, BLOW-IN-DOOR; 16 ELLIPTICAL TUBES, OPEN ENDS

MODEL A_8 = .0518 FT.^{2}; FULL SCALE A_8 = 3.3152 FT.^{2}; SCALE FACTOR = 8:1

	TEST CONDITIONS					ACOUSTIC TEST RESULTS *								
PDC NO.	W_8 (PPS)	P_{T8}/P_o	T_{T8} °R	IDEAL V_J FT/SEC	% BLEED $W_B/W_8 \times 10^5$	PEAK PNdB OVER 320° ARC	ANGLE OF MAX PNdB (DEG.)	$10\log\beta_A^2$	PEAK PNdB $-10\log\beta_A^2$	FWL DIRECTIVITY ON 320° ARC MEASURED FROM NOZZLE EXIT					
										20°	30°	40°	50°	60°	70°
1	3.48	3.22	2308	2846		135.2	50	-27.1	162.3	129.1	131.9	134.2	135.2	131.9	130.0
2	3.78	3.51	2307	2935		137.4	50	-26.1	163.5	129.8	133.0	135.6	137.4	135.9	128.7
3	3.13	3.01	2320	2780		134.4	50	-27.4	161.8	128.2	131.3	133.0	134.4	130.4	127.2
4	2.64	2.51	2325	2569		128.9	40	-28.1	157.0	124.4	127.8	128.9	126.8	125.9	125.5
5	2.07	2.01	2330	2268		123.4	70	-28.7	152.1	120.7	122.5	122.3	123.0	123.1	123.3
6	3.49	3.22	2308	2846		134.4	40	-27.1	161.5	129.1	132.2	134.4	134.4	131.0	129.2

*Data Includes Ground Reflection Interference



DESCRIPTION

Model V-1-2-5 employed a blow-in-door shroud open to ambient air in addition to the primary and secondary shrouds. Shroud gap was 1.5". Equally spaced around the annulus were 16 elliptical tubes, 3/16" wide, with closed ends. Tube penetration was 100% to plug surface. Exit area, A_8 = .0518 ft^2. Material: 321 s.s. for plug, shrouds, blow-in-door, and tubes. Full scale A_8 = 3.3152 Ft^2. Scale factor = 8:1.

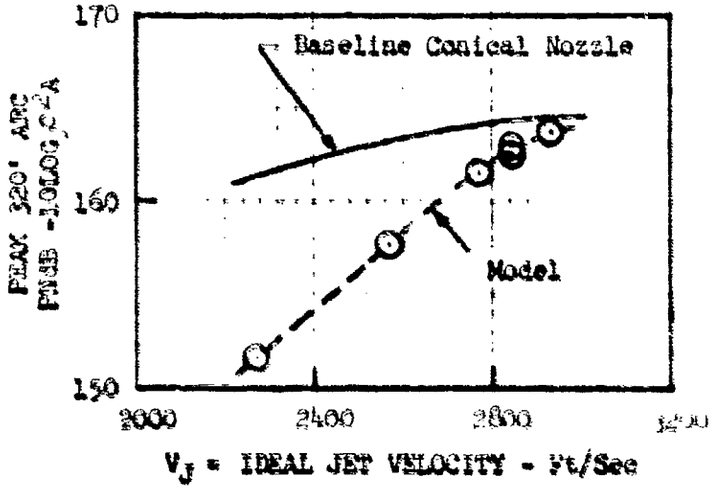


FIGURE V.H.1-10 SCHEMATIC AND 320 FT. ARC JET NOISE LEVEL FOR MODEL V-1-2-5

TABLE V.H.1-11 TEST SUMMARY

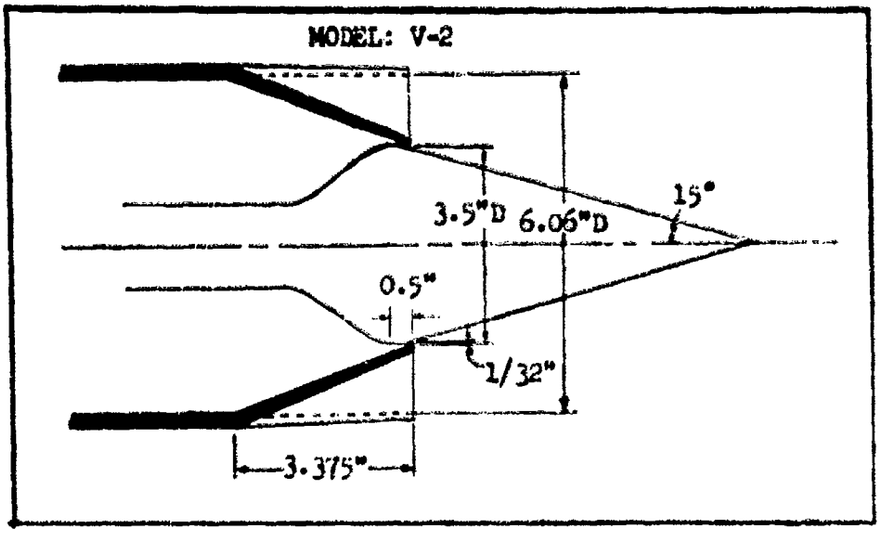
MODEL NO. V-1-2-5

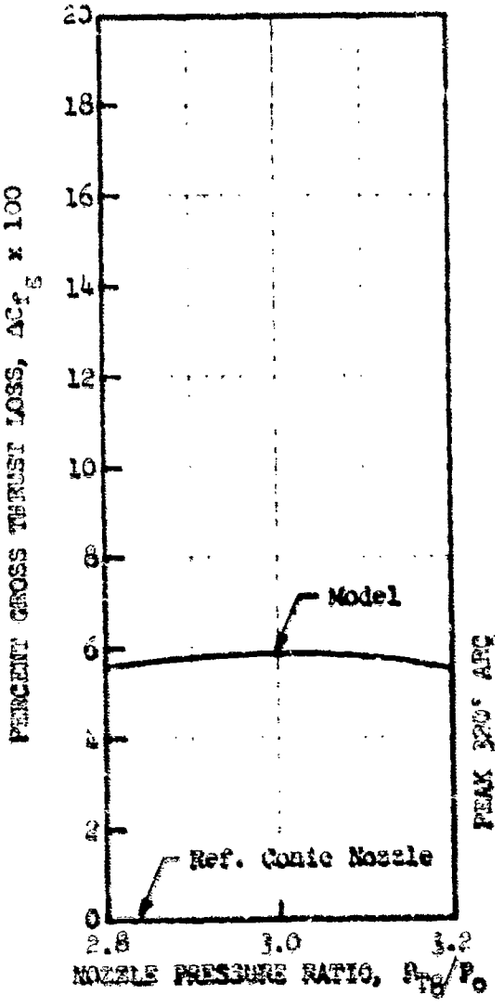
DESCRIPTION 30° PLUG, PRIMARY AND SECONDARY SHROUDS; BLOW-IN-DOOR; 16 ELLIPTICAL TUBES, ENDS CLOSED

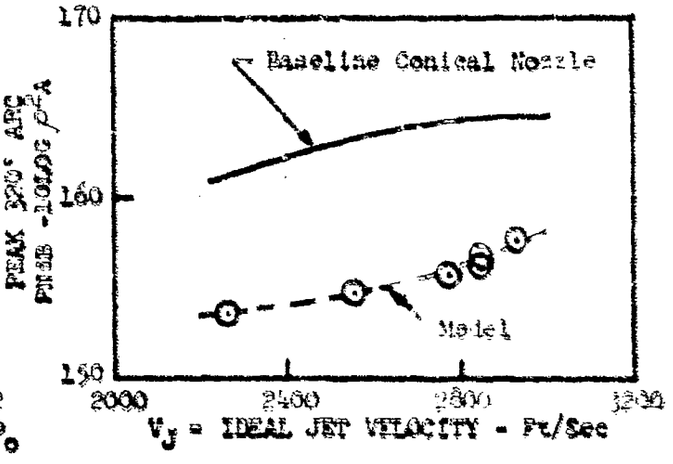
MODEL A_8 = .0518 FT.^{2}; FULL SCALE A_8 = 3.3152 FT.^{2}; SCALE FACTOR = 8:1

	TEST CONDITIONS					ACOUSTIC TEST RESULTS *								
RUN NO.	V_8 (FPS)	P_{T8}/P_∞	T_{T8} °R	IDEAL V_J FT/SEC	% BLEED W_B/W_8 x 100	PEAK PNLB ON 320° ARC	ANGLE OF MAX PNLB (DEG.)	$10\log\beta^2_A$	PEAK PNLB $-10\log\beta^2_A$	PNL DIRECTIVITY ON 320° ARC MEASURED FROM NOZZLE EXIT					
										20°	30°	40°	50°	60°	70°
1	3.55	3.22	2308	2846		135.4	50	-27.1	162.5	128.8	131.6	134.2	135.4	133.1	129.6
2	3.91	3.51	2307	2935		137.1	50	-26.8	163.9	129.3	133.2	135.2	137.1	135.0	131.2
3	3.62	3.01	2310	2774		134.2	50	-27.4	161.6	127.3	130.4	132.8	134.2	131.8	128.2
4	2.49	2.51	2326	2570		129.7	40	-28.1	157.8	125.0	127.2	129.7	128.7	127.3	124.6
5	2.09	2.01	2330	2268		122.9	60	-28.7	151.6	120.4	122.1	122.5	122.6	122.9	122.8
6	3.44	3.22	2310	2847		135.9	50	-27.1	163.0	128.9	132.1	134.6	135.9	132.1	129.5

*Data Includes Ground Reflection Interference







DESCRIPTION

Model V-2 employed a 36-segmented "Flip-Flap" primary shroud with full sidewalls (18 in, 18 out) resulting in 55% blocked area. The 30° plug was used but without the secondary shroud or blow-in-door. Exit area, A_8 = .0588 ft². Material: 321 S.S. Full scale A_8 = 3.7632 Ft². Scale factor = 8:1.

FIGURE V.H.1-11 SCHEMATIC, 320 FT. ARC JET NOISE LEVEL AND AERODYNAMIC TEST RESULTS FOR MODEL V-2

TABLE V.H.1-12 TEST SUMMARY

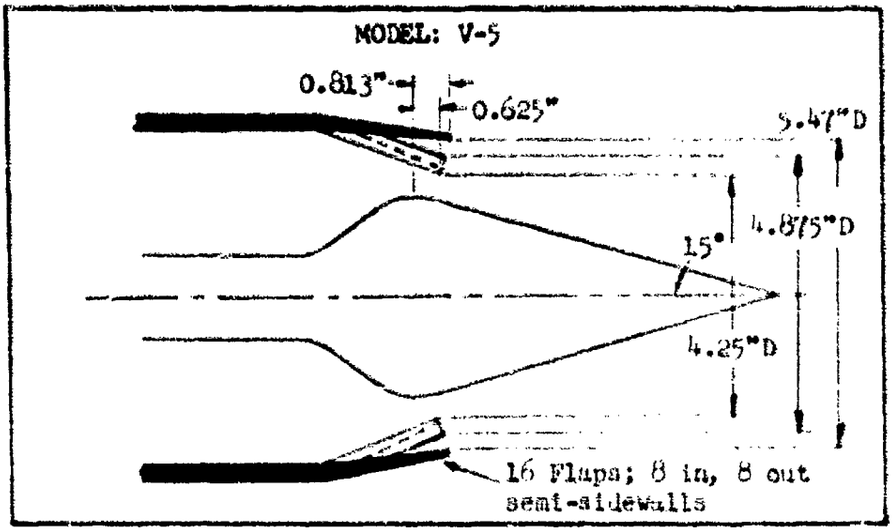
MODEL NO. V-2

DESCRIPTION 30° PLUG, 36-SEGMENTED PRIMARY, "FLIP-FLAPS" (18 IN, 18 OUT)

MODEL A_8 = .0588 FT.^{2}; FULL SCALE A_8 = 3.7632 FT.^{2}; SCALE FACTOR = 8:1

	TEST CONDITIONS					ACOUSTIC TEST RESULTS *								
										PNL DIRECTIVITY ON 320° ARC MEASURED FROM NOZZLE EXIT					
PNC NO.	W_8 (PPS)	P_{T8}/P_0	T_{T8} °R	IDEAL V_j FT/SEC	% BLEED $W_B/W_8 \times 100$	PEAK PNLR ON 320° ARC	ANGLE OF MAX PNLR (DEG.)	$10LOG_{10}F^2A$	PEAK PNLR $-10LOG_{10}F^2A$	20°	30°	40°	50°	60°	70°
1	3.98	3.22	2308	2846		129.6	50	-26.6	156.2	126.4	128.0	129.4	129.6	129.1	128.1
2	4.29	3.50	2304	2930		131.5	50	-26.3	157.8	126.9	128.6	130.4	130.5	129.6	128.9
3	3.71	3.00	2310	2771		128.9	40	-26.9	155.8	125.2	127.5	128.9	128.8	128.4	127.2
4	3.11	2.50	2312	2557		127.3	40	-27.5	154.8	123.4	125.8	127.3	127.1	127.0	125.8
5	2.29	2.01	2315	2261		125.6	50	-28.1	153.7	121.8	124.0	125.6	125.6	124.5	123.7
6	3.94	3.21	2308	2843		130.3	50	-26.6	156.9	126.6	128.2	129.3	130.3	129.9	128.0

*Data Includes Ground Reflection Interference



DESCRIPTION

Model V-5 used a 16-segmented "Flip-Flap" primary shroud (8 in, 8 out) with semi-sidewalls. No secondary shroud was employed. Exit area, A_8 = .0622 ft^2. Material: 321 S.S. for primary and plug. Full scale A_8 = 3.9808 Ft^2. Scale factor = 8:1.

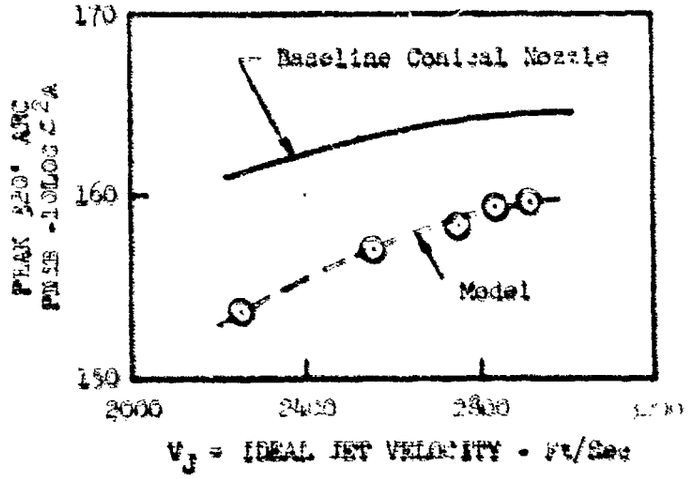


FIGURE V.B.1-12 SCHEMATIC AND 320 FT. ARC JET NOISE LEVEL FOR MODEL V-5

TABLE V.M.1-13 TEST SUMMARY

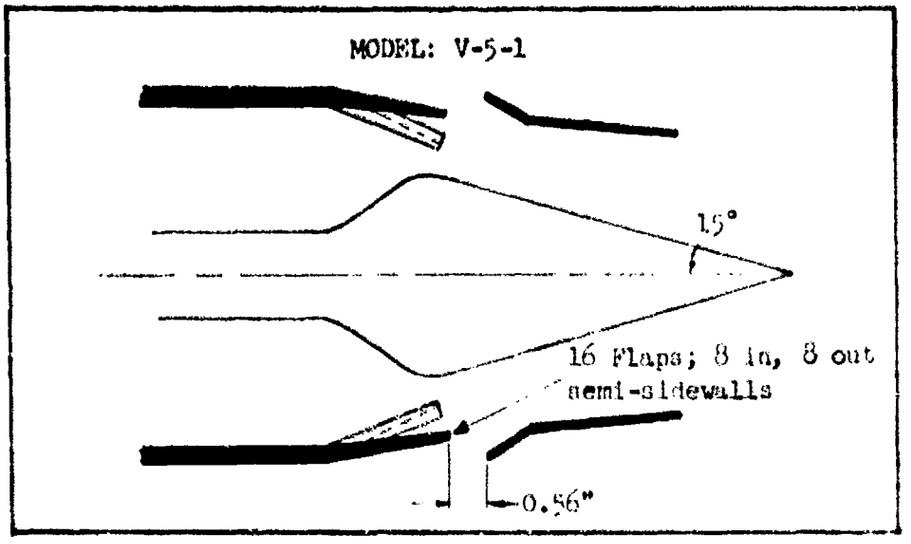
MODEL NO. V-5

DESCRIPTION 30° PLUG, 16 PRIMARY FLAPS (8 IN, 8 OUT), NO SECONDARY SHROUD

MODEL A_8 = .0622 FT.^{2}; FULL SCALE A_8 = 3.9808 FT.^{2}; SCALE FACTOR = 8:1

TEST CONDITIONS						ACOUSTIC TEST RESULTS *									
										PNL DIRECTIVITY ON 320° ARC MEASURED FROM NOZZLE EXIT					
RUN NO.	V_8 (FPS)	P_{T8}/P_0	T_{T8} °R	IDEAL V_j FT/SEC	% BLEED W_B/W_8 x 100	PEAK PNdB ON 320° ARC	ANGLE OF MAX PNdB (DEG.)	$10LOG\beta^2 A$	PEAK PNdB $-10LOG\beta^2 A$	20°	30°	40°	50°	60°	70°
1	4.45	3.21	2302	2838		133.0	50	-26.3	159.3	126.5	128.7	132.0	133.0	131.4	128.0
2	4.82	3.49	2288	2916		133.6	50	-26.0	159.6	127.6	130.4	132.5	133.6	132.2	129.7
3	4.09	2.99	2290	2754		131.7	40	-26.6	158.3	128.6	129.9	131.7	131.3	130.8	128.9
4	3.36	2.50	2308	2554		129.8	50	-27.2	157.0	125.0	127.0	129.3	129.8	128.5	126.9
5	2.64	2.00	2320	2254		125.7	40	-27.9	153.6	122.2	124.4	125.7	125.4	124.7	123.6
6	4.36	3.20	2306	2838		132.9	50	-26.4	159.3	128.0	130.2	131.9	132.9	131.1	128.6

*Data Includes Ground Reflection Interference



DESCRIPTION

Model V-5-1 had a conical secondary shroud with a gap of 1.31". The 16 segmented "Flip-Flap" primary shroud with semi-sidewalls was used. Exit area, A_8 = .0622 ft^2. Material: 321 s.s. for plug and shrouds. Full scale A_8 = 3.9808 Ft^2. Scale factor = 8:1.

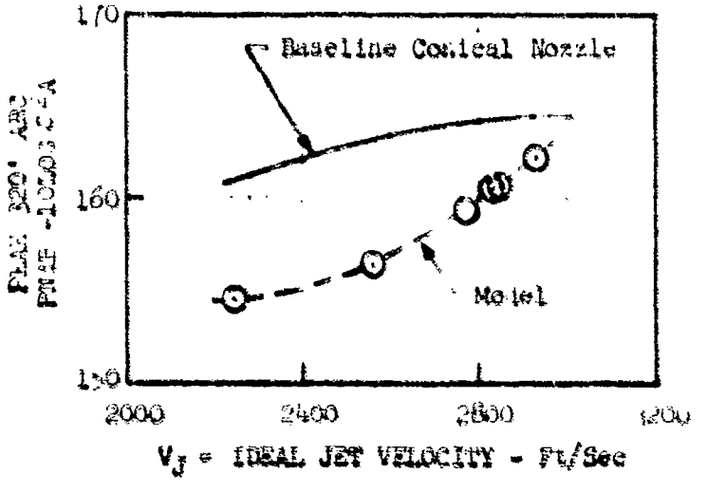


FIGURE V.H.1-13 SCHEMATIC AND 320 FT. ARC JET NOISE LEVEL FOR MODEL V-5-1

TABLE V.H.1-14 TEST SUMMARY

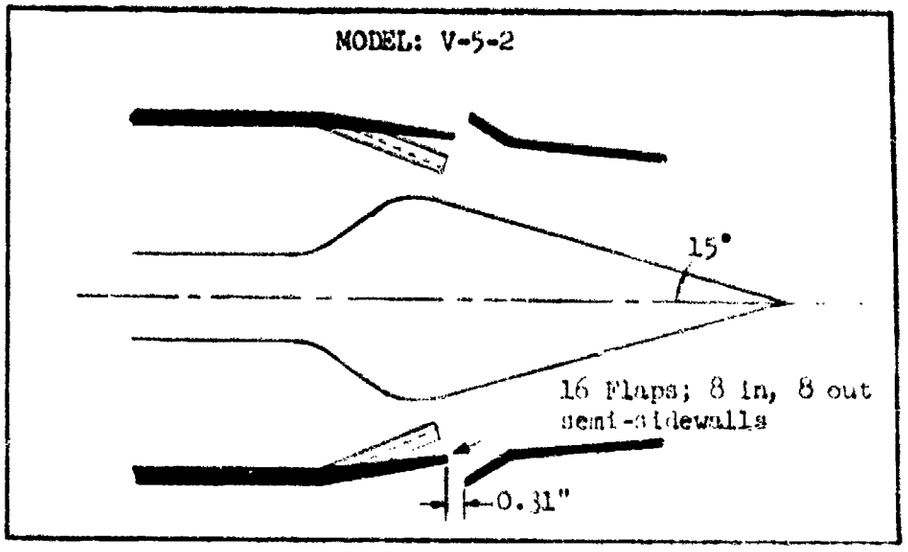
MODEL NO. V-5-1

DESCRIPTION 30° PLUG, 16 PRIMARY FLAPS (8 IN, 8 OUT), SECONDARY SHROUD, 0.56" GAP

MODEL A_8 = .0622 FT.^{2}; FULL SCALE A_8 = 3.9808 FT.^{2}; SCALE FACTOR = 8:1

TEST CONDITIONS						ACOUSTIC TEST RESULTS*									
										PWL DIRECTIVITY ON 320° ARC MEASURED FROM NOZZLE EXIT					
RUN NO.	W_8 (PPS)	P_{T8}/P_∞	T_{T8} °F	IDEAL V_J FT/SEC	% BLEND W_B/W_8 x 100	PEAK PWLB ON 320° ARC	ANGLE OF MAX PWLB (DEG.)	$10\log\beta^2_A$	PEAK PWLB $-10\log\beta^2_A$	20°	30°	40°	50°	60°	70°
1	3.96	3.19	2324	2845		134.4	50	-26.4	160.8	128.9	131.8	133.1	134.3	132.0	128.1
2	4.40	3.48	2319	2928		136.1	50	-26.1	162.2	128.9	133.6	134.7	136.0	134.0	130.6
3	3.74	2.98	2325	2771		132.6	50	-26.7	159.3	127.8	130.7	132.2	132.6	130.0	128.1
4	3.12	2.49	2329	2561		129.1	40	-27.3	156.4	124.8	127.9	129.1	128.1	125.8	-
5	2.45	2.00	2302	2249		126.7	40	-27.8	154.5	126.6	126.0	126.7	125.1	122.9	120.4
6	3.97	3.19	2305	2834		134.1	40	-26.4	160.5	130.5	131.4	134.1	133.6	131.8	128.9

*Data Includes Ground Reflection Interference



DESCRIPTION

Model V-5-2 used the 16 segmented "Flip-Flap" primary shroud with semi-sidewalls. The shroud gap was set at 1.06". Exit area, A_8 = .3622 ft^2. Material: 321 s.s.

Full scale A_8 = 3.9808 Ft^2. Scale factor = 8:1.

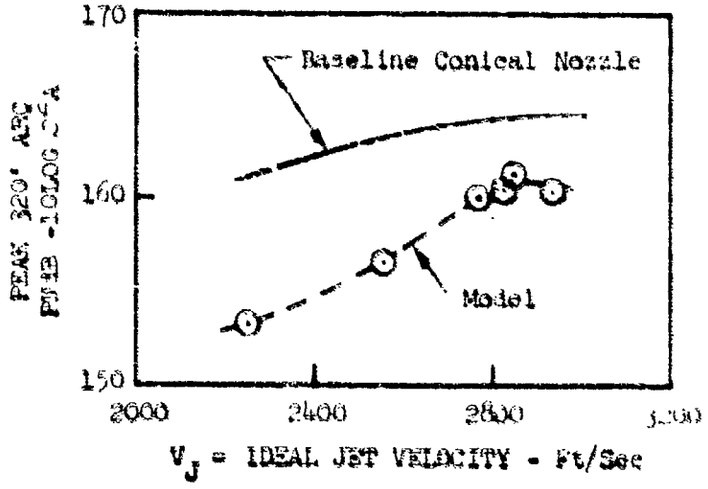


FIGURE V.H.1-14 SCHEMATIC AND 320 FT. ARC JET NOISE LEVEL FOR MODEL V-5-2

TABLE V.H.1-15 TEST SUMMARY

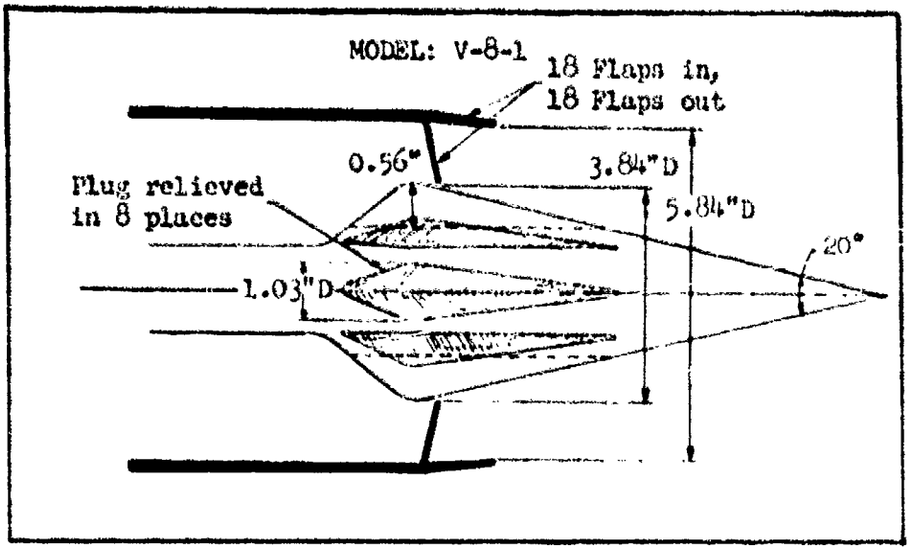
MODEL NO. V-5-2

DESCRIPTION 30° PLUG, 16 PRIMARY FLAPS (8 IN, 8 OUT), SECONDARY SHROUD, 0.31" GAP

MODEL A_8 = .0622 FT.^{2}; FULL SCALE A_8 = 3.9808 FT.^{2}; SCALE FACTOR = 8:1

	TEST CONDITIONS					ACOUSTIC TEST RESULTS*									
RUN NO.	V_8 (FPS)	P_{T8}/P_a	T_{T8} °R	IDEAL V_J FT/SEC	% BLEED W_B/W_8 x 100	PEAK PNdB ON 320° ARC	ANGLE OF MAX PNdB (DEG.)	$10LOG\beta^2_A$	PEAK PNdB $-10LOG\beta^2_A$	PNL DIRECTIVITY ON 320° ARC MEASURED FROM NOZZLE EXIT					
										20°	30°	40°	50°	60°	70°
1	4.78	3.49	2317	2936		134.2	50	-26.1	160.3	131.2	132.5	133.7	134.2	131.1	127.9
2	4.38	3.20	2296	2833		134.1	50	-26.3	160.4	131.7	132.3	133.9	134.1	131.3	129.7
3	4.07	3.00	2306	2766		133.4	50	-26.6	160.0	131.0	131.8	133.4	133.3	131.5	128.8
4	3.32	2.49	2309	2552		129.5	40	-27.2	156.7	127.0	-	129.5	125.6	125.0	126.4
5	2.70	2.01	2308	2254		125.2	40	-27.9	153.1	120.9	124.5	125.2	124.1	121.6	120.1
6	4.38	3.21	2306	2841		134.8	40	-26.4	161.2	128.4	134.0	134.8	134.1	132.0	128.8

*Data Includes Ground Reflection Interference



DESCRIPTION

Model V-8-1 employed a 36-segmented "Flip-Flap" primary shroud (18 in, 18 out) with no sidewalls. A 20°-fluted conical center plug was used. The plug was relieved in 8 places to increase turbulence. Exit area, A_8 = .0920 ft^2. Material: 321 s.s. Full scale A_8 = 5.888 Ft^2.

Scale factor = 8:1.

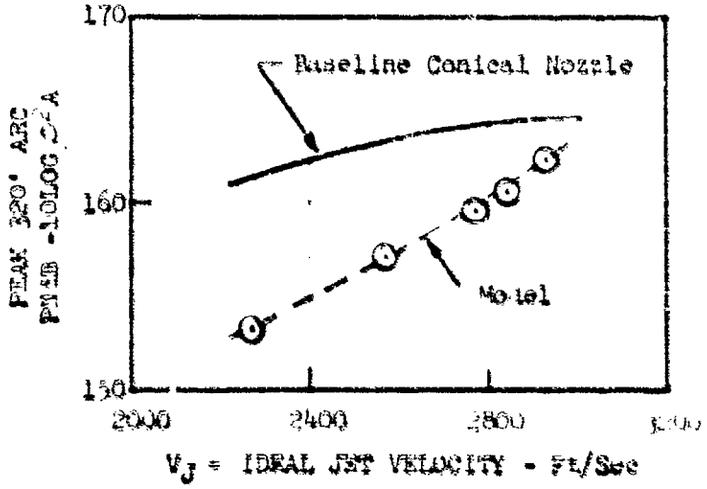


FIGURE V.B.1-15 SCHEMATIC AND 320 FT. ARC JET NOISE LEVEL FOR MODEL V-8-1

TABLE V.H.1-16 TEST SUMMARY

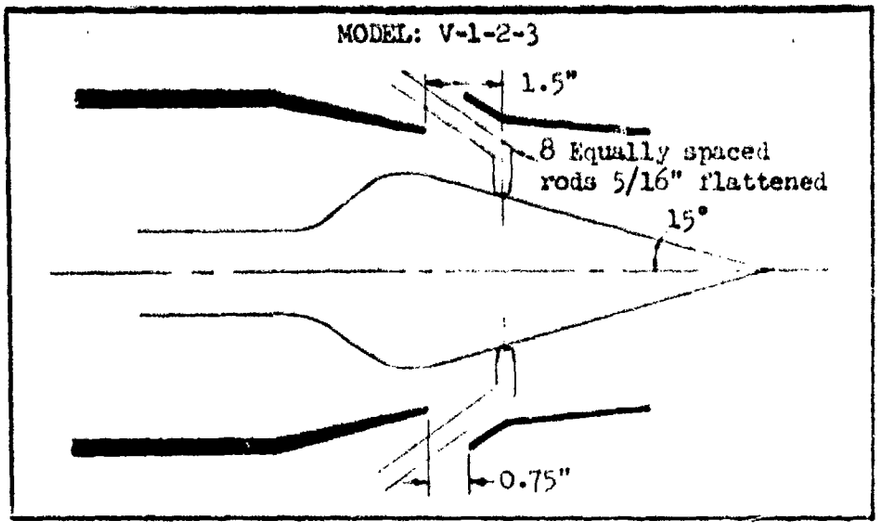
MODEL NO. V-8-1

DESCRIPTION 20° FLUTED PLUG, 36 PRIMARY FLAPS (18 IN, 18 OUT), NO SECONDARY SHROUD

MODEL A_8 = .092 FT.^{2}; FULL SCALE A_8 = 5.888 FT.^{2}; SCALE FACTOR = 8:1

	TEST CONDITIONS					ACOUSTIC TEST RESULTS*								
										PNL DIRECTIVITY ON 320° ARC MEASURED FROM NOZZLE EXIT					
PDS NO.	V_8 (FPS)	P_{T8}/P_0	T_{T8} °R	IDEAL V_j FT/SEC	% BLEED W_B/W_8 x 100	PEAK PNdB ON 320° ARC	ANGLE OF MAX PNdB (DEG.)	$10\log\beta^2_A$	PEAK PNdB $-10\log\beta^2_A$	20°	30°	40°	50°	60°	70°
1	6.02	3.23	2298	2843		136.2	50	-24.5	160.7	129.0	131.7	134.1	136.2	133.8	130.4
2	6.60	3.53	2296	2933		138.2	50	-24.1	162.3	129.1	133.2	135.5	137.7	134.4	132.2
3	5.64	3.02	2300	2772		134.9	50	-24.7	159.6	127.8	131.3	133.5	134.4	131.6	129.3
4	4.68	2.53	2305	2568		131.7	40	-25.4	157.1	125.8	129.9	131.3	130.4	129.0	127.6
5	3.60	2.02	2310	2266		127.2	40	-26.0	153.2	123.8	126.6	126.7	126.7	125.9	125.5
6	6.02	3.23	2298	2843		136.1	50	-24.5	160.6	128.4	131.9	134.4	135.6	133.5	130.4

*Data Includes Ground Reflection Interference



DESCRIPTION

Model V-1-2-3 used an arrangement of 8 equally spaced 3/8" O.D. rods flattened to 5/16" width. Penetration was 100% to plug surface. Shroud gap was 1.5". Exit area, A_8 = .0518 ft^2. Material: 321 s.s. for plug and shrouds; Hastelloy-X for rods. Full scale A_8 = 4.3328 Ft^2. Scale factor = 8:1.

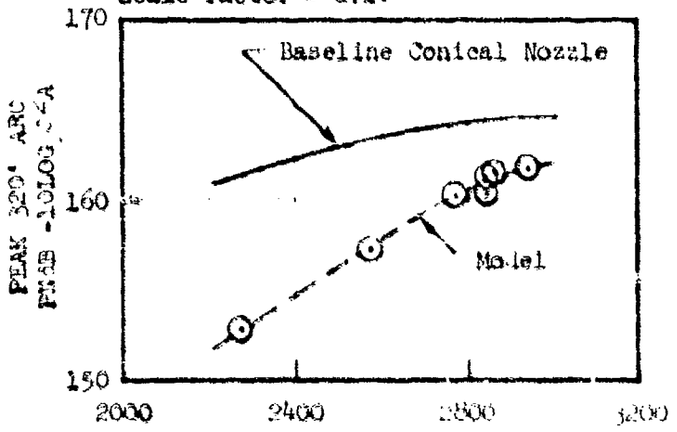


FIGURE V.H.1-16 SCHEMATIC AND 320 FT. ARC JET NOISE LEVEL FOR MODEL V-1-2-3

TABLE V.H.1-17 TEST SUMMARY

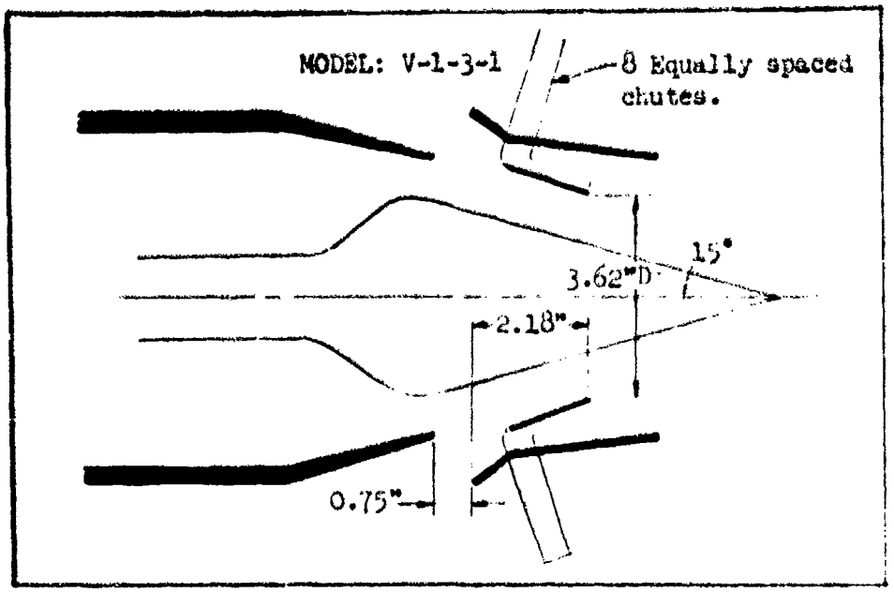
MODEL NO. V-1-2-3

DESCRIPTION 30° PLUG, PRIMARY AND SECONDARY SHROUD; 8 EQUALLY SPACED RODS FLATTENED TO 5/16"

MODEL A_8 = .0677 FT.^{2}; FULL SCALE A_8 = 4.3328 FT.^{2}; SCALE FACTOR = 8:1

	TEST CONDITIONS					ACOUSTIC TEST RESULTS *									
										PNL DIRECTIVITY ON 320° ARC MEASURED FROM NOZZLE EXIT					
ROD NO.	V_8 (FPS)	P_{T8}/P_0	T_{T8} °R	IDEAL V_J FT/SEC	% BLEED $W_B/W_8 \times 100$	PEAK PNLP ON 320° ARC	ANGLE OF MAX PNLB (DEG.)	$10\log\beta^2_A$	PEAK PNLB $-10\log\beta^2_A$	20°	30°	40°	50°	60°	70°
1	4.32	3.24	2306	2852		135.6	50	-25.9	161.5	129.2	133.0	135.1	135.6	133.7	130.9
2	4.70	3.53	2304	2939		136.2	50	-25.6	161.8	129.9	133.4	135.3	136.2	134.4	131.1
3	3.39	2.52	2311	2567		130.3	40	-26.8	157.1	125.9	129.1	130.3	129.7	128.4	125.7
4	2.72	2.02	2314	2268		125.4	50	-27.5	152.9	122.7	124.6	124.8	125.4	124.2	123.0
5	3.94	3.02	2307	2776		134.1	50	-26.2	160.3	128.5	132.0	133.6	134.1	132.9	129.7
6	4.28	3.23	2306	2848		135.2	50	-26.0	161.2	129.3	132.4	134.3	135.2	133.0	130.2
7	4.25	3.23	2306	2848		134.4	50	-26.0	160.4	-	-	-	-	-	-

*Data Includes Ground Reflection Interference



DESCRIPTION

Model V-1-3-1 had 8 equally spaced chutes on the secondary shroud with 50% annulus penetration. Shroud gap was 1.5". Exit area, A_8 = .0677 ft^2. Material: 321 s.s. for plug, shrouds; Hastelloy-X for chutes. Full scale A_8 = 4.3328 Ft^2. Scale factor = 8:1.

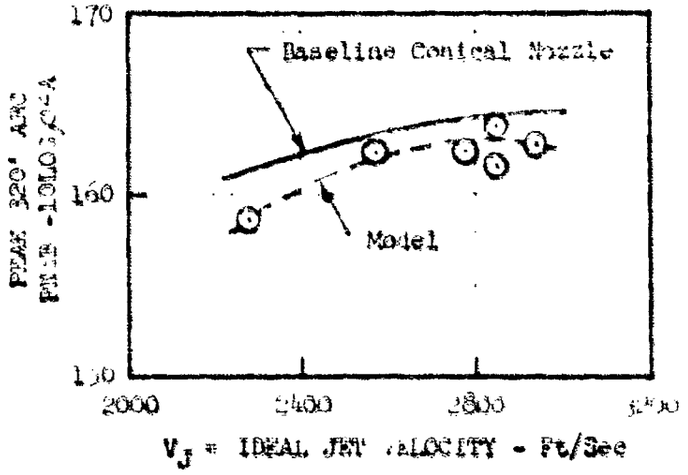


FIGURE V.H.1-17 SCHEMATIC AND 320 FT. ARC JET NOISE LEVEL FOR MODEL V-1-3-1

TABLE V.H.1-18 TEST SUMMARY

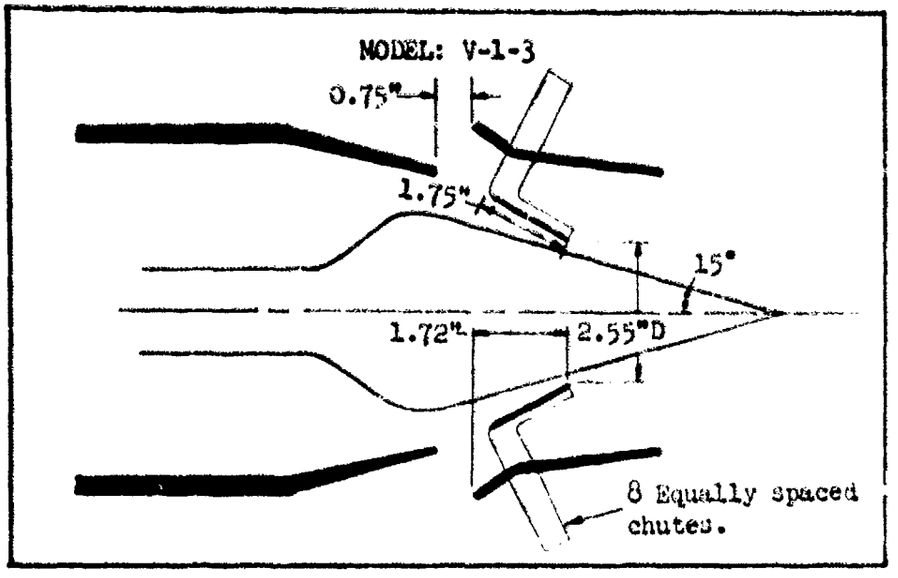
MODEL NO. V-1-3-1

DESCRIPTION 30° PLUG, PRIMARY AND SECONDARY SHROUDS, 8 CHUTES ON SECONDARY, 50% PENETRATION

MODEL A_8 = .0677 FT.^{2}; FULL SCALE A_8 = 4.3328 FT.^{2}; SCALE FACTOR = 8:1

	TEST CONDITIONS					ACOUSTIC TEST RESULTS *								
										PNL DIRECTIVITY ON 320° ARC MEASURED FROM NOZZLE EXIT					
RDG NO.	V_8 (FPS)	P_{T8}/P_0	T_{T8} °R	IDEAL V_j FT/SEC	% BLEED W_B/W_8 * 100	PEAK PNdB ON 320° ARC	ANGLE OF MAX PNdB (DEG.)	$10LOG\beta^2_A$	PEAK PNdB $-10LOG\beta^2_A$	20°	30°	40°	50°	60°	70°
1	4.57	3.24	2306	2852		135.7	50	-25.9	161.6	126.6	135.0	135.6	135.7	135.4	134.9
2	4.96	3.55	2305	2943		137.2	50	-25.6	162.8	133.7	133.0	136.8	137.2	136.4	135.6
3	4.22	3.04	2307	2784		136.2	50	-26.2	162.4	134.9	132.7	135.2	136.2	135.8	133.4
4	3.67	2.54	2312	2576		135.5	50	-26.8	162.3	128.1	130.8	134.2	135.5	133.1	129.3
5	3.03	2.04	2315	2279		131.1	50	-27.5	158.6	124.6	128.5	129.8	131.1	129.4	125.4
6	4.25	3.24	2308	2853		137.9	60	-26.0	163.9	125.6	131.6	135.2	137.8	137.9	133.0

*Data Includes Ground Reflection Interference



DESCRIPTION

Model V-1-3 used the conical primary and secondary shrouds with the 30° plug. Shroud gap was 1.5". Equally spaced around the annulus were 8 chutes on the secondary shroud. The chutes were positioned at 85% penetration to plug. Primary air flowed down the back of each chute to rejoin the main stream. Exit area, A_8 = .0677 ft^2. Material: 321 s.s. for plug and shrouds; Hastelloy-X for chutes. Full scale A_8 = 4.3328 Ft^2. Scale factor=8:1.

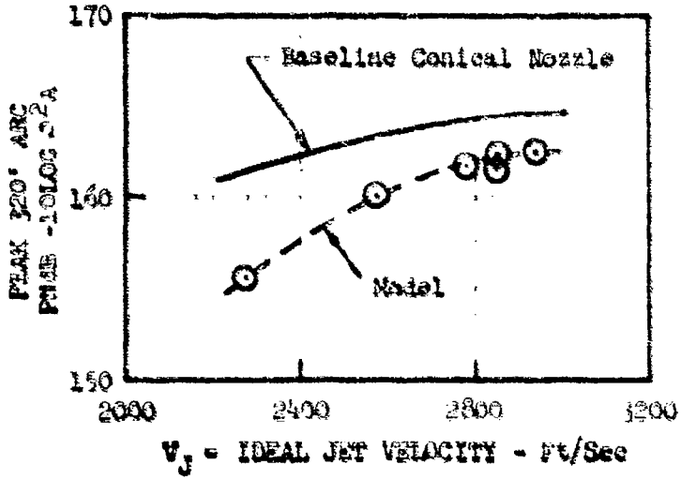


FIGURE V.H.1-18 SCHEMATIC AND 320 FT. ARC JET NOISE LEVEL FOR MODEL V-1-3

TABLE V.H.1-19 TEST SUMMARY

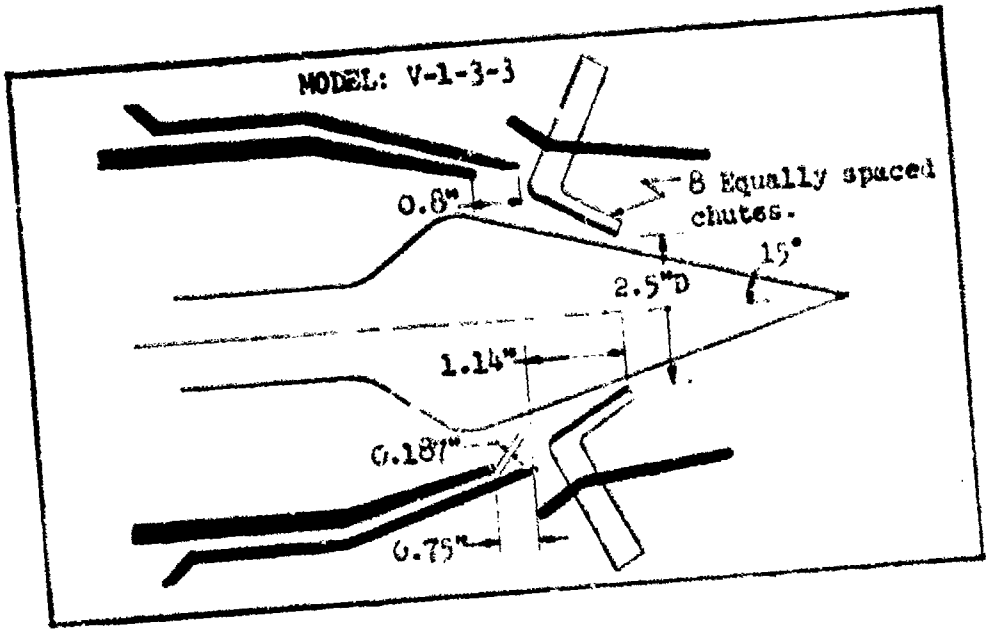
MODEL NO. V-1-3

DESCRIPTION 30° PLUG, PRIMARY AND SECONDARY SHROUDS; 8 CHUTES ON SECONDARY, 85% PENETRATION

MODEL A_8 = .0677 FT.^{2}; FULL SCALE A_8 = 4.3328 FT.^{2}; SCALE FACTOR = 8:1

	TEST CONDITIONS					ACOUSTIC TEST RESULTS *								
										PWL DIRECTIVITY ON 320° ARC MEASURED FROM NOZZLE EXIT					
RUN NO.	W_8 (PPS)	P_{T8}/P_∞	T_{T8} °R	IDEAL V_J FT/SEC	% BLEED W_B/W_8 x 100	PEAK PWLB ON 320° ARC	ANGLE OF MAX PWLB (DEG.)	$10LOG\beta^2_A$	PEAK PWLB $-10LOG\beta^2_A$	20°	30°	40°	50°	60°	70°
1	4.53	3.24	2306	2852		136.7	50	-25.9	162.3	127.5	132.0	134.4	136.7	136.0	131.6
2	4.44	3.54	2305	2943		137.0	50	-25.6	162.6	128.9	132.9	134.7	137.0	135.6	131.7
3	4.26	3.03	2308	2782		135.6	50	-26.2	161.8	127.9	131.5	134.0	135.6	134.2	130.7
4	3.05	2.53	2315	2576		133.3	50	-26.8	160.1	126.7	130.0	131.7	133.3	130.8	127.7
5	2.83	2.03	2320	2277		128.2	50	-27.5	155.7	123.1	127.2	128.1	128.2	126.5	124.1
6	4.67	3.24	2306	2851		135.6	50	-26.0	161.6	128.6	132.2	134.6	135.6	134.4	131.1

* Data Includes Ground Reflection Interference



DESCRIPTION

Model V-1-3-3 had the blow-in-door shroud, open to ambient, in addition to the primary and secondary shrouds. Shroud gap was 1.5". The 8 equally spaced chutes on the secondary shroud were set at 85% penetration depth to plug. Exit area, A_8 = .0677 ft^2. Material: 321 s.s. for plug, shrouds, blow-in-door; Hastelloy-X for chutes. Full scale A_8 = 4.3328 ft^2. Scale factor = 8:1.

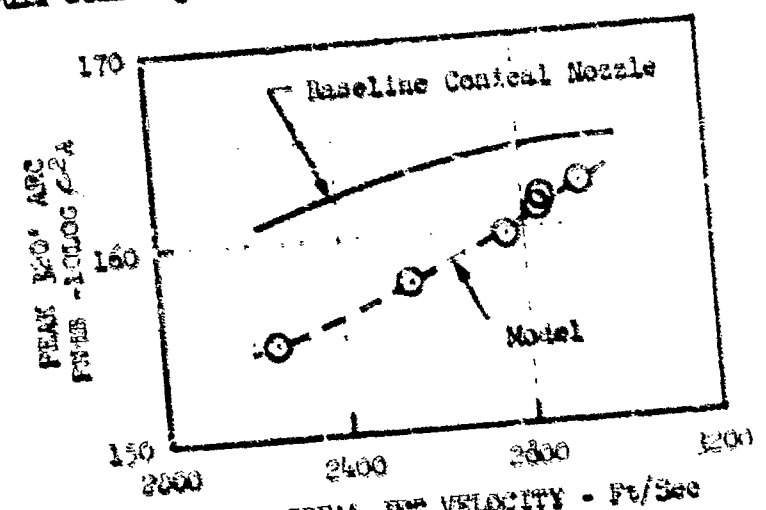


FIGURE V.A.1-19 SCHEMATIC AND 120 FT. ARC JET NOISE LEVEL FOR MODEL V-1-3-3

TABLE V.H.1-20 TEST SUMMARY

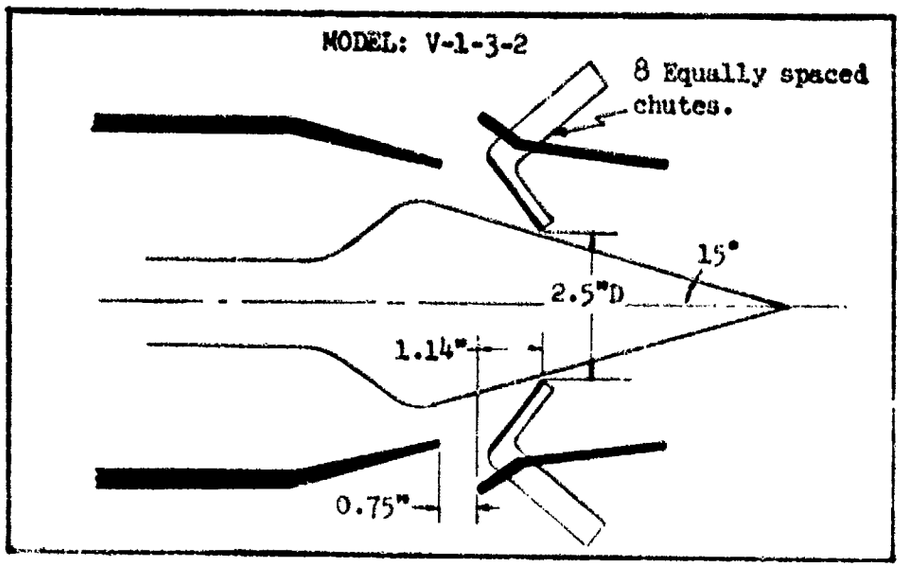
MODEL NO. V-1-3-3

DESCRIPTION 30° PLUG, PRIMARY, SECONDARY SHROUDS, BLOW-IN-DOOR, 8 CHUTES, 85% PENETRATION

MODEL A_8 = .0677 FT.^{2}; FULL SCALE A_8 = 4.3328 FT.^{2}; SCALE FACTOR = 8:1

	TEST CONDITIONS					ACOUSTIC TEST RESULTS *							
										PNL DIRECTIVITY ON 320° ARC MEASURED FROM NOZZLE EXIT					
RUN NO.	W_8 (PPS)	P_{T8}/P_0	T_{T8} °R	IDEAL V_j FT/SEC	% BLEED W_B/W_8 x 100	PEAK PNLB ON 320° ARC	ANGLE OF MAX PNLB (DEG.)	$10\log\mathcal{F}^2_A$	PEAK PNLB $-10\log\mathcal{F}^2_A$	20°	30°	40°	50°	60°	70°
1	4.28	3.21	2306	2840		135.6	50	-26.0	161.6	128.9	132.8	135.0	135.6	133.9	130.5
2	4.76	3.49	2304	2928		136.4	50	-25.7	162.1	130.5	133.8	136.2	136.4	134.4	131.5
3	4.07	2.97	2312	2762		133.5	50	-26.3	159.8	129.6	132.2	133.4	133.5	132.1	129.3
4	3.40	2.49	2312	2553		130.8	50	-26.9	157.7	127.4	130.4	129.7	130.8	128.7	127.2
5	2.64	2.00	2316	2257		127.4	50	-27.5	154.9	123.6	125.7	127.2	127.3	125.7	123.1
6	4.32	3.19	2306	2835		135.1	50	-26.0	161.1	128.8	132.8	134.8	135.1	132.9	129.6

*Data Includes Ground Reflection Interference



DESCRIPTION

Model V-1-3-2 employed the 8 equally spaced chutes on the secondary shroud at 95% penetration depth to plug. Shroud gap was 1.5". Exit area, A_8 = .0677 ft^2. Material: 321 s.s. for plug, shrouds; Hastelloy-X for chutes. Full scale A_8 = 4.3328 Ft^2. Scale factor = 8:1.

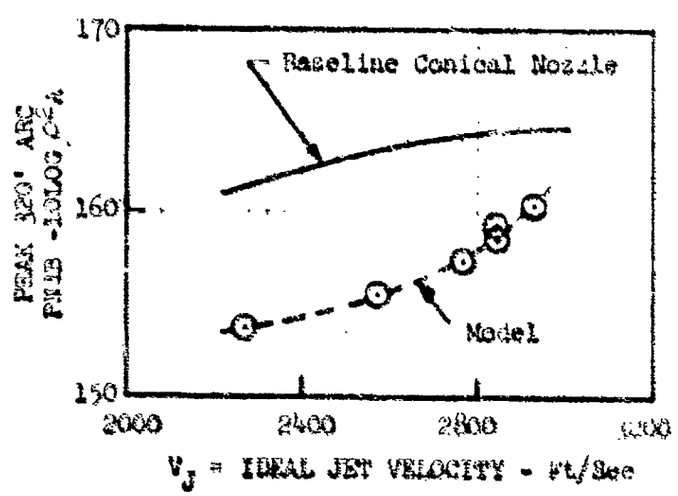


FIGURE V.H.1-20 SCHEMATIC AND 320 FT. ARC JET NOISE LEVEL FOR MODEL V-1-3-2

TABLE V.H.1-21 TEST SUMMARY

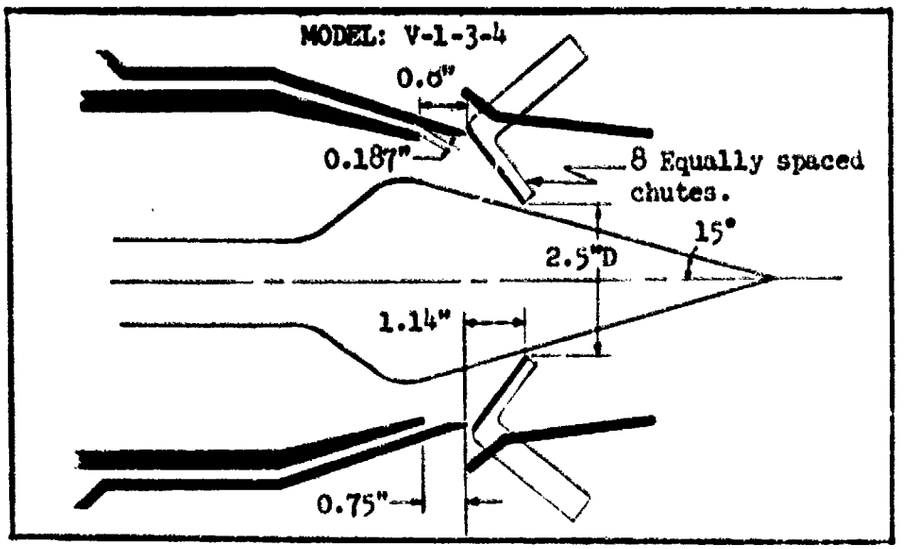
MODEL NO. V-1-3-2

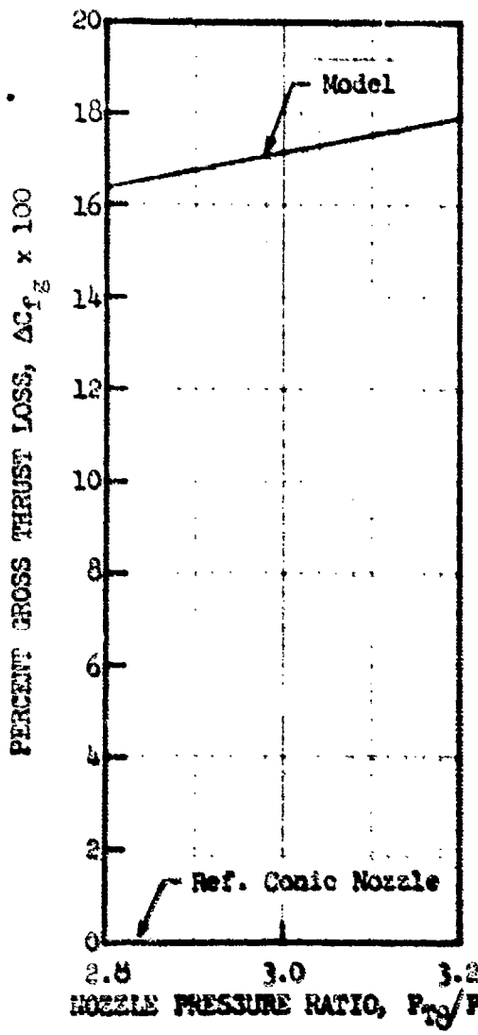
DESCRIPTION 30° PLUG, PRIMARY AND SECONDARY SHROUDS; 8 CHUTES ON SECONDARY, 95% PENETRATION

MODEL A_8 = .0677 FT.^{2}; FULL SCALE A_8 = 4.3328 FT.^{2}; SCALE FACTOR = 8:1

	TEST CONDITIONS					ACOUSTIC TEST RESULTS*								
PLUG NO.	V_8 (FPS)	P_{T8}/P_0	T_{T8} °R	IDEAL V_j FT/SEC	% BLEED W_B/W_8 x 100	PEAK PNdB ON 320° ARC	ANGLE OF MAX PNdB (DEG.)	$10\log\beta^2 A$	PEAK PNdB $-10\log\beta^2 A$	PNL DIRECTIVITY ON 320° ARC MEASURED FROM NOZZLE EXIT				
										20°	30°	40°	50°	60°	70°
1	4.32	3.22	2301	2842		133.4	40	-26.0	159.4	131.6	132.8	133.4	132.4	130.4	127.9
2	4.65	3.51	2293	2926		134.8	40	-25.6	160.4	131.5	134.2	134.8	134.2	131.9	129.5
3	4.46	3.00	2297	2763		131.1	30	-26.2	157.3	129.4	131.1	130.8	130.8	129.3	127.7
4	3.34	2.51	2317	2565		128.8	50	-26.9	155.7	127.5	127.6	128.7	128.8	127.8	126.5
5	2.69	2.01	2340	2273		126.2	50	-27.6	153.8	122.5	123.8	125.6	126.2	125.5	125.1
6	4.21	3.21	2308	2843		132.6	30	-26.0	158.6	130.0	132.6	132.6	131.9	131.0	128.1

*Data Includes Ground Reflection Interference





DESCRIPTION

Model V-1-3-4 used the blow-in-door open to ambient, primary and secondary shrouds. Shroud gap was 1.5". The 8 equally spaced chutes on the secondary shroud were set at 95% penetration. Exit area, A_8 = .0677 ft^2. Material: 321 s.s. for plug, shrouds, blow-in-door; Hastelloy-X for chutes. Full scale A_8 = 4.3328 Ft^2. Scale factor = 8:1.

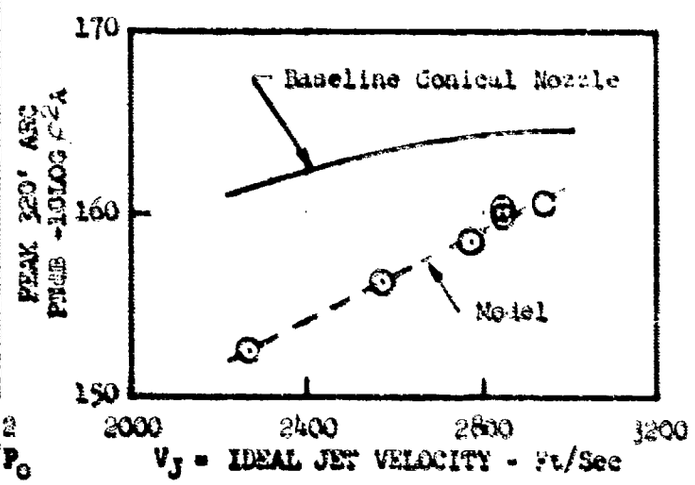


FIGURE V.H.1-21 SCHEMATIC, 320 FT. ARC JET NOISE LEVEL AND AERODYNAMIC TEST RESULTS FOR MODEL V-1-3-4

TABLE V.H.1-22 TEST SUMMARY

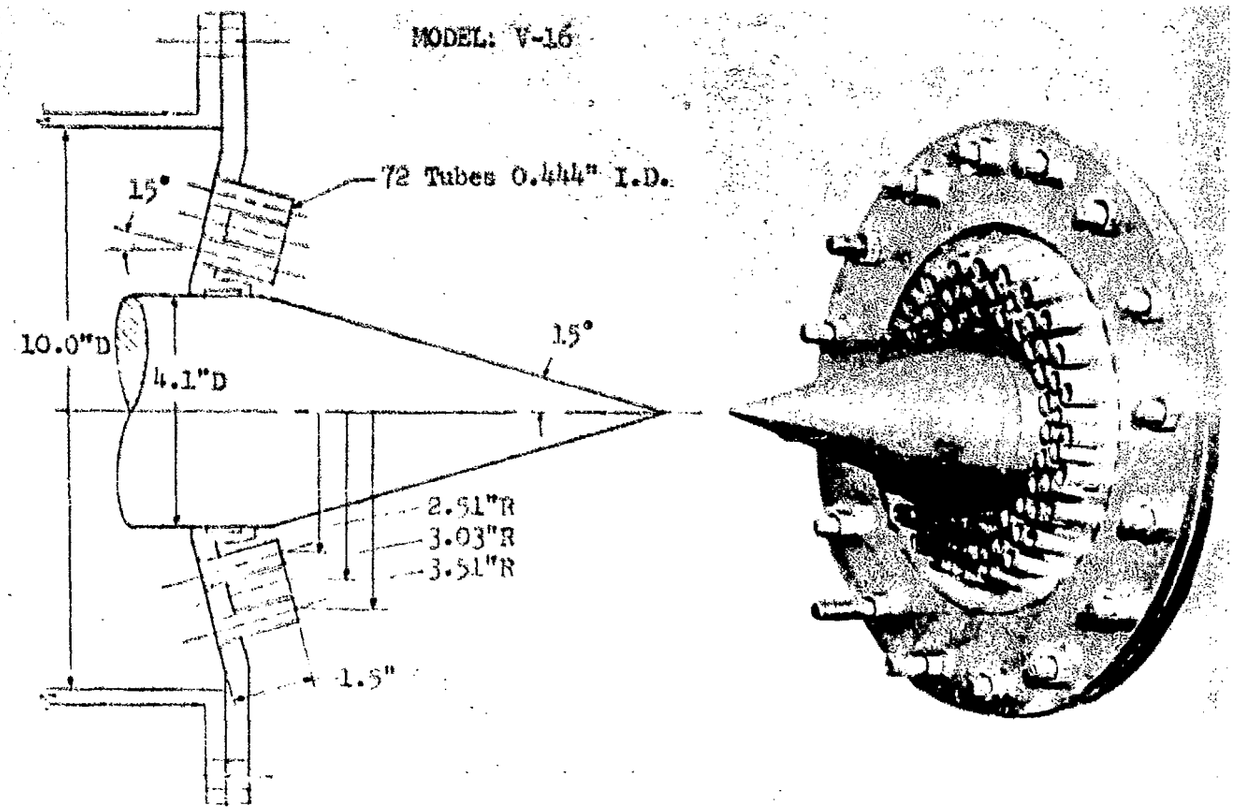
MODEL NO. V-1-3-4

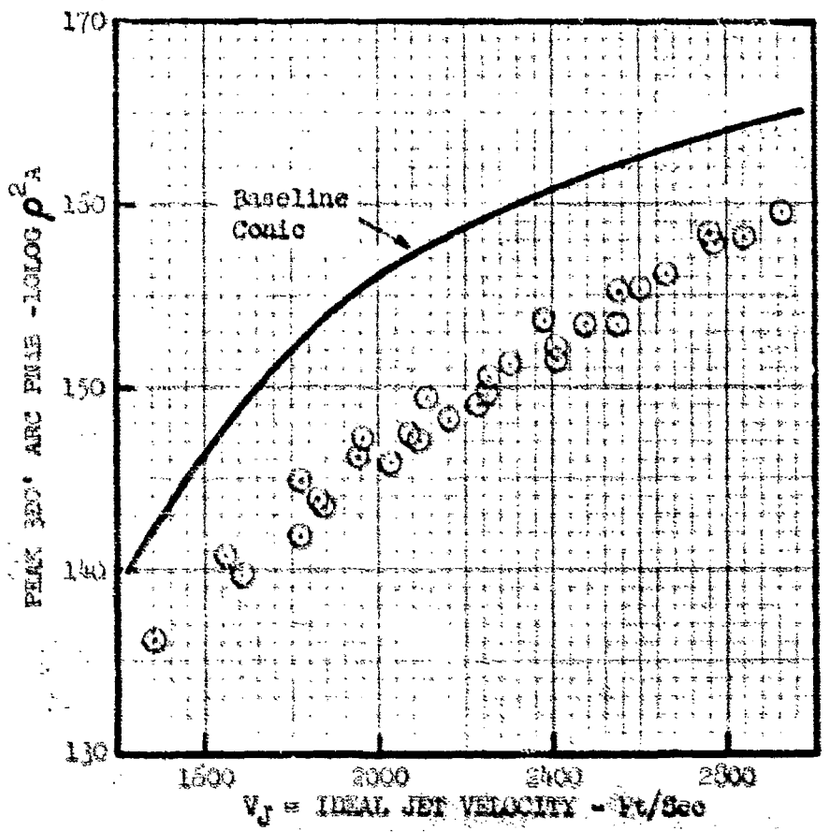
DESCRIPTION 30° PLUG, PRIMARY, SECONDARY SHROUDS, BLOW-IN-DOOR, 8 CHUTES, 95% PENETRATION

MODEL A_8 = .0677 FT.^{2}; FULL SCALE A_8 = 4.3328 FT.^{2}; SCALE FACTOR = 8:1

	TEST CONDITIONS					ACOUSTIC TEST RESULTS *								
										PNL DIRECTIVITY ON 320° ARC MEASURED FROM NOZZLE EXIT				
PNT NO.	V_8 (FPS)	P_{T8}/P_0	T_{T8} °R	IDEAL V_J FT/SEC	% BLEED W_B/W_8 x 100	PEAK PNdB ON 320° ARC	ANGLE OF MAX PNdB (DEG.)	$10\log\beta^2_A$	PEAK PNdB $-10\log\beta^2_A$	20°	30°	40°	50°	60°	70°
1	4.39	3.23	2305	2848		133.9	40	-26.0	159.9	130.1	133.1	133.9	133.1	130.6	128.0
2	4.77	3.53	2304	2939		135.1	40	-25.6	160.7	131.1	133.7	135.1	134.1	132.0	129.7
3	4.08	3.02	2307	2776		132.2	40	-26.2	158.4	129.0	131.8	132.2	131.5	130.2	127.6
4	3.28	2.52	2312	2567		129.3	40	-26.9	156.2	127.1	129.0	129.3	128.6	126.9	125.4
5	2.69	2.02	2314	2268		125.1	50	-27.5	152.6	121.6	123.5	124.1	125.1	124.5	123.1
6	4.33	3.23	2306	2848		134.2	40	-26.0	160.2	130.1	133.3	134.2	133.3	131.1	128.5

*Data Includes Ground Reflection Interference





DESCRIPTION

Model V-16 had a 30° conical plug with 72 tubes, .444" I.D., positioned around the annulus at 15° to axial (tubes parallel to the plug). No secondary shroud was used. Exit area, A_8 = .0774 Ft^2. Material: 321 s.s. Full scale A_8 = 4.9536 Ft^2. Scale factor = 8:1.

FIGURE V.H.1-22 HARDWARE, SCHEMATIC AND 320 FT. ARC JET NOISE LEVEL FOR MODEL V-16

TABLE V.H.1-23 TEST SUMMARY

MODEL NO. V-16

DESCRIPTION 72 TUBES AROUND ANNULUS SET PARALLEL TO 30° CONICAL PLUG

MODEL A_8 = .0774 FT.^{2}; FULL SCALE A_8 = 4.9536 FT.^{2}; SCALE FACTOR = 8:1

	TEST CONDITIONS					ACOUSTIC TEST RESULTS *									
RUN NO.	V_8 (FPS)	P_{T8}/P_o	T_{T8} °R	IDEAL V_J FT/SEC	% BLEED W_B/W_8 x 100	PEAK PWLB ON 320° ARC	ANGLE OF MAX PWLB (DEG.)	$10\log\beta^2_A$	PEAK PWLB $-10\log\beta^2_A$	PWL DIRECTIVITY ON 320° ARC MEASURED FROM NOZZLE EXIT					
										20°	30°	40°	50°	60°	70°
1	4.87	2.00	1000	1482		116.5	30	-19.6	136.1	116.2	116.5	116.4	115.3	114.0	113.3
2	5.96	2.49	1006	1684		120.7	40	-19.1	139.8	120.4	120.2	120.6	119.3	117.3	115.9
3	7.78	2.98	1000	1818		123.5	30	-18.4	141.9	123.5	123.5	123.1	121.0	119.3	117.5
4	3.60	2.00	1516	1822		121.6	40	-23.3	144.9	117.8	121.0	121.5	118.3	118.0	117.2
5	4.93	2.50	1512	2068		124.7	30	-22.6	147.3	123.3	124.7	123.8	122.9	120.9	119.4
6	5.86	3.00	1528	2252		127.5	30	-22.1	149.6	126.9	127.5	126.2	124.7	122.6	121.9
7	6.27	3.19	1520	2303		129.4	30	-21.8	151.2	127.1	129.4	128.2	126.2	124.7	122.7
8	6.83	3.48	1527	2380		131.2	30	-21.5	153.7	129.4	131.2	130.5	127.4	125.1	122.7
9	5.89	3.50	2045	2760		134.3	40	-24.0	158.3	130.2	132.4	134.3	132.5	128.1	125.9
10	5.39	3.19	2037	2664		131.8	40	-24.3	156.1	129.4	131.8	131.8	129.2	126.2	124.5
11	5.05	3.00	2044	2602		130.7	40	-24.6	155.3	126.1	130.3	130.7	127.9	125.7	123.5
12	4.24	2.51	2045	2409		126.2	30	-25.2	151.4	123.4	126.2	125.7	124.9	123.4	121.9
13	3.34	2.00	2043	2117		123.4	30	-25.9	149.3	119.7	123.4	122.6	120.8	120.0	120.0
14	3.09	2.00	2329	2258		123.6	40	-27.0	150.6	120.8	122.9	123.6	122.5	120.5	119.8
15	3.94	2.50	2307	2554		127.3	30	-26.3	153.3	125.2	127.3	127.3	126.3	124.3	122.1
16	4.65	2.98	2322	2771		132.2	40	-25.7	157.9	129.1	131.4	132.2	129.4	126.5	124.7
17	5.15	3.22	2303	2842		132.7	40	-25.4	158.1	127.8	131.7	132.7	131.2	127.8	126.2

*Data Includes Ground Reflection Interference

TABLE V.H.1-23 TEST SUMMARY

MODEL NO. V-16 (Cont.)

DESCRIPTION 72 TUBES AROUND ANNULUS SET PARALLEL TO 30° CONICAL PLUG

MODEL A_8 = .0774 FT.^{2}; FULL SCALE A_8 = 4.9536 FT.^{2}; SCALE FACTOR = 8:1

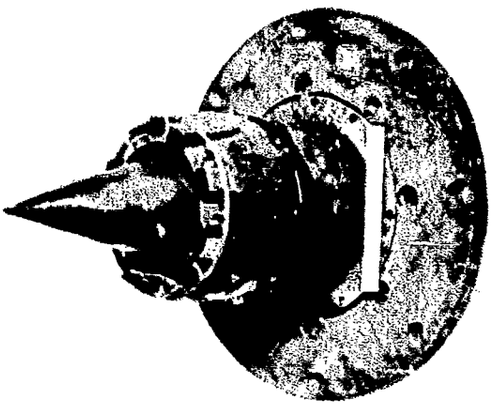
	TEST CONDITIONS					ACOUSTIC TEST RESULTS *								
										PNL DIRECTIVITY ON 320' ARC MEASURED FROM NOZZLE EXIT					
PDC NO.	V_8 (FPS)	P_{T8}/P_o	T_{T8} °R	IDEAL V_J FT/SEC	% BLEED W_B/W_8 x 100	PEAK PNdB ON 320' ARC	ANGLE OF MAX PNdB (DEG.)	$10LOG\beta^2 A$	PEAK PNdB $-10LOG\beta^2 A$	20°	30°	40°	50°	60°	70°
18	5.52	3.48	2317	2932		134.6	40	-25.1	159.7	129.8	132.8	134.6	133.0	129.3	126.6
19	6.31	3.49	1754	2554		132.5	40	-22.7	155.2	130.0	132.3	132.5	129.7	126.4	123.9
20	5.83	3.20	1756	2477		130.5	30	-23.0	153.5	128.6	130.5	129.6	127.2	125.0	123.0
21	5.38	3.00	1763	2416		128.9	30	-23.3	152.2	127.6	128.8	128.3	126.7	124.7	122.2
22	4.58	2.49	1762	2229		125.1	30	-23.9	149.0	124.1	125.1	124.6	123.7	122.7	121.2
23	3.62	2.00	1759	1962		122.6	30	-24.6	147.2	121.3	122.6	121.9	121.0	119.8	118.3
24	4.27	2.00	1246	1652		119.3	30	-21.6	140.9	117.9	119.3	118.8	117.7	116.4	115.1
25	5.37	2.50	1246	1876		122.6	30	-20.9	143.5	122.6	122.6	122.0	120.9	119.6	116.5
26	6.42	3.00	1246	2034		125.6	20	-20.3	145.9	125.8	125.6	124.9	123.7	121.5	119.7
27	6.80	3.19	1252	2090		127.0	20	-20.1	147.1	127.0	126.9	126.2	124.5	122.5	120.8
28	7.40	3.49	1255	2160		128.4	30	-19.8	148.2	127.9	128.4	127.8	126.1	123.6	121.5
29	6.20	3.49	1028	1955		128.1	20	-18.1	146.2	128.1	127.2	124.4	123.9	121.9	120.1
30	7.79	3.19	993	1861		125.8	20	-18.1	143.9	125.8	124.9	123.6	121.9	120.0	119.0

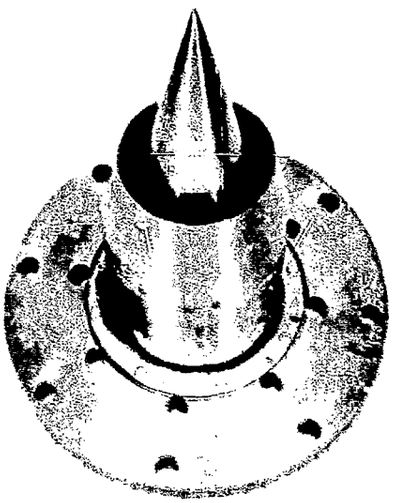
*Data Includes Ground Reflection Interference



MODEL V-2

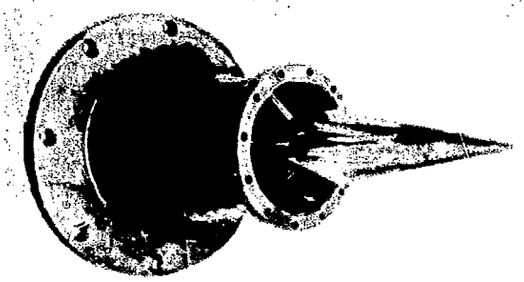
MODEL V-5





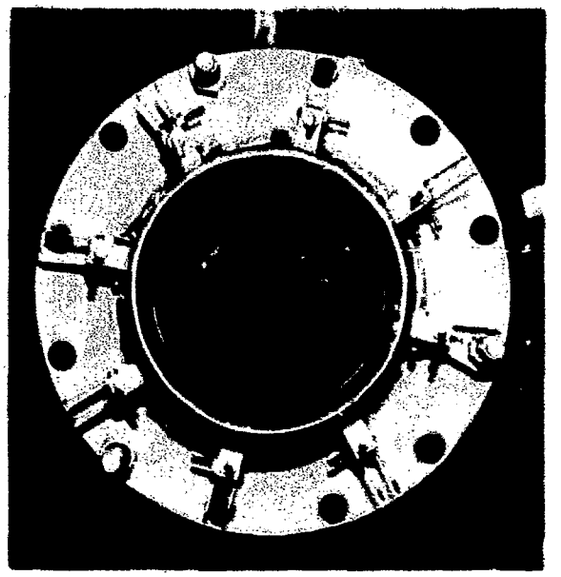
MODEL V-1

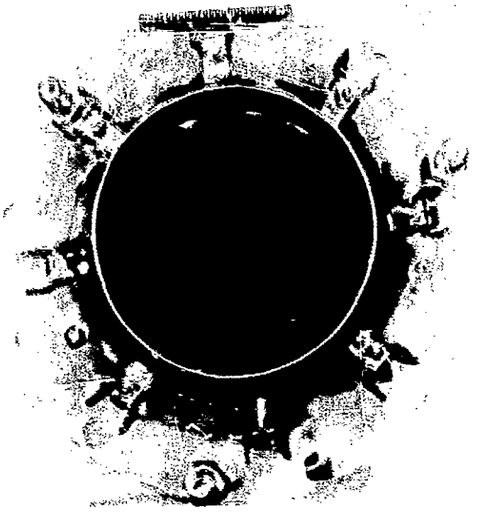
FIGURE V.E.1-23A REPRESENTATIVE CONFIGURATIONS OF ANNULAR PLUG SUPPRESSOR HARDWARE



MODEL V-8-1

MODEL V-1-3





MODEL V-1-3-4

FIGURE V.E.1-23 REPRESENTATIVE CONFIGURATIONS OF ANNULAR PLUG SUPPRESSOR HARDWARE

"PRECEDING PAGE BLANK-NOT FILMED."

V.H.2 MULTI-ELEMENT SPOKE/CHUTE MODEL SUPPRESSOR PARAMETRIC INVESTIGATIONS ON ANNULAR PLUG NOZZLES

"PRECEDING PAGE BLANK-NOT FILMED."

V.H.2 MULTI-ELEMENT SPOKE/CHUTE MODEL SUPPRESSOR PARAMETRIC INVESTIGATIONS ON ANNULAR PLUG NOZZLES

Introduction and Objectives of Test Series

During the latter phases of the Supersonic Transport development program, design studies of high-airflow engines and noise suppression systems were conducted, supported by scale model acoustic and aerodynamic test programs. The recommended engine configuration at the conclusion of the study was a high-airflow turbojet operating without augmentation at liftoff. The engine design was set near 800 pps weight flow and used an annular plug nozzle system. The suppressor concept which provided the most favorable combination of high jet noise suppression for given thrust penalty was in the form of multi-element spoke/chute geometry. The system could be designed to be most beneficial in the liftoff exhaust nozzle velocity range of 2300 to 2500 ft/sec for the high airflow engine.

An extensive model acoustic and aerodynamic static and wind tunnel test program was conducted to determine aero/acoustic performance of individual suppressor designs and to parametrically develop design guidelines. The guidelines were to be used to design a more refined spoke or chute annular plug jet suppressor for the production engine. This section presents the individual models' data and the summary design guidelines.

Test Configurations

o Acoustic

A total of twelve plug nozzle systems were tested at the General Electric, Evendale, JENOTS acoustic facility as per Table V.H.2-1, in addition to a baseline 5.7" D_8 conical nozzle. The twelve systems consisted of (9) multi-element spoke nozzles, (1) multi-element 32-chute nozzle, (1) 12 element deep chute nozzle and (1) baseline unsuppressed plug nozzle. The systems, with the exception of Model 11, simulated the GE4J6H2 exhaust nozzle design and were 1/8th scale of the full size engine design. The initial engine exhaust nozzle design utilized an annular convergent-divergent flowpath with variable flaps and a 10° half-angle plug. The plug would have overlapping leaves at the throat for variable throat areas and a contoured plug end. All the acoustic models

(with the exception of Model 11) simulated the annular convergent-divergent nozzle system with a 10° half-angle plug and contoured plug end. (All initial aerodynamic models, which were identical to the acoustic models, simulated the 10° half-angle plug system. Concurrent with the model aero/acoustic parametric test series, the engine exhaust nozzle design was being changed to a cylindrical translating shroud plug nozzle using a 15° half-angle plug of shorter length; still maintaining the plug variable at the throat area and retaining a contoured plug end. None of the acoustic test models simulated this new geometry, however, three aerodynamic multi-element suppressor nozzles and six non-suppressed plug nozzles were designed around the new cylindrical translating shroud 15° half-angle plug geometry and were aerodynamically tested at FluiDyne Engineering Corporation.)

The acoustic models were designed to investigate variations of spoke and chute geometric parameters, as closely as possible varying one parameter at a time. Doing so allowed acoustic and aerodynamic performance changes to be associated to physical changes so that design guidelines could be formulated.

Model 3 (Figure V.H.2-12) was the basic nozzle around which the geometric parameters were varied. It was an area ratio of 2.0 design and had 32 tapered-planform spokes mounted at 90° to the nozzle centerline. (Area ratio for the annular plug suppressors is defined as the ratio of total annulus area to physical flow area). By comparing other models to Model 3, five geometric parameters were investigated, consisting of 1) area ratio, 2) element number, 3) spoke angle-of-attack to the gas stream, 4) spoke planform shape, and 5) spoke versus chute. These nozzle sets and geometry variations are:

1) Area Ratio Variation - Models 6, 3, and 7 (Figures V.H.2-21, -12 and -24) holding constant a) element number of 32, and b) 90° mount angle to gas stream, while varying area ratio at settings of 1.5, 2.0 and 2.5 respectively.

2) Element Number Variation - Models 2, 3, 4 and 12 (Figures V.H.2-9, -12, -15, and -39) holding constant a) area ratio of 2.0, and b) mount angle to gas stream, while varying element number at settings of 24, 32, 48 and 64, respectively.

3) Spoke Angle-of-Attack Variation - Models 8, 3 and 9 (Figures V.H.2-27, -12, and -30) holding constant a) area ratio of 2.0, and b) element number of 32, while varying the spoke angle-of-attack to the gas stream at settings of 10° forward, normal to the nozzle centerline (90°), and 10° aft, respectively.

4) Spoke Planform Shape Variation - Models 3 and 5 (Figures V.H.2-12 and -18), holding constant a) area ratio of 2.0, b) element number of 32, and c) angle-of-attack to gas stream of 90°, while varying the spoke planform shape from tapered to parallel, respectively.

5) Spoke versus Chute - Models 3 and 10 (Figures V.H.2-12 and -33), holding constant a) area ratio of 2.0, b) element number of 32, c) angle-of-attack to gas stream, and d) planform shape, while changing from solid spoke to ventilated chute designs, respectively.

The remaining suppressor nozzle, Model 11 of Figure V.H.2-36, used a 10° half-angle pointed plug-end design which did not simulate the GE4-J6H2 engine exhaust nozzle geometry. It had 12 deeply ventilated chutes and was of area ratio of 3.0. The nozzle was a model simulation of a NASA, Cleveland J85 size suppressor and was tested as an individual configuration non-related to the parametric study.

Model 1 of Figure V.H.2-6 was the baseline unsuppressed plug nozzle, simulating the exhaust nozzle aerodynamic flowpath with the suppressors mechanism stowed. The multi-element suppressor would be deployed only during run-up, roll, lift-off and climb-out and then would retract within the plug centerbody for storage. The unsuppressed plug geometry was tested as a second baseline configuration to gauge its suppression merit against the industry-standard conical convergent nozzle.

The acoustic measurements at the General Electric, Evendale, JENOTS facility were on a 40 ft. arc at intervals of 10° from 30° (or 20°) through 160° to the exhaust axis. The GE4J6H2 engine running line was simulated over the cycle range of P_{T8}/P_o from 1.4 to 4.0, T_{T8} from 1275 to 2200° R and V_j from 1275 to 3000 ft/sec. Acoustic measurements were taken through 80 kHz, reduced to 1/3 octave band form and scaled by frequency and size to the GE4J6H2 engine

size, using a scale factor of 8:1. All data presented are therefore of simulated engine size and engine freqvency range.

o Aerodynamic

A second set of suppressor nozzles was manufactured with aerodynamically clean external flowpaths for wind tunnel testing at the FluiDyne Engineering Corporation. Testing for internal "static" performance and wind-on "installed" aerodynamic performance was done in FluiDyne's Channel 7 and 10 facilities. (see Section II.E, Volume I.) Sufficient configurations were selected to develop aerodynamic design guidelines to parallel those of the acoustic parametric study. These models were identical to the designs of the acoustic hardware (same model numbers and photographs used in the figures for model identification) based on the full scale annular convergent-divergent exhaust nozzle with a 10° half-angle plug and contoured plug end. The models included:

1) Area Ratio Variation - Models 6, 3 and 7
2) Element Number Variation - Models 2, 3 and 4
3) Spoke Angle-of-Attack Variation - Models 8, 3 and 9
4) Spoke Planform Shape Variation - Models 3 and 5
5) Spoke versus Chute - Models 3 and 10

The models were tested statically (external flow Mach number = 0) and with external flow at M_o = 0.36. A nozzle pressure ratio, P_{T8}/P_o, range of approximately 1.1 through 4.0 was investigated while at M_o = 0 and 0.36. Nozzle discharge coefficient, C_D, and thrust coefficient, C_{fg}, were determined.

In addition to the parametric series of aerodynamic tests, three other suppressed nozzles and six non-suppressed configurations were aerodynamically investigated. As mentioned previously, while the parametric study was in progress the fuel scale engine exhaust nozzle geometry was changed to a cylindrical, translating shroud plug nozzle using a 15° half-angle plug of shorter length, still maintaining the plug variable at the throat area and retaining the contoured plug end.

The three suppressor configurations were designed around this new geometry, (Models 20, 21 and 22 of Table V.H.2-1 and Figure V.H.2-58) and were tested aerodynamically only before contract termination in March, 1971. Two of the

configurations were chute designs, 32 and 24 chutes, respectively for Models 20 and 21, each at area ratio of 1.69; the highest area ratio feasible for storage of chutes within the plug centerbody. The third suppressor configurations, Model 22, was a low C_D spoke design, using 24 spokes at a physical area ratio of 1.38. The anticipated low C_D would provide a higher aerodynamic blockage and a higher effective area ratio with the low physical spoke area for less base drag performance loss.

Of the six non-suppressed model configuration, three were tested statically and with wind-on to determine nozzle performance at important unsuppressed flight points. They are Models 14, 15 and 16 of Figure V.H.2-59 and Table V.H.2-1; again all based on the cylindrical translating shroud 15° half-angle plug geometry. The three models simulated nozzle aerodynamic flowpaths at power cutback/approach (Model 14 at M_o = .36), hold/divert (Model 15 at M_o = 47/.90), and transonic acceleration (Model 16 at M_o = 1.1).

The remaining three non-suppressed model configurations, Models 17, 18, and 19 of Figure V.H.2-61 and Table V.H.2-1, were tested statically to determine supersonic cruise internal performance of the cylindrical translating shroud nozzle system as a function of shroud length.

Presentation and Discussion of Test Results

Presentation of acoustic and aerodynamic test results will be divided into three catgories; a) acoustic models, b) parametric acoustic/aerodynamic comparisons, and c) additional aerodynamic configurations.

o Acoustic Models

Presentation of the individual acoustic models' test results is done in Figures V.H.2-1 through V.H.2-41 and in Tables V.H.2-2 through V.H.2-14, as deliniated in the summary Table V.H.2-1.

The 5.7" D_8 conical convergent nozzle of Figure V.H.2-1 was tested on several days during the test series to establish the unsuppressed baseline to which the other nozzles are referred for suppression. The acoustic results, scaled to engine size, are presented in Table V.H.2-2 and plotted in Figures V.H.2-2, -3 and -4 as 320 ft. arc plus 300 and 1500 ft. sideline normalized peak

PNL as a function of ideal jet velocity. On Figures V.H.2-3 and -4 (lower half) are also plotted similar acoustic results from previous tests of the same baseline nozzle in 1969. Average baseline curves were drawn through the 1969 data (lower half) then transposed to the 1971 data plots (upper half). Baseline data repeated very well and substantiated the use of the average curves for comparison to all other test models. Figure V.H.2-5 presents 1500 ft. sideline PNL distribution as a function of angle from the jet exhaust, for the two test dates. Distribution is smooth as anticipated, except at high jet velocity where the supersonic jet shock tones are present.

Format for presentation of acoustic data for Models 1 through 12 is consistent for each model, as follows:

- Photograph and model description
- Tabulated test conditions and acoustic data summary
- 320 ft. arc normalized peak PNdB versus ideal V_j
- 300 ft. sideline normalized peak PNdB versus ideal V_j
- 1500 ft. sideline normalized peak PNdB versus ideal V_j
- 1500 ft. sideline PNL distribution with angle from jet exhaust

Tables and figures pertaining to individual models are summarized in Table V.H.2-1.

The data for the baseline unsuppressed plug nozzle, Model 1, presented in Figures V.H.2-6, -7 and -8, show that a previous supposition on plug nozzles seems valid in that a somewhat significant suppression level can be realized from a non-suppressed plug nozzle relative to a standard convergent nozzle. The level of suppression is dependent on the plug nozzle design geometry.

Data for the 12 chute/plug nozzle, Model 11, are shown in Figures V.H.2-36, -37 and -38 and indicate a significant suppression level can be attained by this design. Of particular interest is the non-drop-off characteristic of suppression at high jet velocity due to the high area ratio.

The data for the other nozzle systems are discussed in the following parametric acoustic/aerodynamic comparisons.

o Parametric Acoustic/Aerodynamic Comparisons

Results of the multi-element spoke and chute individual model acoustic and aerodynamic tests are presented in this section as parametric comparisons. The individual models' 300 and 1500 ft. sideline peak normalized PNL plots were used to generate PNL suppression curves and are included. The aerodynamic static and wind-on results are also included. Comparisons are presented for the five parametric categories as follows:

		Figures
1)	Area Ratio Variation	V.H.2-43 through -45C
2)	Element Number Variation	V.H.2-46 through -48C
3)	Spoke Angle-of-Attack Variation	V.H.2-49 through -51C
4)	Spoke Planform Shape Variation	V.H.2-52 through -54C
5)	Spoke versus Chute	V.H.2-55 through -57C

The first figure of each set includes model photographs and aerodynamic results for static, $M_o = 0$, and wind-on, $M_o = 0.36$. The second figure of each set compares 300 and 1500 ft. sideline peak PNL suppressions as a function of jet velocity and the specific geometric parameter. The third figure set compares 1500 ft. sideline spectra as a function of the geometric parameter at six incremental jet velocities, nominally from 1300 to 3000 ft/sec. Spectra for the baseline conical nozzle are also included at most jet velocities so that overall spectra suppression can be gauged.

Aerodynamic test results are presented as installed gross thrust coefficient, C_{fg}, not as a ΔC_{fg} referenced to an unsuppressed nozzle system. As a gauge of the true thrust decrement due to the suppressor design, Figure V.H.2-42 presents the baseline unsuppressed plug results for Model 15 at $M_o = 0.0$ and 0.47. The design of Model 15 (see Figures V.H.2-59 and -60) simulated the engine exhaust nozzle flowpath at hold, $M_o = 0.47$, and divert, $M_o = 0.90$, however, the unsuppressed nozzle flowpath at takeoff would be nearly identical. Therefore the presented results would be an accurate baseline at $M_o = 0$ and can be interpolated for $M_o = 0.36$, at which the suppressed nozzles were tested. Thus, a gauge of thrust decrement attributable solely to the suppressor design can be had by comparing

the individual models' gross thrust coefficients to those presented in Figure V.H.2-42.

The area ratio comparison curves of Figure V.H.2-44 (as well as those of later curves) show that high levels of PNL suppression can be attained through use of multi-element annular plug suppressor systems. The trends at the 300 and 1500 ft. sidelines are similar to those previously measured in the multi-tube suppressor series (see Figures V.F.9-20 and -21), with the velocity at which peak suppression occurs increasing with higher area ratio. The area ratio of 2.0 model has the best suppression characteristics except at high jet velocities, where area ratio of 2.5 was optimum. The area ratio of 1.5 model gave lower suppression at all velocities. This model, however, had spokes with somewhat less taper than the other models and this may have contributed somewhat to its poorer than anticipated low velocity suppression.

Figure V.H.2-43 presents the static performance (M_o = 0.0) and effect of external Mach number on installed performance, as a function of area ratio and primary nozzle pressure ratio. The results clearly indicate the necessity for simulating the proper external Mach number in order to obtain meaningful aerodynamic performance data. At M_o = 0.36, the increase in area ratio quite rapidly decreased thrust coefficients due to the larger blockage area and longer spokes. The larger and longer spokes allowed for greater base area, particularly near the center of the nozzle, to which ambient air is not pumped for ventilation. The low base pressure on the spokes creates the largest portion of thrust loss in the form of base drag. The low pressure, combined with the larger base area, resulted in significant performance loss with increased area ratio.

Effect of element number on PNL suppression, Figure V.H.2-47, again shows trends similar to the multi-tube suppressor series (see Figures V.F.9-35 and -36). Peak suppression increases with greater number of elements but at high pressure ratio and velocity, the smaller spacing between flow elements, associated with greater element numbers, appears to be acoustically detrimental. This is due to the separate flows coalescing too early at the high pressure ratios, the noise then being dominated by the coalesced jet still at high jet velocity.

Figure V.H.2-46 shows the effect of element number on static and M_o = 0.36 performance. Each configuration had the same flow and blockage area. As the number of elements decreased the individual element width decreased, lowering pressures on the element base considerably. This results from the flow coalescing in a shorter distance downstream of the base.

Effect of spoke angle-of-attack variation is shown acoustically in Figure V.H.2-50 and aerodynamically in Figure V.H.2-49. The shift of velocity at which peak suppression occurs suggests a relationship similar to an area ratio effect. Directing the flow down the plug (Model 8 with spokes 10° forward = normal to the 10° half-angle plug) gives peak suppression at a low jet velocity. In this case the flow simulates a low area ratio and individual jet streams tend to coalesce close to the nozzle exit plane. Aerodynamic performance with this model is seen to improve over the basic Model 3 nozzle, as directing the flow parallel to the plug surface pressurizes the plug. As the flow angle was increased relative to the plug surface, the static pressures on the plug surface decreased immediately aft of the suppressor throat. The decreased plug pressure was reflected in base pressure on the suppressor elements, resulting in higher base drag and lower performance. The spokes at 90° to the axis (Model 3) and 10° aft (Model 9) simulate an increased area ratio since the flow is initially spreading out from the plug. The highest suppression is thus realized from the 10° aft model.

Results from variation of spoke planform shape from tapered of Model 3 to parallel-sided of Model 5 are shown as an acoustic comparison in Figure V.H.2-53 and an aerodynamic comparison in Figure V.H.2-52. Parallel-sided spokes gave somewhat greater high velocity PNL suppression than the tapered spokes of the same area ratio. With the tapered spokes the spacing between flow elements close to the plug is smaller, causing the core flow to coalesce quicker at high pressure ratio/jet velocity. Suppression capability is thus lowered. Aerodynamic loss is much higher for the parallel sided spoke due to the greater base area at deeper penetration where base pressures are lower.

Acoustic comparison of the ventilated chute (Model 10) versus the solid spoke (Model 3) of Figure 4.H.2-56 indicates the entrained secondary flow through the open-ended chutes was only slightly beneficial acoustically. Aerodynamically, as seen in Figure V.H.2-55, the chutes are far superior due to higher base

pressure and corresponding lower base drag. These trends are similar to those noted for multi-tube suppressors where tube length was investigated. The higher ambient pumping rate through a bundle of long tubes was only slightly beneficial acoustically but considerably increased base pressures, lowering the accompanying base drag and resultant thrust decrement.

o Additional Aerodynamic Configurations

As discussed earlier, while the parametric study was in progress, the full scale engine exhaust nozzle geometry was changed from a convergent-divergent flow path with a 10° half-angle plug to a cylindrical translating shroud flowpath using a 15° half-angle plug. Three additional suppressor configurations were designed around this new geometry and tested aerodynamically before contract termination in March, 1971. Acoustic models were not finalized, so only aerodynamic static and wind-on data are available. Figure V.H.2-58 presents a photograph and test results. Models 20 and 21 were of 32 and 24 chute designs, respectively; each at area ratio of 1.69. The third configuration, Model 22, was a low discharge coefficient (C_D) design, using 24 "V" shaped spokes mounted backwards within an area ratio of 1.38 design. Both static and wind-on aerodynamic results were very promising.

The unsuppressed nozzle configurations of Figure V.H.2-59 were tested statically and with wind-on to determine the basic nozzle system aerodynamic performance at other critical mission points. The nozzles are designed around the cylindrical translating shroud concept with a 15° half-angle plug and simulate exhaust areas and flowpaths at power cutback/approach (Model 14 at M_o = 0.36), hold/divert (Model 15 at M_o = 0.47/0.90), and transonic acceleration (Model 16 at M_o = 1.1). The nozzles were tested at M_o = 0 and at their respective design M_o's and results are presented in Figure V.H.2-60.

The remaining three unsuppressed models are shown in Figure V.H.2-61, along with their aerodynamic test results. They are Models 17, 18, and 19, designed with the exhaust nozzle flowpath geometry at supersonic cruise. They have shroud lengths to simulate full scale dimensions of 18.3", 44.0", and 61.0", respectively. They were tested statically (M_o = 0) to determine the optimum shroud length for best internal nozzle performance at the supersonic cruise nozzle setting. A full scale 44" long shroud was selected as giving the best trade of performance for weight.

A summary of aerodynamic performance results for all test models is included in tabulated form as Table V.H.2-15. In addition to the thrust coefficient data, which has been plotted on the enclosed figures, the table also has nozzle discharge coefficients, C_D.

TABLE V.H.2-1 SUMMARY OF ACOUSTIC AND AERODYNAMIC MODEL SPOKE/CHUTE AND UNSUPPRESSED CONFIGURATIONS

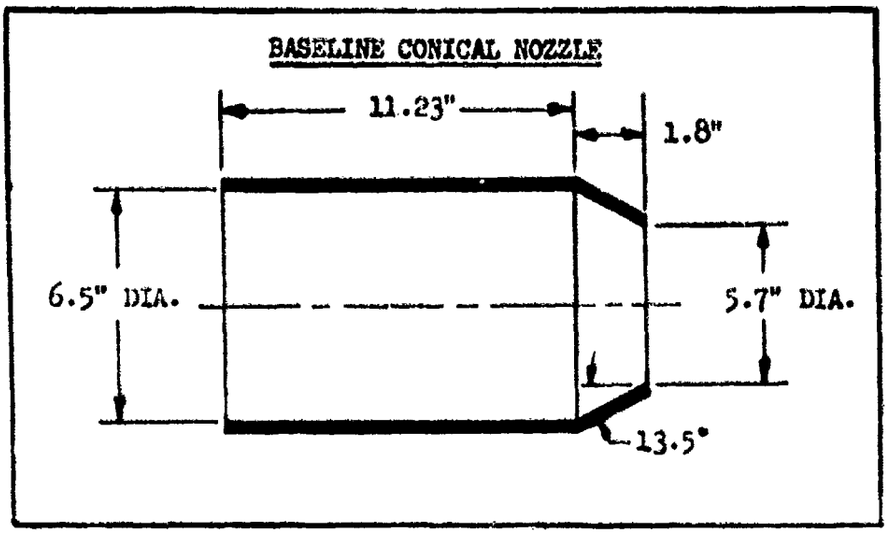
MODEL NO.	ACOUSTIC	AERODYNAMIC	DESCRIPTION	FIGURE NO.	TABLE NO.
5.7	X		Baseline 5.7" I.D. Conic Nozzle	V.H.2-1,-5	V.H.2-2
1	X		Unsuppressed Plug Nozzle	V.H.2-6,-8	V.H.2-3
2	X	X	24 Tapered Spokes @ 90°, A/R = 2.0	V.H.2-9,-11	V.H.2-4,*
3	X	X	32 Tapered Spokes @ 90°, A/R = 2.0	V.H.2-12,-14	V.H.2-5,*
4	X	X	48 Tapered Spokes @ 90°, A/R = 2.0	V.H.2-15,-17	V.H.2-6,*
5	X	X	32 Parallel Spokes @ 90°, A/R = 2.0	V.H.2-18,-20	V.H.2-7,*
6	X	X	32 Tapered Spokes @ 90°, A/R = 1.5	V.H.2-21,-23	V.H.2-8,*
7	X	X	32 Tapered Spokes @ 90°, A/R = 2.5	V.H.2-24,-26	V.H.2-9,*
8	X	X	32 Tapered Spokes @ 10° Fwd., A/R = 2.0	V.H.2-27,-29	V.H.2-10,*
9	X	X	32 Tapered Spokes @ 10° Aft, A/R = 2.0	V.H.2-30,-32	V.H.2-11,*
10	X	X	32 Tapered Chutes @ 90°, A/R = 2.0	V.H.2-33,-35	V.H.2-12,*
11	X		12 Chutes (NASA), A/R = 3.0	V.H.2-36,-38	V.H.2-13
12	X		64 Parallel Spokes @ 90°, A/R = 2.0	V.H.2-39,-41	V.H.2-14
14		X	Unsuppressed 15° Half-Angle Plug Cutback/Approach, M_O = .30	V.H.2-59,-60	*
15		X	Unsuppressed 15° Half-Angle Plug Hold/Divert, M_O = .47/.90	V.H.2-59,-60	*
16		X	Unsuppressed 15° Half-Angle Plug Transonic Accel, M_O = 1.1	V.H.2-59,-60	*
17		X	Unsuppressed 15° Half-Angle Plug Supersonic Cruise, Shroud Length = 18.3"	V.H.2-61	*
18		X	Unsuppressed 15° Half-Angle Plug Supersonic Cruise, Shroud Length = 44"	V.H.2-61	*
19		X	Unsuppressed 15° Half-Angle Plug Supersonic Cruise, Shroud Length = 61"	V.H.2-61	*

* All Aerodynamic Data Are Tabulated in Table V.H.2-15

TABLE V.H.2-1 (Cont.) SUMMARY OF ACOUSTIC AND AERODYNAMIC MODEL SPOKE/CHUTE AND UNSUPPRESSED CONFIGURATIONS

MODEL NO.	ACOUSTIC	AERODYNAMIC	DESCRIPTION	FIGURE NO.	TABLE NO.
20		X	32 Chutes Slanted 15° Forward, A/R = 1.69	V.H.2-58	*
21		X	24 Chutes Slanted 15° Forward, A/R = 1.69	V.H.2-58	*
22		X	24 Low C_D Spokes Slanted 15° Forward, A/R = 1.38	V.H.2-58	*

* All Aerodynamic Data Are Tabulated In Table V.H.2-15



The conical nozzle used as a baseline for this series of annular plug nozzle tests had a convergent section with a 5.713" I.D. Exit Area, A8 = 25.63 in^2, Material: 304 S.S.

TABLE V.H.2-2 TEST SUMMARY

MODEL NO. 5.7 Cone

DESCRIPTION: ● 5.7" I.D. Conical Convergent Baseline Nozzle

DATE: 1-6-71

SCALE MODEL A_8 = 25.63 in^2

FULL SCALE A_8 = 11.33 ft^2

SCALE FACTOR = 8:1

○ DATA INCLUDES GROUND REFLECTION INTERFERENCE

○ ANGLE REFERENCED TO JET EXHAUST

TEST CONDITIONS							ACOUSTIC TEST RESULTS								
								300 FT. ARC		300 FT. SIDELINE		1500 FT. SIDELINE		3128 FT. SIDELINE	
RUN NO.	P_0 PSIA	P_{T8} PSIA	P_{T8}/P_0	T_{T8} °R	IDEAL V_j FT/SEC	W_8 PPS	$10\log_{10}A$	PEAK PNdB	PEAK ANGLE	PEAK PNdB	PEAK ANGLE	PEAK PNdB	PEAK ANGLE	PEAK PNdB	PEAK ANGLE
1	14.620	21.767	1.488	1491	1297	8.07	-4.3	118.8	30	116.5	60	100.6	60	96.7	60
2	14.619	24.535	1.680	1534	1496	8.92	-4.3	124.3	30	120.6	60	104.7	60	101.2	60
3	14.617	27.086	1.853	1571	1620	9.52	-4.5	129.7	30	125.1	60	109.8	60	106.3	60
4	14.617	30.175	2.064	1632	1848	10.50	-4.5	133.6	40	129.5	60	113.9	60	109.9	60
5	14.614	33.251	2.275	1550	2014	11.20	-4.6	137.5	40	133.1	60	117.5	60	113.6	60
6	14.614	36.206	2.477	1636	2145	11.96	-4.6	138.2	50	136.0	50	120.3	50	116.4	50
7	14.617	39.747	2.719	1753	2317	12.81	-4.7	139.8	50	137.7	50	121.9	50	118.0	50
8	14.617	44.319	3.032	1884	2489	13.74	-4.6	143.1	50	140.9	50	125.6	50	121.9	50
9	14.617	48.910	3.346	1955	2659	14.63	-4.6	143.6	50	141.2	50	125.8	50	122.2	50
12	14.616	48.483	3.316	1793	2558	15.17	-4.2	143.7	50	141.6	50	126.3	50	122.5	50

FIGURE V.H.2-1 BASELINE CONICAL NOZZLE SCHEMATIC AND TEST SUMMARY

TABLE V.E.2-2 (Cont.) TEST SUMMARY

MODEL NO. 5.7 Cone

DESCRIPTION: ● 5.7" Conical Convergent Baseline Nozzle

DATE: 2-24-71

SCALE MODEL A_8 = 25.63 in^2

FULL SCALE A_8 = 11.39 ft^2

SCALE FACTOR = 8:1

● DATA INCLUDES GROUND REFLECTION INTERFERENCE

● ANGLE REFERENCED TO JET EXHAUST

TEST CONDITIONS							ACOUSTIC TEST RESULTS								
								320 FT. ARC		300 FT. SIDELINE		1500 FT. SIDELINE		2128 FT. SIDELINE	
PNT. NO.	P_0 PSIA	P_{T8} PSIA	P_{T8}/P_0	T_{T8} °R	IDEAL V_j FT/SEC	W_8 PPS	10Log/A	PEAK PNdB	PEAK ANGLE	PEAK PNdB	PEAK ANGLE	PEAK PNdB	PEAK ANGLE	PEAK PNdB	PEAK ANGLE
3	14.416	22.182	1.539	1271	1337	8.16	-4.1	118.8	30	115.1	30	99.8	30	94.1	30/65
4	14.416	24.501	1.700	1329	1509	8.83	-4.2	123.8	30/40	119.9	40	105.2	40	101.7	40
5	14.416	26.728	1.854	1416	1672	9.35	-4.4	128.9	30	124.4	40	109.5	40	105.9	40
6	14.416	29.515	2.047	1485	1834	10.66	-4.5	134.0	40	129.4	40	114.7	40	111.1	40
7	14.416	32.736	2.271	1587	2017	10.70	-4.6	136.6	40/50	134.4	50	118.5	50	114.7	50
8	14.413	35.916	2.492	1642	2153	11.60	-4.6	139.2	50	137.0	50	120.7	50	116.7	50
9	14.413	39.599	2.747	1756	2330	12.11	-4.6	141.2	50	139.0	50	122.8	50	118.8	50
10	14.413	43.696	3.032	1859	2498	12.99	-4.6	143.0	40	140.5	50	124.3	50	120.3	50
11	14.416	43.827	3.040	1958	2566	12.49	-4.8	141.5	50	141.3	50	125.3	50	121.3	50
12	14.403	44.613	3.097	2086	2669	12.43	-5.1	144.1	50	141.9	50	126.2	50	122.5	50

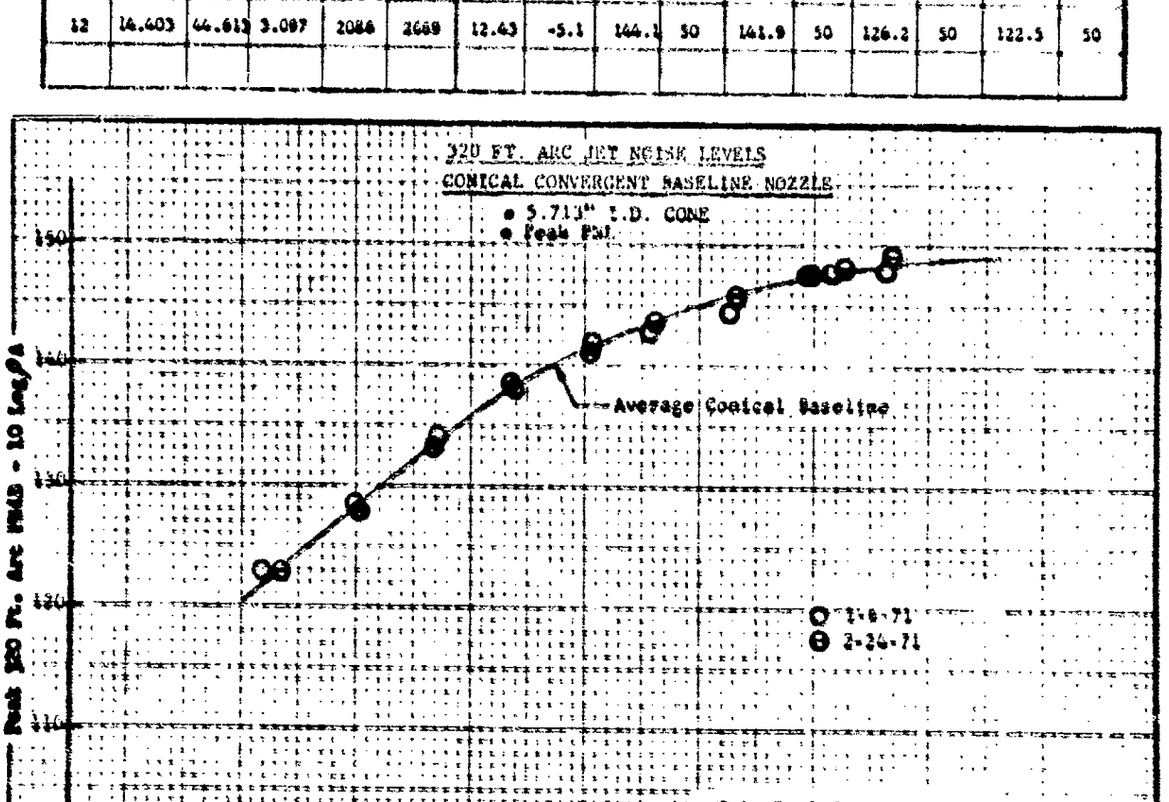
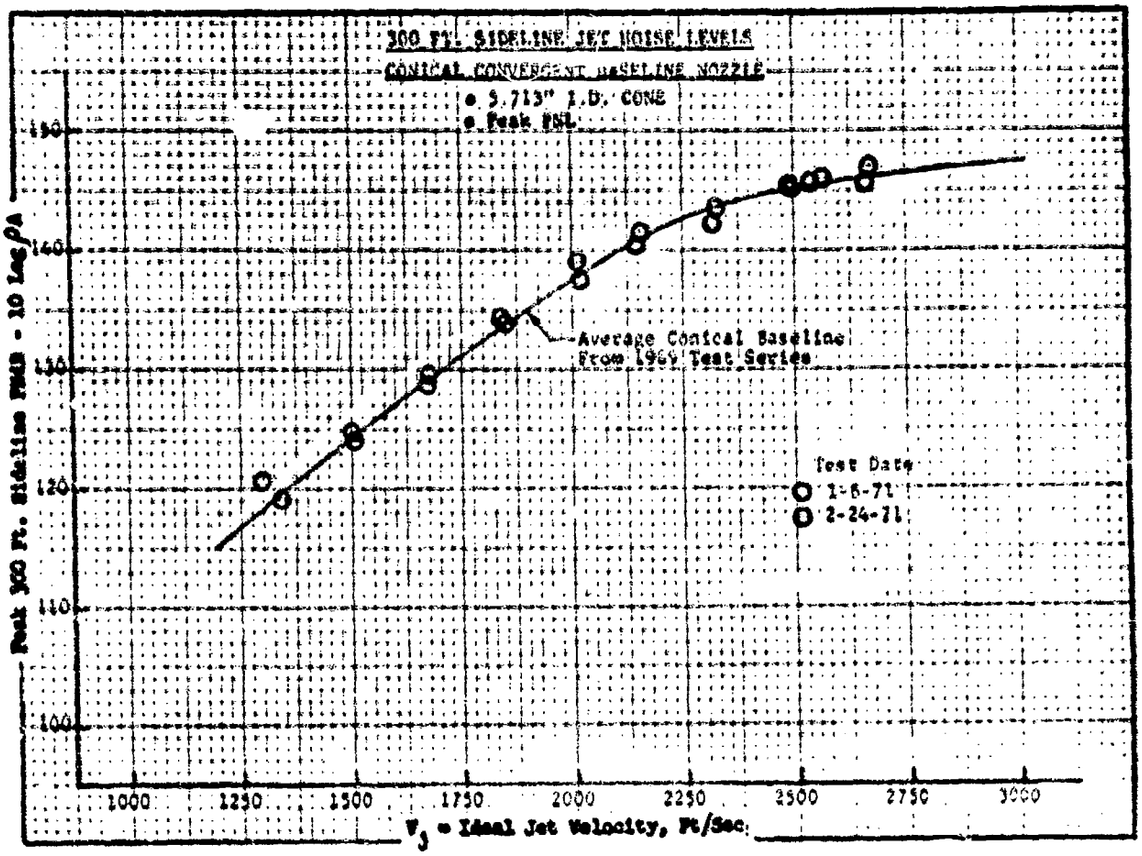


FIGURE V.E.2-2 CONICAL TEST SUMMARY AND BASELINE 320 FT ARC JET NOISE LEVELS



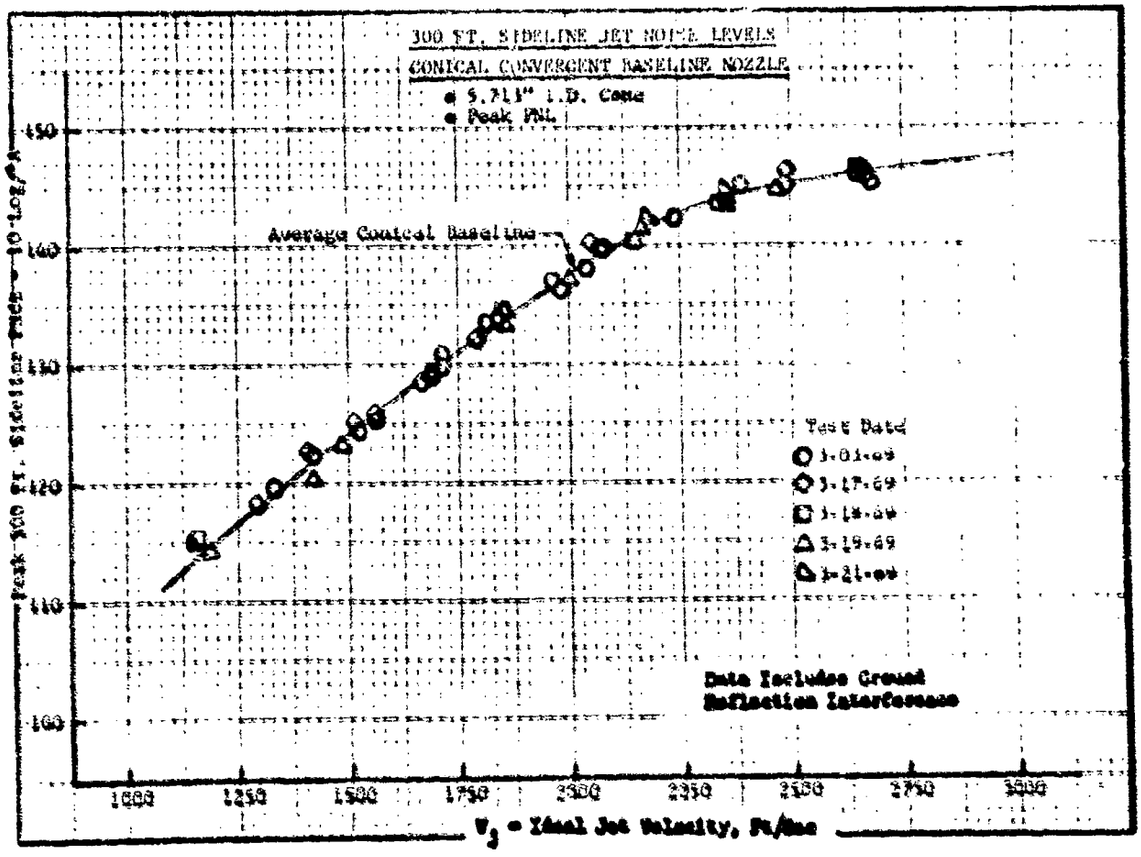
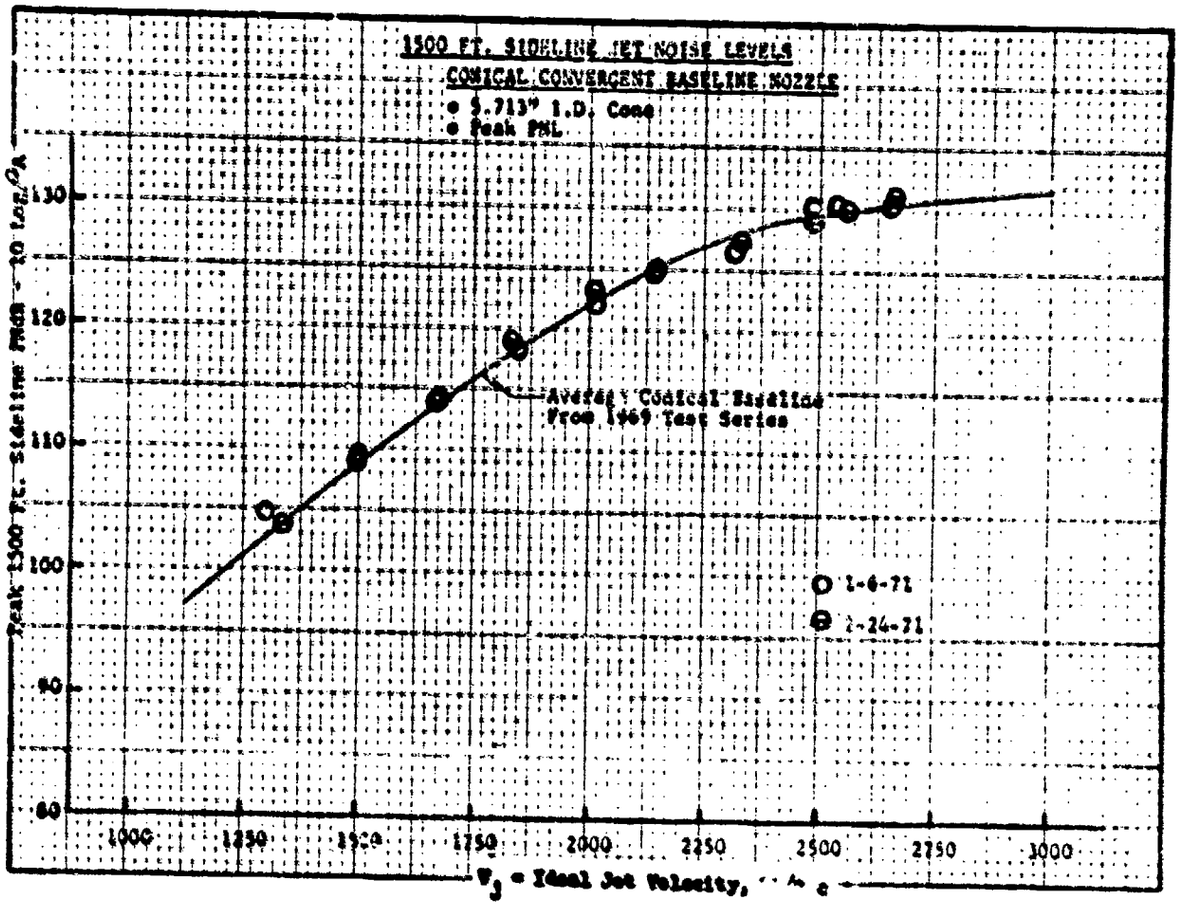


FIGURE V.H.2-3 BASELINE 300 FT SIDELINE JET NOISE LEVELS FROM 1971 AND 1969 TESTS



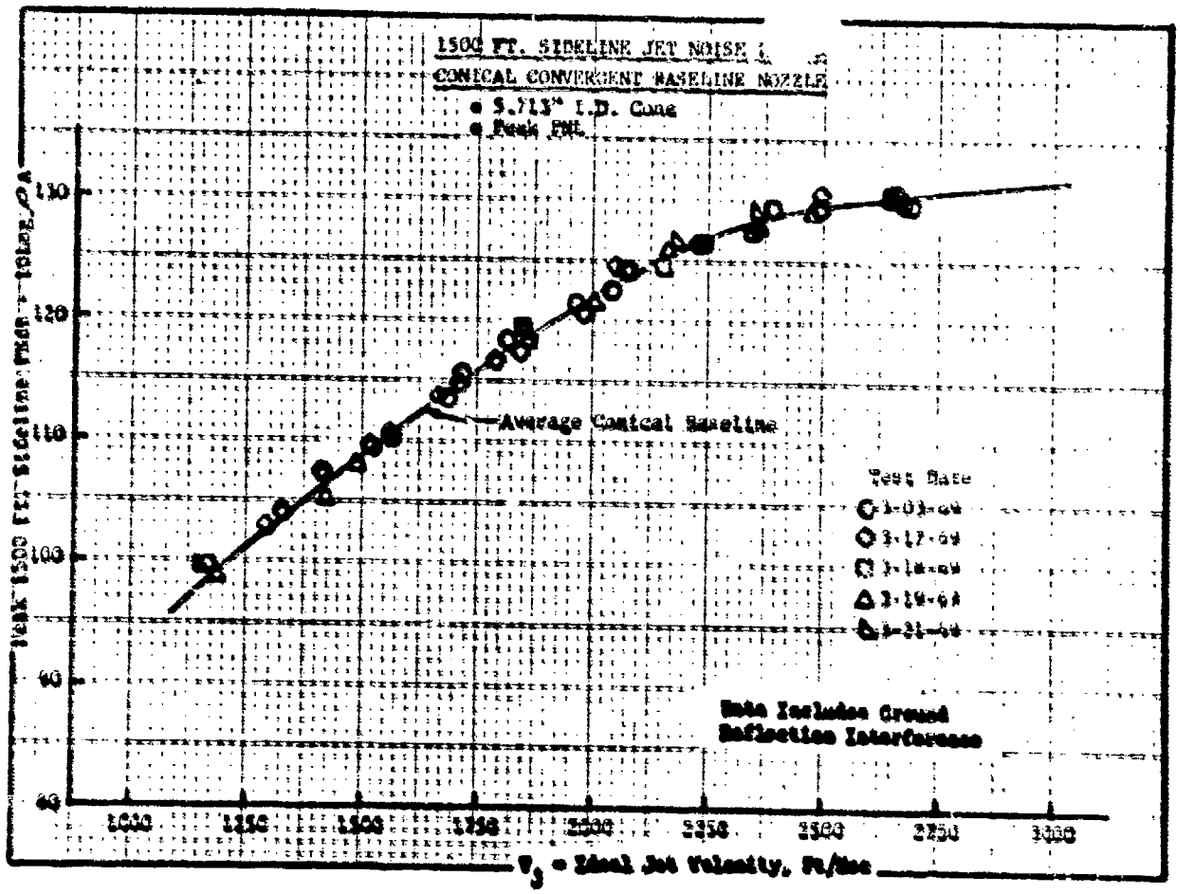
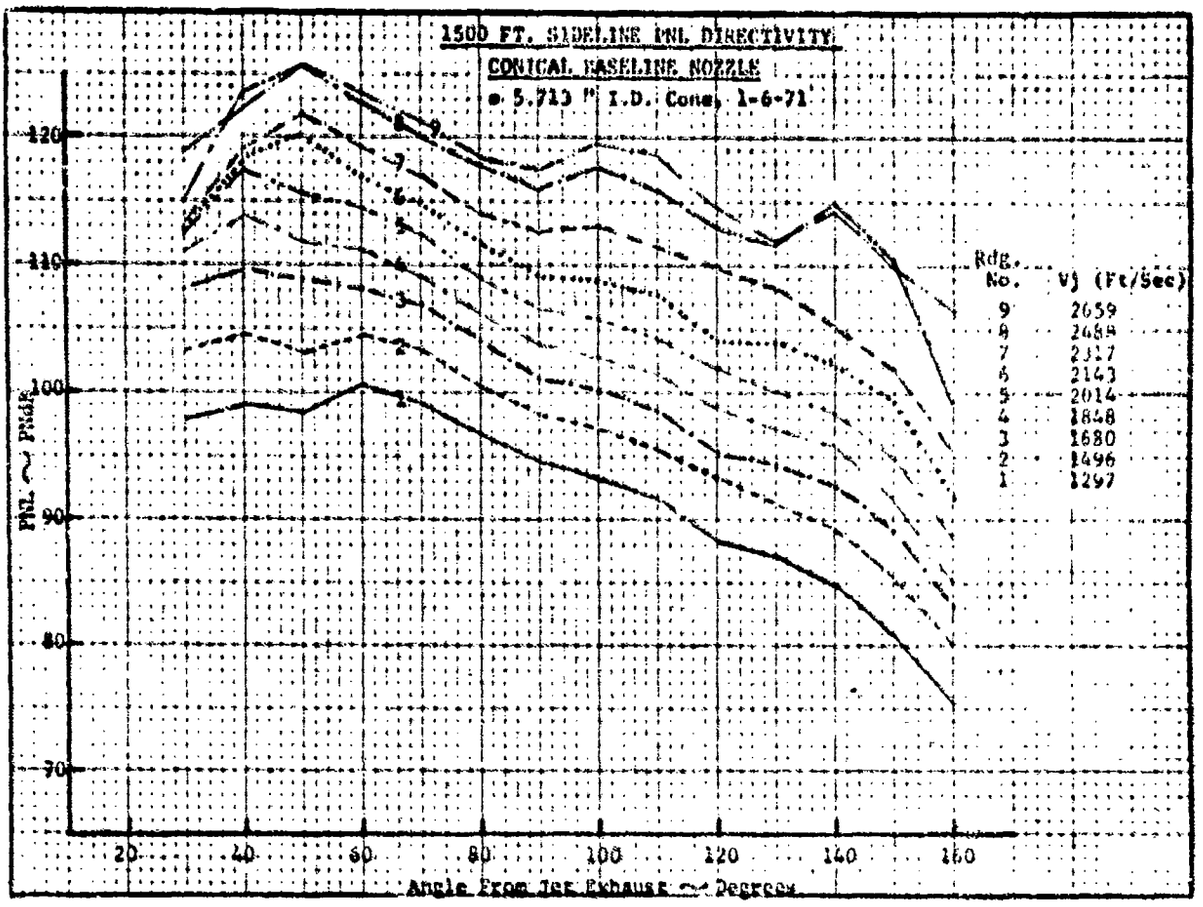


FIGURE V.H.2-4 BASELINE 1500 FT SIDELINE JET NOISE LEVELS FROM 1971 AND 1969 TESTS



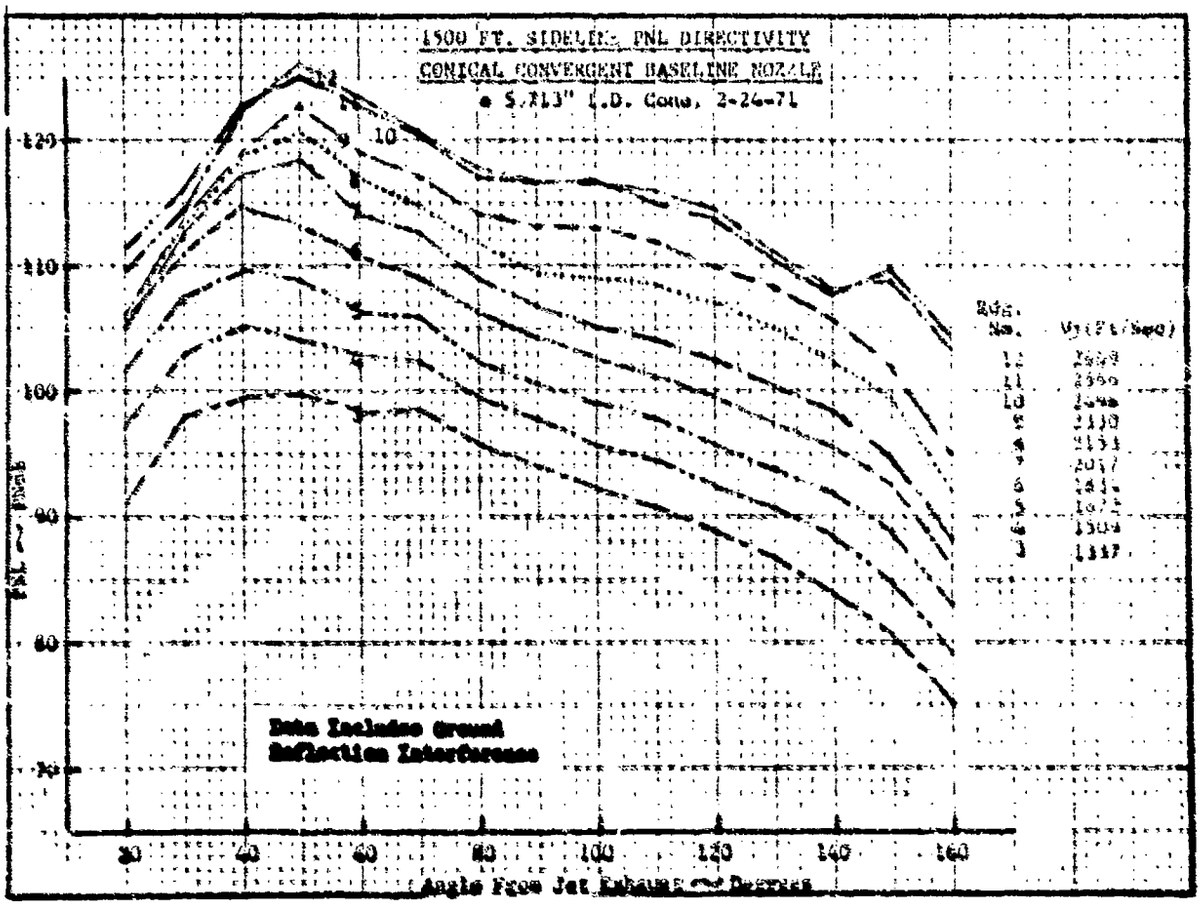
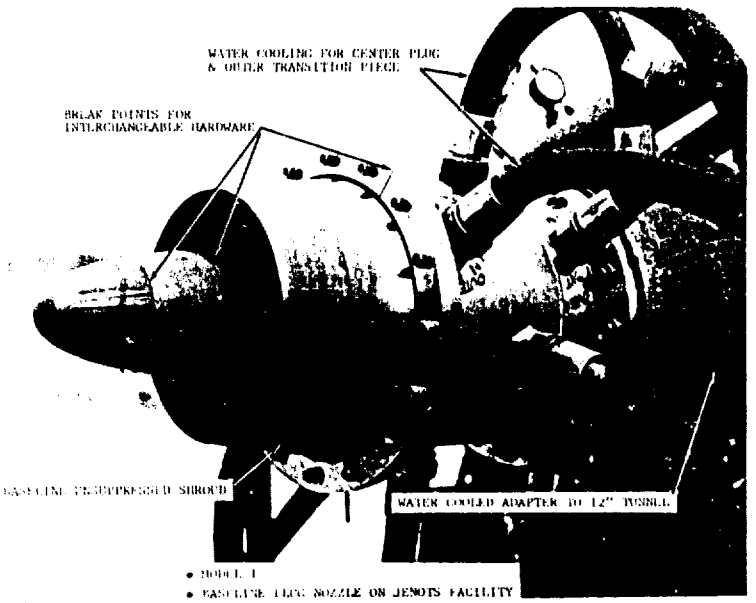


FIGURE V.B.2-5 BASELINE 1500 FT SIDELINE PNL DIRECTIVITY FROM 1971 TESTS



Model 1 was the baseline plug nozzle having an unsuppressed conical primary shroud and a center plug with a 20° cone angle (10° half angle). Both the primary shroud and center plug were water cooled. Exit Area, A_8 = 37.5 in.^{2}, Material: 304 S.S. for both plug and shroud.

TABLE V.H.2-3 TEST SUMMARY

MODEL NO. 1

SCALE MODEL A_8 = 37.5 in.^{2}

DESCRIPTION: Baseline Plug Nozzle With Shroud, 10° Half Angle Plug

FULL SCALE A_8 = 16.67 ft.^{2}

DATE: 1-08-71

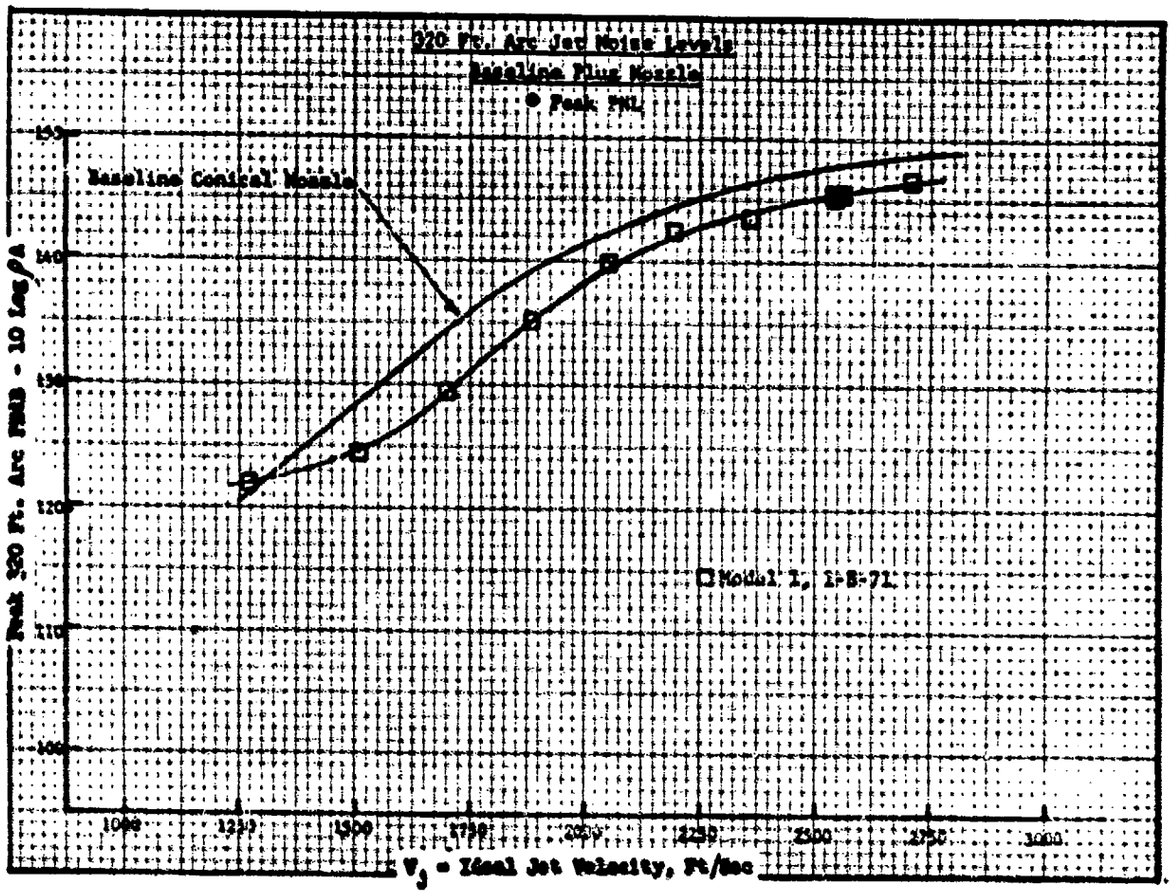
SCALE FACTOR = 8:1

o DATA INCLUDES GROUND REFLECTION INTERFERENCE

o ANGLE REFERENCED TO JET EXHAUST

TEST CONDITIONS							ACOUSTIC TEST RESULTS									
								300 FT. ARC		300 FT. SIDELINE		1500 FT. SIDELINE		2128 FT. SIDELINE	
RDG. NO.	P_0 PSIA	P_{T8} PSIA	P_{T8}/P_0	T_{T8} °R	IDEAL V_j FT/SEC	W_8 PTS	$\Delta C_{L_{OS}}/\rho A$	PEAK PNLB	PEAK ANGLE	PEAK PNLB	PEAK ANGLE	PEAK PNLB	PEAK ANGLE	PEAK PNLB	PEAK ANGLE
1	14.560	21.450	1.473	1277	1274	12.16	-2.5	119.5	60	119	70	102.7	70	98.7	70
2	14.549	24.794	1.704	1325	1510	12.97	-2.5	122.1	60	121.7	70	105.3	70	101.3	70
3	14.544	27.307	1.878	1438	1701	13.49	-2.8	126.6	30	124.9	60	108.4	60	104.3	60
4	14.540	30.713	2.112	1508	1885	14.76	-2.8	132.4	40	128.4	40	113.1	40	109.4	40
5	14.538	34.108	2.346	1585	2051	15.77	-2.8	137.1	40	133.1	40	117.6	40	113.9	40
6	14.537	37.297	2.566	1658	2195	16.92	-2.9	139.5	40	135.5	40	119.9	40	116.2	40
7	14.529	41.106	2.829	1753	2358	18.28	-2.9	140.5	40	136.4	40	121.6	50	117.6	50
8	14.533	45.885	3.157	1871	2546	19.65	-2.9	142.2	50	140	50	123.9	50	120	50
9	14.526	50.263	3.460	1976	2705	20.77	-2.8	143.7	50	141.5	50	125.6	50	121.7	50
10	14.531	55.029	3.787	1667	2560	24.81	-1.8	143.8	50	141.6	50	125.7	50	121.8	50
11	14.525	60.966	4.197	1534	2535	28.58	-1.2	144.3	50	142.2	50	126.2	50	122.4	50

FIGURE V.H.2-6 HARDWARE AND TEST SUMMARY FOR MODEL 1



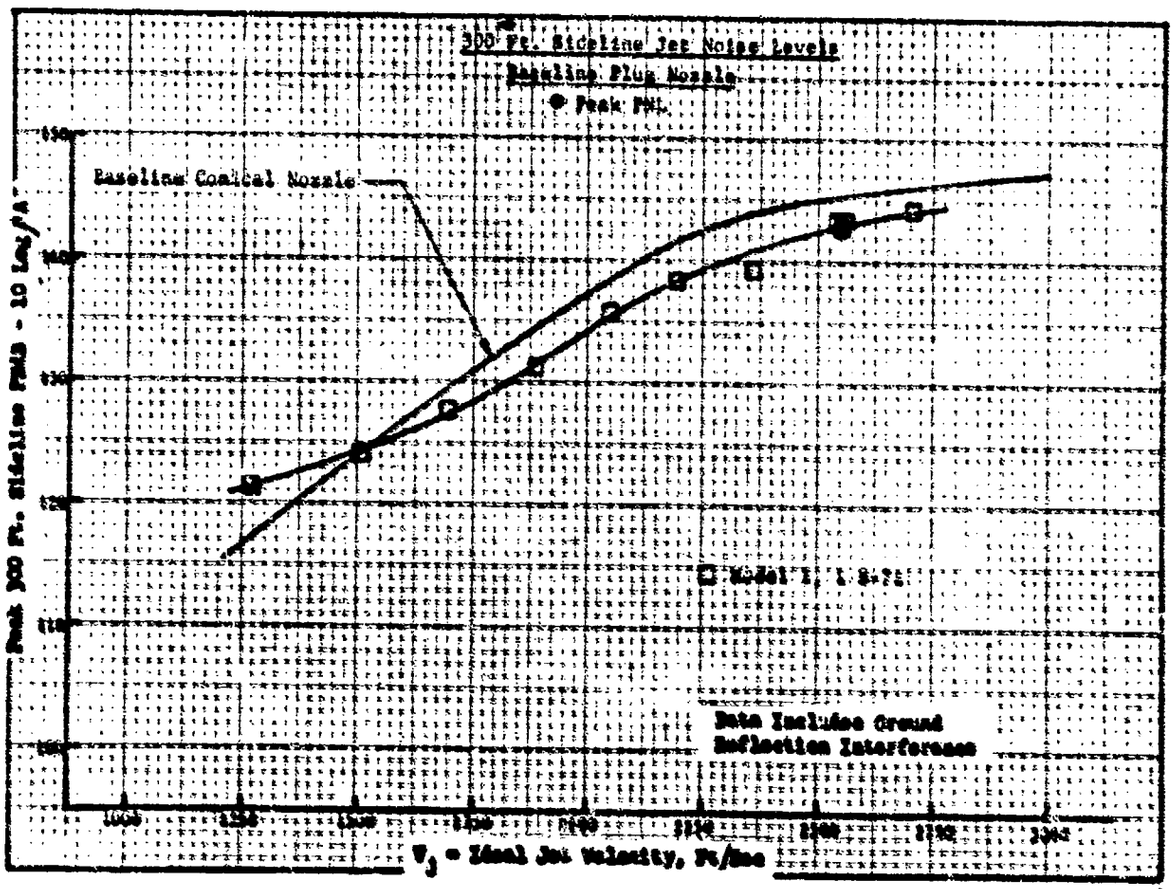
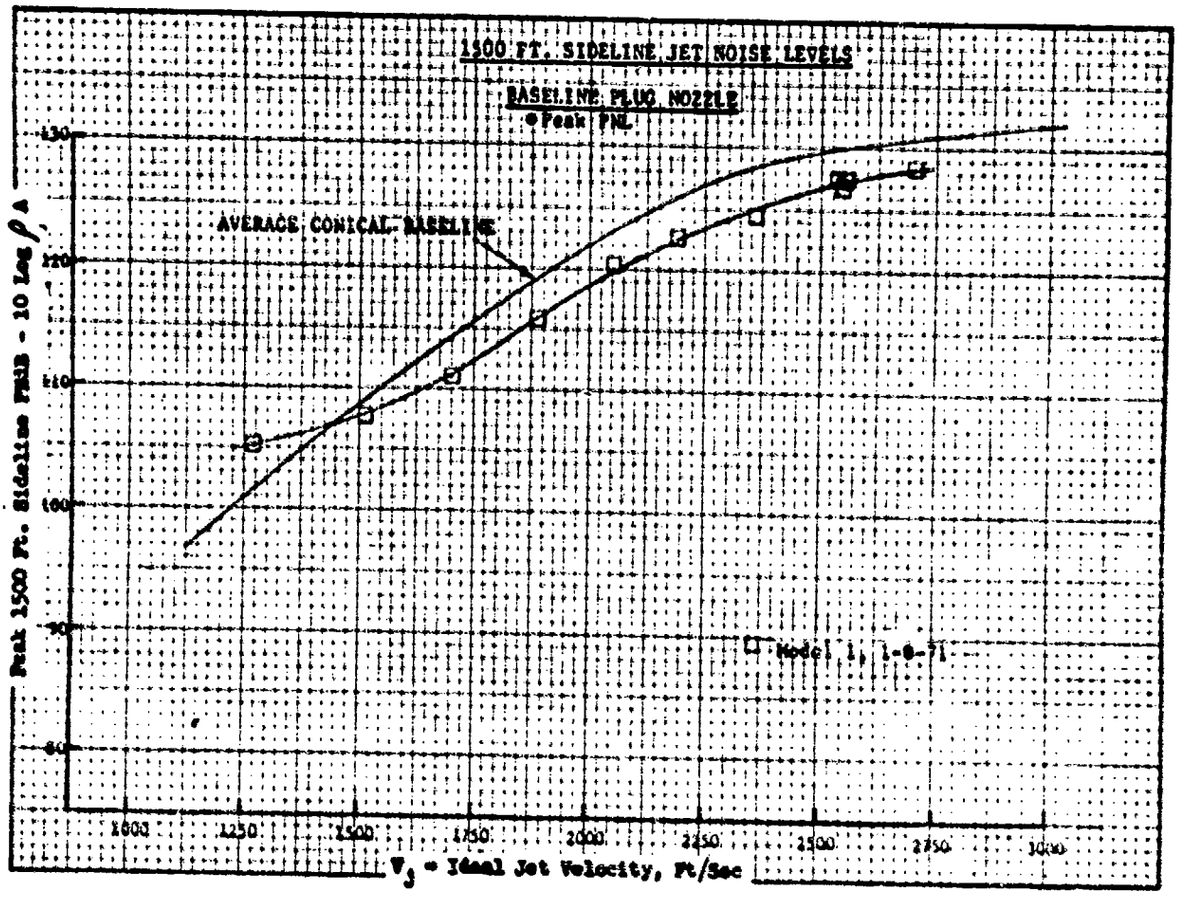


FIGURE V.H.2-7 320 FT ARC AND 300 FT SIDELINE JET NOISE LEVELS FOR MODEL I



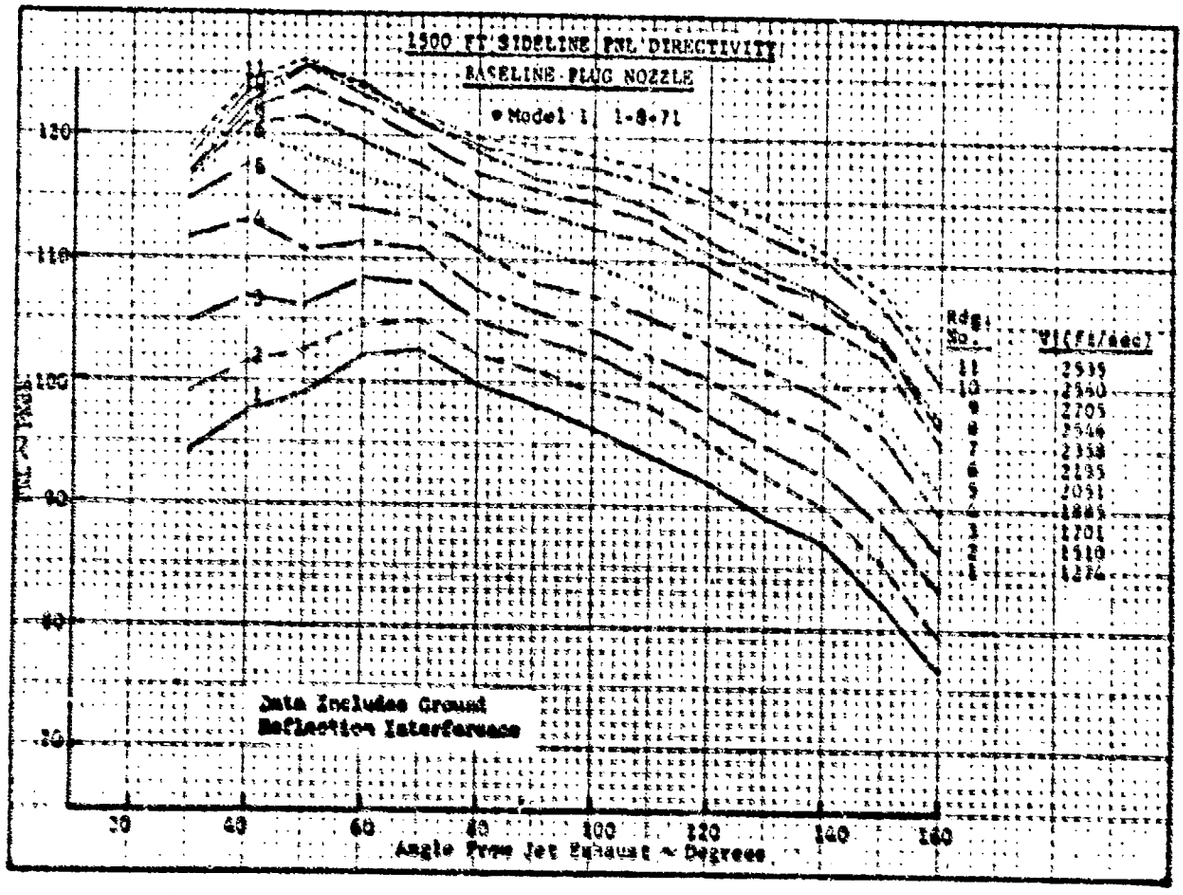
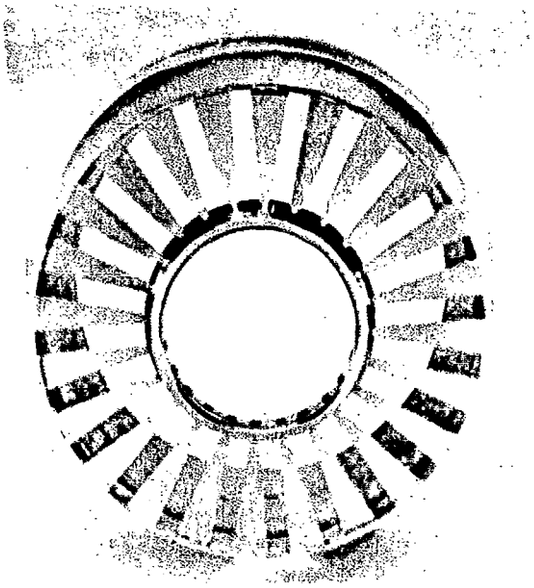


FIGURE V.H.2-8 1500 FT SIDELINE JET NOISE LEVELS AND PNL DIRECTIVITY FOR MODEL 1



- MODEL 2
- 24 TAPERED SPOKES AT 90°
- AREA RATIO = 2.0

Model 2 used the 20° plug with conical primary shroud. The suppressor system consisted of a total of 24 spokes with tapered sides, equally spaced and positioned at 90° to the nozzle axis. Spoke width at tip = .8266; hub = .1875". Exit Area, A8 = 30.83 in^2, Area Ratio = 2.0, Material: 304 S.S. for plug and shroud; RA-333 for spoke suppressors.

TABLE V.H.2-4 TEST SUMMARY

MODEL NO. 2

DESCRIPTION: 24 Tapered Spokes @ 90°, Area Ratio = 2.0

DATE: 1-24-71

SCALE MODEL A_8 = 30.83 $in.^2$

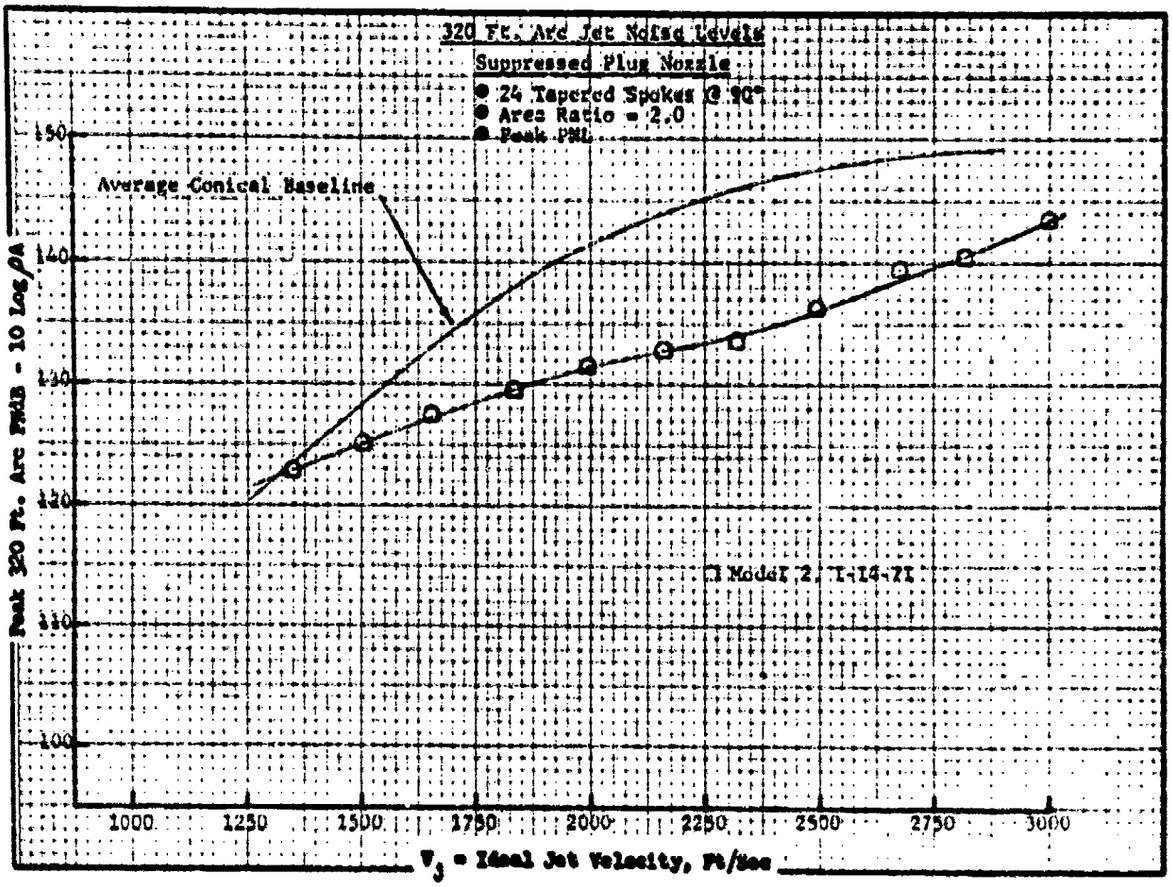
FULL SCALE A_8 = 13.70 $ft.^2$

SCALE FACTOR = 6:1

- DATA INCLUDES GROUND REFLECTION INTERFERENCE
- ANGLE REFERENCED TO JET EXHAUST

TEST CONDITIONS								ACOUSTIC TEST RESULTS							
								320 FT. ARC		330 FT. SIDELINE		1500 FT. SIDELINE		3133 FT. SIDELINE	
RUN NO.	P_0 PSIA	P_{T8} PSIA	P_{T8}/P_0	T_{T8} °R	IDEAL V_j FT/SEC	W_8 PPS	ΔOL_{WA}	PEAK PNLB	PEAK ANGLE	PEAK PNLB	PEAK ANGLE	PEAK PNLB	PEAK ANGLE	PEAK PNLB	PEAK ANGLE
1	14.440	22.34	1.545	1281	1349	9.025	-3.4	119.1	60	119.4	70	101.3	70	96.8	70
2	14.435	24.52	1.696	1331	1507	9.884	-3.4	121.7	70	121.7	70	103.6	70	98.8	70
3	14.437	26.44	1.830	1418	1656	10.550	-3.6	123.9	70	123.9	70	105.9	70	101.2	70
4	14.437	29.39	2.042	1483	1833	11.660	-3.7	125.8	70	125.8	70	107.8	70	103.2	70
5	14.437	32.69	2.261	1559	1990	12.597	-3.7	127.7	70	127.7	70	110.1	70	105.4	70
6	14.437	35.83	2.478	1640	2159	13.351	-3.8	129.1	70	129.1	70	111.4	70	107.1	70
7	14.436	39.65	2.743	1804	2321	14.305	-3.8	129.9	70	129.9	70	112.7	70	108.4	70
8	14.437	44.08	3.049	1839	2490	15.461	-3.7	132.8	60	131.8	70	114.7	70	110.5	70
9	14.436	48.55	3.358	1976	2636	16.343	-3.8	135.7	60	132.6	70	116.3	60	112.5	60
10	14.448	53.84	3.654	2065	2817	17.488	-3.7	136.9	60	133.6	50	118.1	50	114.4	50
11	14.445	59.14	4.019	2190	2995	18.467	-3.7	139.9	50	137.8	50	121.2	50	118.6	50

FIGURE V.H.2-9 HARDWARE AND TEST SUMMARY FOR MODEL 2



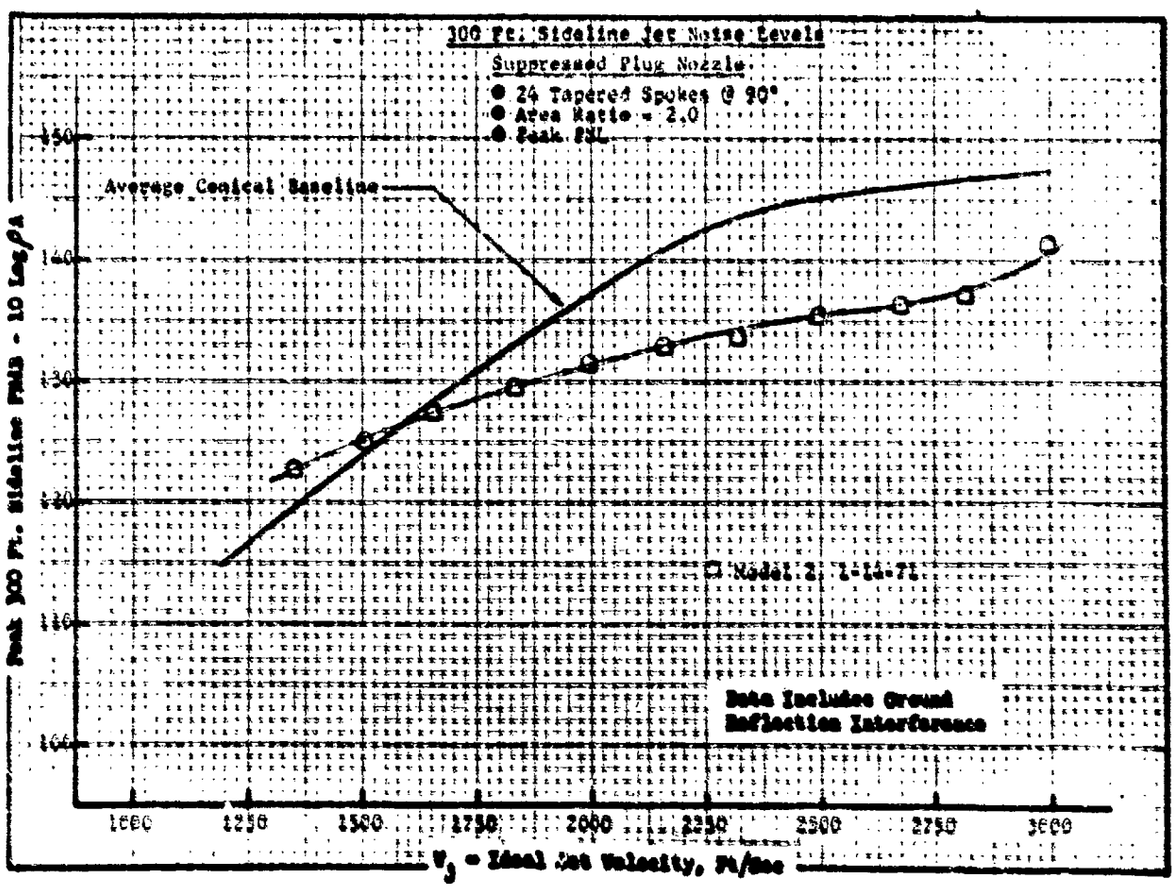


FIGURE V.H.2-10 320 FT ARC AND 300 FT SIDELINE JET NOISE LEVELS FOR MODEL 2

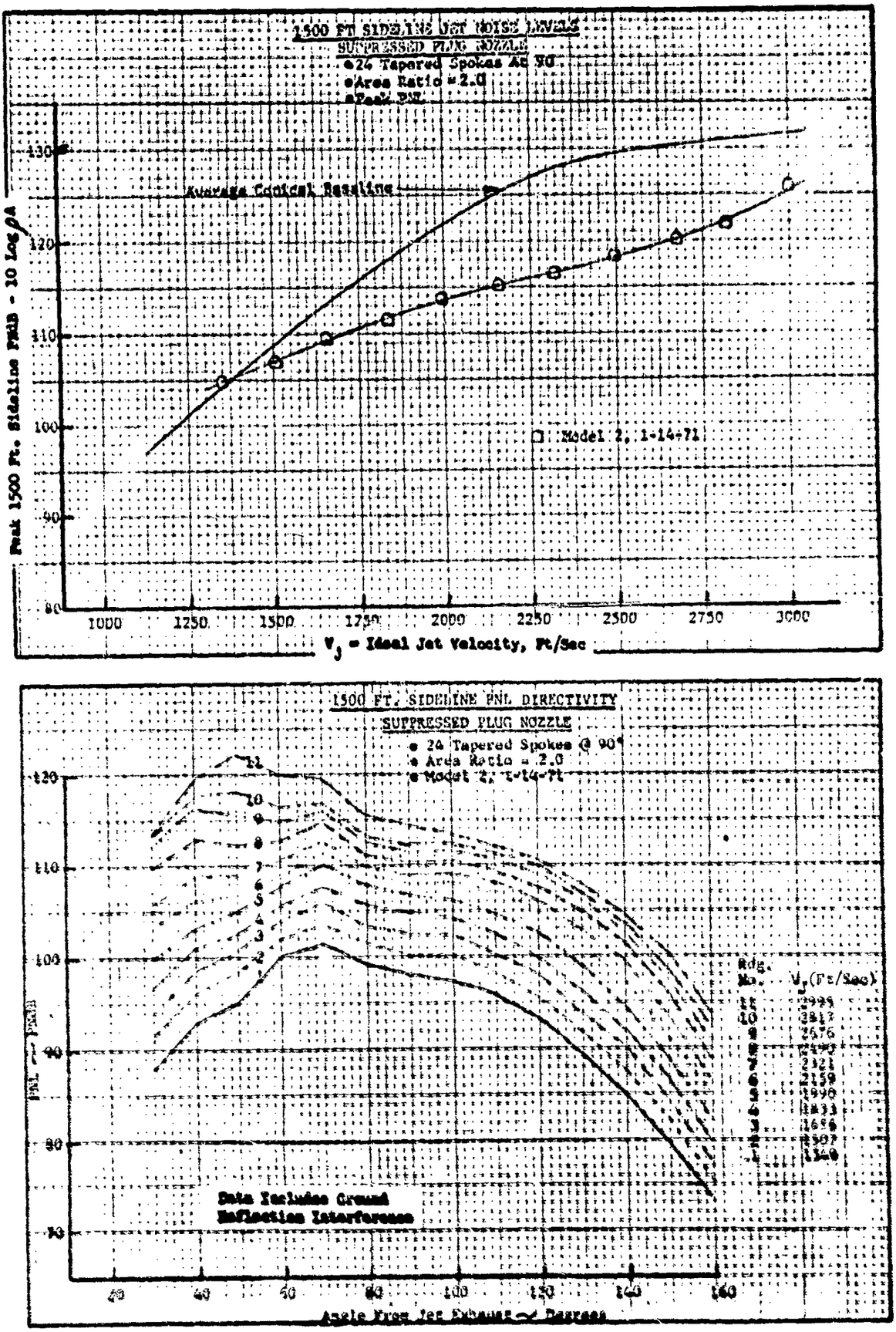
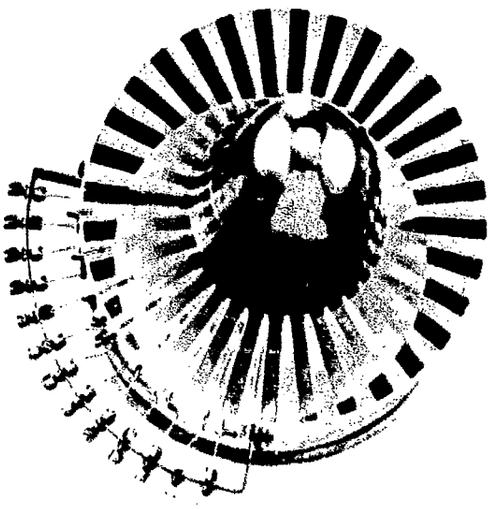


FIGURE V.H.2-11 1500 FT SIDELINE JET NOISE LEVELS AND PNL DIRECTIVITY FOR MODEL 2



- MODEL 3
- 32 TAPERED SPOKES AT 90°
- AREA RATIO = 2.0

Model 3 employed 32 tapered spokes, equally spaced and set at 90° to the nozzle axis. Spoke width at tip = .5712"; hub = .1875". Exit Area, A8 = 30.83 in^2, Area Ratio = 2.0, Material: 304 S.S. for plug and shroud; RA-333 for spoke suppressors.

TABLE V.H.2-5 TEST SUMMARY

MODEL NO. 3

SCALE MODEL A_8 = 30.83 $in.^2$

DESCRIPTION: 32 Tapered Spokes @ 90°, Area Ratio = 2.0

FULL SCALE A_8 = 13.70 $ft.^2$

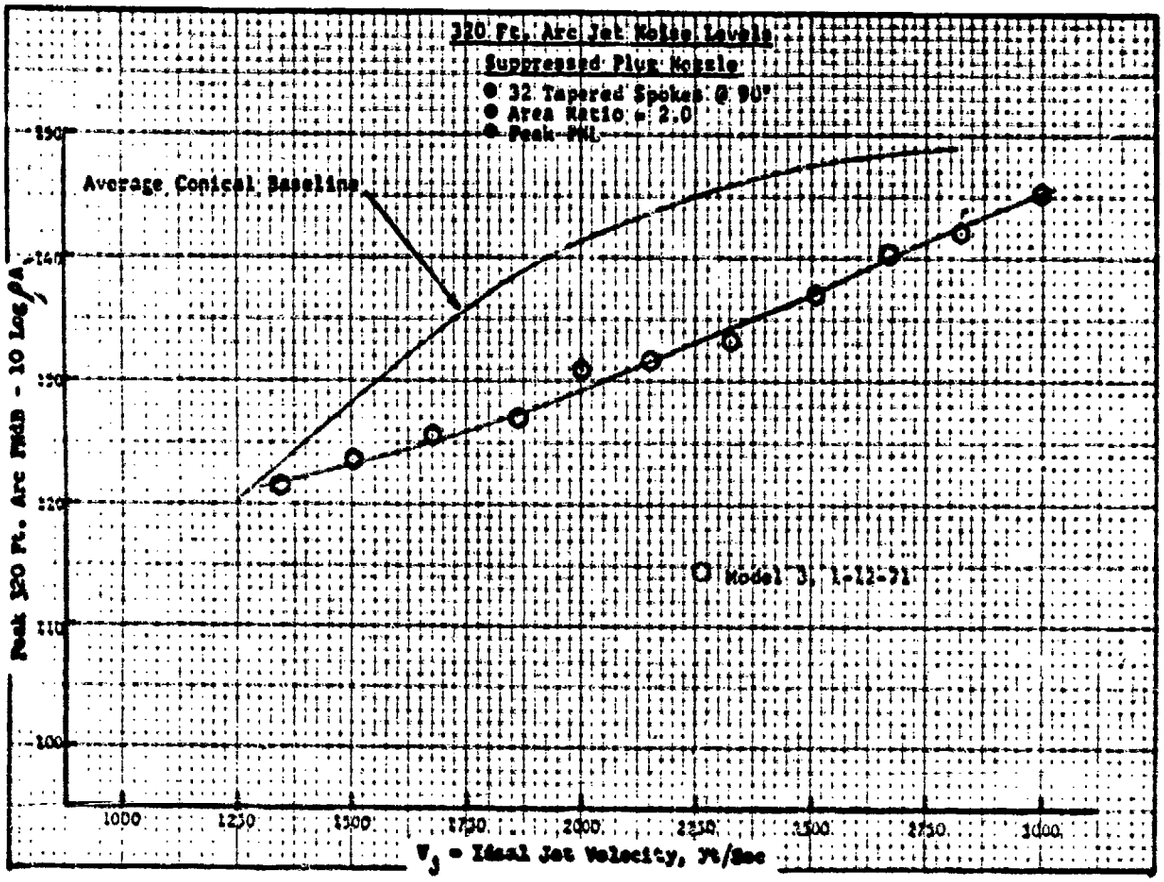
DATE: 1-12-71

SCALE FACTOR = 8:1

- DATA INCLUDES GROUND REFLECTION INTERFERENCE
- ANGLE REFERENCED TO JET EXHAUST

TEST CONDITIONS							ACOUSTIC TEST RESULTS							
								330 FT. ARC		390 FT. SIDELINE		1500 FT. SIDELINE		2138 FT. SIDELINE	
RUN NO.	P_0 PSIA	P_{T8} PSIA	P_{T8}/P_0	T_{T8} °R	IDEAL V_j FT/SEC	W_8 PPS	$10Log_{10}A_1$	PEAK PNdB	PEAK ANGLE	PEAK PNdB	PEAK ANGLE	PEAK PNdB	PEAK ANGLE	PEAK PNdB	PEAK ANGLE
1	14.543	40.(88	3.348	1967	2667	16.55	-3.8	136.5	40	132.5	40	117.1	40	113.3	40
2	14.532	52.877	3.639	2078	2821	17.29	-3.8	138.4	40/50	136.2	50	120.5	50	116.7	50
3	14.533	58.158	4.002	2204	2987	18.49	-3.7	141.7	50	139.6	50	123.9	50	120.1	50
4	14.533	44.814	3.828	1881	2549	15.38	-3.8	133.3	50	130.1	70	113	70	108.9	40
5	14.529	39.853	2.743	1752	2329	14.49	-3.8	129.6	50	128.9	70	111.5	70	107.1	70
6	14.528	36.325	2.500	1644	2159	13.81	-3.7	127.9	70	127.9	70	110.4	70	106.7	70
7	14.529	33.073	2.276	1572	2010	12.51	-3.7	127.2	70	127.2	70	109.5	70	105.8	70
8	14.533	29.497	2.029	1518	1864	11.82	-3.7	123.4	70	123.5	70	105.7	70	101	70
9	14.533	27.060	1.863	1417	1678	10.69	-3.6	123	60	121.7	70	103.7	70	99	70
10	14.533	24.672	1.697	1332	1538	10.15	-3.4	120.3	70	120.4	70	102.2	70	97.6	70
11	14.541	22.329	1.539	1286	1362	9.65	-3.3	118.3	70	118.3	70	100.2	70	95.4	70

FIGURE V.H.2-12 HARDWARE AND TEST SUMMARY FOR MODEL 3



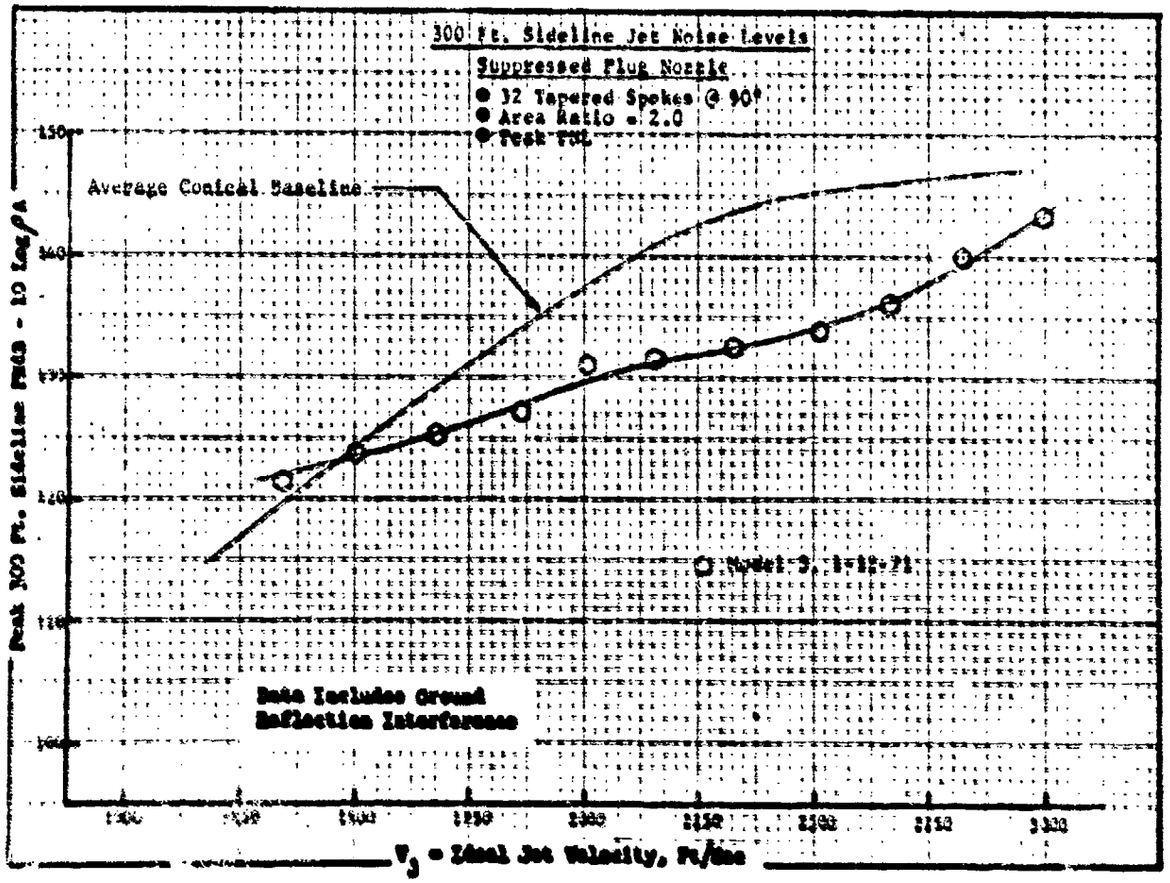
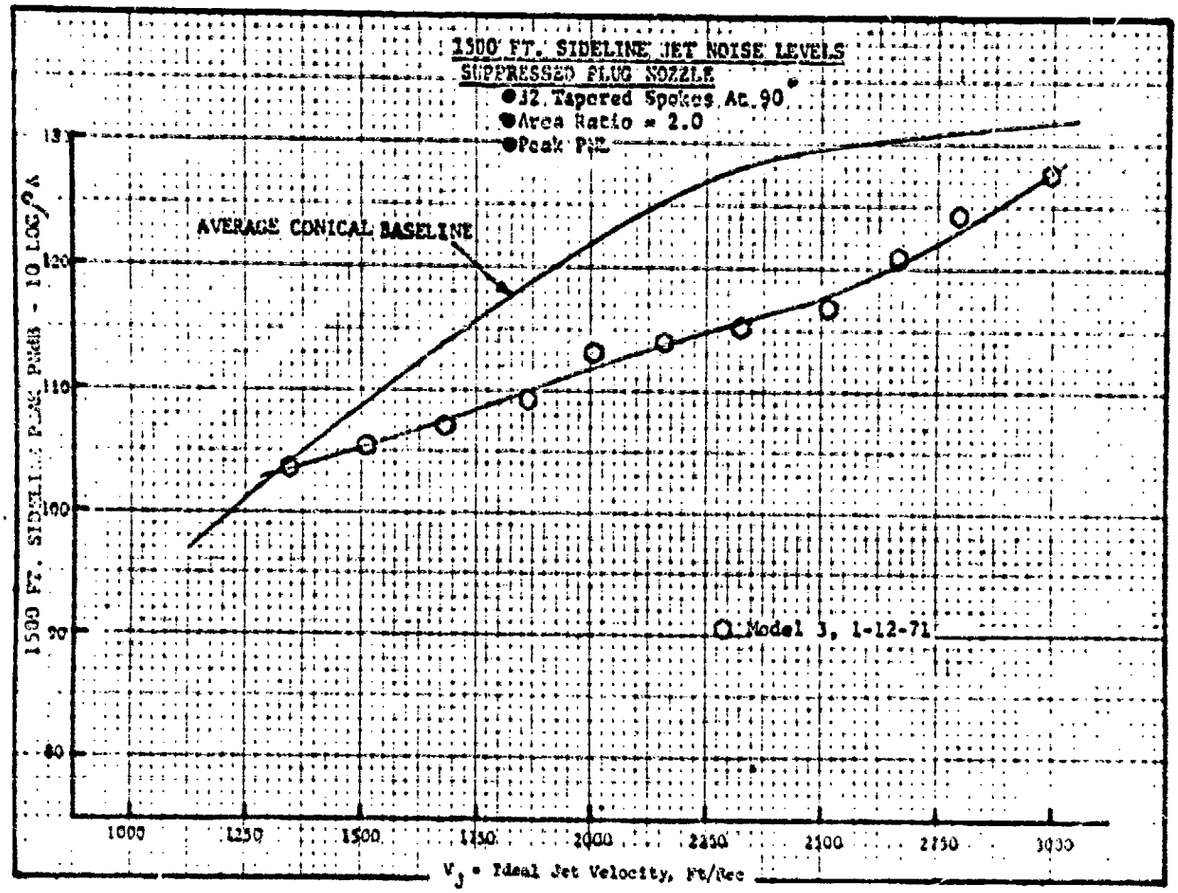


FIGURE V.H.2-13 320 FT ARC AND 300 FT SIDELINE JET NOISE LEVELS FOR MODEL 3



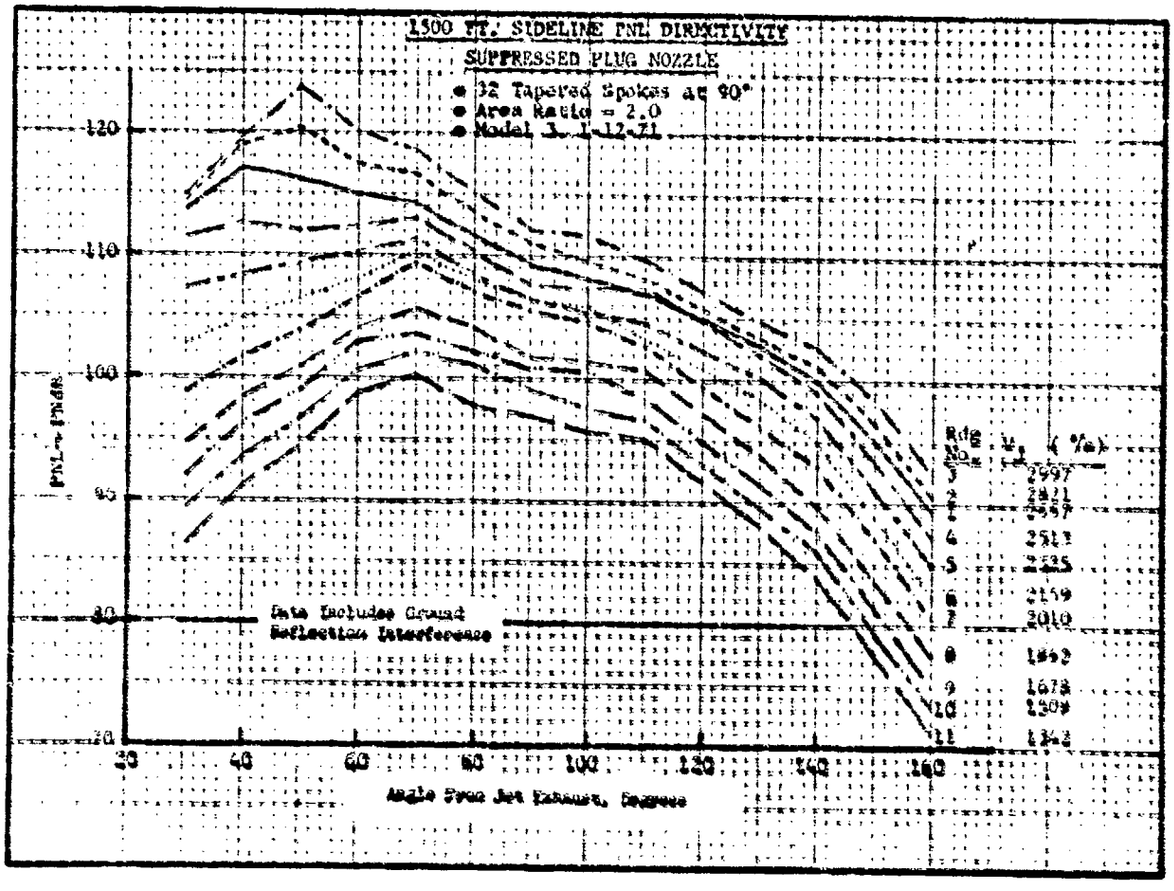
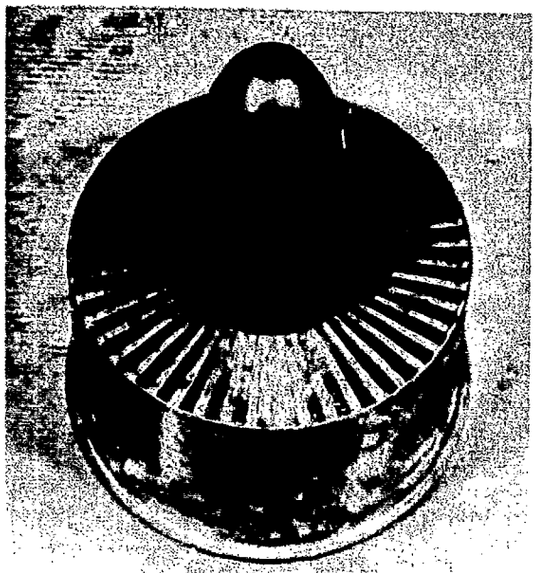


FIGURE V.H.2-14 1500 FT SIDELINE JET NOISE LEVELS AND PNL DIRECTIVITY FOR MODEL 3



- MODEL 4
- 48 TAPERED SPOKES AT 90°
- AREA RATIO = 2.0

Model 4 had 48 tapered spokes, equally spaced and set at 90° to the nozzle axis. Spoke width at tip = .3176"; hub = .1875". Exit Area, A8 = 30.83 in^2, Area Ratio = 2.0, Material: 304 S.S. for plug and shroud; RA-333 for spoke suppressors.

TABLE V.H.2-6 TEST SUMMARY

MODEL NO. 4

DESCRIPTION: 48 Tapered Spokes @ 90°, Area Ratio = 2.0

DATE: 1-25-71

SCALE MODEL A_8 = 30.83 $in.^2$

FULL SCALE A_8 = 13.70 $ft.^2$

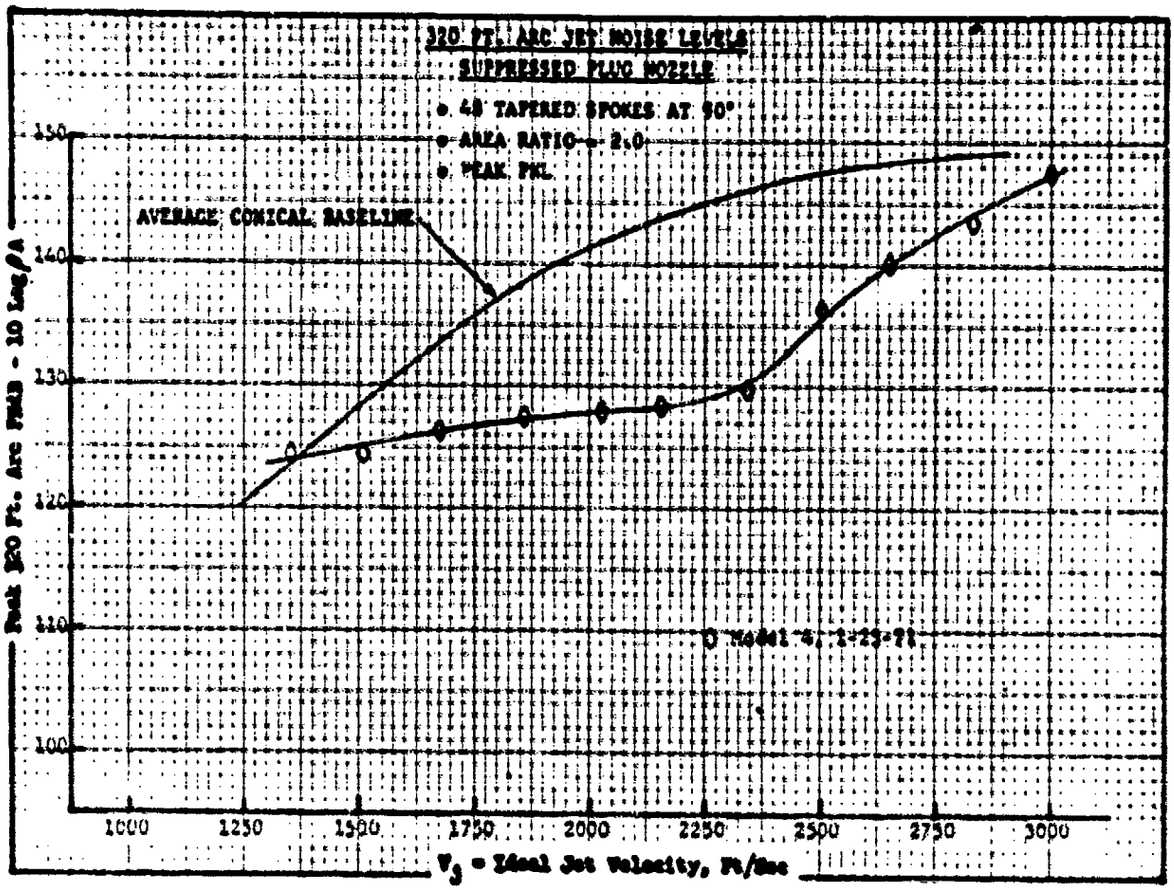
SCALE FACTOR = 8:1

• DATA INCLUDES GROUND REFLECTION INTERFERENCE

o ANGLE REFERENCED TO JET EXHAUST

TEST CONDITIONS								ACOUSTIC TEST RESULTS							
								320 FT. ARC		300 FT. SIDELINE		1500 FT. SIDELINE		2133 FT. SIDELINE	
RUN NO.	P_0 PSIA	P_{T8} PSIA	P_{T8}/P_0	T_{T8} °R	IDEAL V_j FT/SEC	W_8 PPS	$10\log_{10}A_8$	PEAK PNLB	PEAK ANGLE	PEAK PNLB	PEAK ANGLE	PEAK PNLB	PEAK ANGLE	PEAK PNLB	PEAK ANGLE
1	14.381	22.152	1.541	1234	1392	9.55	-3.6	120.9	80	121.4	80	103.2	80	97.8	80
2	14.366	24.281	1.690	1341	1508	10.19	-3.5	120.9	70/80	121.5	80	102.9	80	97.6	80
3	14.357	26.781	1.865	1415	1679	10.82	-3.6	122.7	70	122.7	70	104.1	70	98.8	70
4	14.351	29.767	2.074	1504	1859	11.70	-3.7	123.8	70	123.8	70/80	105.1	70	99.6	70
5	14.351	32.752	2.282	1588	2023	12.71	-3.8	124.2	70	124.3	70	105.9	70	100.7	70
6	14.352	35.882	2.498	1639	2144	13.45	-3.8	124.5	70	124.5	70	106.6	70	102.2	70
7	14.353	39.464	2.753	1765	2338	14.31	-3.9	125.8	50/60	126.7	50	107.9	50	103.7	50
8	14.350	43.848	3.063	1844	2498	15.34	-3.8	132.5	50	127.9	50	111.8	50	107.8	50
9	14.353	48.092	3.358	1937	2650	16.20	-3.8	136.3	40	132.9	50	116.9	40	113.2	40
10	14.345	52.595	3.674	2081	2839	17.21	-3.8	139.8	40	137.6	50	121.6	50	117.6	50
11	14.341	57.861	4.043	2191	3066	18.36	-3.8	143.6	50	141.5	50	125.5	50	121.5	50

FIGURE V.H.2-15 HARDWARE AND TEST SUMMARY FOR MODEL 4



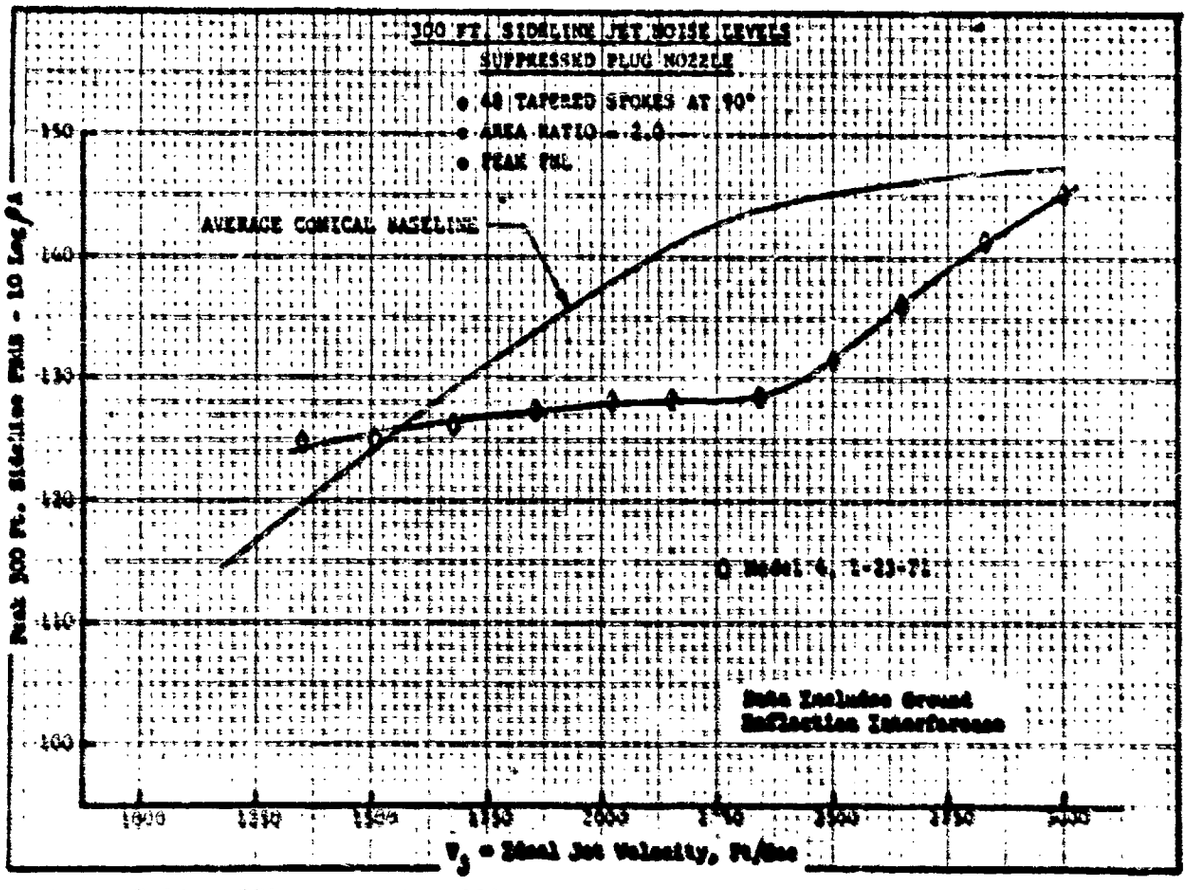
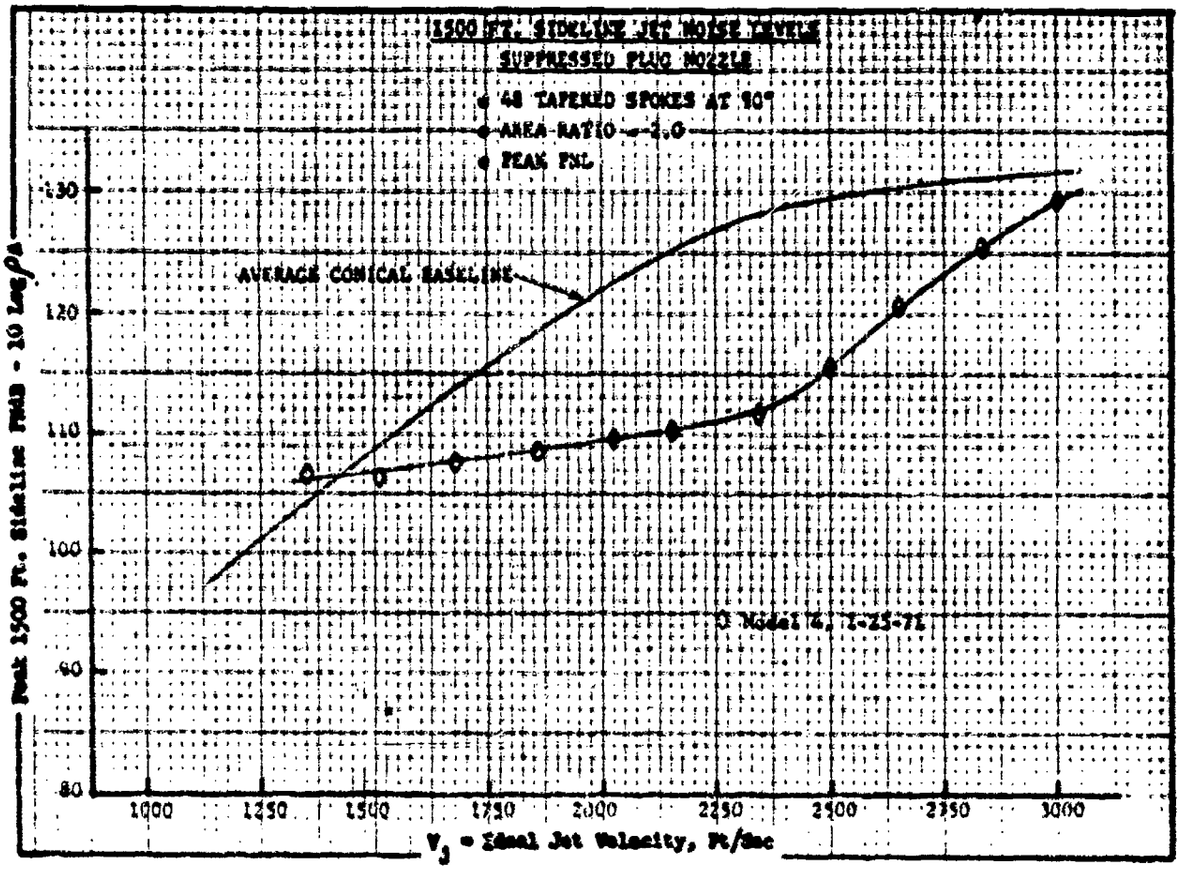


FIGURE V.H.2-16 320 FT ARC AND 300 FT SIDELINE JET NOISE LEVELS FOR MODEL 4



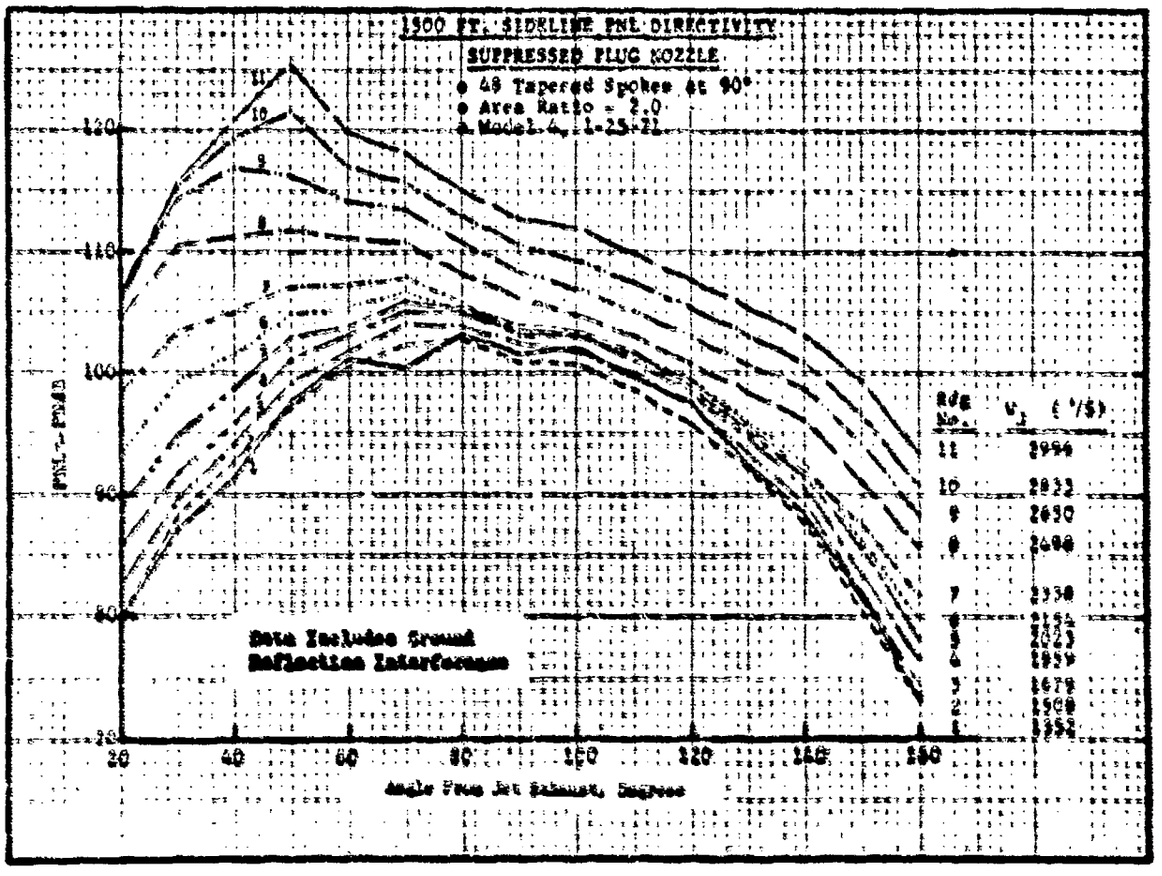
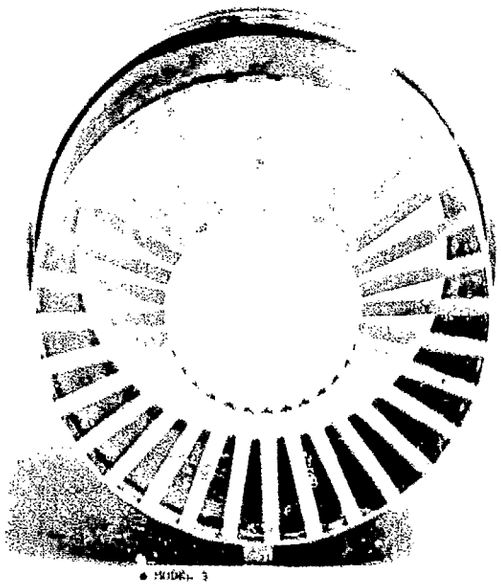


FIGURE V.H.2-17 1500 FT SIDELINE JET NOISE LEVELS AND PNL DIRECTIVITY FOR MODEL 4



- MODEL 5
- 32 PARALLEL SIDED SPOKES AT 90°
- AREA RATIO = 2.0

Model 5 used 32 parallel sided spokes, equally spaced and set at 90° to the nozzle axis. Spoke width at tip = .375"; hub = .375". Exit Area, A8 = 30.83 in^2, Area Ratio = 2.0, Material: 304 S.S. for plug and shroud; RA-333 for spoke suppressors.

TABLE V.E.2-7 TEST SUMMARY

MODEL NO. 5

SCALE MODEL A_8 = 30.83 $in.^2$

DESCRIPTION: 32 Parallel Sided Spokes @ 90°, Area Ratio = 2.0

FULL SCALE A_8 = 13.70 $ft.^2$

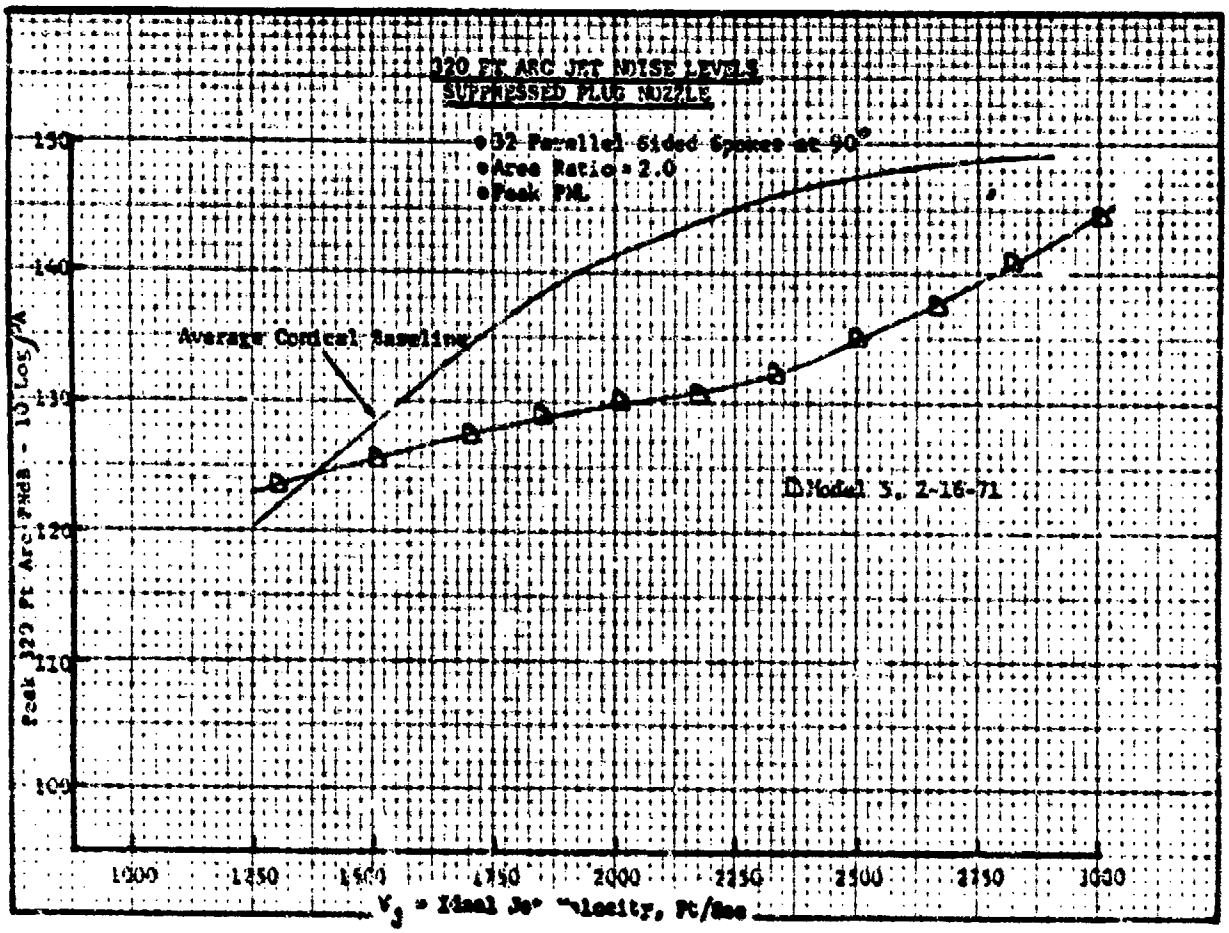
DATE: 2-16-71

SCALE FACTOR = 8:1

- DATA INCLUDES GROUND REFLECTION INTERFERENCE
- ANGLE REFERENCED TO JET EXHAUST

TEST CONDITIONS							ACOUSTIC TEST RESULTS							
								330 FT. ARC		300 FT. SIDELINE		1500 FT. SIDELINE		2128 FT. SIDELINE	
RUN NO.	P_0 PSIA	P_{T8} PSIA	P_{T8}/P_0	T_{T8} °R	IDEAL V_j FT/SEC	V_8 FPS	$\Delta OL_{OJ}/\Delta A$	PEAK PNLB	PEAK ANGLE	PEAK PNLB	PEAK ANGLE	PEAK PNLB	PEAK ANGLE	PEAK PNLB	PEAK ANGLE
1	14.525	21.773	1.499	1283	1304	9.42	-3.4	120.1	90	120.1	90	102.5	90	97.9	90
2	14.523	24.621	1.695	1335	1388	10.27	-2.4	122.2	90	122.2	90	104.2	90	99.6	90
3	14.519	27.295	1.836	1439	1780	11.14	-3.6	123.8	90	123.8	90	105.8	90	101.1	90
4	14.514	29.955	2.064	1469	1892	11.78	-2.7	125.3	90	125.3	90	107.5	90	102.7	90
5	14.509	32.884	2.266	1587	2014	12.70	-3.8	126.3	90	126.4	90	108.7	90	103.9	90
6	14.504	36.129	2.490	1672	2172	13.63	-2.8	126.9	50	126.6	90	109	90	104.4	90
7	14.502	39.793	2.744	1749	2333	14.45	-2.8	128.4	50	127.7	90	110.3	90	106.1	90
8	14.502	44.158	3.045	1859	2498	15.43	-2.8	131.2	50	129.7	90	112.1	90	107.9	90
9	14.503	48.657	3.355	1968	2665	16.61	-3.8	133.8	50	131.6	50	113.2	50	111.2	50
10	14.499	53.998	3.653	2072	2832	17.54	-3.8	137.2	50	134.9	50	116.6	50	114.6	50
11	14.496	58.330	4.049	2186	3030	18.51	-3.7	140.8	50	138.6	50	122.6	50	118.7	50

FIGURE V.E.2-18 HARDWARE AND TEST SUMMARY FOR MODEL 5



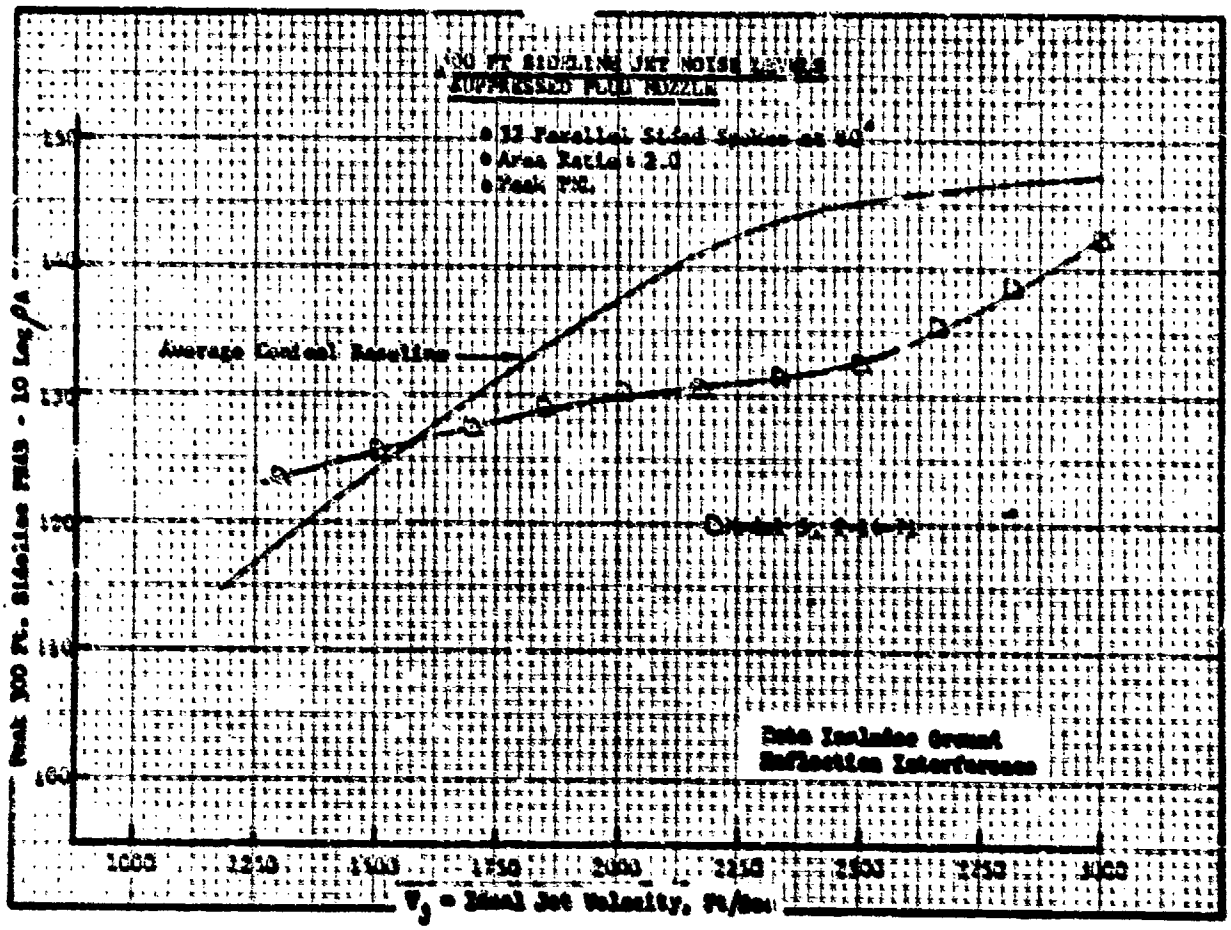
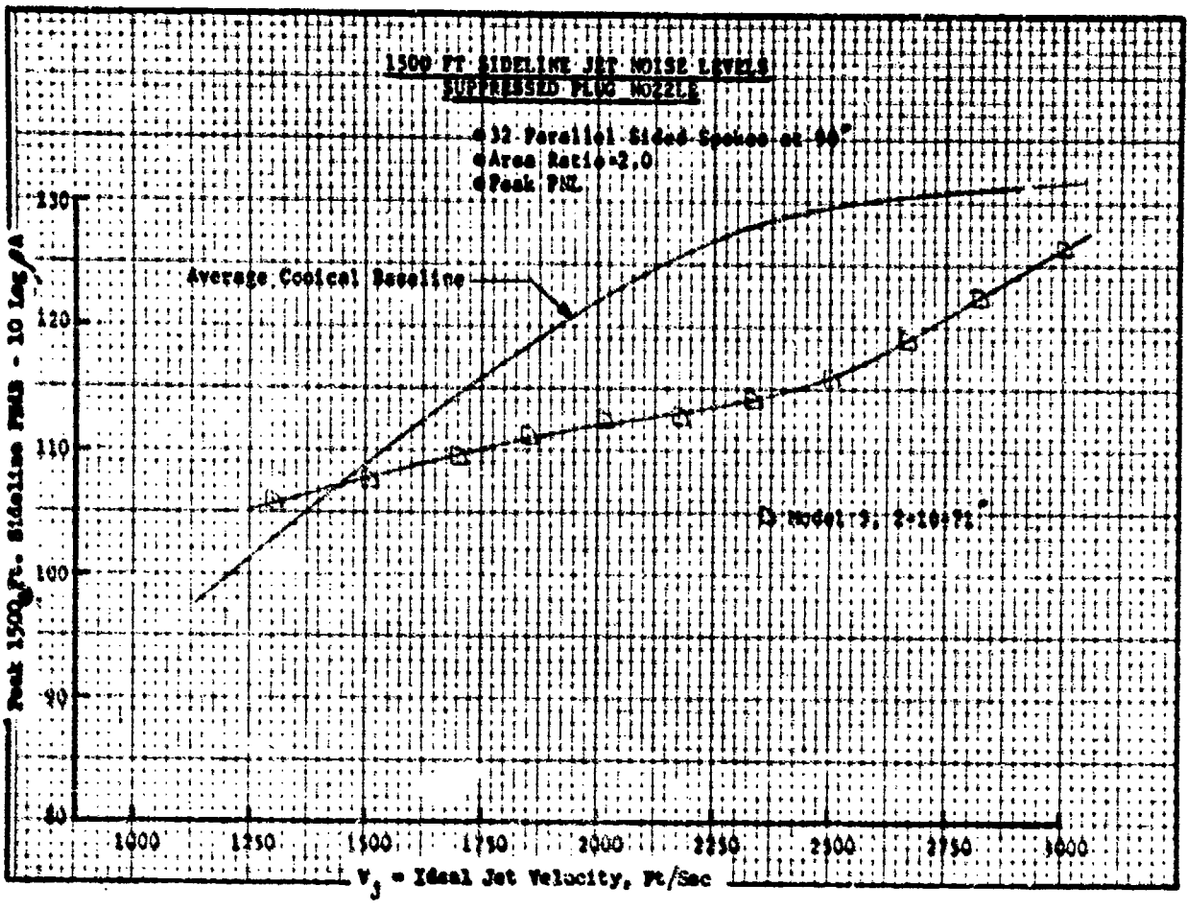


FIGURE V.H.2-19 320 FT ARC AND 300 FT SIDELINE JET NOISE LEVELS FOR MODEL S



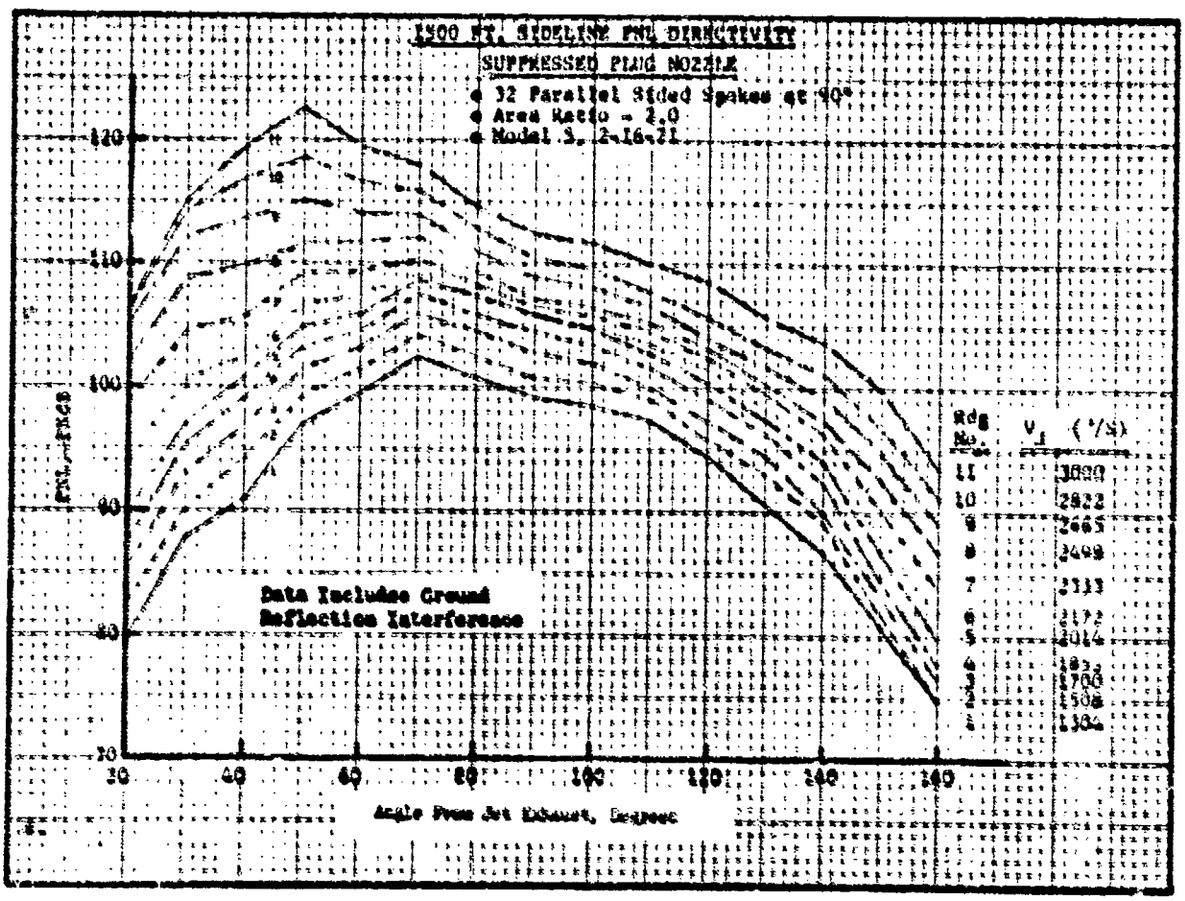
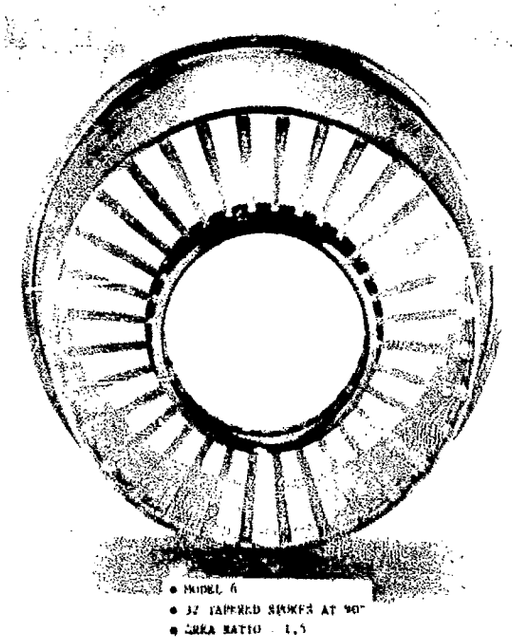


FIGURE V.H.2-20 1500 FT SIDELINE JET NOISE LEVELS AND PNL DIRECTIVITY FOR MODEL 5



Model 6 employed 32 tapered spokes, equally spaced and set at 90° to the nozzle axis. Spoke width at tip = .2814"; hub = .1875". Exit Area, A8 = 30.83 in^2, Area Ratio = 1.5, Material: 304 S.S. for plug and shroud; RA-333 for spoke suppressors.

TABLE V.E.2-8 TEST SUMMARY

MODEL NO. 6

SCALE MODEL A_8 = 30.83 $in.^2$

DESCRIPTION: 32 Tapered Spokes @ 90°, Area Ratio = 1.5

FULL SCALE A_8 = 13.70 $ft.^2$

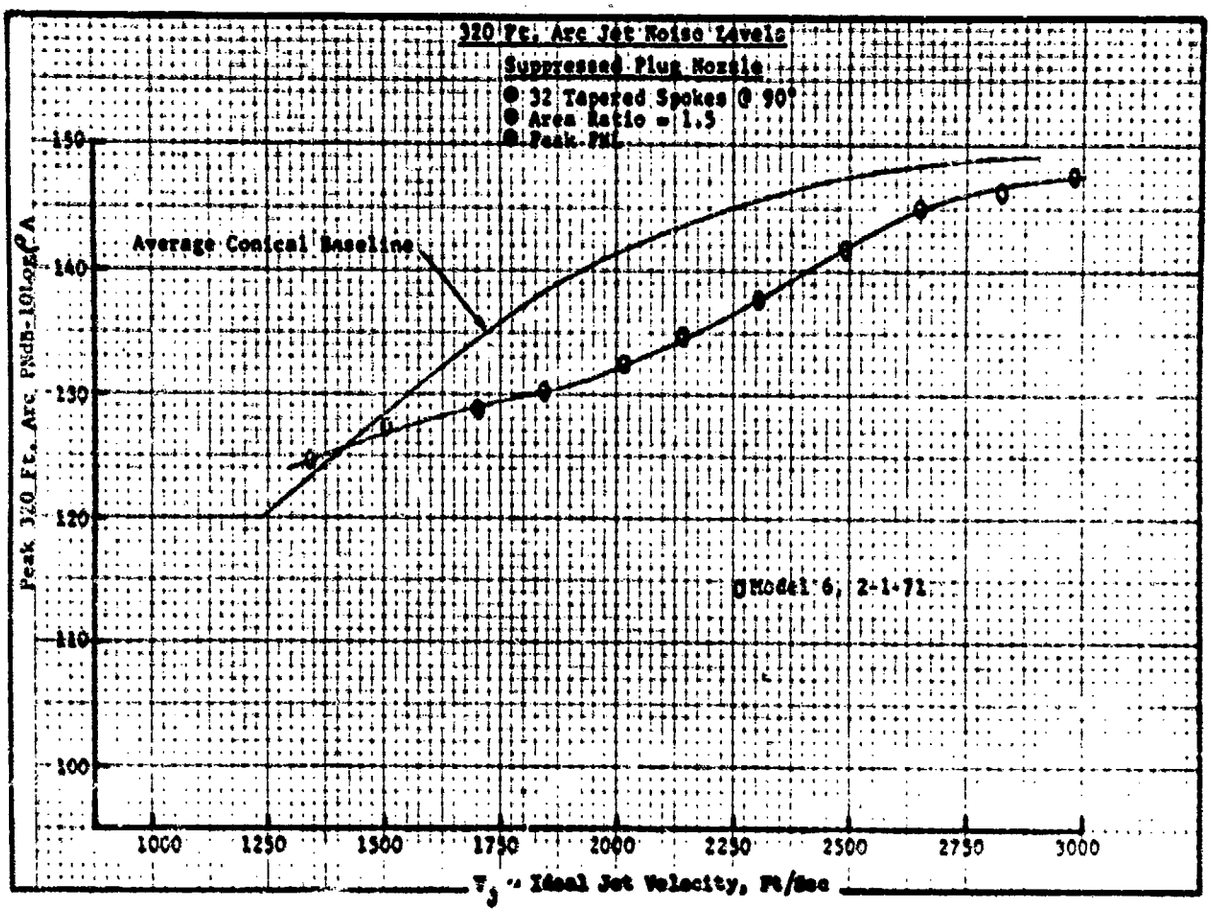
DATE: 2-01-71

SCALE FACTOR = 8:1

- DATA INCLUDES GROUND REFLECTION INTERFERENCE
- ANGLE REFERENCED TO JET EXHAUST

TEST CONDITIONS							ACOUSTIC TEST RESULTS								
								320 FT. ARC		300 FT. SIDELINE		1500 FT. SIDELINE		2128 FT. SIDELINE	
RUN NO.	P_8 PSIA	P_{T8} PSIA	P_{T8}/P_0	T_{T8} °R	IDEAL V_j FT/SEC	V_8 FPS	$10\log_{10}A$	PEAK PNdB	PEAK ANGLE	PEAK PNdB	PEAK ANGLE	PEAK PNdB	PEAK ANGLE	PEAK PNdB	PEAK ANGLE
1	14.543	58.647	4.033	2175	2984	19.1	-3.7	143.9	50	141.7	50	129.7	50	121.8	40
2	14.544	53.095	3.651	2081	2924	17.84	-3.8	142.3	50	140.3	50	124.3	50	120.3	50
3	14.543	48.938	3.365	1925	2848	16.92	-3.7	141.3	50	139.1	50	123.1	50	119.1	50
4	14.543	44.202	3.039	1840	2788	15.93	-3.7	138.1	50	135.9	50	119.7	50	115.7	50
5	14.543	40.875	2.796	1710	2684	14.86	-3.7	134.1	40	1 9	50	114.6	40	110.6	40
6	14.543	35.846	2.448	1654	2599	13.77	-3.7	132.1	30	128.4	70	110.9	40	106.4	40
7	14.544	33.291	2.287	1572	2016	12.8	-3.7	128.2	30	127.1	70	109.1	70	104.5	70
8	14.544	28.915	2.057	1482	1839	12.09	-3.6	126.1	30	125.9	70	107.2	70	102.6	70
9	14.543	27.722	1.949	1432	1706	11.34	-3.6	125.2	70	125.2	70	106.8	70	102.8	60
10	14.542	24.569	1.782	1321	1598	10.44	-3.6	123.8	70/60	123.8	60	105.9	60	100.9	60
11	14.559	22.431	1.541	1296	1340	9.3	-3.3	121.6	70	121.7	60	103.5	60	98.5	60

FIGURE V.E.2-21 HARDWARE AND TEST SUMMARY FOR MODEL 6



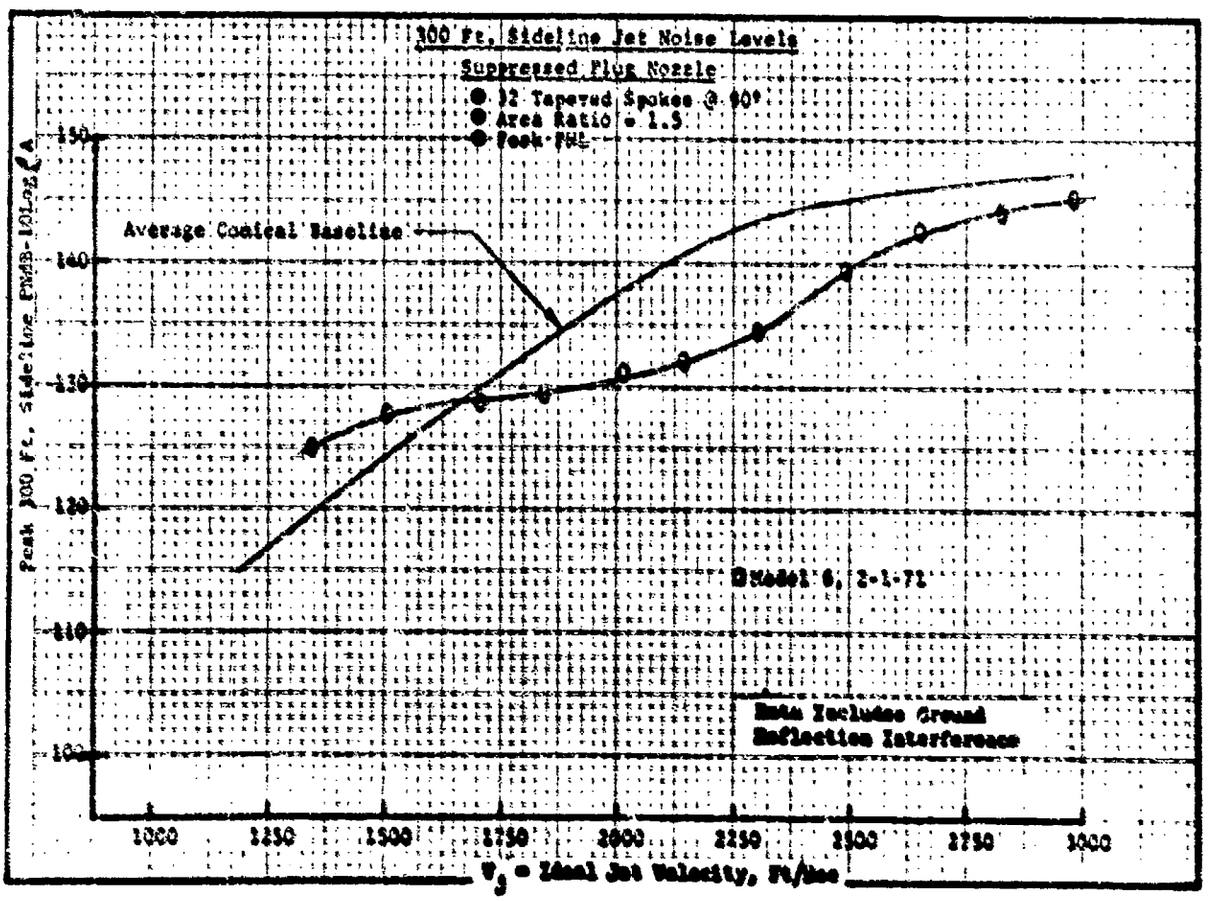
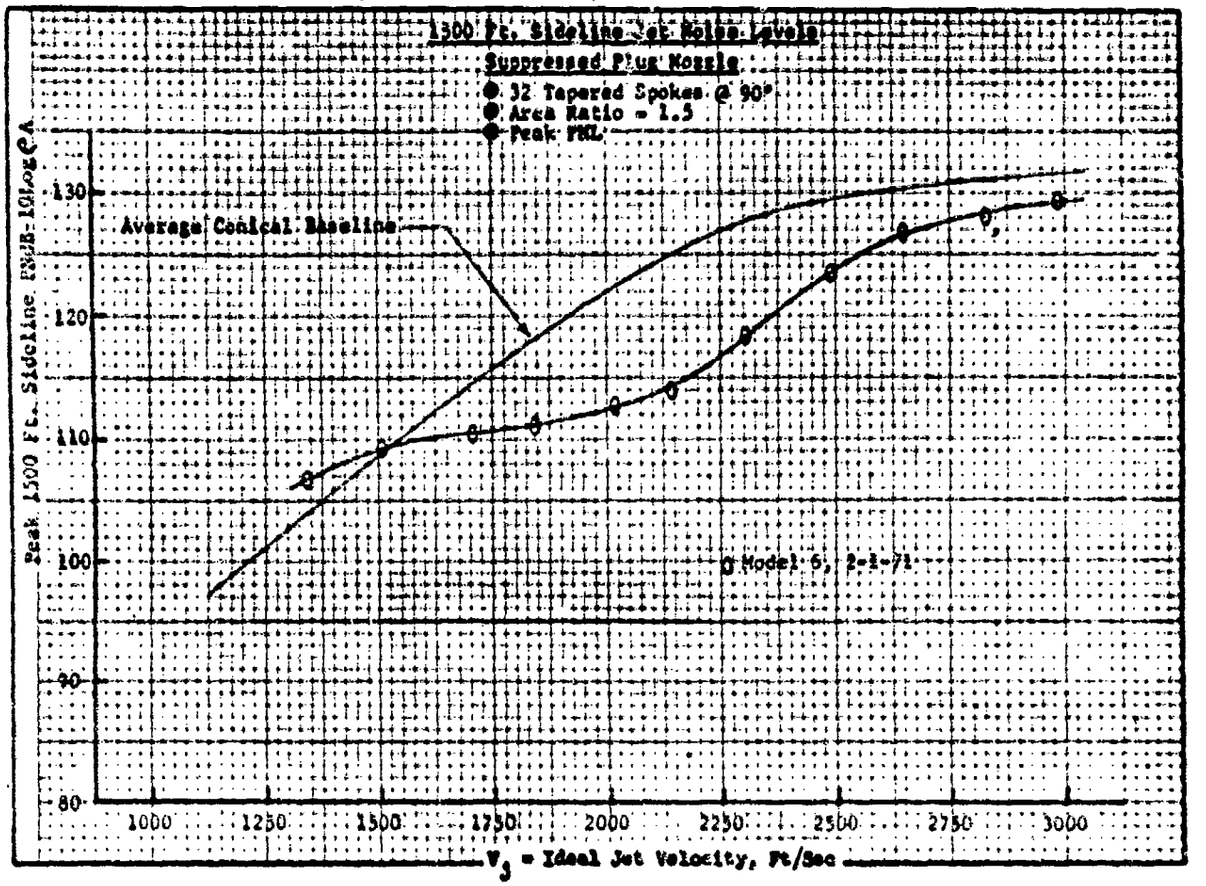


FIGURE V.H.2-22 320 FT ARC AND 300 FT SIDELINE JET NOISE LEVELS FOR MODEL 6



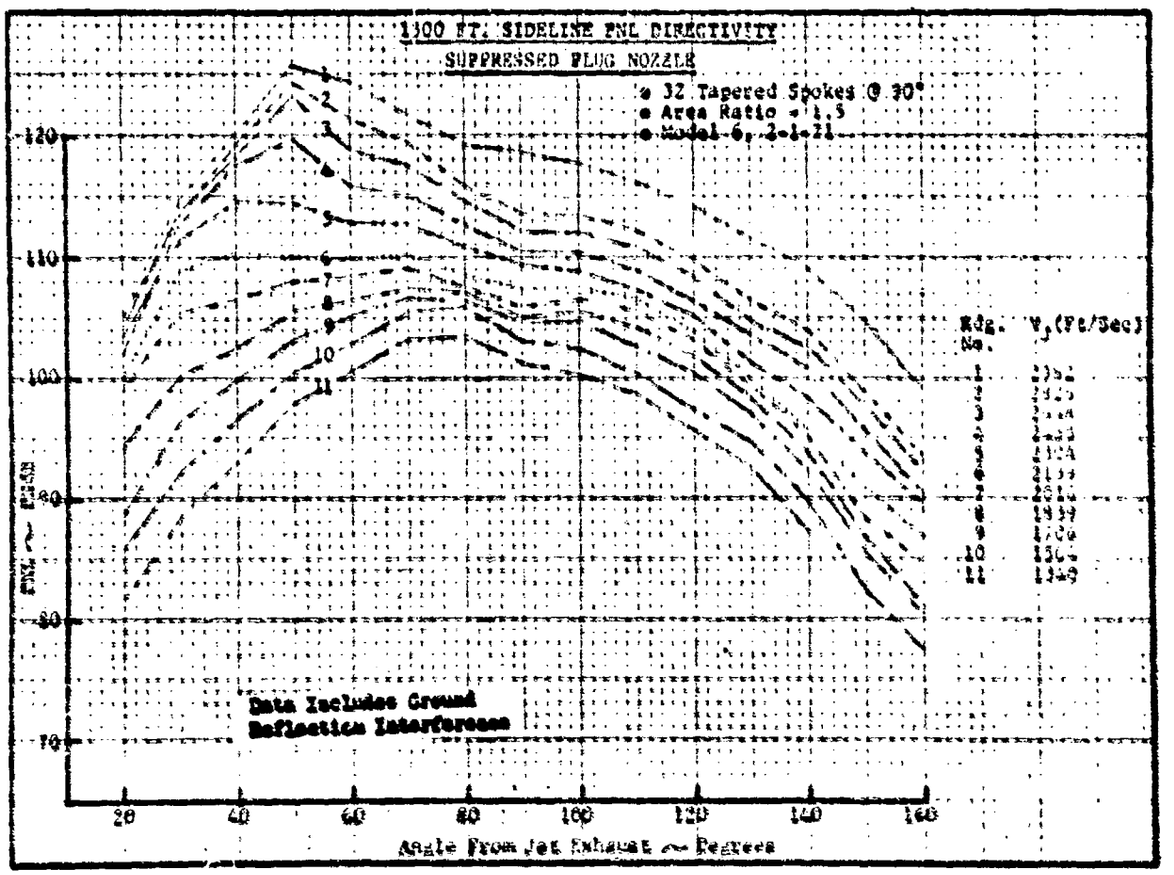
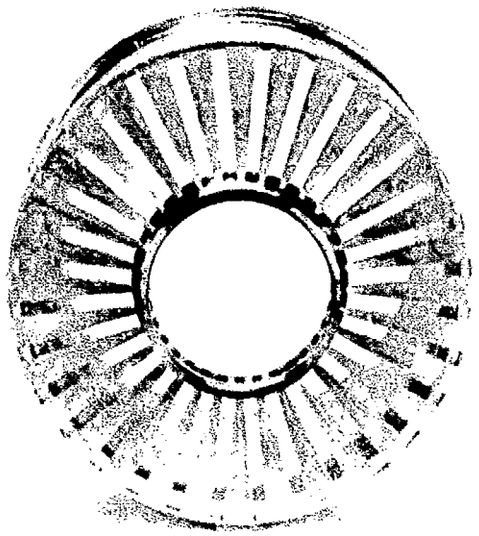


FIGURE V.H.2-23 1500 FT SIDELINE JET NOISE LEVELS AND PNL DIRECTIVITY FOR MODEL 6



- MODEL 7
- 32 TAPERED SPOKES AT 90°
- AREA RATIO = 2.5

Model 7 had 32 tapered spokes, equally spaced and set at 90° to the nozzle axis. Spoke width at tip = .7650"; hub = .1875". Exit Area, A8 = 30.83 in^2, Area Ratio = 2.5, Material: 304 S.S. for plug and shroud; RA-333 for spoke suppressors.

TABLE V.H.2-9 TEST SUMMARY

MODEL NO. 7

DESCRIPTION: 32 Tapered Spokes @ 90°, Area Ratio = 2.5

DATE: 2-08-71

SCALE MODEL A_8 = 30.83 $in.^2$

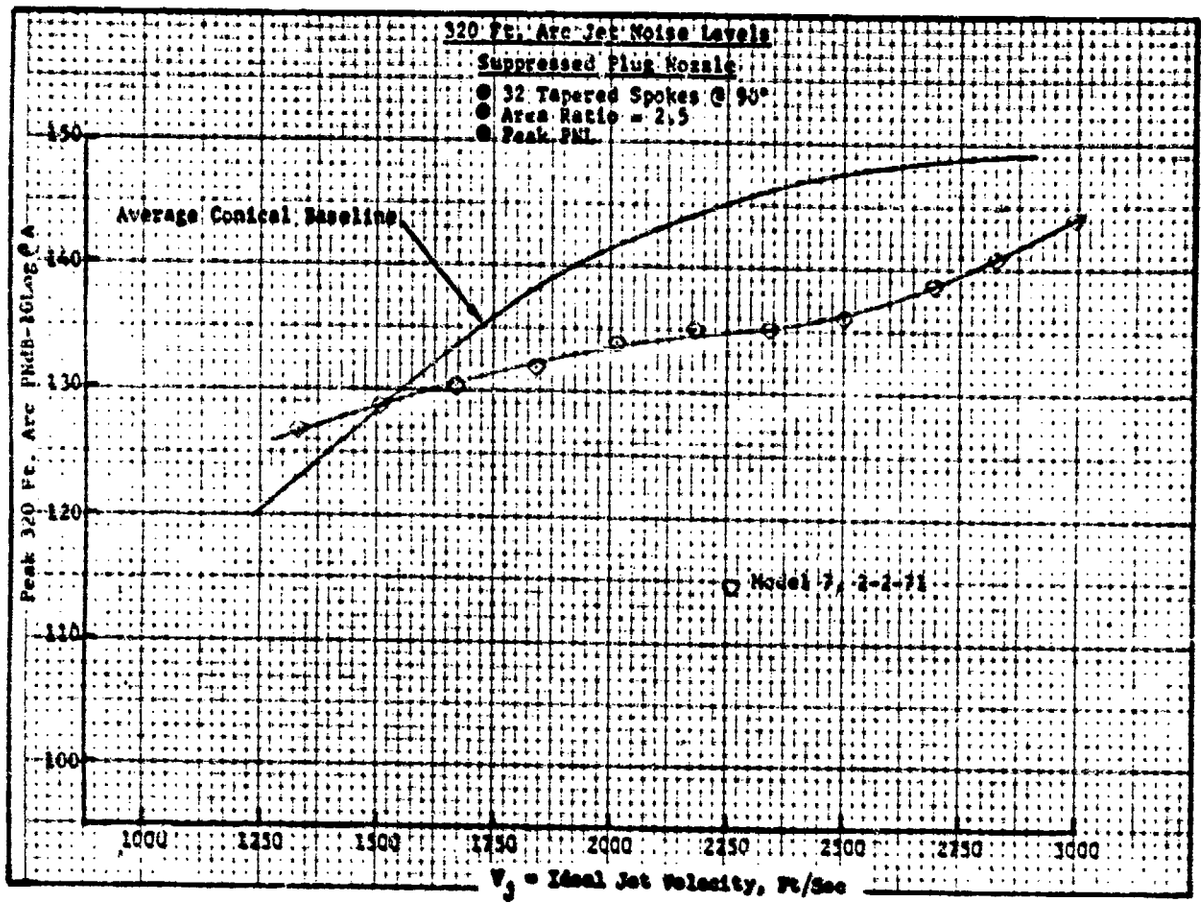
FULL SCALE A_8 = 13.70 $ft.^2$

SCALE FACTOR = 8:1

- DATA INCLUDES GROUND REFLECTION INTERFERENCE
- ANGLE REFERENCED TO JET EXHAUST

TEST CONDITIONS							ACOUSTIC TEST RESULTS									
								320 FT. ARC		300 FT. SIDELINE		1500 FT. SIDELINE		2123 FT. SIDELINE	
PNT. NO.	P_0 PSIA	P_{T8} PSIA	P_{T8}/P_0	T_{T8} °R	IDEAL V_j FT/SEC	W_8 PPS	$10\log_{10}/A$	PEAK PNLB	PEAK ANGLE	PEAK PNLB	PEAK ANGLE	PEAK PNLB	PEAK ANGLE	PEAK PNLB	PEAK ANGLE
1	14.727	22.567	1.532	1278	1335	9.29	-9.3	123.5	80	123.5	80	104.5	80	99.3	80
2	14.713	25.047	1.702	1331	1512	10.29	-9.3	125.5	80	126.1	80	107	80	101.8	80
3	14.738	27.432	1.865	1401	1670	11.03	-9.3	126.8	80	127.4	80	108.4	80	103.2	80
4	14.701	30.283	2.060	1485	1841	11.81	-9.6	128.3	80	128.9	80	109.9	80	104.8	80
5	14.698	33.532	2.280	1591	2071	12.17	-9.2	130.2	80	130.8	80	112.4	80	107.3	80
6	14.696	36.766	2.501	1676	2279	14.69	-9.8	131.2	80	131.8	80	113.5	80	108.5	80
7	14.693	40.319	2.744	1779	2544	14.62	-9.8	131.9	70/80	132.9	80	113.6	80	108.2	80
8	14.693	44.679	3.041	1856	2698	16.03	-9.7	132.3	50	133.3	80	114.1	80	109.4	80
9	14.696	49.633	3.378	1929	2887	16.77	-9.7	133	50	133.3	80	115.2	80	111.2	80
10	14.696	53.932	3.671	2013	3037	17.82	-9.7	137.2	40	134.3	50	118.2	50	114.5	50
11	14.696	58.952	4.012	2193	3290	18.79	-9.7	140.3	30	136.1	50	122	50	118	50

FIGURE V.H.2-24 HARDWARE AND TEST SUMMARY FOR MODEL 7



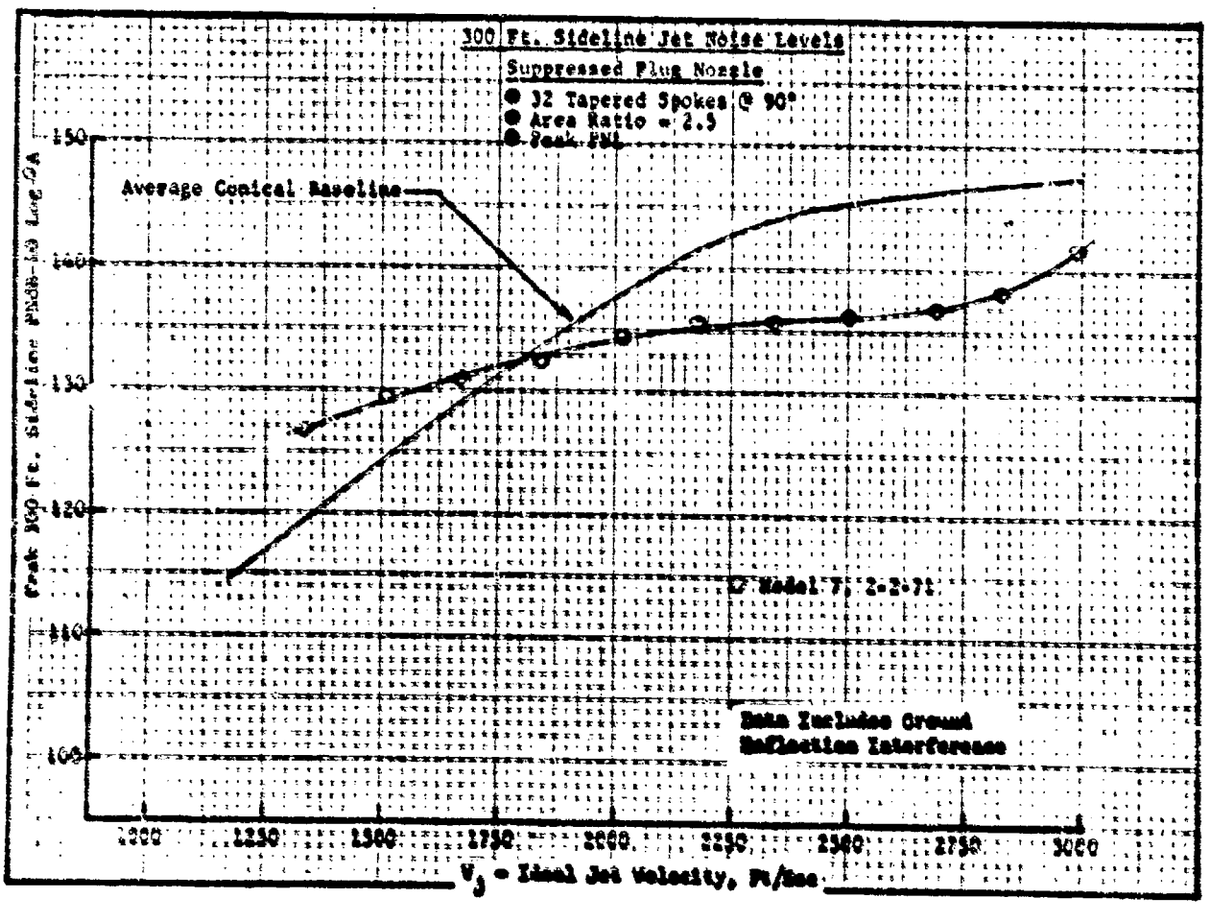
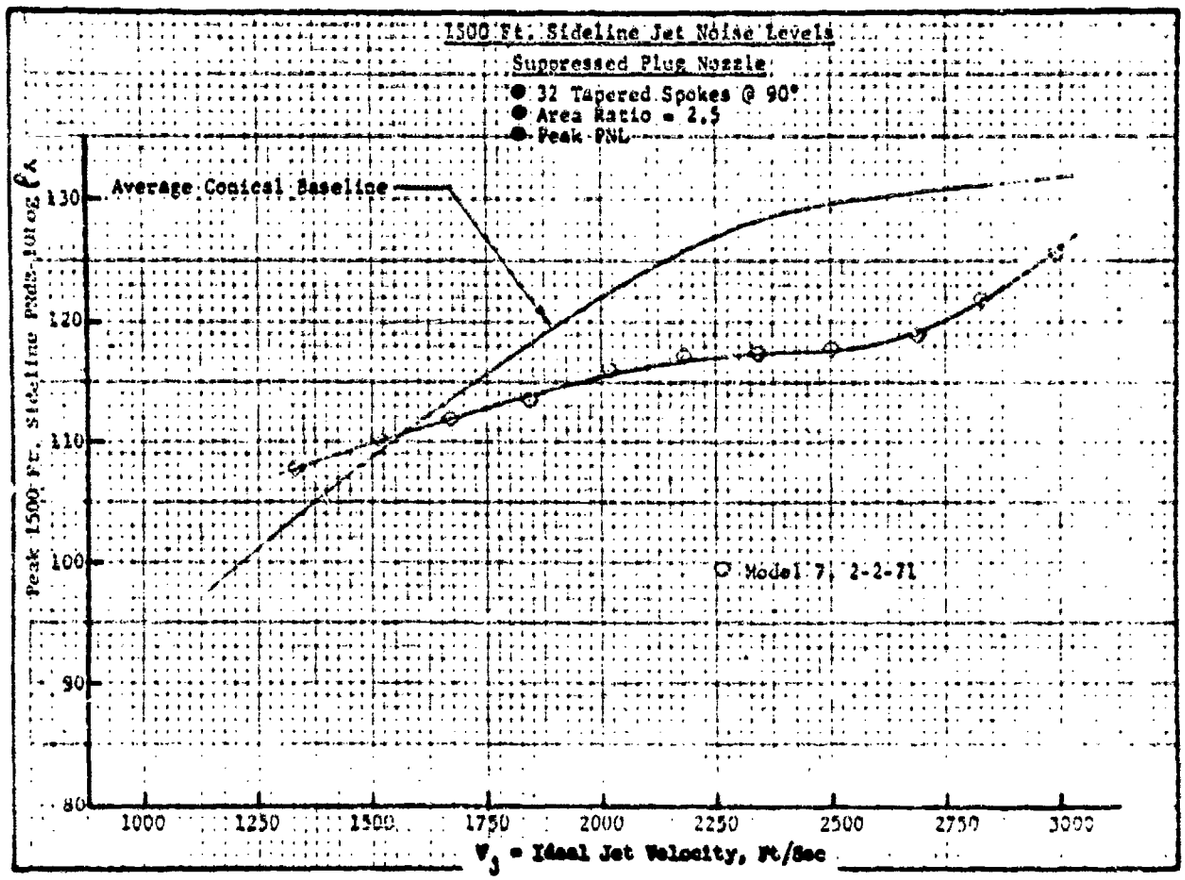


FIGURE V.II.2-25 320 FT ARC AND 300 FT SIDELINE JET NOISE LEVELS FOR MODEL 7



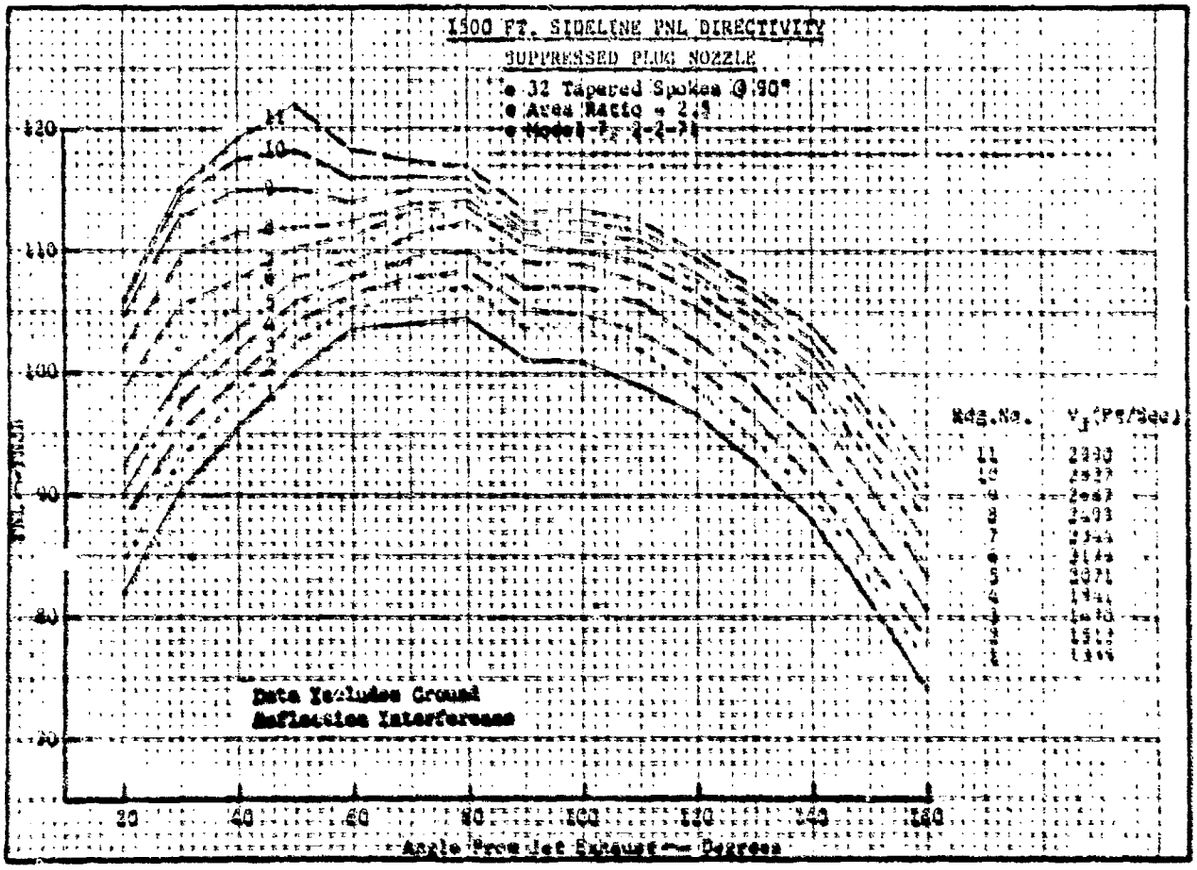
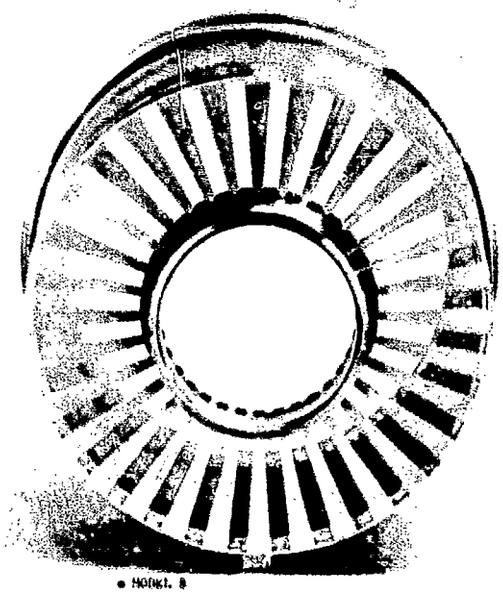


FIGURE V.II.2-26 1500 FT SIDELINE JET NOISE LEVELS AND PNL DIRECTIVITY FOR MODEL 7



- MODEL 8
- 32 TAPERED SPOKES SLANTED 10° FORWARD
- AREA RATIO = 2.0

Model 8 used 32 tapered spokes, equally spaced and tilted 10° forward of the perpendicular to the nozzle axis. Spoke width at tip = .5739"; hub = .1875". Exit Area, A8 = 30.83 in^2, Area Ratio = 2.0, Material: 304 S.S. for plug and shroud; RA-333 for spoke suppressors.

TABLE V.H.2-10 TEST SUMMARY

MODEL NO. 8

: SCALE MODEL A_8 = 30.83 $in.^2$

DESCRIPTION: 32 Tapered Spokes Slanted 10° Foward (Normal to Plug) Area Ratio = 2.0

FULL SCALE A_8 = 13.70 $ft.^2$

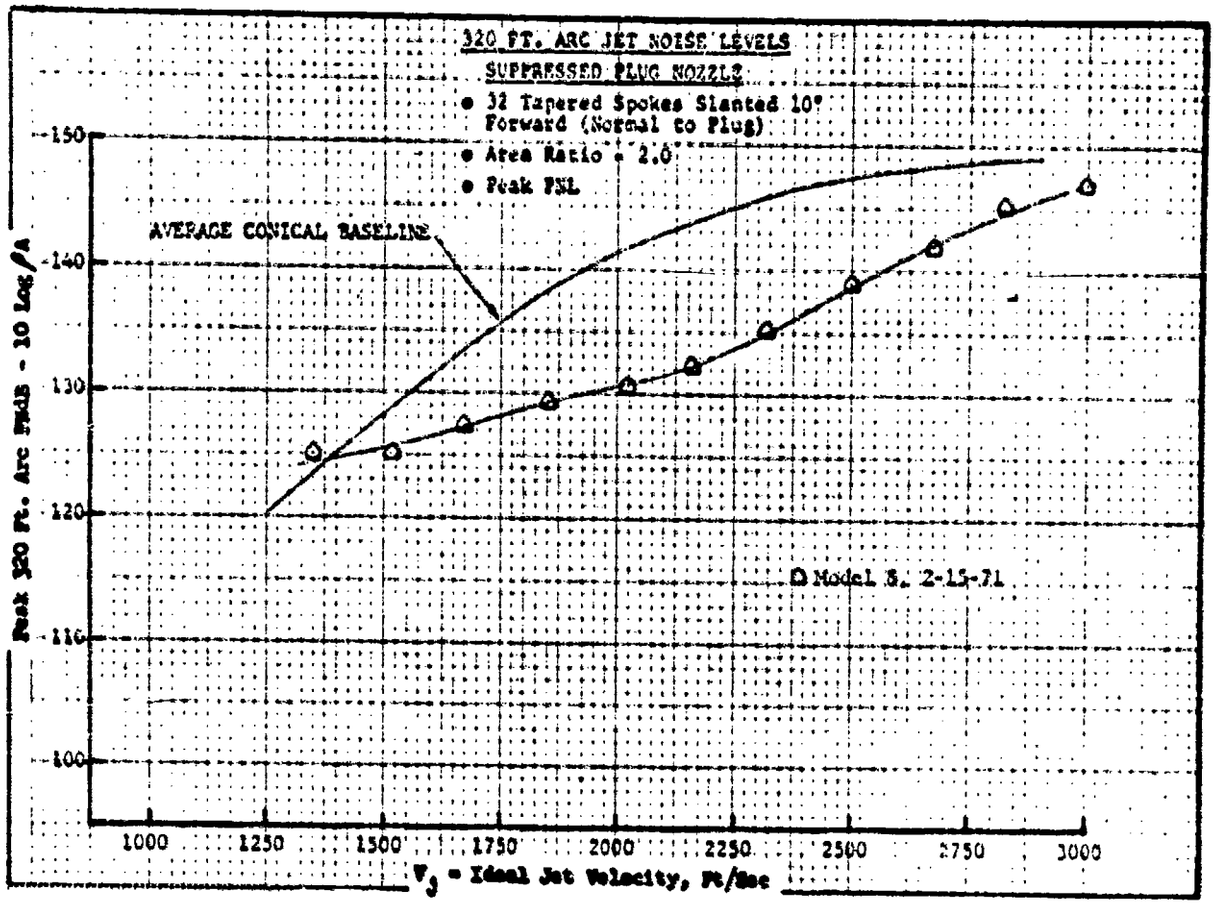
DATE: 2-15-71

SCALE FACTOR = 6:1

- DATA INCLUDES GROUND REFLECTION INTERFERENCE
- ANGLE REFERENCED TO JET EXHAUST

TEST CONDITIONS								ACOUSTIC TEST RESULTS									
									320 FT. ARC		300 FT. SIDELINE		1500 FT. SIDELINE		2125 FT. SIDELINE	
RUN NO.	P_0 PSIA	P_{T8} PSIA	P_{T8}/P_0	T_{T8} °R	IDEAL V_j FT/SEC	W_8 PPS	$10Log^{\Delta A}$	PEAK PNdB	PEAK ANGLE	PEAK PNdB	PEAK ANGLE	PEAK PNdB	PEAK ANGLE	PEAK PNdB	PEAK ANGLE
3	24.430	22.249	1.542	1279	1944	8.99	-3.4	121.9	60	121.1	70	102.8	70	97.8	70
4	24.431	24.604	1.705	1327	1518	10.02	-3.4	121.9	60	121.2	70	103	70	98.3	70
5	24.430	26.847	1.860	1400	1672	10.65	-3.6	123.0	60	123.3	70	104.9	70	100.4	70
6	24.430	29.963	2.076	1487	1851	11.76	-3.7	125.7	70	125.2	70	107.2	70	102.4	70
7	24.430	32.958	2.284	1589	2020	12.68	-3.8	126.9	70	126.6	70	108.9	70	104.2	70
8	24.434	35.876	2.489	1652	2157	13.30	-3.8	128.5	50	127.8	70	110.3	70	105.7	70
9	24.435	39.496	2.730	1744	2316	14.43	-3.8	131.4	40	128.9	50	112.3	50	108.3	50
10	24.435	43.892	3.036	1850	2494	15.36	-3.8	132.4	40	132	50	116.3	50	112.4	50
11	24.443	48.827	3.363	1963	2663	16.12	-3.8	134.1	30	133.8	50	119.8	50	115.9	50
12	24.444	52.766	3.648	2079	2830	17.34	-3.8	141.4	50	139.2	50	122.9	50	118.8	50
13	24.450	58.034	4.016	2208	2996	18.29	-3.7	143.2	50	142	50	125.1	50	121.3	50

FIGURE V.H.2-27 HARDWARE AND TEST SUMMARY FOR MODEL 8



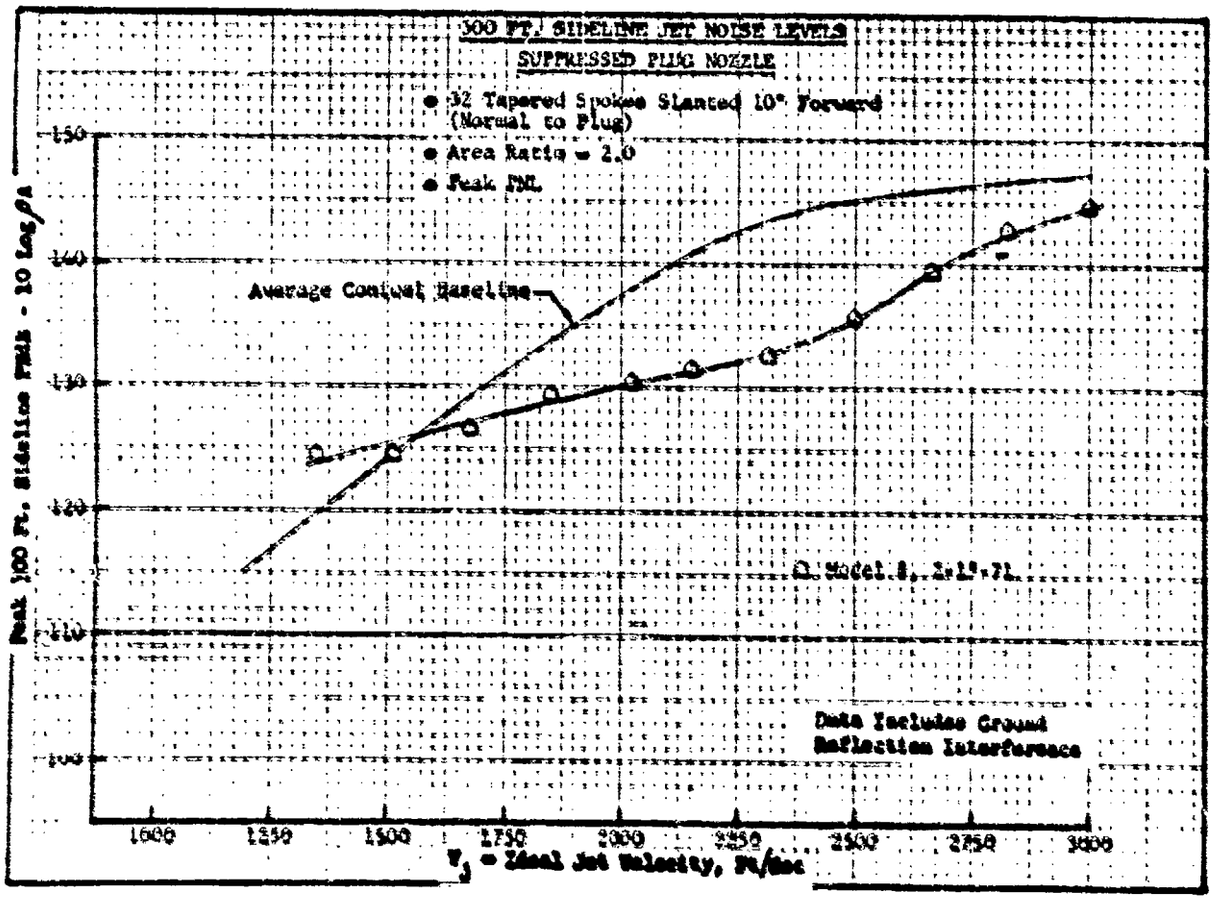
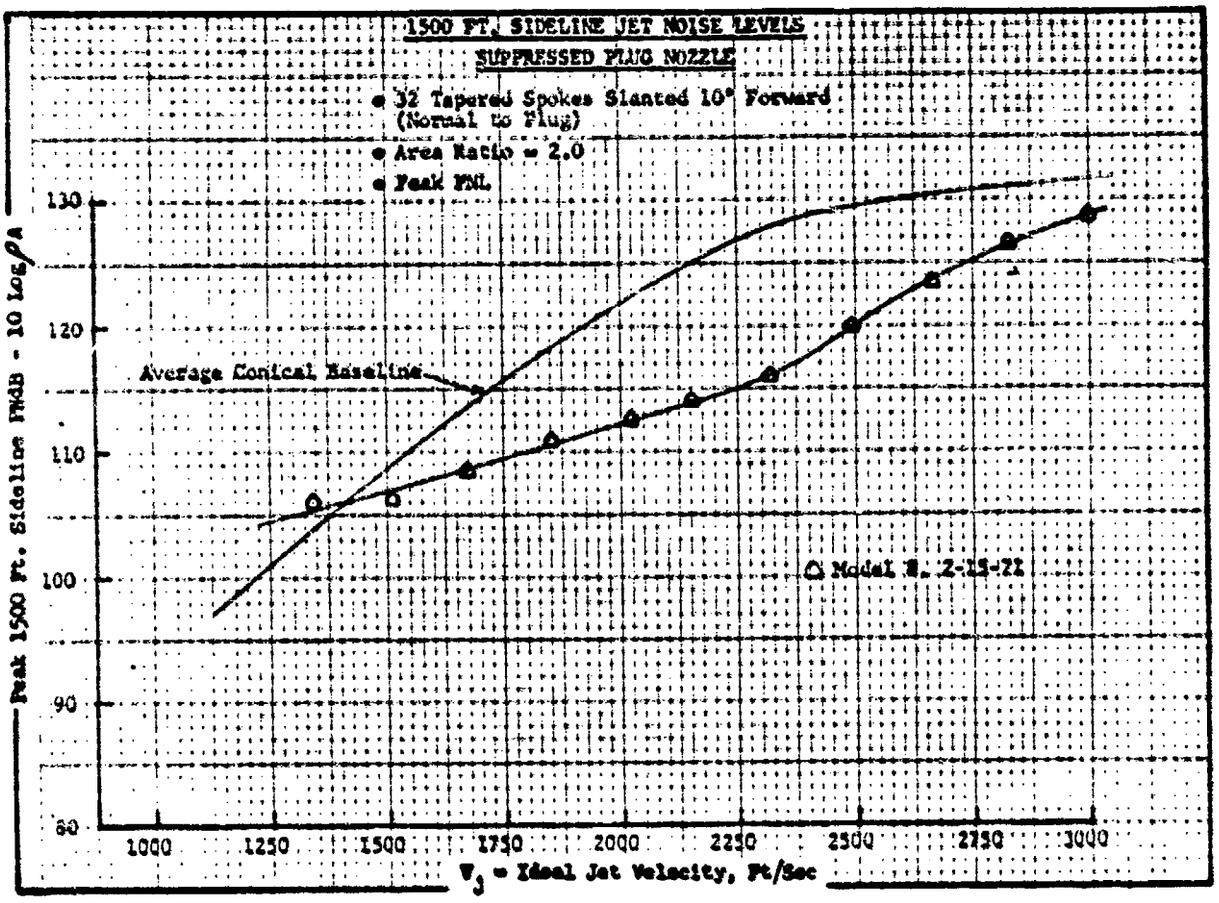


FIGURE V....2-28 320 FT ARC AND 300 FT SIDELINE JET NOISE LEVELS FOR MODEL 8



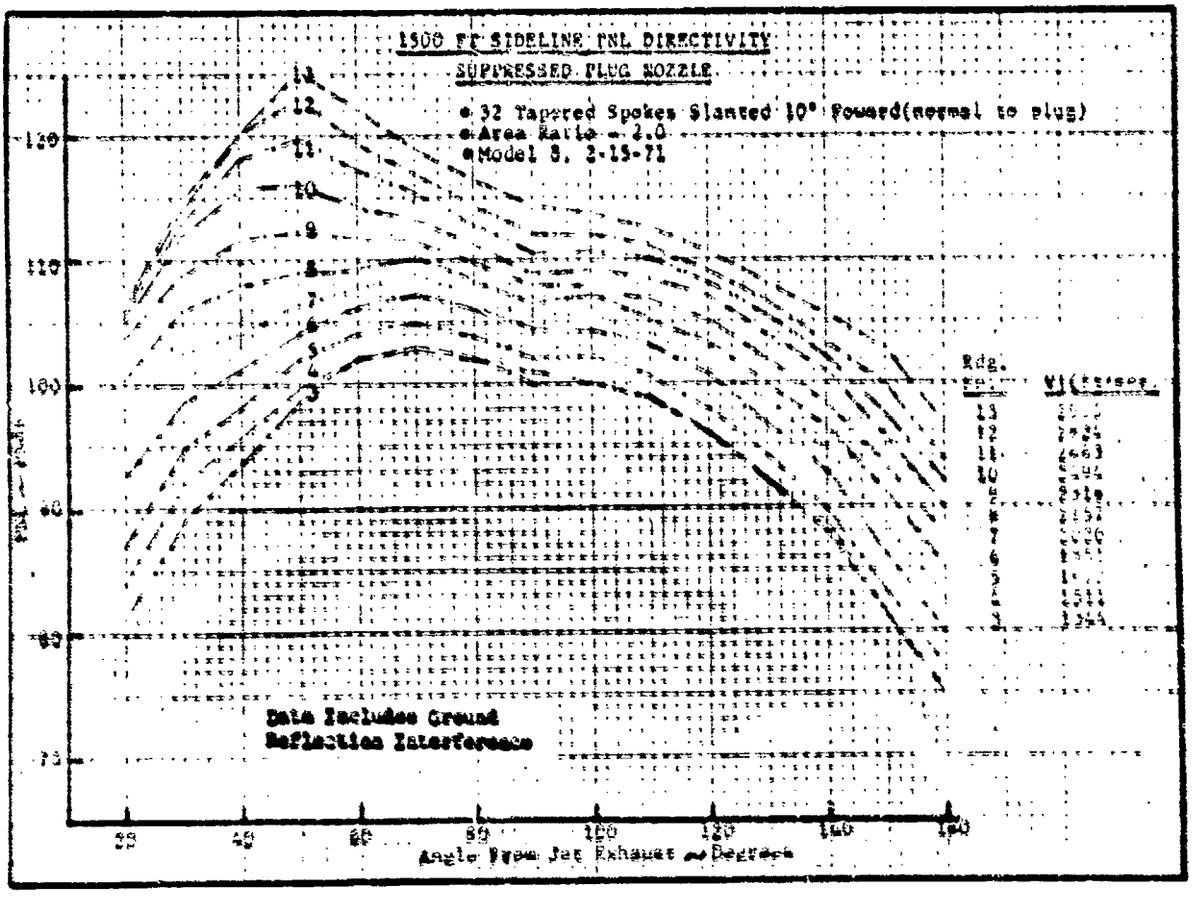
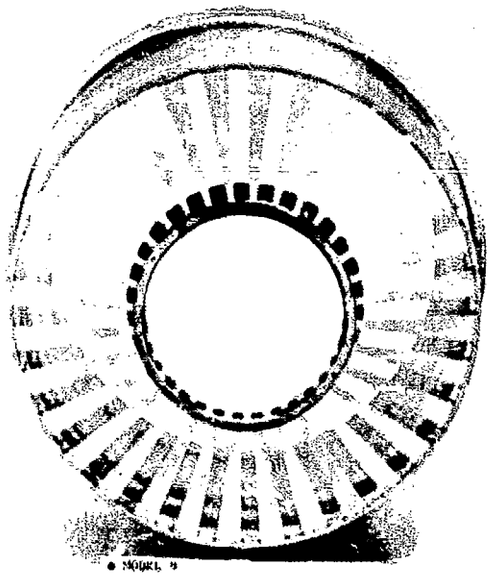


FIGURE V.H.2-29 1500 FT SIDELINE JET NOISE LEVELS AND PNL DIRECTIVITY FOR MODEL 8



- MODEL 9
- 32 TAPERED SPOKES SLANTED 10° AFT
- AREA RATIO = 2.0

Model 9 employed 32 tapered spokes, equally spaced and tilted 10° aft off the perpendicular to the nozzle axis. Spoke width at tip = .5738"; hub = .1875". Exit Area, A_8 = 30.83 in^2, Area Ratio = 2.0, Material: 304 S.S. for plug and shroud; RA-333 for spoke suppressors.

TABLE V.E.2-11 TEST SUMMARY

MODEL NO. 9

DESCRIPTION: 32 Tapered Spokes Slanted 10° Aft, Area Ratio = 2.0

DATE: 6-28-71

SCALE MODEL A_8 = 30.83 $in.^2$

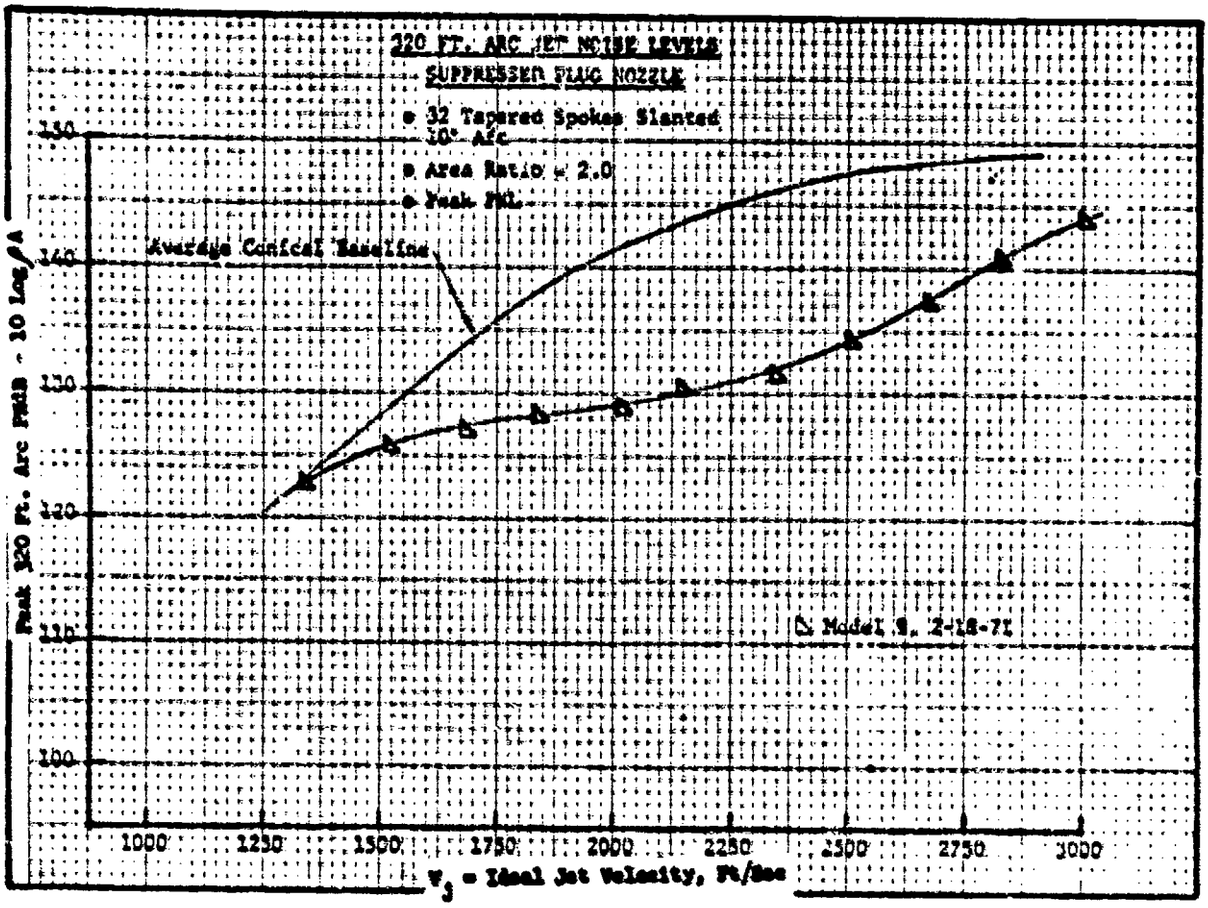
FULL SCALE A_8 = 13.70 $ft.^2$

SCALE FACTOR = 6:1

- DATA INCLUDES GROUND REFLECTION INTERFERENCE
- ANGLE REFERENCED TO JET EXHAUST

TEST CONDITIONS							ACOUSTIC TEST RESULTS									
								320 FT. ARC		320 FT. SIDELINE		1500 FT. SIDELINE		2128 FT. SIDELINE	
PNT. NO.	P_0 PSIA	P_{T8} PSIA	P_{T8}/P_0	Q_{T8} Q_∞	IDEAL V_j FT/SEC	V_8 FPS	$10\log_{10}/A_8$	PEAK PWLS	PEAK ANGLE	PEAK PWLS	PEAK ANGLE	PEAK PWLS	PEAK ANGLE	PEAK PWLS	PEAK ANGLE
1	24.256	21.959	1.140	1269	1337	9.42	-3.4	119.4	30	119.4	30	101.4	30	96.6	30
2	24.591	24.727	1.302	1340	1516	10.59	-3.4	121.4	30	121.4	30	103.6	30	98.8	30
3	24.529	27.163	1.830	1416	1682	11.16	-3.4	123.3	30	123.3	30	105.8	30	101	30
4	24.526	29.031	2.067	1470	1836	12.24	-3.4	124.6	30	124.6	30	107	30	102.3	30
5	24.521	30.113	2.260	1501	2017	13.06	-3.8	125.2	30	125.2	30	107.7	30	103	30
6	24.519	30.830	2.421	1523	2145	13.83	-3.8	126.2	30	126.2	30	109.2	30	104.6	30
7	24.516	30.704	2.755	1573	2333	14.52	-3.8	127.9	30	127.9	30	110.7	30	106.5	30
8	24.500	44.50	3.053	1857	2503	15.38	-3.8	130.5	30	128.3	60	111.3	30	107.1	30
9	24.490	48.55	3.349	1971	2630	16.77	-3.8	133.6	60	130.9	50	114.6	50	110.5	50
10	24.495	53.00	3.457	2032	2832	17.79	-3.8	132.1	60	134.4	50	118.1	50	114	50
11	24.494	53.31	4.316	2221	3003	18.64	-3.8	140.2	50	138	50	121.9	50	118.1	50

FIGURE V.E.2-30 HARDWARE AND TEST SUMMARY FOR MODEL 9



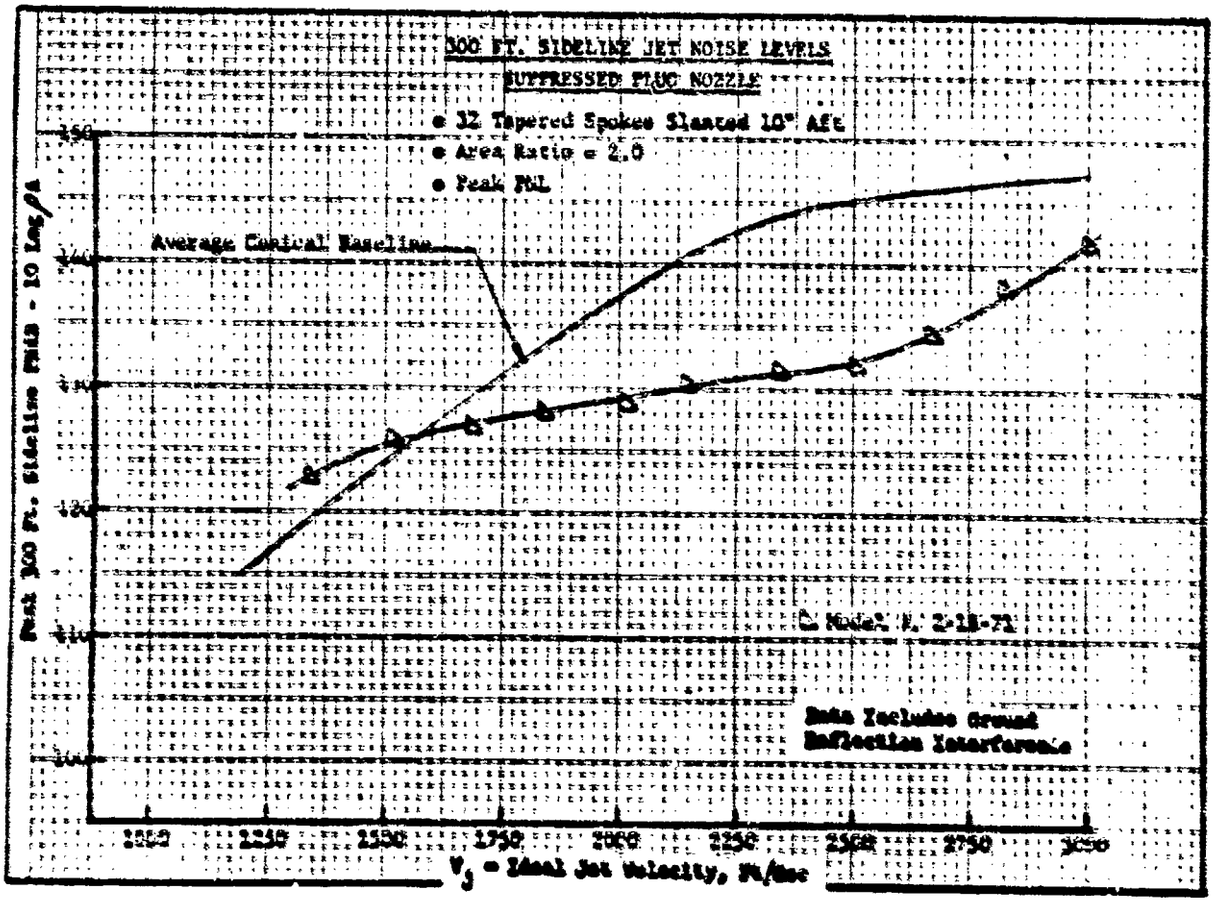
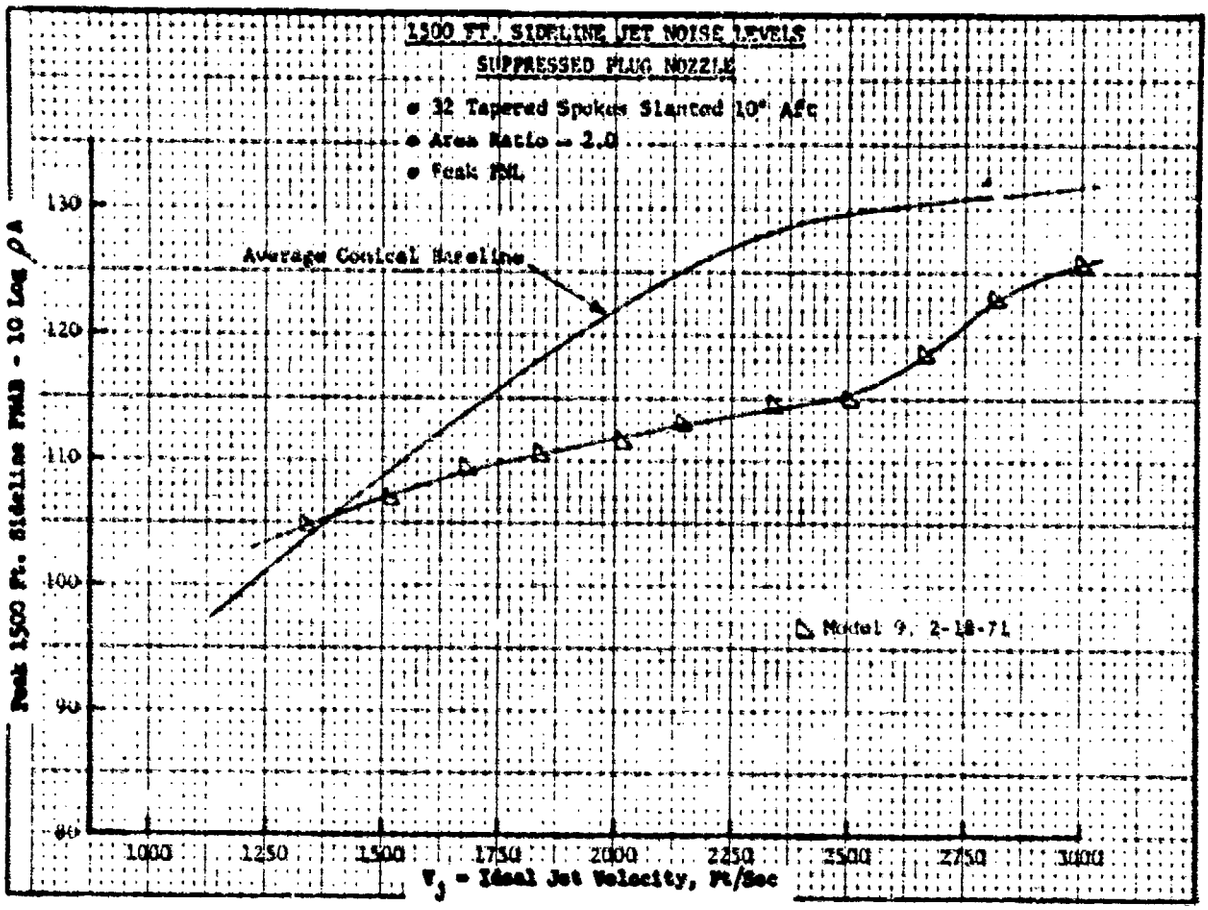


FIGURE V.H.2-31 320 FT ARC AND 300 FT SIDELINE JET NOISE LEVELS FOR MODEL 9



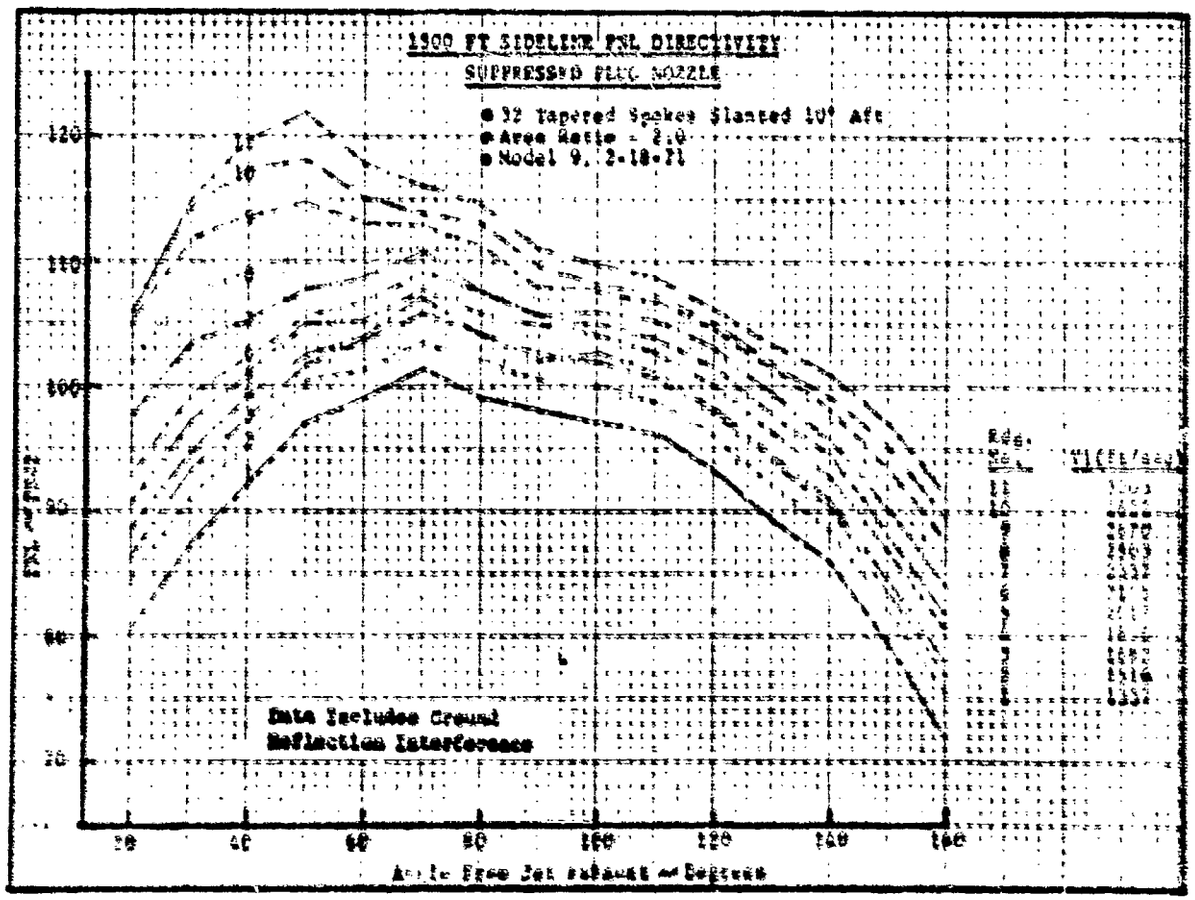
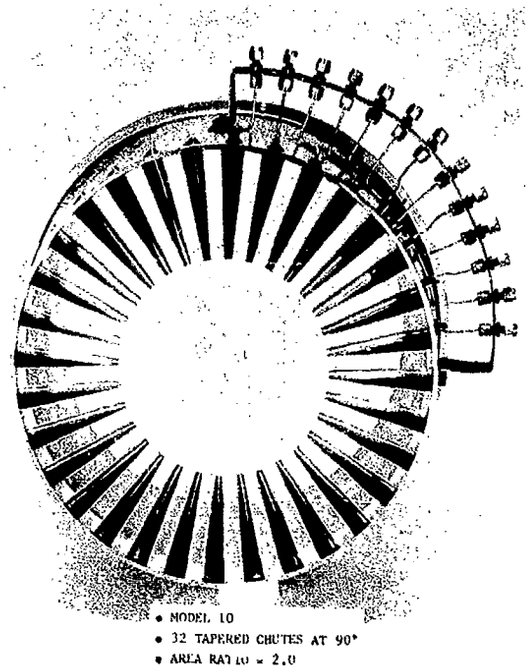


FIGURE V-3-32 1500 FT SIDELINE JET NOISE LEVELS AND PNL DIRECTIVITY FOR MODEL 9



Model 10 had 32 tapered chute suppressors, equally spaced and set at 90° to the nozzle axis. Chute width at tip = .565"; hub = .1875". Exit Area, A8 = 30.83 in^2, Area Ratio = 2.0, Material: 304 S.S. for plug, shroud and chutes.

TABLE V.H.2-12 TEST SUMMARY

MODEL NO. 10

DESCRIPTION: 32 Tapered Chutes @ 90°, Area Ratio = 2.0

DATE: 1-23-71

SCALE MODEL A_8 = 30.83 $in.^2$

FULL SCALE A_8 = 13.70 $ft.^2$

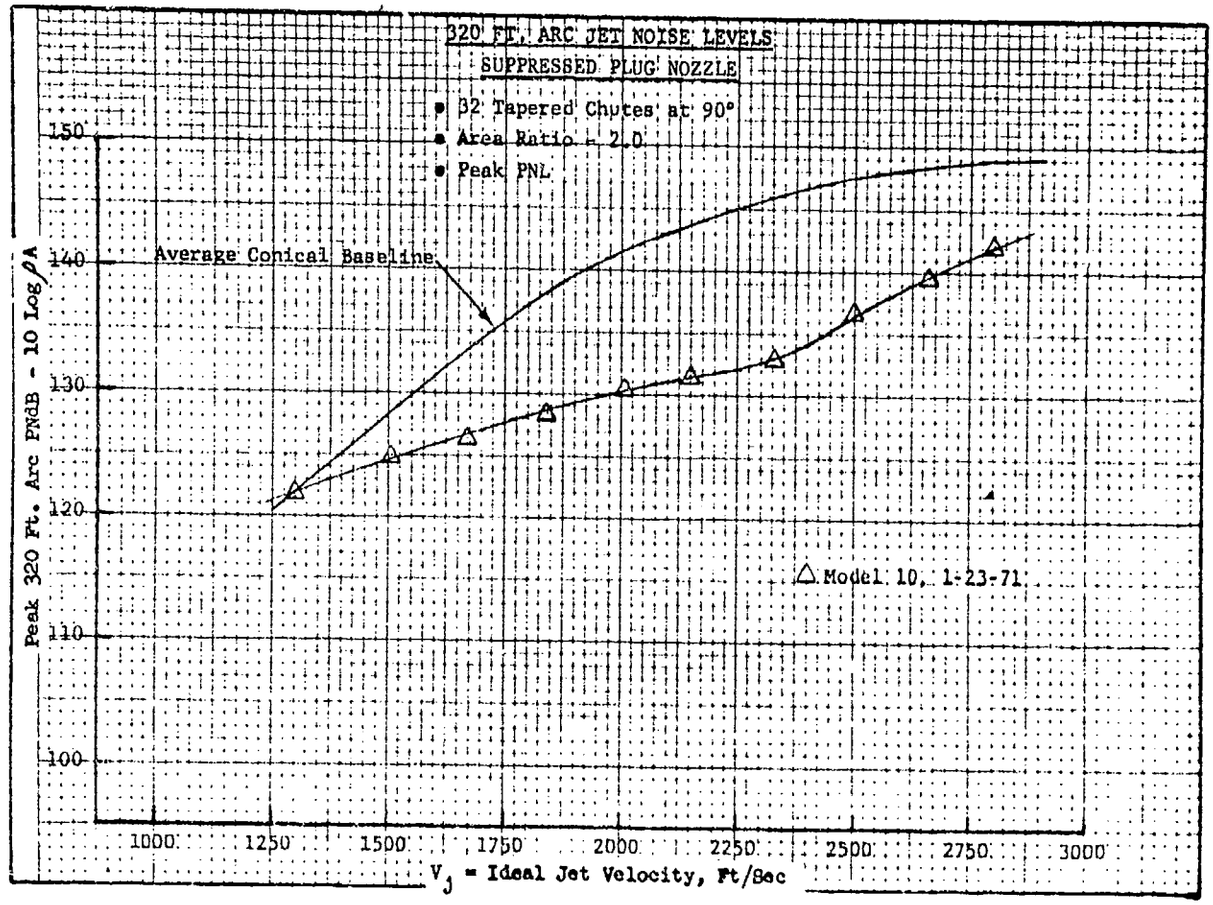
SCALE FACTOR = 8:1

o DATA INCLUDES GROUND REFLECTION INTERFERENCE

o ANGLE REFERENCED TO JET EXHAUST

TEST CONDITIONS							ACOUSTIC TEST RESULTS								
								320 FT. ARC		300 FT. SIDELINE		1500 FT. SIDELINE		2128 FT. SIDELINE	
RDG. NO.	P_O PSIA	P_{T8} PSIA	P_{T8}/P_O	T_{T8} °R	IDEAL V_J FT/SEC	W_8 PPS	10LogρA	PEAK PNdB	PEAK ANGLE	PEAK PNdB	PEAK ANGLE	PEAK PNdB	PEAK ANGLE	PEAK PNdB	PEAK ANGLE
1	14.484	21.684	1.497	1272	1297	9.01	-3.4	118.5	70	118.5	70	100.2	70	95.6	70
2	14.483	24.503	1.692	1337	1507	9.93	-3.4	121.6	70	121.6	70	103.3	70	98.5	70
3	14.480	26.929	1.860	1403	1668	10.67	-3.6	122.8	70	122.8	70	104.8	70	100	70
4	14.478	29.837	2.061	1483	1840	11.51	-3.7	124.7	70	124.7	70	106.9	70	102.1	70
5	14.475	32.860	2.270	1577	2010	12.25	-3.8	126.6	70	126.6	70	108.6	70	103.9	70
6	14.469	35.922	2.483	1642	2150	13.33	-3.8	127.8	50	127.2	70	109.5	70	104.8	70
7	14.469	39.811	2.752	1749	2327	14.31	-3.8	129.2	50	128.7	70	110.9	70	106.4	70
8	14.465	43.862	3.032	1860	2499	15.42	-3.8	132.9	30	129.7	70	112.3	70	108	70
9	14.465	48.330	3.341	1964	2664	16.53	-3.8	136	30/40	132.4	50	116.2	40	112.4	40
10	14.461	52.764	3.649	2039	2798	17.61	-3.7	138.4	40	135.6	50	119.2	50	115.3	40

FIGURE V.H.2-33 HARDWARE AND TEST SUMMARY FOR MODEL 10



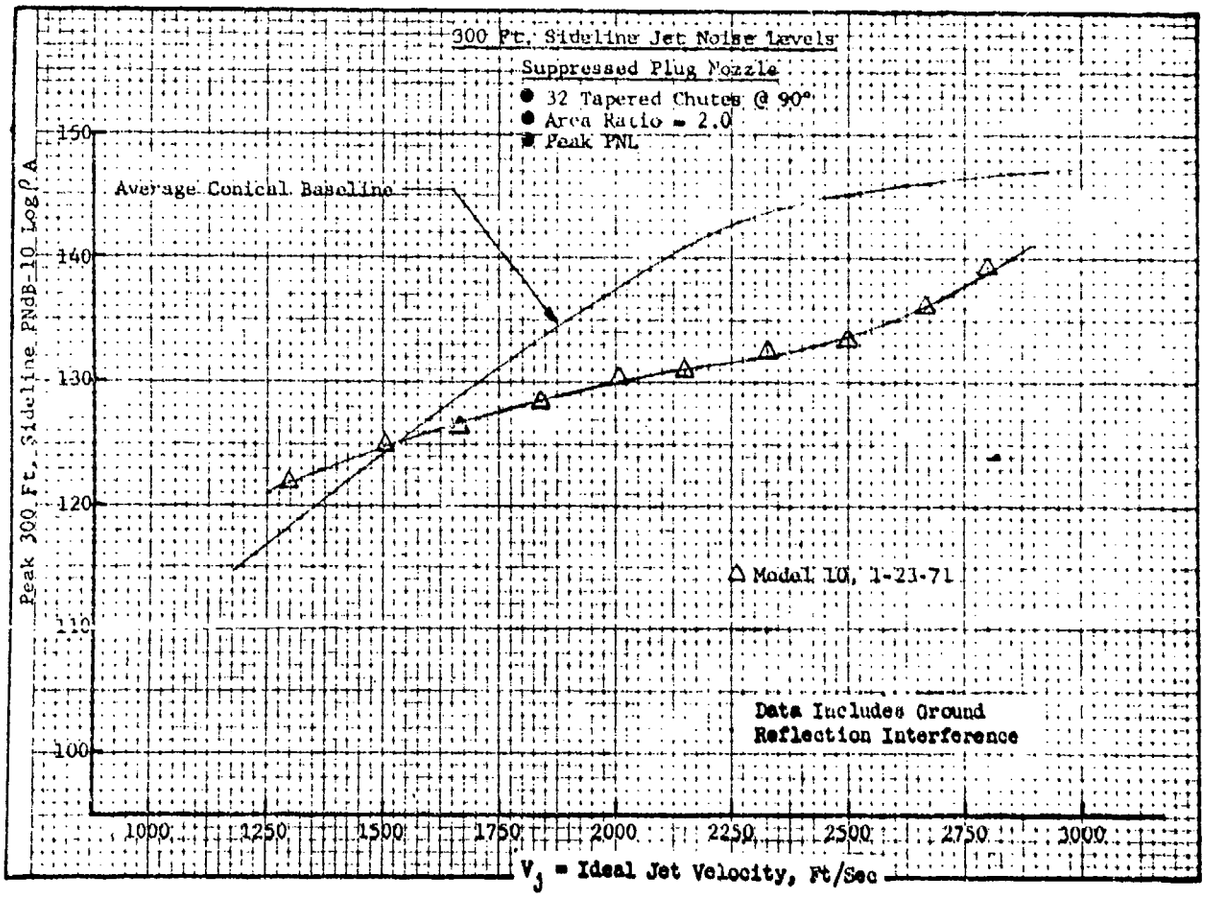
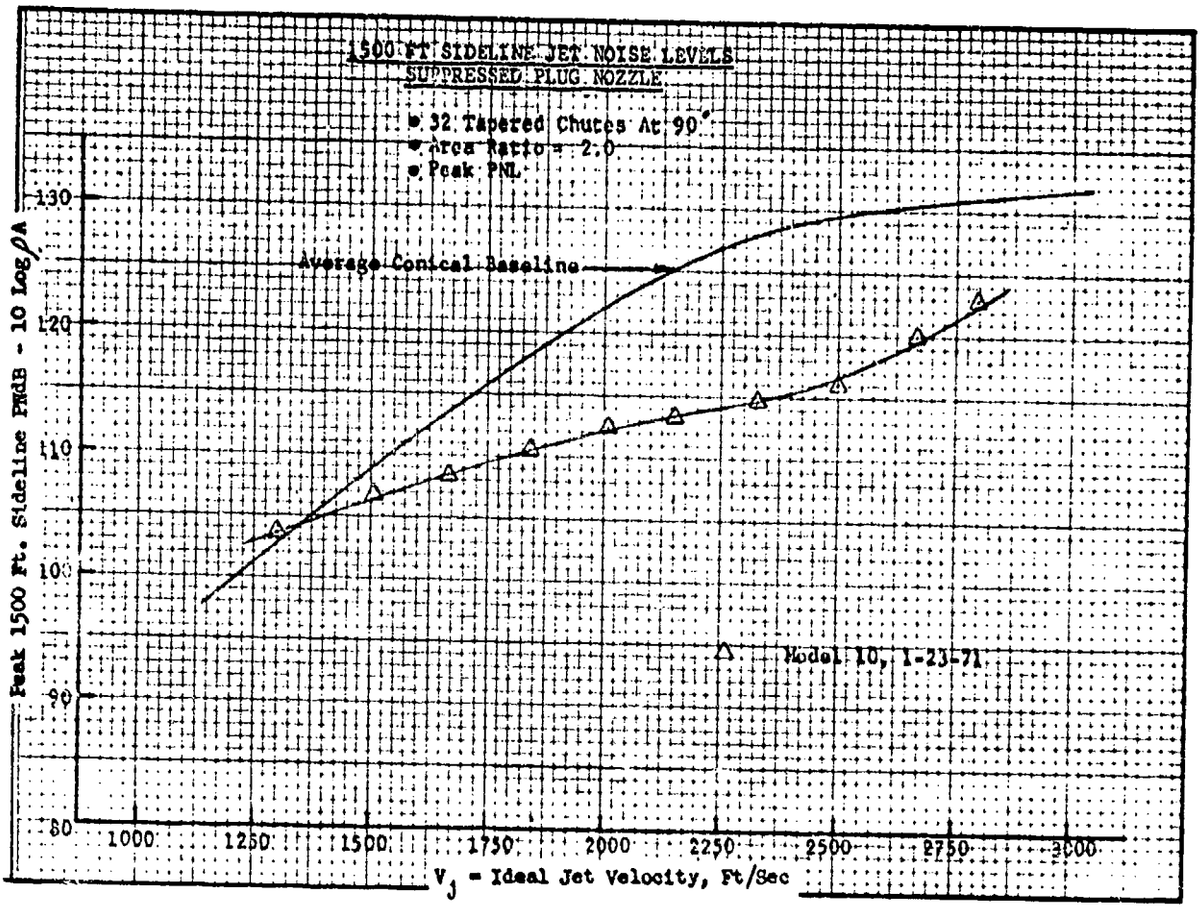


FIGURE V.H.2-34 320 FT ARC AND 300 FT SIDELINE JET NOISE LEVELS FOR MODEL 10



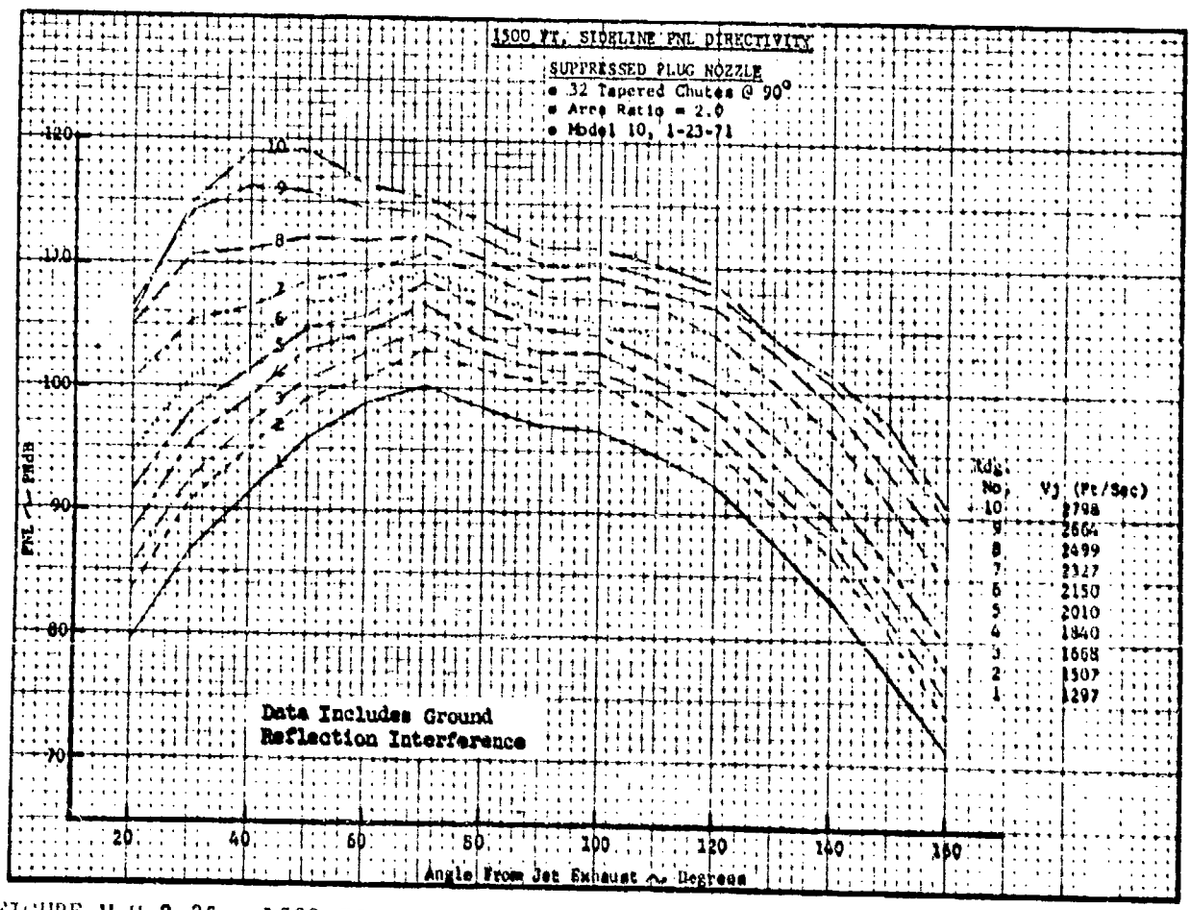
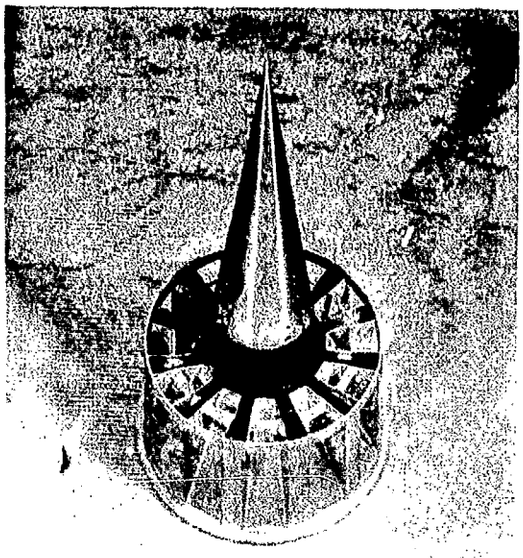


FIGURE V.H.2-35 1500 FT SIDELINE JET NOISE LEVELS AND PNL DIRECTIVITY FOR MODEL 10



- MODEL 11
- NASA CHUTED PLUG NOZZLE
- 12 TAPERED CHUTES SLANTED 10° FORWARD
- 10° HALF ANGLE STRAIGHT PLUG
- AREA RATIO = 3.0

Model 11 was a NASA chuted plug nozzle which had a 20° conical plug and 12 tapered chutes slanted 10° forward off the perpendicular to the nozzle axis. Exit Area, A8 = 17.08 in^2, Area Ratio = 3.0, Material: 304 S.S. for plug, shroud; RA-333 for spoke suppressors.

TABLE V.H.2-13 TEST SUMMARY

MODEL NO. 11

SCALE MODEL A_8 = 17.08 in^2

DESCRIPTION: NASA Chuted Plug Nozzle, 12 Tapered Chutes Slanted 10° Foward (Normal to Plug), 10° Half Angle Straight Plug, Area Ratio = 3.0

FULL SCALE A_8 = 7.59 ft^2

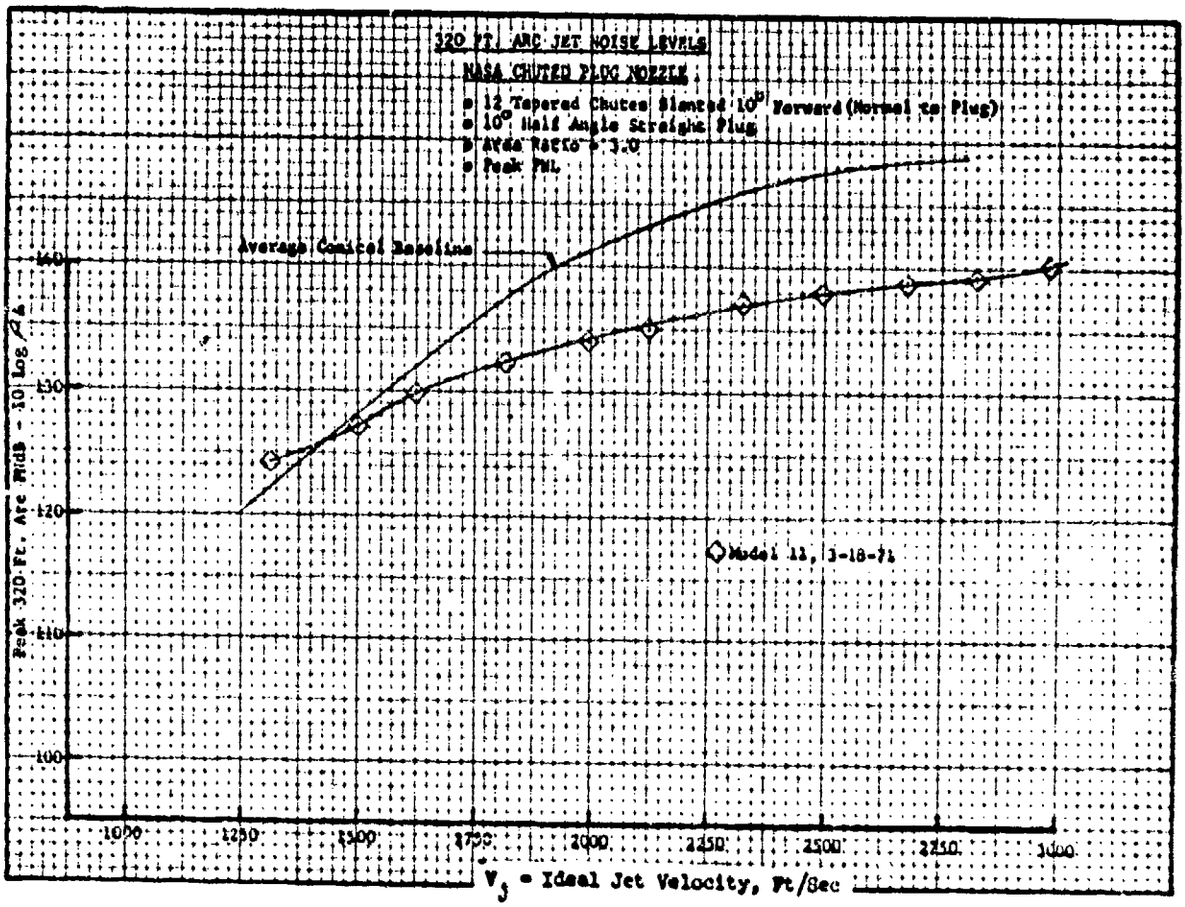
DATE: 3-18-69

SCALE FACTOR = 8:1

- o DATA INCLUDES GROUND REFLECTION INTERFERENCE
- o ANGLE REFERENCED TO JET EXHAUST

TEST CONDITIONS								ACOUSTIC TEST RESULTS									
									320 FT. ARC		300 FT. SIDELINE		1500 FT. SIDELINE		2128 FT. SIDELINE	
RDG. NO.	P_0 PSIA	P_{T8} PSIA	P_{T8}/P_0	T_{T8} °R	IDEAL V_j FT/SEC	V_8 FPS	10Logρ_8	PEAK PNLB	PEAK ANGLE	PEAK PNLB	PEAK ANGLE	PEAK PNLB	PEAK ANGLE	PEAK PNLB	PEAK ANGLE
3	14.521	26.571	1.830	2409	1651	5.777	-6.1	123.8	50	122.1	60	104.9	60	100.6	60
4	14.514	29.358	2.023	1482	1818	6.303	-6.2	126.2	50	124.9	60	107.9	60	103.6	60
5	14.509	32.358	2.230	1585	1995	6.782	-6.4	127.6	60	126.6	60	109.6	60	105.3	60
6	14.516	35.397	2.438	1635	2125	7.293	-6.3	128.8	60	127.9	60	110.9	60	106.6	60
7	14.494	39.019	2.693	1782	2326	7.691	-6.5	130.6	50	129.6	60	112.7	60	108.4	60
8	14.489	43.694	3.016	1862	2495	8.264	-6.4	131.6	60	130.7	60	113.9	70	109.7	70
9	14.489	48.050	3.316	1994	2676	8.665	-6.4	132.4	60	132.2	70	115.4	70	111.2	70
10	14.489	52.264	3.607	2094	2824	9.293	-6.4	132.9	50	132.5	70	115.7	70	111.5	70
11	14.474	57.039	3.941	2203	2980	9.984	-6.4	133.8	50	133.1	70	116.3	70	112.1	70
12	14.460	24.351	1.684	1332	1498	5.681	-6.0	121.1	50	119.1	60	102.2	50	97.9	50
13	14.460	21.670	1.499	1301	1313	4.962	-6.0	118.3	50	116.0	50	99.5	50	95.3	50

FIGURE V.H.2-36 HARDWARE AND TEST SUMMARY FOR MODEL 11



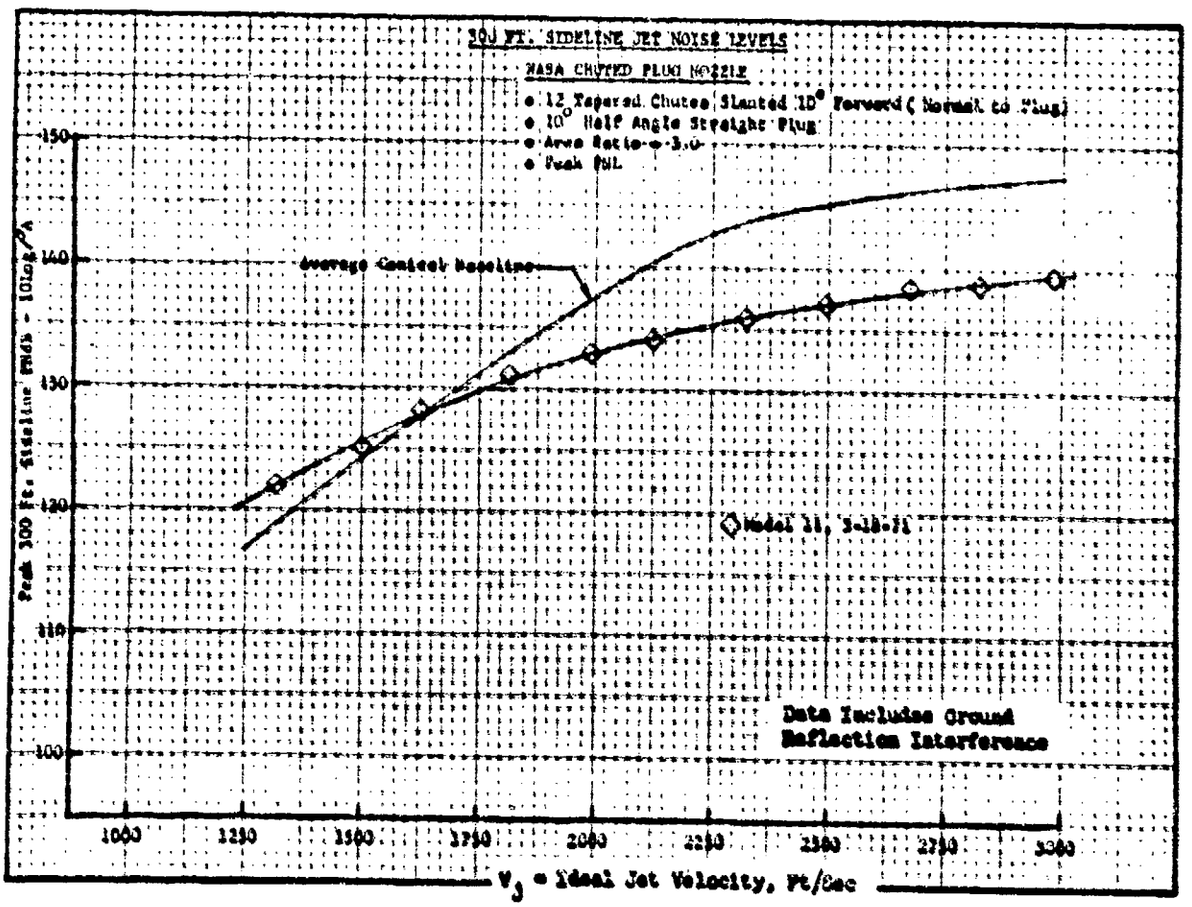
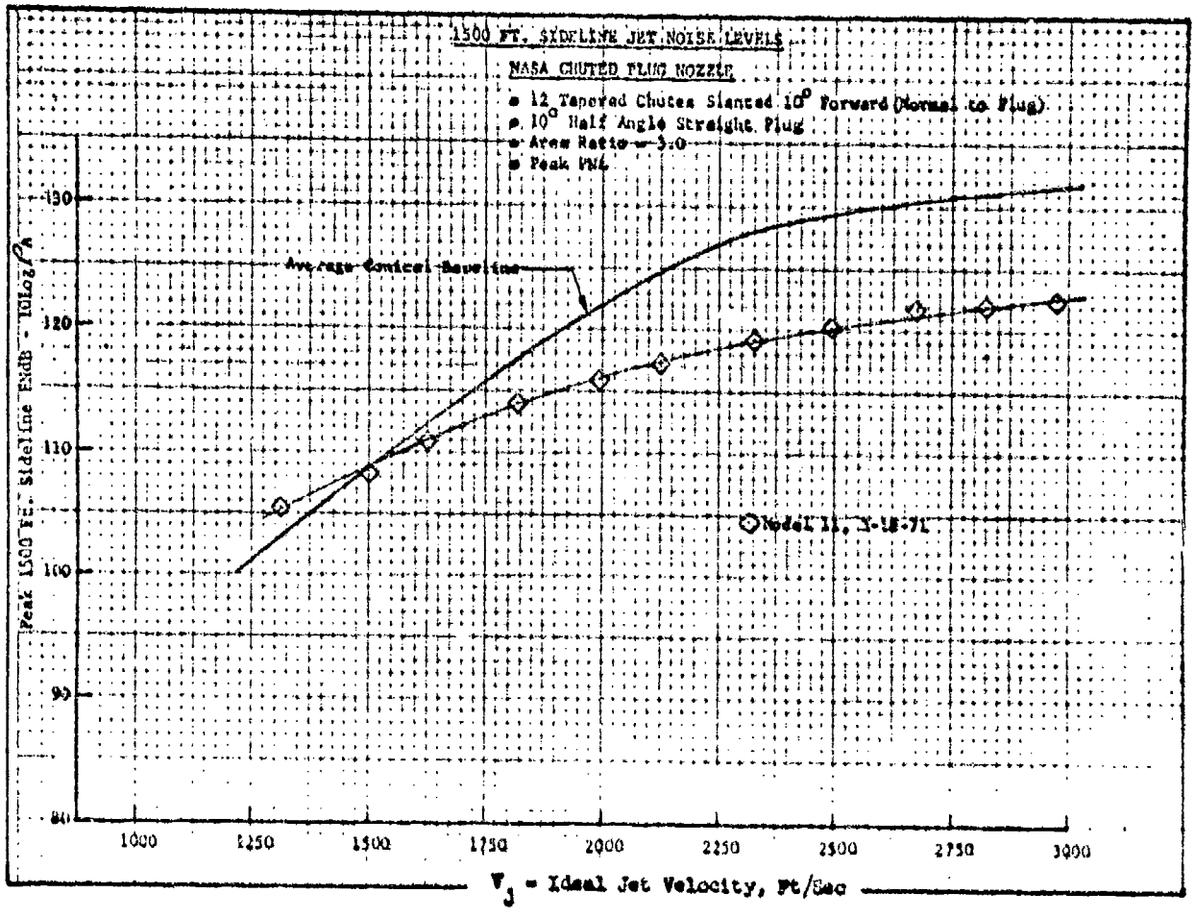


FIGURE V.II.2-37 320 FT ARC AND 300 FT SIDELINE JET NOISE LEVELS FOR MODEL 11



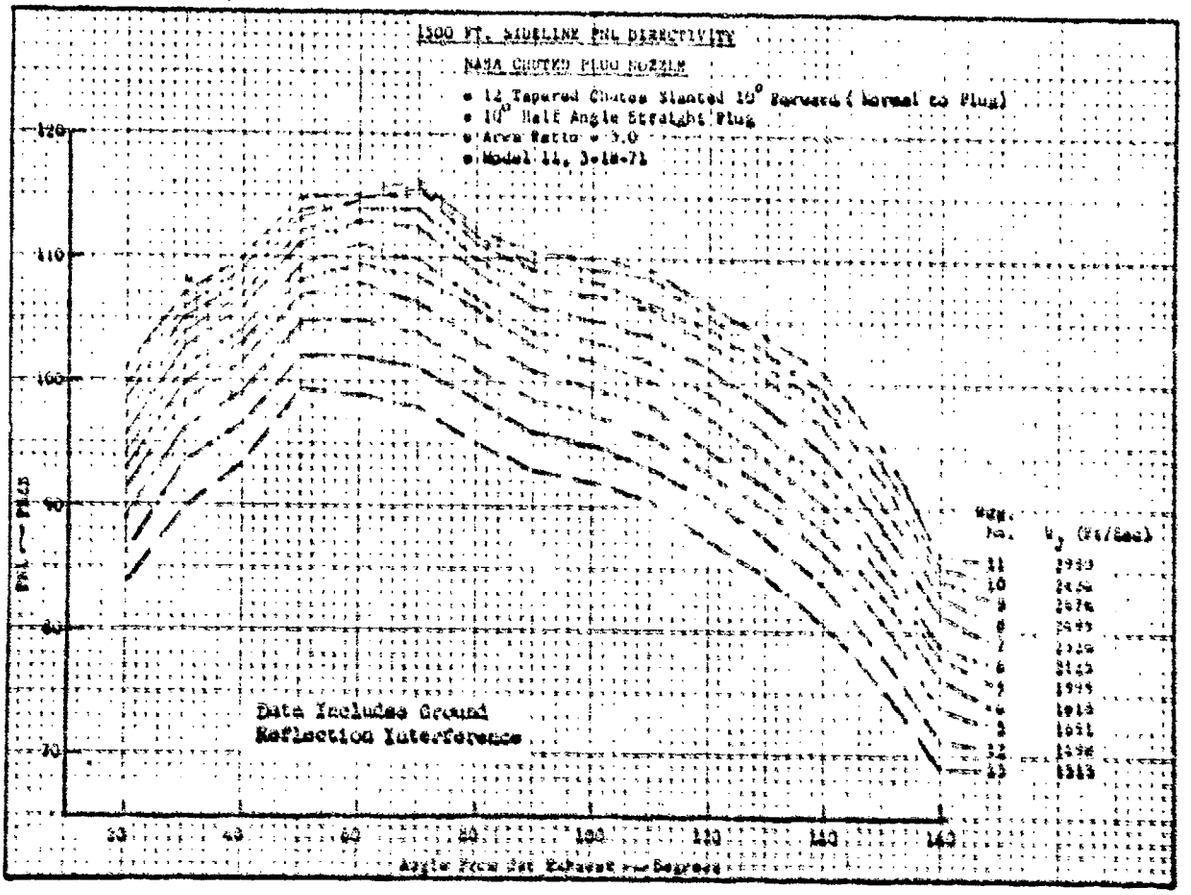
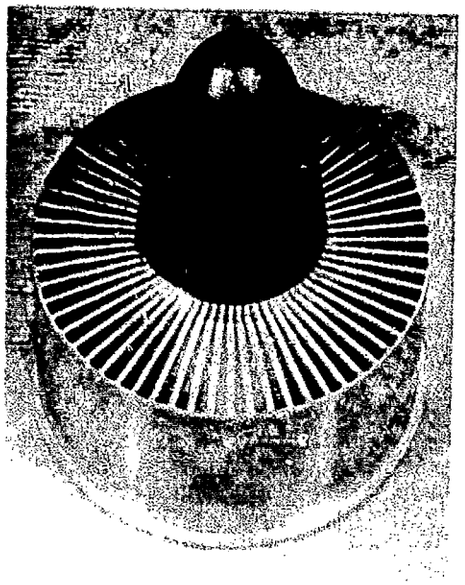


FIGURE V.H.2-38 1500 FT SIDELINE JET NOISE LEVELS AND PNL DIRECTIVITY FOR MODEL 11



Model 12 had 64 parallel sided spokes, equally spaced and set at 90° to the nozzle axis. Spoke width at tip = .1875"; hub = .1875". Exit Area, A8 = 30.83 in^2, Area Ratio = 2.0, Material: 304 S.S. for plug and shroud; RA-333 for spoke suppressors.

- MODEL 12
- 64 PARALLEL SIDED SPOKES AT 90°
- AREA RATIO = 2.0

TABLE V.H.2-14 TEST SUMMARY

MODEL NO. 12

DESCRIPTION: 64 Parallel Sided Spokes @ 90°, Area Ratio = 2.0

DATE: 2-25-71

SCALE MODEL A_8 = 30.83 $in.^2$

FULL SCALE A_8 = 13.70 $ft.^2$

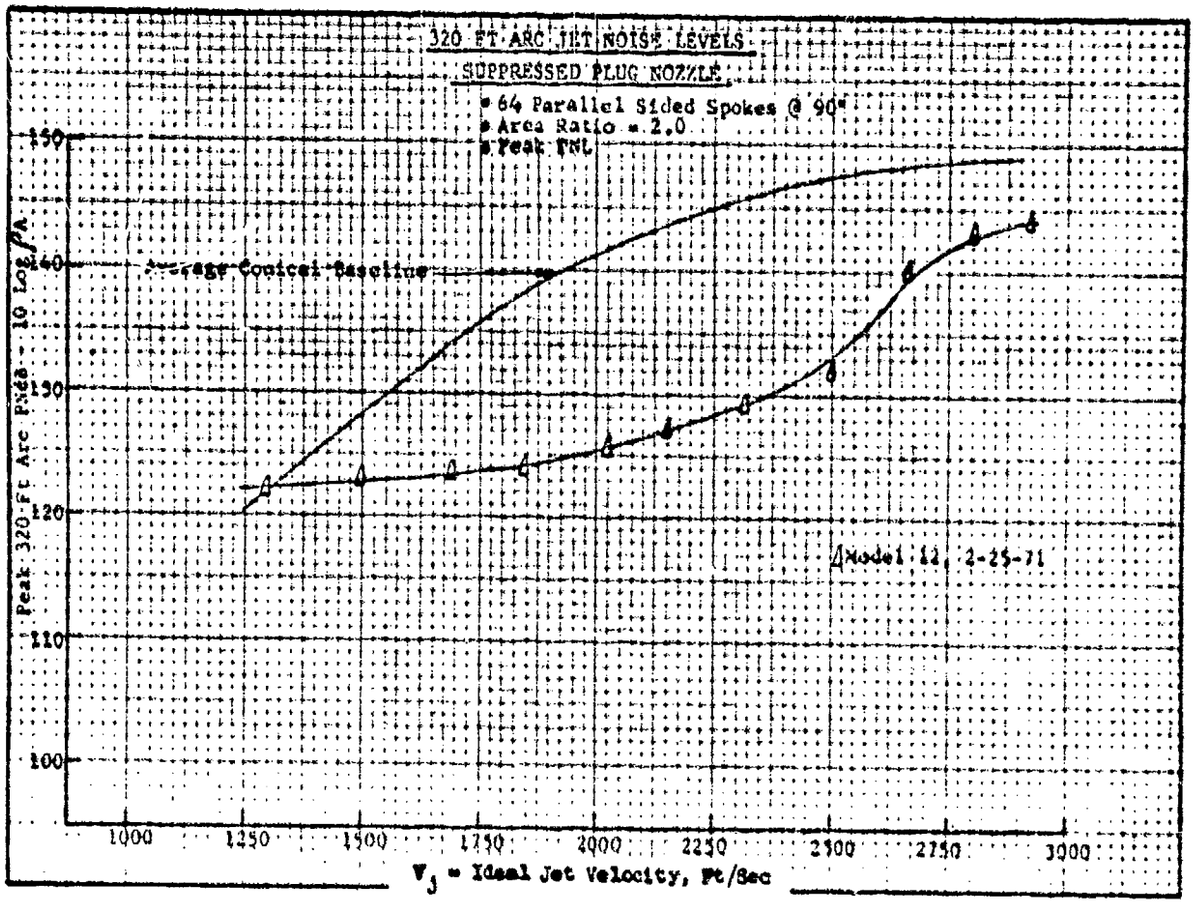
SCALE FACTOR = 8:1

o DATA INCLUDES GROUND REFLECTION INTERFERENCE

o ANGLE REFERENCED TO JET EXHAUST

TEST CONDITIONS							ACOUSTIC TEST RESULTS							
RUN NO.	P_0 PSIA	P_{T8} PSIA	P_{T8}/P_0	T_{T8} °R	IDEAL V_j FPS	W_8 PPS	ΔOL_{eq} PA	320 FT. ARC PEAK PNLA	320 FT. ARC PEAK ANGLE	300 FT. SIDELINE PEAK PNLB	300 FT. SIDELINE PEAK ANGLE	1500 FT. SIDELINE PEAK PNLB	1500 FT. SIDELINE PEAK ANGLE	2133 FT. SIDELINE PEAK PNLB	2133 FT. SIDELINE PEAK ANGLE
1	14.381	21.911	1.496	1272	1295	9.45	-3.4	119	80	119.6	80	100.5	80	95.1	80
2	14.379	24.289	1.690	1315	1499	10.27	-3.4	119.5	70	119.5	70	100.3	70	95.2	70
3	14.367	27.113	1.886	1405	1687	11.13	-3.6	119.9	70	119.9	70/80	101	70	96.3	70
4	14.373	29.637	2.062	1482	1841	11.69	-3.7	120.5	70	120.5	70	102.9	70	98.6	70
5	14.369	33.029	2.299	1580	2026	12.80	-3.8	121.9	70	122	70	105.4	70	101.3	70
6	14.364	35.929	2.501	1638	2169	13.70	-3.7	123.3	70	123.3	70	106.9	70	101.9	70
7	14.364	39.569	2.754	1715	2342	14.55	-3.8	125.6	70	125.7	70	109.4	70	104.4	70
8	14.364	44.299	3.084	1812	2583	15.49	-3.8	129.9	70	129.9	50	113.1	50	109.3	50
9	14.365	48.349	3.367	1955	2669	17.87	-3.8	136.3	50	131.9	40/50	116.6	40	111.9	40
10	14.364	52.699	3.668	2041	2804	18.49	-3.7	139.4	40	136.4	40/50	120.2	40	116.5	40
11	14.363	53.953	3.757	2180	2930	18.15	-3.9	140.4	40	137.1	50	121.3	50	117.5	40/50

FIGURE V.H.2-39 HARDWARE AND TEST SUMMARY FOR MODEL 12



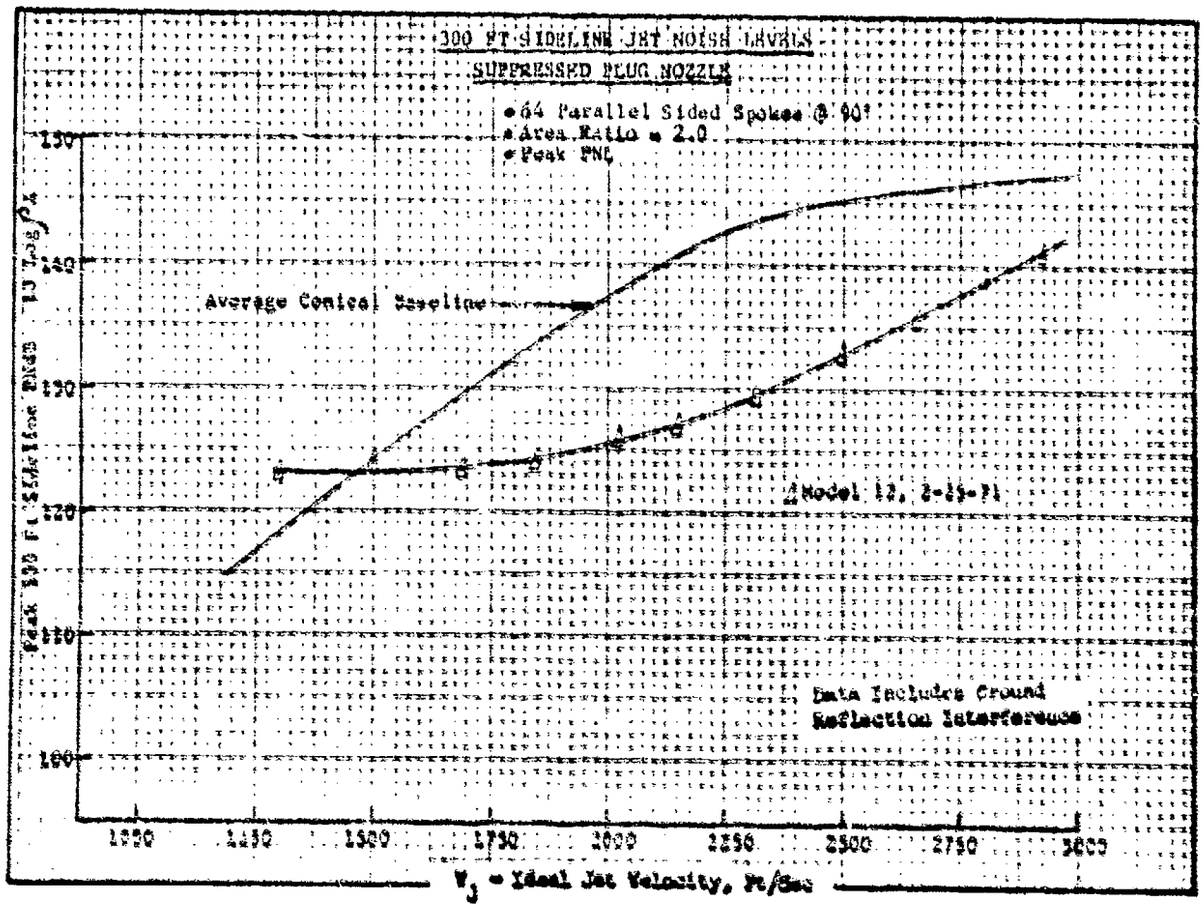
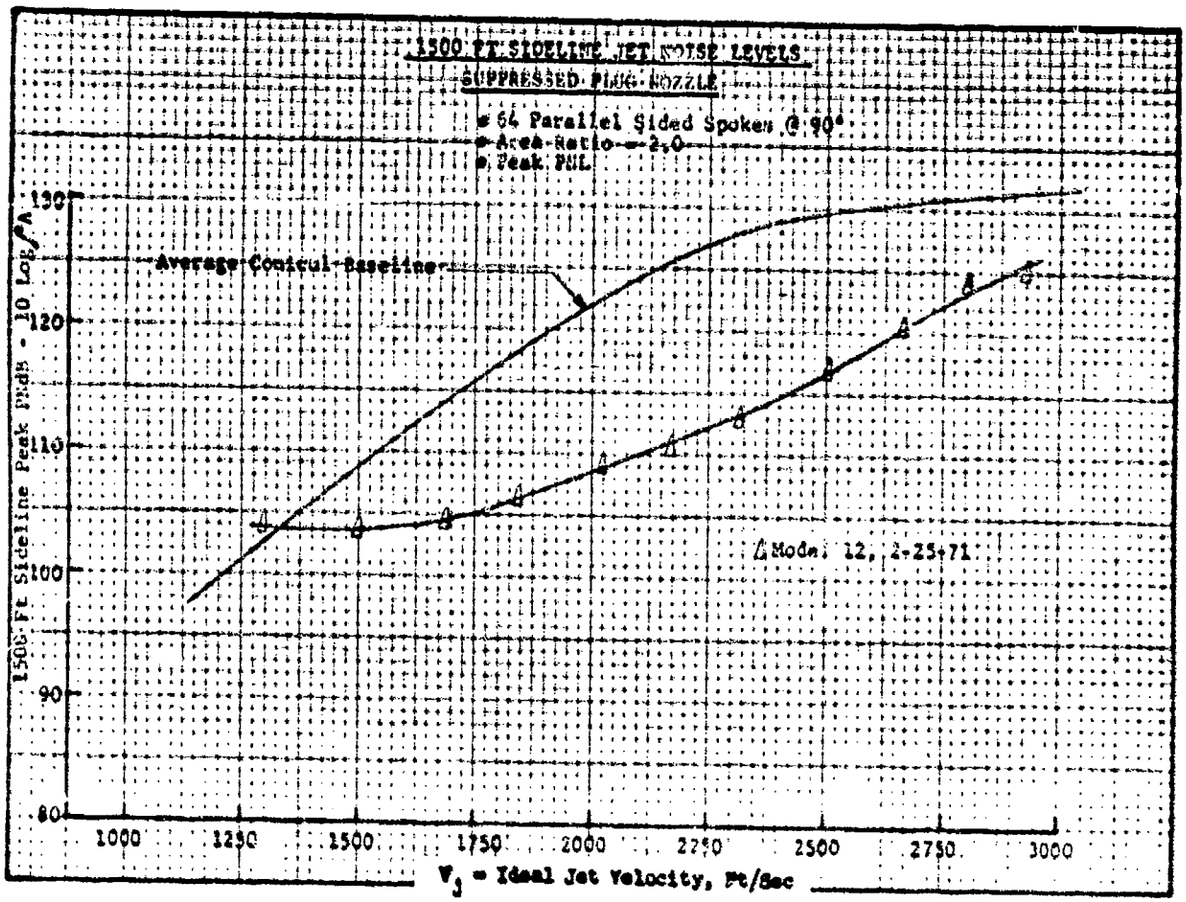


FIGURE V.H.3-40 320 FT ARC AND 300 FT SIDELINE JET NOISE LEVELS FOR MODEL 12



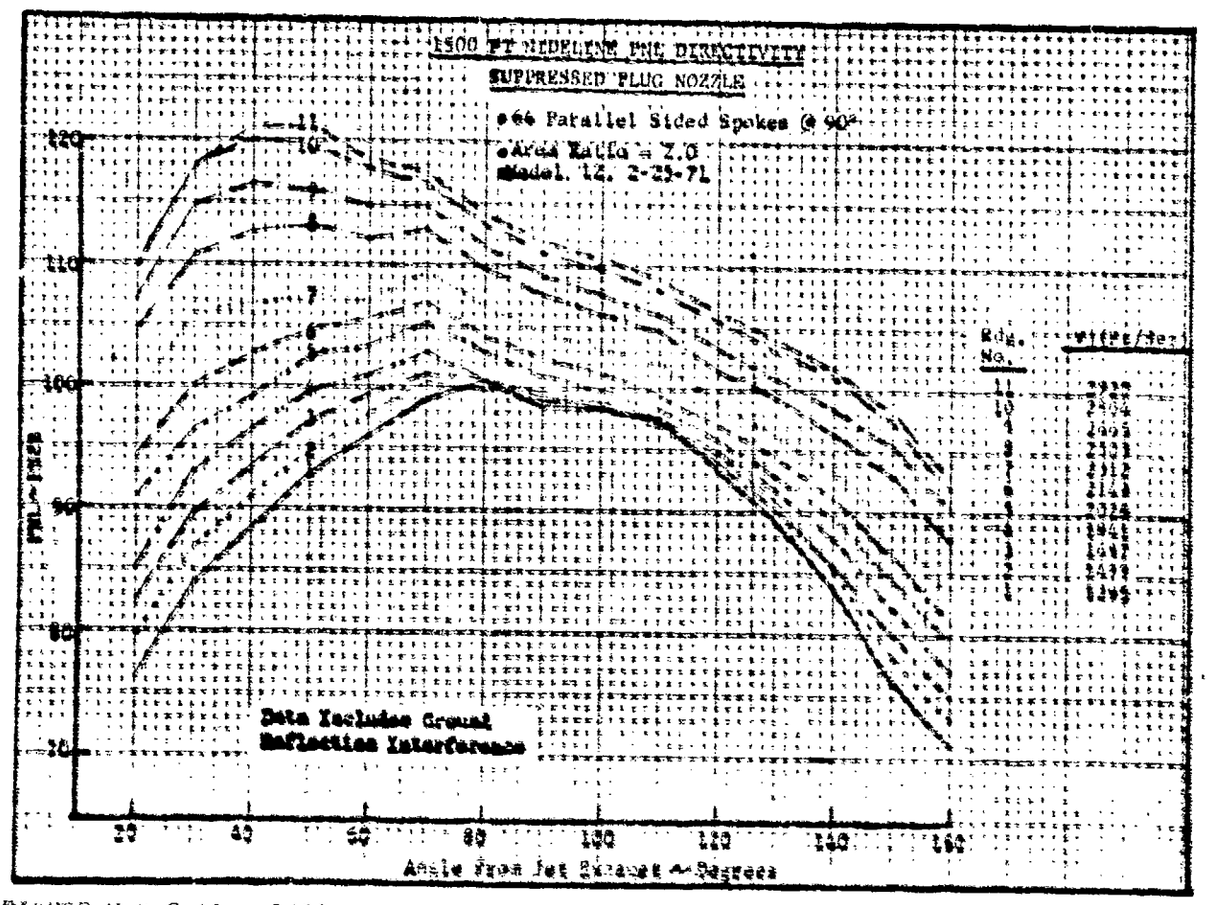


FIGURE V.H.2-41 1500 FT SIDELINE JET NOISE LEVELS AND PNL DIRECTIVITY FOR MODEL 12

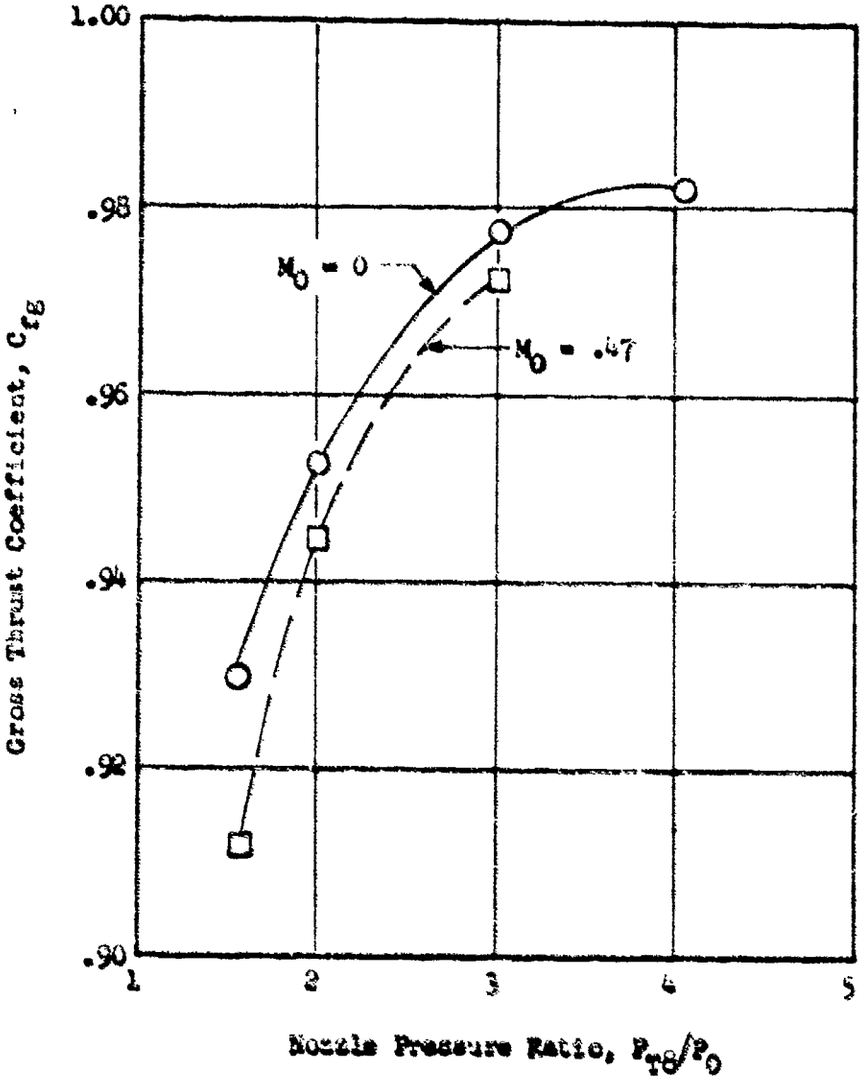
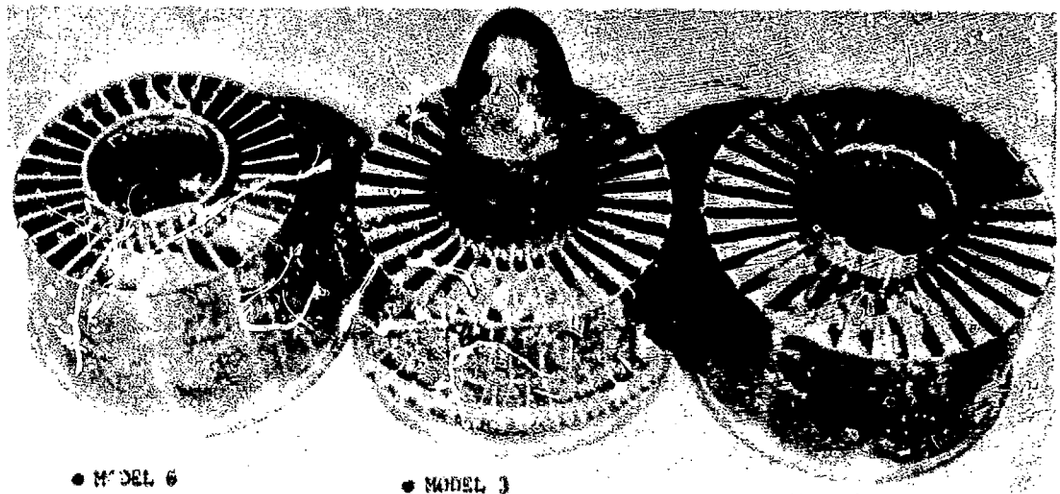


FIGURE V.H.2-42 GROSS THRUST COEFFICIENT VARIATION FOR BASELINE UNSUPPRESSED PLUG NOZZLES



- MODEL 6
- 32 SPOKE
- AREA RATIO = 1.5

- MODEL 3
- 32 SPOKE
- AREA RATIO = 2.0

- MODEL 7
- 32 SPOKE
- AREA RATIO = 2.5

SUPPRESSOR TEST HARDWARE
AREA RATIO VARIATION

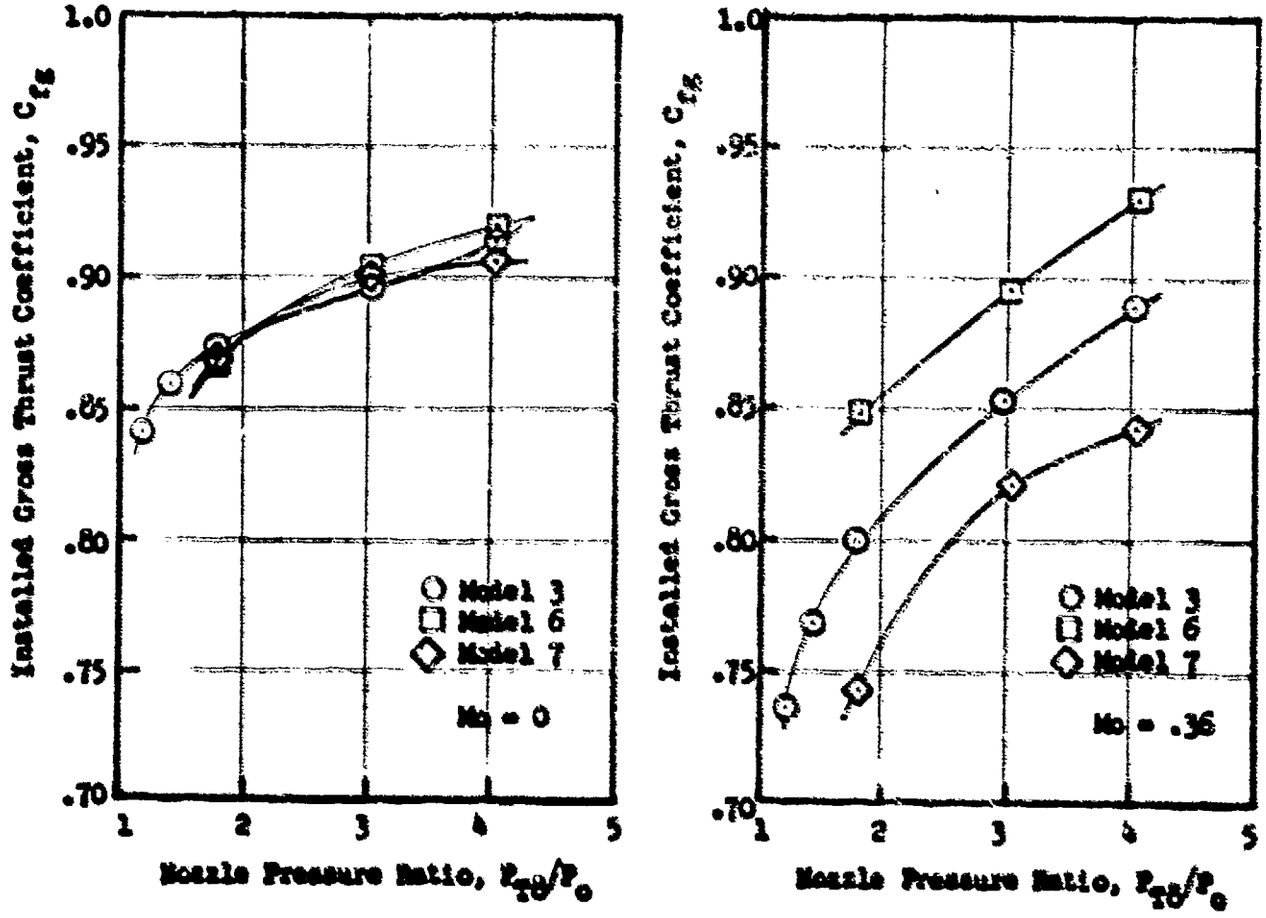
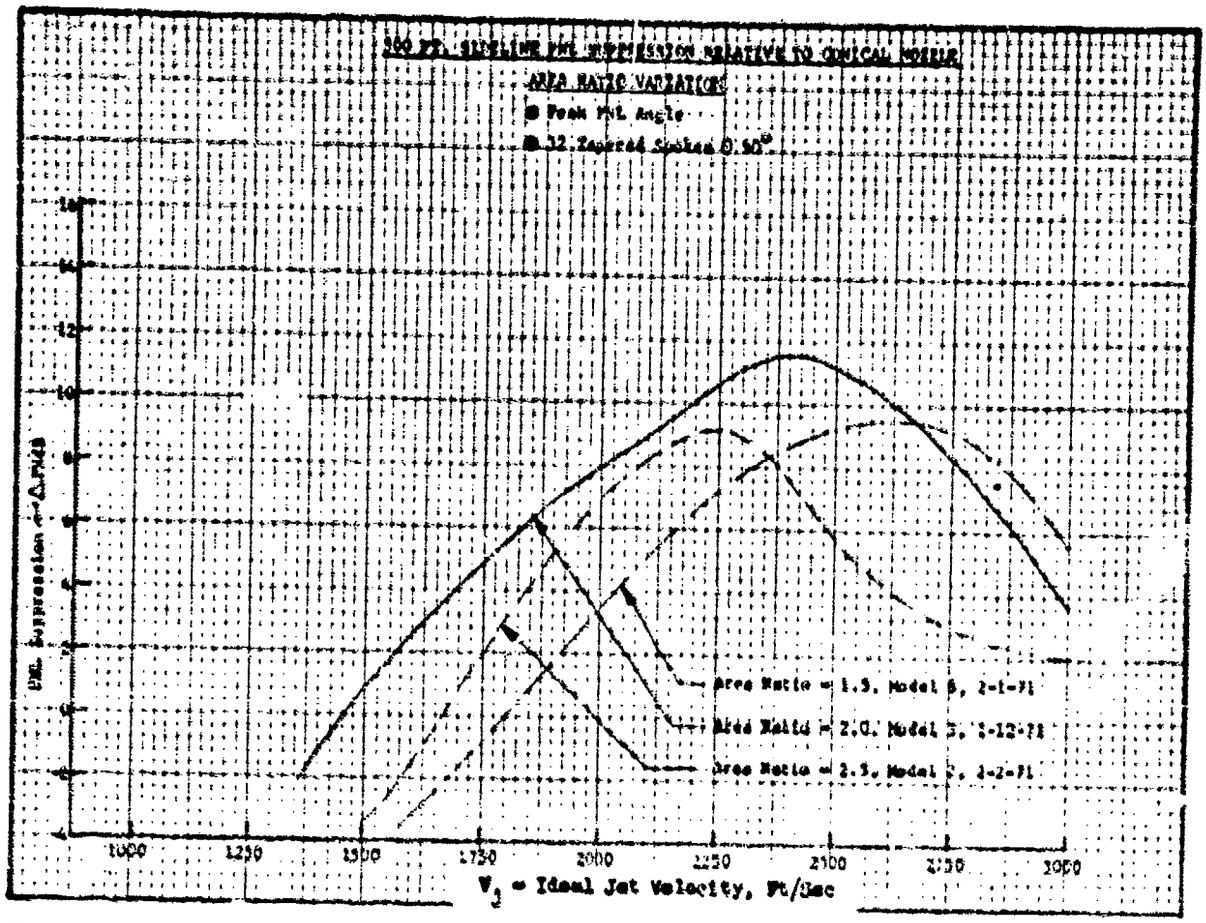


FIGURE V.E.2-43 HARDWARE USED FOR PARAMETRIC INVESTIGATION OF AREA RATIO; AERODYNAMIC TEST RESULTS



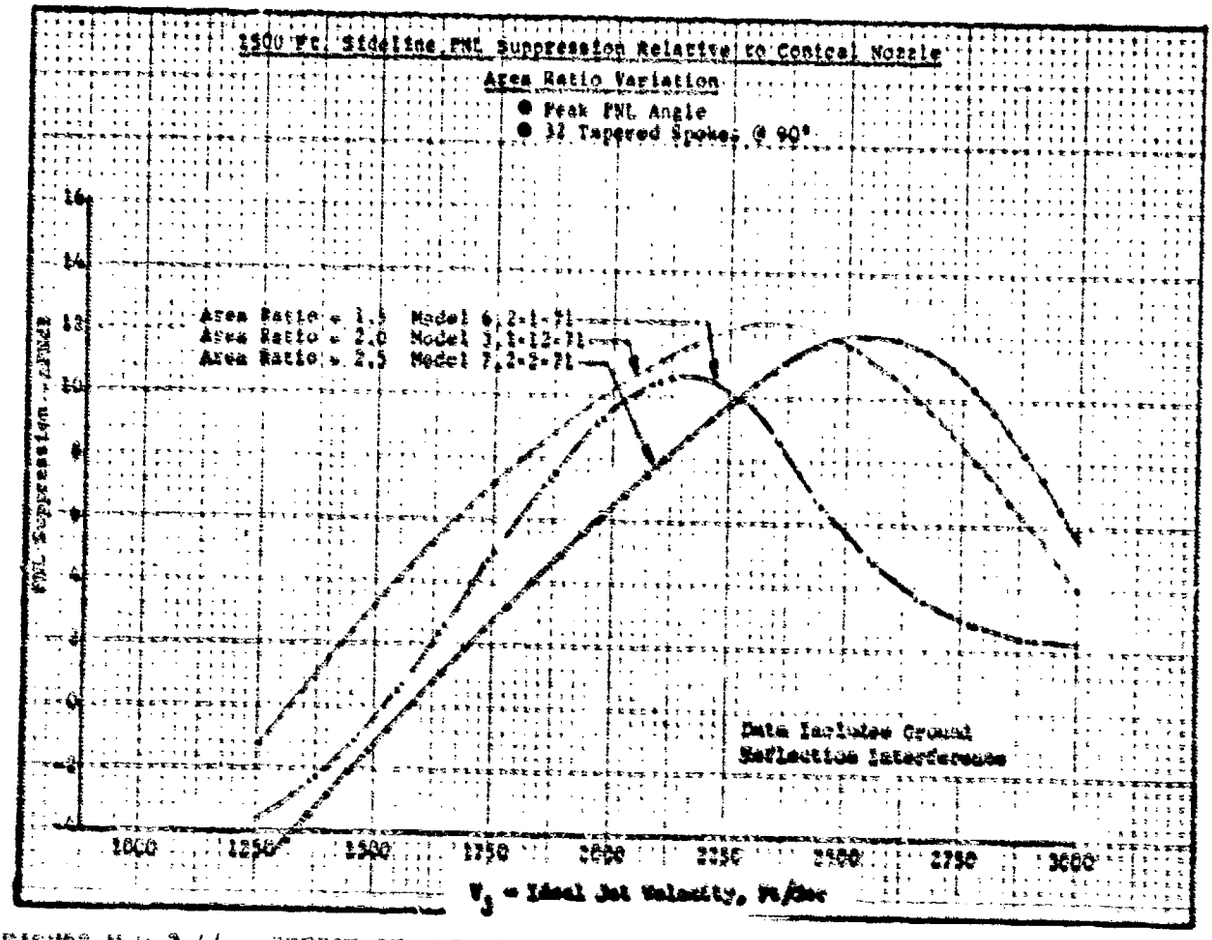


FIGURE V.E.2-44 EFFECT OF AREA RATIO ON 300 FT AND 1500 FT SIDELINE PNL SUPPRESSION FOR PLUG NOZZLE CONFIGURATIONS

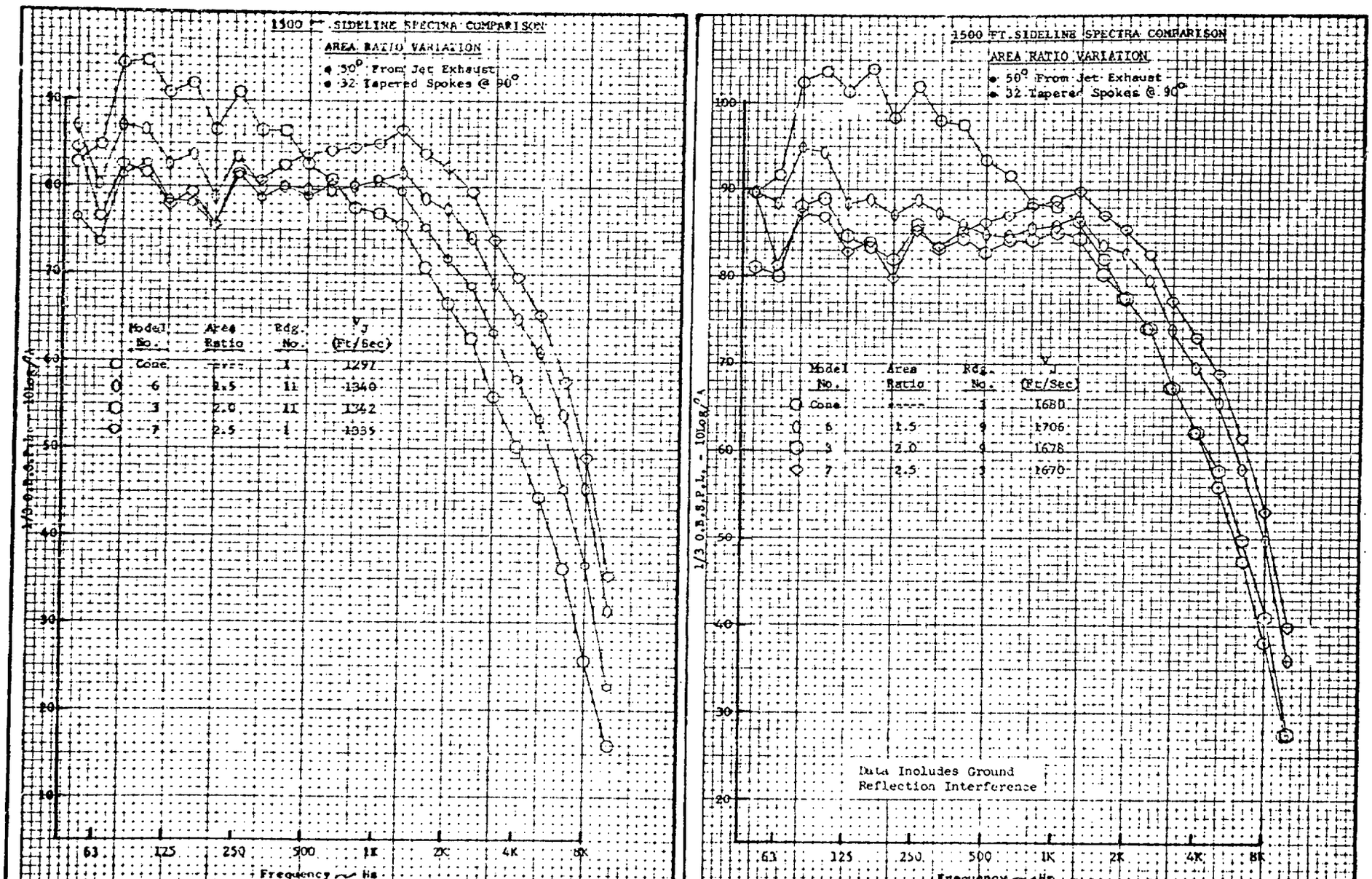


FIGURE V.H.2-45A EFFECT OF AREA RATIO ON 1500 FT SIDELINE SPECTRA

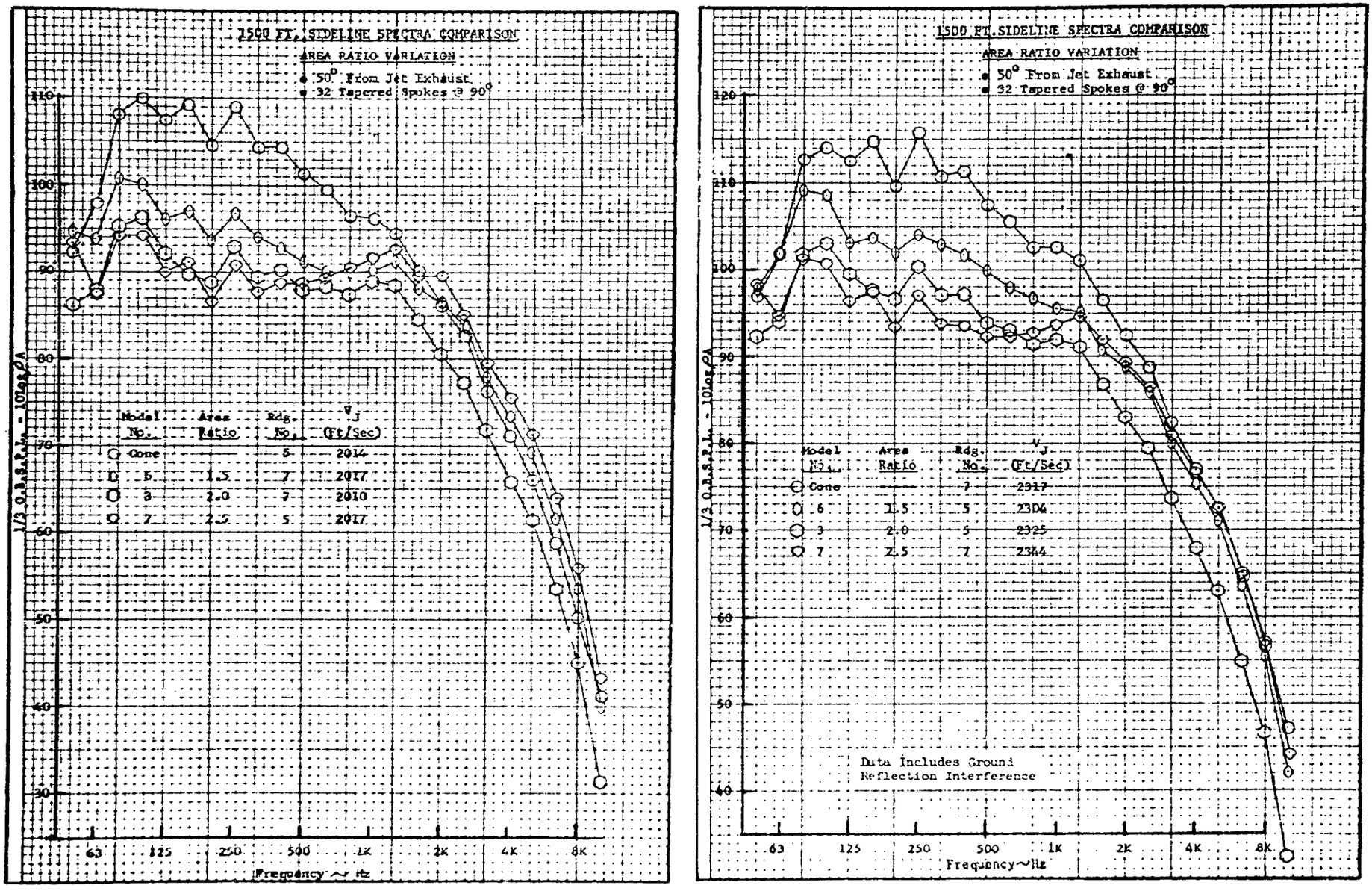


FIGURE V.H.2-45B EFFECT OF AREA RATIO ON 1500 FT SIDELINE SPECTRA

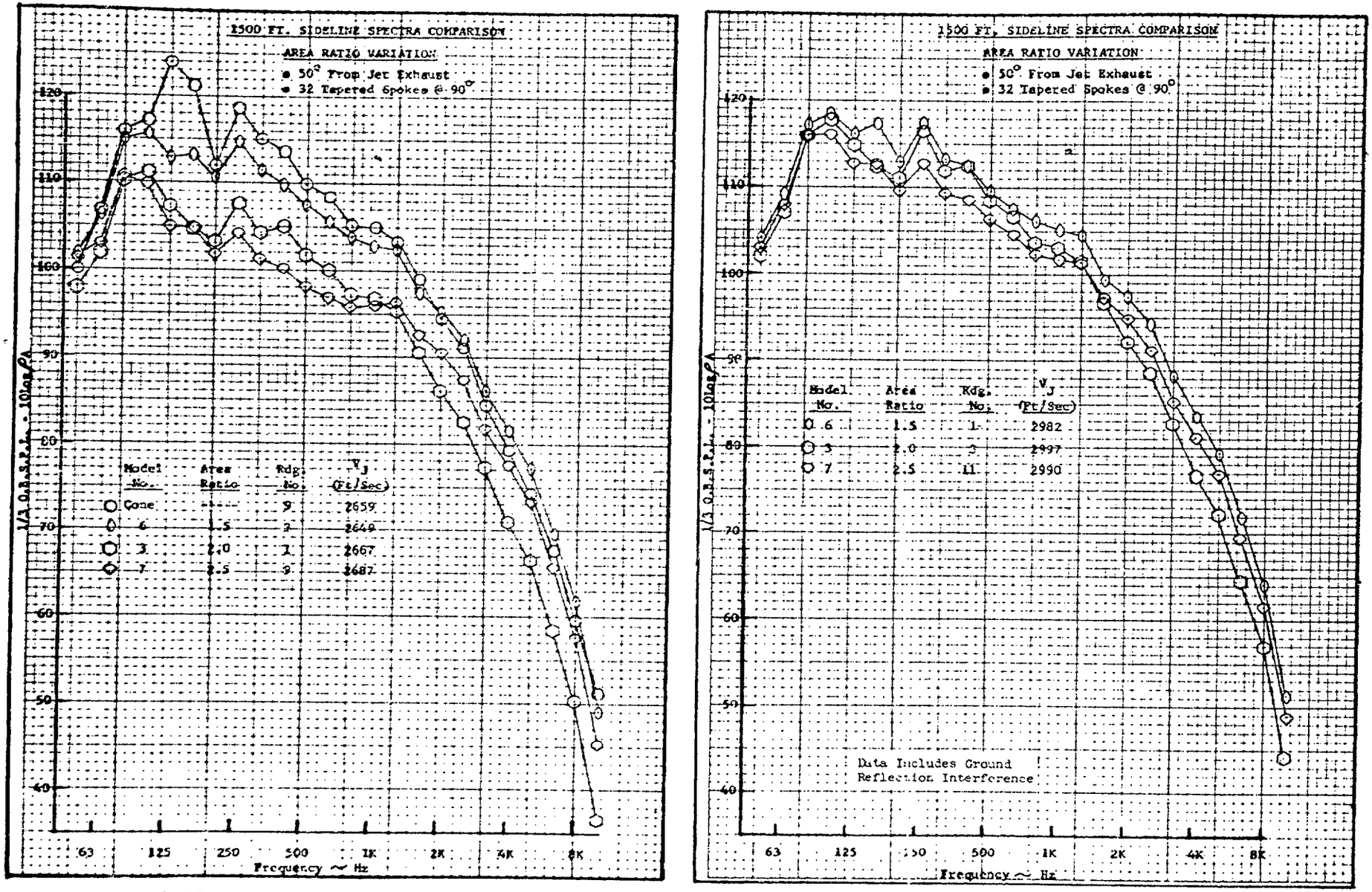
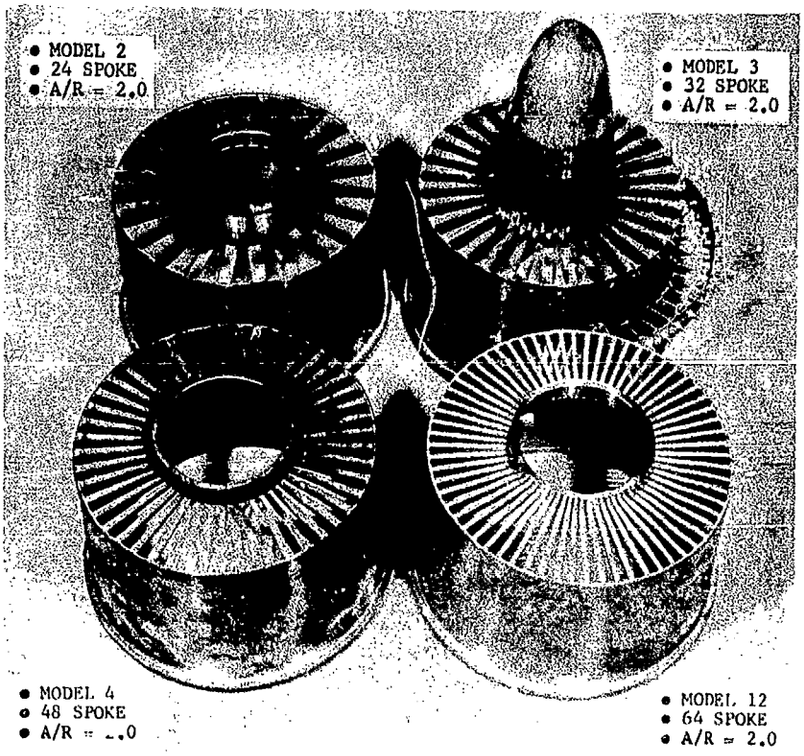


FIGURE V.H.2-45C EFFECT OF AREA RATIO ON 1500 FT SIDELINE SPECTRA



SUPPRESSOR TEST HARDWARE
SPOKE NUMBER VARIATION

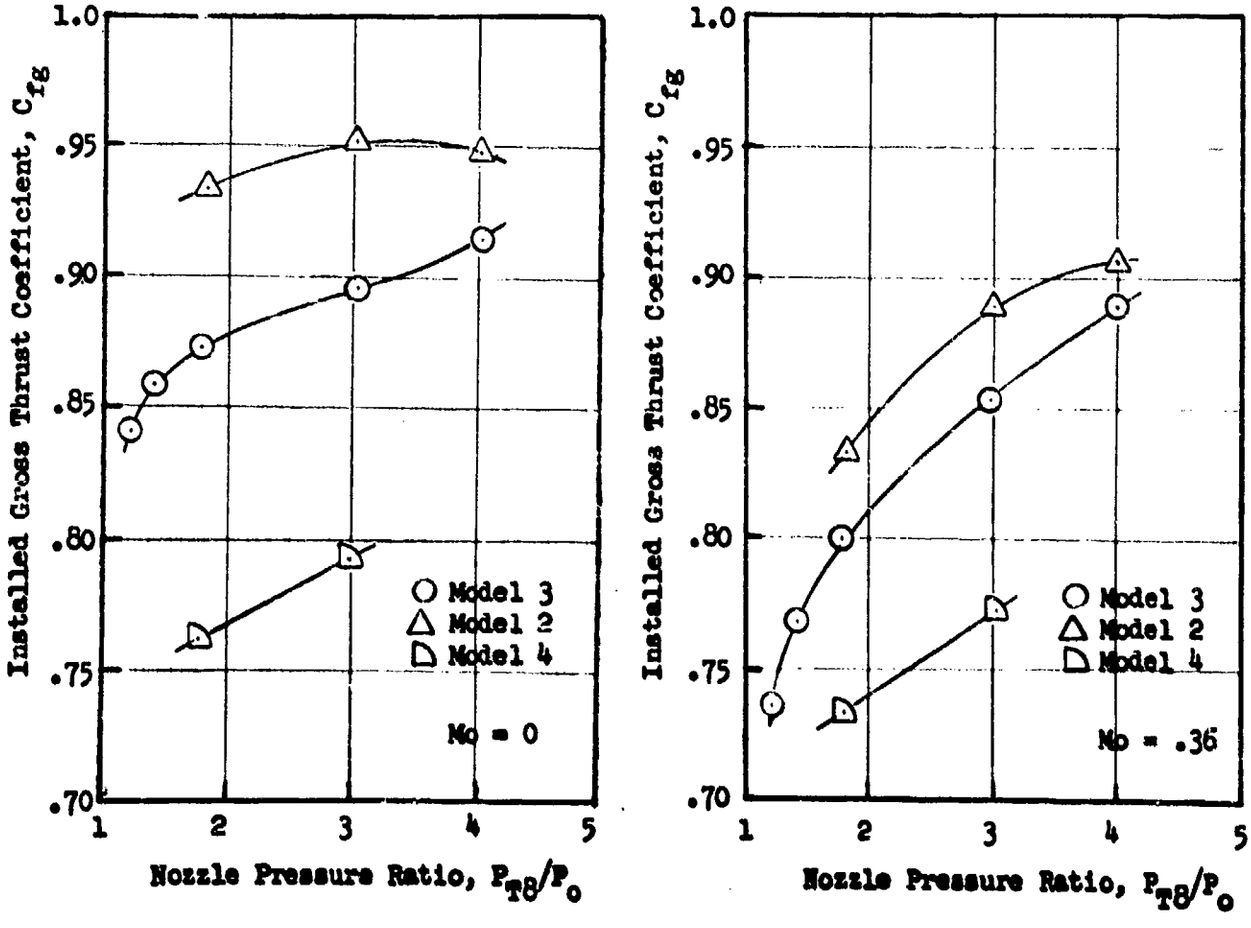
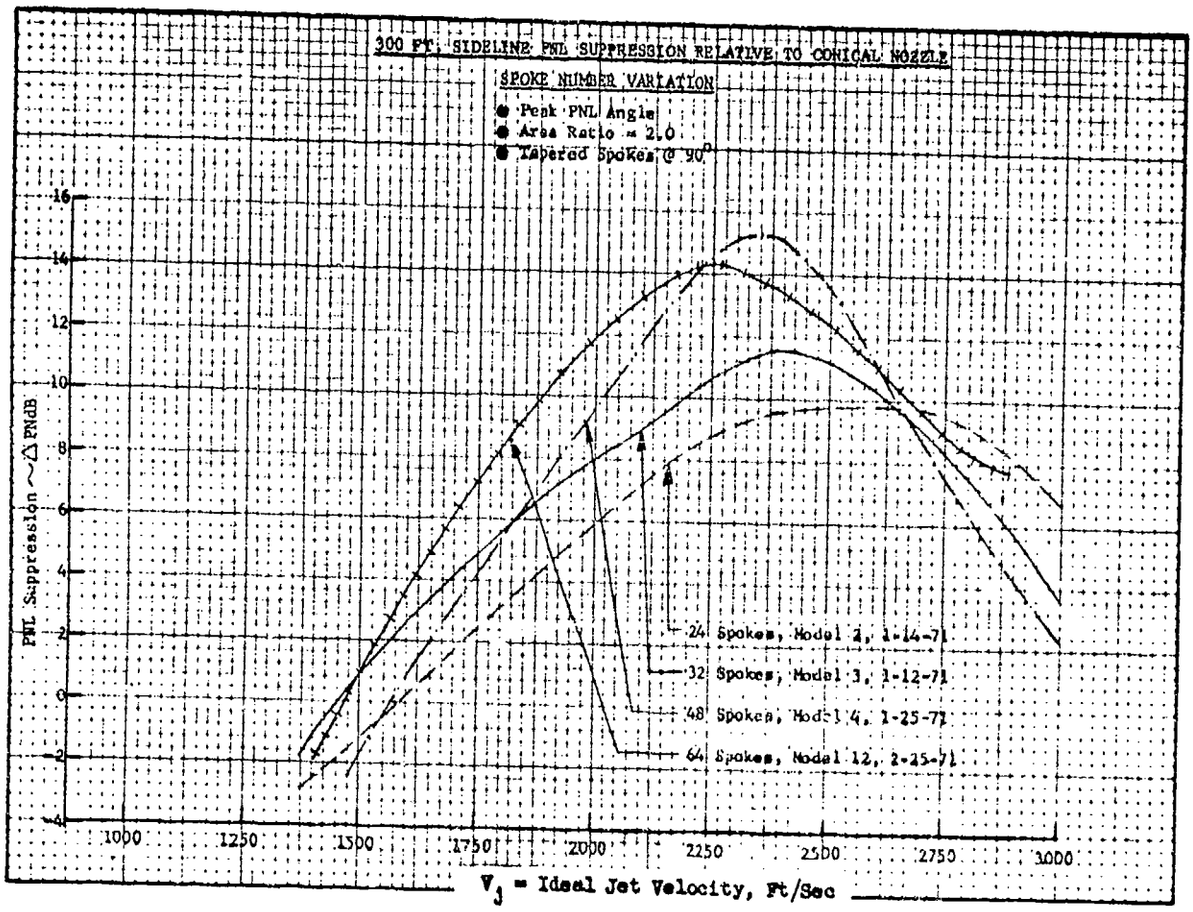


FIGURE V.H.2-46 HARDWARE USED FOR PARAMETRIC INVESTIGATION OF SPOKE NUMBER; AERODYNAMIC TEST RESULTS



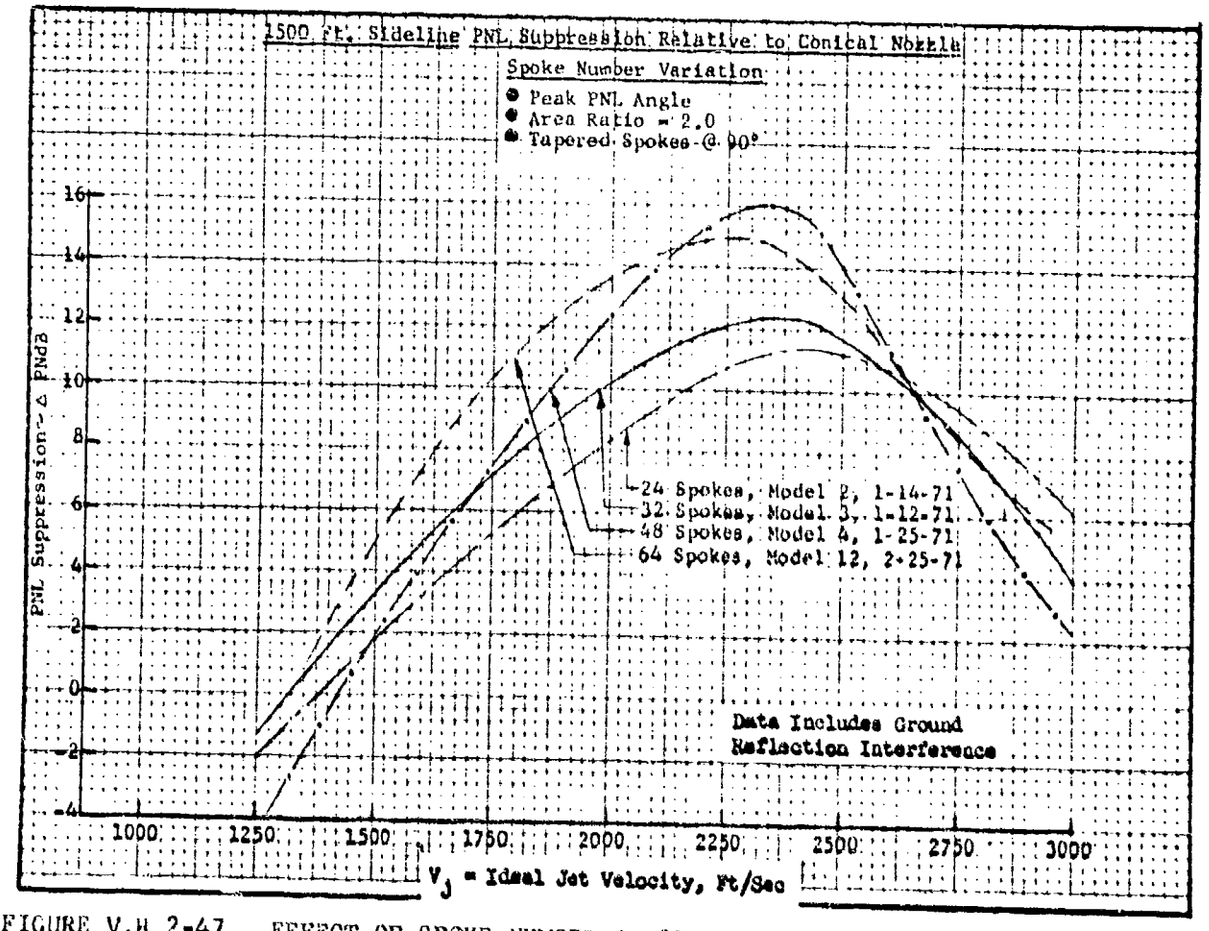
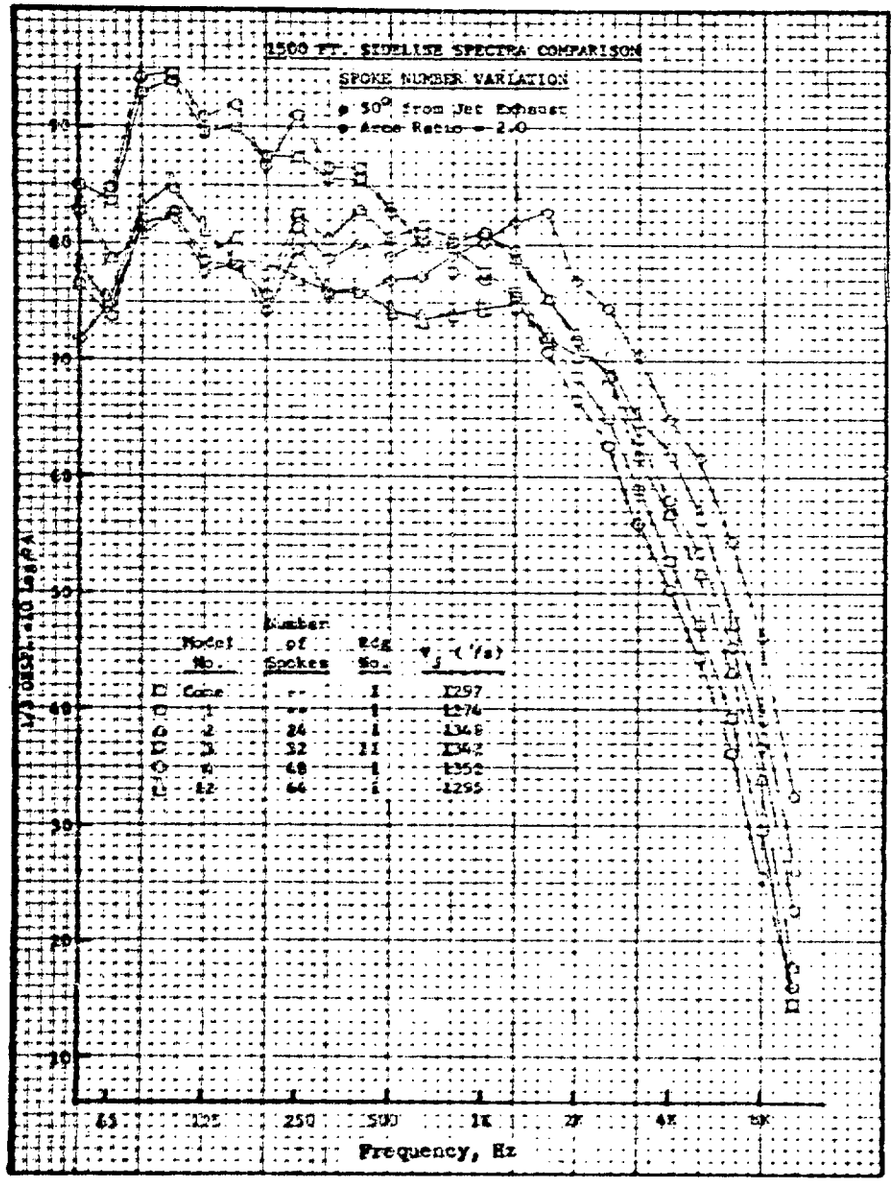


FIGURE V.H.2-47 EFFECT OF SPOKE NUMBER ON 300 FT AND 1500 FT SIDELINE PNL SUPPRESSION FOR PLUG NOZZLE CONFIGURATIONS



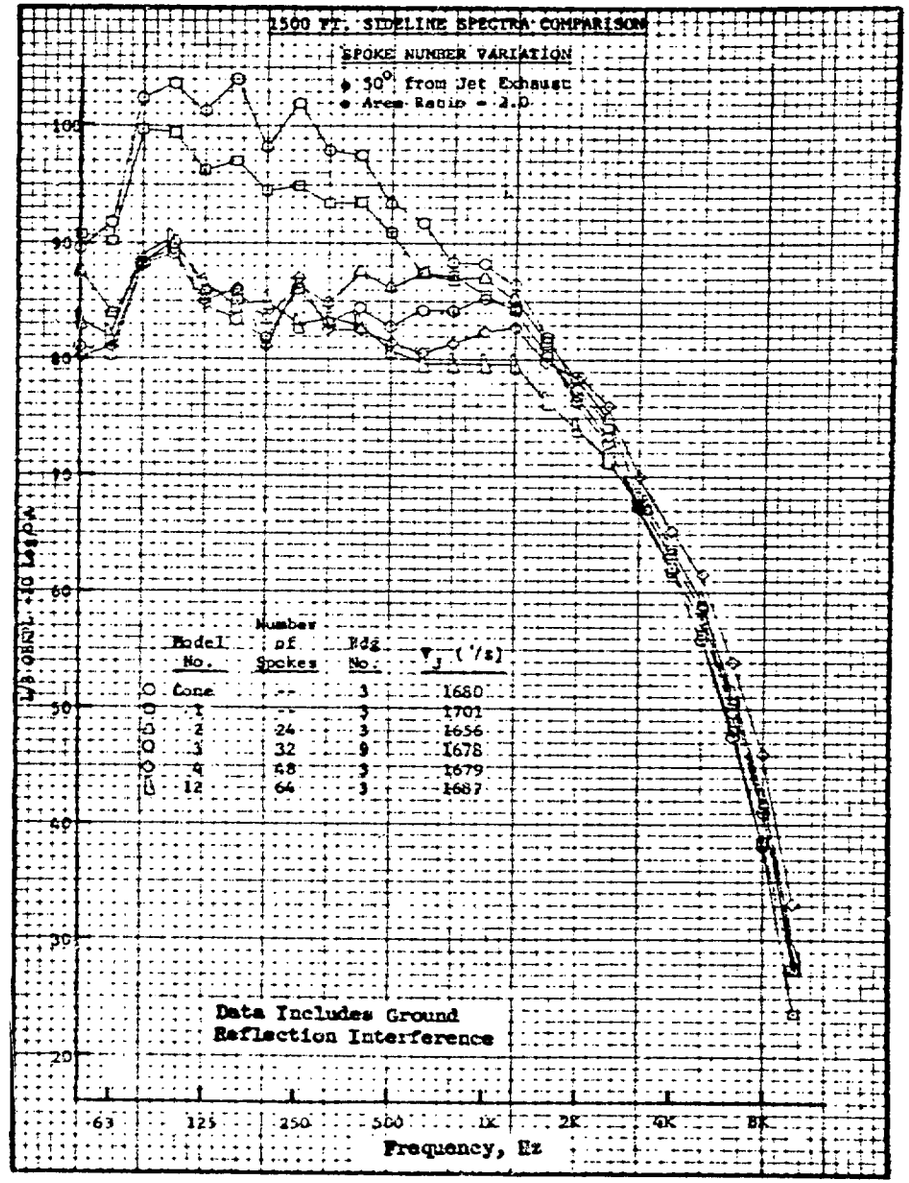


FIGURE V.H.2-48A EFFECT OF SPOKE NUMBER ON 1500 FT SIDELINE SPECTRA

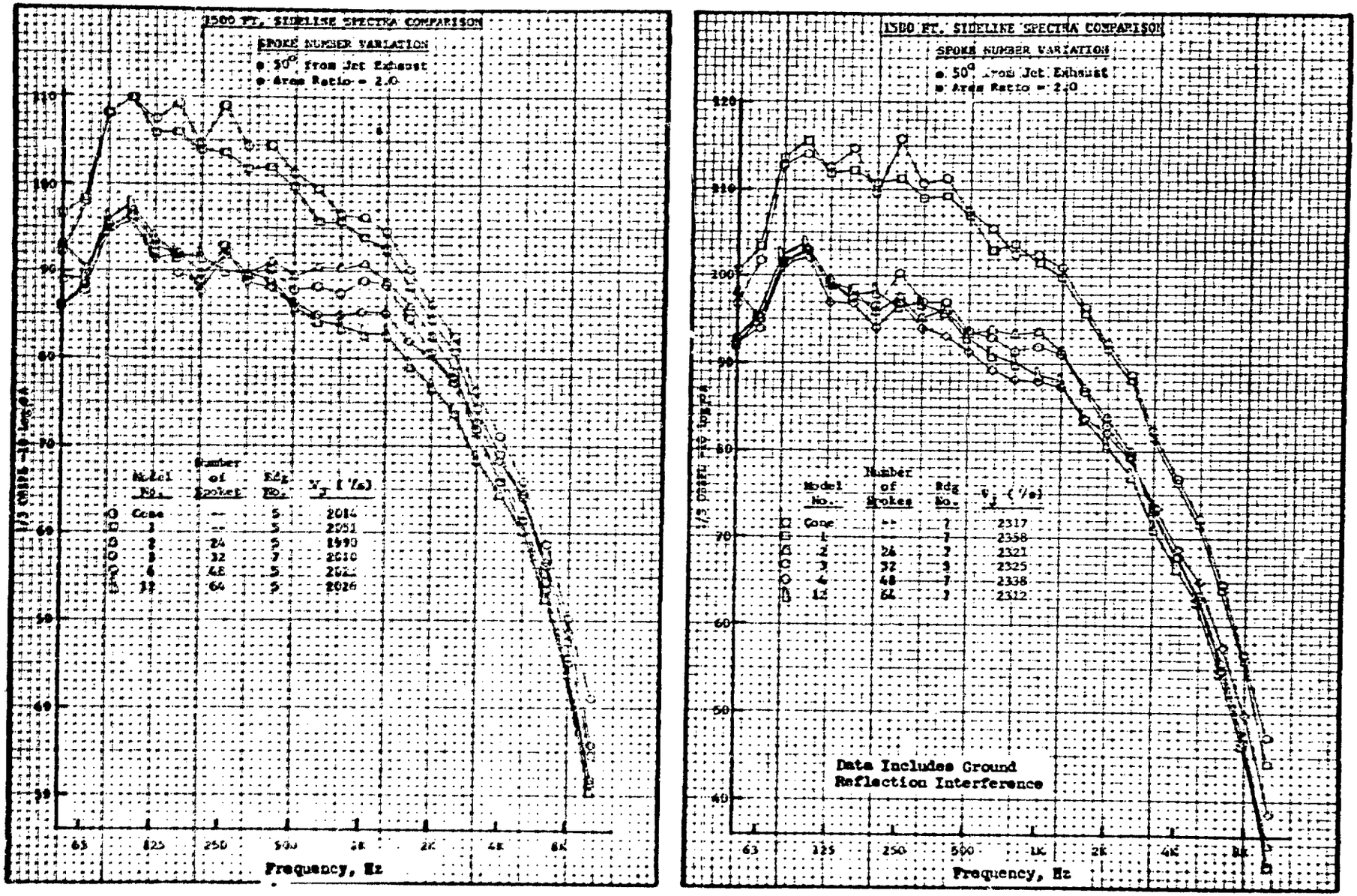
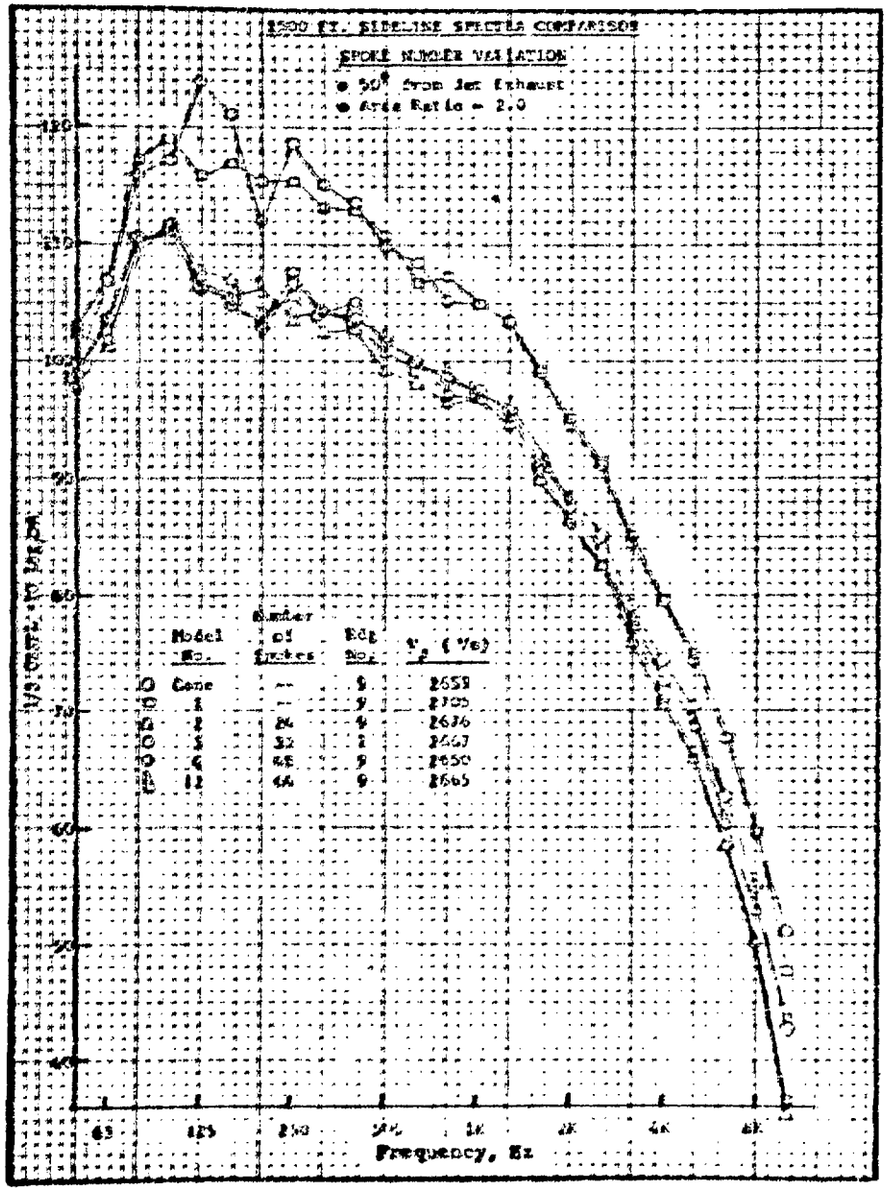


FIGURE V.H.2-48 EFFECT OF SPOKE NUMBER ON 1500 FT SIDELINE SPECTRA



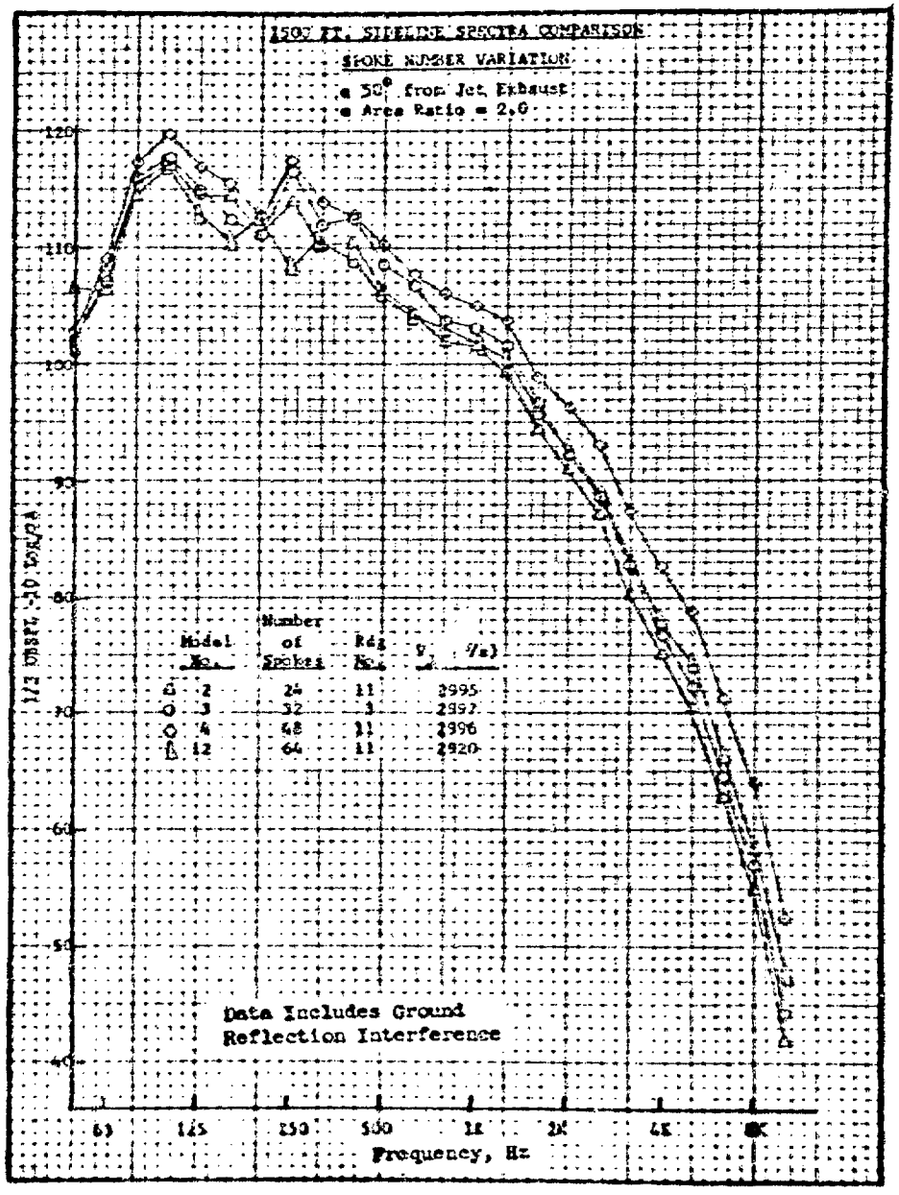
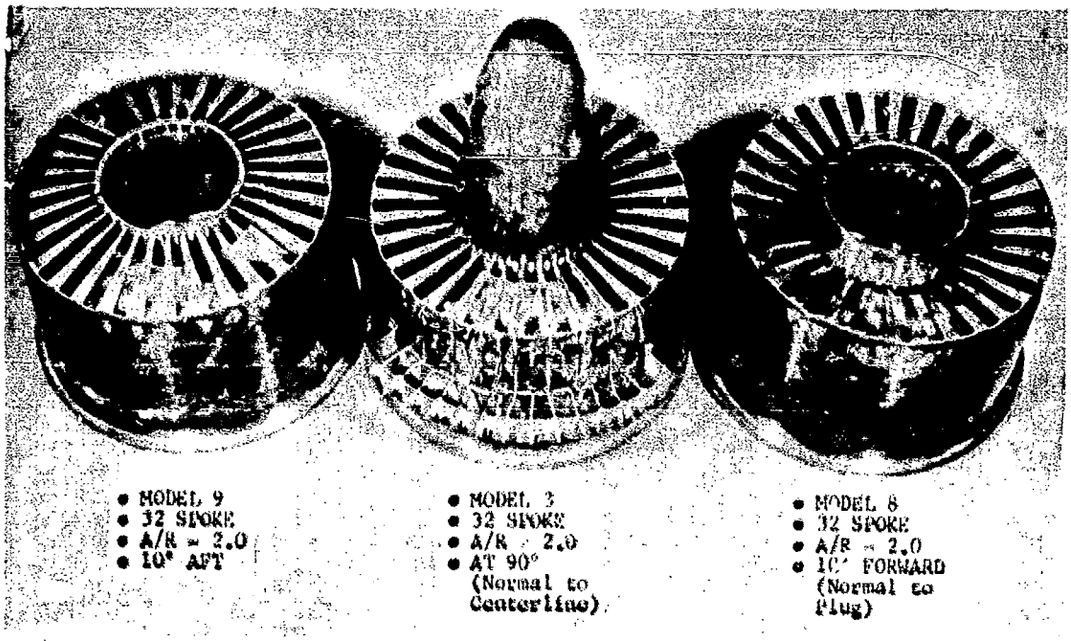


FIGURE V.4.2-48C EFFECT OF SPOKE NUMBER ON 1500 FT SIDELINE SPECTRA



- MODEL 9
- 32 SPOKE
- A/R = 2.0
- 10° AFT

- MODEL 3
- 32 SPOKE
- A/R = 2.0
- AT 90° (Normal to Centerline)

- MODEL 8
- 32 SPOKE
- A/R = 2.0
- 10° FORWARD (Normal to Plug)

SUPPRESSOR TEST HARDWARE
SPOKE ANGLE-OF-ATTACK VARIATION

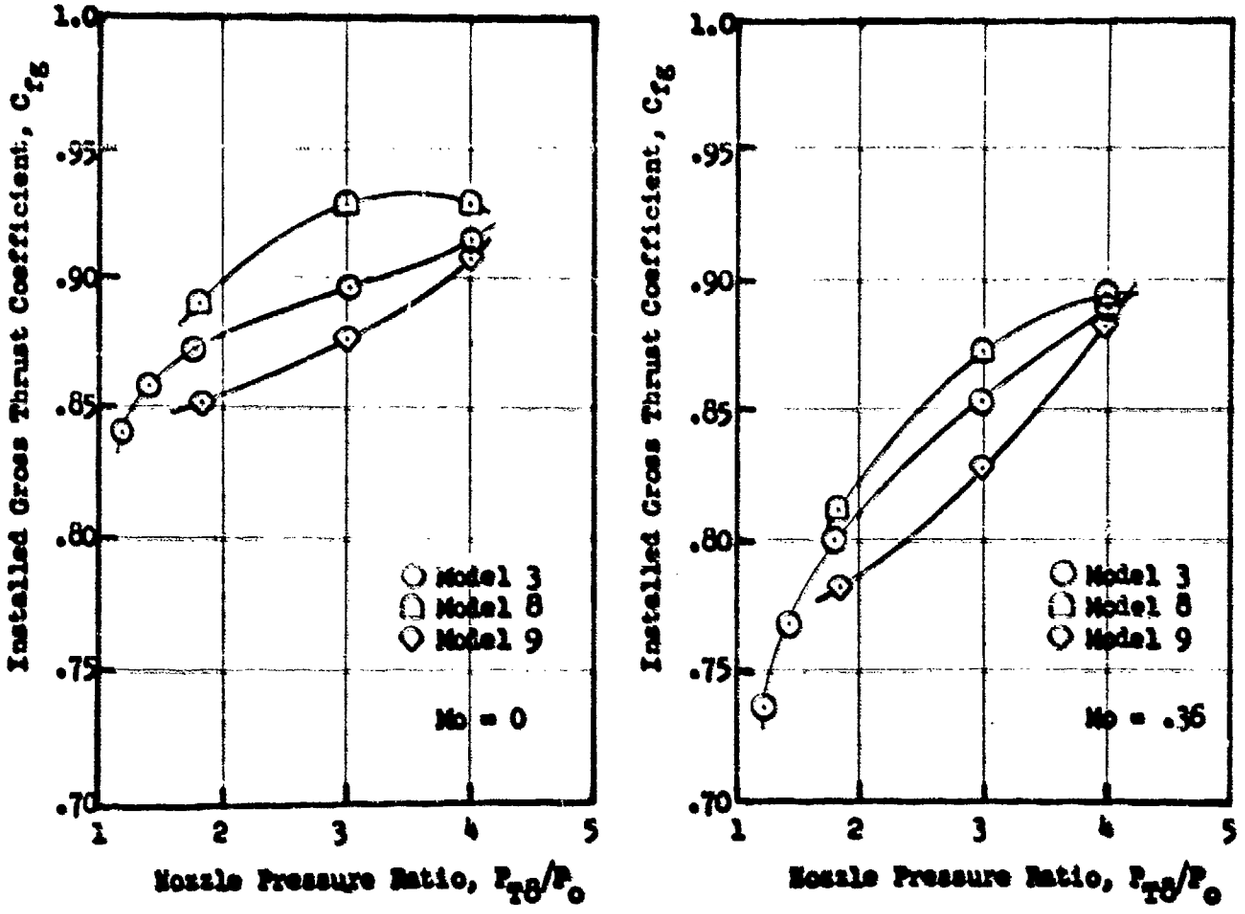
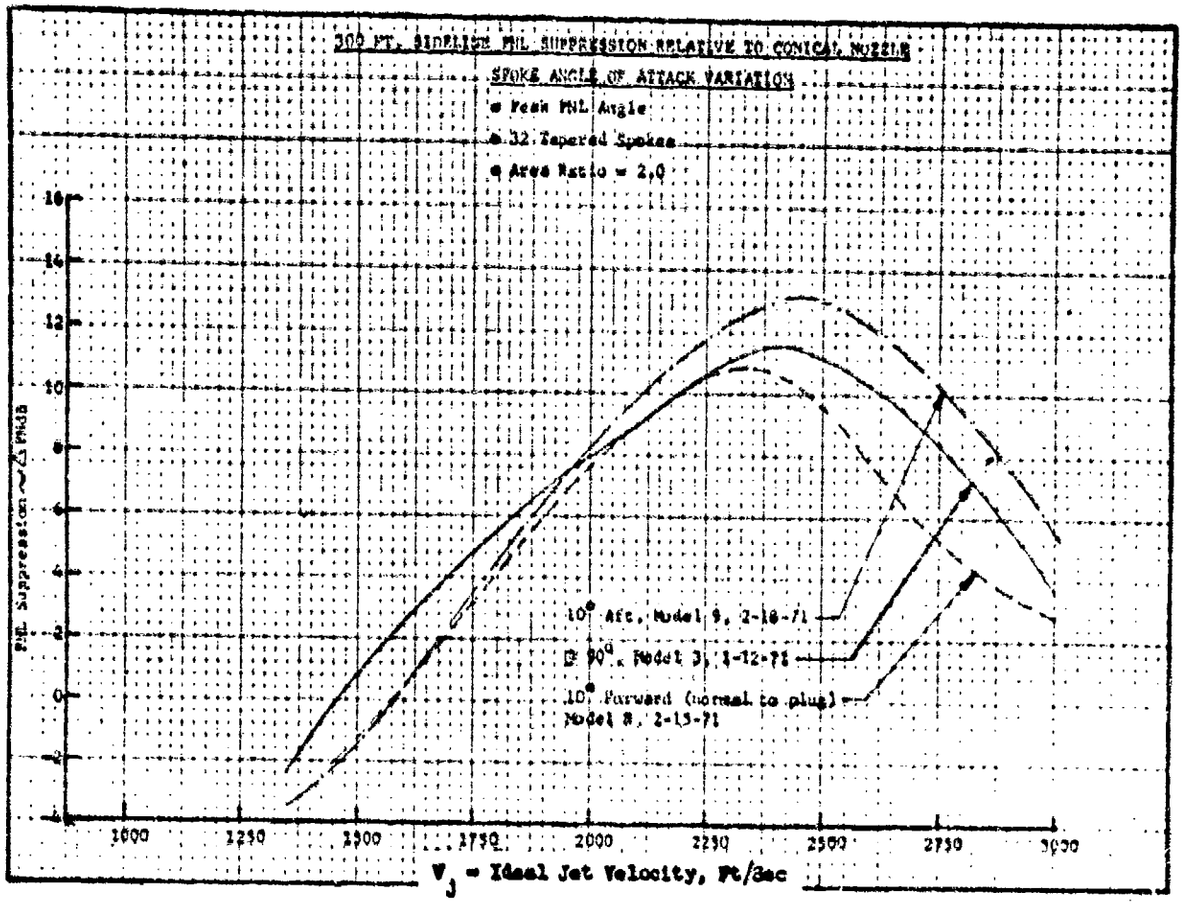


FIGURE V.E.2-49 HARDWARE USED FOR PARAMETRIC INVESTIGATION OF SPOKE ANGLE-OF-ATTACK; AERODYNAMIC TEST RESULTS



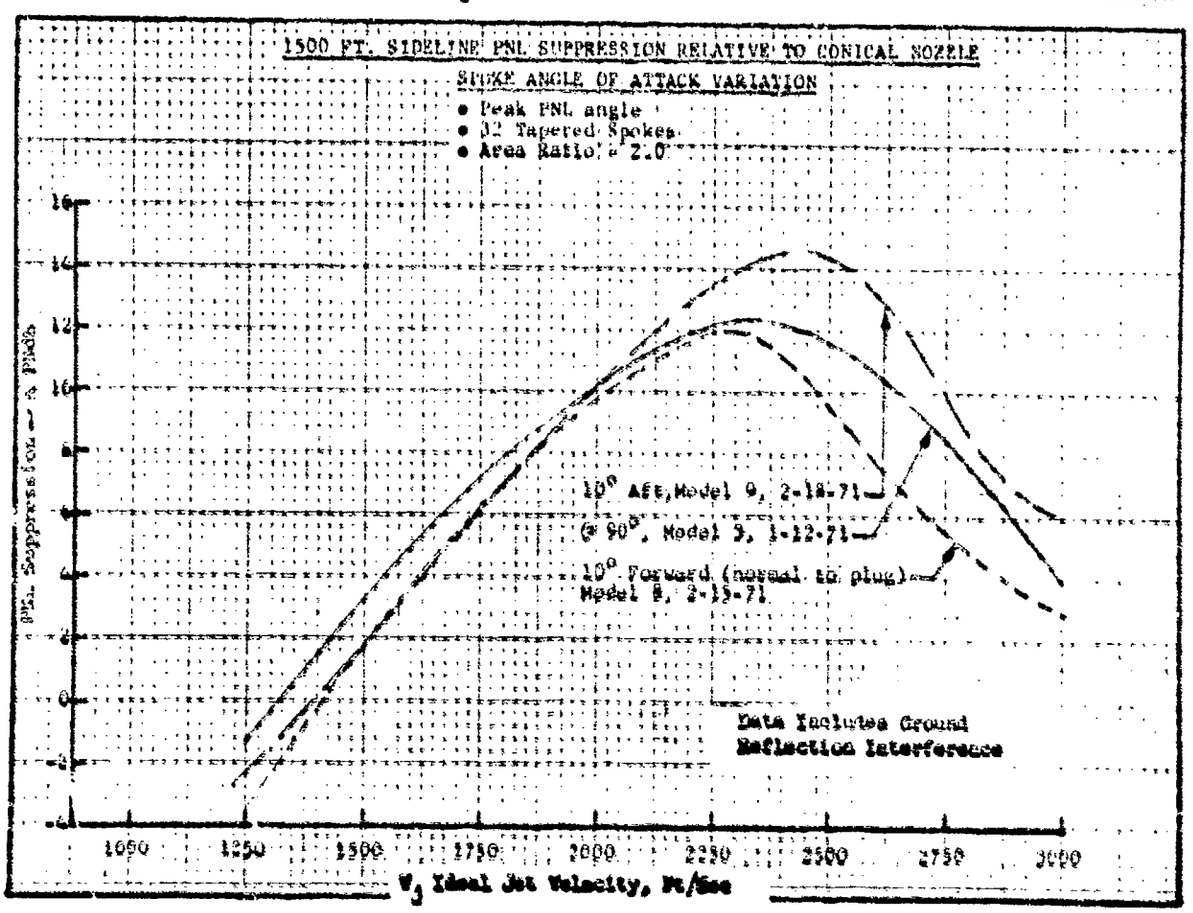
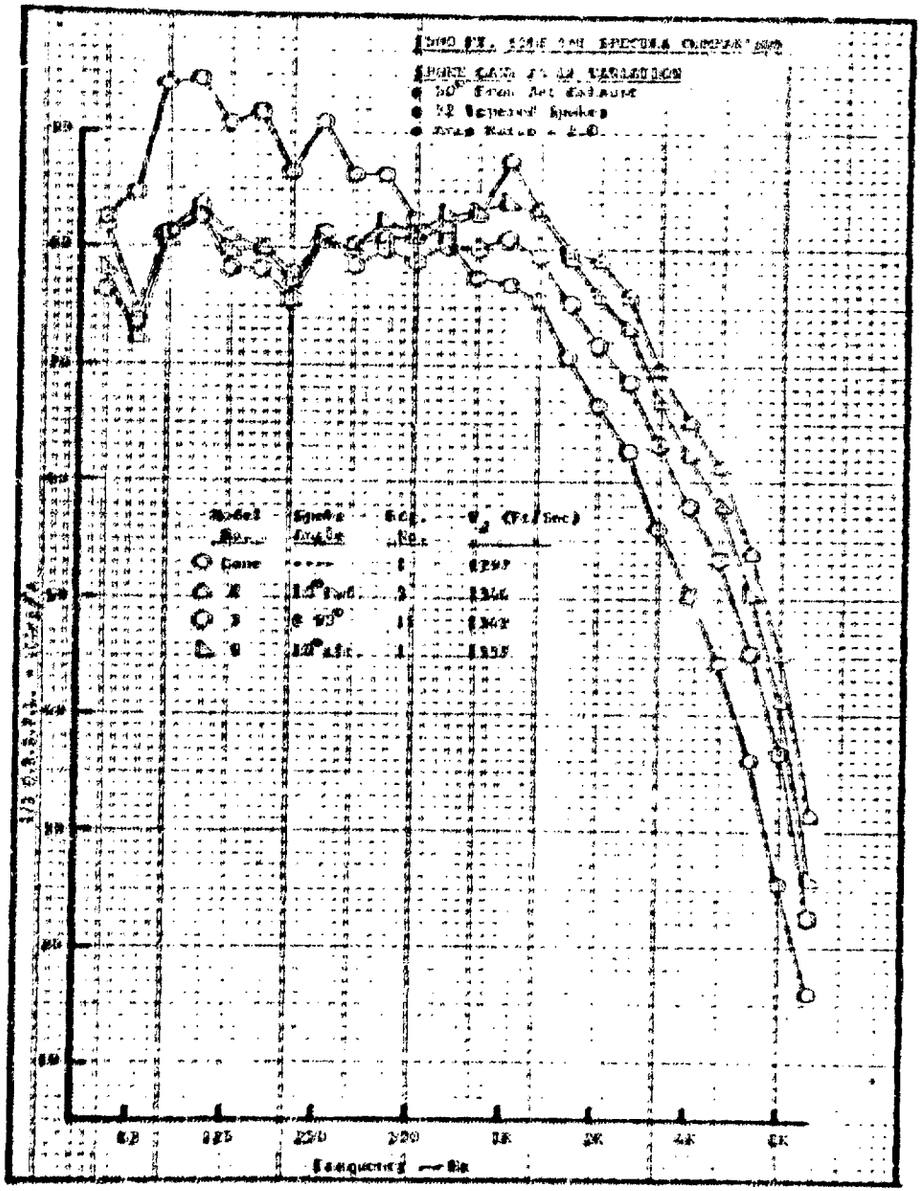


FIGURE V.H.2-50 EFFECT OF SPOKE ANGLE-OF-ATTACK ON 300 FT AND 1500 FT SIDELINE PNL SUPPRESSION FOR PLUG NOZZLE CONFIGURATIONS



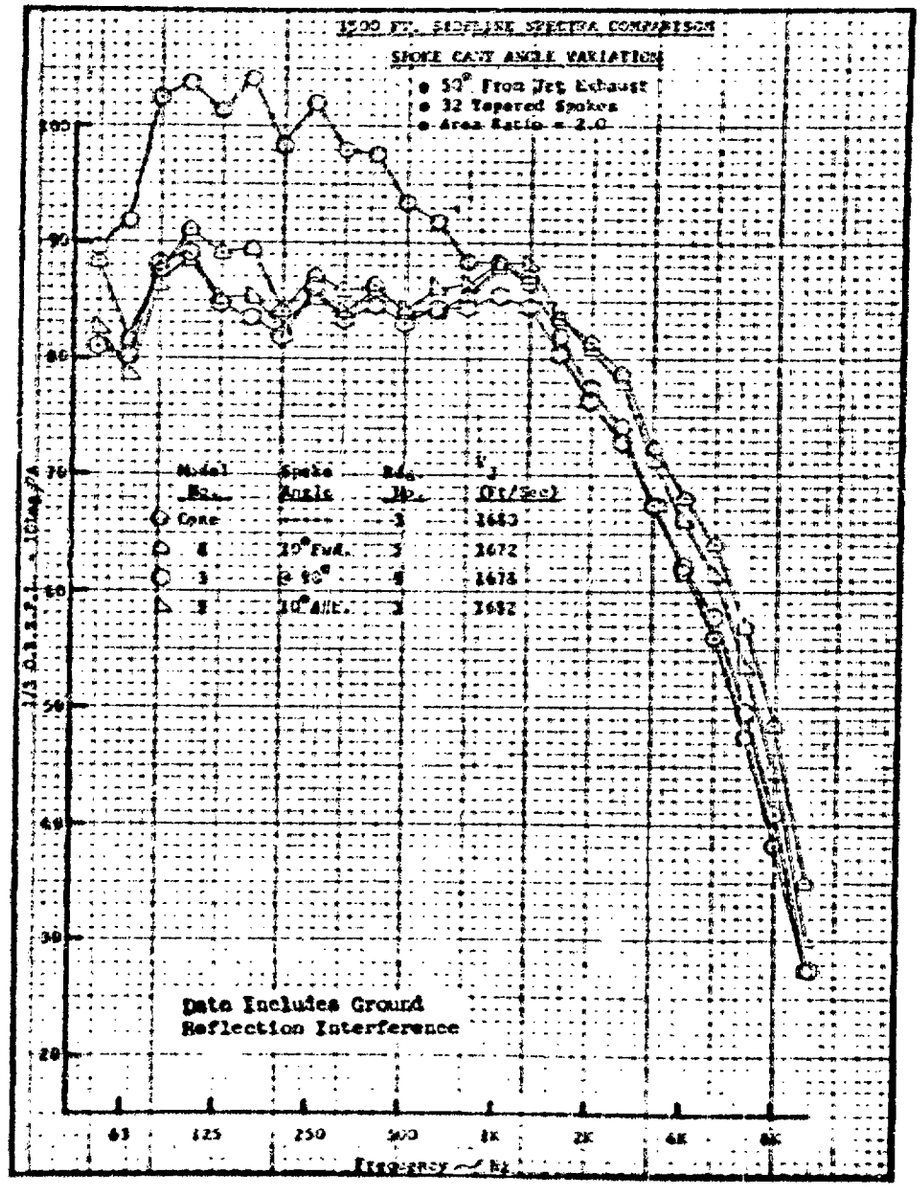


FIGURE V.M.2-51A EFFECT OF SPOKE ANGLE-OF-ATTACK ON 1500 FT SIDELINE SPECTRA

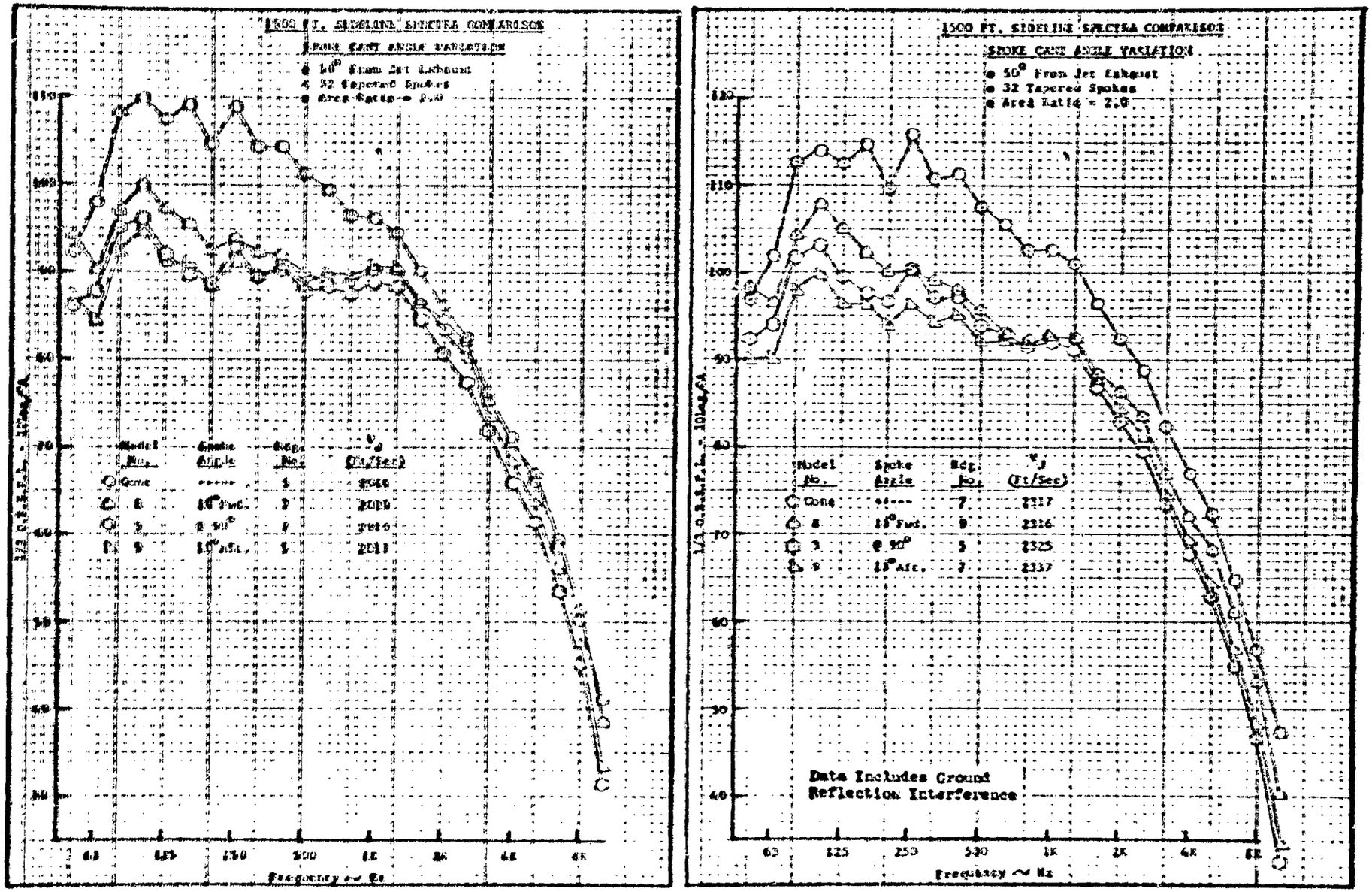


FIGURE V.a.2-51 EFFECT OF SPOKE ANGLE-OF-ATTACK ON 1500 FT SIDELINE SPECTRA

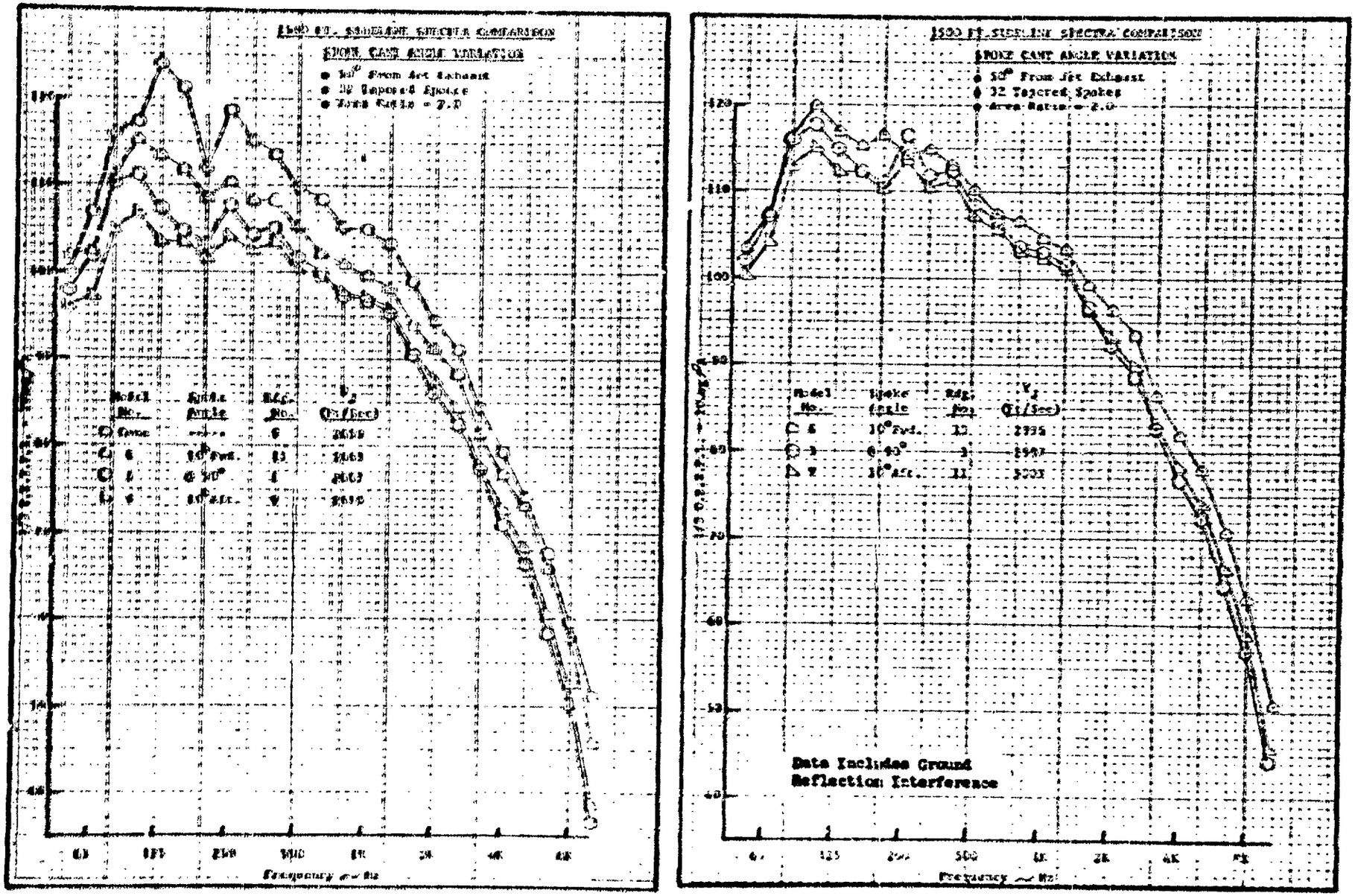
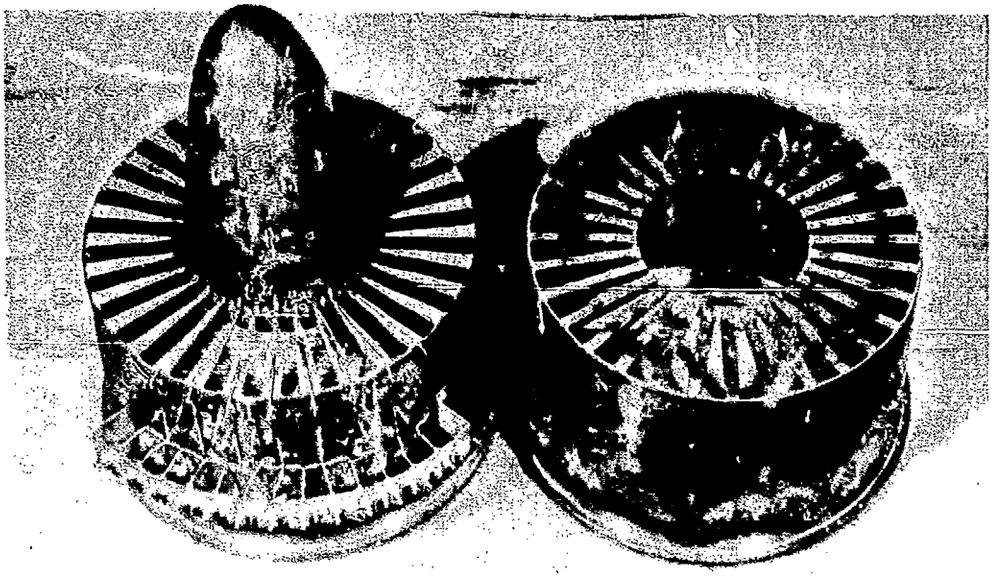


FIGURE V.E.2-51C EFFECT OF SPOKE ANGLE-OF-ATTACK ON 1500 FT SIDELINE SPECTRA



- MODEL 3
- 32 TAPERED SPOKES
- AREA RATIO = 2.0

- MODEL 5
- 32 PARALLEL SIDED SPOKES
- AREA RATIO = 2.0

SUPPRESSOR TEST HARDWARE
TAPERED VS PARALLEL SIDED SPOKES

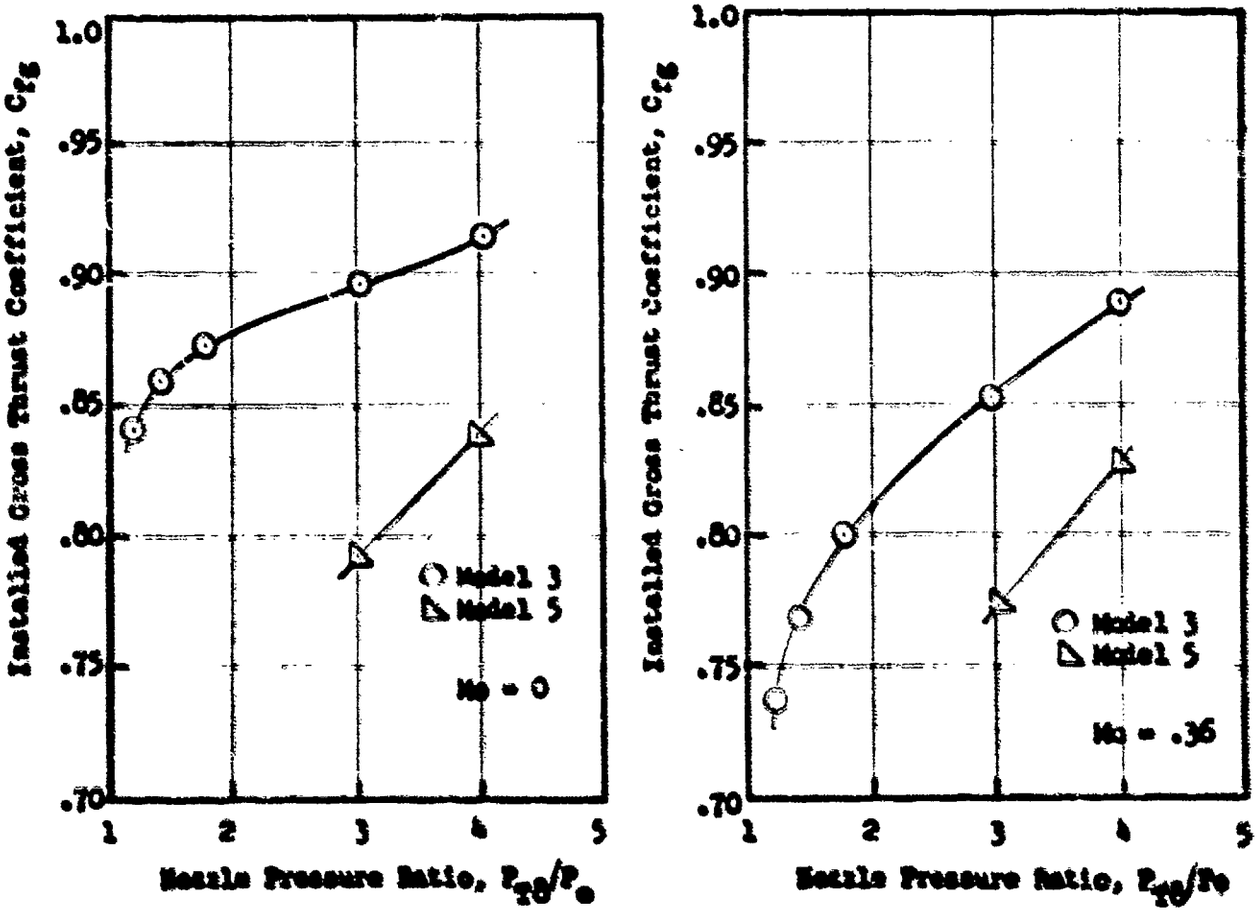
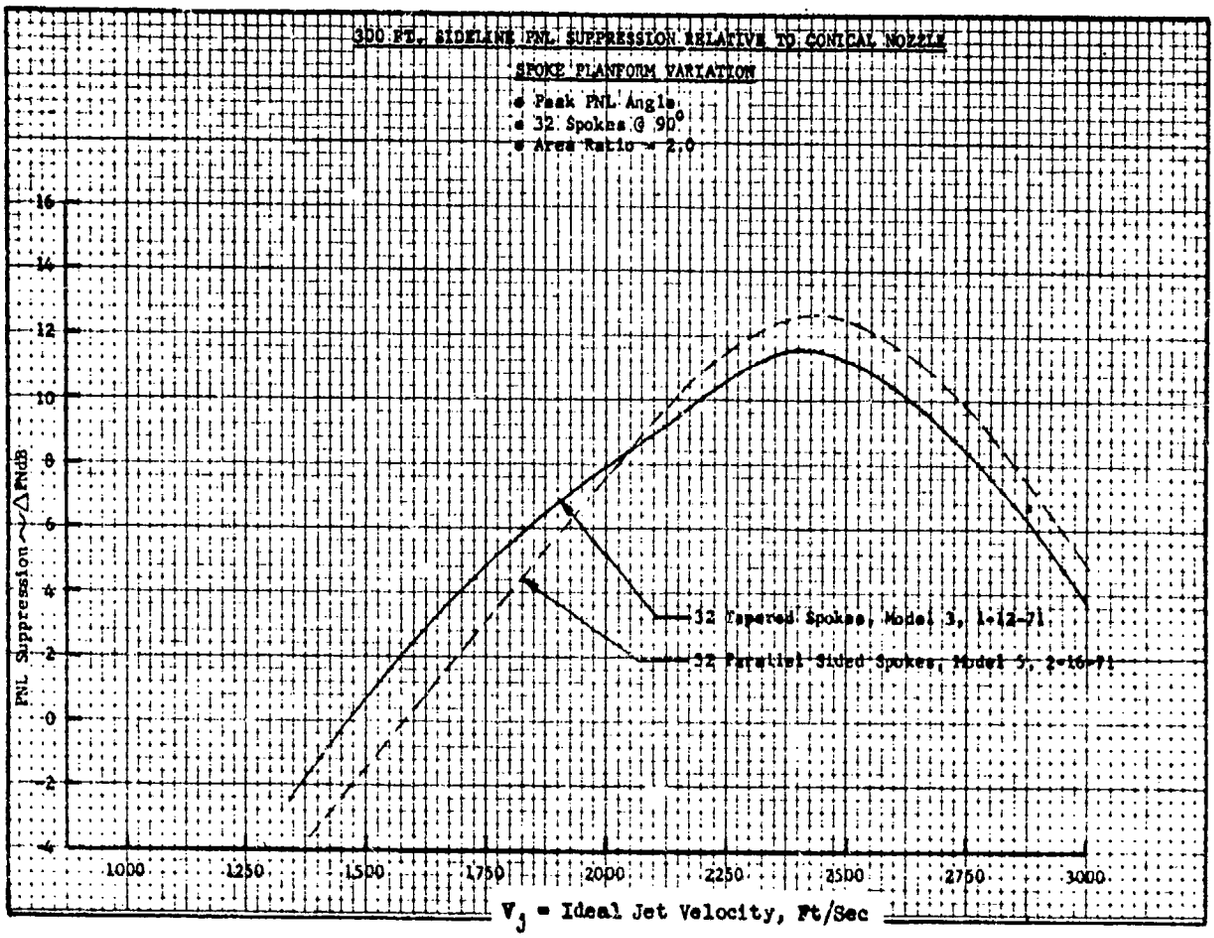


FIGURE V.E.2-52 HARDWARE USED FOR PARAMETRIC INVESTIGATION OF SPOKE PLANFORM; AERODYNAMIC TEST RESULTS



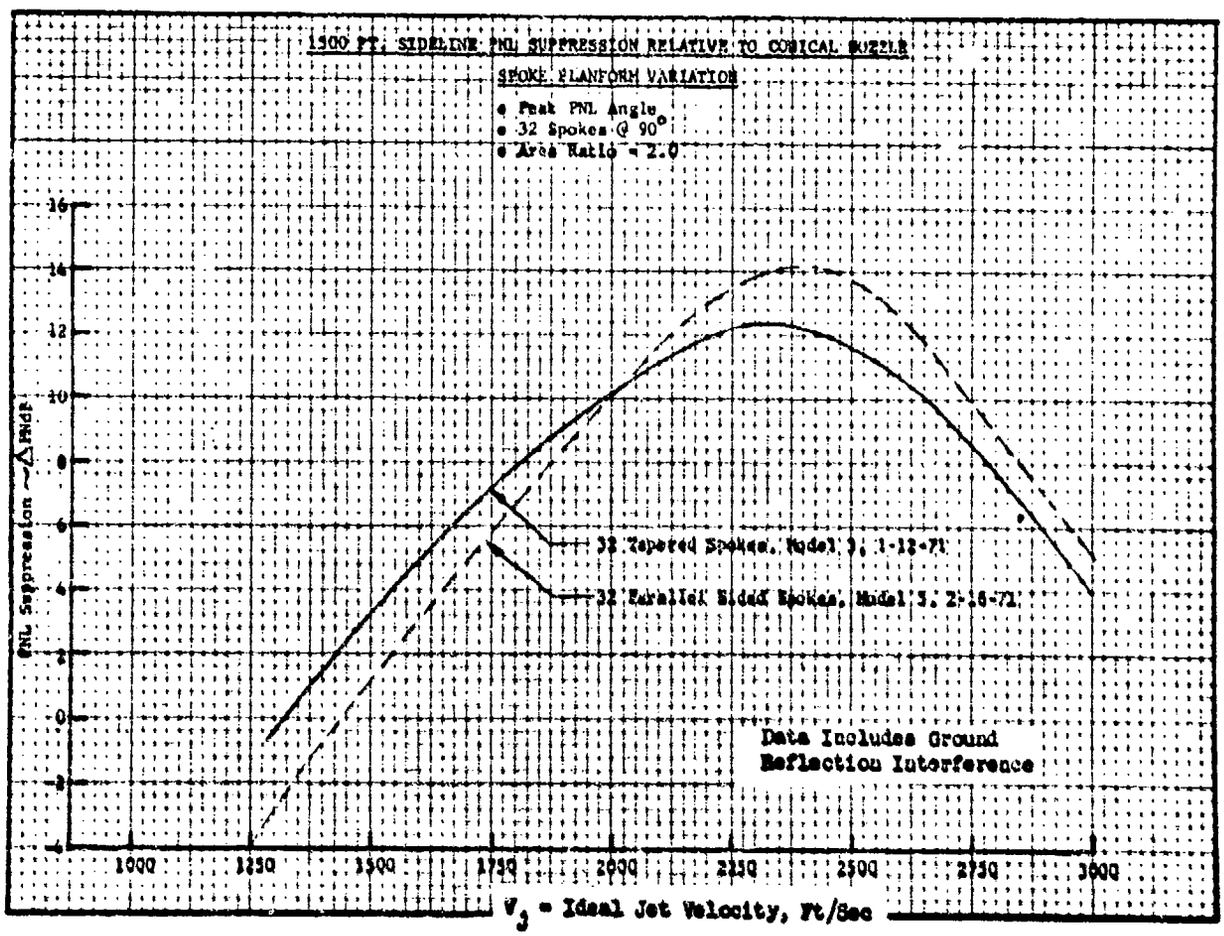
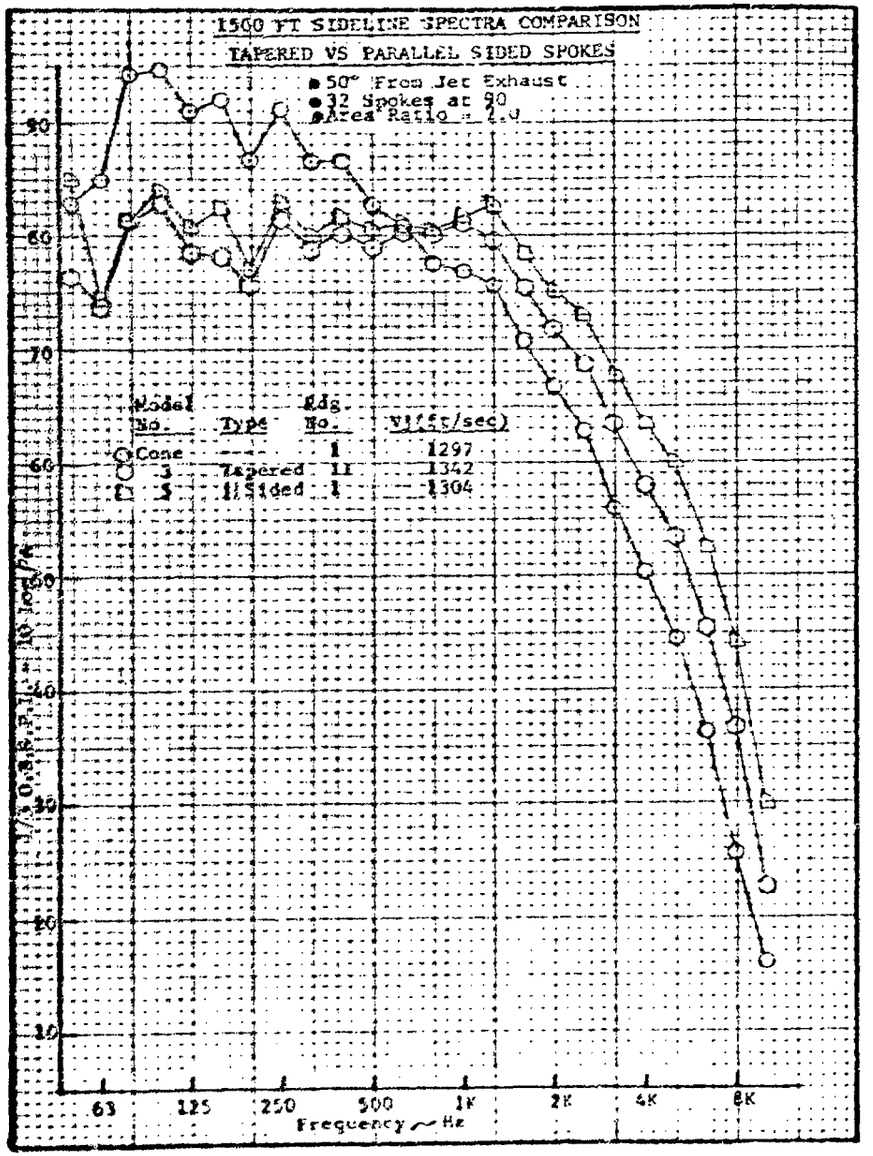


FIGURE V.H.2-53 EFFECT OF SPOKE PLANFORM ON 300 FT AND 1500 FT SIDELINE PNL SUPPRESSION FOR PLUG NOZZLE CONFIGURATIONS



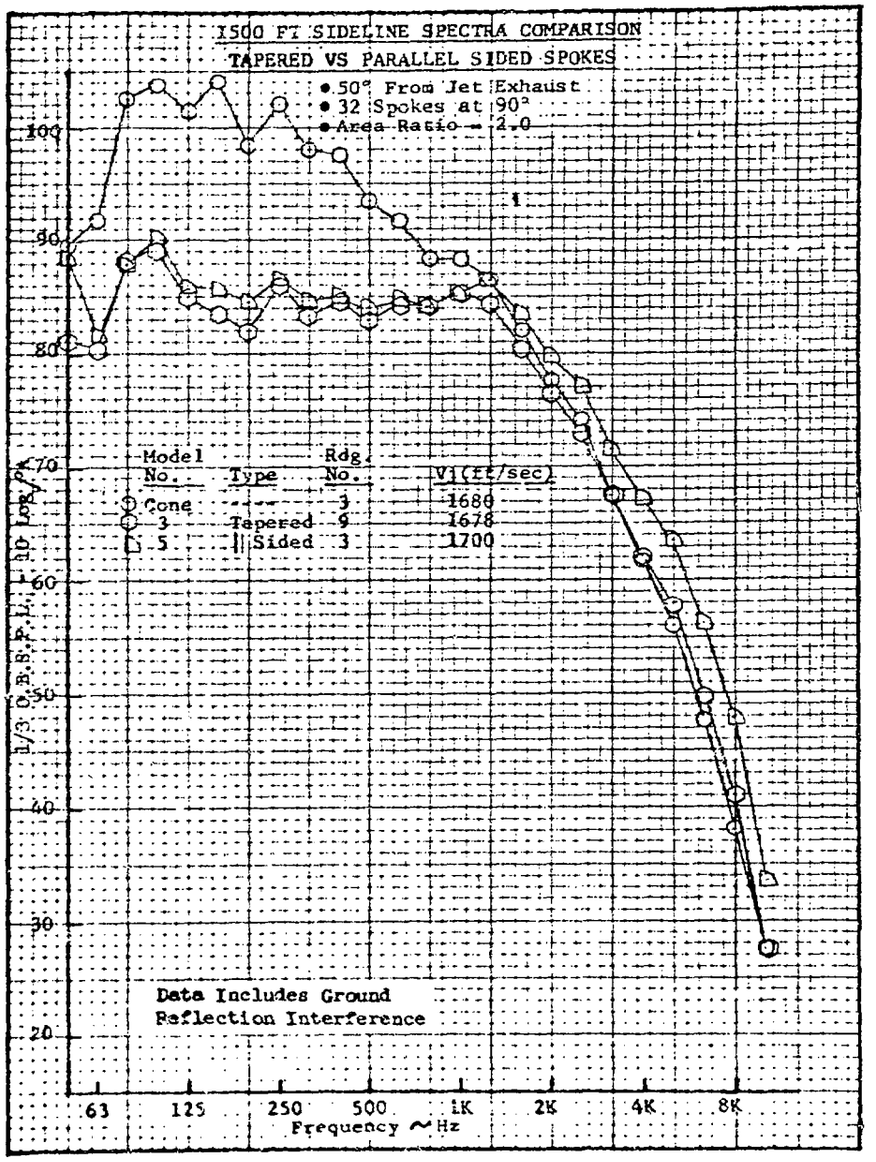
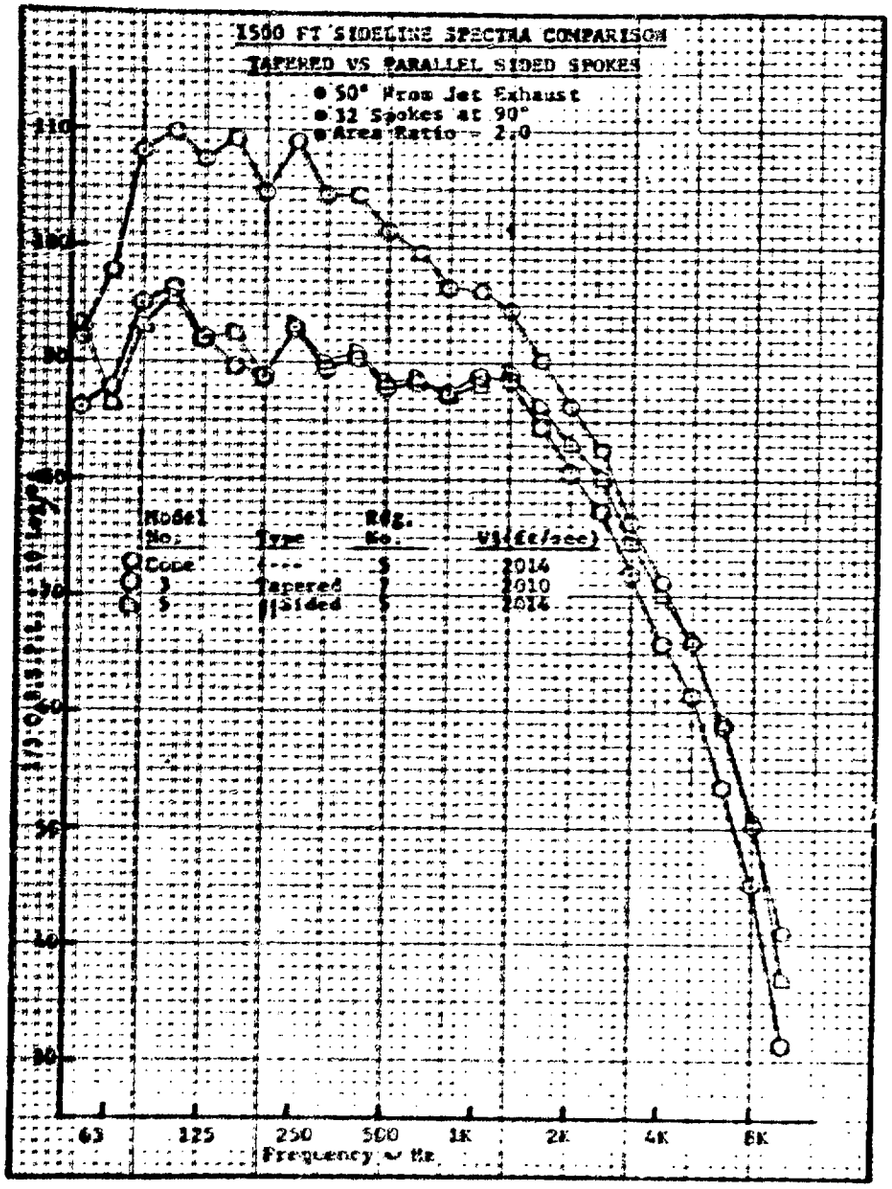


FIGURE V.H.2-54A EFFECT OF SPOKE PLANFORM ON 1500 FT SIDELINE SPECTRA



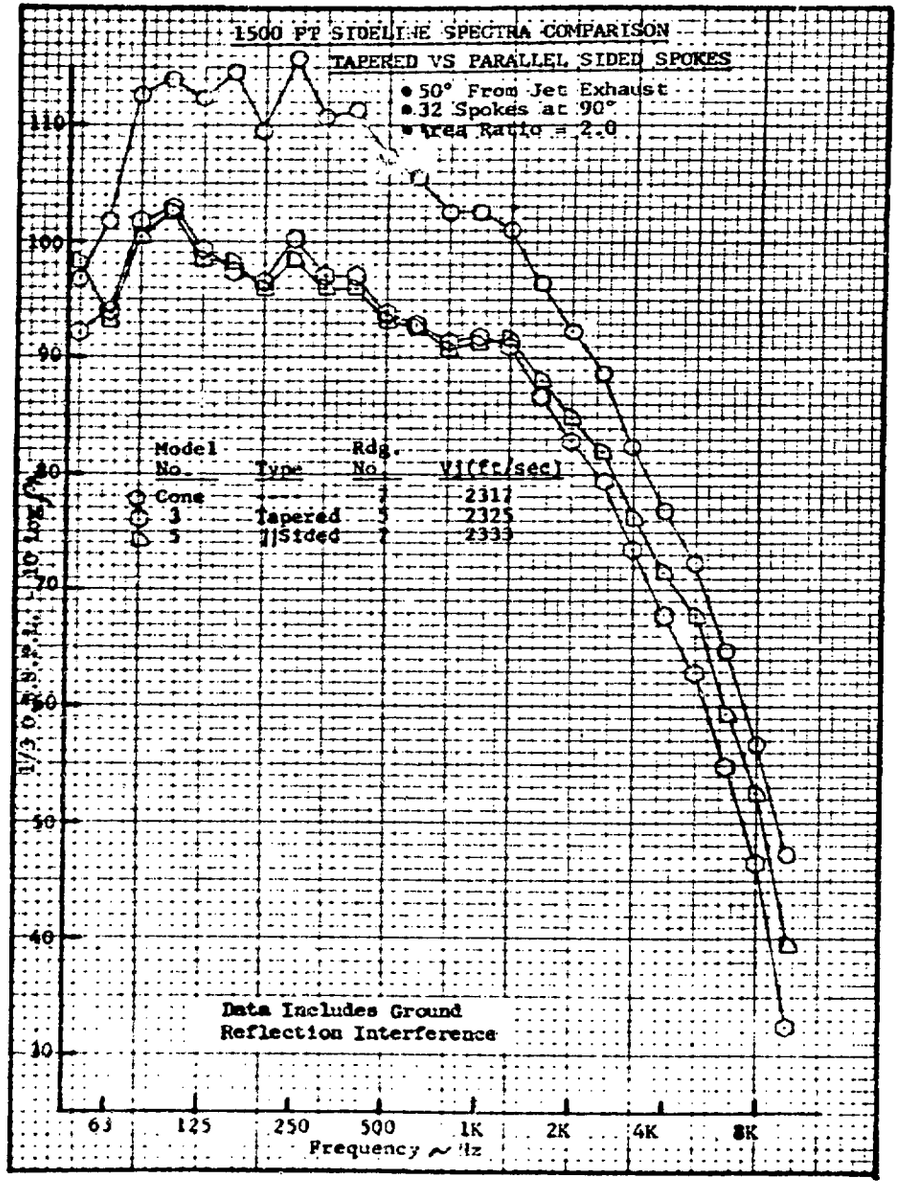
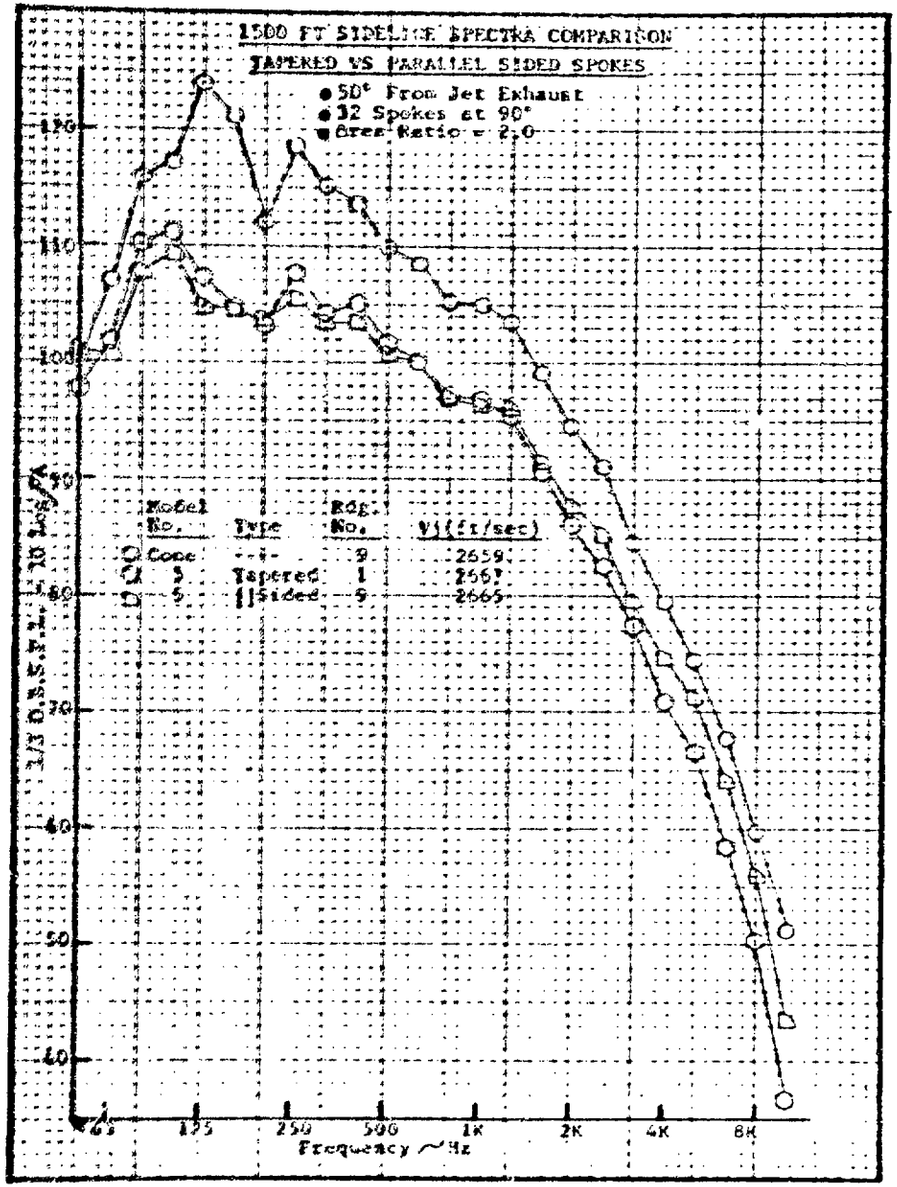


FIGURE V.H.2-54B EFFECT OF SPOKE PLANFORM ON 1500 FT SIDELINE SPECTRA



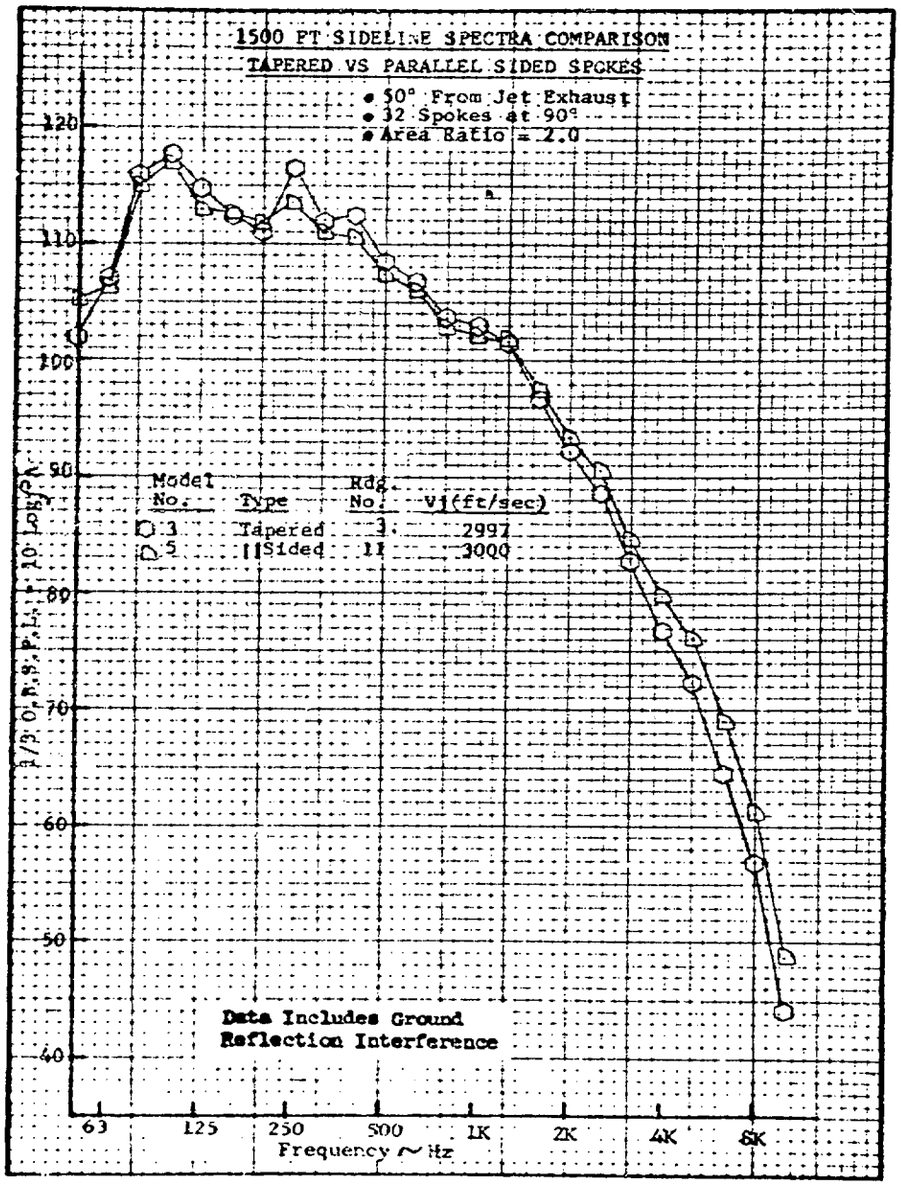
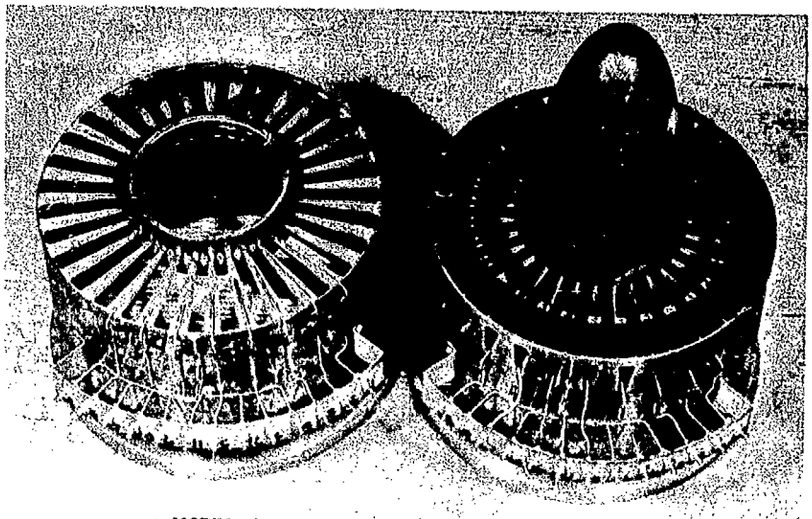


FIGURE V.A.2-54C EFFECT OF SPOKE PLANFORM ON 1500 FT SIDELINE SPECTRA



- MODEL 3
- 32 SPOKE
- A/R = 2.0

- MODEL 10
- 32 CHUTE
- A/R = 2.0

SUPPRESSOR TEST HARDWARE
CHUTES VS SPOKES

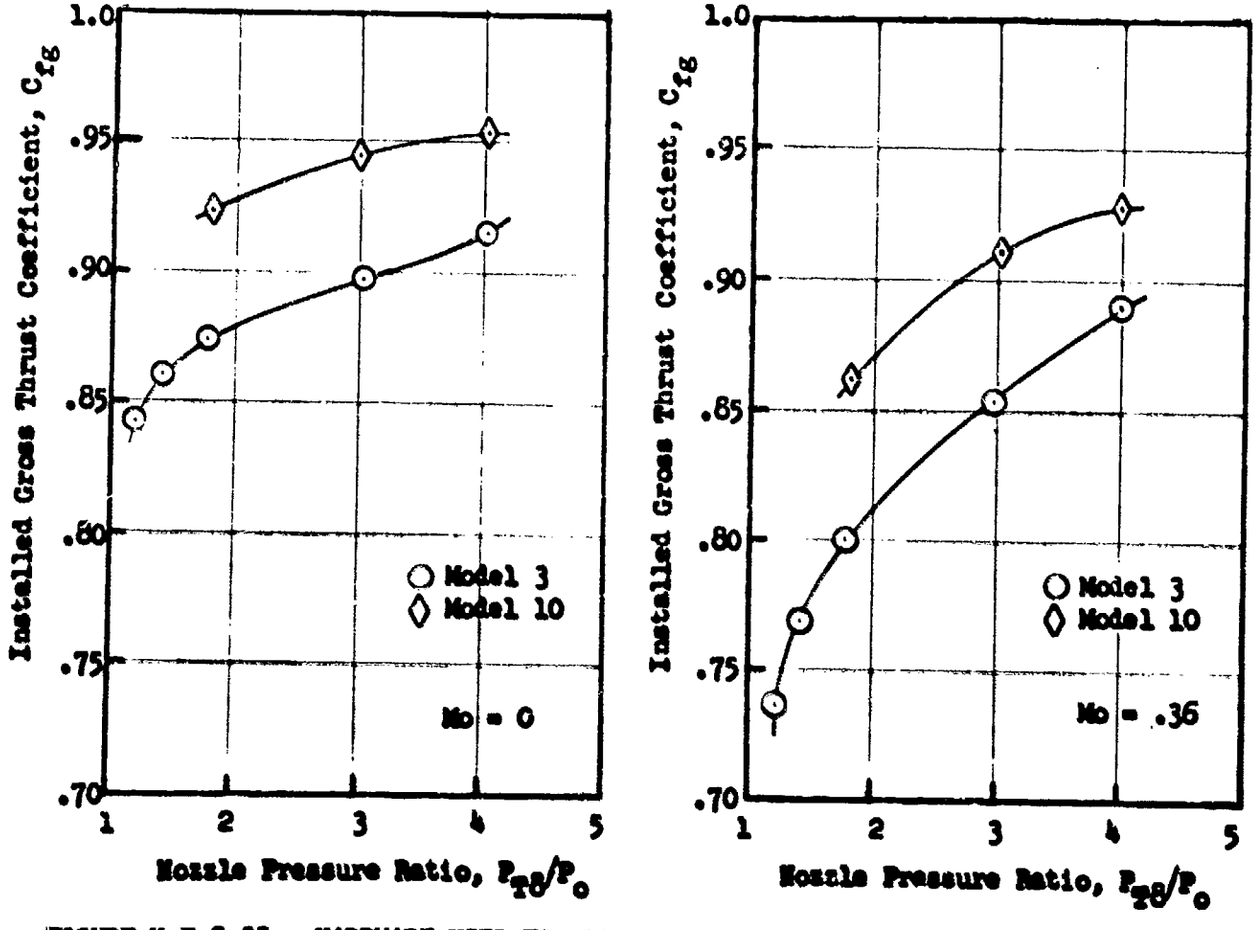
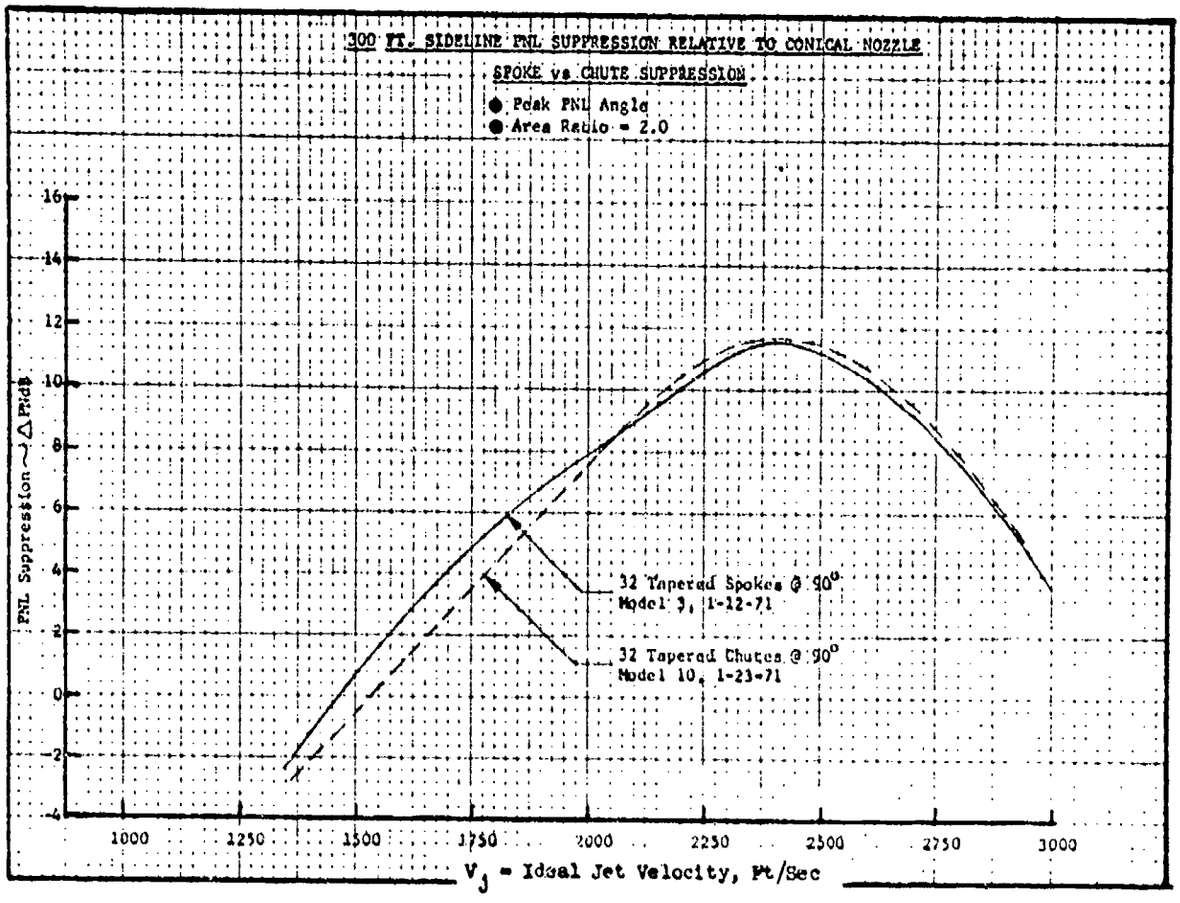


FIGURE V.E.2-55 HARDWARE USED FOR PARAMETRIC INVESTIGATION OF CHUTES VS SPOKES; AERODYNAMIC TEST RESULTS



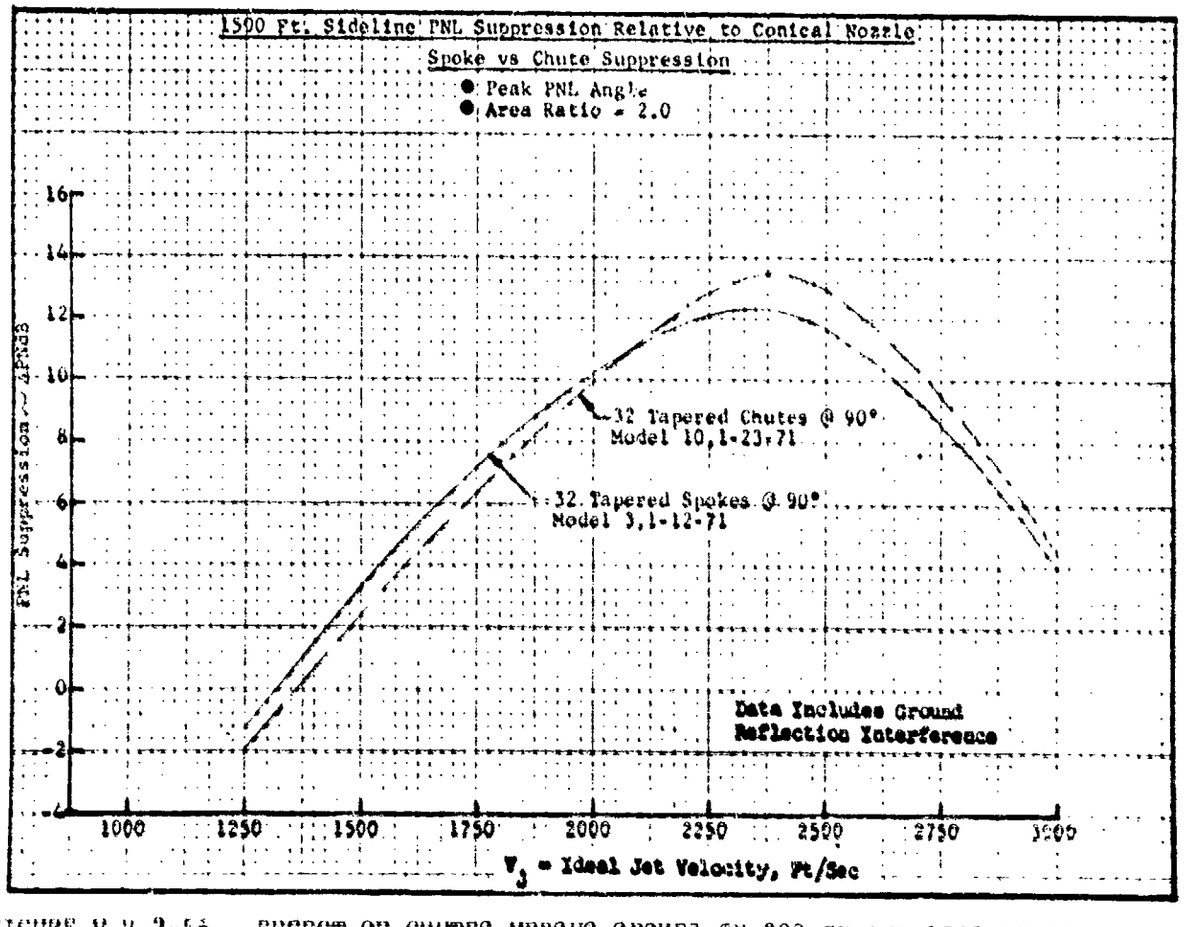
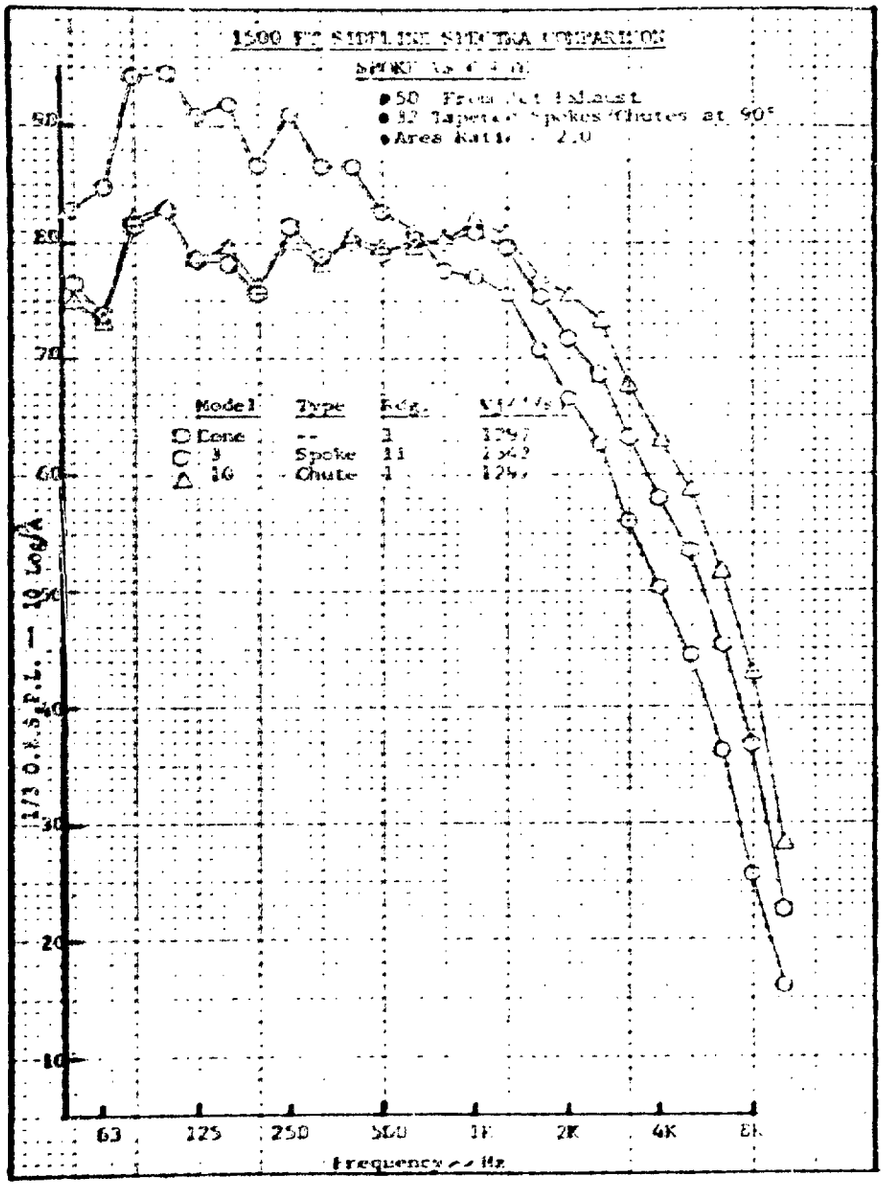


FIGURE V.H.2-56 EFFECT OF CHUTES VERSUS SPOKES ON 300 FT AND 1500 FT SIDELINE PNL SUPPRESSION FOR PLUG NOZZLE CONFIGURATIONS



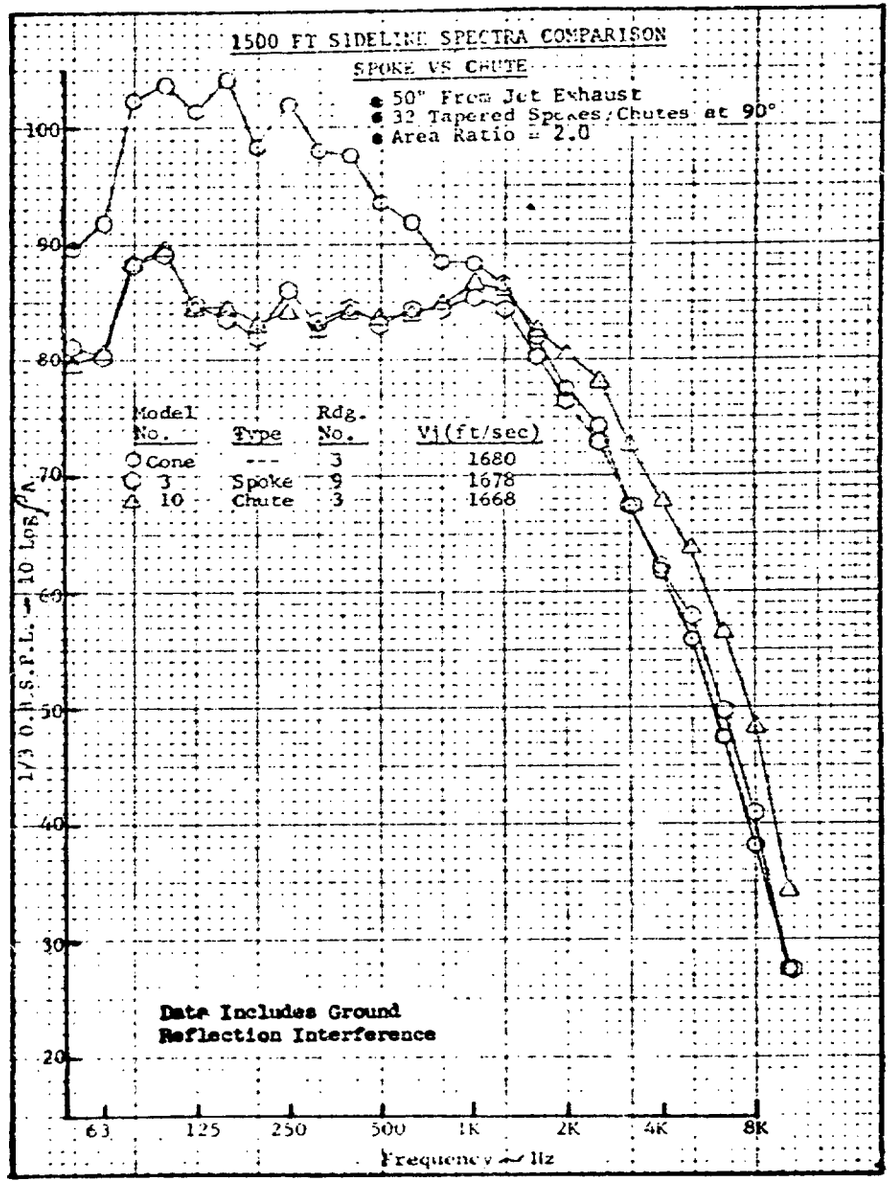
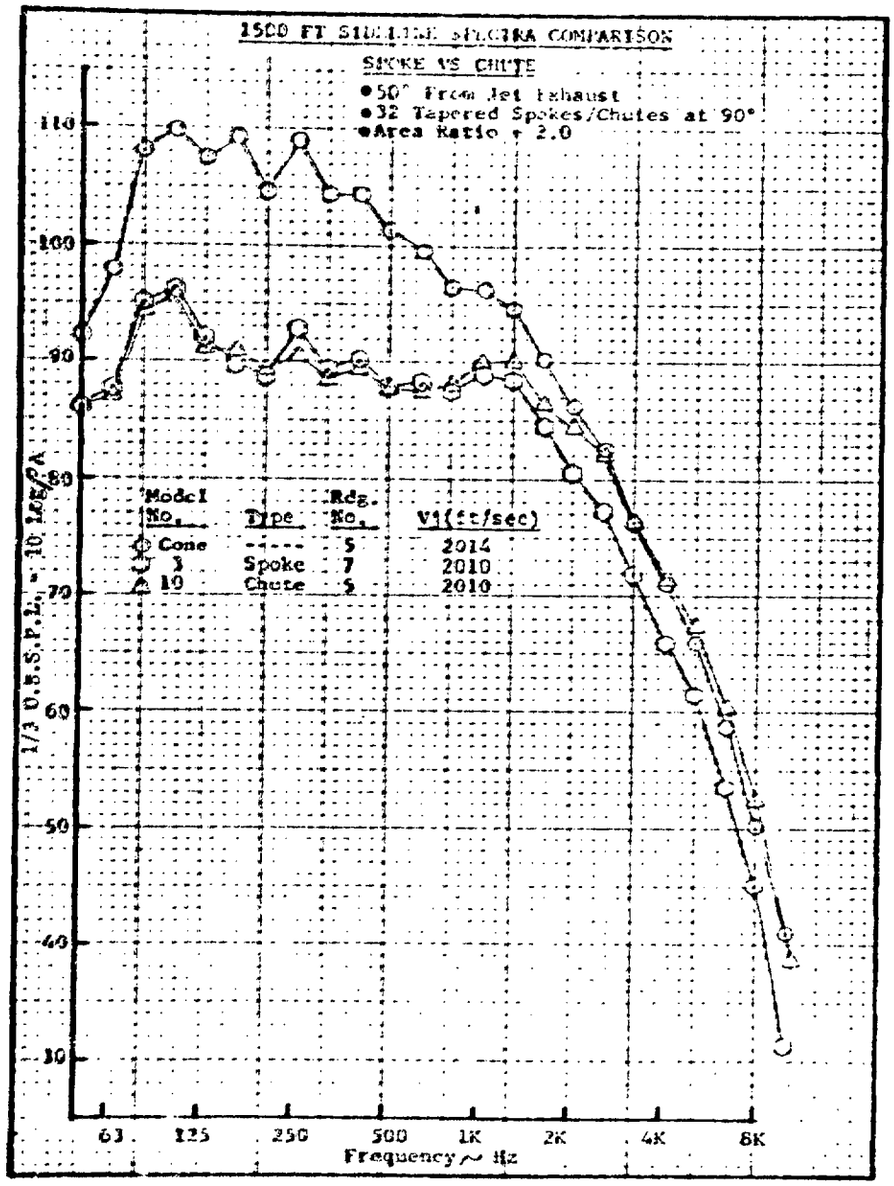


FIGURE V.B.2-57A EFFECT OF CHUTES VERSUS SPOKES ON 1500 FT SIDELINE SPECTRA



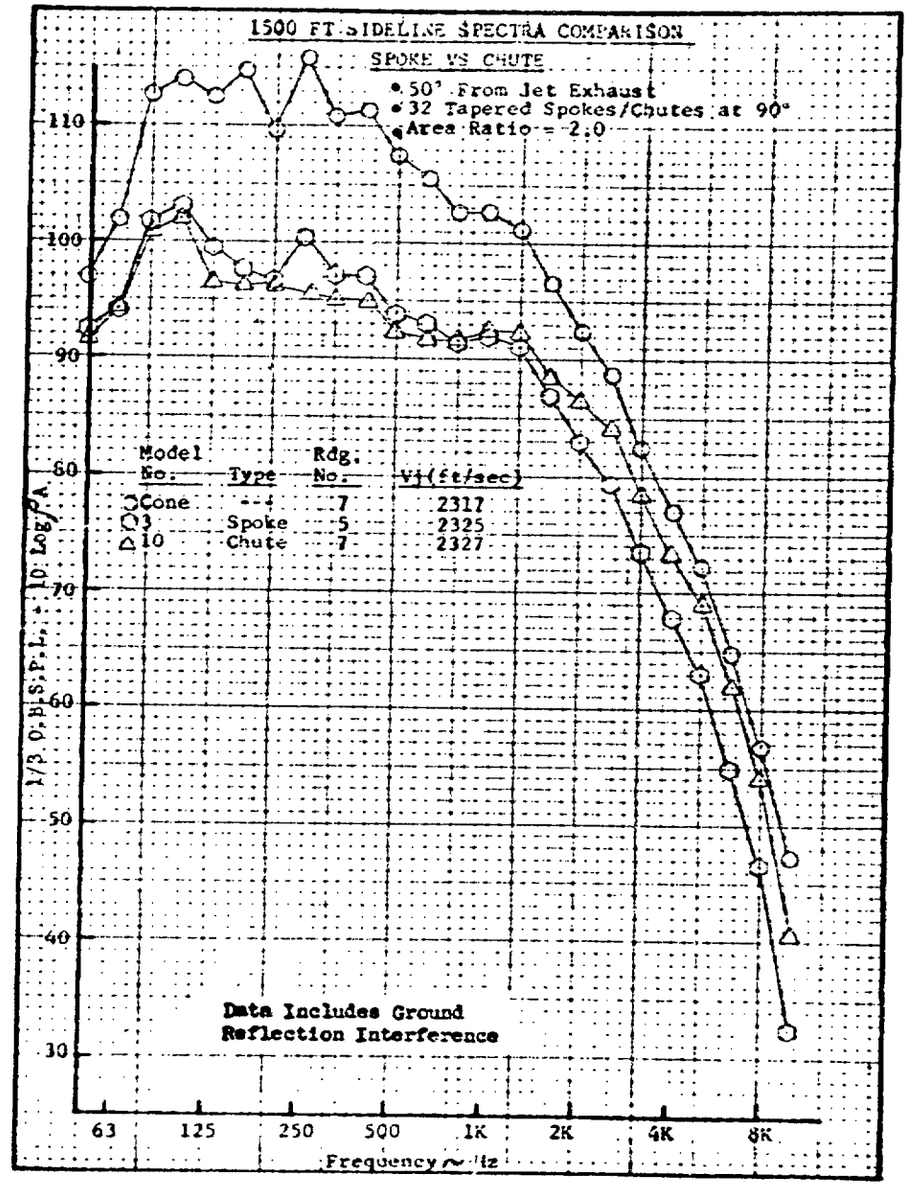
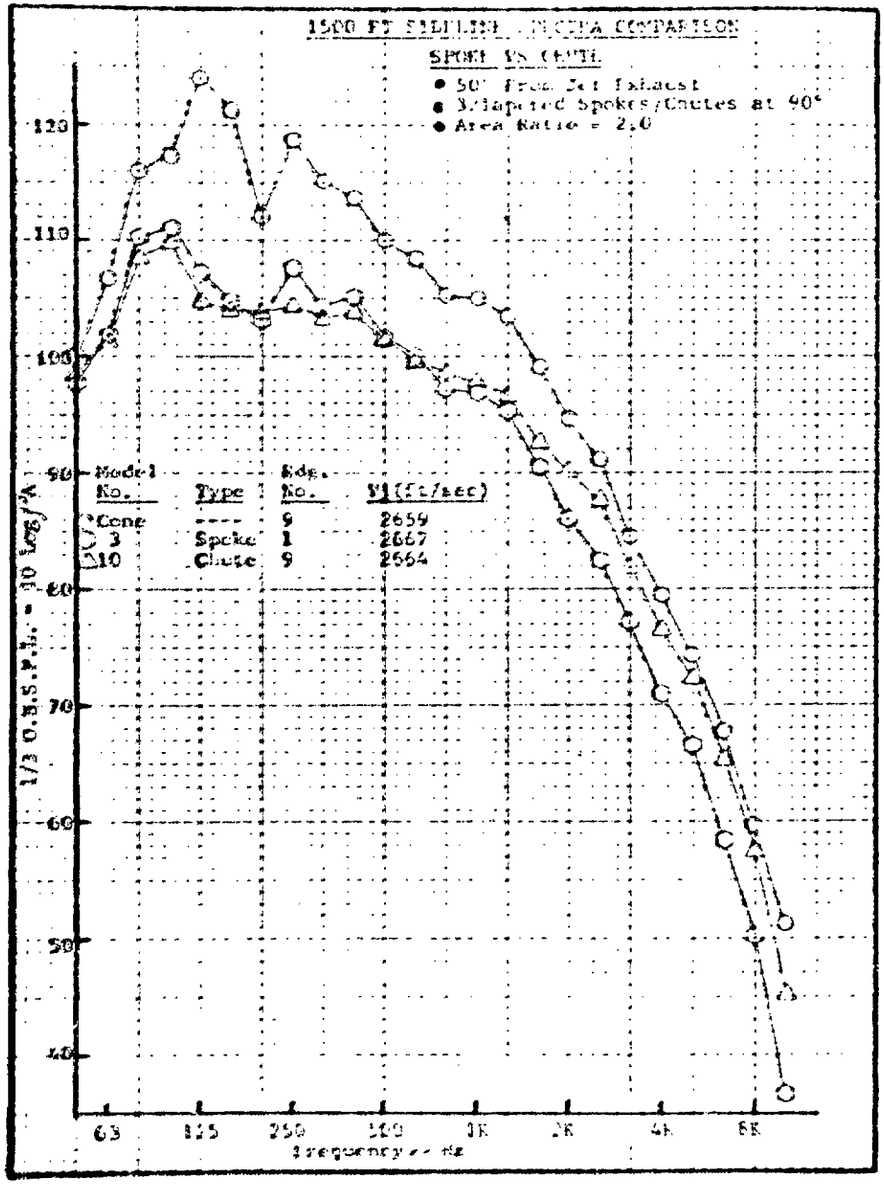


FIGURE V.H.2-57P EFFECT OF CHUTES VERSUS SPOKES ON 1500 FT SIDELINE SPECTRA



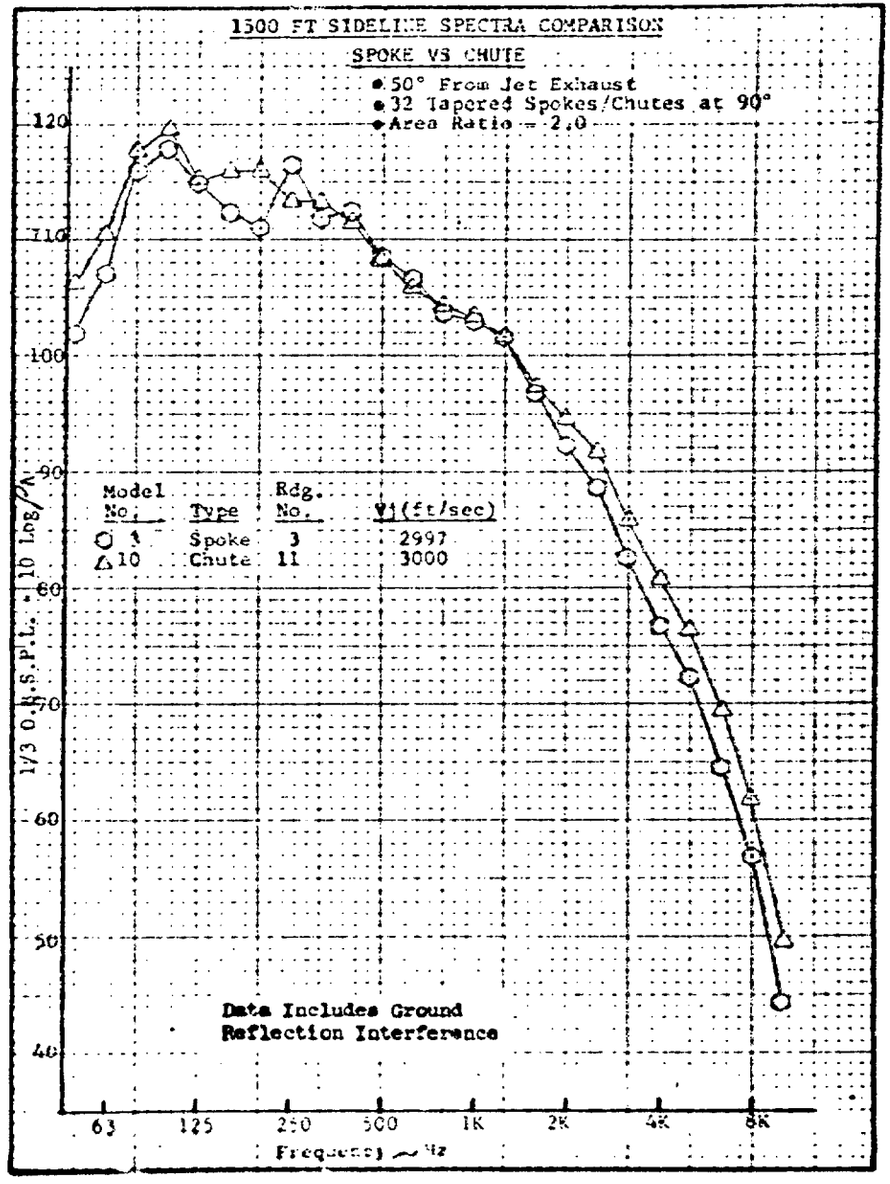
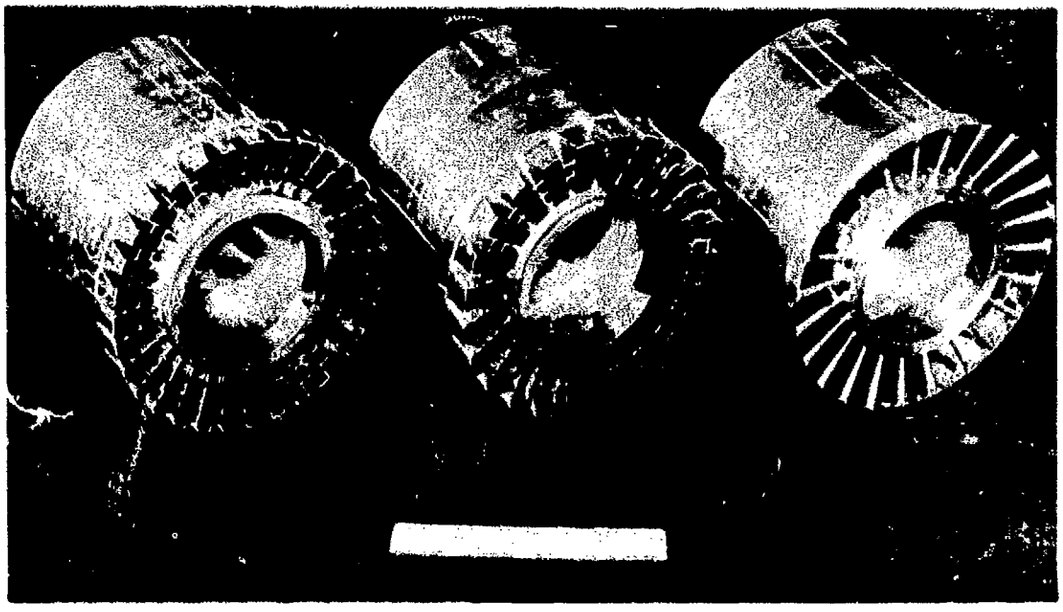


FIGURE V.1.2-57C EFFECT OF CHUTES VERSUS SPOKES ON 1500 FT SIDELINE SPECTRA



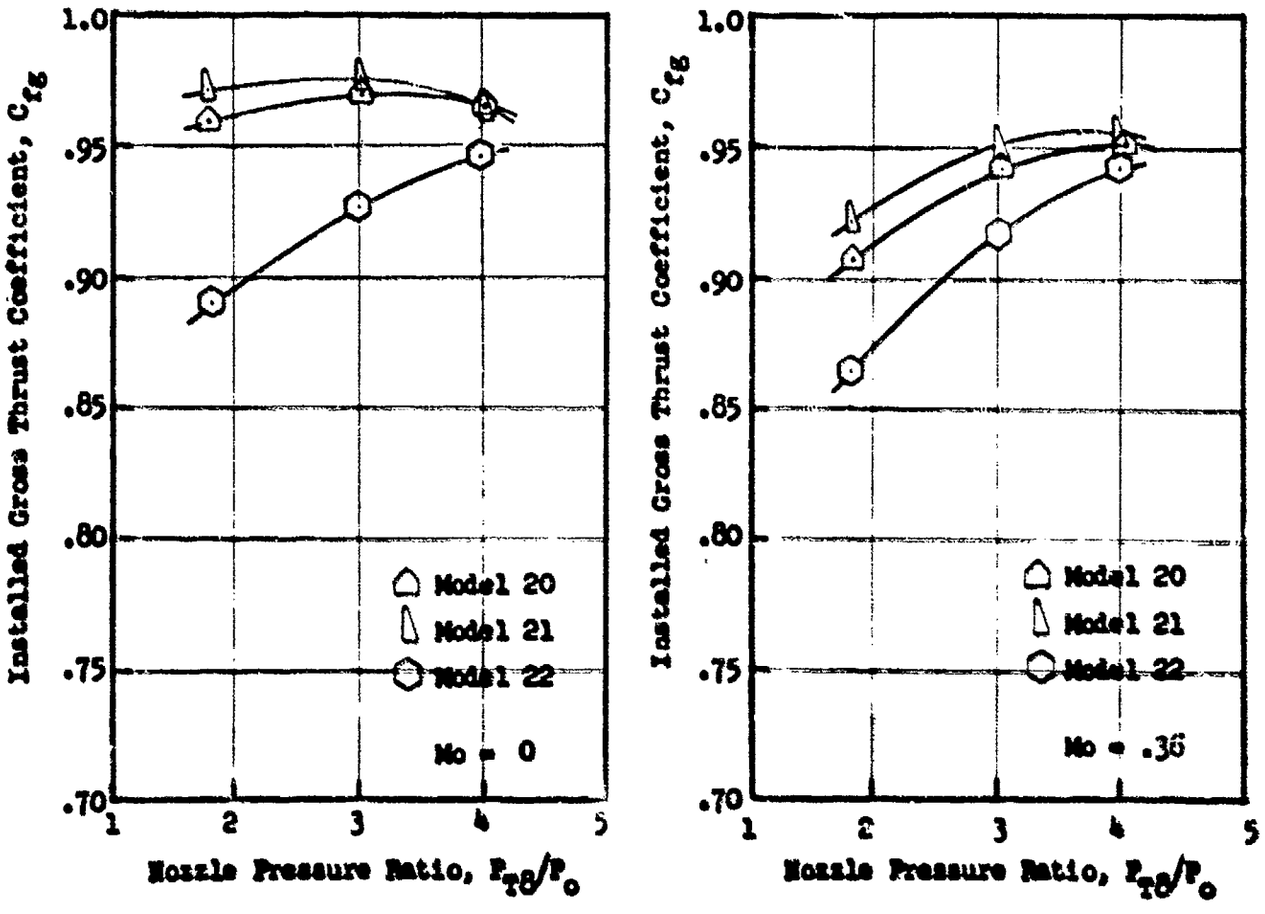
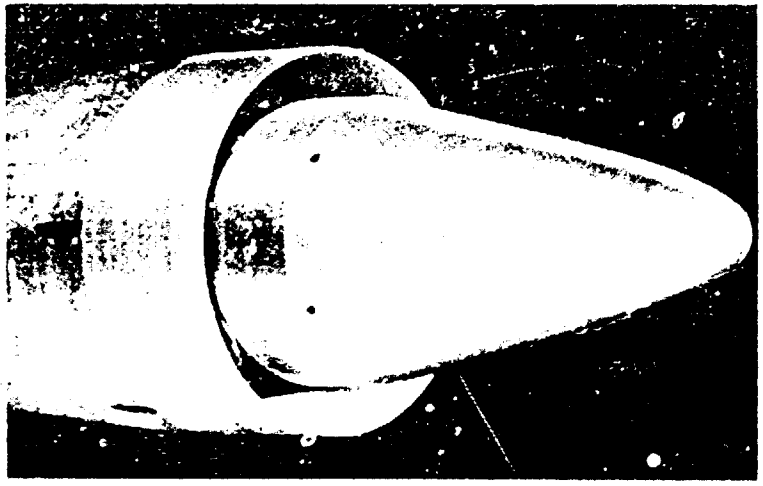
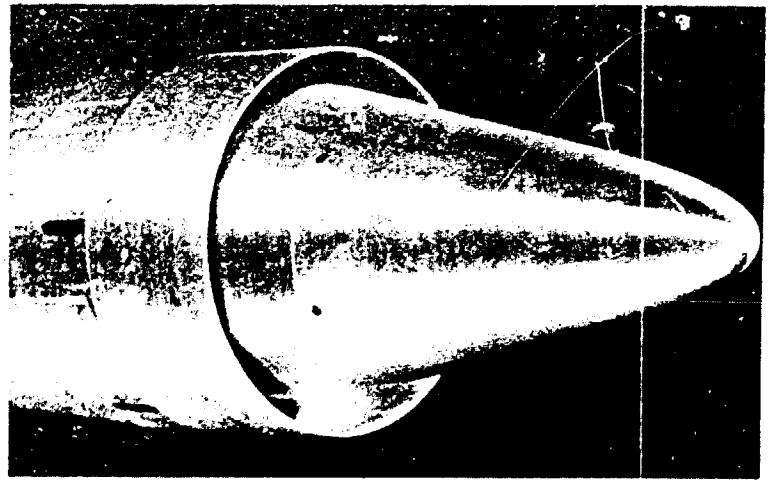


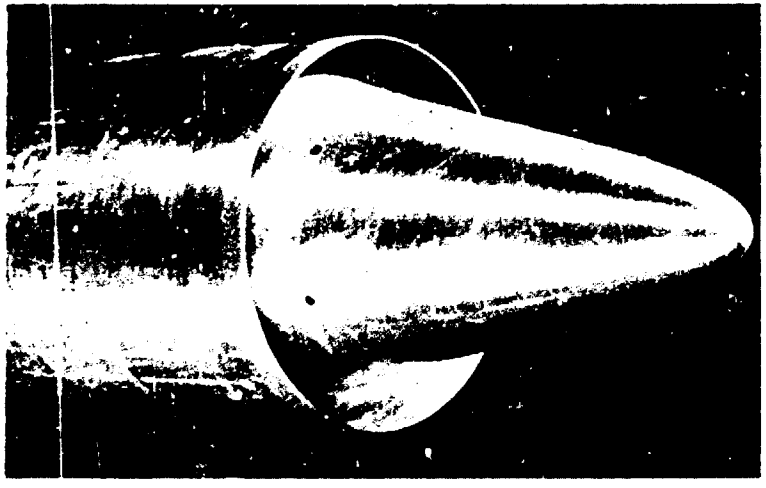
FIGURE V.E.2-58 SUPPRESSED NOZZLE HARDWARE AND AERODYNAMIC RESULTS



A. CUTBACK/APPROACH



B. HOLD/DIVERT



C. TRANSONIC ACCEL

FIGURE V.H.2-59 UNSUPPRESSED PLUG NOZZLE HARDWARE SHOWING FLIGHT MODE CONFIGURATIONS

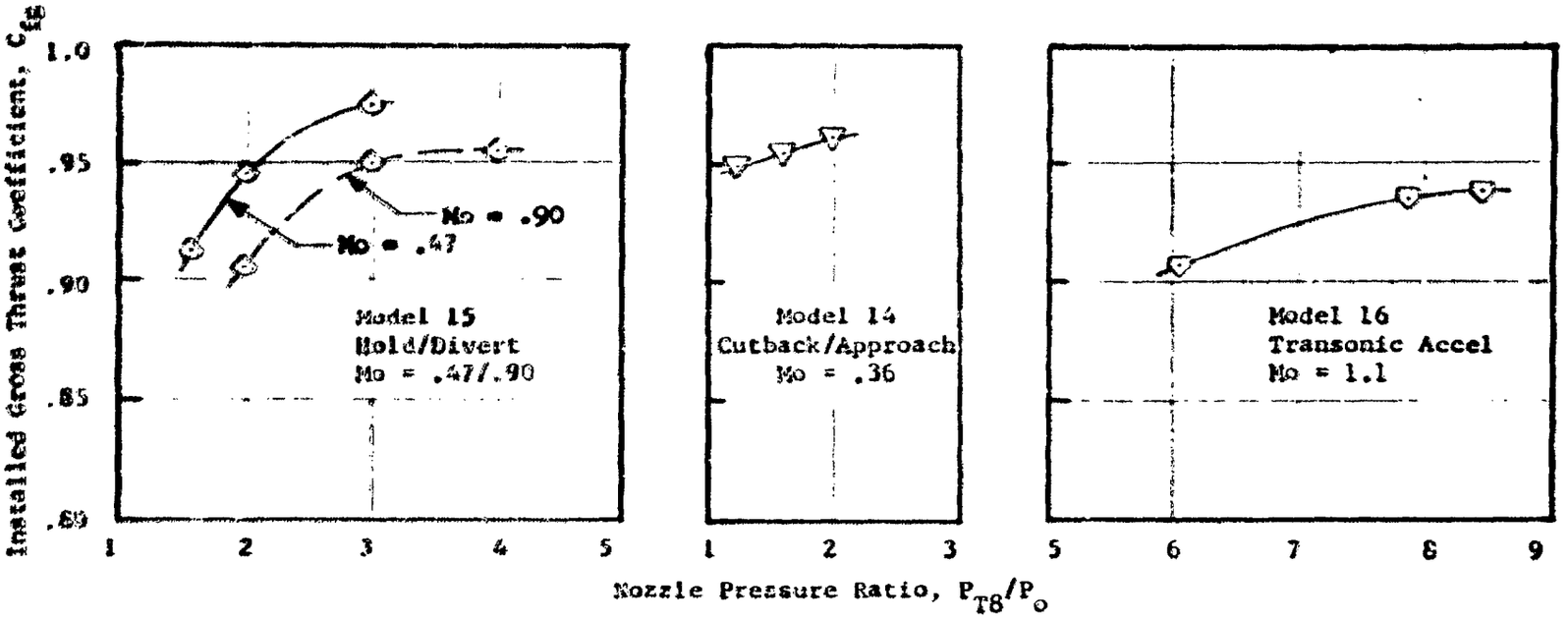
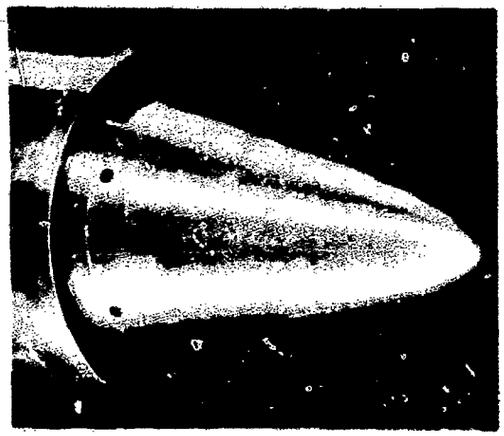
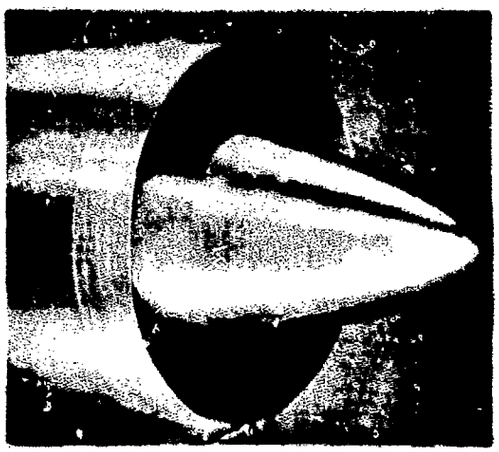


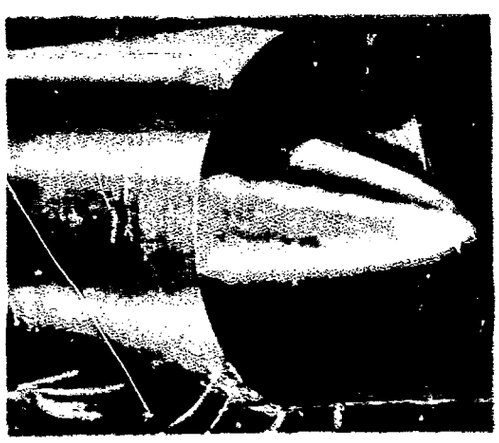
FIGURE V.H.2-60 FLIGHT MODE TEST RESULTS ON UNSUPPRESSED PLUG NOZZLES



18.3" SHROUD



44.0" SHROUD



61" SHROUD

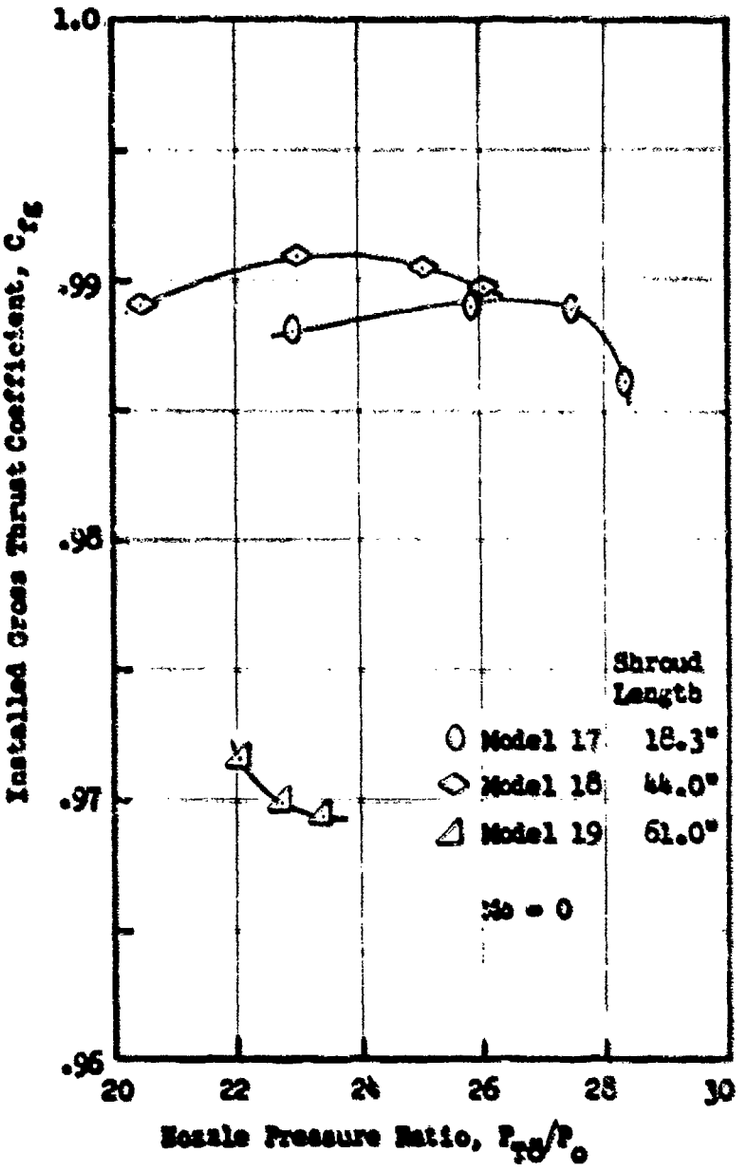


FIGURE V.E.2-61 SIMULATED FULL SCALE SHROUD LENGTH VARIATION EFFECTS

TABLE V.H.2-15 SUMMARY OF AERODYNAMIC TEST RESULTS ON SCALE MODEL NOZZLES

MODEL CONFIGURATION (SCALE FACTOR 8:1)	MACH NUMBER M_o	NOZZLE PRESSURE RATIO, P_{T8}/P_o	THRUST COEFFICIENT C_{fg}	DISCHARGE COEFFICIENT C_D
Model 2 - △	0	1.810	.9325	.8481
24 Spokes @ 90°	0	3.020	.9513	.9016
Area Ratio = 2.0	0	4.038	.9486	.9099
Model A_8 = 14.910 in^2	.359	1.806	.8324	.8634
	.352	3.002	.8892	.9049
	.356	4.006	.9055	.9106
Model 3 - ○	0	1.043	-	.8229
32 Spokes @ 90°	0	1.207	.8407	.8359
Area Ratio = 2.0	0	1.408	.8590	.8508
Model A_8 = 15.098 in^2	0	1.794	.8730	.8808
	0	3.031	.8955	.9190
	0	4.044	.9140	.9218
	.354	1.225	.7365	.8751
	.357	1.419	.7686	.8720
	.358	1.795	.8003	.8867
	.360	2.986	.8539	.9203
	.356	4.005	.8894	.9205
Model 4 - ▷	0	1.798	.7621	.8918
48 Spokes @ 90°	0	2.995	.7931	.9189
Area Ratio = 2.0	.357	1.800	.7340	.8939
Model A_8 = 14.648 in^2	.362	3.021	.7721	.9176
Model 5 - ▷	0	3.007	.7922	.8940
32 Spokes @ 90°	0	3.983	.8392	.8944
Parallel Sides	.356	3.012	.7724	.8934
Area Ratio = 2.0	.357	3.999	.8270	.8938
Model A_8 = 14.972 in^2				
Model 6 - □	0	1.799	.8660	.8792
32 Spokes @ 90°	0	3.019	.9084	.9072
Area Ratio = 1.5	0	4.038	.9390	.9063
Model A_8 = 15.012 in^2	.364	1.802	.8492	.8783
	.361	3.019	.8952	.9067
	.365	4.039	.9300	.9053
Model 7 - ◇	0	1.804	.8681	.8399
32 Spokes @ 90°	0	3.001	.9004	.8923
Area Ratio = 2.5	0	4.029	.9059	.8997
Model A_8 = 15.457 in^2	.364	1.806	.7426	.8534
	.367	3.024	.8218	.8935
	.370	4.058	.8434	.8999

TABLE V.H.2-15 SUMMARY OF AERODYNAMIC TEST RESULTS ON SCALE MODEL NOZZLES (Cont.)

MODEL CONFIGURATION (SCALE FACTOR 8:1)	MACH NUMBER M_o	NOZZLE PRESSURE RATIO, P_{T8}/P_o	THRUST COEFFICIENT C_{fg}	DISCHARGE COEFFICIENT C_D
Model 8 - ∩	0	1.816	.8904	.8527
32 Spokes 10° Forward	0	3.002	.9295	.8984
of Perpendicular	0	4.008	.9292	.9040
to Plug Centerline	.355	1.802	.8108	.8585
Area Ratio = 2.0	.355	2.990	.8730	.9993
Model A_8 = 15.198 in^2	.362	3.992	.8945	.9057
Model 9 - ◇	0	1.830	.8522	.8683
32 Spokes, 10° Aft	0	3.008	.8762	.9072
of Perpendicular	0	4.004	.9089	.9108
to Plug Centerline	.350	1.804	.7829	.8743
Model A_8 = 15.978 in^2	.361	2.991	.8280	.9045
	.358	.3989	.8821	.9049
Model 10 - ◇	0	1.807	.9224	.9706
32 Chutes @ 90°	0	3.004	.9449	.9788
Area Ratio = 2.0	0	4.034	.9536	.9807
Model A_8 = 14.655 in^2	.361	1.825	.8616	.9740
	.365	3.036	.9107	.9770
	.360	3.987	.9278	.9803
	.499	1.771	.8391	.9763
	.500	3.000	.8875	.9809
	.501	4.015	.9186	.9803
Model 14 - ▽	0	1.597	.9619	.9879
Unsuppressed	0	2.004	.9673	.9692
15° Plug	.356	1.215	.9486	1.0252
Cutback/Approach	.356	1.590	.9541	.9865
Mode, M_o = .36	.356	1.996	.9601	.9676
Model A_8 = 18.038 in^2				
Model 15 - ◇	0	1.562	.9319	1.0095
Unsuppressed	0	1.996	.9527	.9808
15° Plug	0	3.010	.9771	.9809
Hold/Divert	0	4.053	.9821	.9814
Mode, M_o = .47/.90	.468	1.562	.9118	1.0052
Model A_8 = 12.969 in^2	.468	2.001	.9446	.9779
	.469	3.012	.9724	.9812
	.895	1.979	.9051	.9813
	.898	3.009	.9487	.9820
	.895	4.005	.9530	.9806

TABLE V.H.2-15 SUMMARY OF AERODYNAMIC TEST RESULTS ON SCALE MODEL NOZZLES (Concluded)

MODEL CONFIGURATION (SCALE FACTOR 8:1)	MACH NUMBER M_o	NOZZLE PRESSURE RATIO, P_{T8}/P_o	THRUST COEFFICIENT C_{fg}	DISCHARGE COEFFICIENT C_D
Model 16 - ♡	0	5.932	.9733	.9833
Unsuppressed	0	7.678	.9833	.9834
15° Plug	0	8.980	.9850	.9834
Transonic Accel	1.094	6.046	.9053	.9814
Mode, M_o = 1.1	1.099	7.852	.9332	.9828
Model A_8 = 11.290 in^2	1.097	8.435	.9369	.9811
Model 17 - ○	0	22.961	.9883	.9827
Supersonic Cruise	0	25.894	.9892	.9823
Shroud Length*= 18.3"	0	27.537	.9887	.9823
Model A_8 = 12.975 in^2	0	28.346	.9861	.9826
Model 18 - ◇	0	20.472	.9890	.9840
Supersonic Cruise	0	23.011	.9909	.9809
Shroud Length*= 44"	0	25.050	.9904	.9830
Model A_8 = 12.998 in^2	0	26.023	.9897	.9824
Model 19 - ◿	0	22.064	.9716	.9814
Supersonic Cruise	0	22.744	.9699	.9825
Shroud Length*= 61"	0	23.410	.9694	.9823
Model A_8 = 12.958 in^2				
Model 20 - ⌂	0	1.794	.9595	.9615
32 Chutes 15° Forward	0	3.024	.9695	.9661
of Perpendicular	0	4.011	.9649	.9675
to Plug Centerline	.357	1.812	.9061	.9639
Area Ratio = 1.69	.359	3.030	.9408	.9638
Model A_8 = 14.709 in^2	.356	4.028	.9510	.9668
Model 21 - ⌂	0	1.799	.9708	.9786
24 Chutes 15° Forward	0	3.017	.9761	.9853
of Perpendicular	0	4.029	.9649	.9848
to Plug Centerline	.357	1.825	.9218	.9827
Area Ratio = 1.69	.355	3.032	.9517	.9852
Model A_8 = 14.697 in^2	.354	3.997	.9559	.9844
Model 22 - ⬡	0	1.802	.8896	.8199
24 Low C_D Spokes 15°	0	3.001	.9260	.8669
Fwd. of Perpendicular	0	3.990	.9464	.8690
to Plug Centerline	.356	1.815	.8641	.8280
Area Ratio = 1.38	.359	3.004	.9167	.8635
Model A_8 = 19.030 in^2	.361	3.992	.9413	.8662

*Simulated Full Scale

"PRECEDING PAGE BLANK-NOT FILMED."

VI. SYSTEM STUDIES

"PRECEDING PAGE BLANK-NOT FILMED."

VI.A CHOKED INLET - GE4 ENGINE

"PRECEDING PAGE BLANK-NOT FILMED."

VI.A CHOKED INLET-GE4 ENGINE

Test Purpose and Configuration Setup

Acoustic tests of a choked inlet were performed in 1968 at the General Electric Peebles Proving Grounds, Site 4D, at Peebles, Ohio. The full scale GE4 Block I Engine 435-002 was used with The Boeing Company's axisymmetric variable position centerbody inlet. Purpose of the test was to determine the acoustic effectiveness of a choked inlet on the suppression of compressor noise radiation from the GE4 engine during typical cutback and approach cycle conditions.

A photograph of Engine -002 with the sharp lip inlet, as mounted on the Site 4D thrust stand, is shown in Figure VI.A-1. Schematically, Figure VI.A-2 illustrates the geometric features of the varible inlet system including the reference centerbody location, L. The inlet centerbody throat area was varied by axial movement of the inlet centerbody. Tests were conducted at the four throat areas of 815, 1005, 1135, and 1215 sq. in., as shown. As the minimum inlet area setting, acoustic measurements were taken both with the inlet doors closed and open. The photograph in Figure VI.A.-1 shows the inlet doors. At the other configuration settings, the inlet takeoff doors were fully closed. For all the tests a 1318 in^2 conical primary exhaust nozzle was fitted to the engine.

Acoustic data were obtained simultaneously from microphones located at a 250 ft. radius from the engine at nozzle centerline heights and at 10° increments from 0° to 160° to the inlet axis. The acoustic data were reduced in 1/3 octave band form, corrected to a 59° F, 70% relative humidity standard day, and with calculations of OASPL and PNL at the 250 ft. arc. The arc data were extrapolated to the 300 and 1500 ft. sidelines using standard SAE procedures.

Data Presentation and Results

Table VI.A-1 summarizes all test configurations, engine speeds, inlet throat Mach number and 300 ft. sideline peak PNdB levels. In Figures VI.A-3, -4 and -5 the acoustic results are shown in terms of PNdB levels at 300 ft. sideline versus angle to the inlet axis for nominal engine speeds of 4000, 5000, and 4700 rpm. For angles up to 90° to the inlet axis, considerable attenuation was achieved by choking the inlet PNL suppressions of up

to 15 PNdB were attached for the angles close to the inlet axis at the lowest speed. The suppression decreases with increase in rpm due to the increase in jet noise contribution to the total engine noise output. Although the choked inlet gave considerable suppression in the forward quadrant, the 300 ft. sideline peak PNdB level was not reduced by more than 1 to 3 PNdB. This is more clearly shown in Figure VI.A-6 which plots the normalized 300 ft. sideline PNdB levels for each inlet configuration versus ideal jet velocity. Included on the graph are earlier measured data from standard bellmouth inlet testing with the 1318 in^2 primary exhaust nozzle. A mean line is drawn through the test data with the inlet throat choked and again shows only limited peak 300 ft. sideline suppression. At typical cutback and approach conditions, the choked inlet would then provide from 1 to 3 peak sideline PNdB suppression. On an EPNdB basis, the suppression would be considerably higher due to the change in PNL directivity. For comparison, the SAE jet noise prediction line, extrapolated below 1000 ft/sec is included on the figure. Even with the choked inlet removing compressor noise, the peak sideline PNdB are still considerably higher than what would be predicted by the SAE procedure.

To more clearly show the effect of inlet choking on compressor noise radiation, 1/3 octave band spectra at 30° and 110° to the inlet axis are illustrated in Figures VI.A-7 and -8, respectively; both on the 250 ft. measuring arc. At 30° the compressor noise dominates the unchoked spectra, and suppression by choking is obtained at all frequencies above 400 Hz. The first stage fundamental tone, at a frequency of 1400 Hz, is reduced by approximately 18 dB. Harmonics of this tone plus tones from other compressor stages and broadband noise are also shown to be considerably attenuated. At the angle of peak 300 ft. sideline PNdB, 110° to the inlet, the spectra for before and after choking are similar except for a slight reduction of the stage 1 compressor fundamental tone (1400 Hz) down to the noise floor from the other engine/jet sources.

Narrowband analyses, in 50 Hz bandwidth, were also performed on the recorded data to further understand the effect of inlet choking on far field noise. Data for nominal engine speeds of 4000, 4500 and 4700 rpm, at 30° and 110° to the inlet are presented for both unchoked and choked inlet conditions as follows:

Engine Speed rpm	Inlet Throat Mach No.	Angle From Inlet	Figure No.
4013	0.25	30°	VI.A-9A
4006	1.00	30°	VI.A-9B
4013	0.26	110°	VI.A-9C
4006	1.00	110°	VI.A-9D
4506	0.385	30°	VI.A-9E
4496	1.00	30°	VI.A-9F
4506	0.385	110°	VI.A-9G
4496	1.00	110°	VI.A-9H
4703	0.465	30°	VI.A-9I
4679	1.00	30°	VI.A-9J
4703	0.465	110°	VI.A-9K
4679	1.00	110°	VI.A-9L

- The data show, in general, that both broadband noise and tones are considerably reduced, especially at the front of the engine, but, at the angle of peak PNdB, the reductions are much less marked.
- The broadband compressor noise seems to be more effectively suppressed by the sonic inlet than the tones.
- Tones still exist in the choked inlet spectra and tend to stand out more clearly with no "broadband skirts".
- At the lower engine speed, 4000 rpm, the tones from the 5th, 6th, 7th and 8th compressor stages were not reduced by choking at the 110° inlet angle of peak PNdB on the 300 ft. sideline (see Figures VI.A-9C and -9D). These two contribute about 2 PNdB to the total noise level at the condition.

Additional 1/3 octave band spectra plots are included at the three nominal engine speeds of 4000, 4500, and 4700 rpm in Figures VI.A-10, -11 and -12, respectively. They compare the 300 ft. sideline, 110° peak PNdB angle spectra for choked and unchoked inlet and show the attained spectra suppression. Also included on each curve is the estimated free field jet

noise spectra for the particular jet exhaust velocity associated with the cycle point. The three figures all show that choking the inlet does not completely remove the compressor noise and that even at 4700 rpm the peak 300 ft. sideline noise is influenced by turbomachinery generated noise.

Subsequent to the 1968 test, The Boeing Company determined that, to satisfy the power cutback engine airflow requirements and still maintain reasonable inlet distortion levels, it would be required to reconfigure the inlet in the sound suppression mode to have the inlet doors partially open (total door inlet area = 8.6% main lip area). Due to this geometry change, an acoustic retest of the choked inlet was performed at Peebles Site 4D during April, 1969, using the GE4 Engine 435-003. The purpose of the test was to determine change in attained suppression with the partially opened doors.

In this second test series the engine primary nozzle area was fixed at 1560 in^2 so that the Block I engine would operate statically with the same absolute jet velocity as the relative velocity of the production type turbojet during a typical approach cycle. This was done to simplify the process of obtaining "in flight" predictions from measured static data. To determine the effect of opening the blow-in-doors on the far field noise, parametric tests were run for a range of centerbody positions from 0" to 30" (see Figure VI.A-2) with doors closed and partially open. In all cases a bellmouth inlet was attached to the front of the sharp-edged inlet, as per Figure VI.A-13. This was to prevent flow separation at the inlet lip which became somewhat of a problem in the 1968 test series.

Steady state acoustic measurements were again taken on the 250 ft. arc. In addition, noise data were recorded during a slow engine acceleration for each test configuration. Typical of the data thus obtained is Figure VI.A-14 showing the 250 ft. arc 30° and 110° to inlet variation in compressor stage 1 fundamental tone sound pressure level with physical rpm and main inlet Mach number. The configuration is with the centerbody at the 16 inch position and with the inlet doors open at 8.6%. This again shows the drop in noise at the front of the engine with increase in inlet Mach number, but no variation at the 110° position; similar to the 1968 test results.

A typical approach condition was simulated at 4530 rpm with a) the centerbody set at 24 inches with doors closed, and b) at 16 inches with doors open at 8.6%; both conditions attaining approximately 0.85 main inlet Mach number. Figure VI.A-15 shows the 30° and 110° 1/3 octave band spectra for the test points and Figure VI.A-16 shows their PNdB directivity, both at the 300 ft. sideline. The data show that partially opening the blow-in-doors at approach power setting did not appreciably alter the far field noise levels.

Conclusions

- At angles close to the inlet and at low speed, choking the inlet reduced the far field 300 ft. sideline noise up to 15 PNdB. However, level of suppression decreases with increasing speed and at angles further from the inlet.
- Sideline peak PNL is reduced by only 1 to 3 PNdB due to other engine/jet noise predominance at the aft quadrant peak noise angle.
- On an EPNL basis, suppression could be expected to be considerably higher than the peak PNL suppression due to the large change in directivity pattern from unchoked to choked inlet operation.
- 1/3 Octave band spectra at 30° show reduction up to 18 dB for the band containing the compressor 1st stage fundamental tone. Harmonics of this tone plus tones from other stages and broadband noise are also considerably suppressed. This suppression decreases with increasing angle from the inlet.
- From narrowband analysis, the compressor broadband noise seems to be more effectively reduced than the tones. The tones still exist in the choked inlet spectra but tend to stand out of the broadband noise more clearly.
- Partially opening the inlet blow-in-doors (to satisfy power cutback engine airflow requirements) had no appreciable effect on the sonic inlet far field noise suppression.

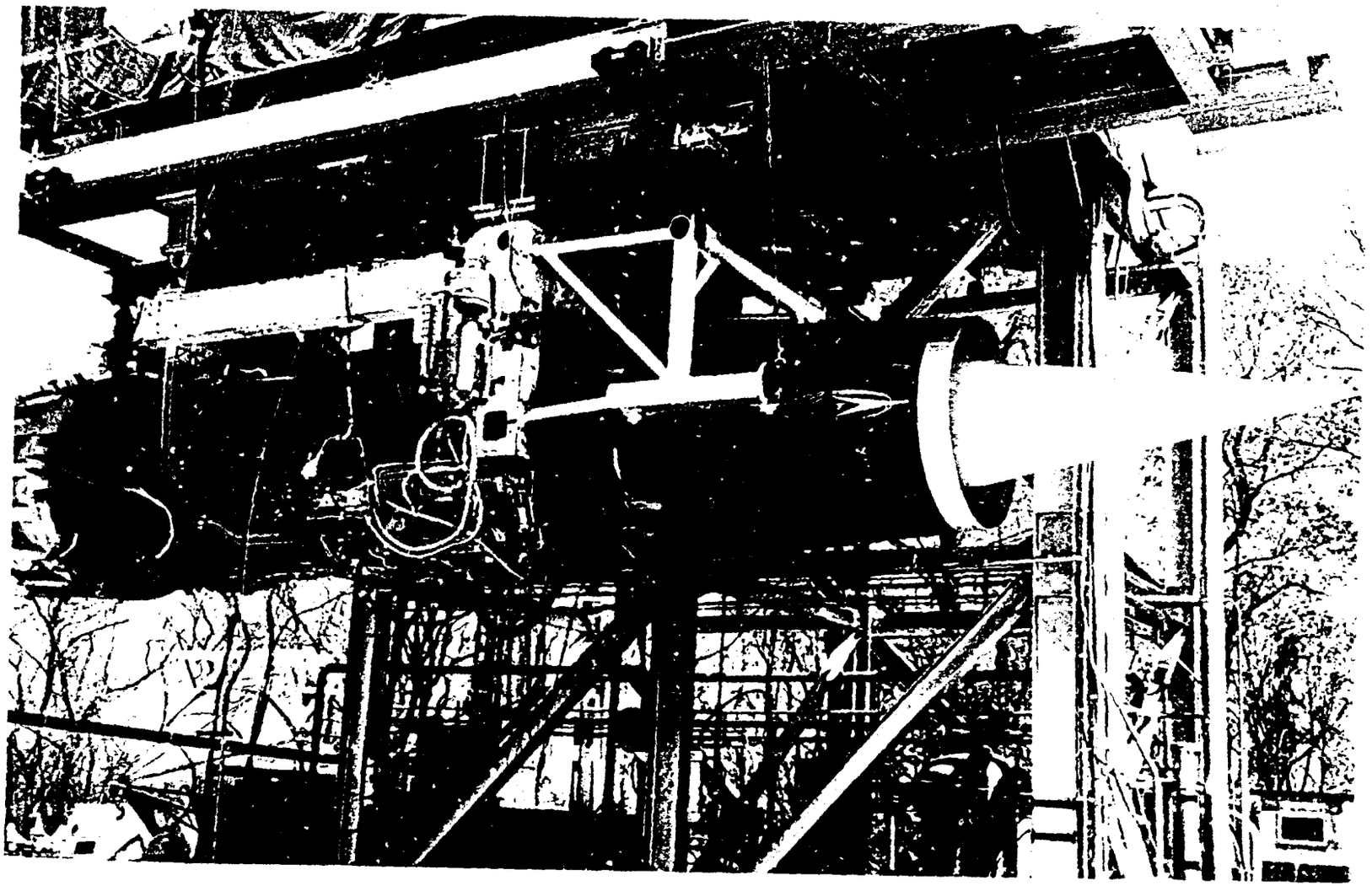
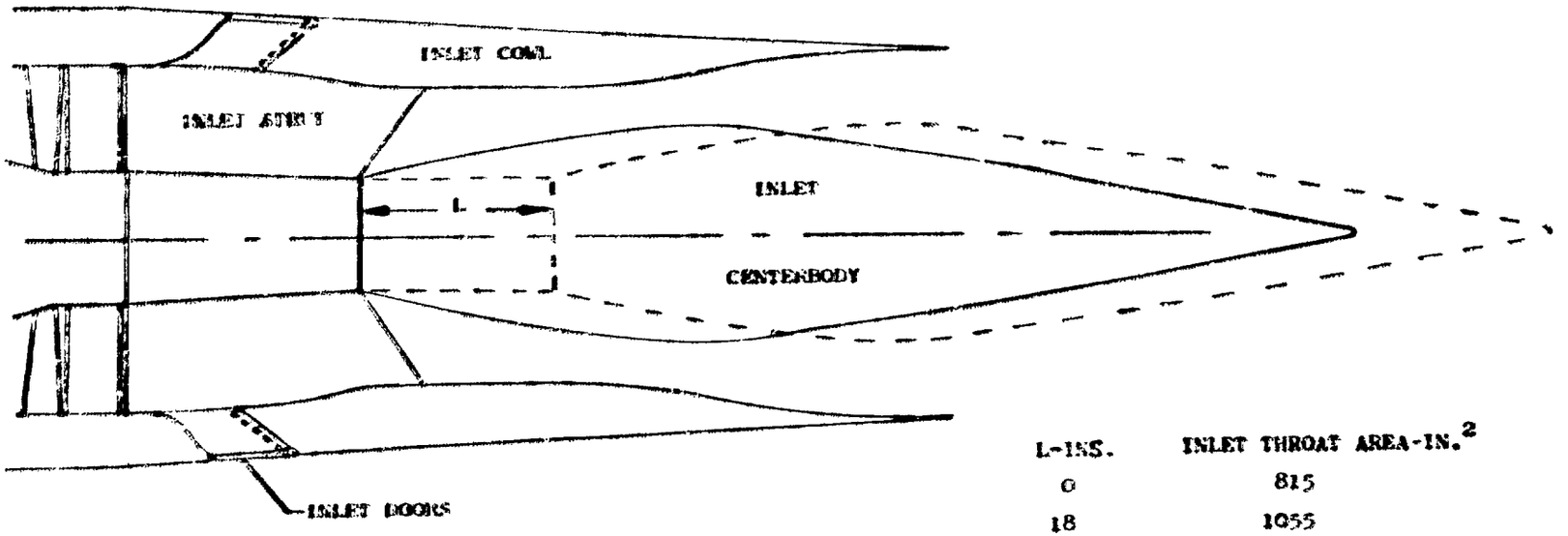


FIGURE VI.A-1 GE4 ENGINE 435-002 WITH BOEING INLET-SHARP EDGED LIP - PEEBLES SITE 4D



L-INS.	INLET THROAT AREA-IN.^{2}
0	815
18	1055
24	1135
30	1215

FIGURE VI.A-2 SCHEMATIC OF BOEING INLET FOR GE4 ENGINE TEST

TABLE VI.A-1 CHOKED INLET - GE4 ENGINE 435-002 - TEST SUMMARY

Reading No.	Run No.	Bellmouth	T/D Doors	Throat Area	Condition Simulated	% $N/\sqrt{\theta}$	Inlet M_N	300° SL Peak PNdB
229	45	Off	Open	1215 in^2	Take-Off	60.6	.125	101.7
230						71.4	.175	104.6
231						96.6	.525	123.0
233						96.7	.55	123.2
234						92.3	.465	117.8
241						78.5	.26	108.0
242						88.1	.385	114.3
247	47	Off	Closed	1215 in^2	Noise-Hi Pwr	60.5	.245	99.3
248						79.6	.455	107.7
249						89.4	.70	113.7
250						92.4	1.0	116.9
251						92.6	1.0	117.2
255	48	Off	Closed	815 in^2	Noise-Lo Pwr	61.8	.40	99.2
256						71.0	.515	102.5
257						78.8	.80	106.5
258						80.6	1.0	107.8
259						82.4	1.0	107.7
264	49	Off	Closed	1135 in^2	Noise-Hi Pwr	61.1	.26	99.2
265						80.2	.495	108.7
266						90.0	.85	114.7
267						91.1	1.0	115.5
268						93.2	1.0	116.2
275	50	Off	Closed	1055 in^2	Noise-Lo Pwr	61.2	.28	99.6
276						79.5	.53	107.2
277						89.0	1.0	112.5
278						91.9	1.0	115.1

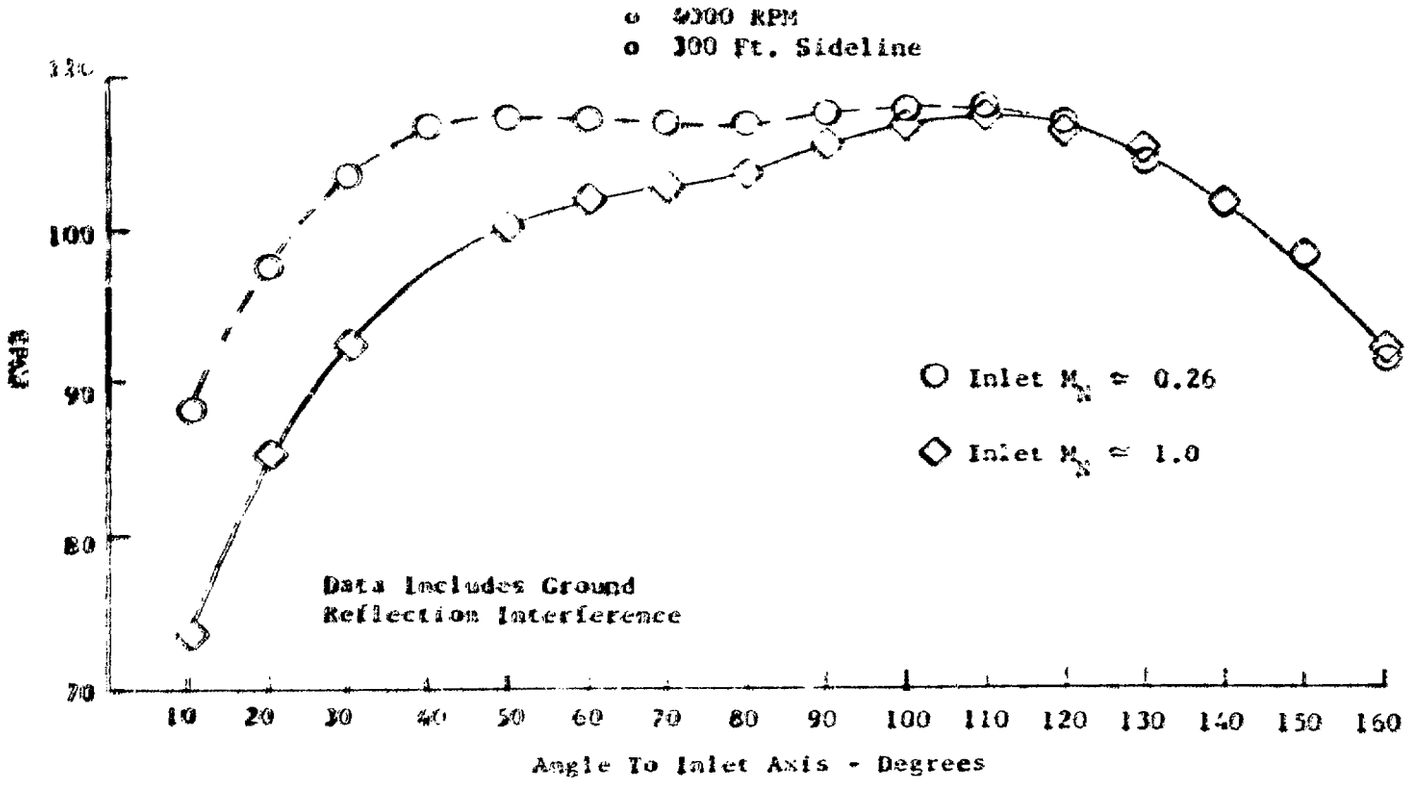


FIGURE VI.A-3 EFFECT OF CHOKED INLET ON 300 FT. SIDELINE PNL DIRECTIVITY AT 4000 RPM

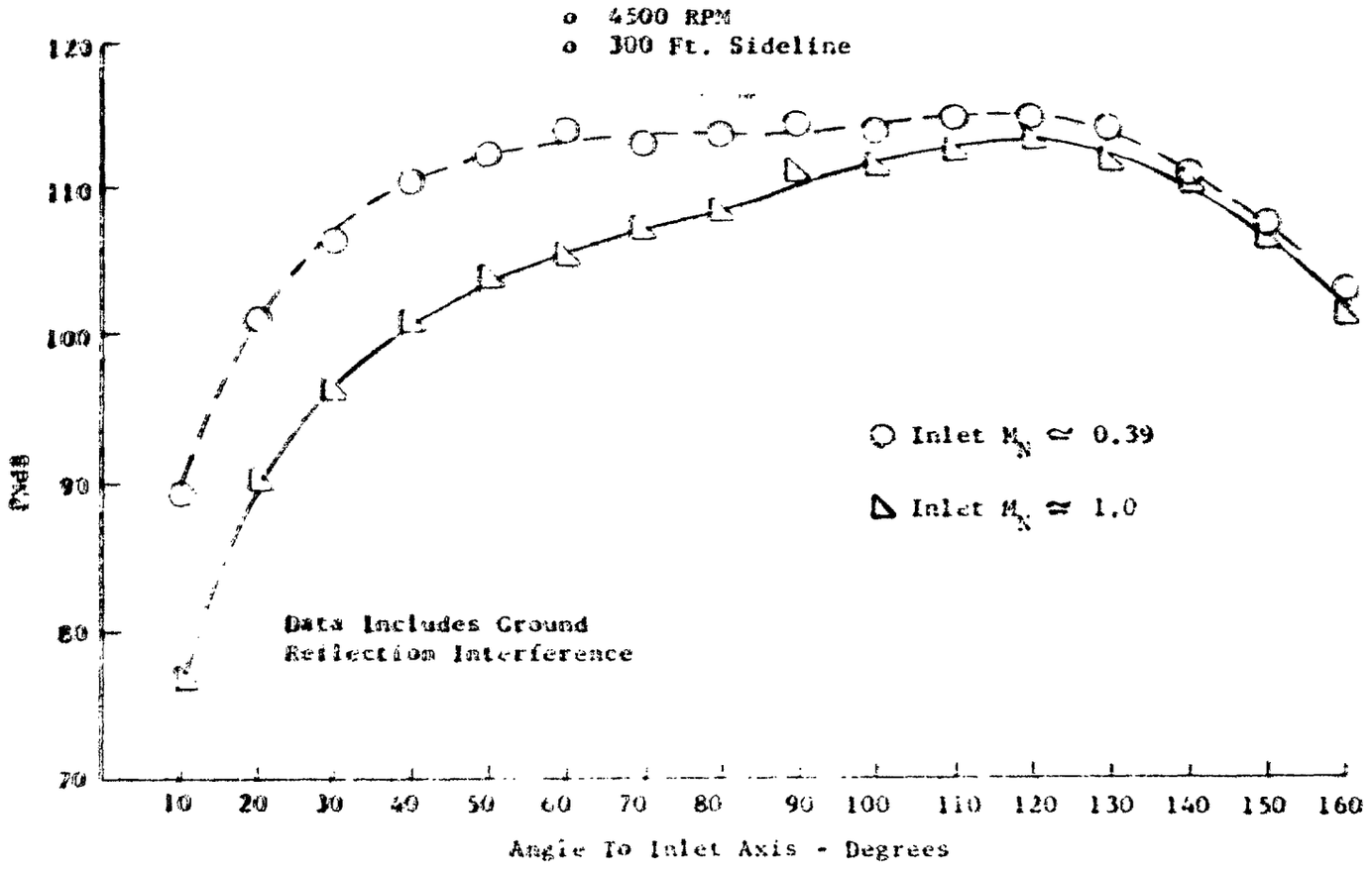


FIGURE VI.A-4 EFFECT OF CHOKED INLET ON 300 FT. SIDELINE PNL DIRECTIVITY AT 4500 RPM

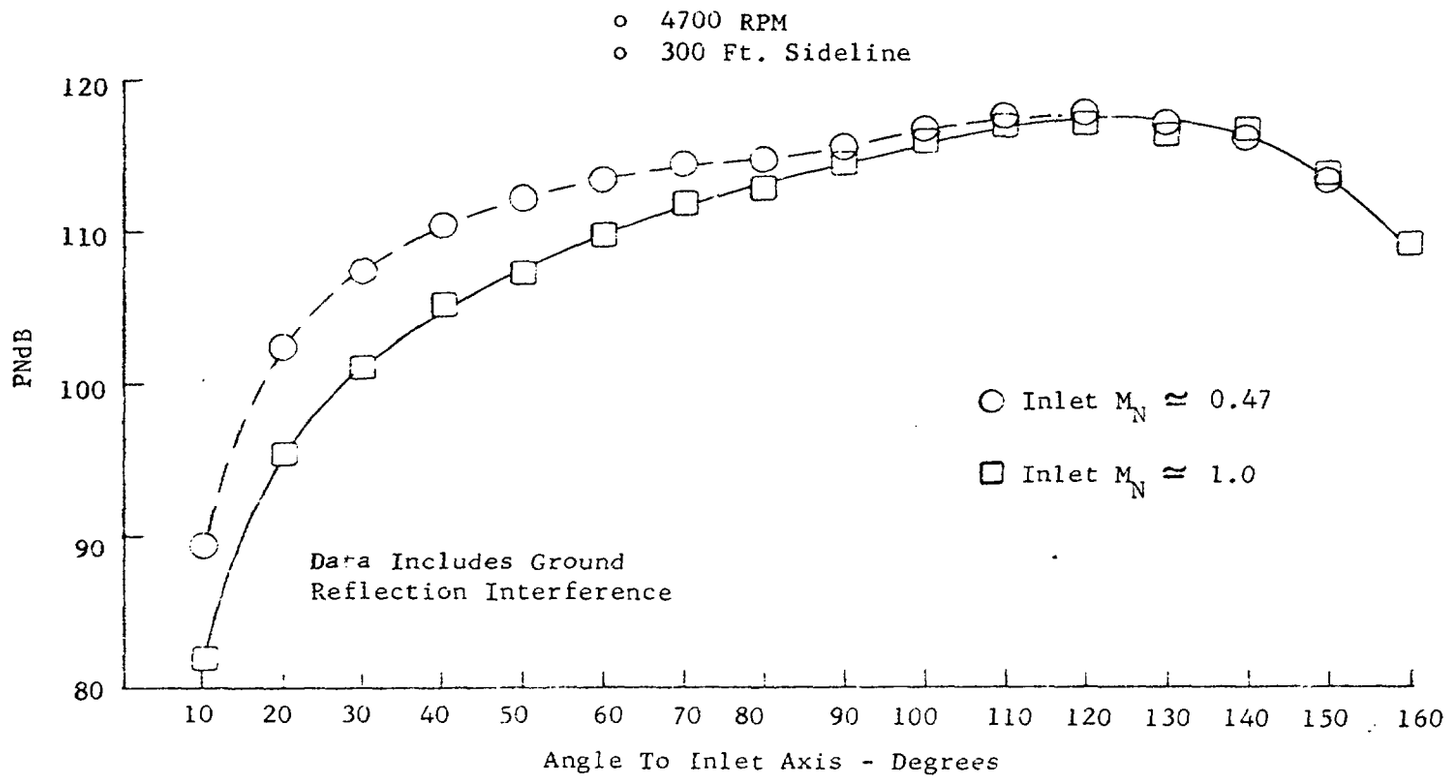


FIGURE VI.A-5 EFFECT OF CHOKED INLET ON 300 FT. SIDELINE PNL DIRECTIVITY AT 4700 RPM

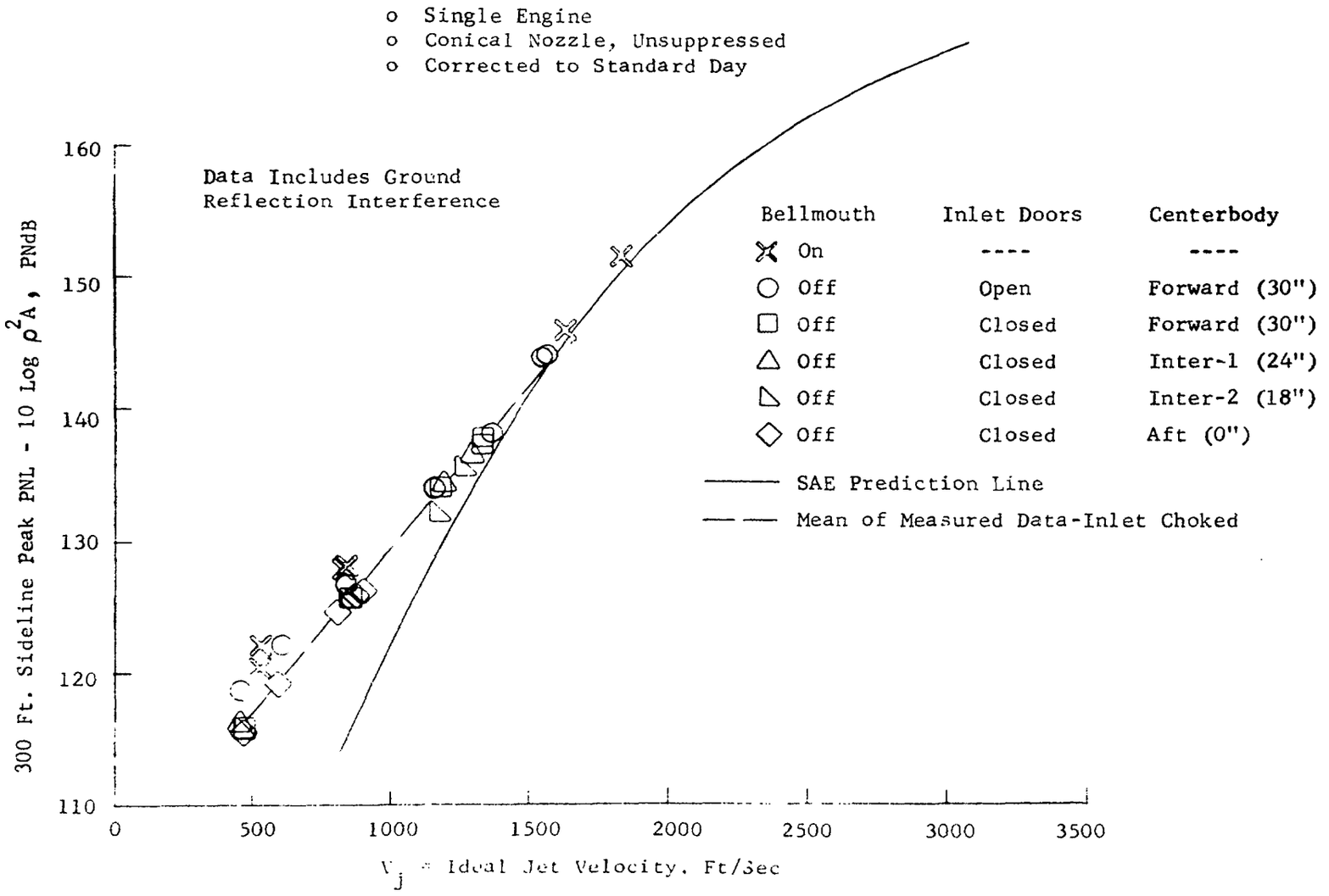


FIGURE VI.A-6 EFFECT OF CHOKED INLET ON 300 FT. SIDELINE PEAK PNL

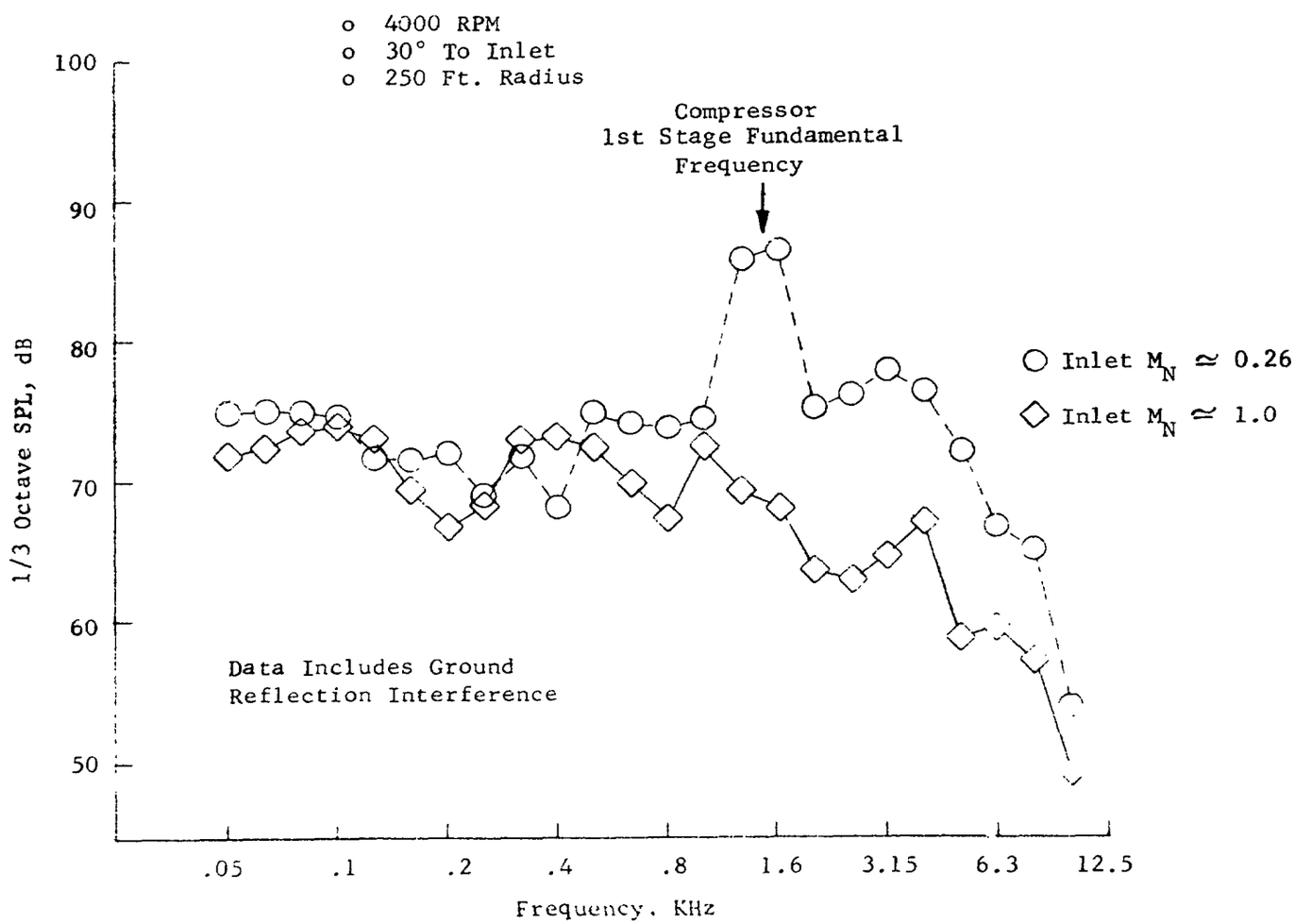


FIGURE VI.A-7 EFFECT OF CHOKED INLET ON 250 FT. ARC SPECTRA AT 30° TO THE INLET

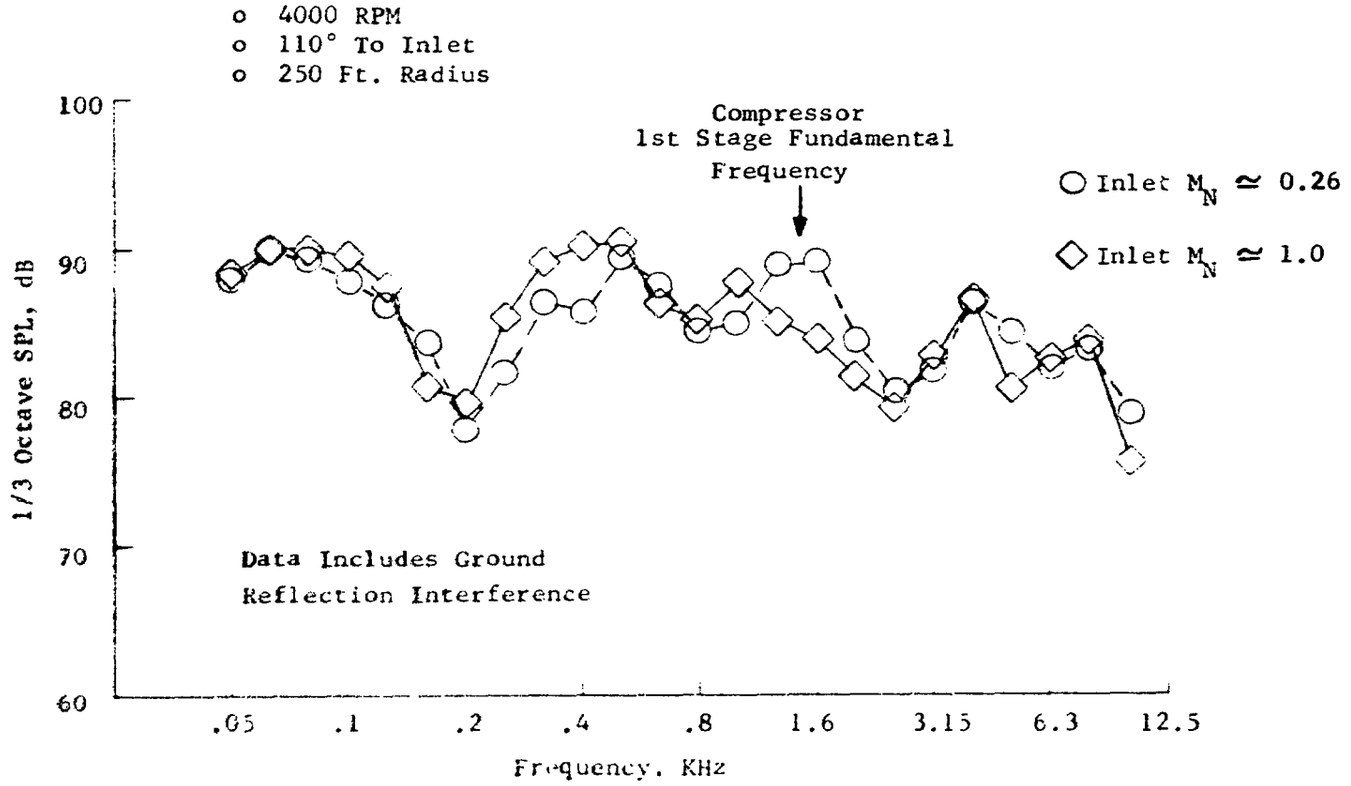


FIGURE VI.A-8 EFFECT OF CHOKED INLET ON 250 FT. ARC SPECTRA AT 110° TO THE INLET

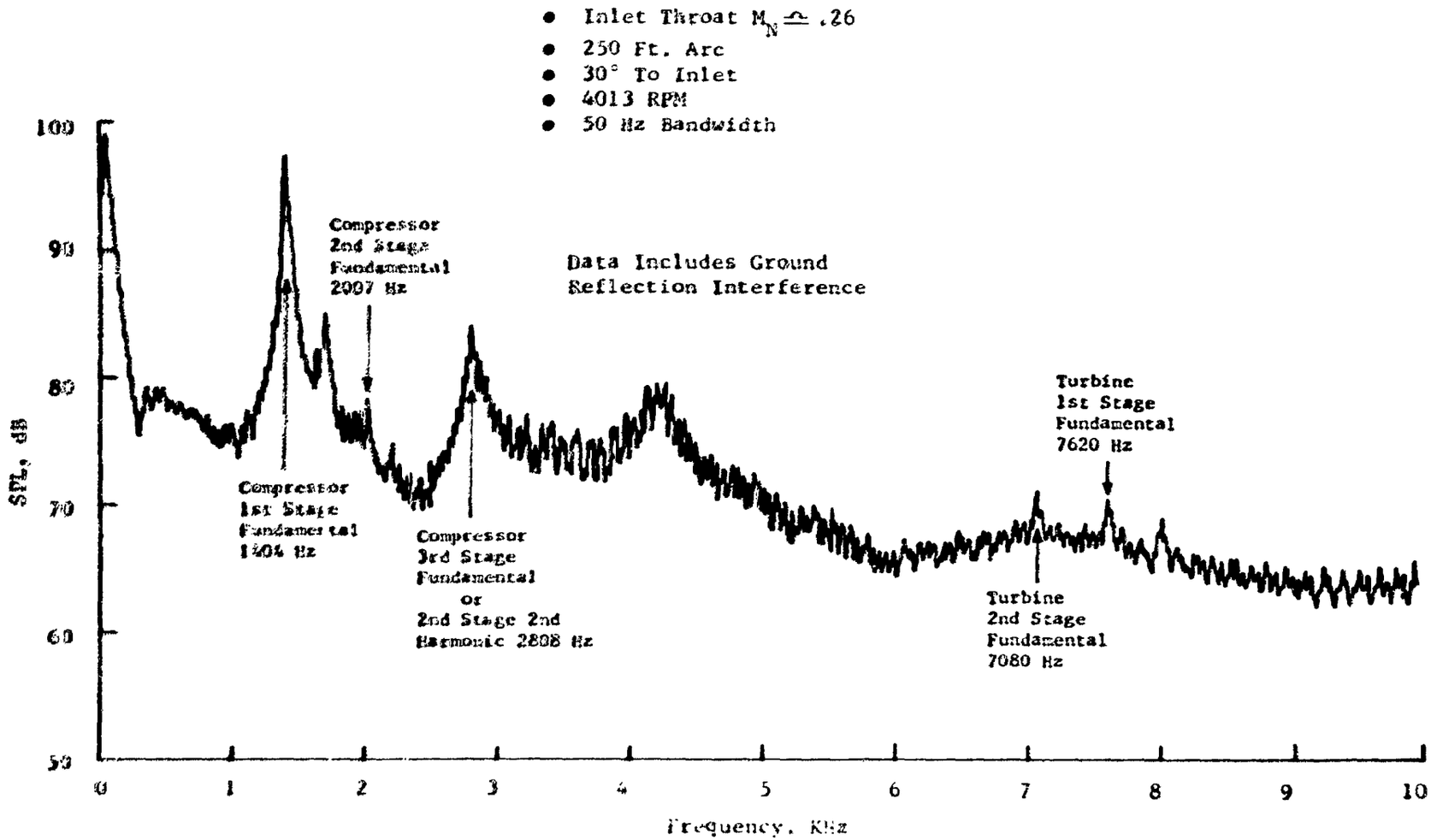


FIGURE VI.A-9A NARROWBAND ANALYSIS OF GE4 CHOKED INLET ACOUSTIC TEST

- Inlet Throat $M_N \leq 1.0$
- 250 Ft. Arc
- 30° To Inlet
- 4006 RPM
- 50 Hz Bandwidth

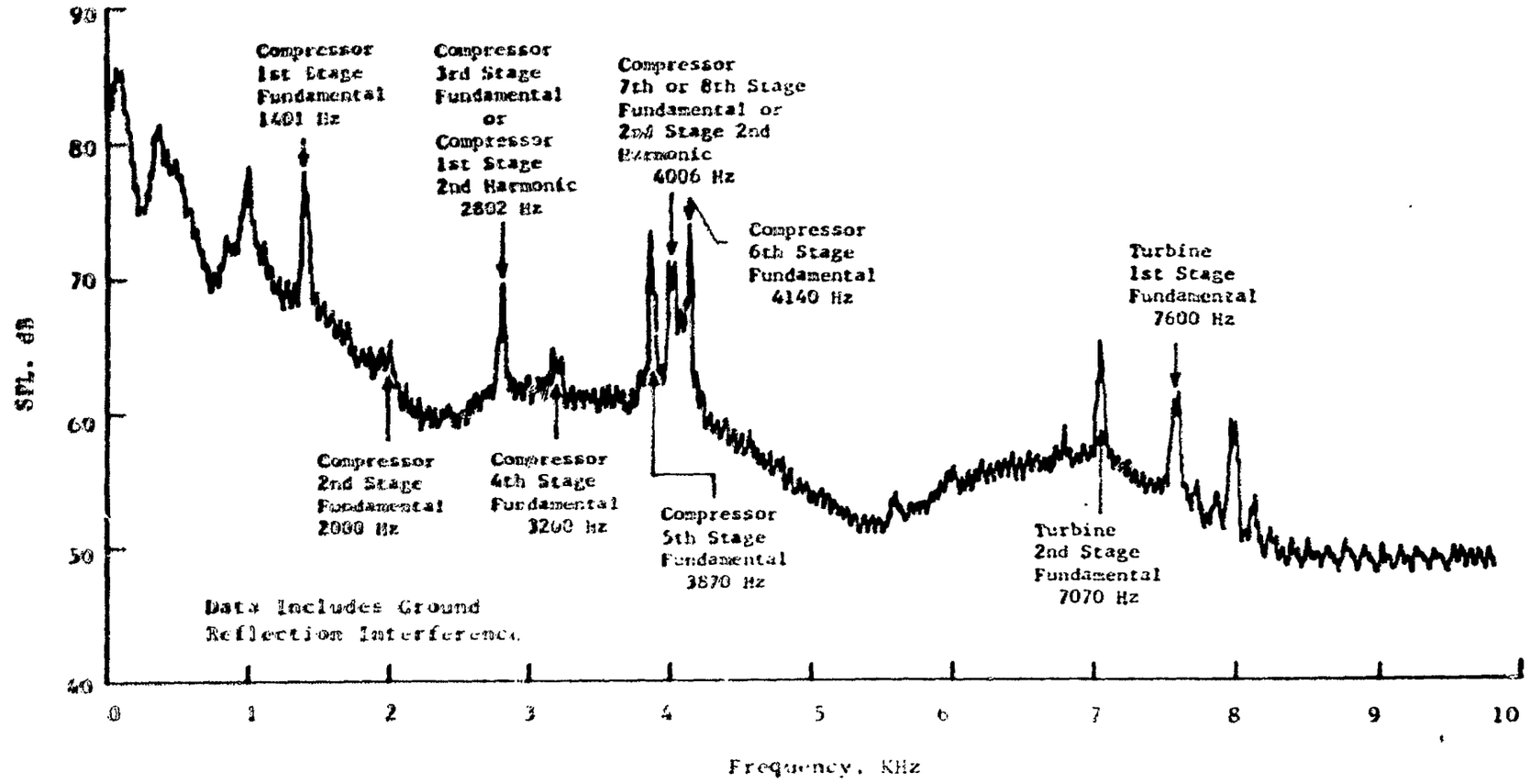


FIGURE Y1.A-9B NARROWBAND ANALYSIS OF GE4 CHOKED INLET ACOUSTIC TEST

- Inlet Throat $M_N \simeq .26$
- 250 Ft. Arc
- 110° To Inlet
- 4013 RPM
- 50 Hz Bandwidth

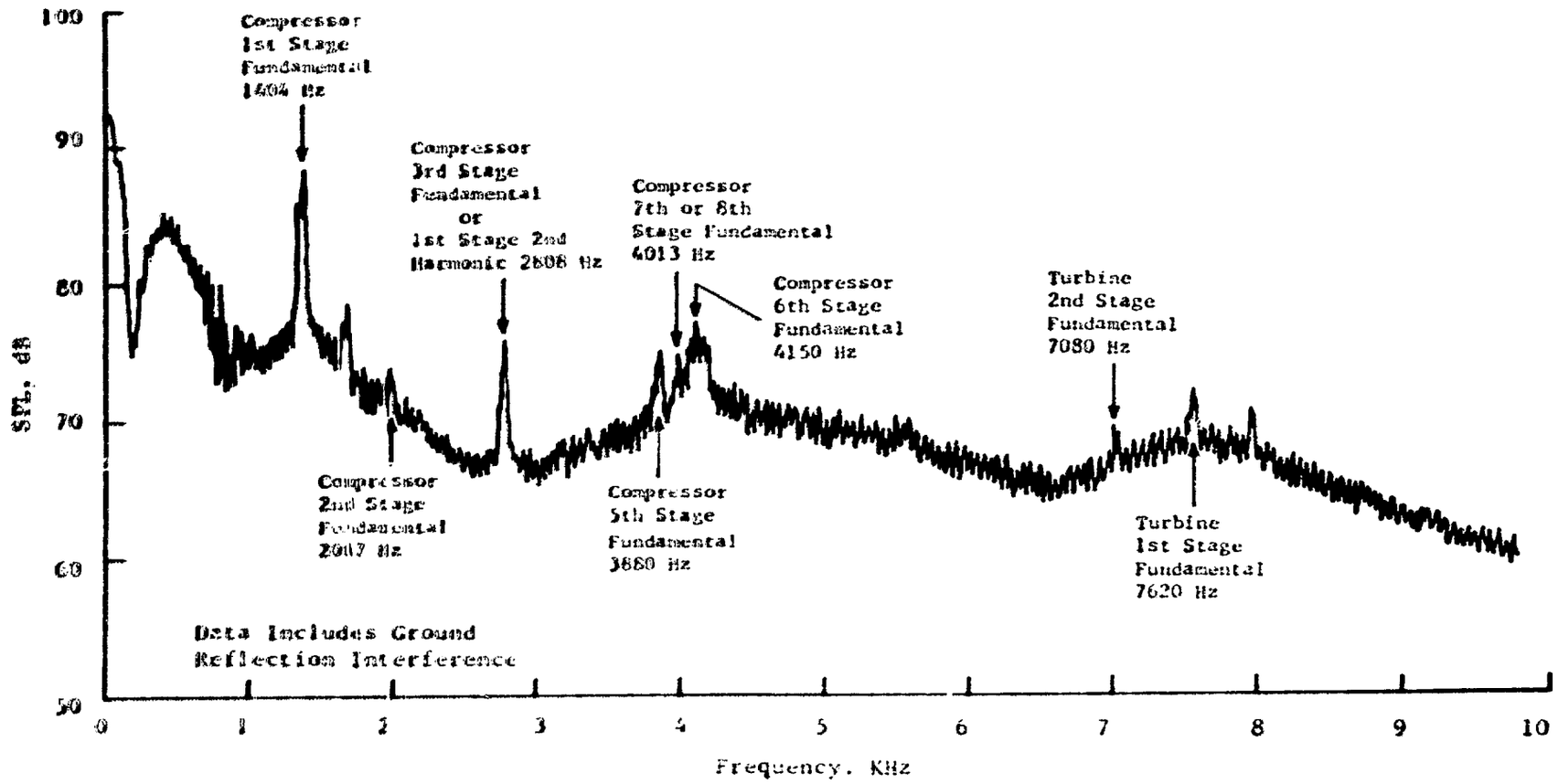


FIGURE VI.A-91 NARROWBAND ANALYSIS OF GE4 CHOKED INLET ACOUSTIC TEST

- Inlet Throat $M_N \triangleq 1.0$
- 250 Ft. Arc
- 110° To Inlet
- 4006 RPM
- 50 Hz Bandwidth

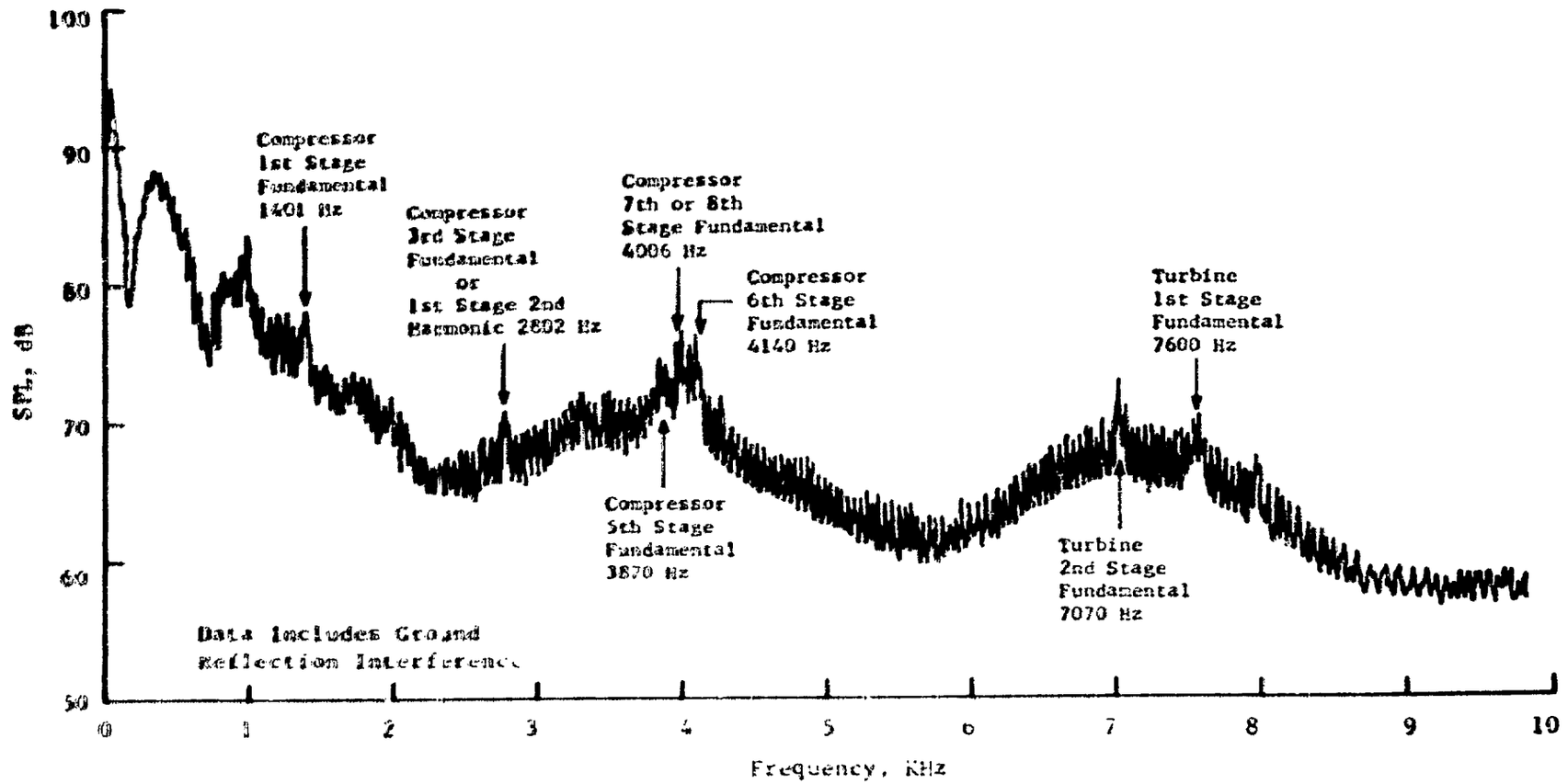


FIGURE 11.A-90 NARROWBAND ANALYSIS OF GE4 CHOKED INLET ACOUSTIC TEST

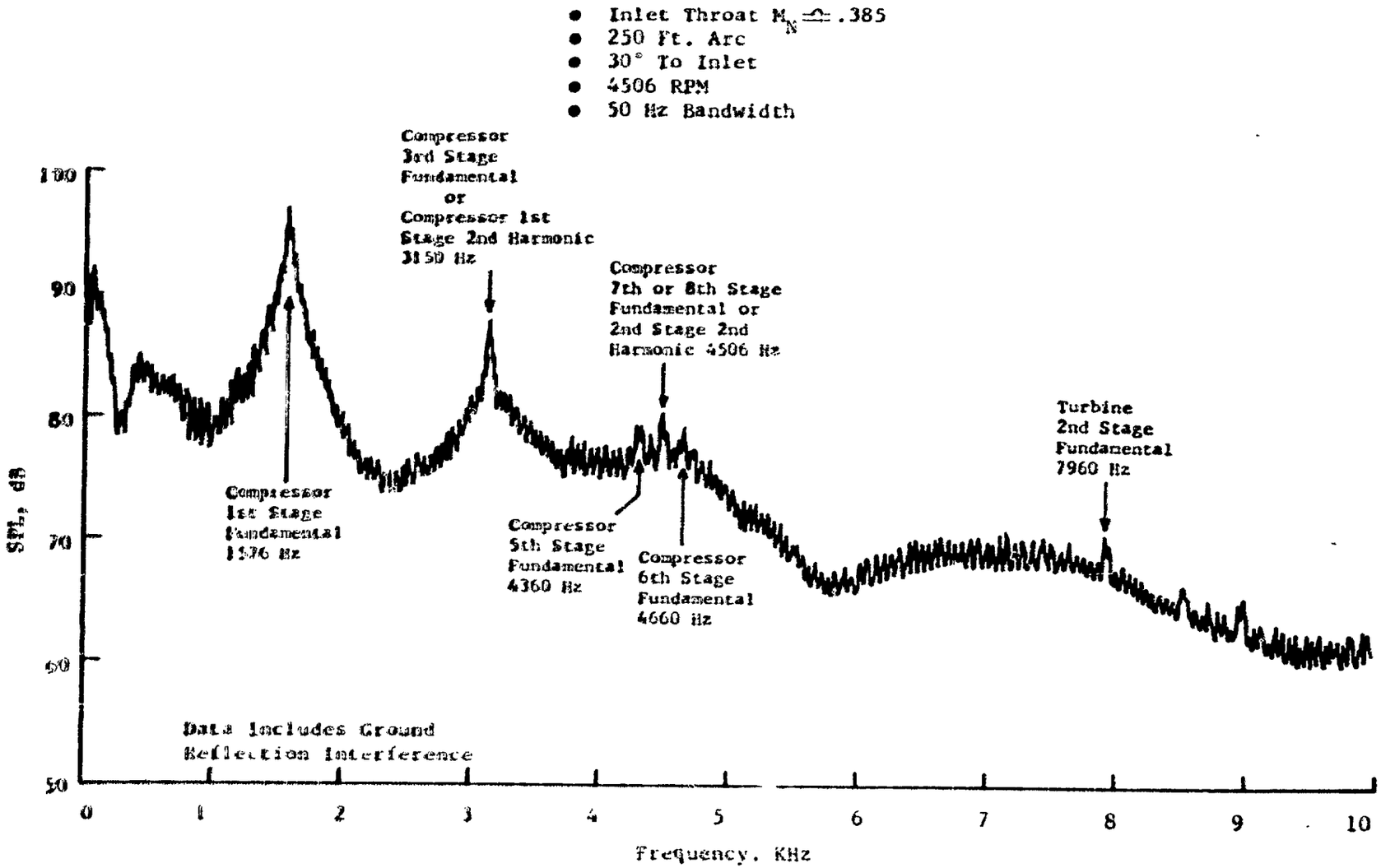


FIGURE VI.A-91 NARROWBAND ANALYSIS CE4 CHOKED INLET ACOUSTIC TEST

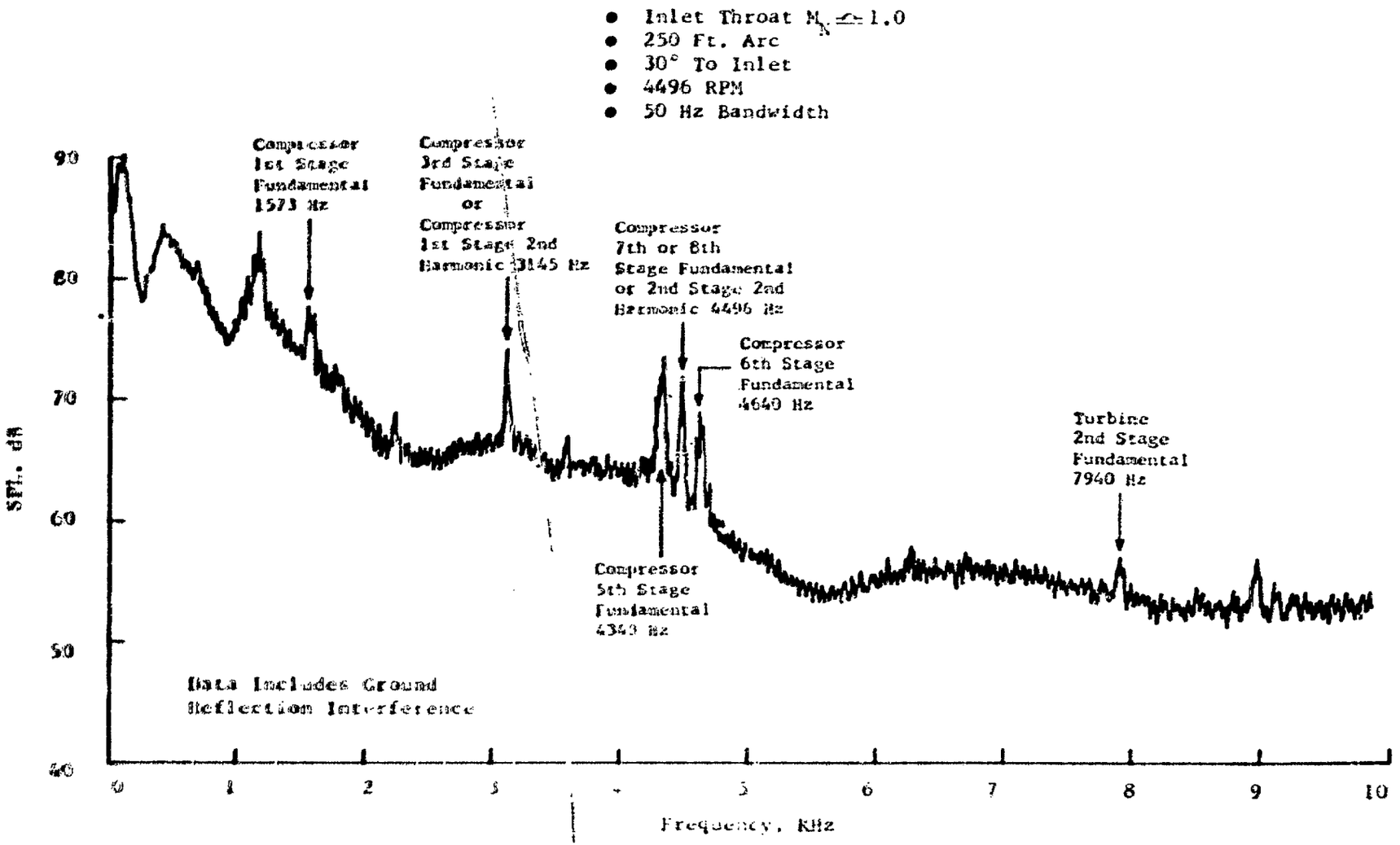


FIGURE VI.A-9 NARROWBAND ANALYSIS [illegible] CHOKED INLET ACOUSTIC TEST

- Inlet Throat $M_N \triangleq .385$
- 250 Ft. Arc
- 110° To Inlet
- 4506 RPM
- 50 Hz Bandwidth

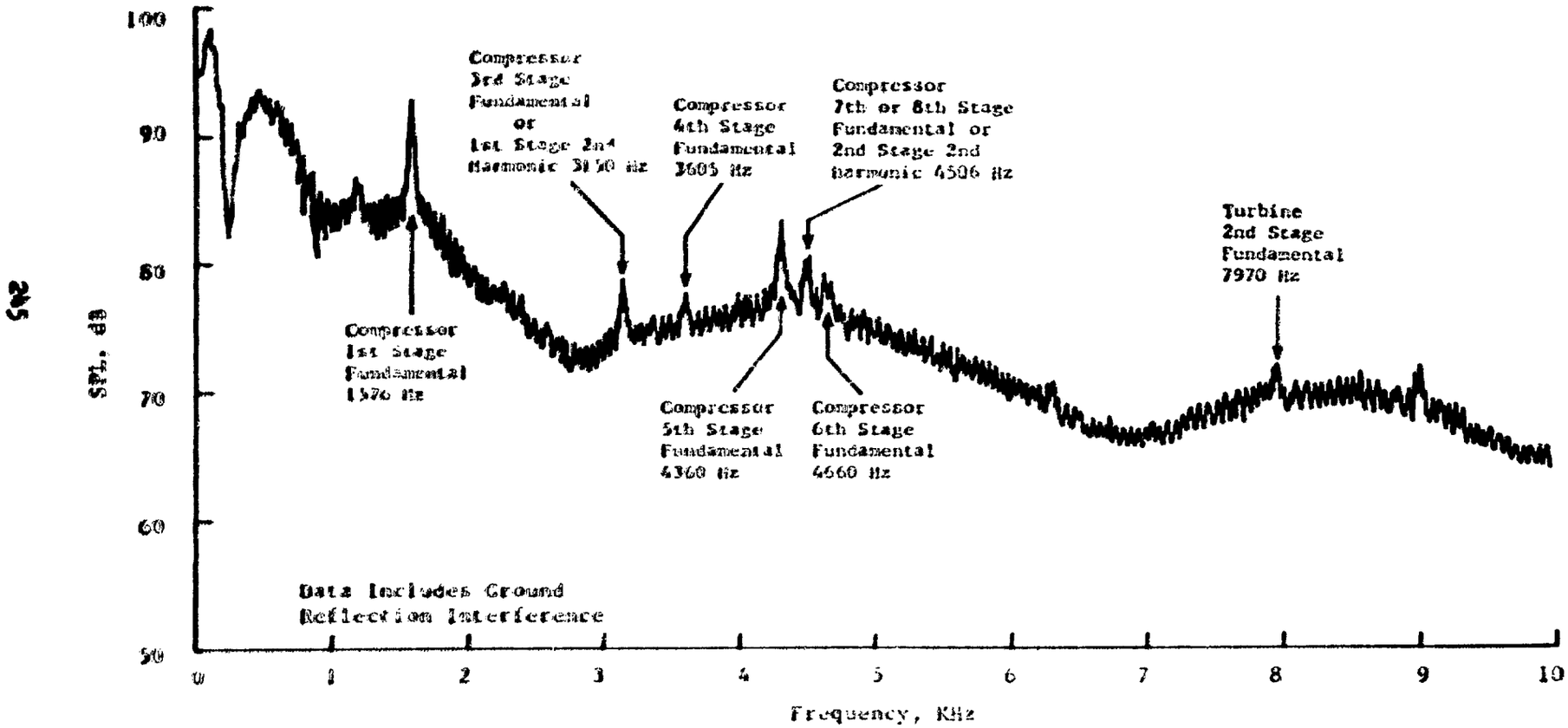


FIGURE VI.A-9 NARROWBAND ANALYSIS GE4 CHOKED INLET ACOUSTIC TEST

- Inlet Throat $M_x \cong 1.0$
- 250 Ft. Arc
- 110° To Inlet
- 4496 RPM
- 50 Hz Bandwidth

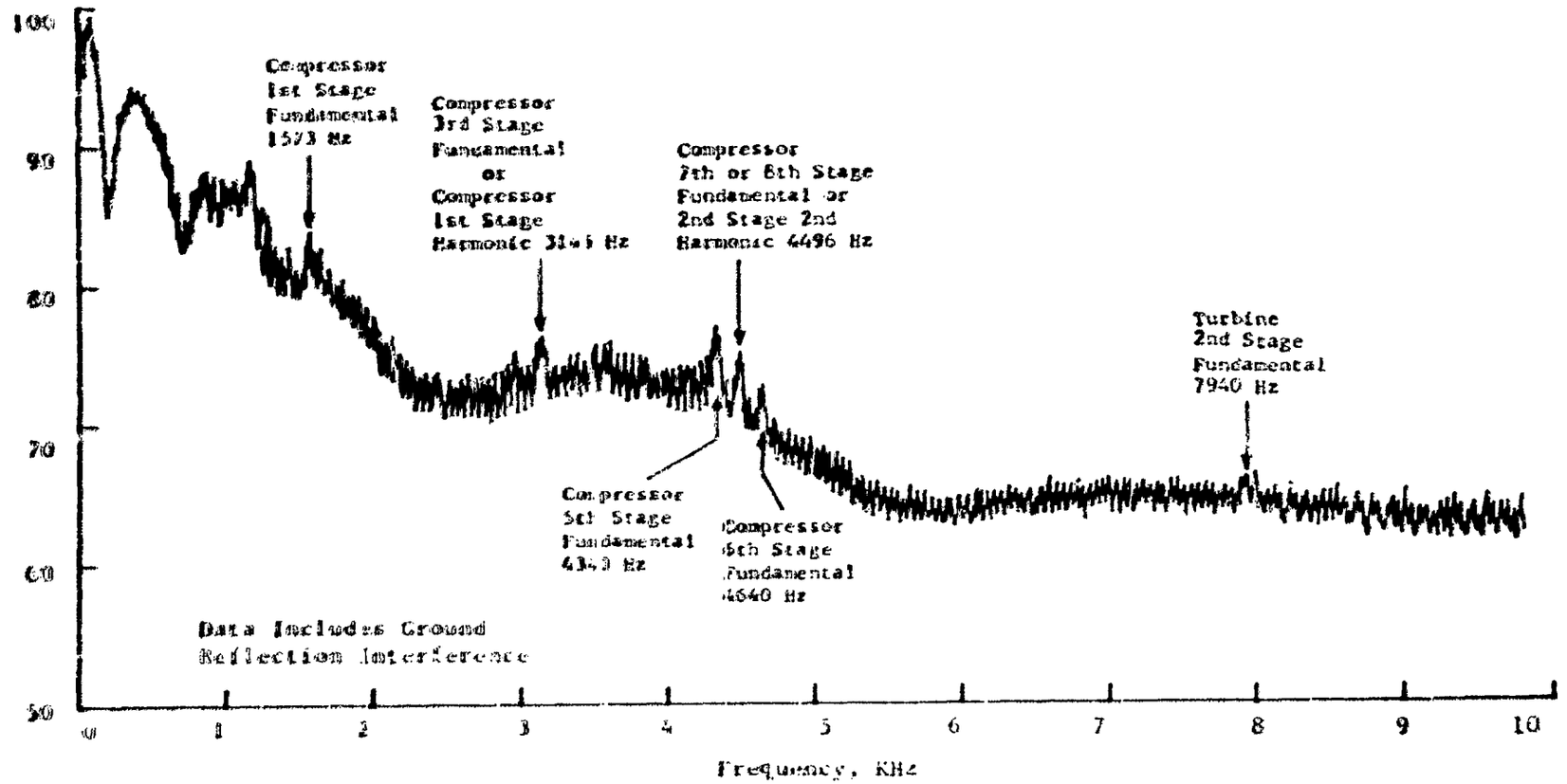


FIGURE VI.A-93 NARROWBAND ANALYSIS GE4 CHOKED INLET ACOUSTIC TEST

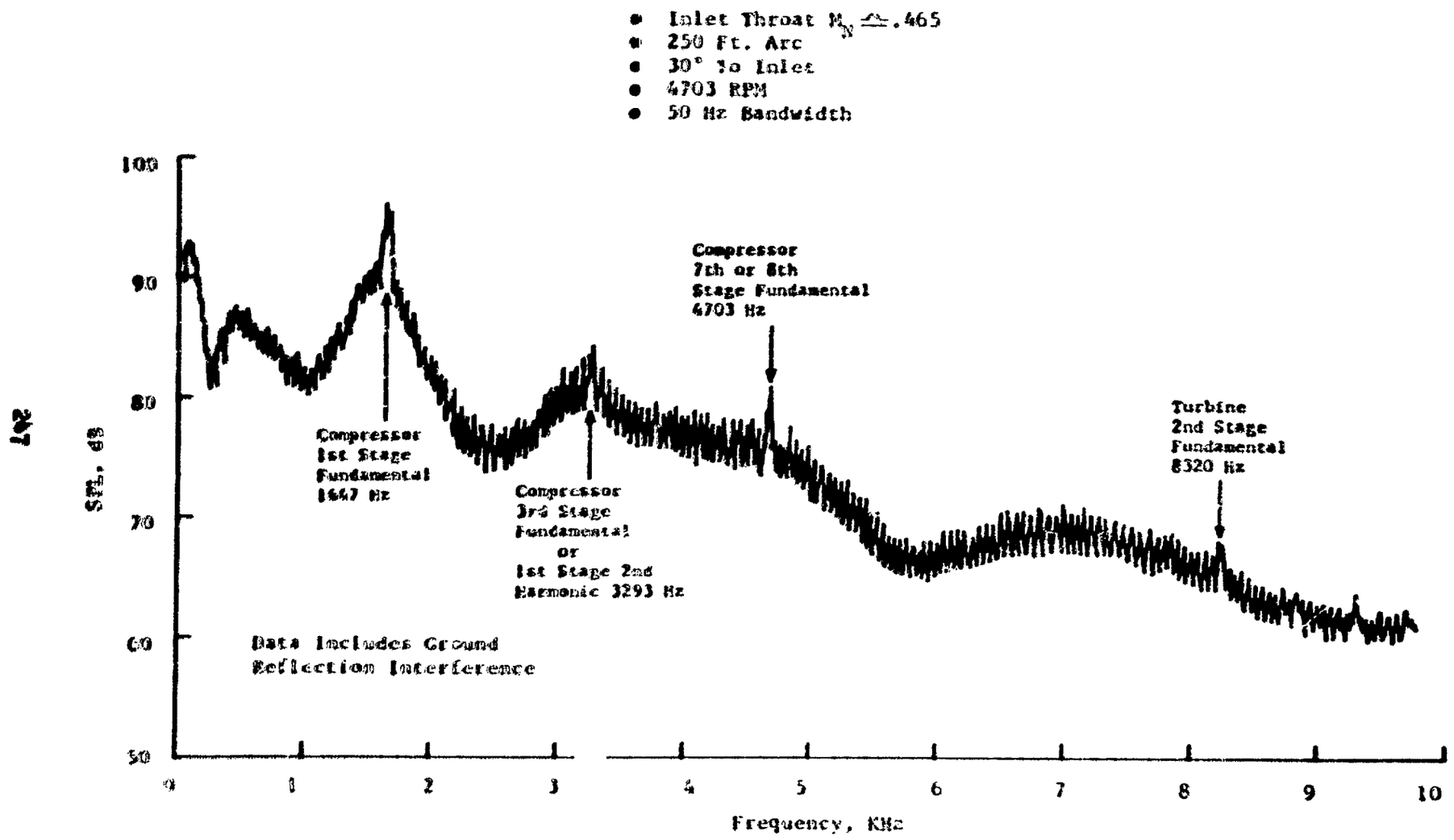


FIGURE VI.A-91 NARROWBAND ANALYSIS GE4 CHOKED INLET ACOUSTIC TEST

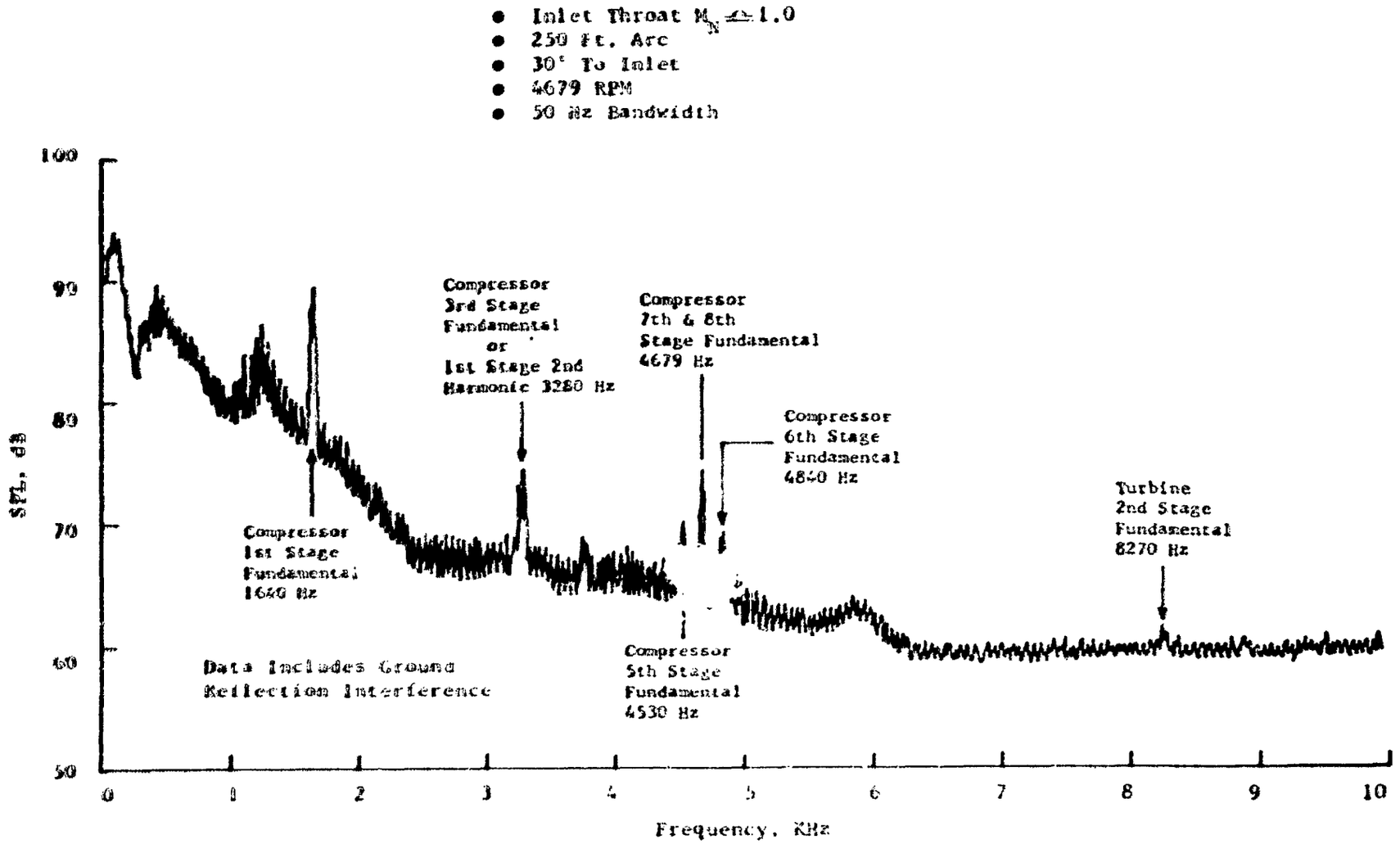


FIGURE VI.A-9 NARROWBAND ANALYSIS GE4 CHOKED INLET ACOUSTIC TEST

- Inlet Throat M_N = .465
- 250 Ft. Arc
- 110° To Inlet
- 4703 RPM
- 50 Hz Bandwidth

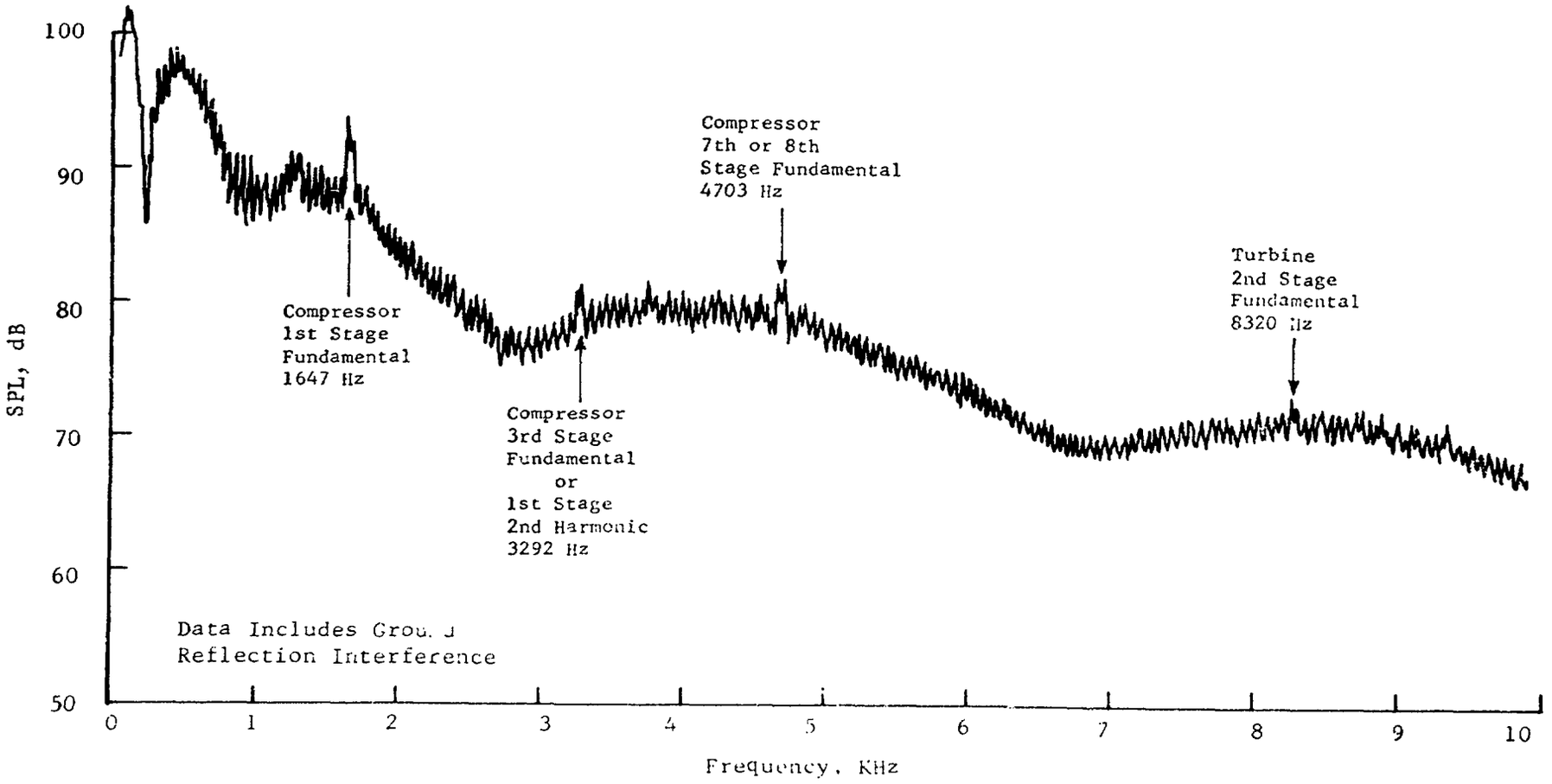


FIGURE VI.A-9K NARROWBAND ANALYSIS GE4 CHOKED INLET ACOUSTIC TEST

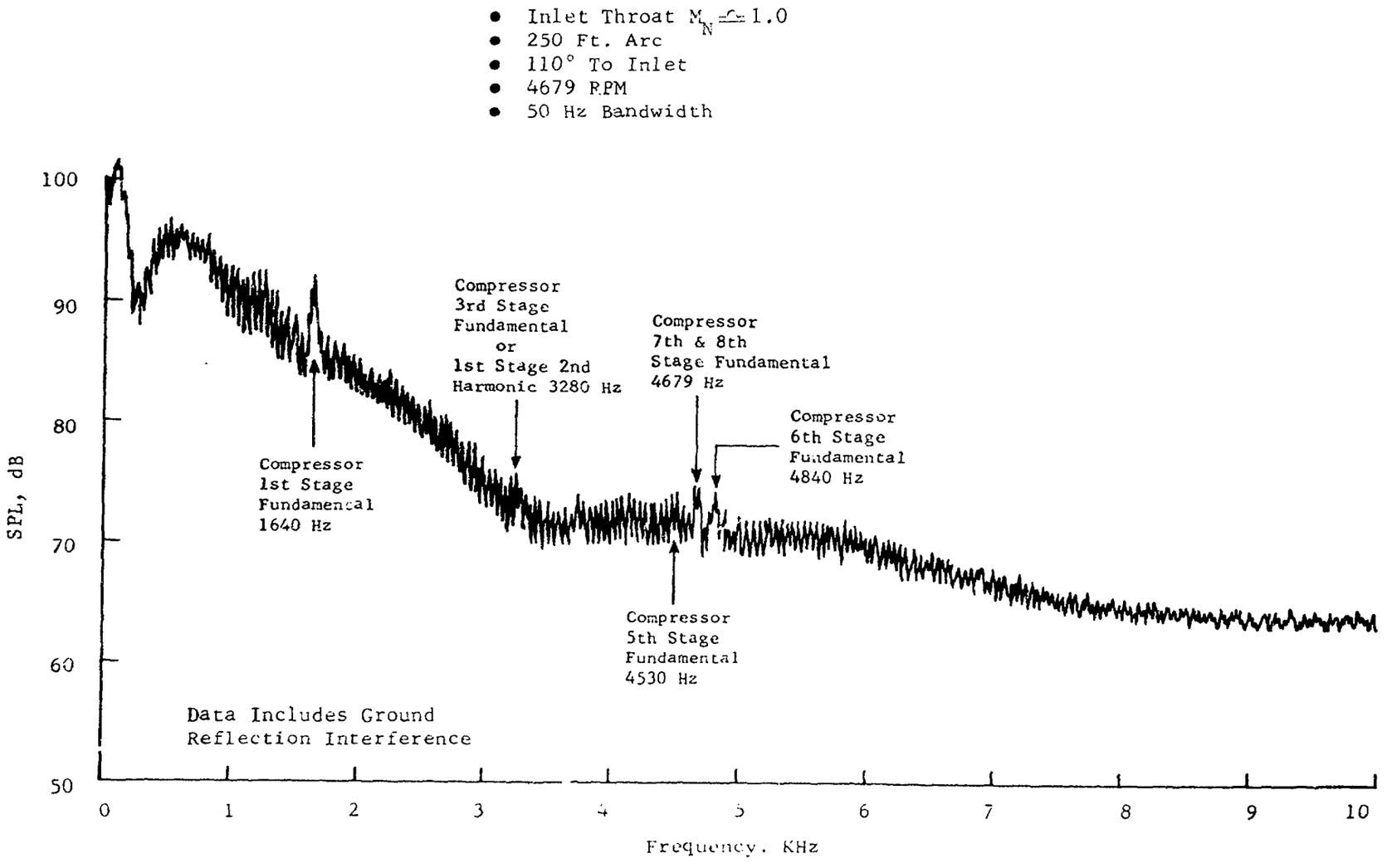


FIGURE VI.A-9L NARROWBAND ANALYSIS GE4 CHOKED INLET ACOUSTIC TEST

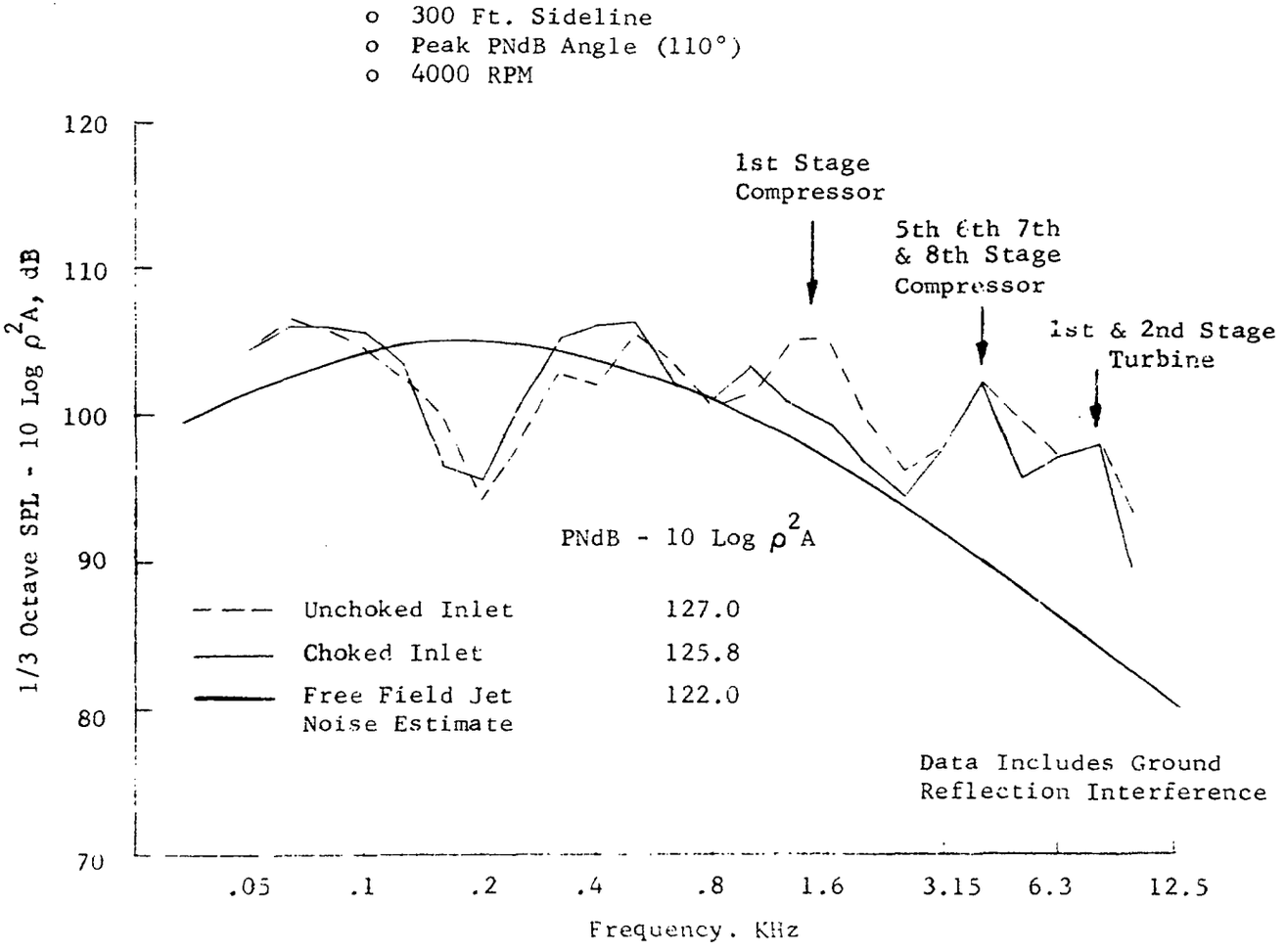


FIGURE VI.A-10 EFFECT OF CHOKED INLET ON 300 FT. SIDELINE SPECTRA AT 110° & 4000 RPM

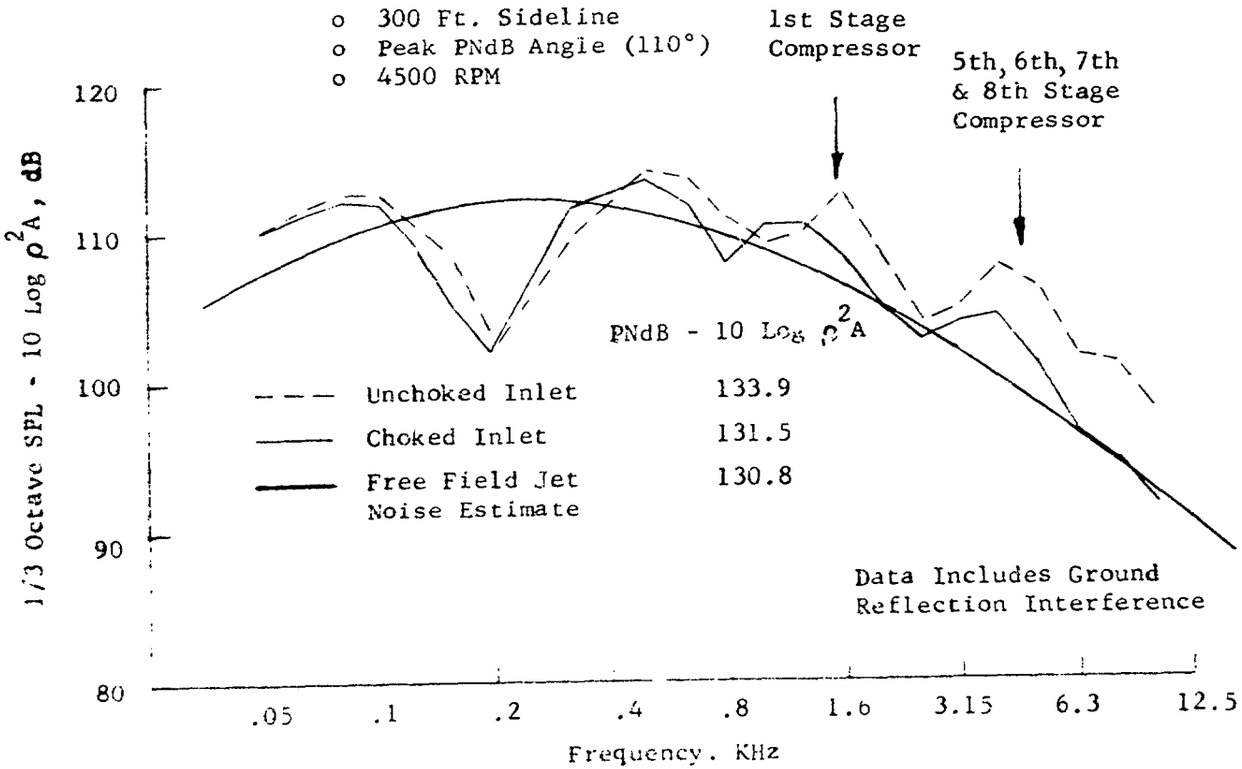


FIGURE VI.A-11 EFFECT OF CHOKED INLET ON 300 FT. SIDELINE SPECTRA AT 110° & 4500 RPM

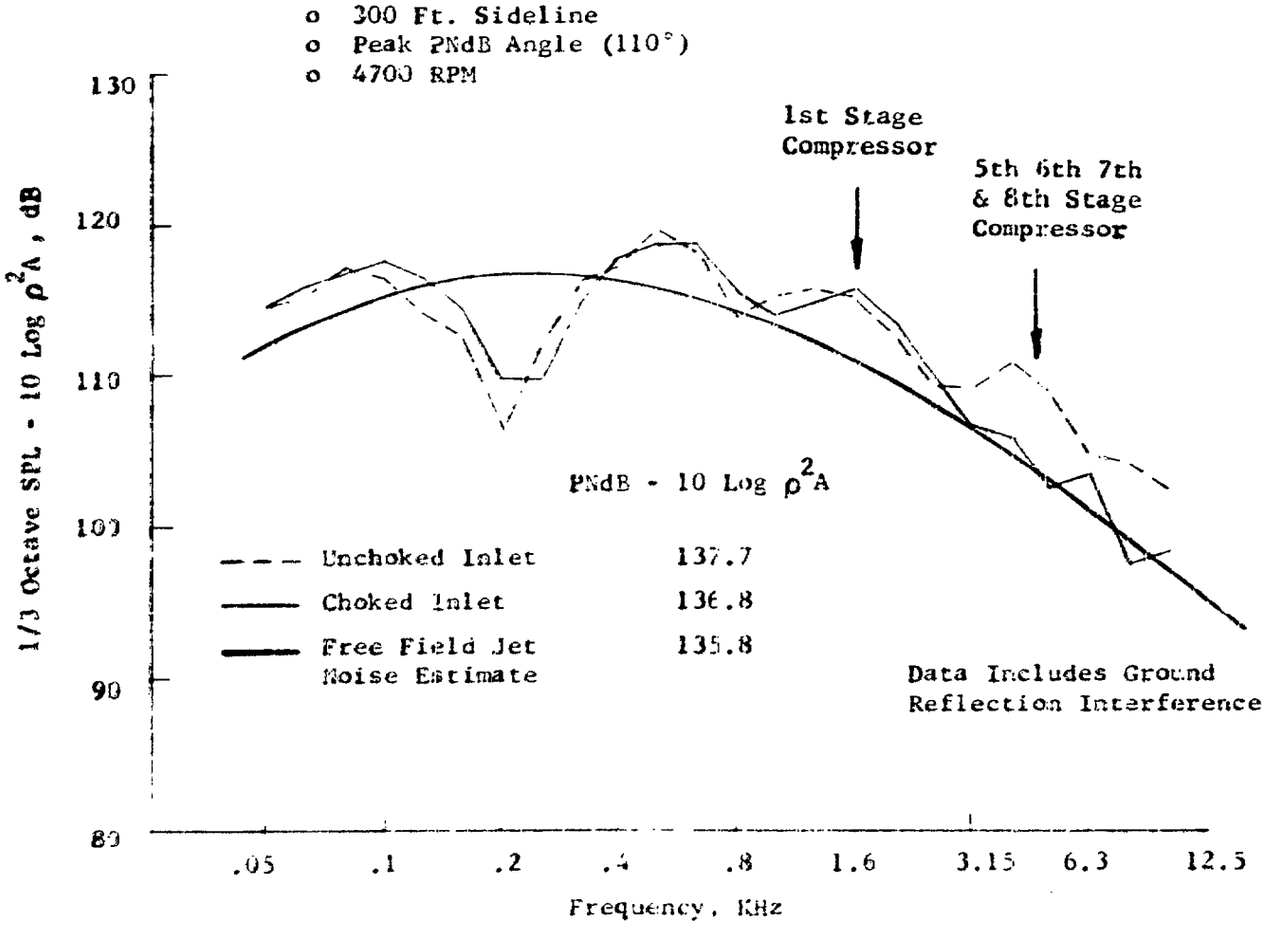


FIGURE VI.A-12 EFFECT OF CHOKED INLET ON 300 FT. SIDELINE SPECTRA AT 110° & 4700 RPM

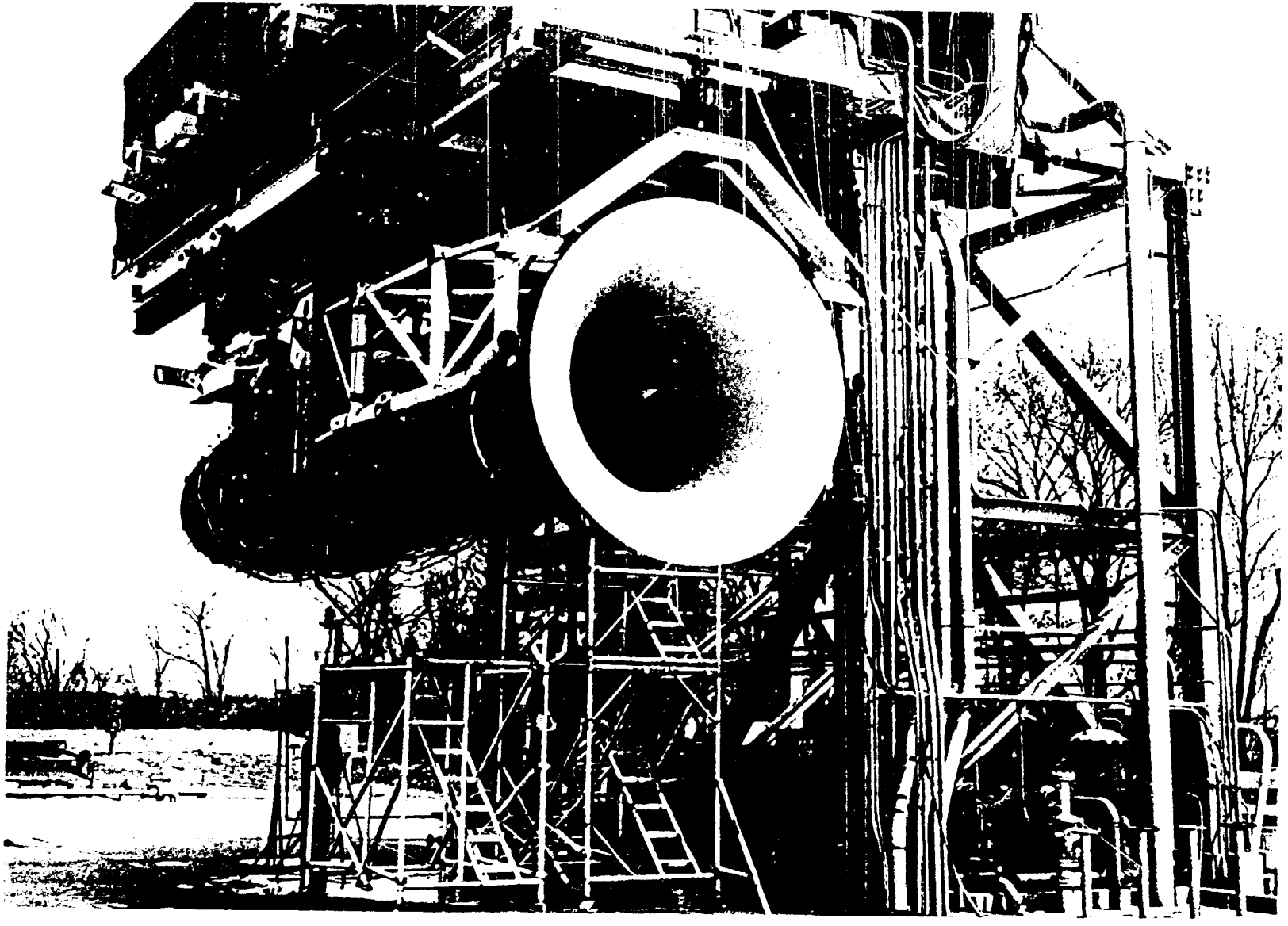


FIGURE VI.A-13 GE4 ENGINE 435-003 WITH BOEING INLET-BELLMOUTH - PEEBLES SITE 4D

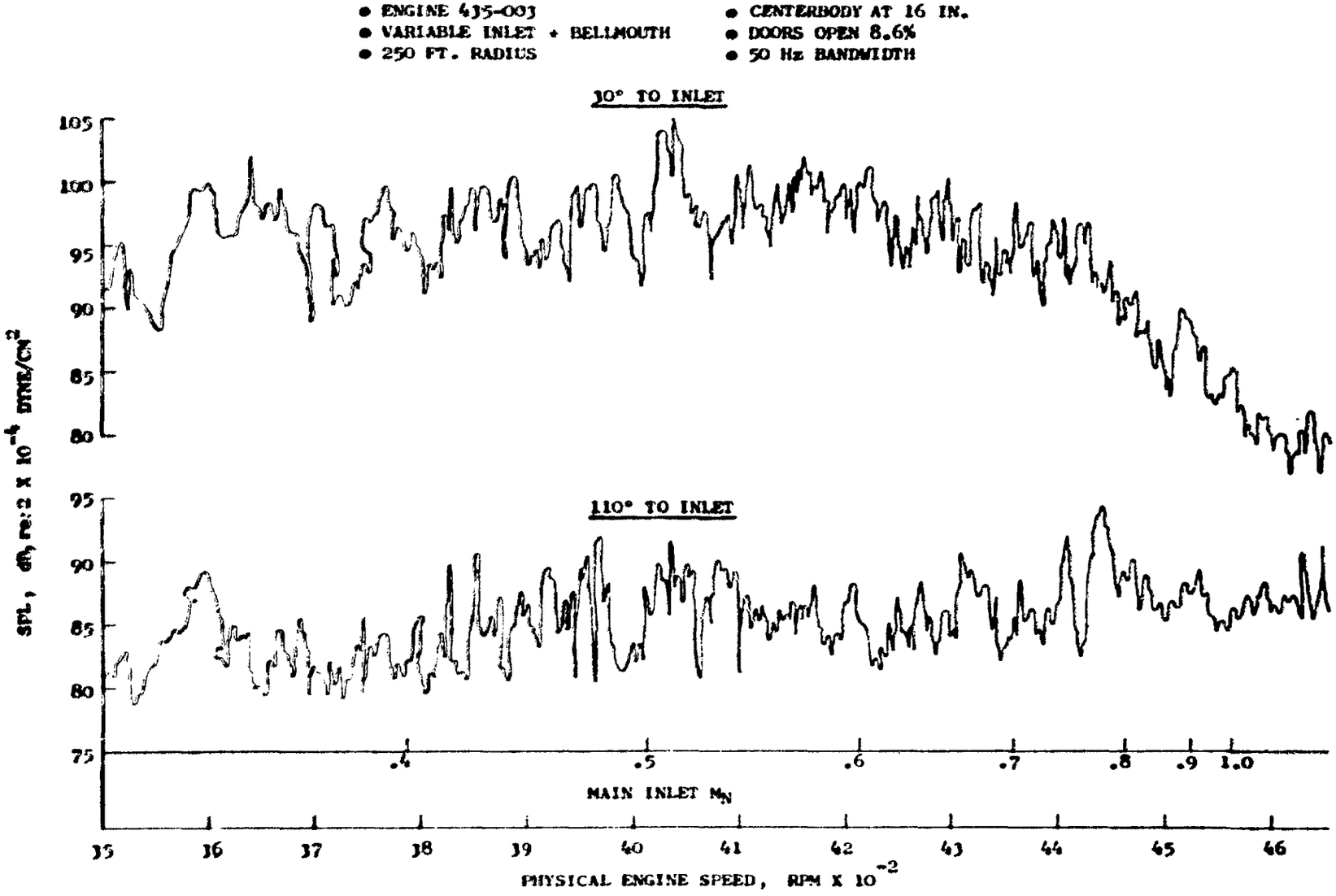


FIGURE VI.A-1 - EFFECT OF MAIN INLET MACH NUMBER ON COMPRESSOR FIRST STAGE FUNDAMENTAL TONE

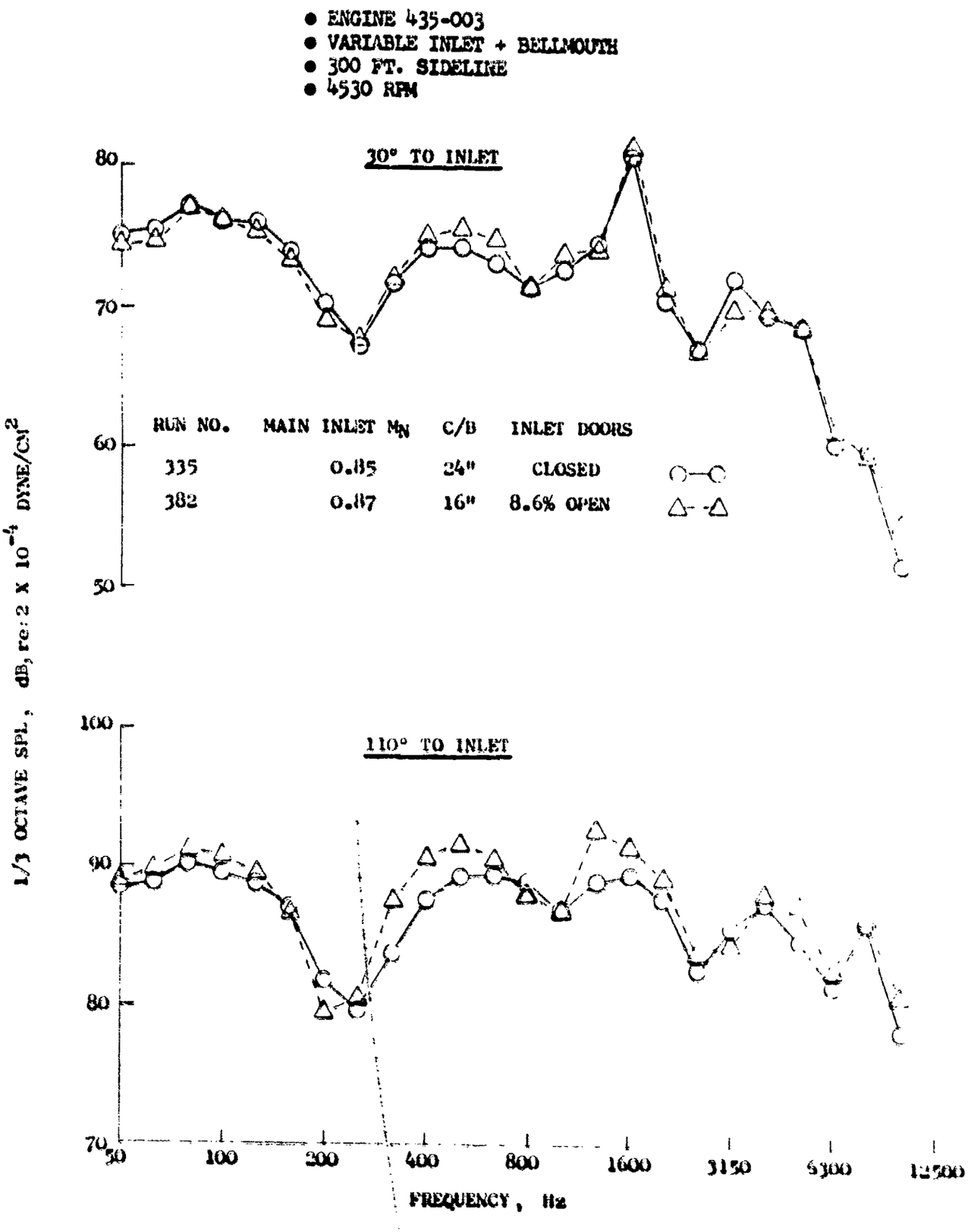


FIGURE VI.A-15 EFFECT OF VARIABLE INLET DOOR OPENING ON FAR FIELD SPECTRA AT 30° & 110° TO INLET

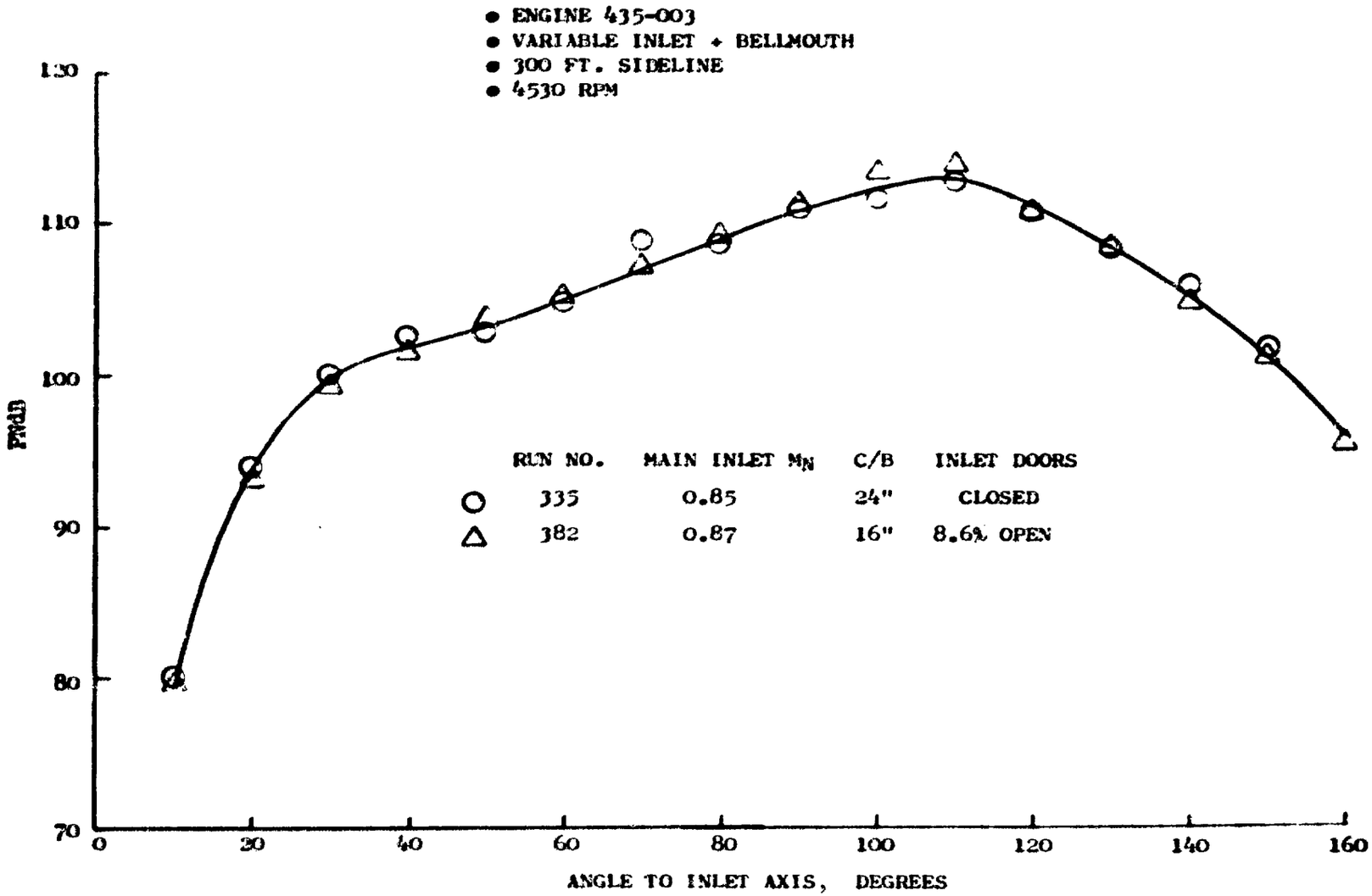


FIGURE VI.A-16 EFFECT OF VARIABLE INLET DOOR OPENING ON FAR FIELD PNL DIRECTIVITY

"PRECEDING PAGE BLANK-NOT FILMED."

VI.B EXHAUST NOZZLE OPEN AREA SCHEDULE - GE4 ENGINE

"PRECEDING PAGE BLANK-NOT FILMED."

VI.B EXHAUST NOZZLE OPEN AREA SCHEDULE - GE4 ENGINE

Objectives of Test Series

At a given exhaust nozzle throat setting, a variable A_8 exhaust system, such as that planned for the GE4 engine, could be advantageously used to lower jet noise. At approach and/or cutback thrust settings, operation of the nozzle at a larger than normal A_8, on the "open area schedule", would produce the required thrust but at a lower than normal jet exhaust velocity, thereby lowering the generated jet noise. To evaluate this open area schedule effectiveness, acoustic tests were performed using GE4 Engines 435-002 and 435-003 at the Peebles Proving Ground Site 4D acoustic facility.

Test Configurations

Using GE4 Engine 435-002, four fixed area conical convergent nozzles at A_8's = 900, 1000, 1200, and 1300 in^2, were used to simulate A_8 positions of the variable exhaust system. On GE4 Engine 435-003, three fixed area conical convergent nozzles were used at A_8's of 1200, 1300, and 1560 in^2. Acoustic measurements were taken on a 250 ft. arc at each 10° increment from 0° to 160° from the inlet axis. Various thrust settings were set while using each nozzle within the range of 10,000 to 34,000 lbs. With Engine 435-002, acoustic measurements were also taken while using a Two Stage Ejector Nozzle (TSEN) with the 1000 and 1200 in^2 primary nozzles giving D_5/D_8 ratios of 1.37 and 1.26, respectively.

Presentation and Discussion of Test Results

Acoustic results of the Engine 435-002 test series are shown in Figure VI.B-1; 500 ft. sideline peak PNdB as a function of measured gross thrust. The figure shows measurements using the four bare conical primary nozzles and the two cone-plus-TSEN systems. Almost exact agreement is seen with the SAE predicted lines for the four fixed A_8's. Measurements with the cone-plus-TSEN systems are identical levels to the bare conical nozzles. For a typical thrust setting of 28,000 lb., inspection of the curves shows a PNL suppression of 7 PNdB by increasing nozzle A_8 from 900 to 1300 in^2, thus verifying the effectiveness of the open area schedule.

Further measurements with Engine 435-003, using 1300 and 1560 in^2 A_8 nozzles and over a lower range of thrust settings, are shown in Figure VI.B-2 with the Engine 435-002 data. The data are again 300 ft. sideline peak PNdB as a function of measured gross thrust. For exhaust areas up to 1300 in^2 and thrust levels above 20,000 lbs., the agreement between engines and between engine and SAE prediction is good. Below this thrust level and for the larger exhaust area the measured data was nearly 10 dB above SAE. At these low power settings the internally generated turbomachinery noise predominates over the jet noise and causes the measurements to diverse from predicted levels. A comparison of spectra at the 80° from exhaust peak PNL angle is done in Figure VI.B-3. The spectra are for 1300 and 1560 in^2 A_8's with the engine operating at constant thrust of 15,000 lbs. The plot shows low frequency noise levels from the jet are approximately equal in level, but at frequencies above 1 KHz the noise level from the 1560 in^2 nozzle is greater due to running the engine at higher rpm to maintain the same thrust setting.

Figure VI.B-4 shows the 300 ft. sideline peak PNdB, normalized to account for the A_8 variance, as a function of ideal jet velocity. The SAE line, also normalized, is included for comparison. The data show that, for a given jet velocity, the larger nozzle areas generate higher engine noise levels. Thus, at the low power settings and more open A_8's, the acoustic output is dominated by the internally generated noise component over the pure jet noise. The internally generated turbomachinery noise increases with increase in rpm and engine rpm increases with increase in A_8, for a given jet velocity.

Conclusions

- Open area schedule is effective in reducing the jet noise component of engine total noise levels and follows that predicted by the SAE procedure.
- At low thrust settings and with large A_8's, the GE4 measured noise became dominated by internally generated turbomachinery noise, overshadowing the open area effectiveness in reducing the pure jet noise component.

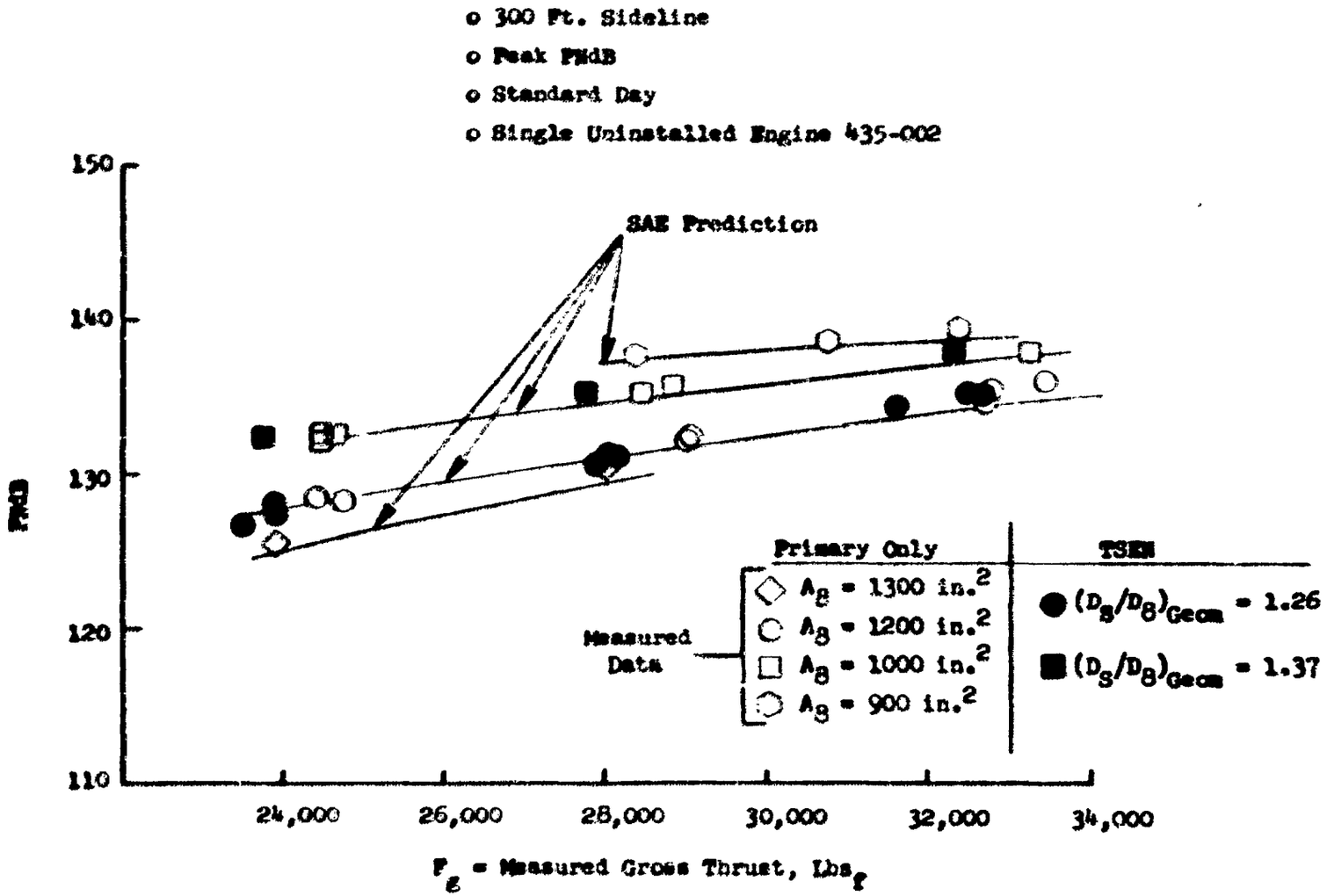


FIGURE VI.B-1 EFFECT OF EXHAUST NOZZLE OPEN AREA SCHEDULE ON GE4 ENGINE 435-002 NOISE LEVELS

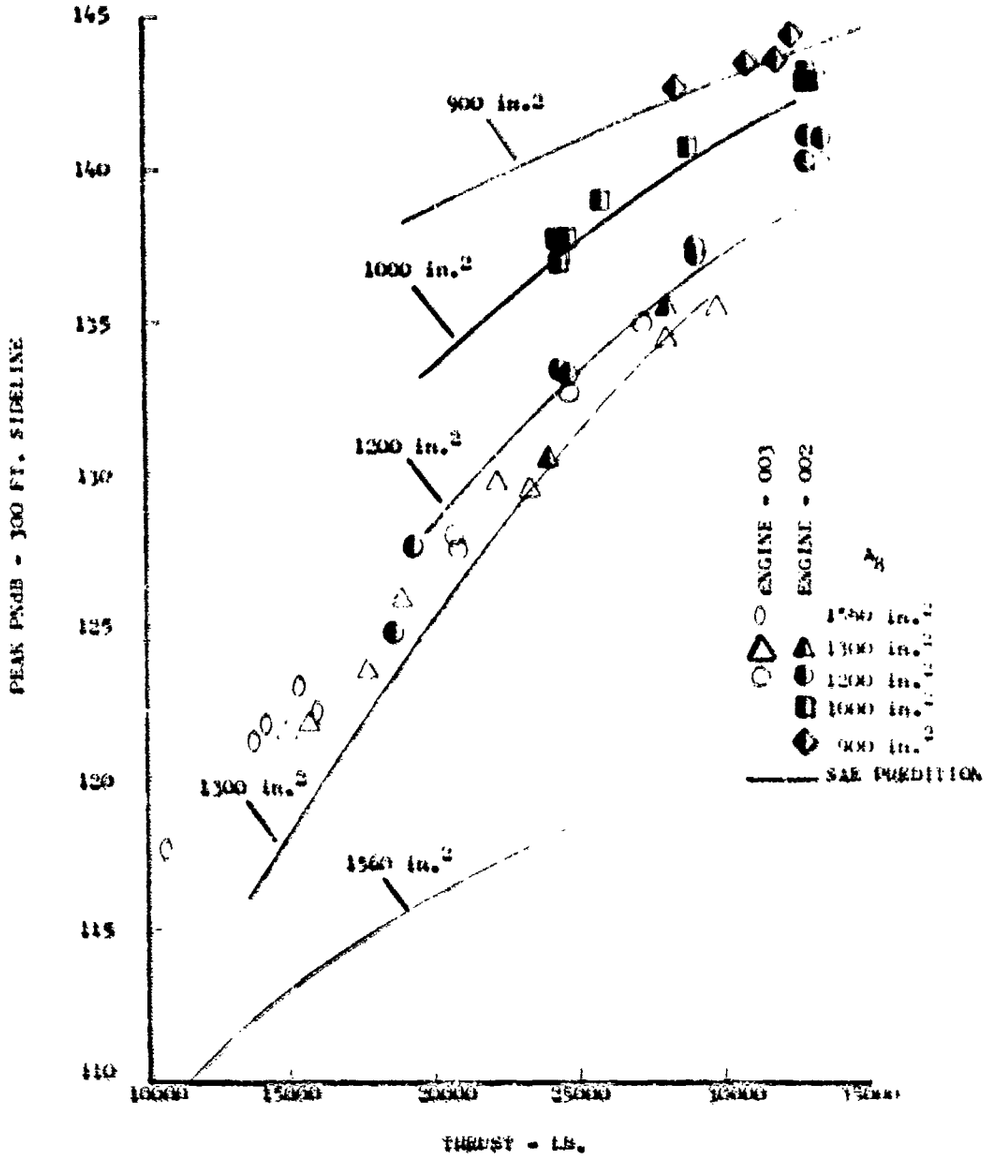


FIGURE VI.3-2 EFFECT OF [illegible] AREA SCHEDULE ON GE6 PEAK PNL

- 300 Ft. Sideline
- 80° From Jet Exhaust
- F_N = 15,000 Lbs.
- Engine 435-003

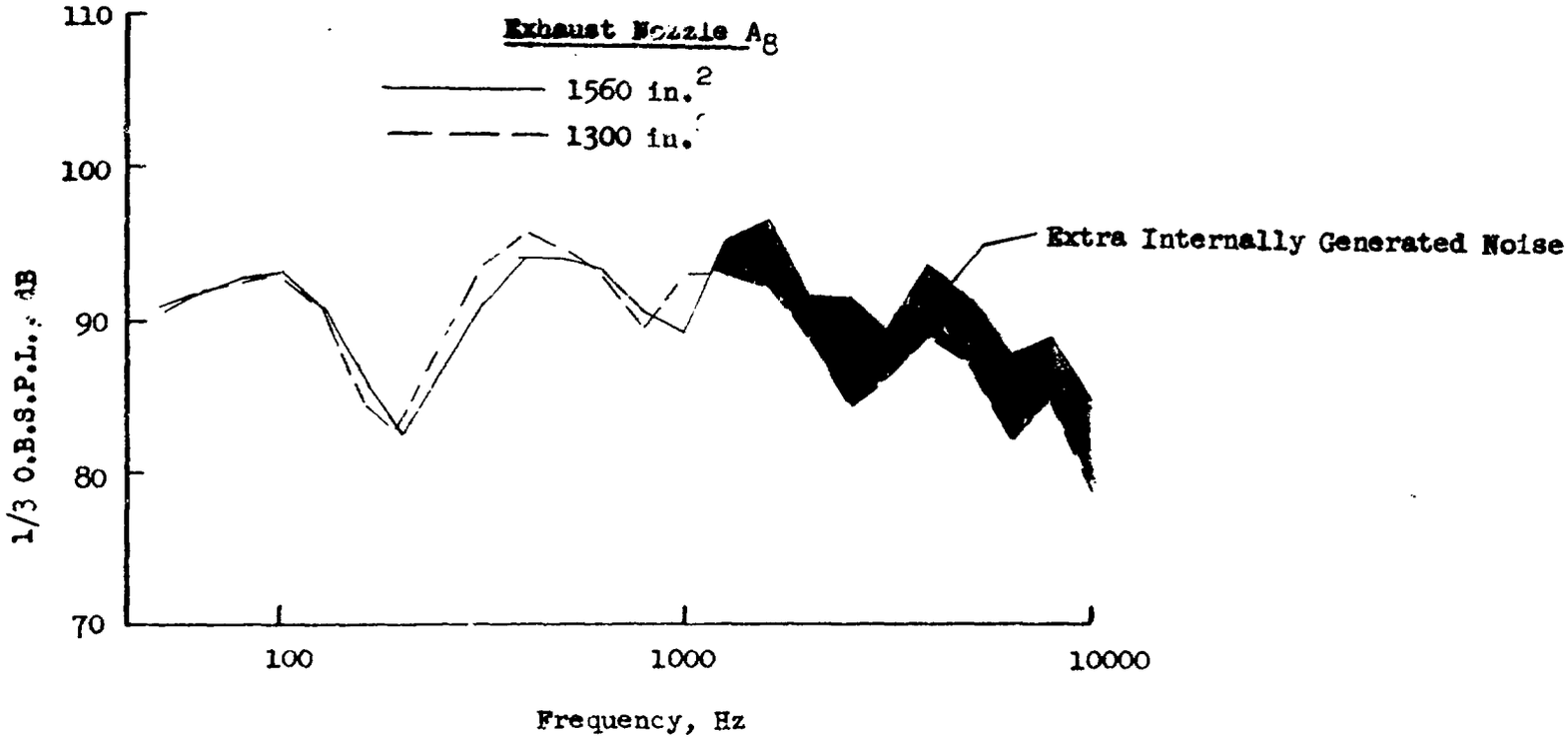


FIGURE VI.B-3 EFFECT OF A_8 ON GE4 NOISE SPECTRA AT CONSTANT THRUST

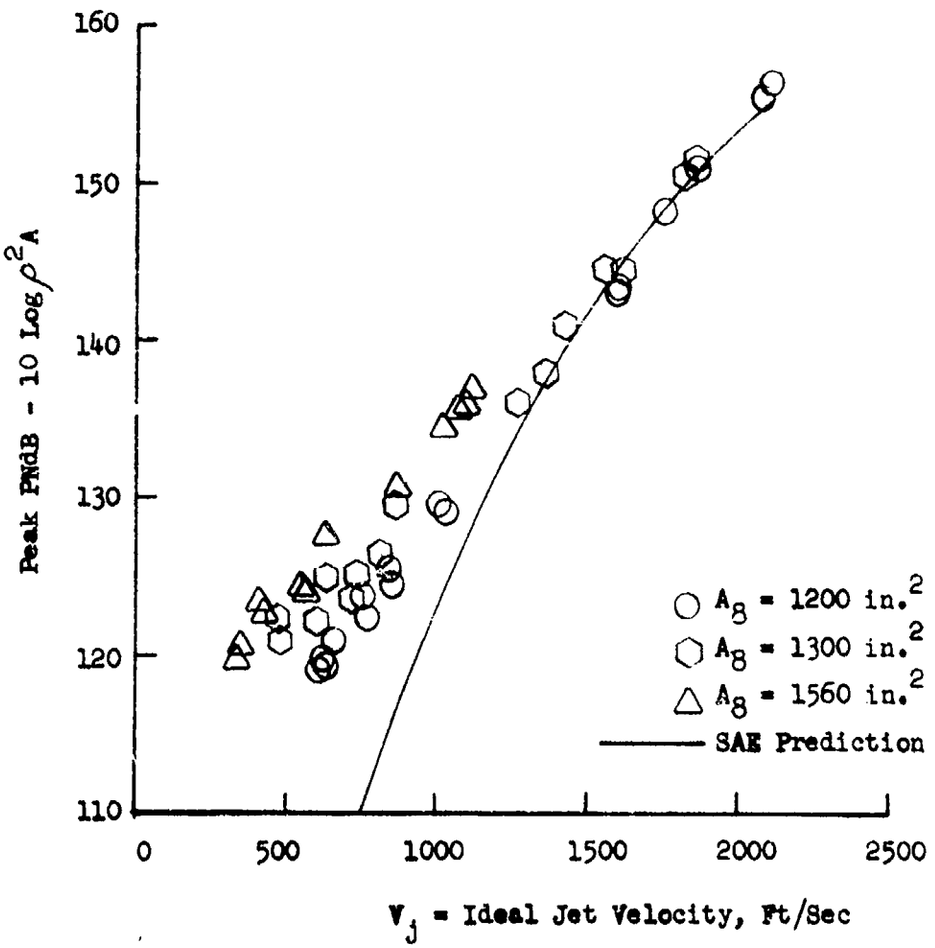


FIGURE VI.B-4 NORMALIZED GE4 NOISE LEVELS AS A FUNCTION OF JET VELOCITY

VI.C TURBOMACHINERY NOISE ON GE4 ENGINE

"PRECEDING PAGE BLANK-NOT FILMED."

VI.C TURBOMACHINERY NOISE INVESTIGATION - GE4 ENGINE

The GE4 engine was identified as having a turbomachinery noise problem, particularly at the low thrust settings of approach, and to a lesser extent, at power cutback. The peak noise in the aft quadrant of the GE4 engine is relatively unaffected by employing a choked inlet (See Section VI.A - Choked Inlet - GE4 Engine). Narrowband analyses suggest that, at this angle, the spectrum is highly influenced by noise components from the turbomachinery which are either transmitted through the engine exhaust ducting and exhaust nozzle or through the engine casing. In either case, noise from the compressor or turbine could have significance.

A series of diagnostic tests were planned and partially completed toward the goal of determining the source and magnitudes of turbomachinery noises, their respective propagation paths to the far field, and their contribution to the far field total engine acoustic level. Investigated areas of interest included:

- Compressor source noise identification with acoustic probes (Section VI.C-1)
- Compressor tip shroud treatment study (Section VI.C-2)
- Noise source identification with directional microphone array (Section VI.C-3)
- J79 Turbomachinery noise test (Section VI.C-4)
- GE4 engine 435-007 near and far field acoustic measurements (Section VI.C-5).

"PRECEDING PAGE BLANK-NOT FILMED."

VI.C.1 COMPRESSOR SOURCE NOISE IDENTIFICATION WITH ACOUSTIC PROBES

"PRECEDING PAGE BLANK-NOT FILMED."

VI.C.1 COMPRESSOR SOURCE NOISE IDENTIFICATION WITH ACOUSTIC PROBES

Objectives of Tests

Several attempts were made to identify source turbomachinery predominant tones and their acoustic levels by using traversing acoustic probes within a compressor, while undergoing component aerodynamic testing, and during tests of a final engine configuration. These tests included:

Phase I. - Probe measurements within the Block II compressor inlet duct while undergoing component aerodynamic tests in a tank facility.

Phase II. - Probe measurements within the FTS (Flight Test Status) compressor inlet and exhaust diffuser while undergoing component aerodynamic tests in a tank facility.

Phase III. - Probe measurements within the FTS compressor inlet while assembled in the GE4 engine 435-007.

The probes were to identify a) which compressor tones propagated forward and aft of the compressor, and b) their relative acoustic levels near the source to gauge their potential for propagation forward through the inlet, aft through the engine duct and nozzle, or through the casing to the far field.

Presentation of Test Results

The test results for Phases I, II and III are presented in Figures VI.C.1-1 through -9. Figure VI.C.1-1 schematically shows the traversing probes set up in the FTS compressor for Phase II measurements. Phase I measurements within the Block II compressor were similar to the inlet probes of Figure VI.C.1-1. Figure VI.C.1-2 compares the Block II and FTS compressor IGV, first stage rotor and stator designs. Figure VI.C.1-3 shows the inlet duct acoustic probe within the GE4 engine 435-007 at Peebles for Phase III testing.

Typical data obtained in narrowband form are shown in Figures VI.C.1-4, -5 and -6 from the Phase II work with the FTS compressor tank test. The data of Figures VI.C.1-4 and VI.C.1-5 were obtained from intermediate (-46.3") axial probe measurements at an immersion depth of approximately 50% of the annulus height for corrected compressor speeds of 64% and 89.9%, respectively. Both plots emphasize the predominance of first stage rotor fundamental and harmonic

tones; however, with the higher speed point, multiple peaks show increasing predominance and are labeled as to origin. Figure VI.C.1-6 is typical of the compressor diffuser probe data with all stage tones defined. This plot shows the predominance of the stage 9 compressor tone and the presence of all other stage tones having propagated through the compressor.

By integration of tone sound pressure levels across the annulus ducts, tone power levels can be calculated. Of significance from the Phase II test with the FTS compressor is the comparison of forward and aft propagated tone power levels for each compressor stage, as shown in Figure VI.C.1-7. It is observed that the forward propagated noise is dominated by the first stage only, whereas for aft propagation, stages 4 through 9 are the major contributors. The forward propagated tones should be considerably reduced by the choked inlet. However, the attenuation factors to be applied to the aft propagated noise, either due to transmission through the engine casing and nacelle, or due to propagation through the combustor and turbine, are not known.

Looking further at the predominant first stage compressor fundamental tone, the duct power level is presented as a function of corrected speed in Figure VI.C.1-8. The plot includes data from all three test phases, namely, the Block II and FTS tank (component) tests and the FTS engine test. The FTS tank data was initially 10 dB low due to a recording error but is now shown corrected and complies fairly well with the Block II data. Trend lines drawn through the data show that the FTS tank test levels at high corrected speed are slightly under the Block II tank test levels due to the difference in design, as seen in Figure VI.C.1-2. The FTS engine test data follows the FTS tank test trend line quite closely.

Power levels for fundamental tones of all the compressor stages are shown at various engine speeds in Figure VI.C.1-9 from the Phase III FTS engine test. They indicate that forward propagated noise is dominated by first stage fundamental tone with the second stage contributing somewhat at several speeds. From stages 3 through 9 the levels are 10 to 20 dB below those of stage 1.

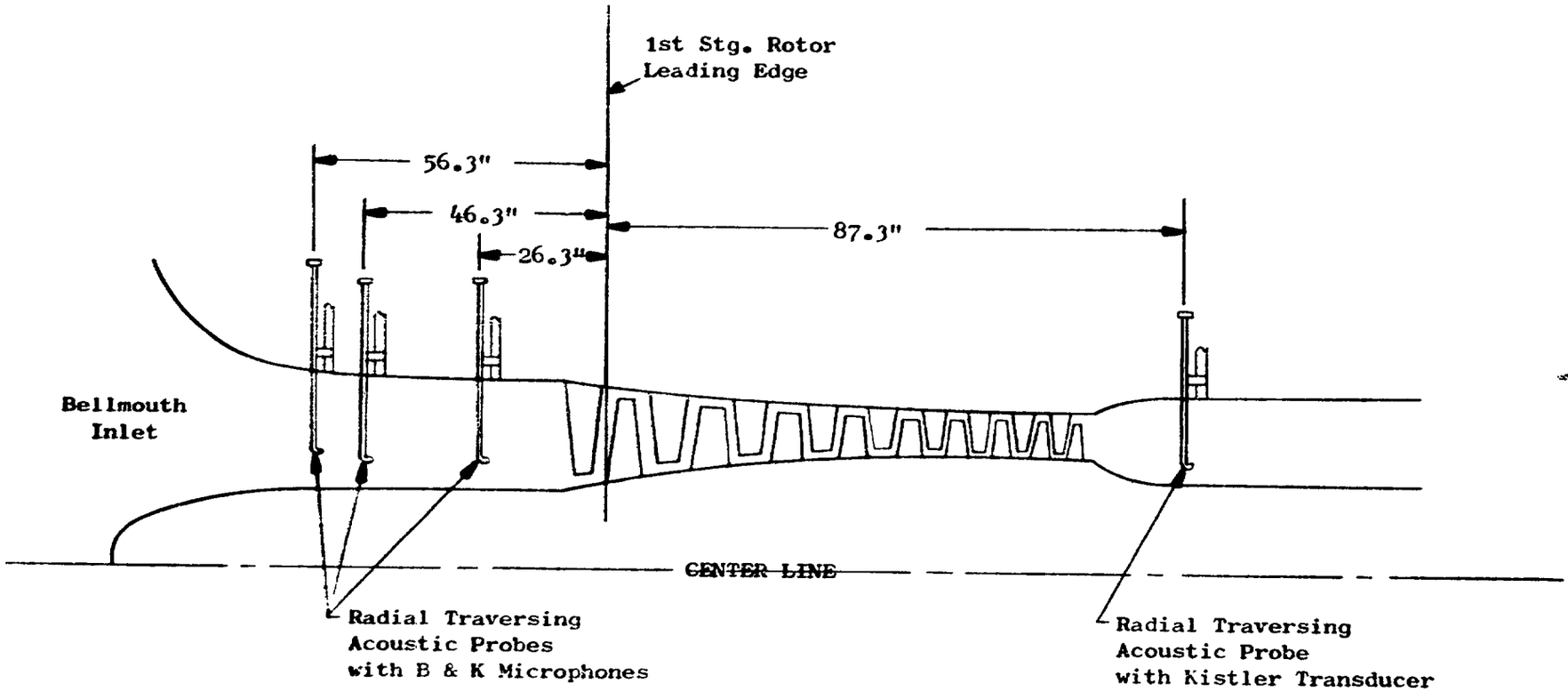


FIGURE VI.C.1-1 SCHEMATIC OF FTS COMPRESSOR TEST VEHICLE

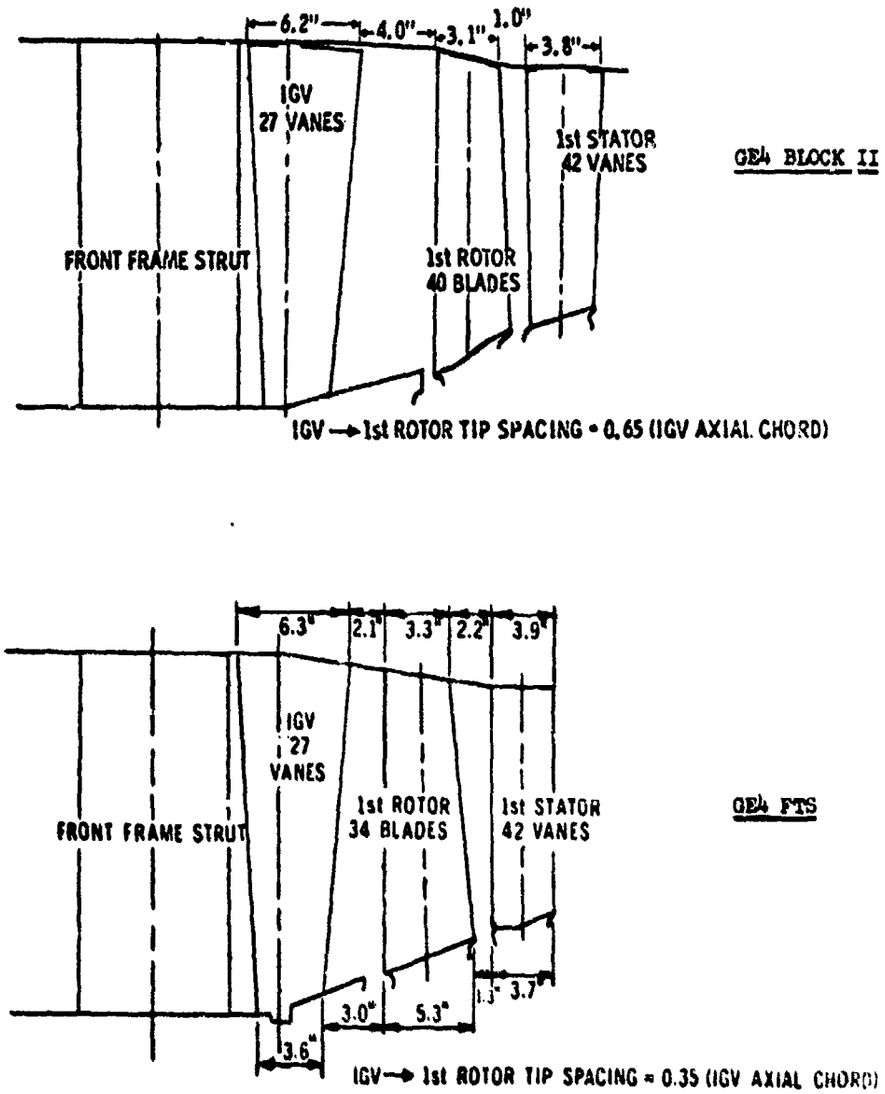


FIGURE VI.C.1-2 GE4 COMPRESSOR GEOMETRY

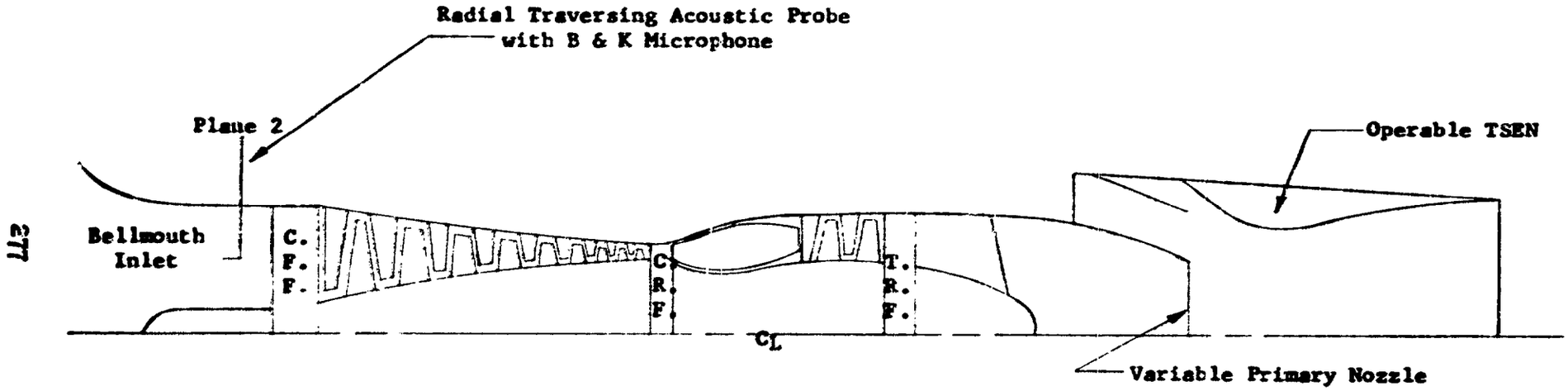


FIGURE VI.C.1-3 SCHEMATIC OF GE4 ENGINE 435-007 WITH INLET ACOUSTIC PROBE

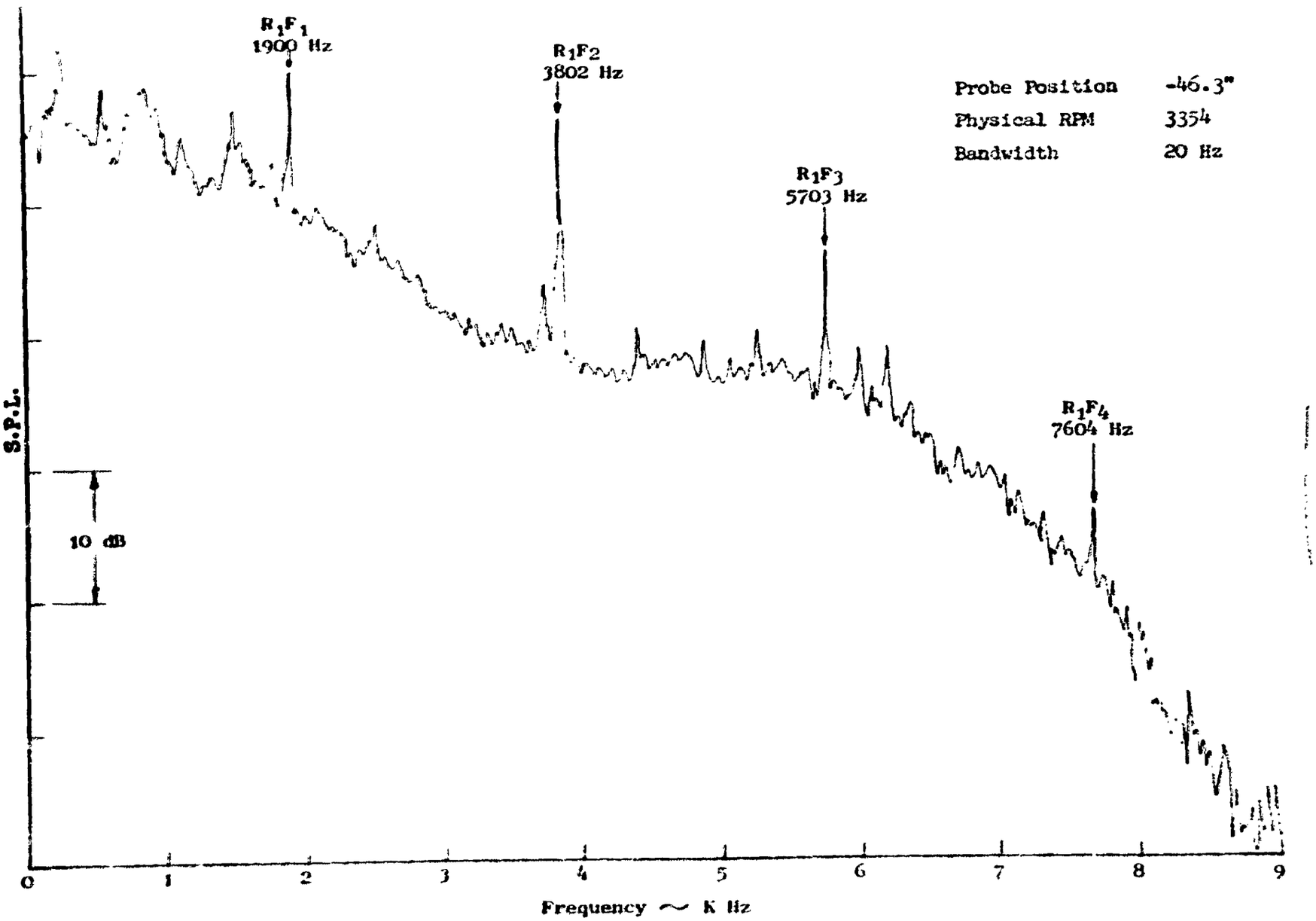


FIGURE VI.C.1-4 FTS COMPRESSOR TANK TEST - ACOUSTIC NARROWBAND PLOT

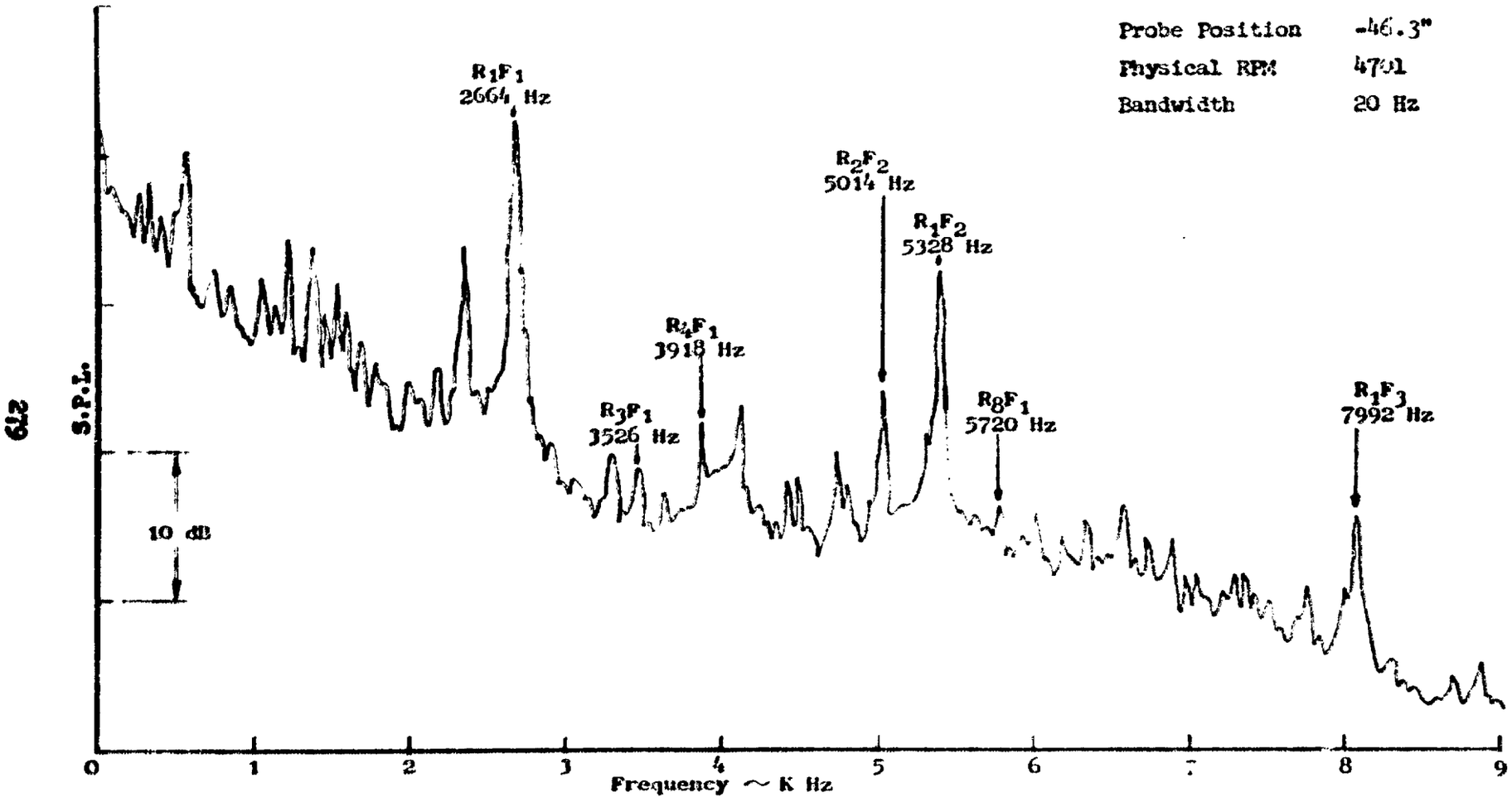


FIGURE VI.C.1-5 FTS COMPRESSOR TANK TEST - ACOUSTIC NARROWBAND PLOT

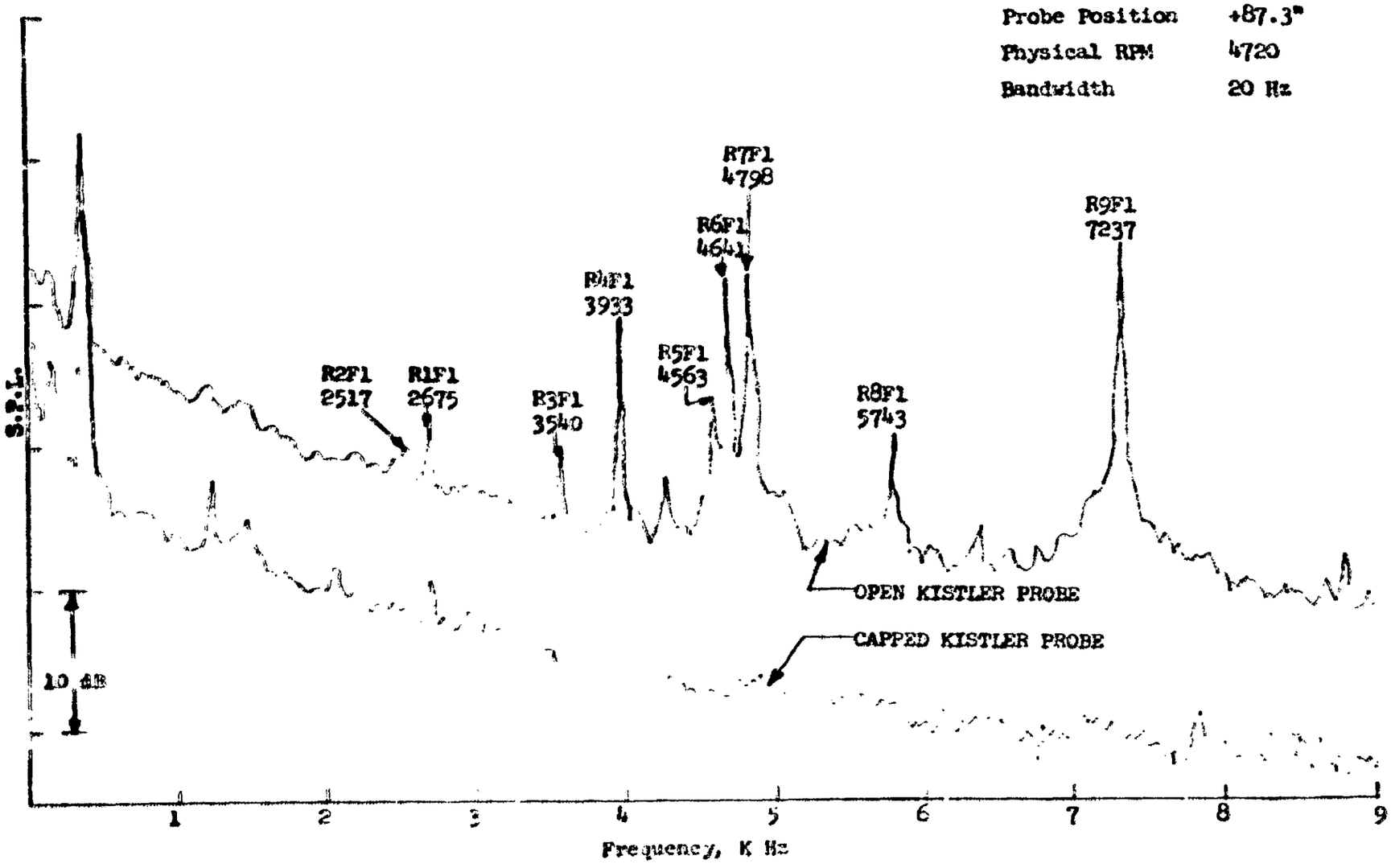


FIGURE VI.C.1-6 GE4 FTS COMPRESSOR TANK TEST - ACOUSTIC NARROWBAND PLOT

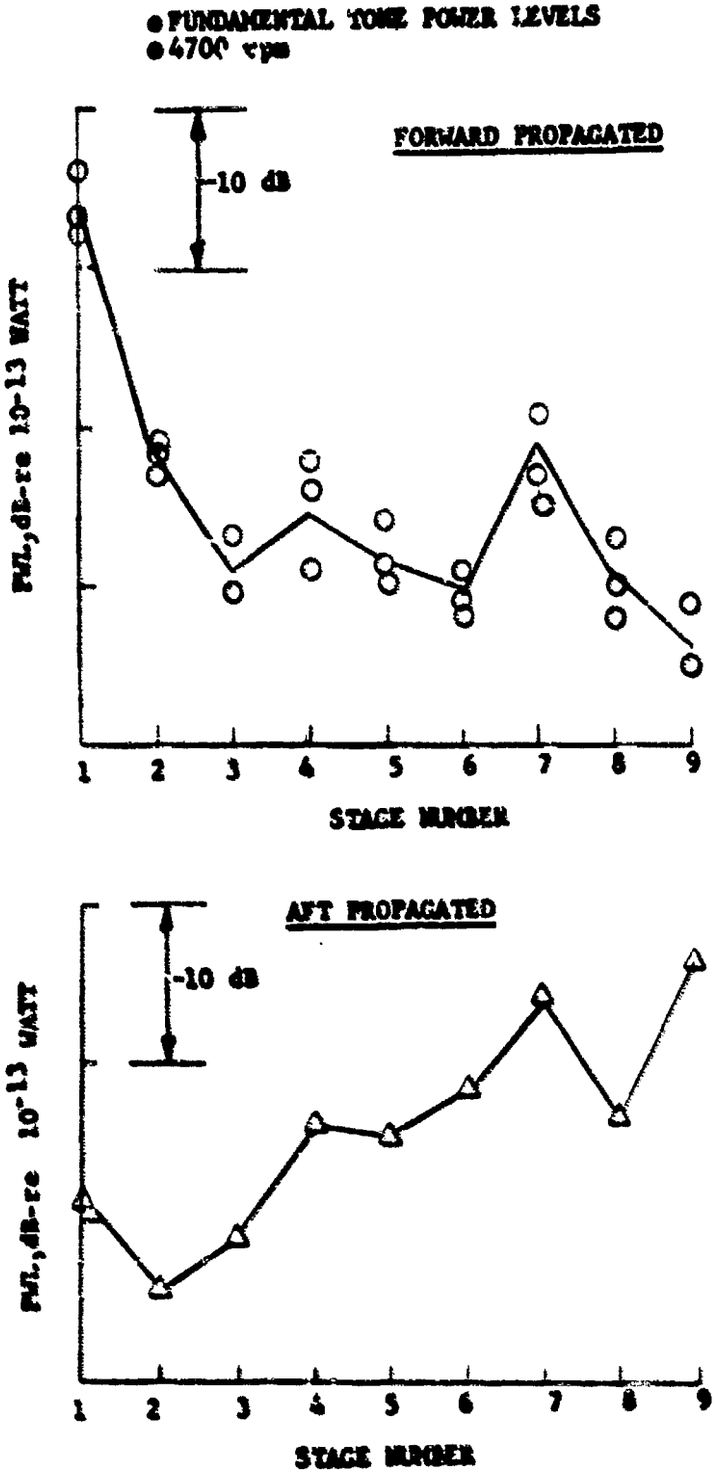


FIGURE VI.C.1-7 GE4 FTS COMPRESSOR TANK TEST - FORWARD & AFT PROPAGATED FUNDAMENTAL TONE POWER LEVELS

- o FIRST STAGE FUNDAMENTAL TONES
- o PROBE MEASUREMENTS IN INLET

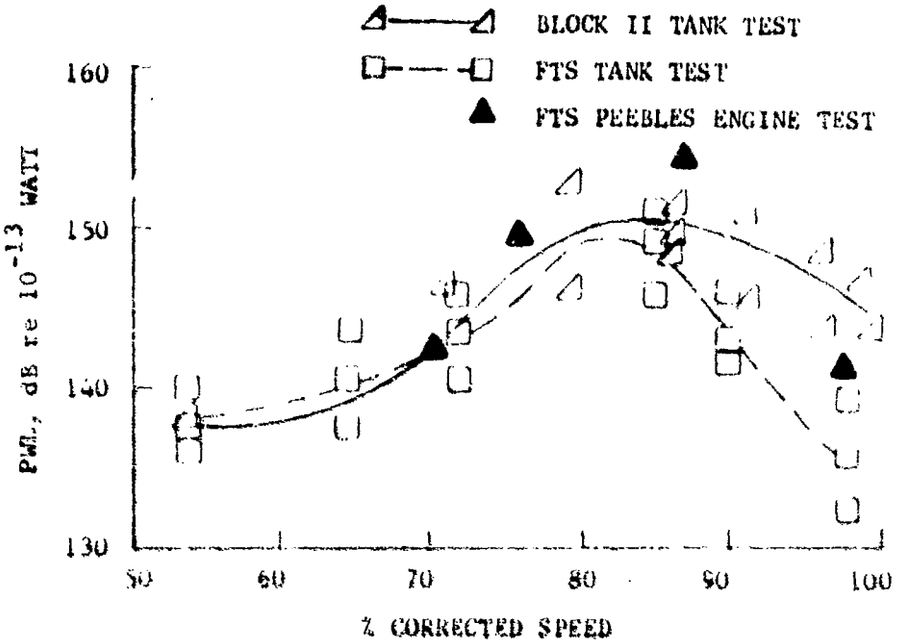


FIGURE VI.C.1-8 GE4 BLOCK II & FTS COMPRESSOR TESTS - FIRST STAGE FUNDAMENTAL TONE POWER LEVELS

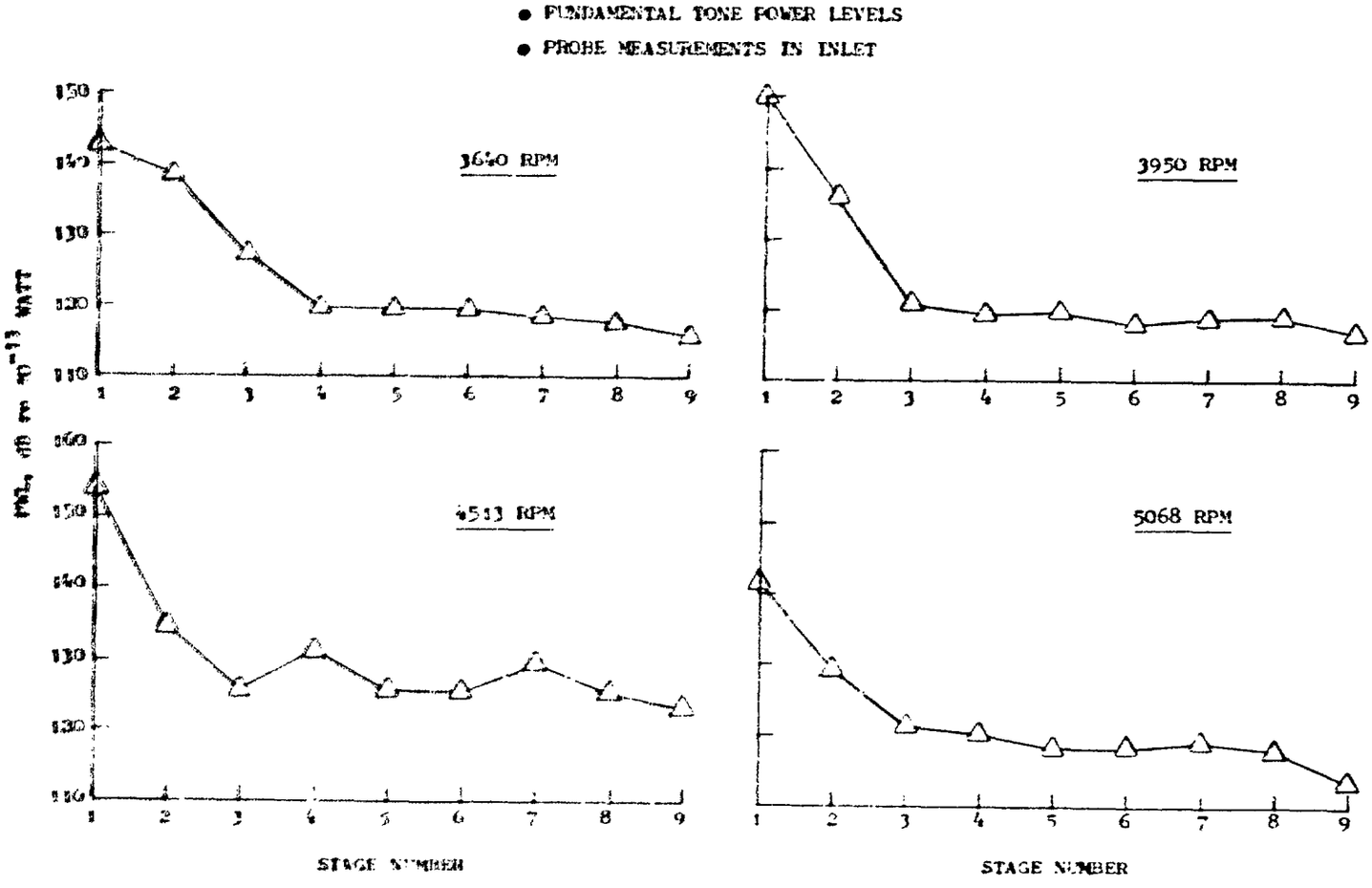


FIGURE VI.C.1-9 GE4 FTS COMPRESSOR NOISE LEVELS - PEEBLES ENGINE TEST

"PRECEDING PAGE BLANK-NOT FILMED."

VI.C.2 COMPRESSOR TIP SHROUD TREATMENT STUDY

"PRECEDING PAGE BLANK-NOT FILMED."

VI.C.2 COMPRESSOR TIP SHROUD TREATMENT STUDY

Objectives of Tests

Compressor tip shroud treatment was investigated as a possible means of noise suppression at the generation source. The design of the GE4 compressor included cavities over the rotor tip shrouds which could have possibly been modified to accept acoustic liner treatment. A schematic of the concept is shown in Figure VI.C.2-1 together with generalized trends of acoustic suppression of aft propagated noise. Two suppression effects would be anticipated.

- o Tip treatment effect - this is the effect of the treatment reducing the noise generated at the tip for a given blade row. This effect should be equal for all stages.
- o Lined duct effect - this is the effect of the treatment acting on noise produced by previous stages and would have a lesser effect with higher stage number.

Test Configurations and Presentation of Results

A series of tests were conducted to obtain preliminary data to check the viability of tip treatment effectiveness before incorporation into elaborate engine hardware. The tests were performed on an available 15" diameter, low tip speed, single stage compressor which was modified in the blade tip region to accept various lengths and types of acoustic treatment. Figure VI.C.2-2 is a schematic of the vehicle showing possible variations of acoustic treatment as replacements for the blade tip seals. The 15 in. compressor rig did not simulate the GE4 compressor operating conditions; however, the principles of acoustic suppression developed could be applied to the GE4 design.

The first test series used a bulk absorber treatment consisting of a 22.5% open perforated face plate with one inch of Cerafelt CR400 filler. The rig utilized eight equally spaced rods simulating IGV's for the purpose of generating IGV/blade interaction noise at the blade passing frequency. Similar tests were run with no rods ahead of the blades to determine changes in treatment effectiveness as a function of noise generation mechanism. Results of the tests are shown in Figures VI.C.2-3, -4 and -5 illustrating the effectiveness of treatment widths of three-blade chords and single blade row only with IGV's (Figures VI.C.2-3

and -4) and treatment width of three-blade chords without IGV's (Figure VI.C.2-5). The plots show that for bulk absorptive treatment over the blade row only, suppression was attained at frequencies up to the second harmonic of the blade passing frequency. When the treatment width was increased to three chord lengths, suppression was attained at all frequencies except the fundamental blade passing frequency. The results showed that 1 - 2 dB suppression could be gained from the bulk type treatment, although with modified designs higher suppression could possibly be attained throughout the frequency range, including the blade passing frequency and harmonics.

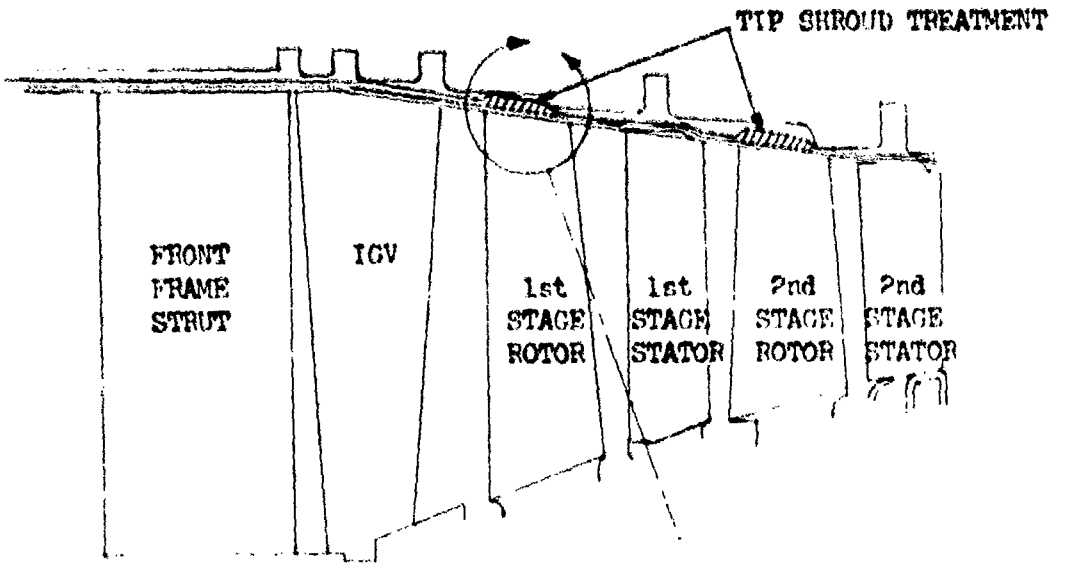
The second test series evaluated a more practical type of single-degree-of-freedom (SDOF) treatment insert, tested in three combinations of location and area. The first test utilized a three-blade-chord width treated area, the second used a one-blade-chord width treatment over the blade row and the third test used the same one-blade-chord width treatment directly aft of the blade row. Results of time averaged 1/3 octave Δ SPL's indicate that, within its design range, the SDOF treatment is at least as good as a bulk type suppressor and exceeds the bulk type suppressor performance at the blade passing frequency since suppression is not lost at this point.

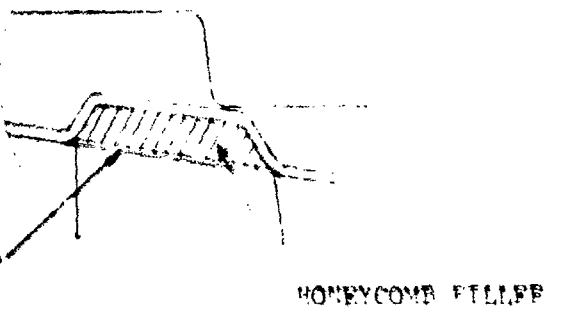
Variable rotor-speed tests indicate no trends of suppression variation with speed as per Figure VI.C.2-6. All variations of suppression seem to be of a random nature. Extrapolation with respect to tip speed could, therefore, suggest that the attained insert suppression may still exist, possibly to the point where blade tip speed becomes sonic, where noise generation characteristics change. Figure VI.C.2-7 illustrates a typical 6% bandwidth probe spectrum of the baseline model and corresponding 1/3 octave time averaged suppression level as a function of frequency attained by SDOF treatment over the blade row only.

Applying these results of the more practical SDOF material to the CF4 compressor configuration could then possibly be accomplished through use of the plot in Figure VI.C.2-8. The plot indicates that up to 3 dB tip treatment suppression could be attained on each treated compressor stage. In addition, if all stages were treated, the lined duct effect indicates additional suppression gain for aft propagated noise for the first four compressor stages.

Conclusions

- Acoustic treatment internal to the engine, such as compressor tip shroud treatment and compressor diffuser treatment, can be used to help control noise at it's origin of generation.
- Initial tests in a single stage low speed compressor indicate that practical materials such as SDOF will give moderate suppression levels when applied in the tip shroud region.





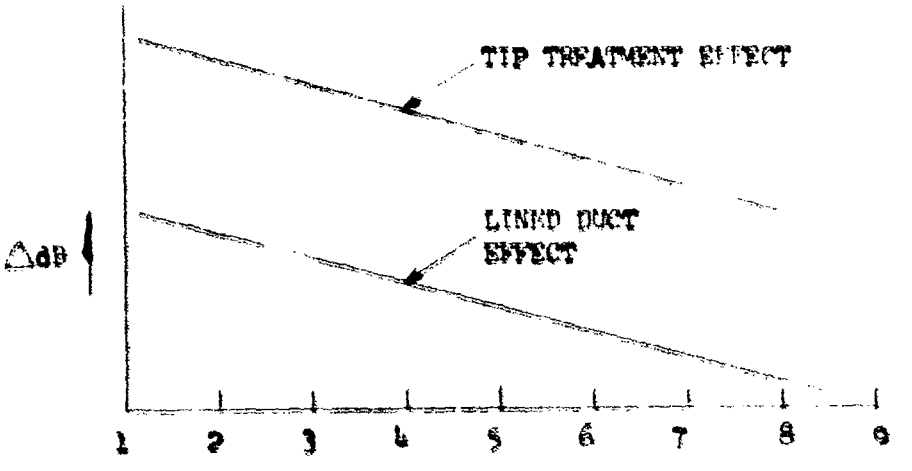


FIGURE VI.C.2-1 GE4 COMPRESSOR TIP SHROUD TREATMENT

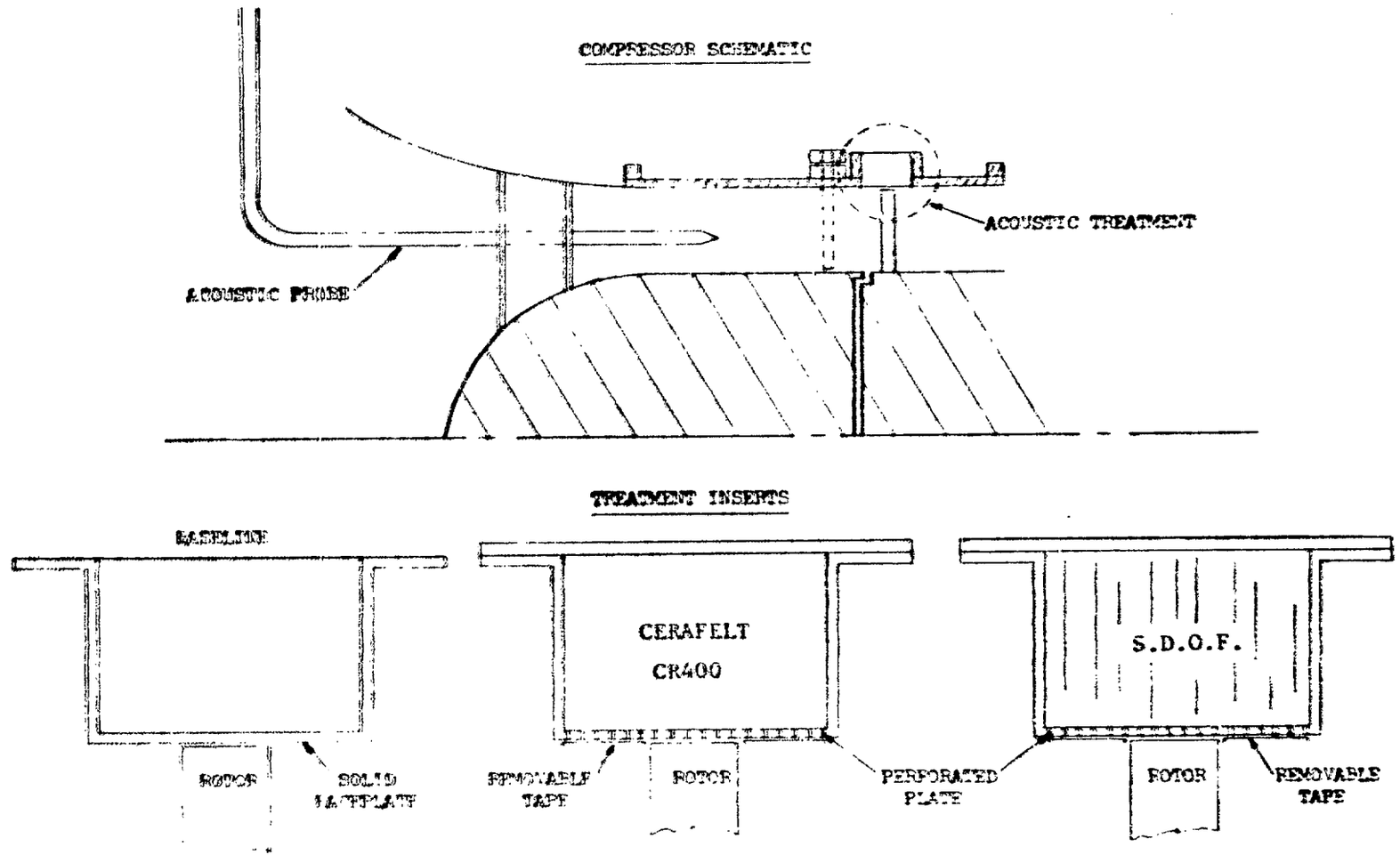


FIGURE VI.C.2-2 SCHEMATIC OF 15" COMPRESSOR & TIP TREATMENT VARIATIONS

- o Bulk Absorber
- o 22½% Open Perforated Plate
- o CR400 Cerafelt
- o Treatment Width 3 Blade Chords
- o With IGV's
- o Results of Four Repeat Runs

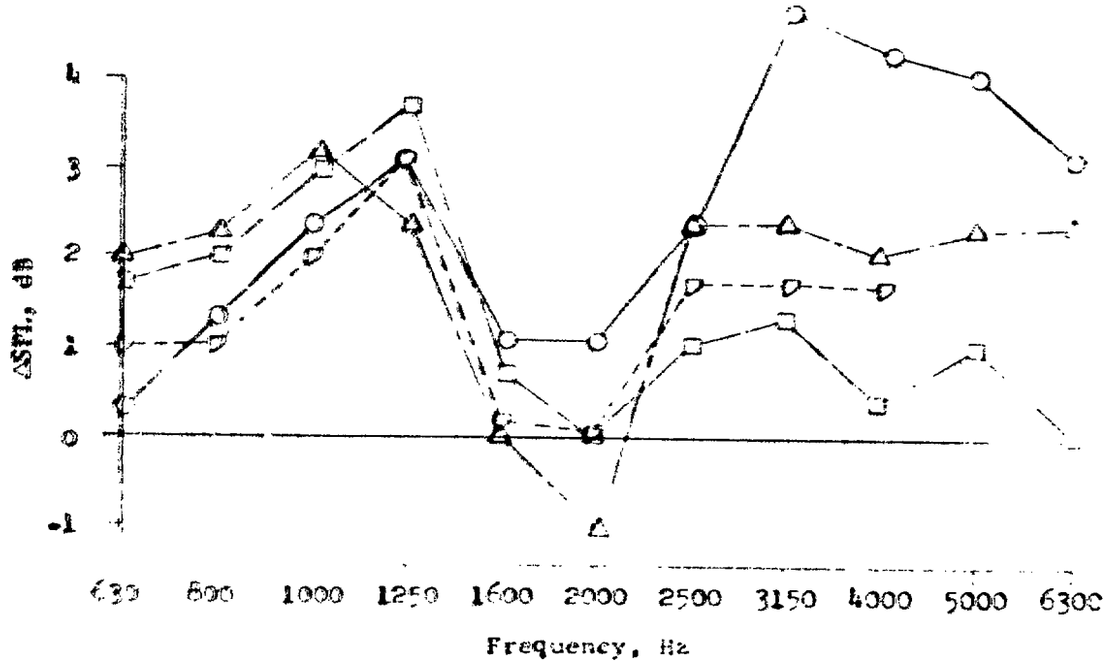


FIGURE VI.C.2-3 TIP SHROUD TREATMENT EFFECTIVENESS - 3 BLADE CHORD WIDTHS - WITH IGV'S

- o Bulk Absorber
- o 22½% Open Perforated Plate
- o CR400 Cerafelt
- o Treatment Over Blade Row Only
- o With IGV's
- o Results of Four Repeat Runs

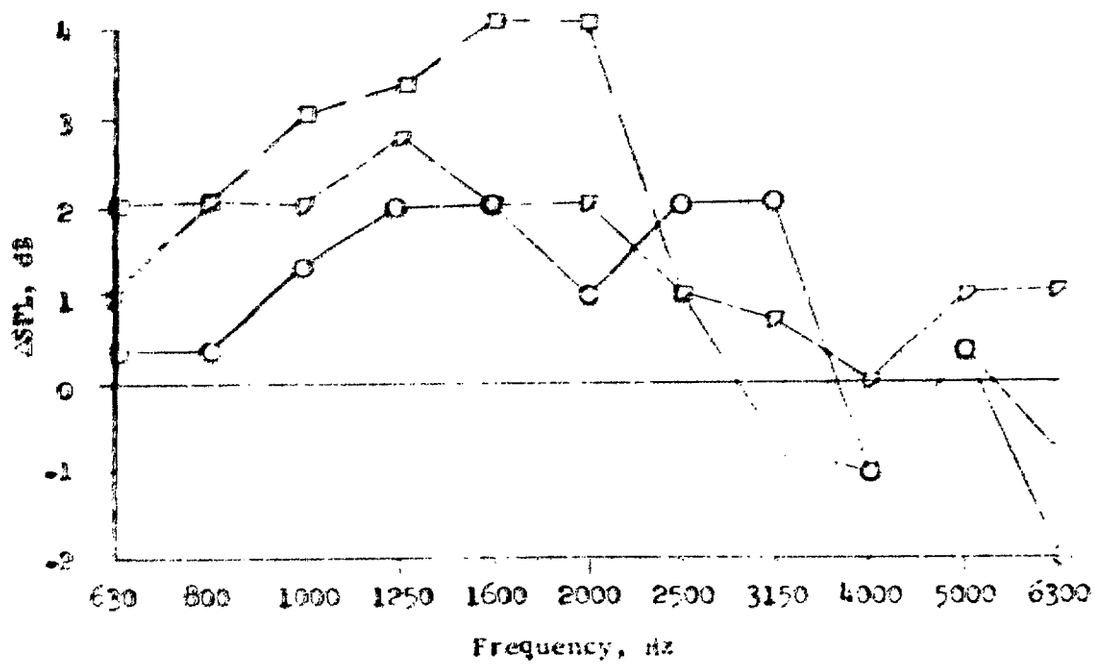


FIGURE VI.C.2-[illegible] TIP SHROUD TREATMENT EFFECTIVENESS - SINGLE BLADE CHORD WIDTH - WITH IGV'S

- o Bulk Absorber
- o 22½% Open Perforated Plate
- o CR400 Cerafelt
- o Treatment Width 3 Blade Chords
- o Without IVG's
- o Results of Four Repeat Runs

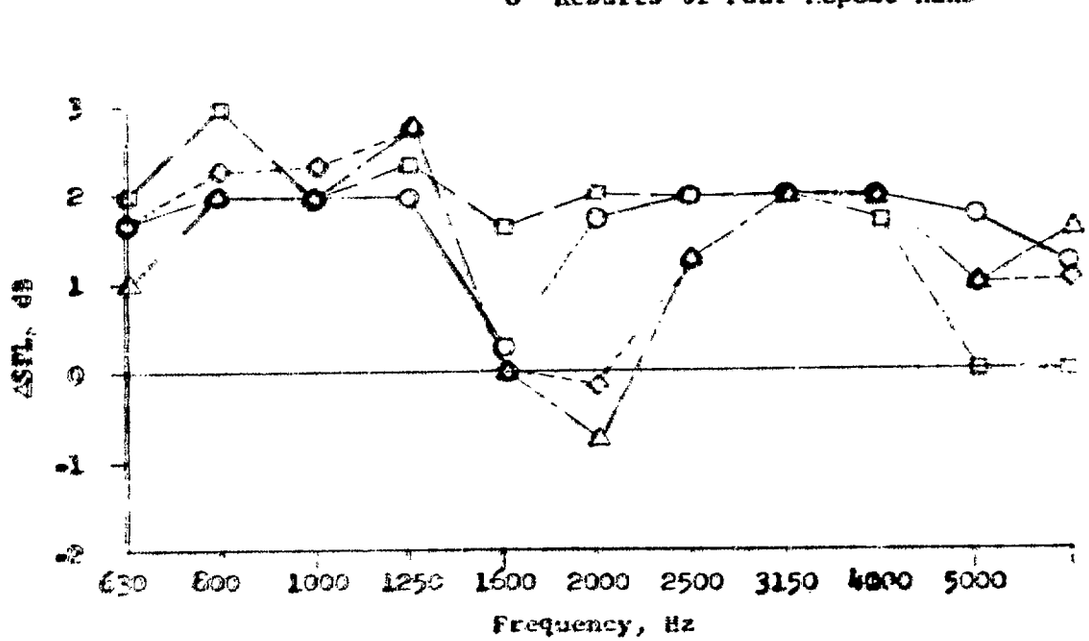


FIGURE VI.C.2-5 TIP SHROUD TREATMENT EFFECTIVENESS - 3 BLADE CHORD WIDTHS - WITHOUT IGV'S

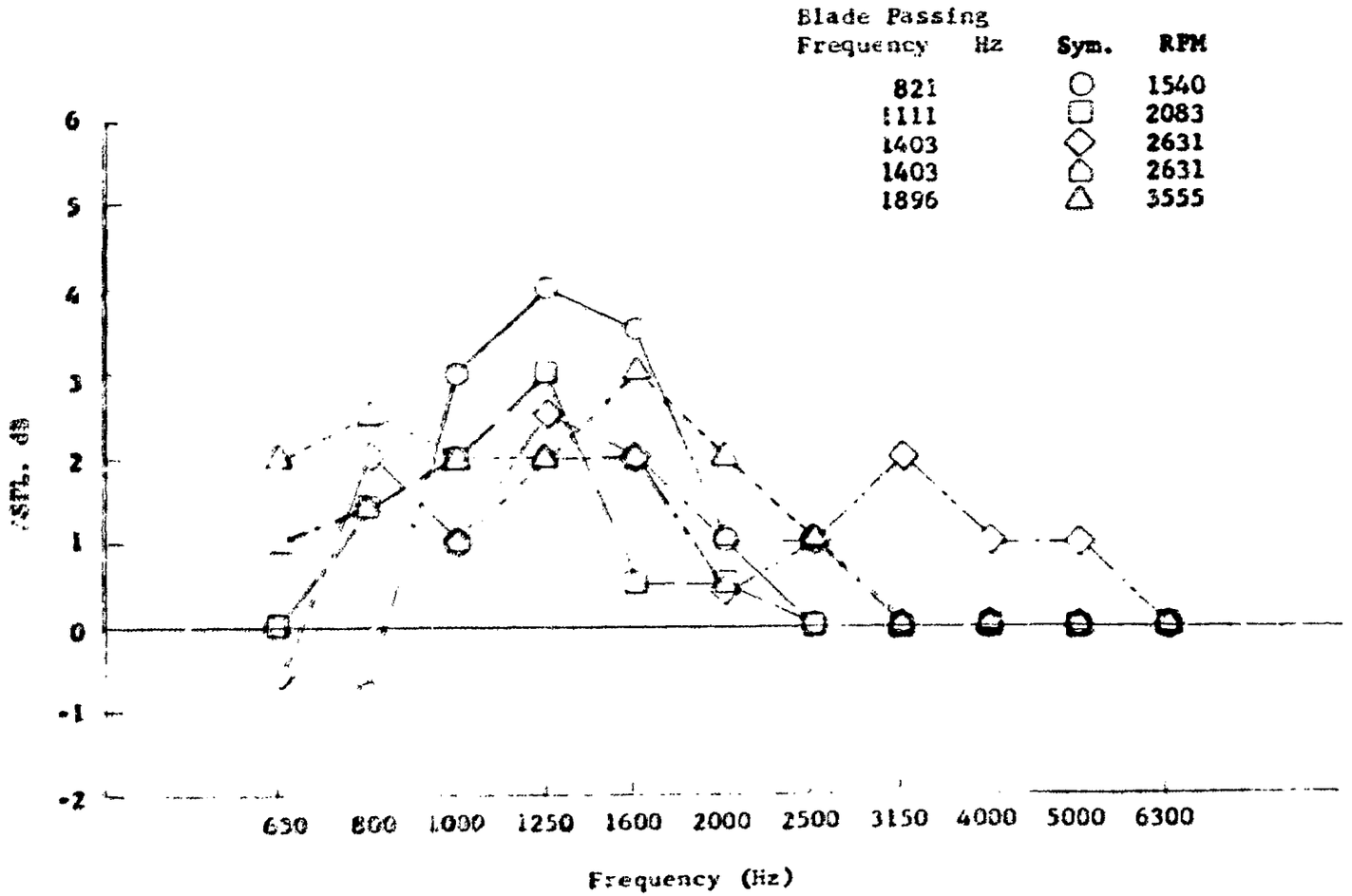


FIGURE VI.C.2-6 TIP SHROUD TREATMENT EFFECTIVENESS - SDOF OVER BLADE ROW ONLY

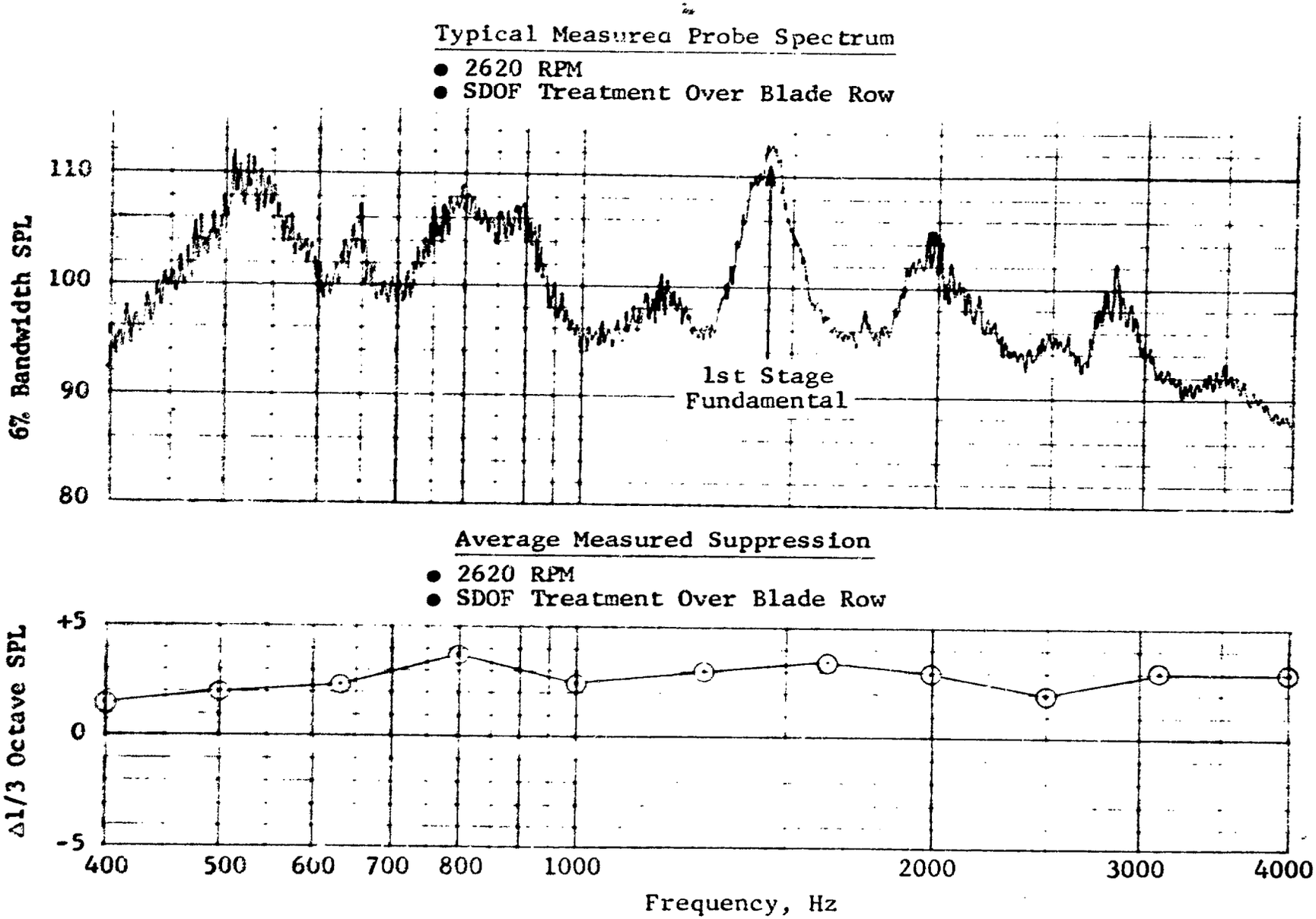


FIGURE VI.C.2-7 TIP SHROUD TREATMENT EFFECTIVENESS - NARROWBAND ANALYSIS & 1/3 OCTAVE BAND SUPPRESSION

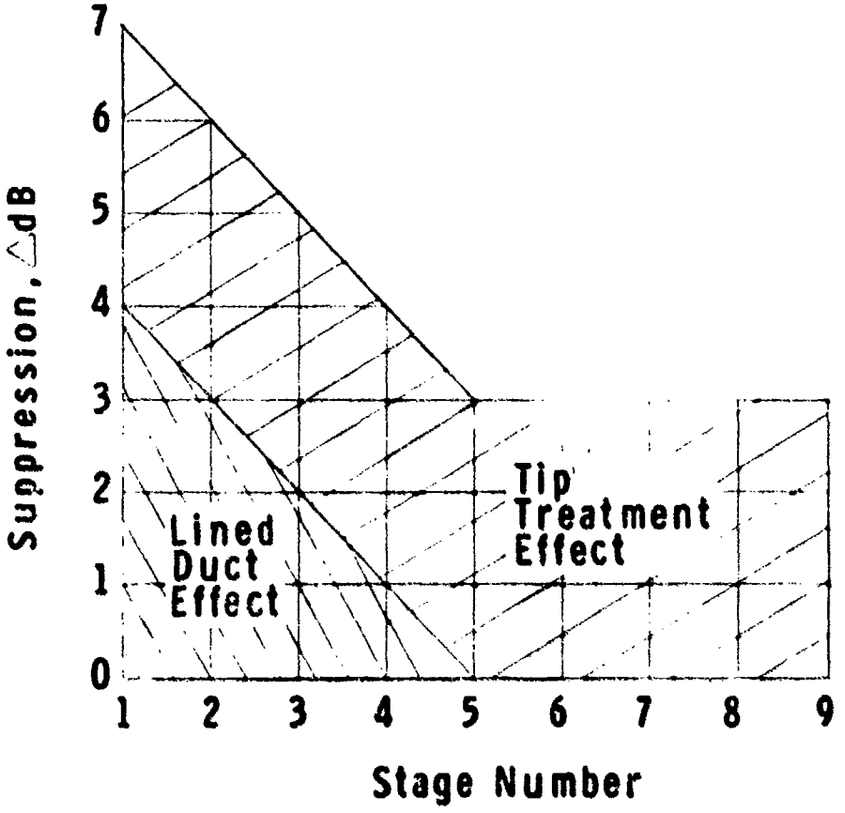


FIGURE VI.C.2-8 ESTIMATED GE4 TIP SHROUD SUPPRESSION

"PRECEDING PAGE BLANK-NOT FILMED."

VI.C.3 NOISE SOURCE IDENTIFICATION WITH DIRECTIONAL MICROPHONE ARRAY

"PRECEDING PAGE BLANK-NOT FILMED."

VI.C.3 NOISE SOURCE IDENTIFICATION WITH DIRECTIONAL MICROPHONE ARRAY

Test Objectives and Configuration

Another acoustic tool for turbomachinery analysis was introduced in the GE4 acoustic test series to help identify major turbomachinery noise source location. It is a directional microphone array, shown in Figure VI.C.3-1, consisting of a linear array of 14 one-inch Hewlett-Packard microphones. The microphones are mounted on an arc of 100 ft. radius on a 15 ft. beam. The array, with its related acoustic systems and recorder, is on a movable trailer. Positioning of the array is accomplished by aiming a sighting telescope at the anticipated noise source.

The array works on the principle of the phase relationship of acoustic signals approaching the microphones. When pointed at a particular noise source, the array will distinguish between this signal and signals of the same frequency arriving from an off-axis source. Data from all possible source locations are necessary to accurately determine the amplitude of the major source.

The array is designed so that it will have an effective frequency range of 2000 to 5000 Hz with a depth-of-field of $\pm$ 20 ft. and can discriminate between sources of equal magnitude separated by 3 ft. The array sensitivity versus off-axis angle is shown in Figure VI.C.3-2.

Use of the array of the GE4 was limited to two speed points of 85% and 95% with the inlet unchoked. The array was located at 110° and 130° to the inlet axis on a 100 ft. radius centered about the engine mid-point. The array was aimed at:

- 5 ft. forward of the Boeing inlet lip
- Boeing inlet lip
- Inlet blow-in doors
- Cowling opposite stage 1 compressor
- Cowling opposite turbine mid-point
- TSEN blow-in doors
- Exhaust D_9
- 5, 10, and 15 ft. aft of D_9

Presentation of Test Results

A typical analysis of the resultant data is presented in Figure VI.C.3-3 showing 50 Hz bandwidth pure tone SPL's and their relation to generation sources along the engine. The symbols are actual measurements and the lines are the data corrected to eliminate the contribution from off-axis major lobes.

Results show that compressor first stage fundamental and harmonics radiate primarily from the area of the Boeing inlet blow-in doors and from off-axis major lobes.

Results show that compressor first stage fundamental and harmonics radiate primarily from the area of the Boeing inlet blow-in doors and from the cowling opposite the compressor first stage. A detailed analysis of measurements for identification of all source locations was not completed.

Conclusions

- By use of specialized acoustic tools, source locations can be pinpointed and their relative contribution to the engine far field acoustic signature can be established.

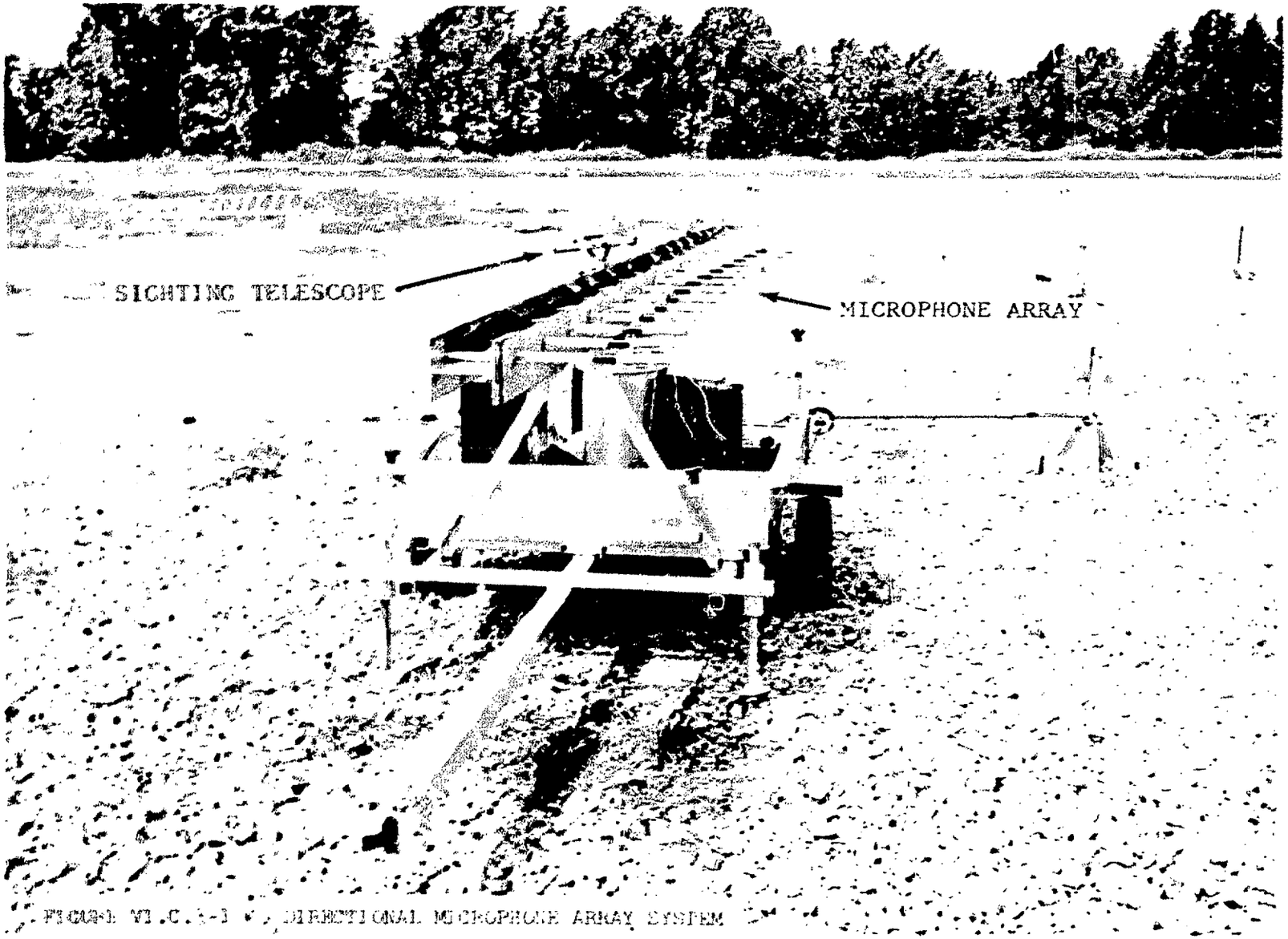


FIGURE VI.C.3-1 DIRECTIONAL MICROPHONE ARRAY SYSTEM

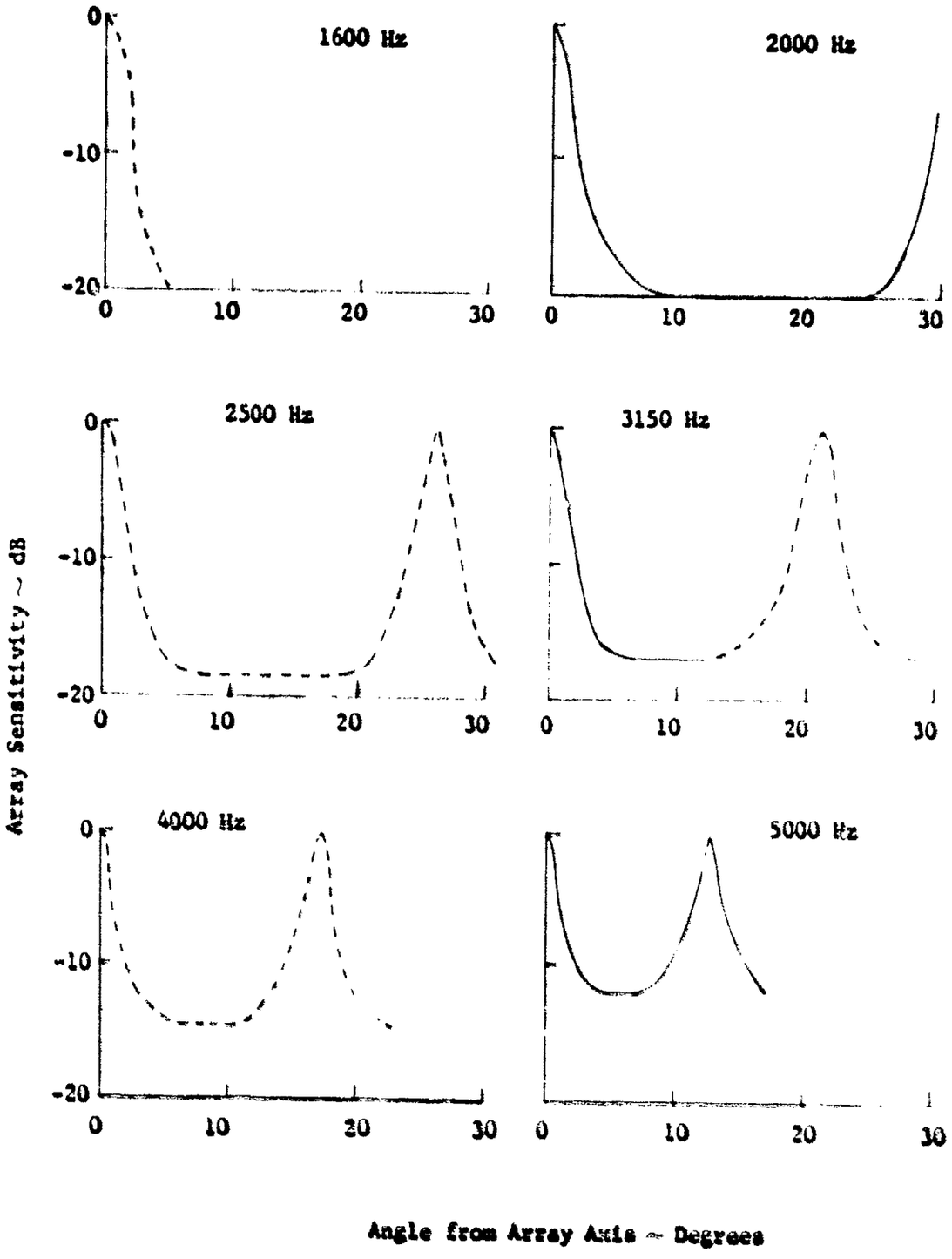


FIGURE VI.C.3-2 BEAM PATTERNS OF DIRECTIONAL ACOUSTIC ARRAY

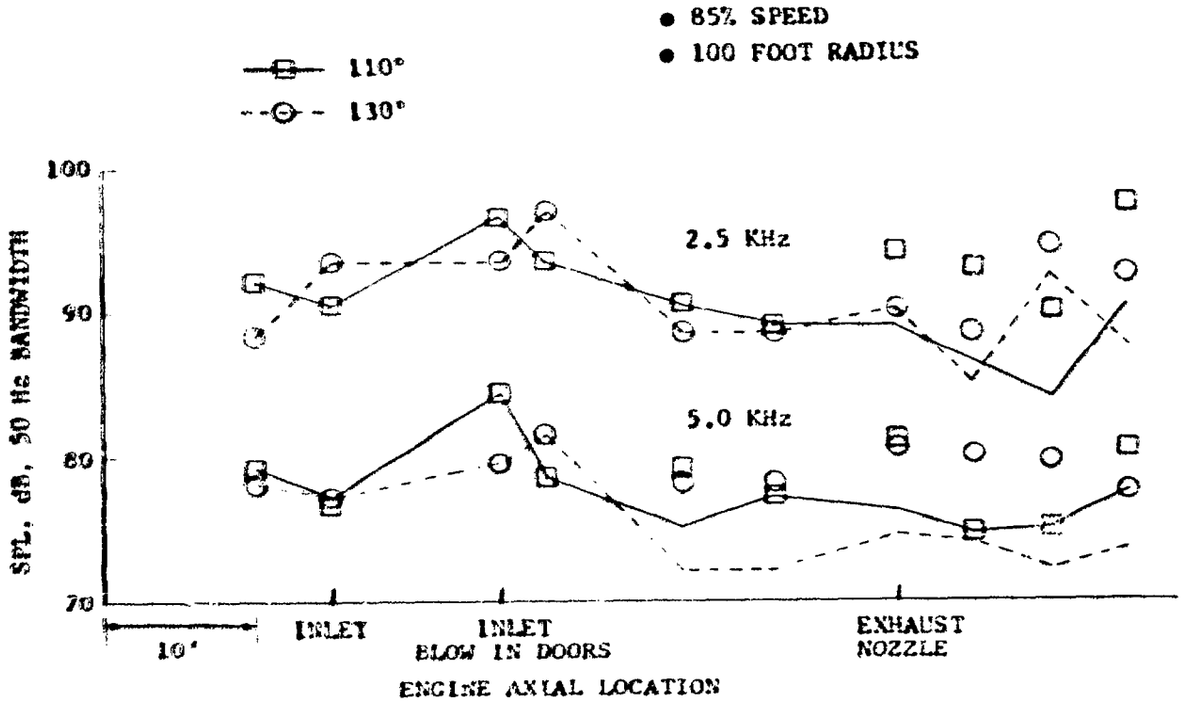


FIGURE VI.C.3-3 GE4 FIRST STAGE COMPRESSOR TONE SOURCE LOCATIONS

"PRECEDING PAGE BLANK-NOT FILMED."

VI.C.4 J79 TURBOMACHINERY NOISE TEST

"PRECEDING PAGE BLANK-NOT FILMED."

VI.C.4 J79 TURBOMACHINERY NOISE TEST

Test Objectives and Configuration

As an aid in evaluating the relative magnitudes of casing transmitted and exhaust duct propagated turbomachinery noises, a test series using a J79 engine was conducted. The test vehicle was permanently fitted with a CJ805-23 core inlet suppressor (See Figure VI.C.4-1) to eliminate, as much as possible, the forward propagated noise emanating through the inlet. The exhaust nozzle was a large fixed area (613 in^2) conical nozzle, designed to lower the exhaust velocity and hence jet noise, allowing the aft propagated turbomachinery noise to dominate over the jet noise. A long annular acoustically lined exhaust duct was used prior to the exhaust nozzle for two configurations with half-length acoustic treatment and full-length acoustic treatment. For half-length treatment, solid sheet stainless steel was used to cover one-half of the duct suppressor treatment, effectively eliminating the treatment in the covered area. A shorter, non-annular, non-treated duct was used for the baseline engine configuration, (see Figure VI.C.4-1).

Acoustic instrumentation consisted of: a) radial traversing acoustic probes mounted at planes 2, 5 and 7; b) a series of casing microphones spaced 6 inches from the casing; c) a near field array of 32 microphones arranged in four rows of 8 microphones, each with 6 ft. spacings; and d) far field microphones on a 150 ft. arc at 10° intervals from 0° to 160° from the inlet axis. The test vehicle and acoustic instrumentation, as set up at Edwards Air Force Base, are shown in Figure VI.C.4-2.

Presentation of Test Results

The plane 5 and 7 acoustic probes were used to determine the effectiveness of the exhaust suppressor in lowering aft propagated turbomachinery noise. The magnitude of casing transmitted turbomachinery noise was gauged by comparing far field suppression to duct suppression. Through use of the near field microphone array and narrowband data reduction, tone contours were generated which aided in identifying turbomachinery noise sources and their propagation paths to the far field.

In Figure VI.C.4-3 the 200 ft. sideline peak PNdB for the J79 is plotted against jet velocity for the untreated, half-treated, and fully treated duct configurations. Comparison is also made to predicted jet noise using the SAE procedure. There is 3.5 to 6 PNdB reduction in noise between the baseline and fully suppressed configurations, but there is very little difference between the full and one-half suppressor configurations. Figure VI.C.4-4 presents far field 1/3 octave band power level reductions using half and fully treated exhaust ducts referenced to the untreated duct. It also presents the probe measured duct power level reductions and the predicted level of duct treatment effectiveness based on scale model acoustic tests in a heated duct.

Predicted and measured duct suppression levels agreed well at high frequency for both full and half treated exhaust ducts at length to height ratios of 6 and 3. Comparing the far field and duct measured PNL suppressions shows the level of turbomachinery noise suppression experienced in the far field was not near that of the level measured within the duct. This indicates that sources other than aft duct propagated turbomachinery noise, namely casing transmitted noise, contributed to the far field acoustic levels.

Figure VI.C.4-5 shows a typical far field 40 Hz narrowband analysis of the baseline, full suppressor, and half treated suppressor at 120°, the maximum sideline PNdB angle, corrected for atmospheric attenuation. The suppression curve, relative to the untreated duct is also shown. Additional suppression gain in the far field from one-half to full length ducts is not near the level anticipated from probe measurements.

Figure VI.C.4-6 is a comparison of 40 Hz narrowband analyses from: a) a strain gage mounted to the combustor casing; and b) a microphone located at the same axial plane and spaced 6" away from the casing. From the comparison it is evident that the casing is highly pure tone excited from the engine turbomachinery and that many of these same high frequency tones are strongly transmitted to the surrounding near field.

To substantiate accuracy of the near field method of contour plotting as an aid in identifying the noise sources, the tone generated by the radial bevel gear in the external gearbox was analyzed. Figure VI.C.4-7 shows constant level contours obtained from the near field array from 40 Hz narrowband

analysis. The source of the tone is identified by an X on the schematic, located in the back of a dolly wheel, thus the double lobe in contours. Baseline versus suppressed contours are unchanged except by wind shift, indicating the method of analysis will identify tone source locations. Applying the technique to a turbomachinery source is done typically in Figure VI.C.4-8.

The 15th and 17th compressor stages of 121 blades each, in combination, generate an internal tone which is identifiable in the 150 foot arc far field narrowbands. Analysis of their near field baseline and suppressed contours, at an engine speed of 6893 rpm and tone frequency of 13,900 Hz, shows a predominant shift toward the internal source location when the jet suppressor is added. This indicates casing transmission is a strong secondary noise source, and that near field method of analysis will be a good aid in identifying magnitudes and sources of turbomachinery noise.

Conclusions

- The J79 engine, as tested, provided a useful vehicle for turbomachinery noise investigation.
- Reduction of aft propogated turbomachinery noise through use of duct acoustic treatment was effective within the duct; however, far field noise levels were not equivalently lowered. This indicates casing radiated turbomachinery noise was of a sufficient level to influence far field measurements.
- Near field tone contour plotting proved a valuable aid in determining primary sources of turbomachinery noise and its propagation paths to the far field.
- The analysis technique was established which would be applied to CF4 acoustic measurements planned, using engine 435-007 at the Peebles test facility.

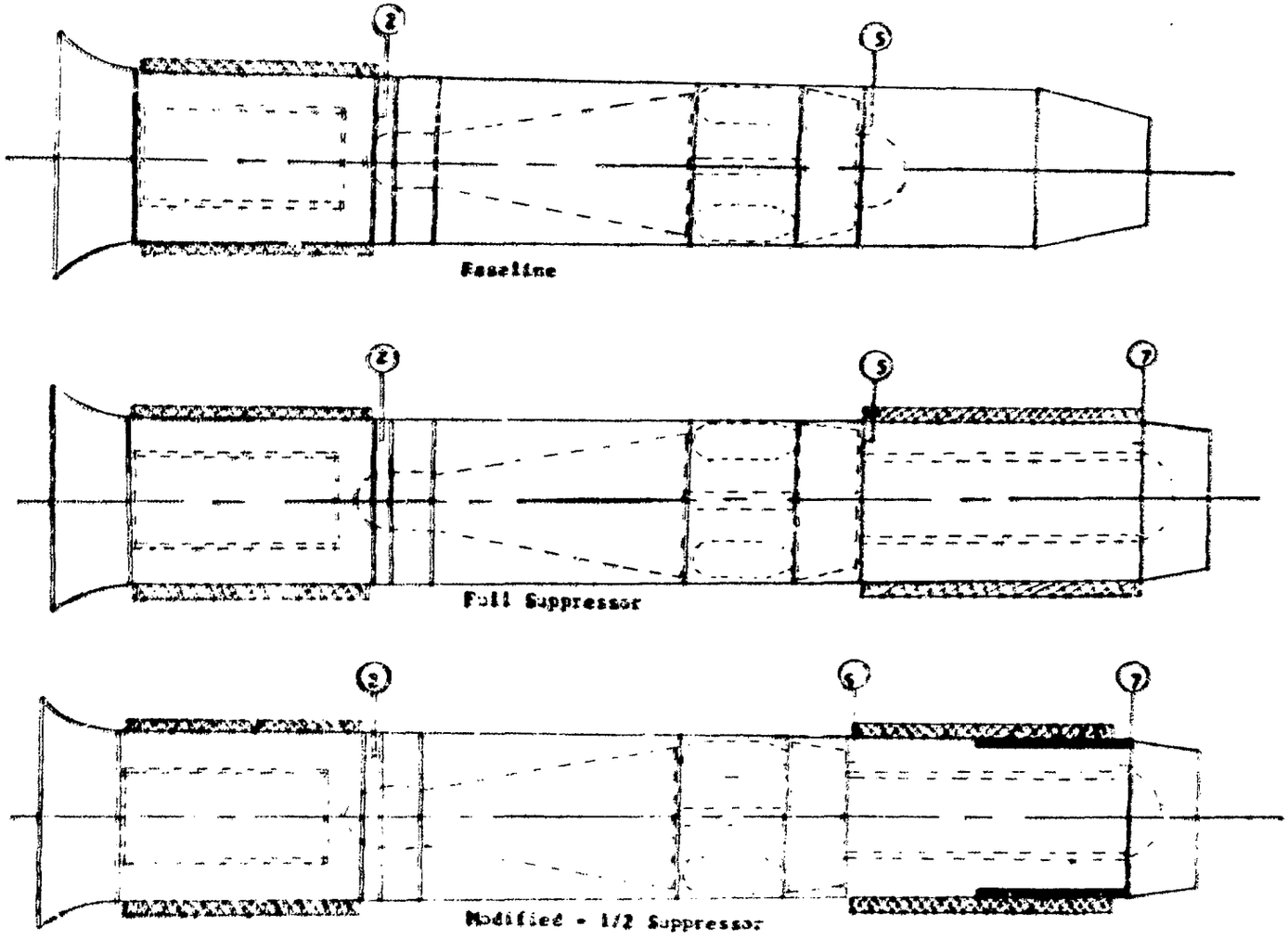


FIGURE VI.C.4-1 SCHEMATIC OF J79 TURBOMACHINERY NOISE TEST VEHICLE

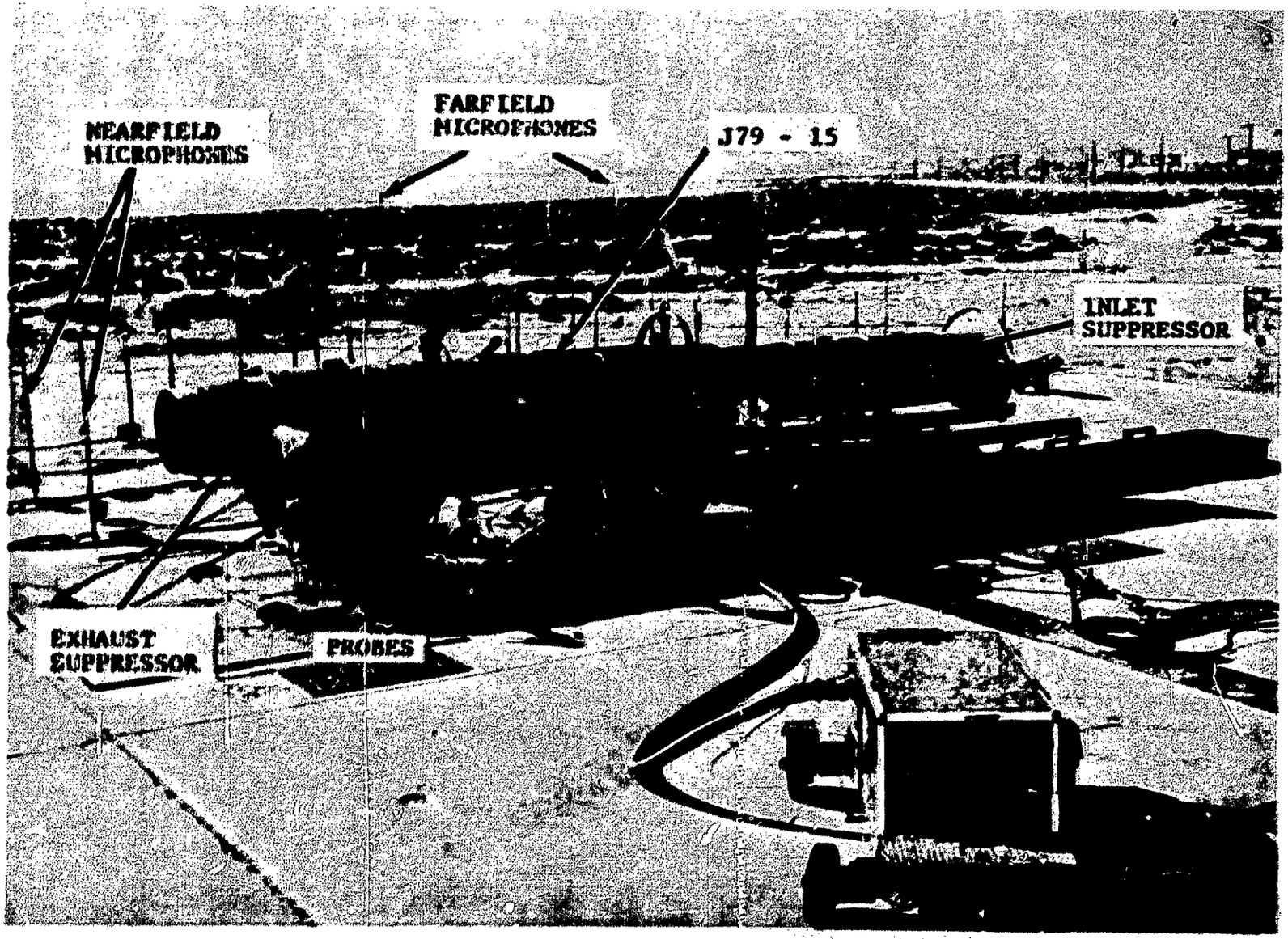


FIGURE VI.C.4-2 J79-15 NEAR/FAR FIELD TURBOMACHINERY NOISE TEST

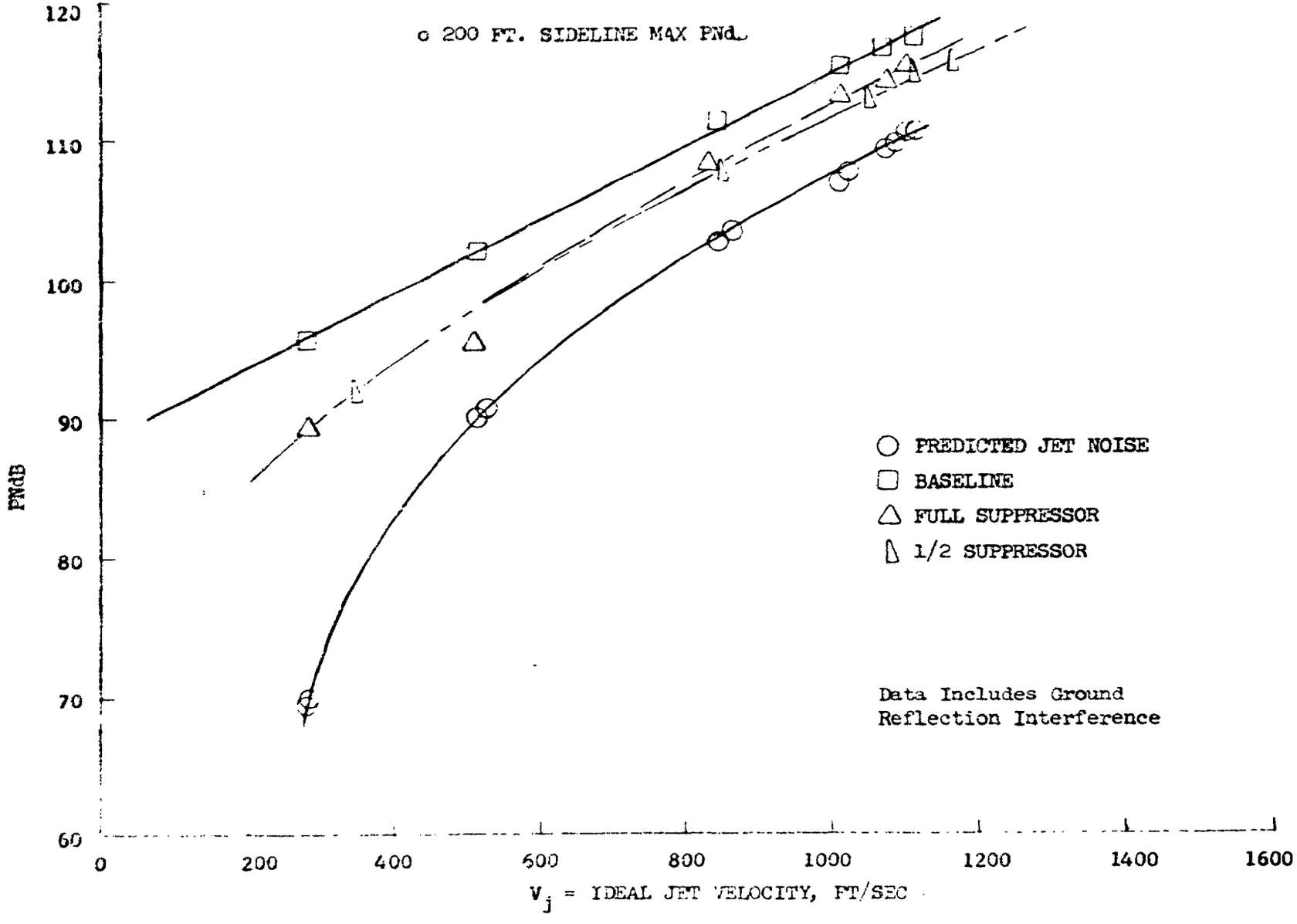
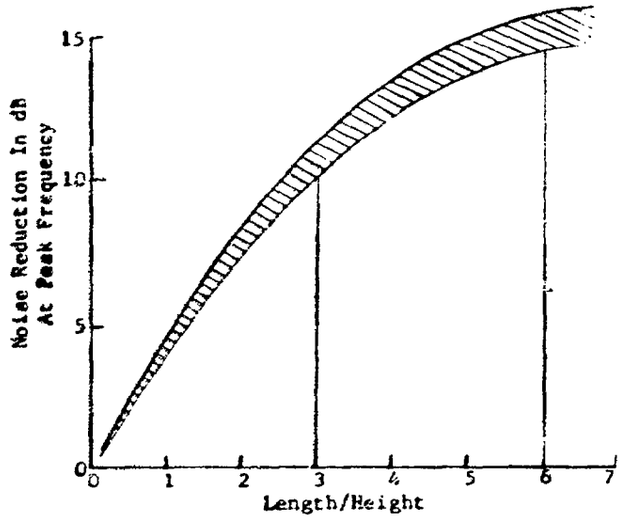
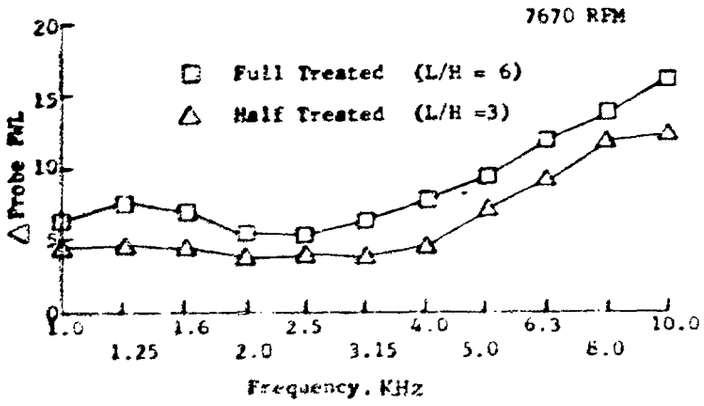


FIGURE VI.C.4-3 COMPARISON OF MEASURED AND PREDICTED J79 PERCEIVED NOISE LEVELS



ACOUSTIC DUCT DATA

Temperature	1000 F
Velocity	750 Ft/Sec
Duct Height	8 Inches
Panel Depth	1.5 Inches
Peak Frequency	10,000 Hz
Mach No.	.41



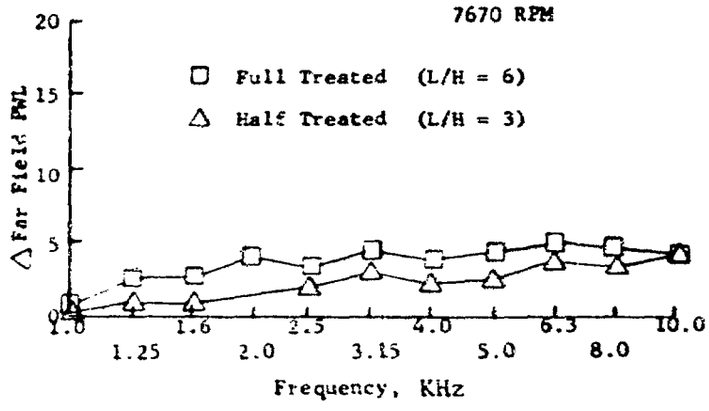


FIGURE VI.C.--- 379 TURBOMACHINERY NOISE SUPPRESSOR PERFORMANCE - FAR FIELD & DUCT SOUND POWER LEVEL REDUCTIONS

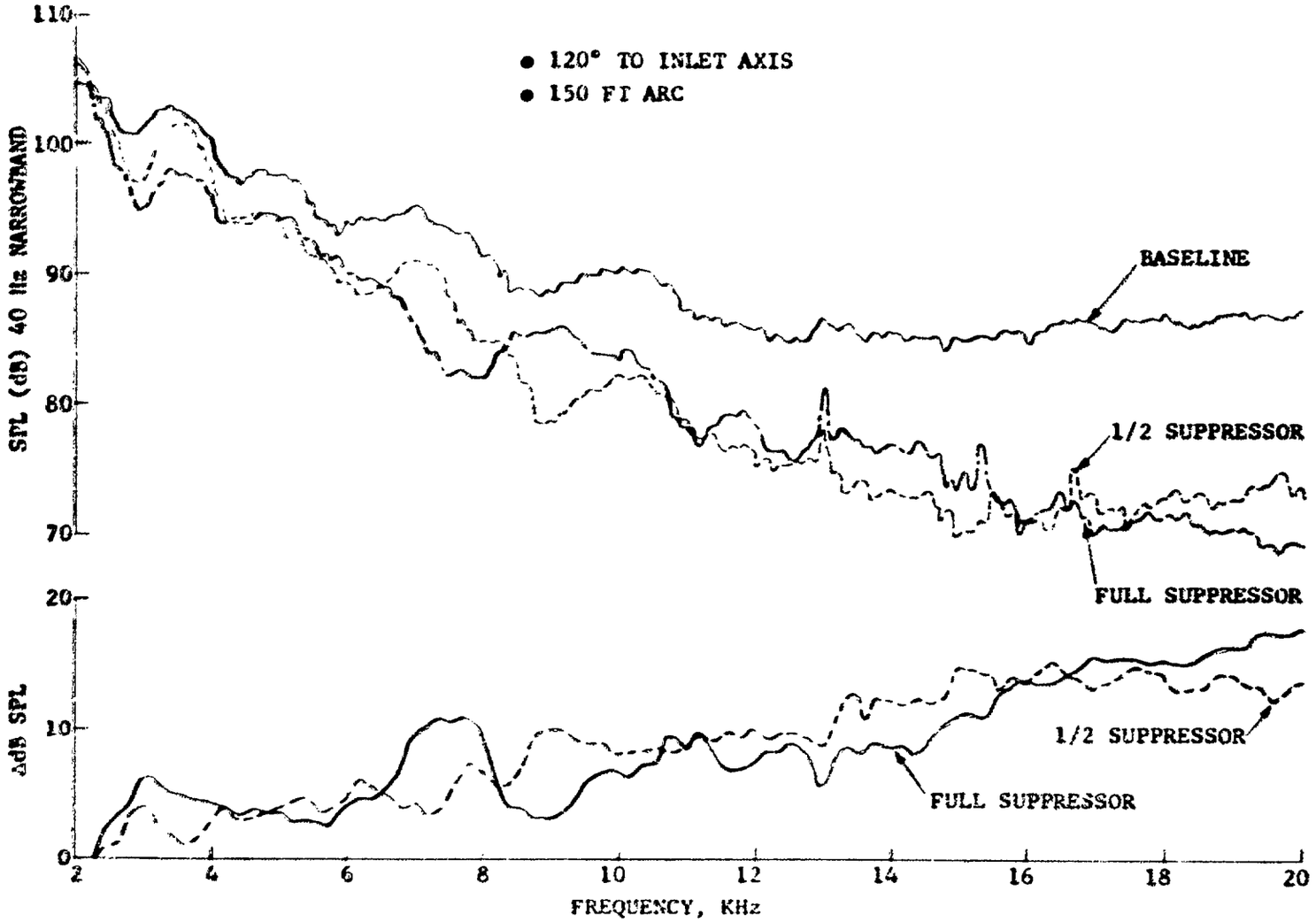


FIGURE VI.C.4-5 J79 TURBOMACHINERY NOISE SUPPRESSOR PERFORMANCE - NARROWBAND ANALYSIS

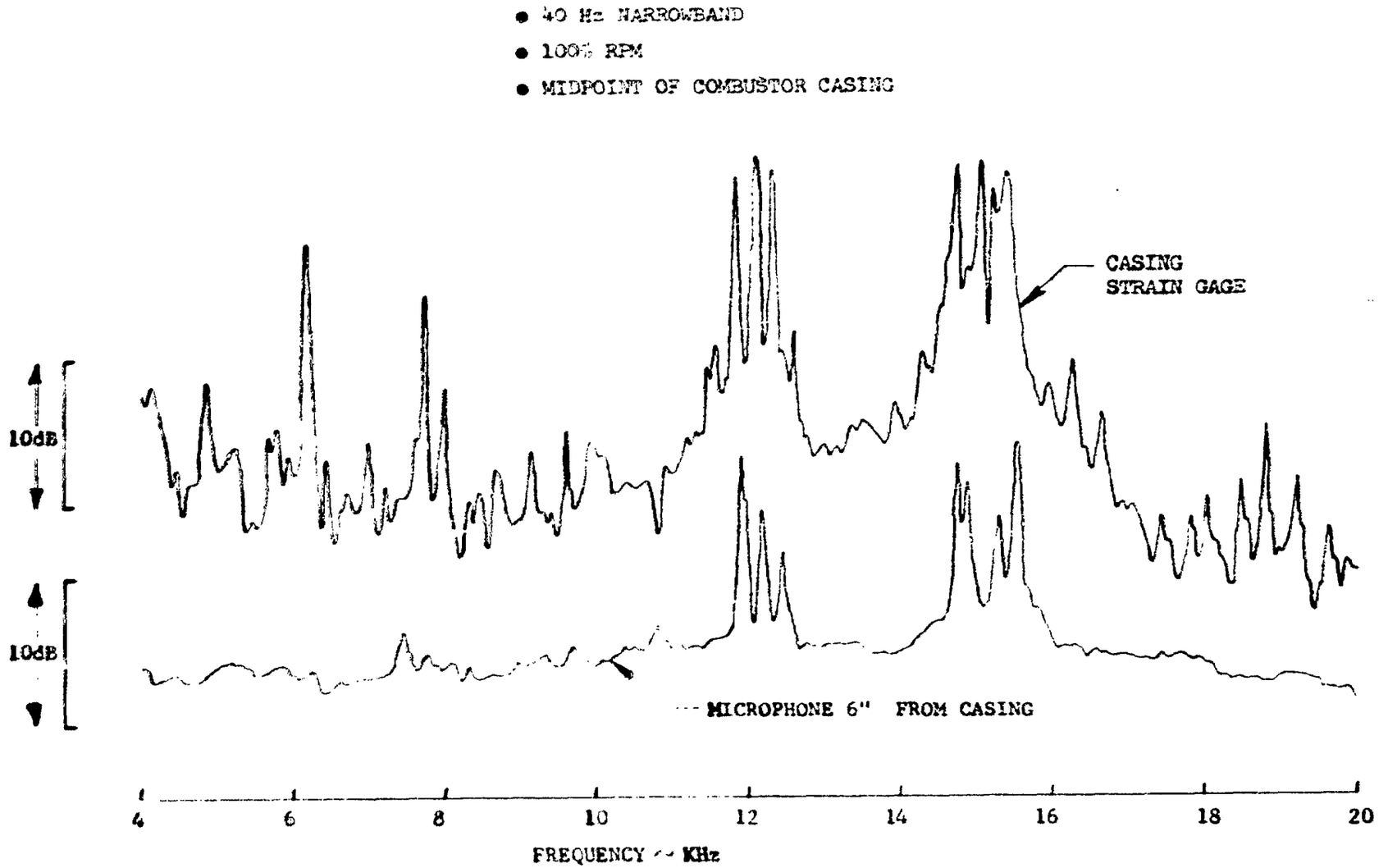


FIGURE VI.C.4-6 COMPARISON OF J79 CASING STRAIN GAGE AND MICROPHONE SPECTRA

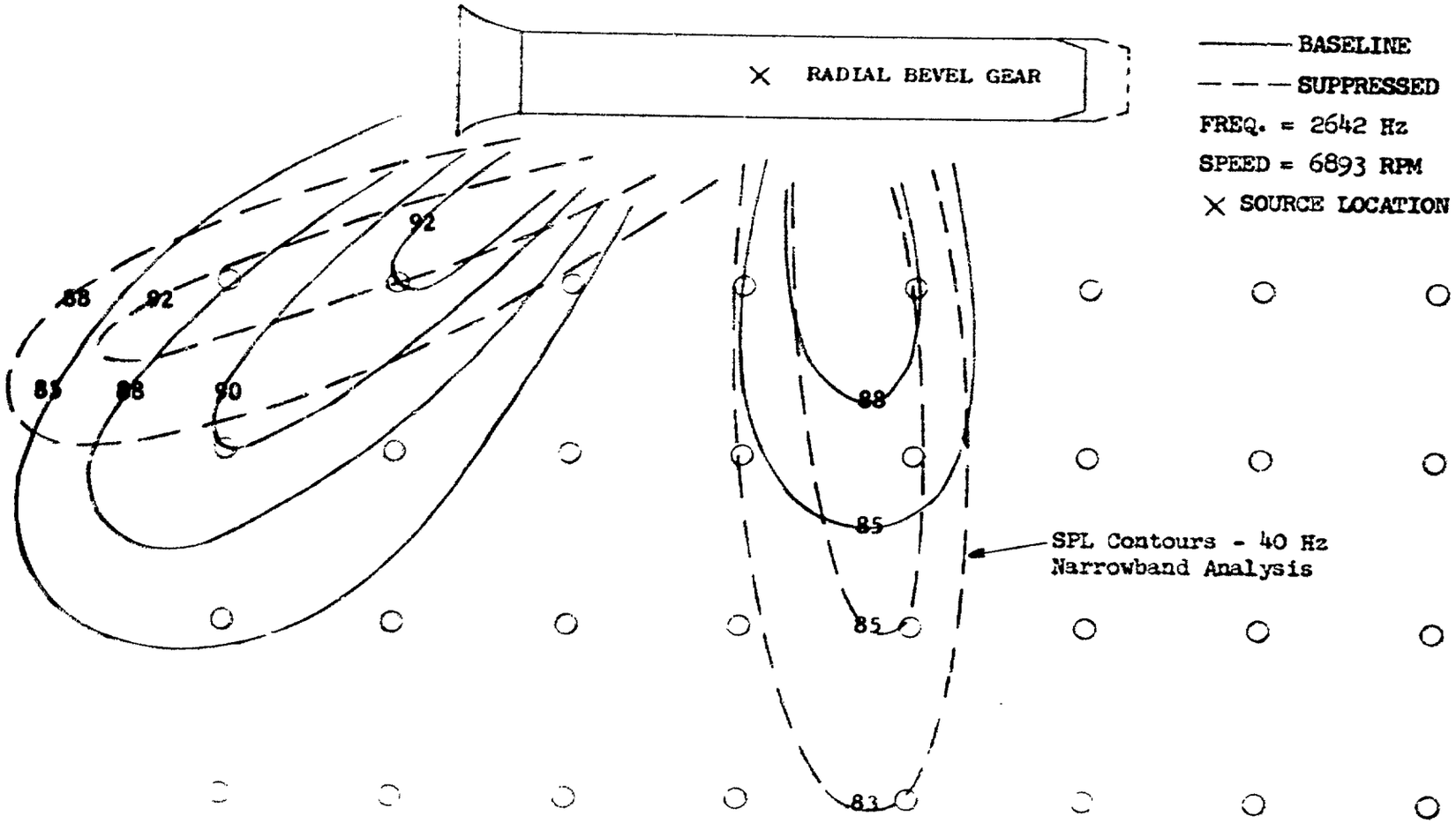


FIGURE VI.C.4-7 NEAR FIELD ARRAY NOISE CONTOURS OF TONE FROM RADIAL BEVEL GEAR

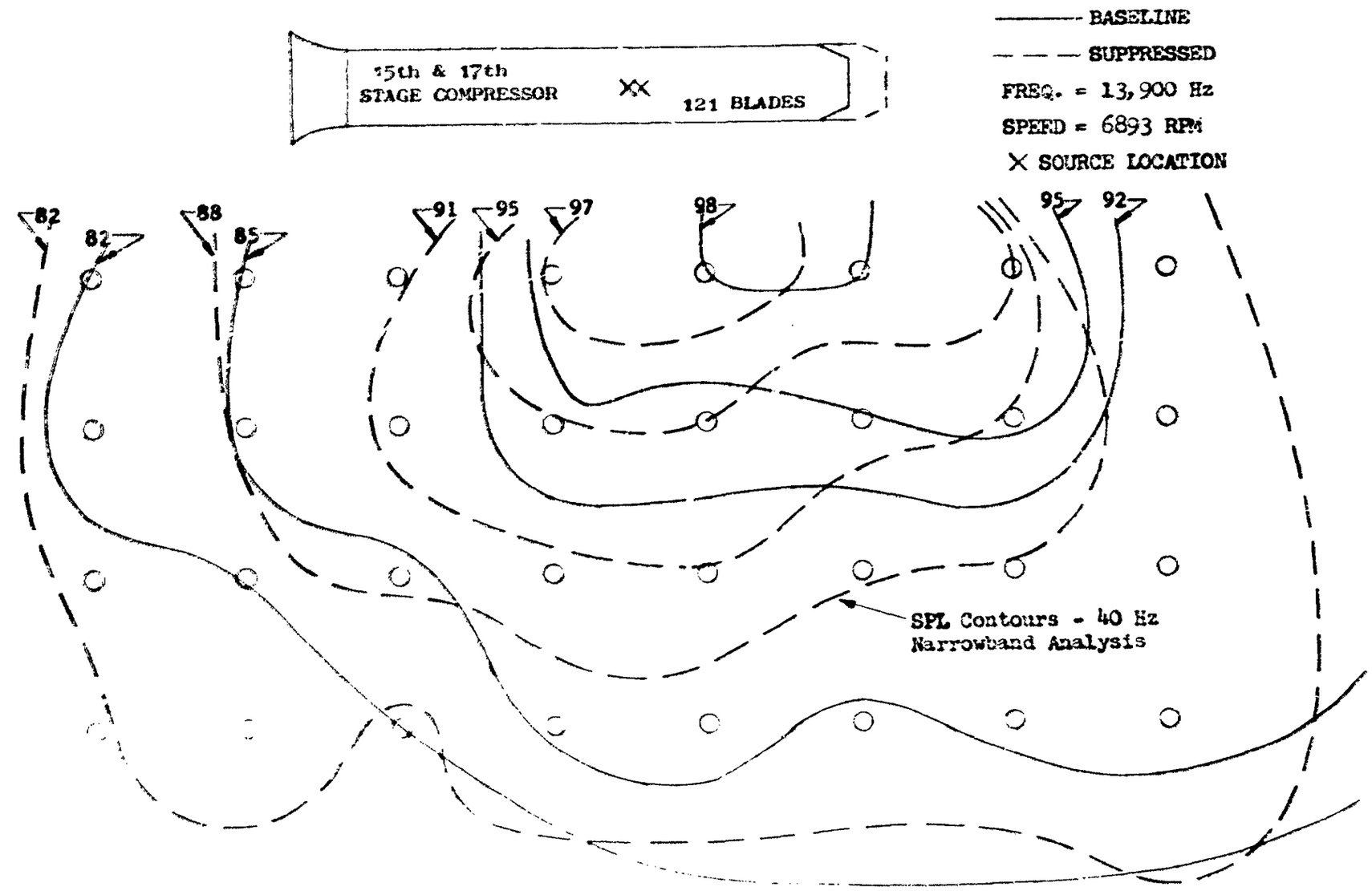


FIGURE VI.C.4-8 NEAR FIELD ARRAY NOISE CONTOURS OF TONE FROM 15th & 17th COMPRESSOR STAGES

"PRECEDING PAGE BLANK-NOT FILMED."

VI.C.5 GE4 ENGINE 435-007 NEAR AND FAR FIELD ACOUSTIC MEASUREMENTS

"PRECEDING PAGE BLANK-NOT FILMED."

VI.C.5 GE4 ENGINE 435-007 NEAR AND FAR FIELD ACOUSTIC MEASUREMENTS

Test Objectives and Configuration

For an initial investigation of turbomachinery noise characteristics of the Flight Test Status (FTS) engine, as well as for far field acoustic status, engine 435-007 was tested at Peebles Pad 4D as per Figure VI.C.5-1. The test also fulfilled the objective of establishing the aircraft environmental noise levels. To accomplish these objectives, the acoustic array consisted of the following:

- The normal far field array of microphones on the 250 ft. arc centered on the engine axis at plane 8, at 10° intervals, from 0° to 160° from the inlet axis.
- Twenty-one near field microphones in a matrix designed to help identify predominant noise source locations on the engine and their propagation paths to the far field.
- Fourteen near/far field microphones in a pattern specified by Boeing to identify aircraft environmental noise levels.
- Five near field microphones within the close proximity of the engine casing, located to identify major casing propagated pure tones and their levels.
- Plane 2 acoustic probe within the inlet annulus to identify engine-internal forward-propagated pure tone levels. (Results of the probe measurements were discussed in Section VI.C.1 COMPRESSOR SOURCE NOISE IDENTIFICATION WITH ACOUSTIC PROBES.)

Presentation of Test Results

All of the data acquired was reduced and partially analyzed before SST contract termination in March, 1971; however, detailed analysis to fulfill all of the initial goals was not completed. The initial analysis did show good results which are presented herein.

For far field acoustic measurements, both the normal (open) and loiter A_8 cycle schedules were followed. The 250 ft. arc noise measurements were

extrapolated to the 300 ft. sideline and are compared to SAE predictions in Figure VI.C.5-2. The data show good agreement with SAE in the predominant jet noise region with the exception of high jet velocity, where engine 435-007 levels were slightly lower. Typically the divergence from SAE due to turbomachinery noise occurred at jet velocities below 1400 to 1500 ft/sec.

FTS engine 435-007 noise levels are compared to Block I measurements on engines 002 and 003 in Figure VI.C.5-3. The normalized measurements agree well, again with the exception of high jet velocity, where the FTS levels were slightly under the Block I average.

Directivity and spectra comparisons of FTS and Block I data are shown in Figures VI.C.5-4 through -9. At high and low jet velocities, agreement is quite favorable showing almost identical noise characteristics. At high jet velocity (Figures VI.C.5-4 and -6) the minor differences in Block I and FTS noise levels occurs mainly at the angles of maximum noise, whereas at low jet velocity (Figure VI.C.5-8) the peak noise levels are the same but the variance at other angles is larger. Spectral characteristics do shift somewhat due to variance in ground effects and turbomachinery blading but, in general, acoustic agreement between the two engines is very good.

The measurements do point out that, at low and intermediate jet velocities, the turbomachinery generated noise will be a major problem in the FTS engine. To exemplify the variance of turbomachinery noise content with engine speed, Figure VI.C.5-10 presents far field 110°, 20 Hz bandwidth, narrowband plots at 79, 88, and 98% corrected speeds. At low speed, all compressor and turbine stage fundamentals were present and predominant. However, they tended to become masked by the overriding jet noise as speed increased, and were unidentifiable at high engine speed. Figure VI.C.5-11 exemplifies the change in noise levels between the normal (open) and loiter A_8 schedules at the same engine speed. The compressor/turbine tones and broadband turbine noise levels were of the same magnitude, while the jet noise was reduced considerably at the lower jet velocity, larger A_8 nozzle setting.

The near field microphone array was used to generate contour plots of fundamental tones, serving as visual aids in identifying predominant modes

of pure tone radiation from the engine and their respective propagation paths to the far field. Typical plots are shown in Figure VI.C.5-12 and -13 for fundamental tones of the compressor 9th stage and turbine 2nd stage. The contours show both tones had predominant sources within the exiting jet stream, with the possibility of casing radiation adding significantly to that prime source.

Figure VI.C.5-14 typifies results from the microphones located within near proximity of the engine casing. Significance of this data is that the compressor casing microphone was picking up forward stages compressor tones through the casing, the combustor microphone had a predominant stage 9 compressor tone, and the plane 5.8 microphone exhibited high turbine tone levels. At low rpm the acoustic levels were of sufficient magnitude where contribution to the far field noise levels was considered possible.

In a similar test with GE4 engine 435-004, acoustic measurements were taken with and without an engine cowling while microphones were located approximately 6" from the nearest casing or cowling surface. Figure VI.C.5-15 shows the casing radiated high frequency noise substantially lowered by the addition of the engine cowling. Low frequency noise, not expected to be internally generated or casing transmitted, is essentially unaltered. Readings at various engine speeds were taken and the magnitude of reduction seems fairly consistent and independent of speed. Figure VI.C.5-15 data presentation is at 85% speed.

In response to the Boeing Company's request for aircraft environmental noise levels, acoustic measurements were taken at all the microphone locations in Figure VI.C.5-1 for: 1) idle, 2) 100% rpm, 3) max dry, and 4) partial reheat settings. Figures VI.C.5-16 through -19 define typical overall sound pressure levels at each measuring station for the four cycle points.

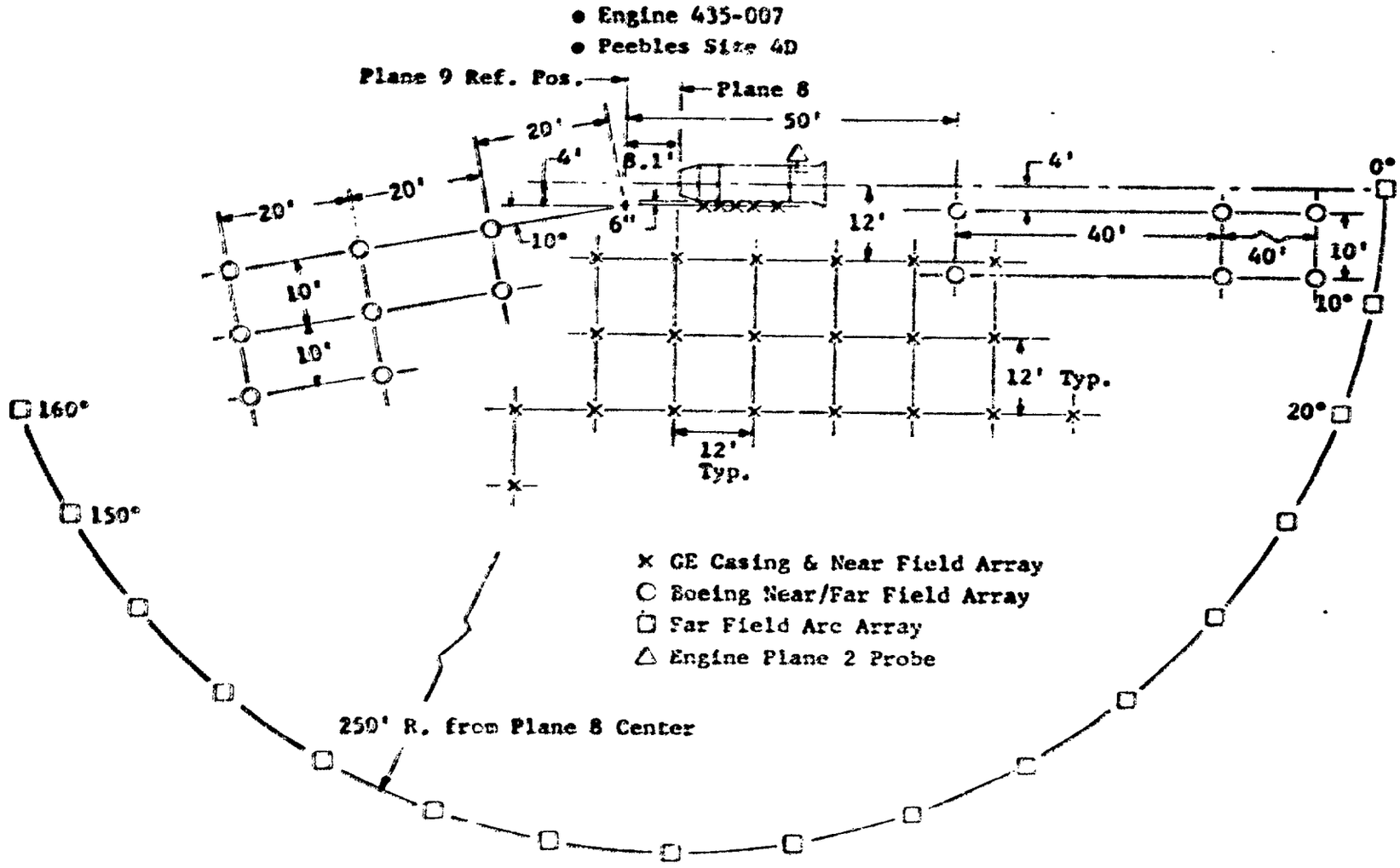


FIGURE VI.C.5-1 GE4 ACOUSTIC MICROPHONE ARRAY

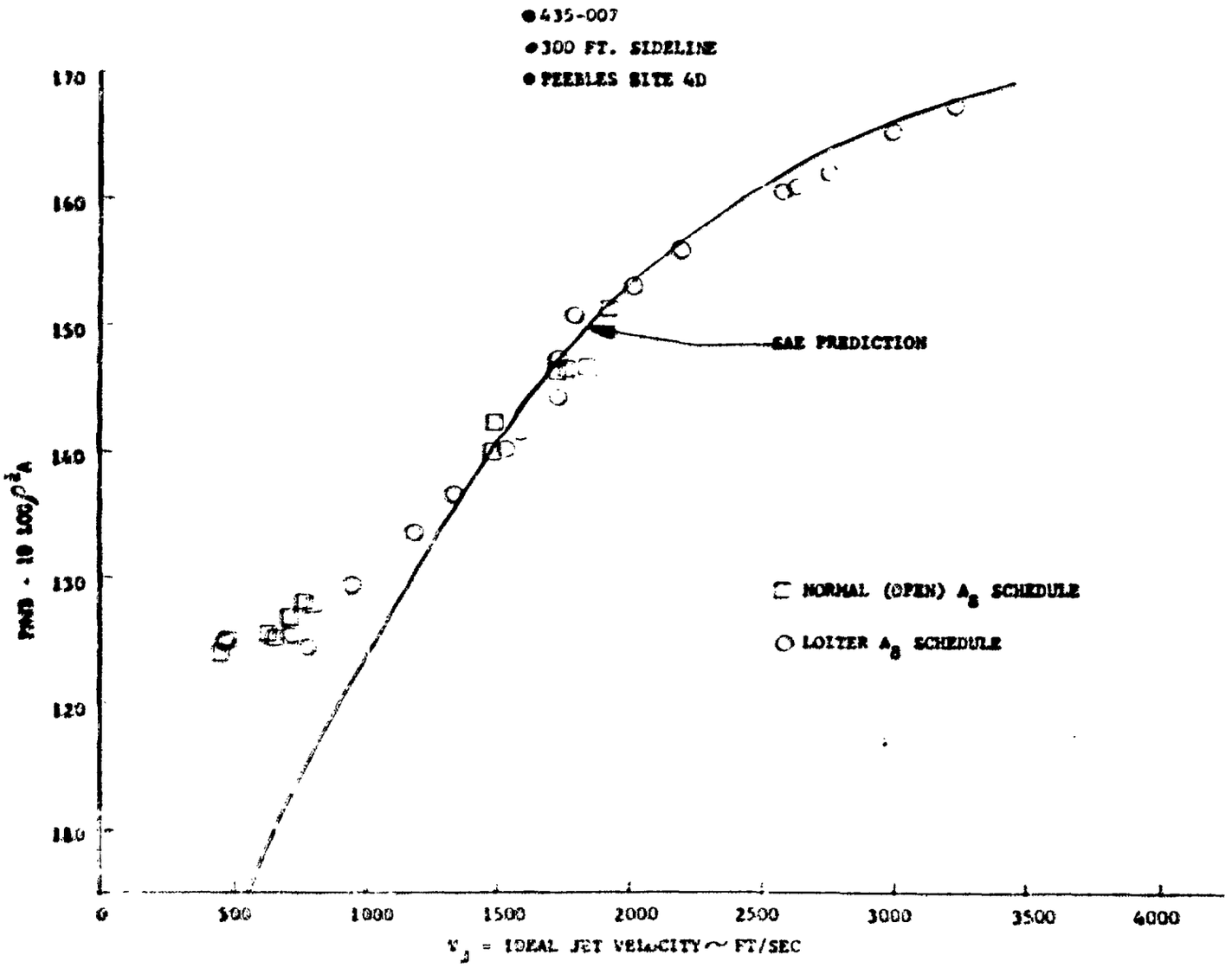


FIGURE VI.C.5-2 GE4 FTS ENGINE FAR FIELD NOISE LEVELS

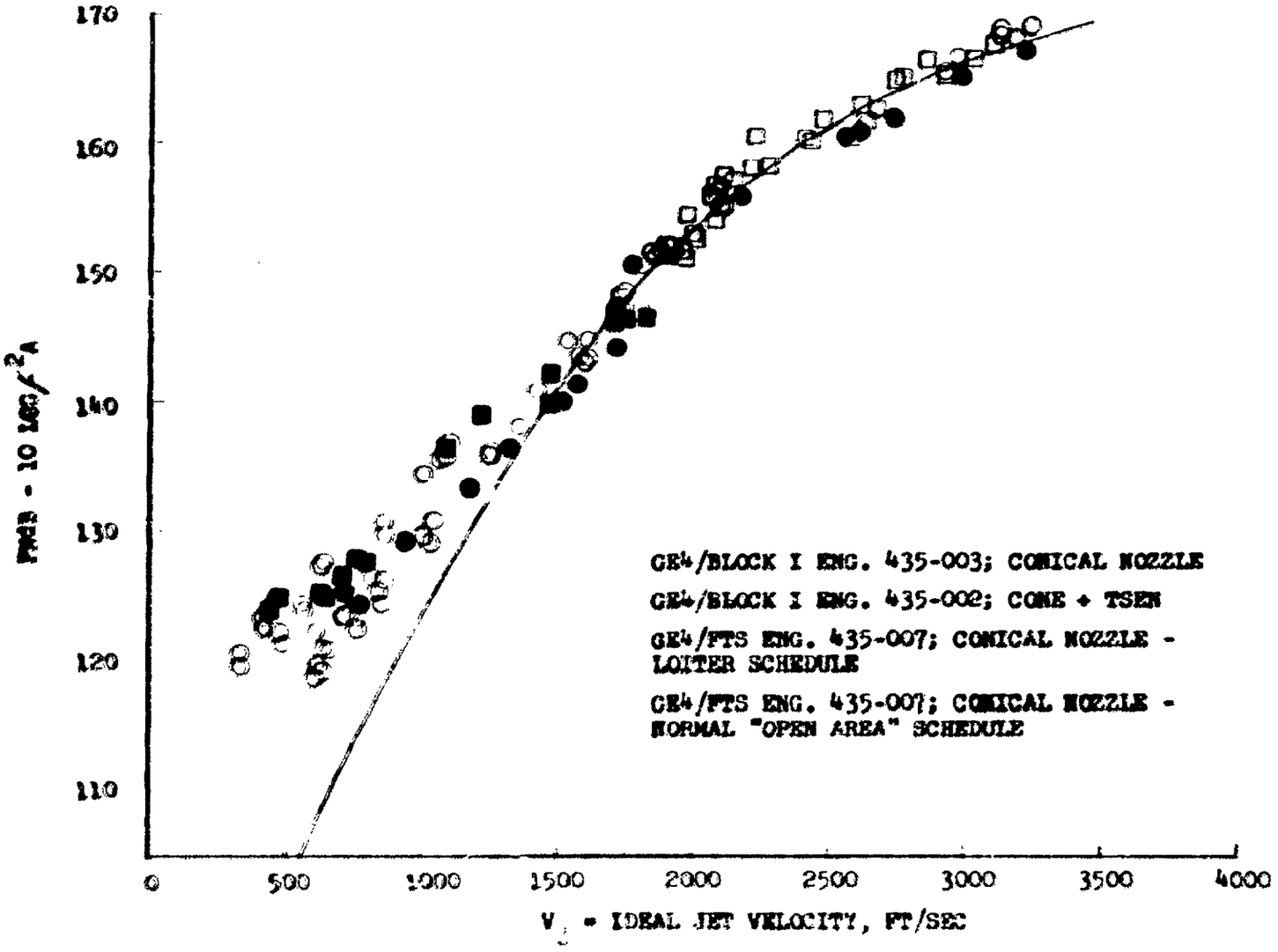


FIGURE VI.C.5-3 COMPARISON OF GE4 BLOCK I & FTS ENGINE FAR FIELD NOISE LEVELS

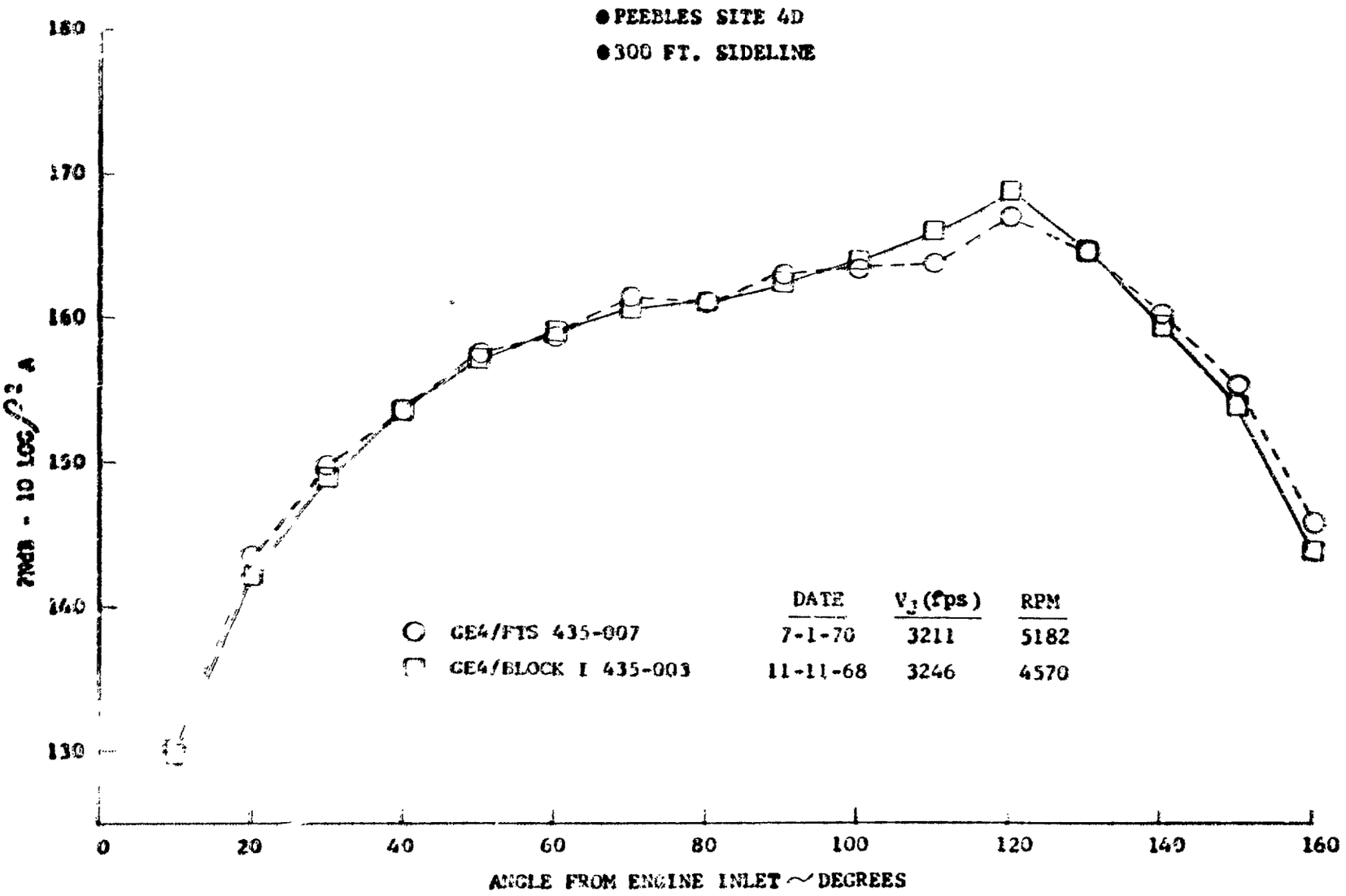


FIGURE VI.C.5-4 GE4 BLOCK I & FTS DIRECTIVITY COMPARISON AT HIGH JET VELOCITY

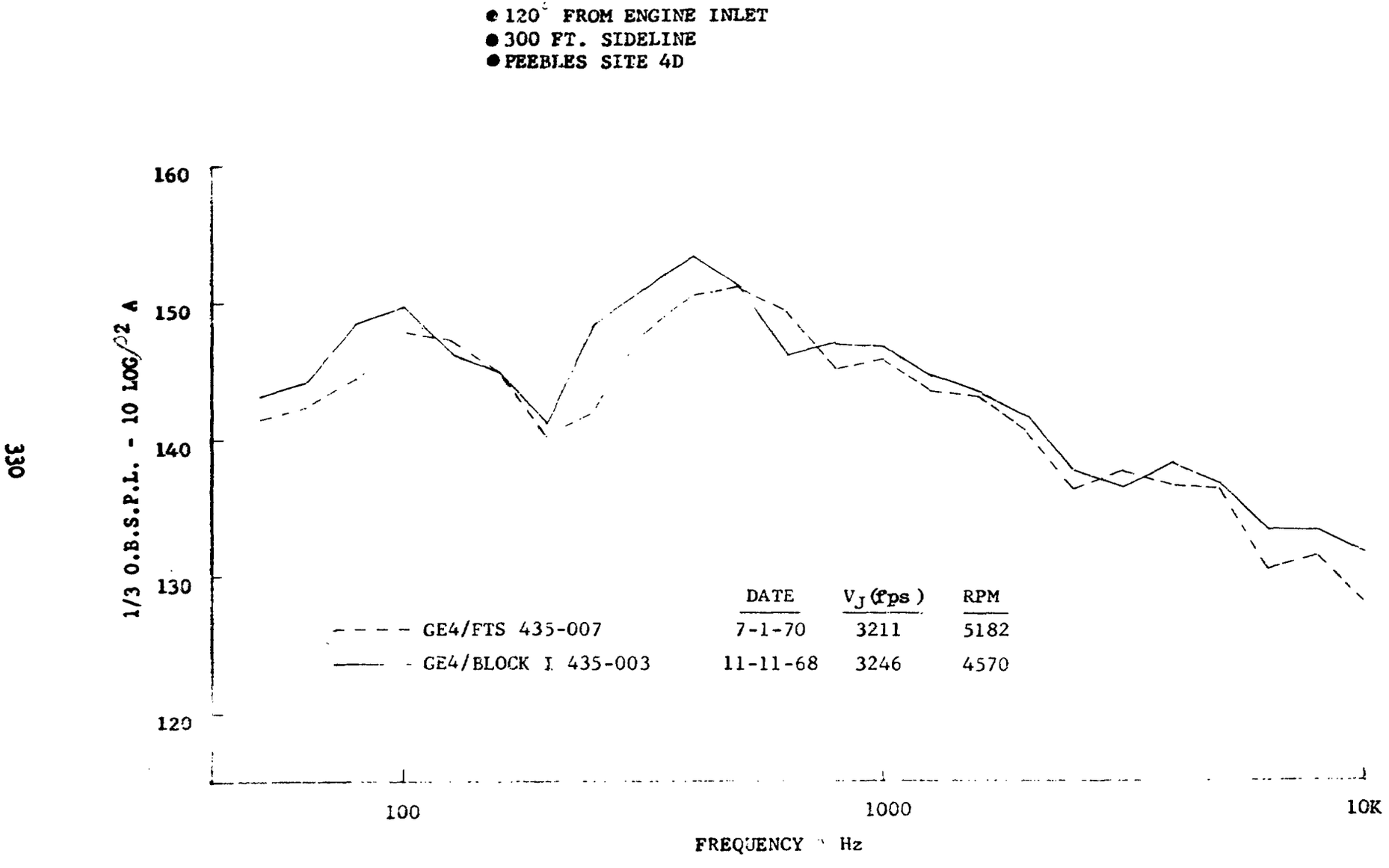


FIGURE VI.C.5-5 GE4 BLOCK I & FTS SPECTRA COMPARISON AT HIGH JET VELOCITY

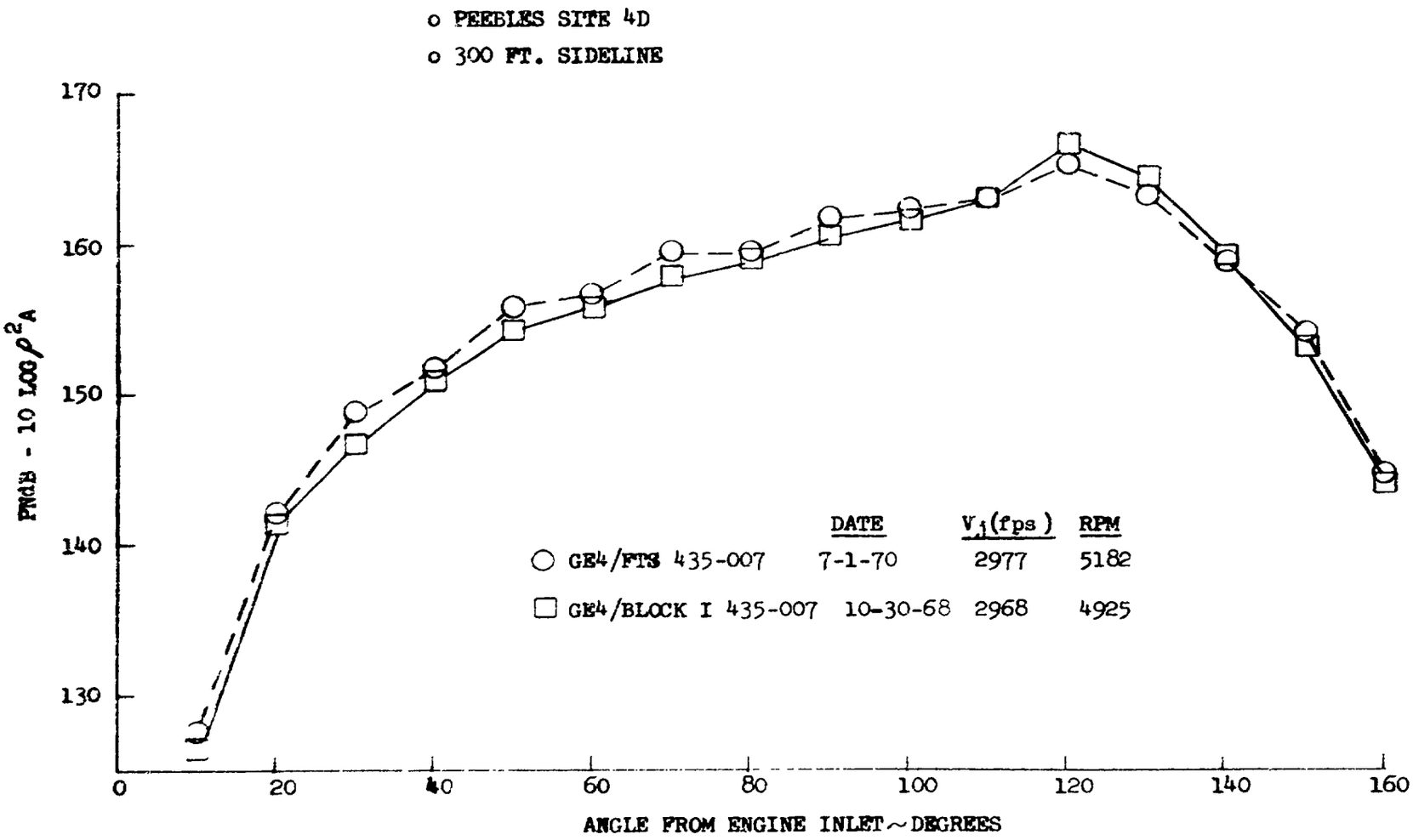


FIGURE VI.C.5-6 GE4 BLOCK I & FTS DIRECTIVITY COMPARISON AT HIGH JET VELOCITY

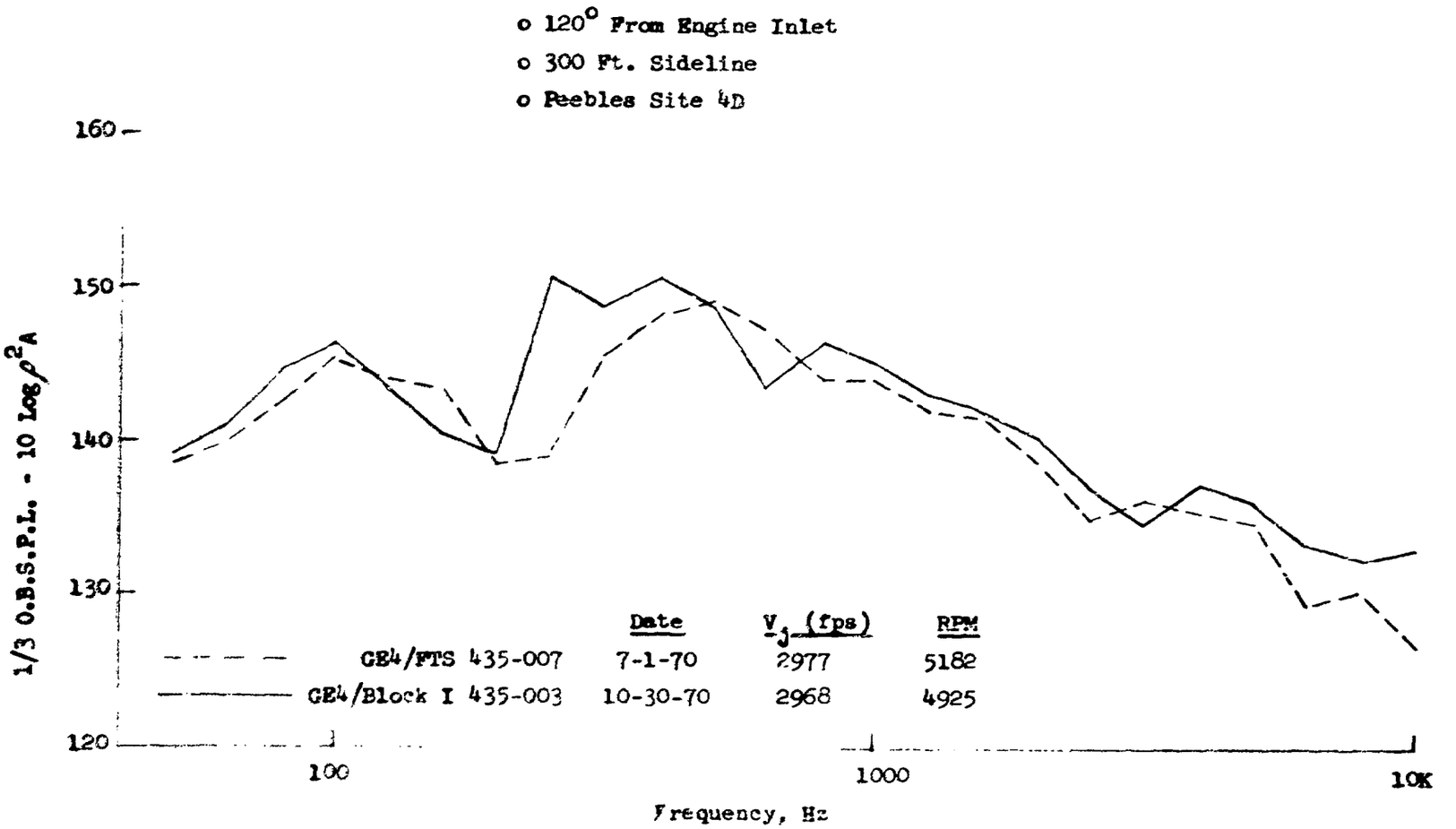


FIGURE VI.C.5-7 GE4 BLOCK I & FTS SPECTRA COMPARISON AT HIGH JET VELOCITY

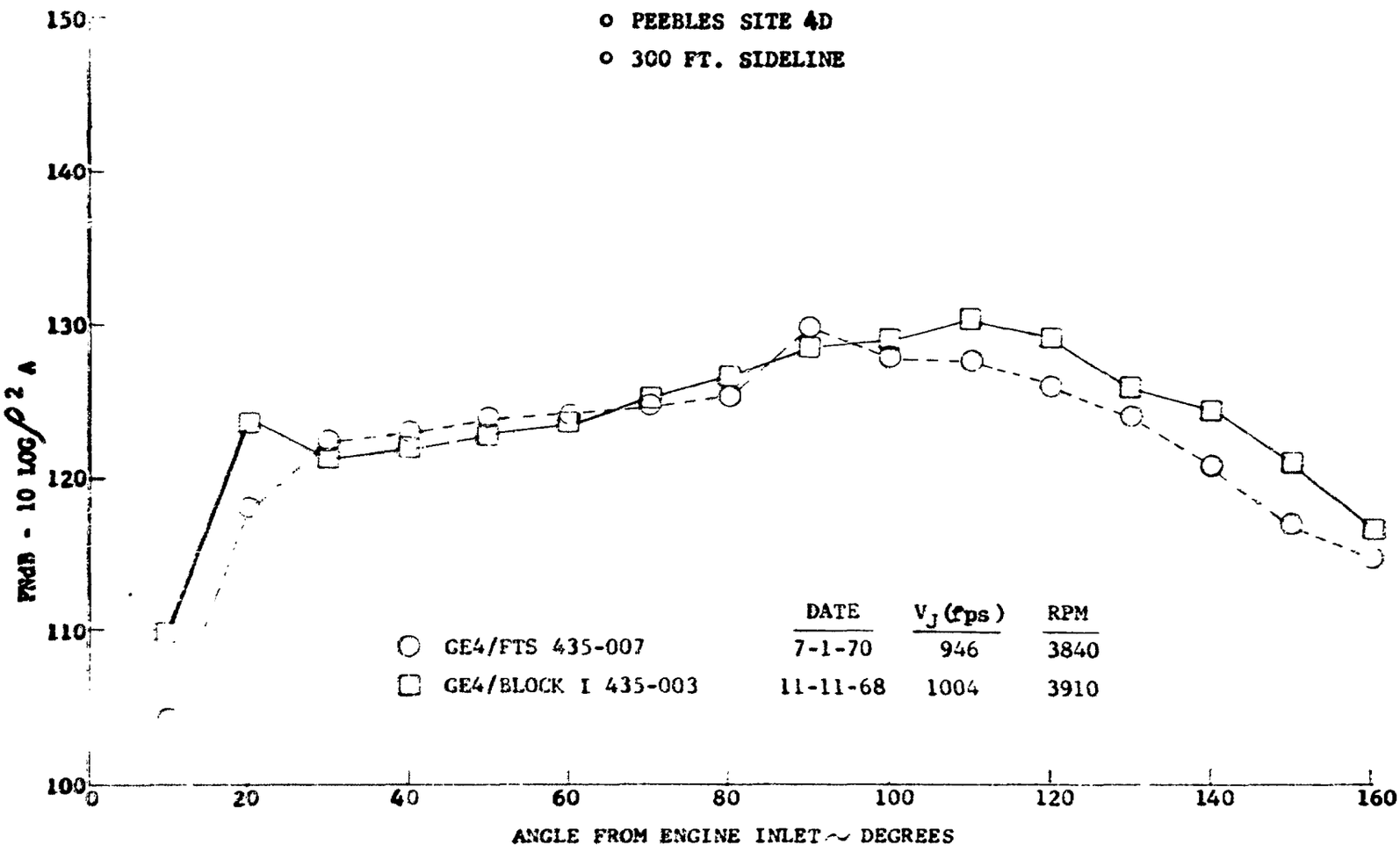


FIGURE VI.C.5-8 GE4 BLOCK I & FTS DIRECTIVITY COMPARISON AT LOW JET VELOCITY

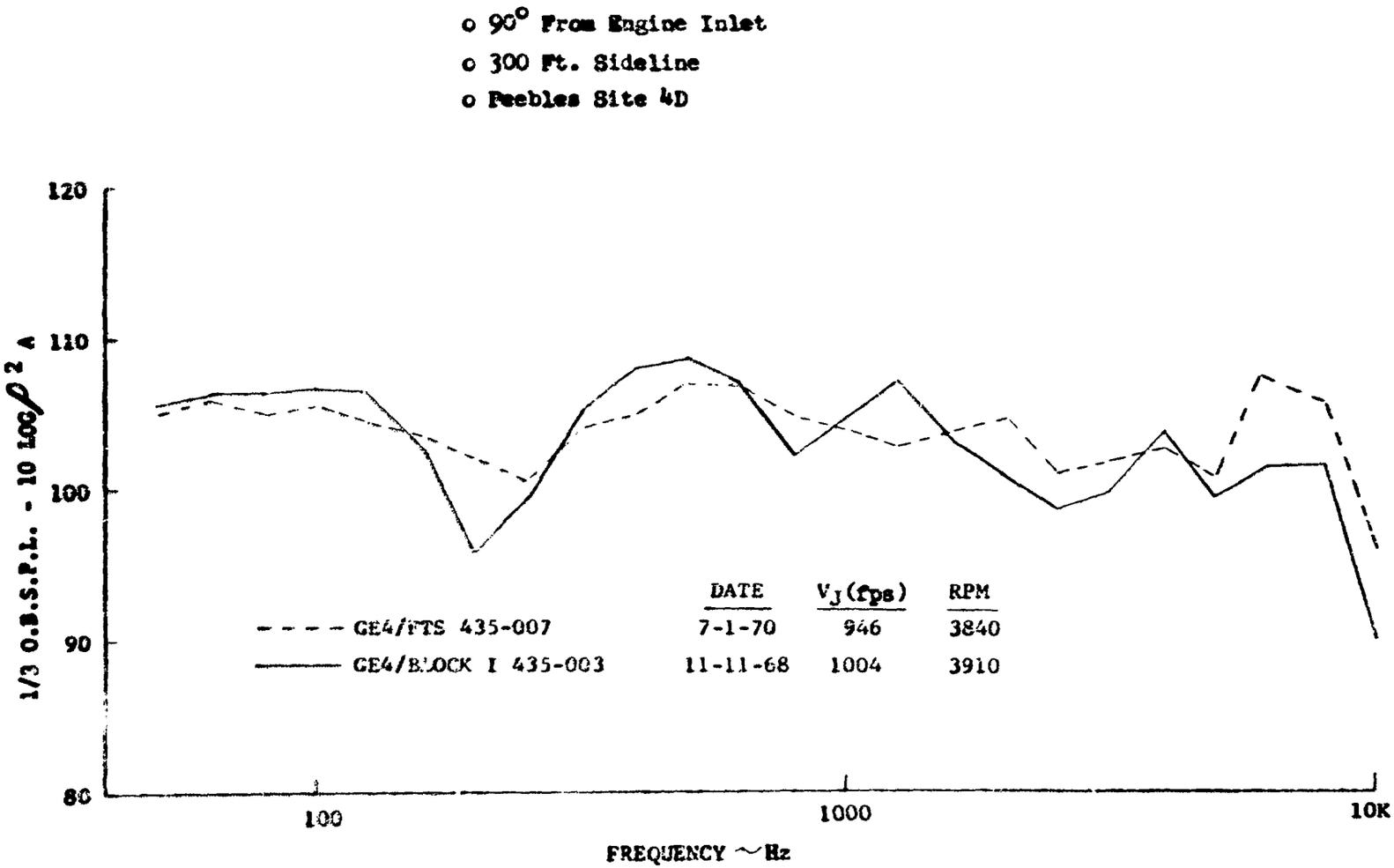


FIGURE VI.C.5-9 GE4 BLOCK I & FTS SPECTRA COMPARISON AT LOW JET VELOCITY

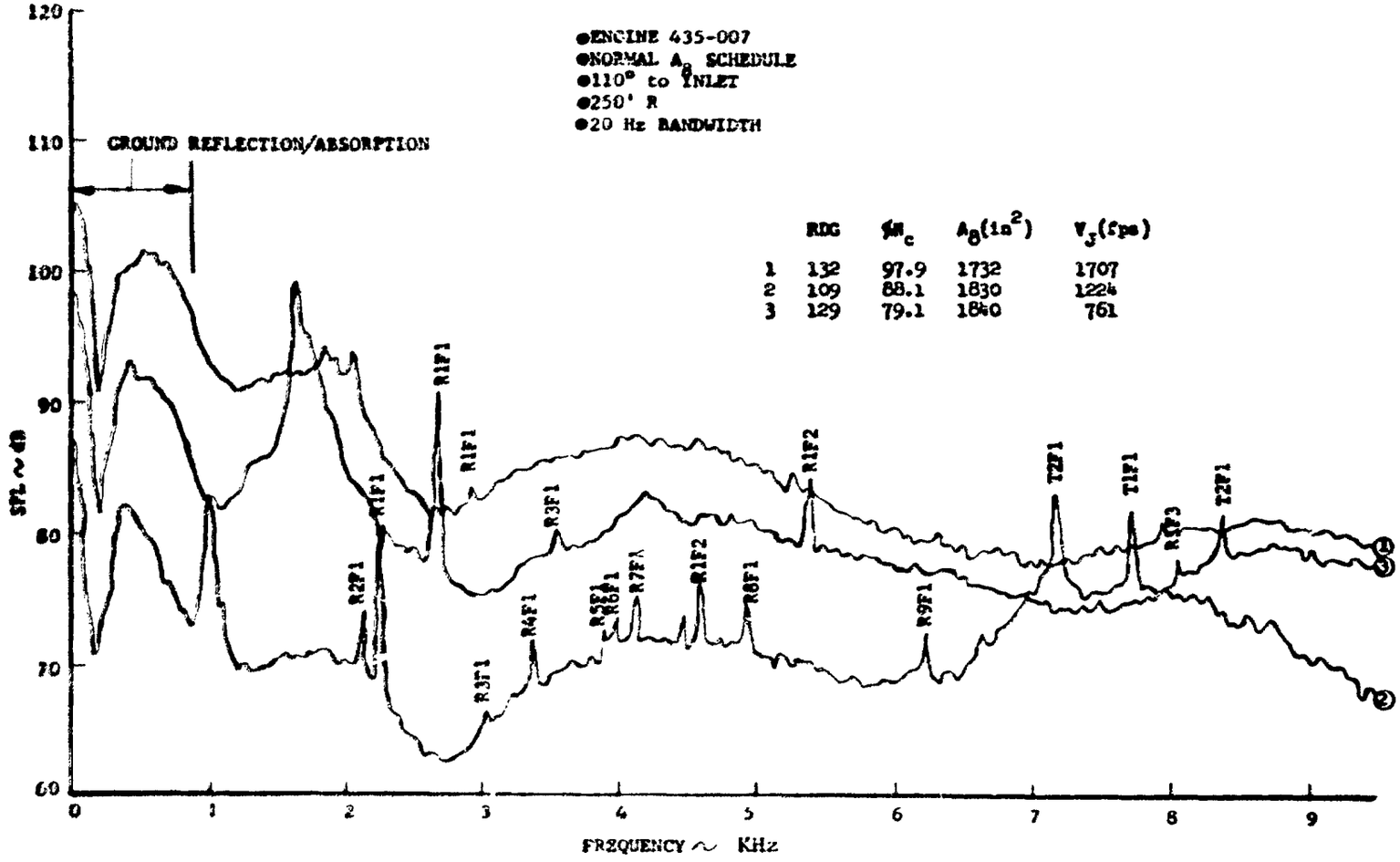


FIGURE VI.C.5-10 GE4 NOISE DATA - NARROWBAND SPECTRA AT SEVERAL ENGINE SPEEDS ON NORMAL A_8 SCHEDULE

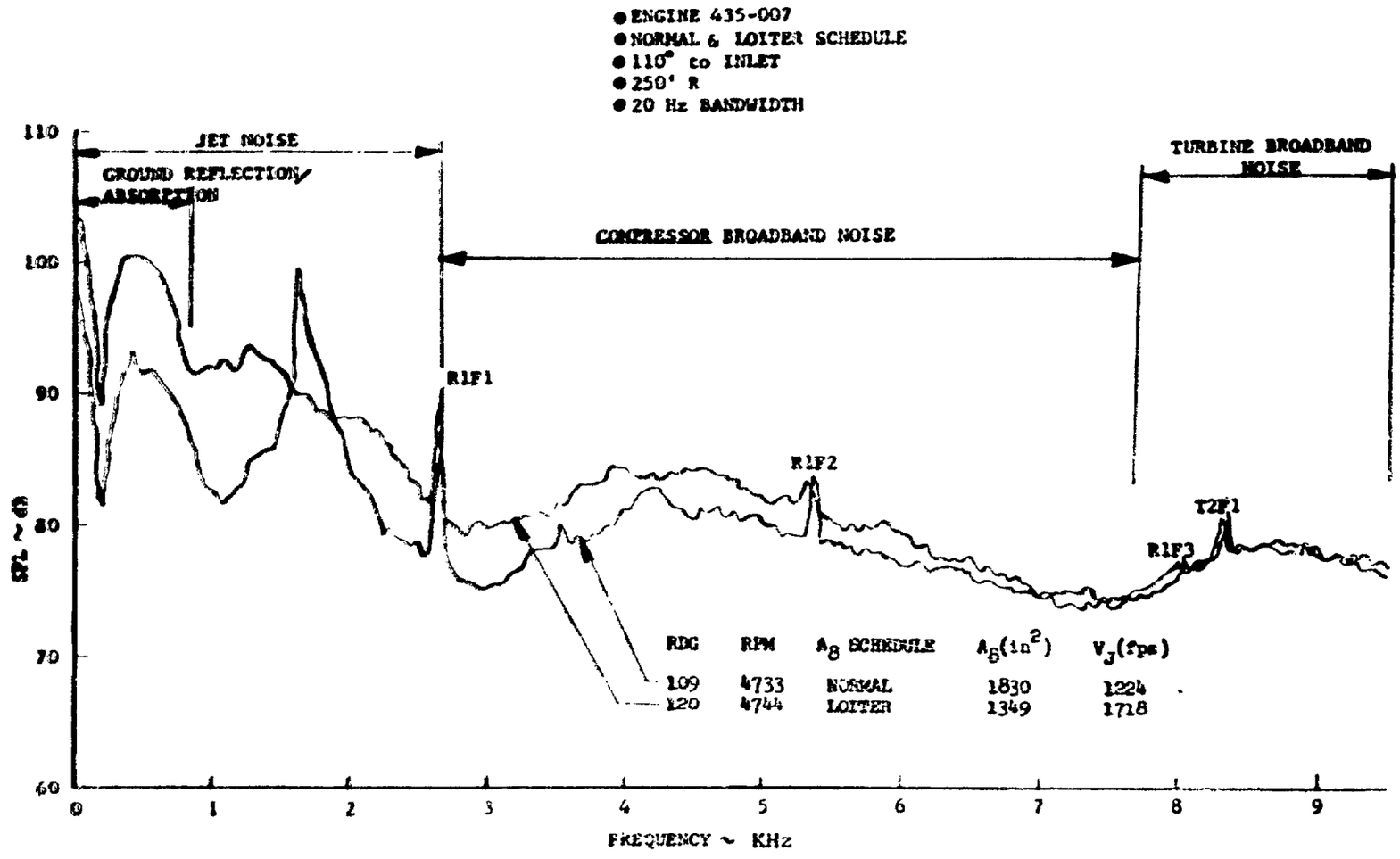


FIGURE VI.C.5-11 GE4 NOISE DATA - NARROWBAND SPECTRA VARIATION WITH NORMAL & LOITER A_8 SCHEDULE

- STG. 9 COMPRESSOR FUNDAMENTAL; 7242 Hz
- 4723 RPM, NORMAL A_8 SCHEDULE
- ENGINE 435-007
- LEVELS FROM 20 Hz NARROWBANDS

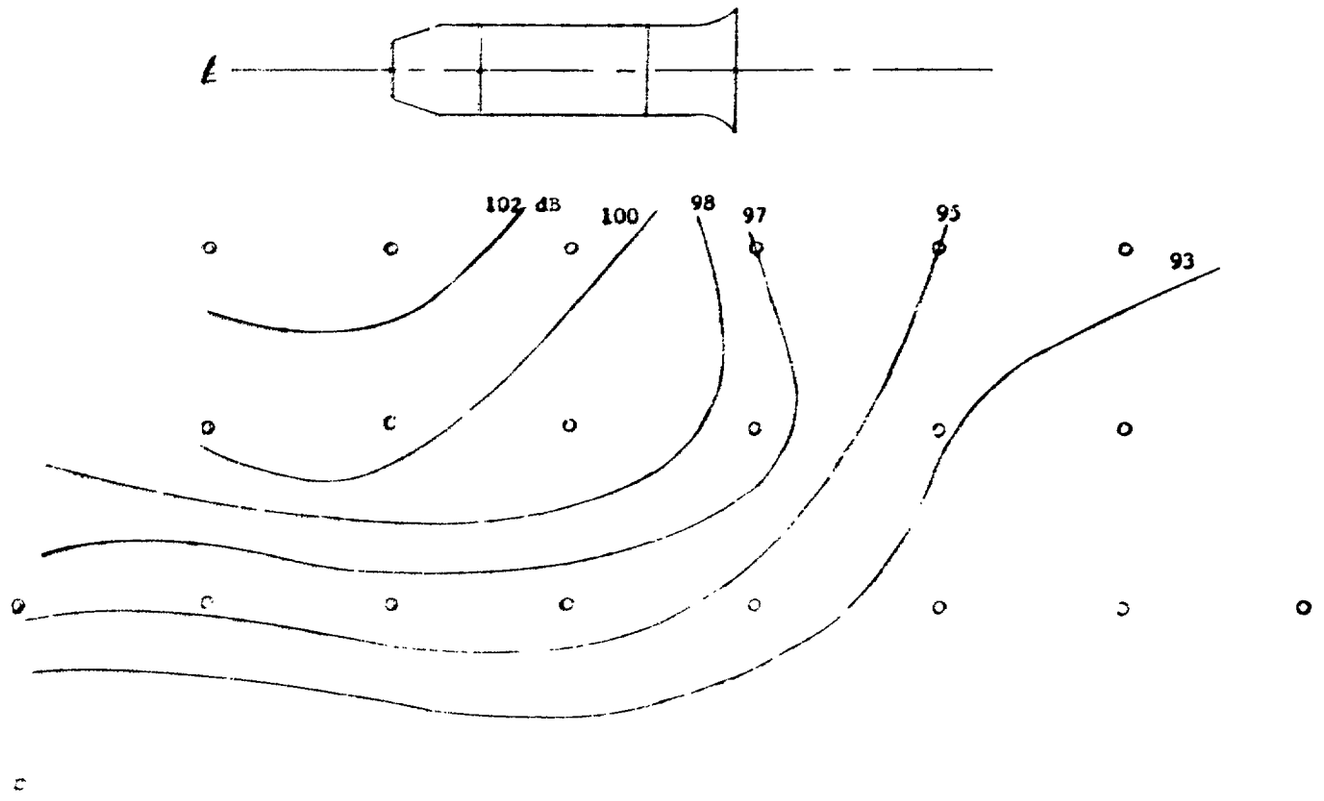


FIGURE VI.C.5-12 GE4 NEAR FIELD NOISE CONTOURS - STAGE 9 COMPRESSOR FUNDAMENTAL PURE TONE

- STG. 2 TURBINE FUNDAMENTAL; 8344 Hz
- 7423 RPM, NORMAL A_8 SCHEDULE
- ENGINE 435-007
- LEVELS FROM 20 Hz NARROWBANDS

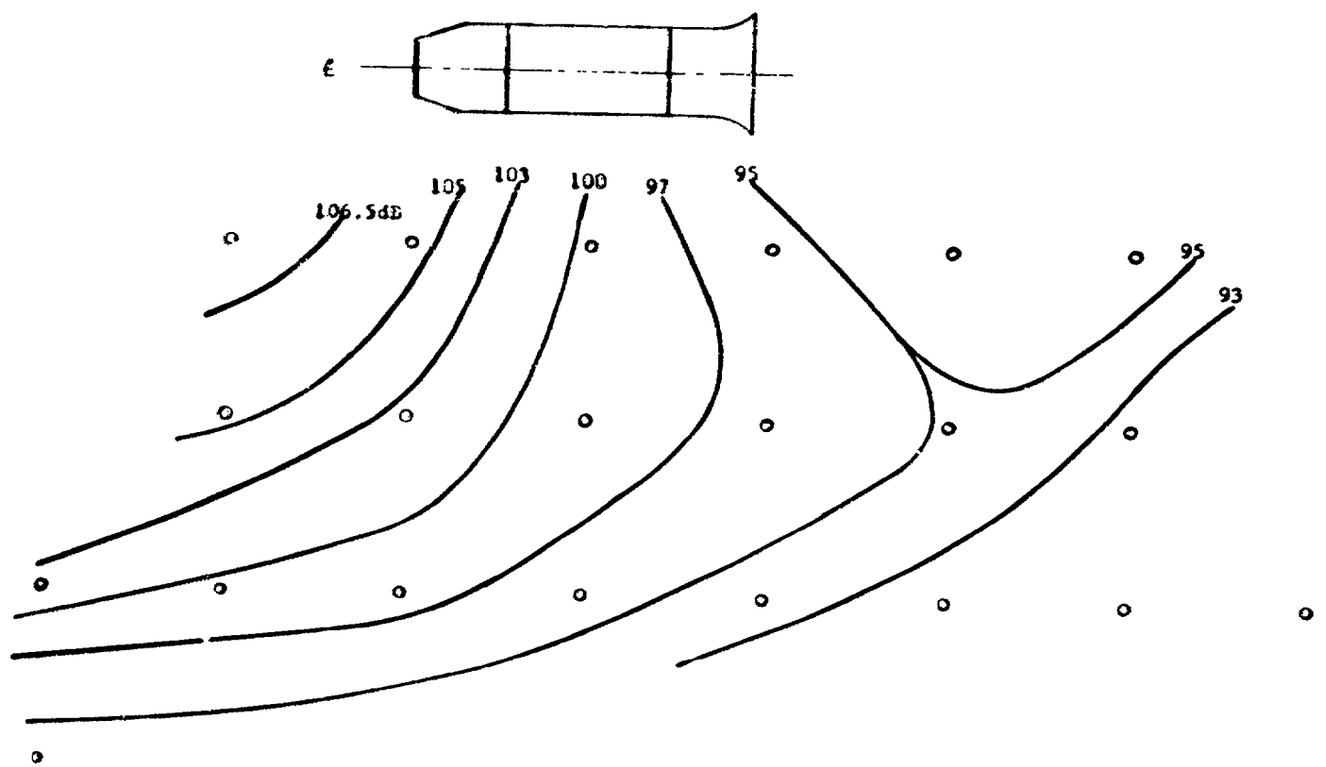


FIGURE VI.C.5-13 GE4 NEAR FIELD NOISE CONTOURS - STAGE 2 TURBINE FUNDAMENTAL PURE TONE

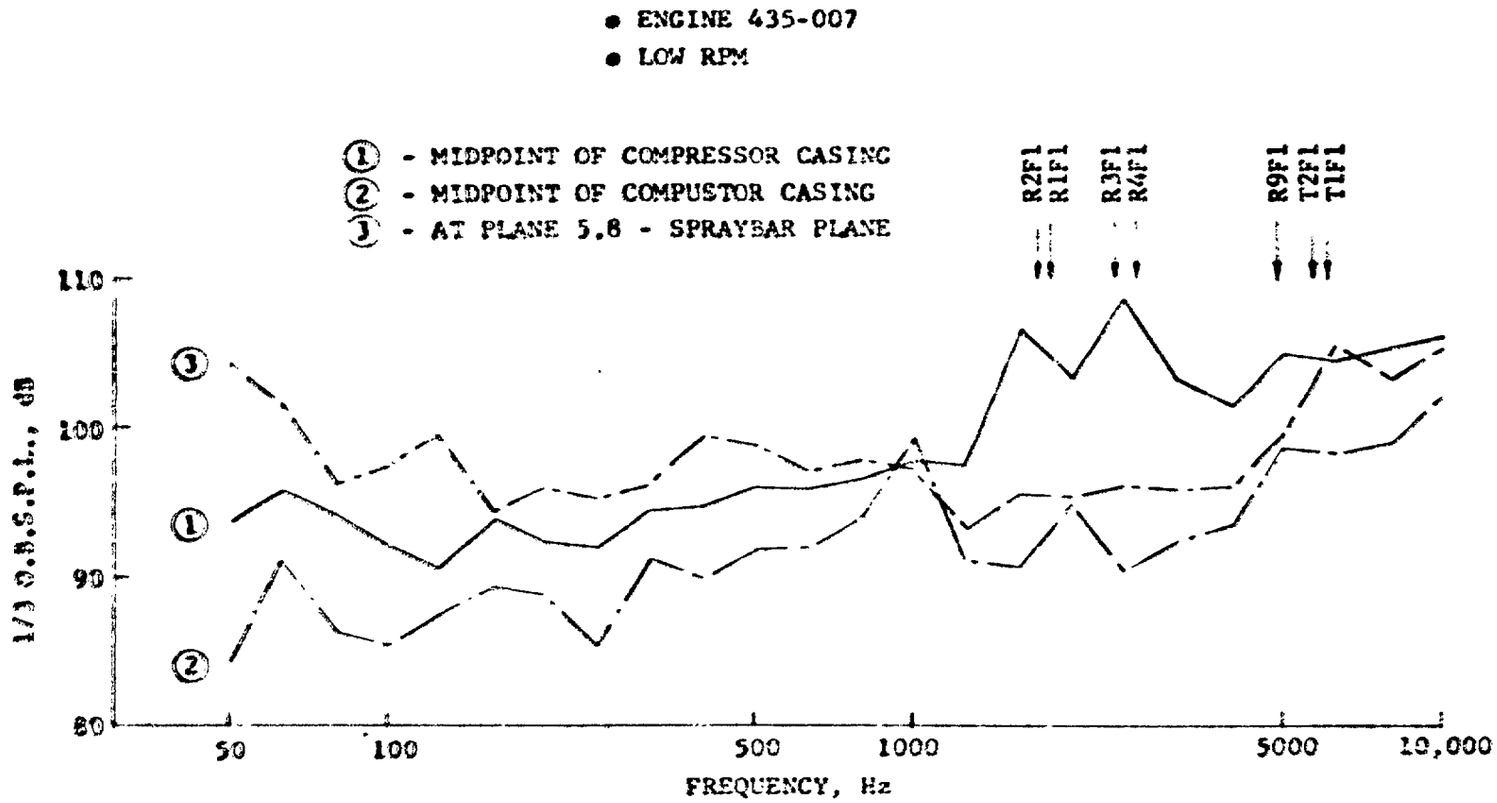


FIGURE VI.C.5-14 GE4 NEAR FIELD CASING MICROPHONE NOISE LEVELS

- GE4 Engine 435004
- With & Without Engine Cowling
- Mics Located ≈ 6" From Nearest Casing/Cowling Surface
- 85% Speed

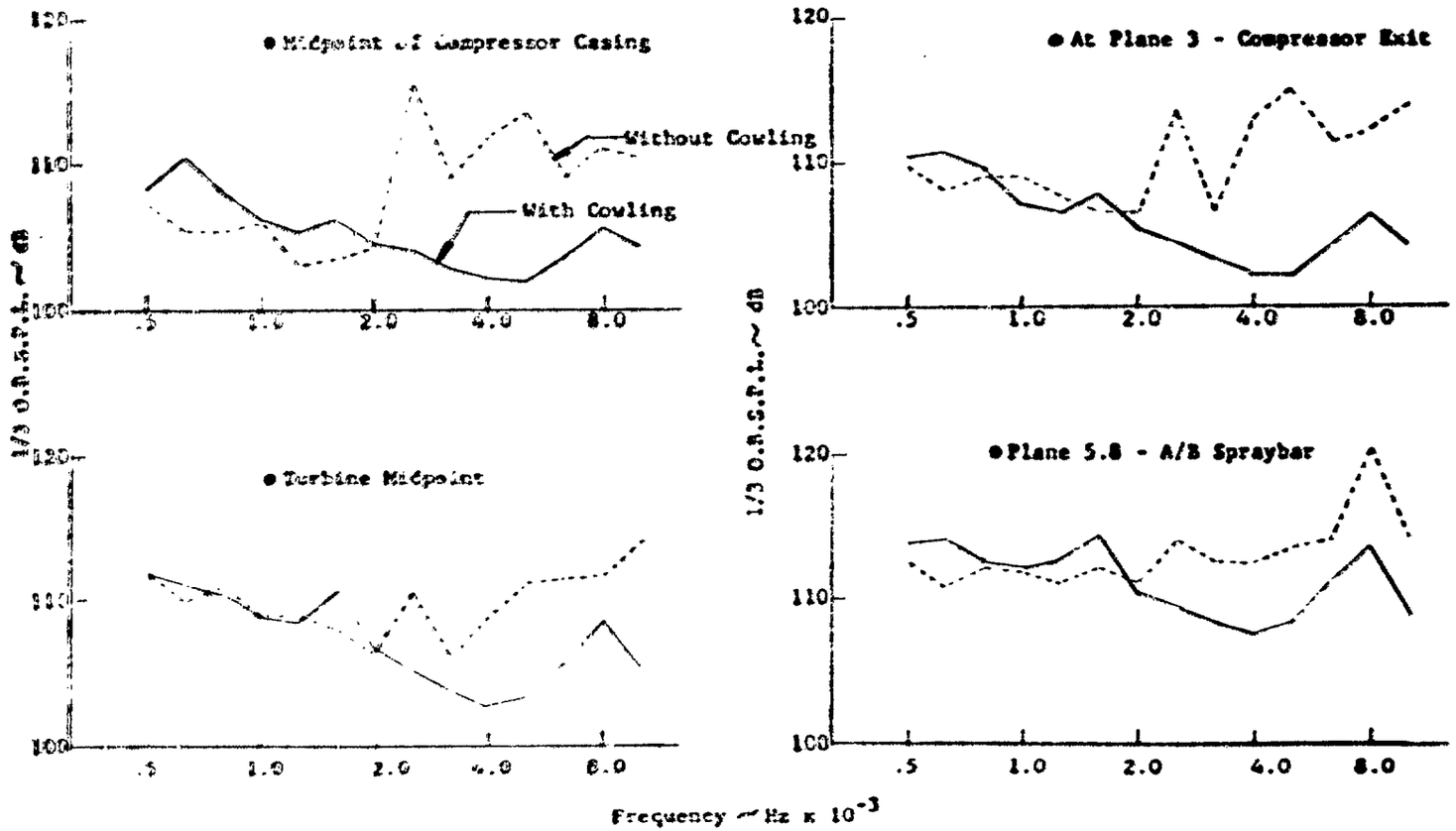


FIGURE VI.C.5-15 GE4 NEAR FIELD NOISE REDUCTION BY ENGINE COWLING

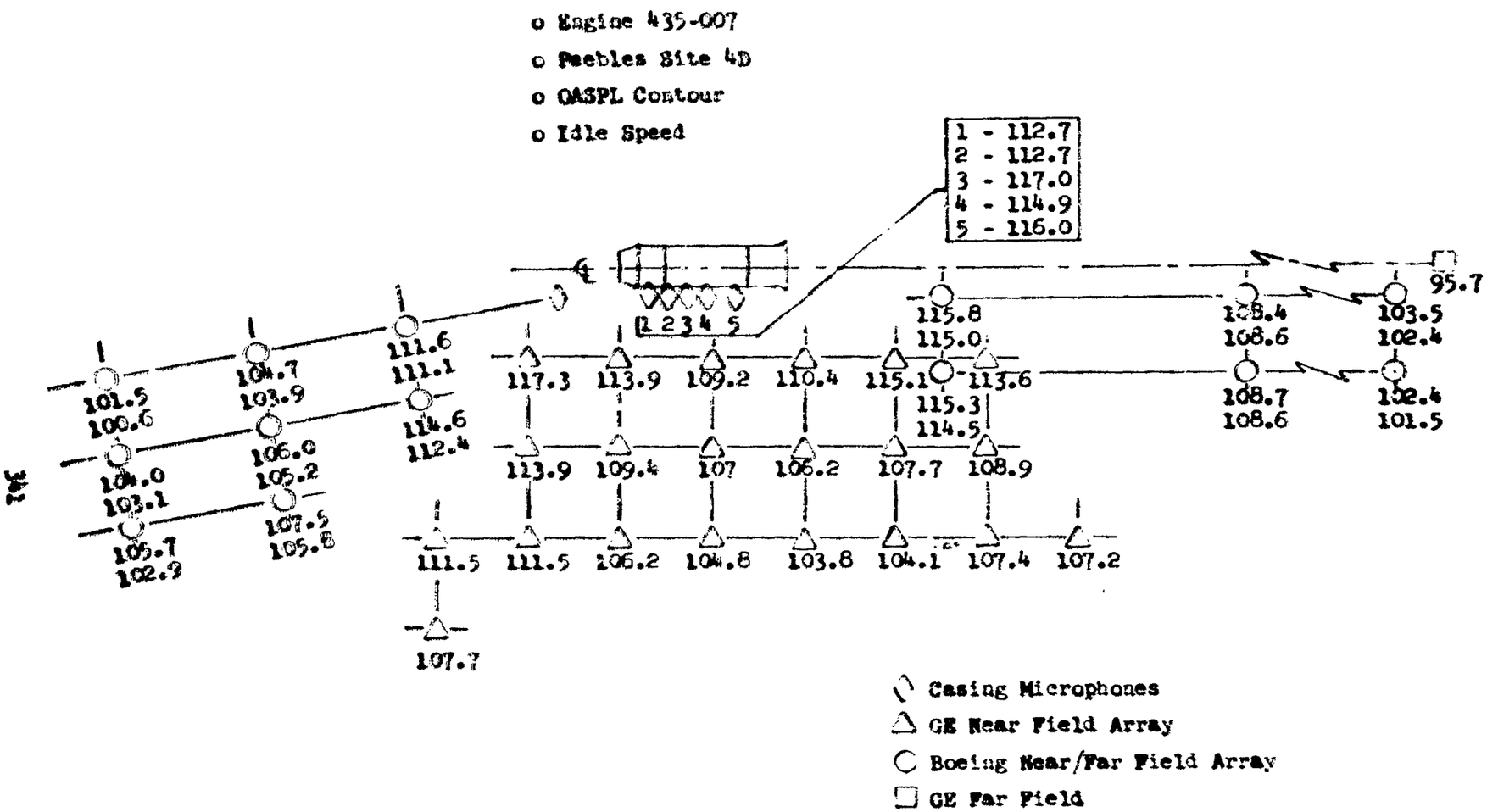


FIGURE VI.C.5-16 GE4 NEAR/FAR FIELD OVERALL SOUND PRESSURE LEVELS AT IDLE

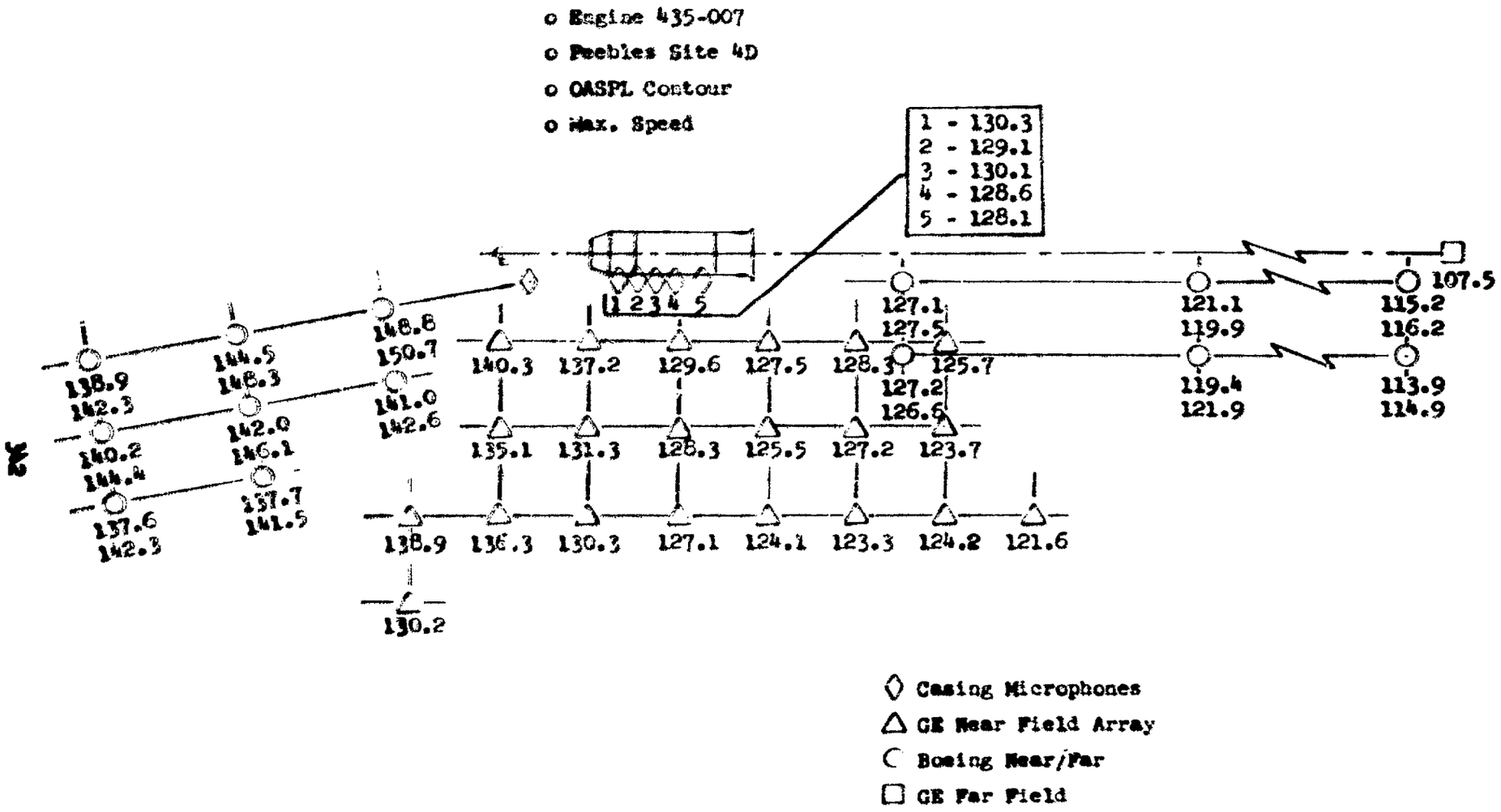


FIGURE VI.C.5-17 GE4 NEAR/FAR FIELD OVERALL SOUND PRESSURE LEVELS AT MAXIMUM SPEED

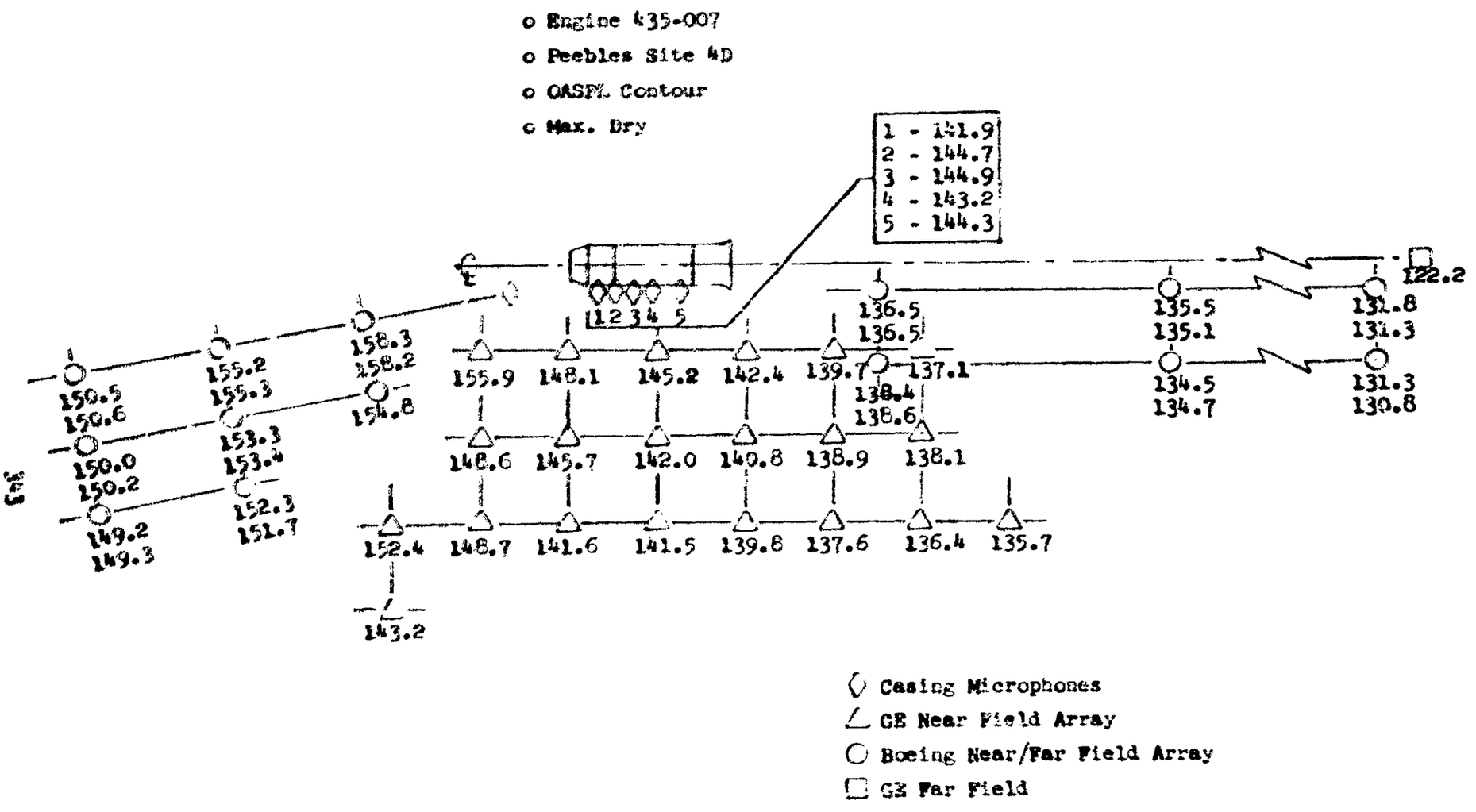


FIGURE VI.C.5-15 GE4 NEAR/FAR FIELD OVERALL SOUND PRESSURE LEVELS AT MAXIMUM DRY

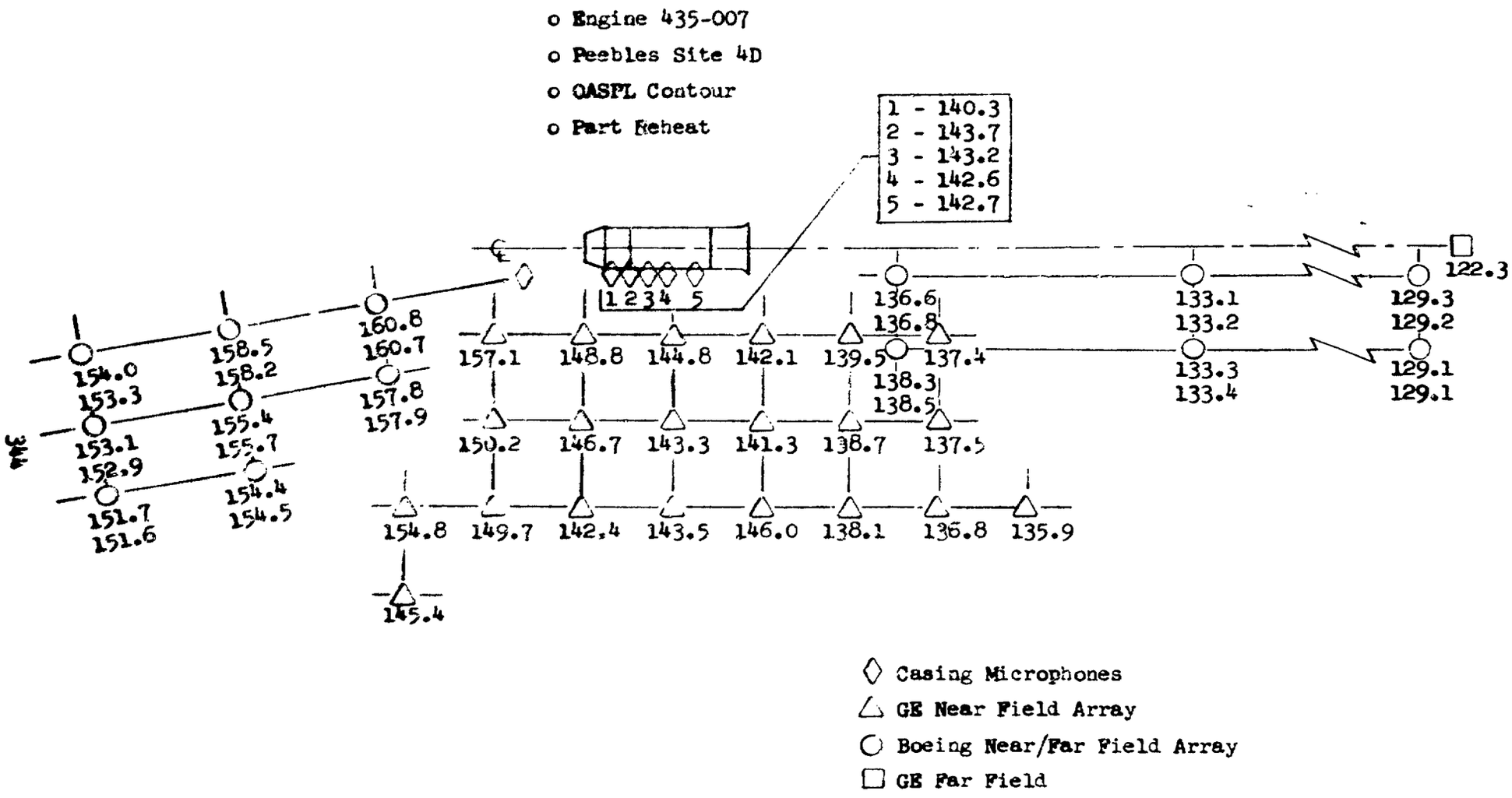


FIGURE VI.C.5-19 GE4 NEAR/FAR FIELD OVERALL SOUND PRESSURE LEVELS AT PART REHEAT

VII. GENERAL ELECTRIC CORPORATE RESEARCH AND DEVELOPMENT CENTER'S FUNDAMENTAL JET NOISE WORK

"PRECEDING PAGE BLANK-NOT FILMED."

VII. GENERAL ELECTRIC CORPORATE RESEARCH AND DEVELOPMENT CENTER'S FUNDAMENTAL JET NOISE WORK

The General Electric Corporate Research and Development Center of Schenectady, New York, was supported by the Federal Aviation Administration through the General Electric Flight Propulsion Division of Evendale, Ohio, throughout the Supersonic Transport program, to perform fundamental jet noise investigations. Their effort has been duly summarized in the report included as Section VII.A, authored by H.T. Nagamatsu and R.E. Sheer, Jr.

As their work was primarily a research program initiated to study the physics of noise generation from supersonic jets and the suppression mechanisms of jet noise, no major attempt was made to gas-dynamically or geometrically simulate the GE4 exhaust nozzle systems. To obtain flow and acoustic characteristics of supersonic jets, experimental research was conducted to determine the mean and fluctuating flow parameters in the jet plume as well as near and far field acoustic measurements. Suppressor configurations were investigated to obtain knowledge regarding the correlation between the flow and acoustic characteristics.

A description of the Corporate Research and Development Center's test facilities have been included in Section II.D. Primarily, test models were of small scale and far-field acoustic measurements were taken on a 10 ft. hemispherical arc to obtain overall sound pressure level, power spectra levels and overall power levels. Normally data were acquired to 16 KHz, and to 80 KHz in the latter part of the program; however, no attempt was made to scale basic measurements of the small scale nozzles to the GE4 engine size. Therefore, all results presented in Section VII.A are model scale results, unlike the scaled data of all the other sections of this summary document.

"PRECEDING PAGE BLANK-NOT FILMED."

VII.A SUPERSONIC JET NOISE SUPPRESSOR RESULTS AND PREDICTION METHODS

"PRECEDING PAGE BLANK-NOT FILMED."

VII.A SUPERSONIC JET NOISE SUPPRESSOR RESULTS AND PREDICTION METHODS

H.T. Nagamatsu and R.E. Sheer, Jr.
Mechanical Engineering Laboratory
General Electric Corporate Research and Development Center
Schenectady, New York

VII.A.1 INTRODUCTION

One of the critical problems for the supersonic transport aircrafts is the jet exhaust noise during take-offs from metropolitan airports. The control of this noise is essential for the successful development of the supersonic transports for commercial use. The jet noise suppression is difficult because of the large thrust required for take-off with supersonic jet exhaust velocities. For plain jets the available experimental flow and acoustic data at supersonic jet velocities is very limited and the information regarding the methods of reducing the supersonic jet noise is being developed for the design of supersonic aircrafts for military and commercial uses. A research program was initiated to study the physics of noise generation from supersonic jets and the suppression mechanisms of jet noise. To obtain the flow and acoustic characteristics of supersonic jets, experimental research was conducted to determine the mean and fluctuating flow parameters in the jet plume as well as the near- and far-field acoustic measurements, and the results are presented in Refs. 1-3. Based upon the experimental results for the supersonic jets, a supersonic jet noise theory was developed by Nagamatsu and Horvay,[4,5], which contained the flow and acoustic characteristics of supersonic jets. Also, sound suppressors of various configurations were investigated at supersonic exhaust velocities to obtain knowledge regarding the correlation between the flow and acoustic characteristics for these suppressors as discussed in Refs. 6-13.

Lassiter and Hubbard[14] investigated the use of wire screen in the subsonic jet flow and observed the reduction in the magnitude of the fluctuating pressure at lower frequencies. For a choked supersonic jet the magnitude of the screen component was reduced by the use of four small auxiliary orifices placed at the nozzle exit. Mercer[15] summarized the results on the effects of small protuberances, "teeth", on the acoustic characteristics of jet engines and found

that the total acoustic power generated is practically unchanged with some change in the power spectra. Several noise-suppression nozzles for jet engines with approximately 5,000 and 10,000 pounds thrust were investigated by Coles and Callaghan[16]. These nozzles achieved sound power level reduction of about 5 dB with small thrust loss by the mixing interference of adjacent jets produced by multiple-slot nozzles. More current status of the jet engine noise due to fan and compressor and jet exhaust has been summarized by Greatrex[17], and also some of the current jet noise suppressors are discussed.

Extensive supersonic jet noise suppressor configurations were investigated by The Boeing Company and General Electric Company for the development of the supersonic transport, SST. Schairer and colleagues have summarized the acoustic and thrust results for the multiple-tube, multiple-chute, and multiple-spoke suppressor configurations in Ref. 18. From the thrust loss standpoint the multiple-tube suppressors give the greatest suppression for a given thrust loss compared to other configurations. Harris[19] compared the acoustic data between the model and full-scale results for the GE4 engine for the SST airplane and found excellent agreement in terms of directivity and spectra at jet velocities above 1750 ft/sec for the convergent nozzle. Various reverse flap suppressor configurations were investigated with the model scale jet noise facility. Jet plume characteristics of 72-tube and 72-hole primary suppressor nozzles were determined with a model scale GE4 engine in Ref. 20, and in this study the thrust loss was also determined. Stringas[21] has summarized the flow, acoustic, and thrust characteristics of multiple-tube, multiple-spoke, and multiple-chute suppressor configurations that were investigated for the GE4 engine. Both hot and cold jet flow data obtained in model scale facilities are presented in these references.

This report presents the results of the investigations that were conducted to determine the flow and acoustic characteristics of subsonic and supersonic jets produced by contoured and convergent nozzles. Acoustics of shock waves produced by choked nozzle, detached shock waves from rods and secondary impinging jets, and transition shock waves in shrouds will be discussed. Comparisons are made regarding the supersonic jet noise suppression with long shroud, rods, and induced flow for parallel flow and convergent nozzles at a jet Mach number

of 1.5. The flow and acoustic characteristics were determined for the reverse slotted cone suppressor configurations for supersoic jet Mach number. The results of the studies that were conducted to determine the flow, acoustic, and thrust characteristics of multiple tubes with and without multiple shrouds are summarized. These flow and acoustic results for the various supersonic suppressor configurations were analyzed and methods of acoustic performance prediction for supersonic jet noise suppressors are predicted.

VII.A.2 CHARACTERISTICS OF SUBSONIC AND SUPERSONIC JETS

Flow

To obtain flow and acoustic characteristics of subsonic and supersonic jets, nozzles of various configurations and exit diameters were investigated as discussed in Ref. 1. Both optical photographs and axial surveys with impact pressure, total temperature, and piezoelectric impact pressure probe were used to determine the flow phenomenon existing in the jets with the reservoir at room temperatures. All of the axial surveys and acoustic measurements were obtained with the 2 in. diameter convergent nozzle designed for an exit Mach number of 1.5 and 2 in. diameter throat in Ref. 8.

The shadowgraph photographs[2] of the flow from a convergent nozzle with an exit diameter of 1 in., taken with a 0.4 μ sec. spark source, are presented in Figure VII.A-1 for jet Mach numbers of 1.0 and 1.4. For the sonic Mach number the photograph indicates the outer edge of the jet boundary and the initial boundary layer around the jet at the nozzle exit. At a jet Mach number of 1.4, the shock bottles are distinct close to the jet exit but farther downstream the shock bottles are smaller and not as distinct because of the lower supersonic Mach number. With a convergent nozzle operated at supersonic jet velocities the shock bottles occur because of the inertia effects of the air as shown in Refs. 22 and 23. Schlieren, interferometer, and shadowgraph photographs were taken of the flow from a convergent nozzle with an exit diameter of 1/8 in. for jet Mach numbers of sonic and 1.4 in Ref. 1. With these different features of the subsonic and supersonic jets.

The axial variations of the flow velocity along the jet axis of a 2 in. diameter convergent nozzle were determine in Ref. 1 by means of impact and

total temperature probes from the jet exit to 80 in. downstream. In Figures VII.A-2A and 2B the Mach number and velocity distributions along the axis for a jet Mach number range of 0.60 to 1.4 are presented as a function of distance from the jet exit. Over the jet Mach number range of 0.60 to 1.0, the axial variations of the flow velocity with distance were quite similar with the core extending on the axis to approximately five diameters, and downstream of the core region the velocity decay of the fully developed turbulent jet was proportional to x^{-1} as indicated in Figure VII.A-2B and Refs. 24 and 25. For supersonic jet exhaust Mach numbers of 1.2 and 1.4, the location of the sonic velocity on the axis moves farther downstream from the nozzle exit, and for Mach 1.4 the sonic location was approximately 13.7 diameters as indicated in Figures VII.A-2A and 2B. But even for supersonic jet exhaust velocities the decay of the jet velocity in the subsonic regions, as indicated in Figure VII.A-2B, is proportional to x^{-1} as observed for sonic and subsonic jet exhaust Mach numbers. Thus, the decay of the jet velocity in the fully developed turbulent jet in the subsonic region seems to be independent of the initial jet exhaust Mach number for jets with reservoir at room temperature.

In Ref. 1, a 1/4 in. diameter quartz piezoelectric pressure transducer with a response time of 20 microseconds was used to measure the pressure fluctuations on the face of the probe along the jet axis for various jet Mach numbers. The rms values of the pressure fluctuations for the 2 in. diameter convergent nozzle are presented in Figure VII.A-3 as a function of distance from the nozzle exit. It was shown in Ref. 2 that the rms value is related to the local turbulent velocity fluctuations for subsonic velocities. For the subsonic Mach number range of 0.60 to 1.0, the variations of the impact pressure fluctuation with distance were quite similar with peak pressure fluctuations occurring at approximately 9 diameters from the jet exit. And the decay in the piezoelectric impact pressure fluctuations downstream of the peak value was proportional to $x^{-1.75}$ as indicated in Figure VII.A-3. For supersonic jet Mach numbers the peak pressure fluctuations were greater than those observed for subsonic jets and the location of the peak fluctuations was in the vicinity of the sonic velocity on the jet axis as indicated in Figure VII.A-3. Downstream of the sonic location on the axis, the pressure fluctuations decayed as $x^{-1.75}$, similar

to that observed for sonic and subsonic jet exhaust velocities. Thus, the maximum piezoelectric pressure fluctuations on the axis for subsonic jets occurs in the "adjustment region" of the jet while for supersonic jets the peak fluctuations occur in the vicinity of the sonic velocity on the axis. The contours of mean velocity and pressure fluctuations for a 1 in. diameter convergent nozzle at Mach numbers of 0.6 to 1.4 were determined in Ref. 2. The peak fluctuations occurred near the sonic region for supersonic jets.

One of the significant aerodynamic differences between the subsonic and supersonic jet is the length of the jet core, defined as the distance from the jet exit where the velocity on the axis is equal to that at the nozzle exit. A Summary of the available published data on the jet core length and the length of the sonic region for supersonic jets[4] of various diameters and temperatures are presented in Figure VII.A-4. The supersonic length is the distance from the jet exit to the sonic velocity on the axis for supersonic jet exhaust velocities. For subsonic jet exhaust velocities[2,26,27] the core length is approximately 4 diameters, and in Ref. 1 with a convergent nozzle of low turbulence level in the reservoir the core length was approximately 5 diameters for subsonic jet Mach numbers of 0.60 to 1.0.

For contoured supersonic nozzles the core lengths have been determined by various investigators[8,23-25,28] and the empirical equation for the core length is given by[4]

$$L_c = \ell_c/D = 5.22M_j^{0.9} + 0.22 \qquad \text{(VII.A-1)}$$

For convergent nozzles at pressure ratios greater than the critical values for supersonic Mach numbers, there is no uniform core region because of the shock bottles[1,2,22,23]. The length of the supersonic region for both cold and hot jets and for convergent and contoured nozzles of various exit diameters is presented in Figure VII.A-4. The length of the supersonic region relative to the jet diameter as a function of the jet Mach number is given by[4]

$$L_s = \ell_s/D = 5M_j^2 + 0.8 \qquad \text{(VII.A-2)}$$

Within the experimental accuracy the effects of jet temperature, dimension of the nozzle, and the shape of the nozzle are small on the supersonic length compared to the jet exhaust Mach number as discussed in Ref. 4.

Acoustics

In Ref. 1 the overall sound pressure levels were determined for a convergent nozzle operated over a Mach number range of 0.60 to 1.4 and the results are presented in Figures VII.A-5 and 6. For subsonic jet velocities the variation of the overall sound pressure level with angular position was quite simiare with the maximum pressure level closest to the jet axis. Similar results were observed by other investigators[14,29,30] with room temperature subsonic jets. For supersonic jet Mach numbers the far-field directivity patterns are different from those observed for subsonic jets are shown Figure VII.A-5. Due to the existence of the shock bottles the sound pressure level remains nearly constant with angular position from the jet axis[22]. When the supersonic jet is perfectly expanded through contoured nozzles to the ambient air, there are no shock bottles as shown in Refs. 8, 23-25, and 28. In Ref. 8 it was observed that the overall sound pressure level decreased with the angular position from the jet axis for a contoured nozzle because of no shock bottles in the supersonic jet flow.

The sound power spectra corresponding to the sound pressure level distribution for the convergent nozzle at various Mach numbers are presented in Figure VII.A-6. In obtaining these 1/3-octave frequency band power spectra in Ref. 1, the sound pressure levels were measured with a microphone at eight angular positions from the jet axis over a frequency range of 40 Hz to 16 KHz. For subsonic jet Mach numbers of 0.60 to 1.0 the power spectra are quite similar to those observed by other investigators[14,29,30]. At a jet Mach number of 1.4 the maximum power occurred at a higher frequency than that observed for subsonic jet Mach numbers. In this figure the overall acoustic power output calculated from the microphone data are tabulated for the various jet Mach numbers.

Near-field pressure fluctuations have been determined for subsonic jets by the use of microphones in Refs. 1, 14, 29, and 30. The near-field pressure fluctuations for the convergent nozzle determined in Ref. 1 are presented in

Figure VII.A-7 with the microphone placed at a radial distance of 2 nozzle diameters from the nozzle exit for jet Mach numbers of 0.60 to 1.40. For subsonic jet Mach numbers of 0.60 to 1.0 the variation of the sound pressure level with axial distance were quite similar indicating the same type of acoustic radiation from subsonic jets. But for supersonic jet Mach numbers of 1.2 and 1.4, the sound pressure levels at the jet exit location increased appreciably from that of the sonic jet, and the increased in the sound pressure levels with distance was not as large as that observed for subsonic jets. This difference in the near-field pressure distribution is caused by the appearance of the Mach waves for supersonic jets as discussed in Ref. 1. Lassiter and Hubbard[14] observed the similar change in the near-field pressure field as the jet velocity was incerased from subsonic to supersonic jet Mach numbers relative to the ambient velocity of sound.

From the near-field microphone measurements at a radial distance of 2 diameters from the nozzle exit, the acoustic intensity and acoustic power transmitted through a cylir lrical surface were calculated in Refs. 1 and 5. By assuming that the sound emission from the circular jet is axially symmetric, the sound transmission per unit length through a cylindrical surface containing the microphone was calculated in terms of unit diameter length by[1]

$$W_d = \frac{D}{\rho_a c_a} \int_0^{2\pi} \bar{p}^2 \, r \, d\theta \qquad \text{(VII.A-3)}$$

where $\bar{p}$ is the rms sound pressure, and the results for supersonic jets are presented in Figure VII.A-8. At the jet exit plane, the acoustic power propagation per unit length is appreciably less than that at the sonic location for the Mach 1.4 jet. The acoustic power distribution can be approximated in the supersonic region by a linear variation and the scatter is due to the presence of shock bottles for convergent nozzles operated at supersonic Mach numbers. For a contoured nozzle at a jet Mach number of 2.49, Potter and Jones[28] observed a similar linear variation of the acoustic power radiation from the supersonic region of the jet.

In Figure VII.A-8 the overall acoustic power propagating through the cylindrical surface containing the microphone was obtained by integrating the acoustic power distribution

$$W \triangleq \int_0^{L_s} w_d \, 2\pi r \, d(x/D) + \int_{L_s}^{\infty} w_{d_s} \, 2\pi r \, L_s^6 (x/D)^{-6} \, d(x/D) \qquad \text{(VII.A-4)}$$

where w_{d_s} is the acoustic power transmission per unit diameter length at the sonic location, L_s. It was assumed that the acoustic radiation decayed as x^{-6} in the fully developed turbulent sonic region of the jet[31,32]. Rather encouraging agreement was observed for supersonic jet Mach numbers of 1.2 and 1.4 between the overall sound power levels determined from the far-field and near-field microphone data as indicated in Figure VII.A-8 and discussed in Ref. 1.

VII.A.3 ACOUSTICS OF SHOCK WAVES IN SUPERSONIC JETS

Contoured and Convergent Nozzles, Shock Bottles

To investigate the differences in the flow and acoustic characteristics for contoured and convergent nozzles at supersonic Mach numbers, a contoured nozzle designed for an exit Mach number of 1.5 with a throat diameter of 2 in. and a convergent nozzle with an exit diameter of 2 in. were constructed and investigated in Ref. 8. Both nozzles were operated at a pressure ratio of 3.7 with a corresponding jet Mach number of 1.5 and the results are presented in Figures VII.A-9 through 11. With the convergent nozzle the Mach number distribution along the jet axis, Figure VII.A-9, varied in the initial shock bottle region[1-3], as shown in Figure VII.A-1. After the disappearance of the shock bottles or diamonds, the Mach number along the jet axis decreased monotonically with distance as x^{-1}. For the contoured nozzle the velocity along the jet axis decreased initially more gradually than the convergent nozzle. But the location of the sonic velocity on the jet axis occurred closer to the jet exit than that observed for the convergent nozzle. Once the jet became fully turbulent and subsonic the velocity decay with distance was the same for both nozzles. Evidently the existence of shock bottles for the convergent nozzle decreases the mixing of the primary jet with the ambient air and lengthens the supersonic region for the same pressure ratio and throat diameter.

The sound pressure levels as a function of angular position from the jet axis for contoured and convergent nozzles at a nominal jet Mach number of 1.5 are presented in Figure VII.A-10 from Ref. 8. For the contoured nozzle with with parallel exit velocity and static pressure equal to the ambient pressure, the sound pressure level was highest near the jet axis and decreased with the angular position as observed by others[14,28] with contoured nozzles at supersonic Mach numbers. With the convergent nozzle the sound pressure level was about the same as for the parallel flow jet near the axis but was higher at all angular positions greater than approximately 50°. This difference is caused primarily by the shock bottles from the convergent nozzle as shown in Refs. 1, 2, and 23.

Comparison of the sound power spectra for contoured and convergent nozzles were obtained in Ref. 8 for a jet Mach number of 1.5 are the results are presented in Figure VII.A-11. In this figure the sound power spectra below 100 Hz has some scatter because the microphone measurements were conducted on a radius of 10 ft. from the jet exit. Hence, for frequencies less than 100 Hz the wave length is greater than 10 ft. so that the microphone is in the near-field for these lower frequencies. For frequencies up to approximately 3000 Hz the sound power spectra for the convergent nozzle was lower than for the contoured nozzle, but for frequencies above 3000 Hz the sound power spectra for the convergent nozzle was higher than for the parallel flow nozzle and the difference became greater as the frequency increased. This difference in the sound power spectra for these nozzles with the same pressure ratio and mass flow is caused primarily by the shock bottles present with the convergent nozzle. It is interesting to note that even with the shock waves present in the jet from the convergent nozzle the difference in the overall sound power levels for these two types of nozzles was only 3.1 dB as indicated in Figure VII.A-11. Thus, shock bottles do produce additional acoustic radiation compared to a parallel supersonic flow with the same mass flow and Mach number, but the increase is small compared to the overall sound power level from supersonic jets.

Detached Shock Waves from Small Rods and Secondary Jets

An investigation was conducted to determine the effects of detached shock waves produced by small circular rods and secondary jets on the flow and acoustic

characteristics of supersonic jets in Refs. 6-8, and 13. For these investigations the primary nozzle throat diameter was 2 in., and the six rods were 1/4 in. diameter and the length varied from 1/4 to 3/4 in. Six secondary jets were located transversely to the primary jet with the jet diameter of 1/8 in. as discussed in Ref. 13. The primary jet was operated at pressure ratios of 3.2 and 3.7 with corresponding nominal Mach numbers of 1.4 and 1.5. In Ref. 8 the six rods were placed in the supersonic region for the parallel flow from a contoured nozzle and downstream of the convergent nozzle exit.

The purpose of the detached shock waves from the rods was to decrease the region of the supersonic flow and to increase the mixing of the primary jet with the ambient air by producing six convolutions around the primary jet surface by the rods. The axial Mach number distribution determined from the impact pressure and total temperature surveys for a convergent nozzle at a pressure ratio of 3.2 with a corresponding nominal jet Mach number of 1.4 is presented in Figure VII.A-12. The axial Mach number distribution is not continuous in the vicinity of the jet exit because of the existence of the shock bottles for a convergent nozzle. With the six rods of 1/4 in. length, the sonic location on the jet axis was decreased from approximately 13.3 diameters for the plain jet to 9.5 diameters with the rods. Thus, the interaction of the detached shock waves from the rods with the shock bottles for the convergent nozzle decreased the length of the supersonic region by approximately 29 percent.

In Figure VII.A-12B the effects of six small rods upon the sound pressure level distribution as a function of the angle from the jet axis are shown. With the rods the sound pressure level was decreased nearly 6 dB from that of plain jet at the 19.1° location and at other angular positions that sound pressure level was also less than for the plain convergent jet at a Mach number of 1.4. The corresponding power spectra for these two jet configurations are presented in Figure VII.A-12C. At the lower frequencies the power level with the six rods was only slightly less than for the plain jet, and the greatest reduction of approximately 9 dB occurred at a frequency of about 1800 Hz. But at higher frequencies the power level approached the plain jet values. The overall sound power level reduction with the six rods of 1/4 in. length was 5.7 dB from the plain convergent jet at a Mach number of 1.4 as discussed in Ref. 12.

While with a contoured nozzle at a Mach number of 1.5 in Ref. 8 the six rods of 1/4 in. length increased the overall sound power level by 3.9 dB from that of the plain jet. Hence, these acoustic results for the convergent and contoured nozzles at supersonic Mach numbers indicate that the detached shock waves from small rods at the periphery of the jet will reduce or increase the overall sound power level from plain convergent and contoured nozzles respectively. With the contoured nozzle operated at the ideal pressure ratio for a given design jet Mach number, the detached shock waves from the small rods produced noise which is greater than the reduction in the primary jet noise due to the decrease in the length of the supersonic region by the rods. Consequently, the overall sound power level with the six rods was higher than for the plain jet.

The effects of the length of the six 1/4 in. diameter rods with a 2 in. diameter convergent nozzle on the flow and acoustic characteristics for a pressure ratio of 3.7 and corresponding nominal Mach number of 1.5 were investigated in Ref. 8 and the results are presented in Figures VII.A-13A and 13B. For the rod the lengths of 1/4, 1/2, and 3/4 in. the variations of the sound pressure level with angular position were similar as indicated in Figure VII.A-13A. The largest difference between the various rod lengths occurred only at the 19.1° position and for angles greater than 43.8° the sound pressure levels for various rod lengths were practically identical with a nearly constant reduction from the plain convergent nozzle configuration. The corresponding power spectra for the six rods of various lengths are presented in Figure VII.A-13B. For the 1/4 in. rod length the power spectra is lower that the plain convergent jet at all frequencies with the largest reduction of approximately 10 dB occurring at a frequency of about 4500 Hz. With these rods the overall sound power level was decreased 5.7 dB from that of the plain jet. Increasing the rod length to 1/2 and 3/4 in. reduced the overall sound power level by 6.2 and 6.0 dB respectively as indicated in Figure VII.A-13B. And the greatest reduction of approximately 20 dB from the plain jet occurred at 1000 Hz for the 3/4 in. length. Hence, these results with six rods and a convergent nozzle at supersonic Mach numbers indicate there is an optimum rod length for suppression of the jet exhaust noise.

Transition Shock Waves in Shrouds

Long shrouds were investigated in Refs. 6, 8, and 13 to determine the effects of shielding and induced flow upon the suppression of jet exhaust noise from contoured and convergent nozzles at supersonic Mach numbers. The shroud in these references was 58 in. long with an inside diameter of 4 in. and it was used with supersonic nozzles with a throat diameter of 2 in. A sketch of the convergent nozzle and shroud configuration is shown in Figure VII.A-14A. With this shroud the acoustic and flow investigations were conducted at a jet Mach number of 1.5. The shroud was investigated with and without induced flow and rods and the results[8] are presented in Figures VII.A-14B through 14F. All of these tests were conducted with room temperature air exhausting to the ambient atmosphere away from the building as described in Refs. 1, 8, and 10.

With the 4 in. diameter shroud placed with the entrance 3.25 in. upstream of the 2 in. diameter convergent nozzle exit[8] and the entrance to the shroud closed so that no induced flow was permitted to enter the shroud, the pressure distributions along the 58 in. long shroud with and without six 1/4 in. diameter rods of various lengths are presented in Figure VII.A-14B. Without the six rods the pressure in the shroud ahead of the nozzle exit was extremely low. But downstream of the nozzle exit the shroud pressure increased rapidly over the initial 5 in. as indicated in the figure. This very rapid pressure rise would indicate that the supersonic jet exhaust was going through transition shock waves to subsonic velocity similar to the flow phenomenon in the diffuser region of transonic and supersonic wind tunnels. For locations farther downstream of the initial 5 in. from the nozzle exit the shroud pressure was close to the outside ambient pressure. This would imply that the corresponding jet flow in the shroud was subsonic over most of the shroud length.

In Figure VII.A-14C the radial Mach number profiles at the exit of the 58 in. long shroud with and without induced flow are shown for various configurations. With no induced flow and without the rods, the exit Mach number is approximately 0.58 at the axis and decreased slowly over the shroud cross section. The axial Mach number variations with distance from the shroud exit for these configurations are presented in Figure VII.A-14D. Without the induced

flow the Mach number along the axis downstream of the shroud exit remained nearly constant at approximately 0.56 for a distance of nearly 5 diameters before decreasing. Similar results were observed for subsonic jets from a 2 in. diameter convergent nozzle in Ref. 1. But upstream of the shroud exit the flow Mach number was not constant but increased towards the nozzle exit as indicated in the figure. This variation of the flow Mach number with distance is due to the subsonic viscous flow within the shroud.

When the six rods of 1/4 and 3/4 in. lengths were inserted at the periphery of the supersonic jet exit with no induced flow in the shroud, the pressure within the shroud at the nozzle exit increased with the rod length as indicated in Figure VII.A-14B. The interaction of the detached shock waves from the rods with the primary supersonic jet exhaust caused the flow to become subsonic very close to the nozzle exit. Again from the 5 in. location from the exit, the shroud pressure was very close to the ambient pressure, which indicated the existence of subsonic flow over most of the long shroud. In Figure VII.A-14C the radial Mach number distributions at the exit of the 58 in. shroud are presented with and without the rods and induced flow. With the induced flow and without rods, the radial Mach number at the axis was approximately 0.93 and it decreased monotonically towards the outer edge of the shroud. For this configuration the shroud static pressure distribution in Ref. 8 indicated that the primary jet remained supersonic over a distance of approximately 25 in. from the nozzle exit. With the six rods of 1/4 in. length and induced flow, the axial Mach number at the shroud exit was approximately 0.78 and it remained nearly constant across the shroud, indicating a subsonic jet with uniform velocity. The shroud pressure distribution for this configuration in Ref. 8 indicated that the flow became subsonic very close to the convergent nozzle exit.

In Figure VII.A-14D the axial Mach number distributions are presented for the shroud with the induced flow and with and without the rods. Without the rods the Mach number variation downstream of the shroud exit was not constant over the initial 5 diameters as observed for the case with no induced flow or with induced flow and with six rods. Also, upstream of the shroud exit the Mach number increased towards the nozzle exit. With the six rods and induced flow the flow velocity was nearly constant over a distance of approximately 5

diameters before decreasing with distance. And upstream of the shroud exit the Mach number increased slowly similar to the case of no induced flow. For this condition the induced flow was approximately 45 percent of the primary jet mass flow[8]. Thus, a supersonic primary jet decreased in velocity by weak shock waves from small rods and induced flow through a shroud with uniform velocity at the shroud exit can be considered aerodynamically as a subsonic jet with uniform velocity with the diameter of the jet equal to that of the shroud. But, if the velocity at the shroud exit is not uniform, the jet does not have the flow characteristic of a uniform subsonic jet downstream of the shroud exit.

The overall sound pressure levels and the power spectra for the plain convergent jet and with the long shroud without induced flow and with rods are presented in Figures VII.A-14E and 14F. For these conditions the 2 in. diameter convergent nozzle was operated at a pressure ratio of 3.7 which corresponds to a jet Mach number of 1.5. Also, in these figures the acoustic results[1] for the convergent nozzle at a Mach number of 0.60 are presented for comparison purposes, since the flow Mach number at the shroud exit in Figure VII.A-14C with no induced flow was approximately 0.58. The variations of the overall sound pressure levels with angular position from the jet axis are presented in Figure VII.A-14E. For the subsonic jet Mach number of 0.60 the overall sound pressure level decreases continuously from the jet axis as observed in Refs. 1, 14, 29 and 30. But for the supersonic jet Mach number of 1.5 from a convergent jet, the sound pressure decreases to approximately 44° and then remains nearly constant due to the presence of the shock bottles.

With the long shroud and induced flow for a primary jet Mach number of 1.5, the overall sound pressure levels are very similar with and without the rods. There was a decrease of approximately 20 dB at the 19.1° angular position from that of the plain jet, and over the angular positions of 44° to 60° the sound pressure level was approximately 5 dB from that of the plain jet. For larger angular positions the reduction in the sound pressure level increased to approximately 20 dB at 146.4°, with the case of no rods producing the greatest reduction. The difference in the overall sound pressure level reduction from the plain jet for the various rod lengths was not very large. Based upon the Mach number at the shroud exit of approximately 0.58, Figure VII.A-14C, the overall

sound pressure level variation with angular position should approach the distribution of a plain jet at a Mach number of 0.60, obtained in Ref. 1 and shown in Figure VII.A-14E. The increase in the overall sound pressure level for the plain jet at a Mach number of 0.60 due to the larger mass flow through the shroud and slightly lower velocity is only a few dBs. Therefore, the difference in the overall sound pressure levels with the shroud attached to a primary jet at a nominal Mach number of 1.5 with no induced flow and that for the plain jet at a Mach number of 0.60, which is approximately the same Mach number as existing at the shroud exit, is caused primarily by the transition shock waves through which the supersonic flow becomes subsonic within the shroud. By comparing these sound pressure level curves, it is evident that the transition shock wave is increasing the sound pressure level by approximately 20 dB at the 19.1° location and has the largest increase of about 30 dB at the 60° position. This large increase at this location is due mainly to the refraction[32] of the acoustic waves produced by the transition shock waves located close to the nozzle exit.

By using 191 tubes, in Ref. 33 and with each tube enclosed by a hexagonal shroud and with no induced flow through the shrouds, the flow at the multi-shroud exit was subsonic with the primary tube Mach number of 1.4 and the overall sound pressure levels were approximately 10 dB lower than for the single shroud with no induced flow for a primary jet Mach number of 1.5 shown in Figure VII.A-14E. Thus, by breaking the large transition shock waves existing downstream of the primary nozzle exit within the shroud with no induced flow from a single large primary nozzle to many smaller transition shock waves from multiple small tube nozzles with each tube enclosed in a shroud, the overall sound pressure level is decreased considerably from that existing for an equivalent single nozzle with a shroud.

The sound power level spectra for a plain convergent nozzle at Mach numbers of 0.60 and 1.5 and with rods and shroud with no induced flow are presented in Figure VII.A-14F from data obtained in Refs. 1 and 8. The power spectra were determined from the microphone measurements obtained at a radius of 10 ft. from the jet and shroud exits. The power spectra was obtained up to 16 KHz, which was the limit of the tape recorder. Since these data were obtained, power spectra

have been obtained up to 80 KHz and the power spectra for the plain jet decreased continuously for frequencies between 16 KHz and 80 KHz, for a jet Mach number of 1.4. With the primary jet at a pressure ratio of 3.7 and nominal Mach number of 1.5, the use of a 58 in. long shroud with no induced flow through the shroud decreased the power spectra at all frequencies from that of the plain jet as shown in Figure VII.A-14F, for various rod lengths. Again the difference in the power spectra due to the various rod lengths was small as observed for the overall sound pressure levels in Figure VII.A-14E. At 1000 Hz the power spectra for the shroud with no induced flow was approximately 22 dB less than that for the plain Mach 1.5 jet. For frequencies less than 1000 Hz the power spectra with the shroud were slightly higher than that existing for the plain subsonic jet at a Mach number of 0.60. But for frequencies greater that 1000 Hz the difference in the power spectra for the Mach 0.60 jet and the Mach 1.5 jet with the shroud became very large with a difference of approximately 30 dB at 16 KHz. At these high frequencies the power spectra for the shroud with rods of various lengths approached that of the plain jet at a Mach number of 1.5. Since the Mach number at the shroud exit was approximately 0.58, the difference in the power spectra for frequencies higher than 1000 Hz for the plain jet at Mach numbers of 0.60 and the shroud with and without rods is caused mainly by the transition shock waves in the shroud. The noise from these shock waves is greatest at the higher frequencies, and thus, for an efficient supersonic jet noise suppressor it is imperative to minimize the noise from the transition shock waves in the suppressor to fully utilize the noise reduction from decreased velocity at the exit of the suppressor.

The overall sound power level reductions from a plain jet at a Mach number of 1.5 with the shroud and no induced flow were 9.4, 8.5, and 9.0 dB for six rod lengths of 0, 1/4, and 3/4 in. respectively as indicated in Figure VII.A-14F. But the difference in the overall sound power level between the 2 in. convergent jet at Mach numbers of 0.60 and 1.5 was 36.6 dB and the difference corrected to the same mass flow by Lighthill's subsonic jet noise equation[31]

$$W = 10^{-4} \frac{m}{2} \frac{\rho}{\rho_a} \left(\frac{c_j}{c_a}\right)^5 c_j^2 M_j^7 \qquad \text{(VII.A-5)}$$

existing for the Mach 1.5 jet is 34.5 dB. This overall sound power level difference is approximately 25 dB greater than that observed with the shroud, which had an exit Mach number of approximately 0.58. Hence, the transition shock waves in the shroud from the Mach 1.5 jet are generating large amounts of acoustic power to the ambient air.

VII.A.4 PARALLEL FLOW AND CONVERGENT NOZZLES WITH RODS, SHROUD, AND INDUCED FLOW

Parallel Flow Nozzle with Rods, Shroud, and Induced Flow

An investigation was conducted with both parallel flow and convergent nozzles[8] with six small rods placed at the nozzle exit and a 4 in. diameter 58 in. long shroud located at the nozzle exit as shown in Figures VII.A-14A and 15A. For both nozzles the throat diameter was 2 in. and the reservoir conditions were the same with a pressure ratio of 3.7 which corresponds to a Mach number of 1.5 for the expansion of the jet to the ambient pressure. The long shroud was used to obtain information regarding the suppression of a Mach 1.5 jet by inducing the ambient air through the shroud and shielding the acoustic radiation from the supersonic portion of the jet to the outside. Six 1/4 in. diameter rods were used in conjunction with the induced flow through the shroud to determine the effectiveness of weak detached shock waves from the six rods interacting with the supersonic primary jet in reducing the noise. Both flow and acoustic characteristics were determined for both nozzles with the rods, shroud, and induced flow to correlate the reduction in the overall sound power level of the plain supersonic jet with the change in the flow variables. The available literature for this type of correlation between the reduction in the acoustic power level with the corresponding change in the flow characteristics is still very limited.

For the parallel flow nozzle with a throat diameter of 2 in. the nozzle was attached to the reservoir section as shown in Figure VII.A-15A. With this nozzle configuration the 4 in. diameter shroud was either attached directly to the nozzle exit for the no induced flow condition or was moved downstream 1 in. to permit the ambient air to enter the shroud. The six 1/4 in. diameter rods were placed at the nozzle exit by the use of a ring section as shown in Figure VII.A-15A. To simplify the surveys of the jet exhaust with impact, total

temperature, and piezoelectric impact pressure probes, the air supply from the compressors to the nozzle was approximately room temperature and a detailed description of the jet exhaust noise facility is presented in Ref. 8.

The shroud pressure distributions for the single shroud of 4 in. diameter and a length of 58 in. and with the second shroud of 5-3/4 in. diameter and a length of 36 in. attached to the exit of the contoured nozzle, Figure VII.A-15A, operated at a jet Mach number of 1.5 are presented in Figure VII.A-15B. With the single shroud and no induced flow the shroud pressure at the nozzle exit is approximately 0.32 of the ambient pressure. The shroud pressure increased rapidly from this low value and attained nearly 0.5 of the ambient pressure at approximately 3 in. from the nozzle exit. This result indicates that the supersonic jet flow is going through transition shock waves to subsonic velocity close to the nozzle exit. From 10 in. downstream of the nozzle exit the shroud pressures close to the ambient pressure. With the shroud moved back 1 in. from the nozzle exit, cf. Figure VII.A-15A, which permitted ambient air to be induced into the 58 in. long shroud, the pressure ratio at the shroud entrance was approximately 0.46 and remained close to this pressure for nearly 15 in. before increasing slowly to the ambient pressure at the shroud exit. Thus, with the induced flow through the shroud the primary jet velocity remains supersonic over a longer distance that with no induced flow. When the second 5-3/4 in. diameter shroud was placed at the end of the first shroud, the shroud pressures remained low for the first shroud with the pressure at the shroud exit of approximately 0.76 of the ambient pressure. The pressures in the second shroud increased from 0.76 to ambient pressure at the exit as shown in Figure VII.A-15B. With the single 58 in. long shroud and 1 in. gap the induced flow through the shroud was .66 of the primary jet mass flow and by using the two shrouds in series with gaps for outside air to enter the shrouds, the induced mass flow was slightly greater than the primary jet mass flow as indicated in Table VII.A-1 from Ref. 8.

From the impact pressure and total temperature probe surveys, the local flow Mach number, velocity, temperature, and density were determined and the calculated quantities from these measurements are presented in Table VII.A-1 for a Mach number 1.5 flow condition for the plain jet. The experimental Mach

number distribution across the exit of the contoured nozzle is presented in Figure VII.A-15C. The Mach number is slightly lower at the axis of the nozzle and increased slightly to the outer edge with the average Mach number of approximately 1.5. With the 58 in. long shroud and no induced flow, the flow Mach number is nearly constant, at 0.58, across the shroud exit. The shroud pressure distribution for this configuration indicated in Figure VII.A-15B that the flow became subsonic close to the nozzle exit. When the shroud was moved downstream from the nozzle exit by 1 in. the Mach number at the shroud exit, over the initial 0.75 in. from the axis was approximately sonic and for greater radial distance the velocity decreased slowly as shown in Figure VII.A-15C. For this configuration with induced flow the ambient air had not mixed completely with the primary jet to produce uniform velocity at the exit of the 58 in. shroud. By the addition of the second larger shroud at the exit of the first shroud, the Mach number at the second shroud exit was approximately 0.74 on the axis and decreased to approximately 0.4 at the outer radius. Even for this long total length for both shrouds, the flow velocity at the shroud exit was still not uniform. The ratios of the maximum and average velocity at the shroud exit to the primary jet velocity are presented in Figure VII.A-15D as a function of the ratio of the mass flows of the induced air and primary jet for the single shroud and two shroud configuration. Without the shock waves from the six small rods and induced flow, the velocity at the shroud exit is not uniform and the effects will be discussed further with the convergent nozzle configuration in the next section of the report.

By measuring the sound pressure levels at eight angular positions from 19.1° to 146.4° on a 10 ft. radius from the nozzle or shroud exits, the overall sound pressure level variations with angular position are shown in Figure VII.A-15E for various nozzle configurations. For the plain jet at a Mach number of 1.5 the overall sound pressure level decreases continuously from the value closest to the jet axis to the maximum angular position, similar to a subsonic jet[1,14,29]. With parallel flow nozzles the shock bottles do not exist for supersonic Mach numbers so that the sound pressure level decreases with angular position, which is not the case with the convergent nozzle, Figure VII.A-10, as discussed in Ref. 1. The sound pressure levels for the long shroud without the induced flow were approximately 15 dB lower at the 19.1° location than for

the plain jet but at the 60° location the sound pressure level was about the same as for the plain jet. And at larger angular positions from the jet axis the sound pressure level became lower than the plain jet. With a gap of 1 in. between the shroud entrance and the nozzle exit the overall sound pressure levels were always lower than the plain jet values with the greatest reduction of approximately 12 dB occurring at the 19.1° location. By the addition of six 1/4 in. diameter rods of 3/4 in. length to the shroud with the gap, the overall sound pressure levels were decreased even more with approximately 20 dB reduction at the 19.1° location from the plain jet value. Even for this configuration the peak overall sound pressure level occurred at the 60° location due probably to the refraction of the acoustic waves in the shroud as discussed in Ref. 32. For the combination of the two shrouds with gaps, the overall sound pressure levels were all much lower than that for the plain jet with approximately 20 dB reduction at the 19.1° locations. But at angular positions greater than 99.6° the overall sound pressure level increased and approach the plain jet value for this configuration as shown in Figure VII.A-15E. This increase could be due to the acoustic radiation from the entrance of the second larger diameter shroud.

From the tape recorded microphone data obtained at the eight angular positions, the third-octave band sound power level was obtained as a function of the frequency for the various configurations[10], and the results are presented in Figure VII.A-15F. For the plain jet at a Mach number of 1.5 the power spectra continuously increased from the low frequency to a peak at approximately 3700 Hz before decreasing. Since the microphone was placed on a 10-ft. radius from the jet exit, there is some scatter in the power spectra for frequencies lower than 100 Hz because the microphone at these lower frequencies was in the near-field.

When the 58 in. long shroud was attached to the nozzle with no gap, the resultant flow in the shroud produced organ pipe effects as shown by the power spectra in Figure VII.A-15F. At low frequencies the power level was lower than that for the plain jet and at approximately 150 Hz the organ pipe effect produced an appreciable increase in the power level. Over the frequency range of approximately 600 to 6500 Hz the power spectra was lower than that for the

plain jet and at higher frequencies the power spectra was close to that for the plain jet. The organ pipe effect on the power spectra was eliminated by using a 1 in. gap between the shroud entrance and nozzle exit to permit induced flow of approximately 66 percent of the primary jet mass flow, Table VII.A-1. With this arrangement the power level was lower than that for the plain jet at all frequencies with the greatest reduction of nearly 9 dB occurring at approximately 7300 Hz, and the overall sound power level was 5.9 dB less than the value for the plain jet. The addition of the second shroud with gaps for both shrouds decreased the power spectra from that of the 58 in. shroud with the gap and the overall power level was 9.4 dB lower that that for the plain jet. By the addition of six 1/4 in. diameter rods of 3/4 in. length to the single 58 in. long shroud with a 1 in. gap, the power level was lower than the plain jet at all frequencies and the overall sound power level was decreased 12.1 dB from the plain jet at a Mach number of 1.5.

The overall sound power level reduction of a parallel flow Mach 1.5 jet is presented in Figure VII.A-15G as a function of the induced mass flow ratio for single and two shrouds and with six rods. Also, in this figure the overall sound power level reduction calculated from Lighthill's prediction, Eq. (VII.A-5) is presented as a function of the induced mass flow ratio. In the calculation the experimental measured flow quantities were used and the results are presented in Table VII.A-1. There is a large difference between the observed overall sound power level reduction from the plain jet and that calculated by Lighthill's equation. One of the primary differences is due to the fact that Lighthill's subsonic jet noise equation applies to jets with uniform exit velocity while the velocity at the shroud exits were not uniform without the six rods, as shown in Figure VII.A-15C. With the addition of the six 1/4 in. diameter rods of 3/4 in. length to the 58 in. long shroud with gap, the experimental overall sound power level reduction from the plain jet approached the value calculated by Lighthill's equation because of the uniform velocity at the shroud exit as will be shown with the convergent nozzle in the next section.

Convergent Nozzle with Rods, Shroud, and Induced Flow

Investigations were conducted with both contoured and convergent nozzles with the same throat diameter of 2 in. to investigate the supersonic jet noise

reduction with small rods, shroud, and induced flow[8,10]. This study was made to determine with which type of nozzle it would be possible to achieve the greatest noise reduction for a supersonic jet Mach number of 1.5. Therefore, these two different types of nozzles were operated with the same throat and reservoir conditions, with six 1/4 in. diameter rods, with a shroud of 4 in. diameter and a length of 58 in., and with a gap between the nozzle exit and shroud entrance to permit induced flow.

The possible configurations for the convergent nozzle with various rods and shroud arrangement are shown in Figure VII.A-14A. For the shroud open condition the entrance to the long shroud was located 3-1/4 in. upstream of the 2 in. diameter convergent nozzle exit. At the first static pressure location for the shroud, which was upstream of the nozzle exit as indicated in Figure VII.A-16A, the shroud pressure was approximately 0.61 of the ambient pressure. For a location 5 in. downstream of the nozzle exit the shroud pressure was only 0.31 of the ambient pressure and the pressure ratio increased to approximately 0.35 at the 22 in. location. These low shroud static pressures indicate the large aspirating effects of the 2 in. diameter supersonic jet mixing within the 4 in. diameter shroud. At these low pressure conditions the primary jet expands to a higher Mach number than 1.5 calculated for the condition of the reservoir air expanding isentropically to the ambient pressure condition. The pressure in the shroud increased rapidly over a region of 22 to 33 in. and at the shroud exit the pressure approached the ambient value.

Six 1/4 in. diameter rods of various lengths were placed 1/2 in. downstream of the nozzle exit, cf Figure VII.A-14A, and the shroud pressure distributions for the different rod lengths with induced flow through the shroud are presented in Figure VII.A-16A. For a rod length of 1/4 in. the shroud pressure ratio over the entrance region was approximately 0.66 and the pressure increased rapidly over the distance of 3 to 7 in. from the nozzle exit. The shroud pressure was equal to the ambient pressure at a distance of 20 in. from the nozzle exit and remained above ambient pressure over the rest of the shroud length. Evidently the shock waves from the six rods of 1/4 in. length were strong enough to interact with the primary jet shock bottle system and decrease the jet velocity and increase the mixing with the induce air. For other rod lengths of 1/2 and

3/4 in. the shroud pressures were increased over that of the rod length of 1/4 in. for the distance of 22 in. from the nozzle exit and became equal to the ambient pressure at this location. But for distances greater than this to the shroud exit the pressure was close to the ambient and less than for the 1/4 in. length configuration as indicated in Figure VII.A-16A. The detached shock waves from the six rod lengths of 1/2 and 3/4 in. were stronger than that with the rod length of 1/4 in. so that the interaction of the stronger shock waves with the primary jet waves decreased the primary jet velocity by a greater amount.

In Figure VII.A-14C the radial Mach number distributions at the end of the 58 in. long shroud with and without induced flow and with six rods of 1/4 in. length are presented for a primary jet Mach number of 1.5. With the gap between the shroud and the nozzle closed, cf. Figure VII.A-14A, the flow Mach number at the shroud exit was nearly constant at a Mach number of approximately 0.58, which is similar to what was observed with the parallel nozzle flow with shroud as shown in Figure VII.A-15C. When the gap was opened to permit induced flow, the flow Mach number was not constant across the shroud exit but decreased from a Mach number of 0.92 at the axis to approximately 0.65 at the outer edge of the shroud. This corresponds to an average velocity of 736 ft/sec and total mass flow of .167 slugs/sec as shown in Table VII.A-2. The Mach number at the shroud exit, with a gap and six rods of 1/4 in. length, determined from the impact pressure surveys made in line with the rods and between the rods are presented in Figure VII.A-14C. Within the experimental accuracy the radial flow Mach number distribution across the shroud exit determined from these impact surveys were practically identical. The shock waves from the six rods increased the mixing of the primary jet and the induced flow with a resultant nearly constant Mach number across the shroud of approximately 0.77. This corresponded to an average flow velocity of 771 ft/sec and a total mass flow rate of .177 slugs/sec as shown in Table VII.A-2. Thus, the six rods of 1/4 in. length made the velocity at the shroud exit nearly constant and increased the induced flow compared to the case of the shroud without the rods.

Surveys were conducted along the axis of the jet with impact pressure and total temperature probes inside and downstream of the 4 in. diameter 58 in. long shroud and the results for the variation of the axial Mach number for the different configurations are presented in Figure VII.A-14b. Again with the gap closed for the shroud, the flow Mach number was subsonic both inside and downstream of the shroud. At the shroud exit the Mach number was approximately 0.55 and remained nearly constant for 18 in., which corresponds to an axial distance to shroud diameter ratio of 4.5. For a uniform subsonic jet at a Mach number of 0.6, the uniform core region extended to approximately 5 diameters as observed in Ref. 1.

With the gap opened between the shroud and the nozzle and without the six rods, the axial Mach numbers upstream and downstream of the shroud exit were not constant but varied much more than the case with no induced flow as shown in Figure VII.A-14D. The axial Mach number decreased continuously with distance from a value of 0.9 at the shroud exit. This type of axial variation of the flow velocity is due to the fact that the velocity at the shroud exit was not uniform as indicated in Figure VII.A-14C. The mixing of the primary jet and the induced flow was not completed before reaching the end of the 58 in. long shroud. When the six rods of 1/4 in. length were placed downstream of the nozzle exit with the gap for induced flow, the velocity decayed more slowly within the shroud and decreased to a Mach number of 0.78 at the exit as shown in Figure VII.A-14D. Downstream of the shroud the flow velocity remained nearly constant for approximately 4 diameters or 16 in. before decreasing with distance. For this configuration the velocity at the shroud exit was nearly uniform, Figure VII.A-14C, and consequently, the flow from the shroud was like a uniform subsonic jet.

In Figure VII.A-16B the rms values of the piezoelectric impact pressure fluctuations are presented for the various configurations. For the plain nozzle the peak pressure fluctuations occurred at approximately 28 in. from the nozzle exit, which was slightly ahead of the sonic location. One inch downstream of the nozzle exit the rms value of the piezoelectric pressure fluctuations was approximately 0.45 mv and the peak value was nearly 5 mv in the vicinity of the sonic velocity on the axis. By placing the long shroud at the nozzle exit with no gap for the ambient air to enter the shroud, the piezoelectric

pressure fluctuations along the axis from the shroud exit remained relatively low and increased gradually to a peak value of approximately 1 mv at the 30 in. location.

With the gap opened between the shroud and the nozzle, Figure VII.A-14A, the rms value of the piezoelectric impact pressure fluctuations was 2 mv at 1 in. downstream of the shroud exit and remained close to this value over a distance of nearly 30 in. as indicated in Figure VII.A-16B. With the addition of six rods of 1/4 in. length the rms value of the piezoelectric pressure fluctuations was 0.4 mv at 1 in. downstream of the shroud exit, which is one-fifth of the value for the case without the rods. The piezoelectric pressure fluctuations for these configurations remained low over the distance of 30 in. For these configurations of the shroud velocities across the shroud exit were nearly the same, Table VII.A-2, but the piezoelectric impact pressure fluctuations were much higher for the non-uniform radial velocity distribution across the shroud without the rods.

The overall sound pressure levels as function of angular position from the convergent nozzle axis with six rods of various lengths and shroud opened are presented in Figure VII.A-16C. As discussed previously the overall sound pressure level for the plain nozzle at a Mach number 1.5 remains nearly constant for angles greater than 44° because of the shock bottles. The overall sound pressure levels for the shroud with the gap closed and opened are quite similar as indicated in Figure VII.A-14E and 16C with the peak occurring at 60° from the jet axis. The lowest overall sound pressure levels were obtained with the six rods of 1/4 in. length for the shroud with induced flow. At the 19.1° angular position the overall sound pressure level was approximately 20 dB less than the value for the plain jet and the smallest reduction of approximately 12 dB from the plain nozzle occurred at the 60° position. For larger angular positions the reduction of the overall sound pressure level increased to approximately 25 dB at the 146.4° location, Figure VII.A-16C. For longer rod lengths of 1/2 and 3/4 in. the overall sound pressure levels increased with increasing rod length relative to the 1/4 in. rod length configuration for all angular positions except at the 19.1° location. Evidently the noise from the interaction of the detached shock

waves from the six rods and the primary shock bottle system increased with the length of the rods with a corresponding increase in the overall sound pressure level.

The sound power level spectra for the convergent nozzle at a Mach number of 1.5 with various configurations of rods, shroud, and induced flow are presented in Figure VII.A-16D. With the long shroud and with the gap closed, the sound power spectra was shown in Figure VII.A-14F to be lower than the plain jet overall of the frequency range and approached the plain jet spectra at the higher frequencies. The overall sound power level reduction from the plain jet for this configuration was 9.4 dB as shown in Table VII.A-3. With the gap and without the six rods, Figure VII.A-16D, the sound power spectra was higher than the case with the gap closed over the frequency range of 100 to 4000 Hz, as seen by comparing Figures VII.A-14F and 16D. For higher frequencies the sound power levels were very close for these two configurations and the overall sound power level reduction with the gap was 11.2 dB from that of the plain jet. By the use of six rods of 1/4 in. leng . and the shroud with gap, the sound power levels were much less than that for the plain jet with nearly 25 dB reduction at approximately 4500 Hz. The overall sound power level reduction was 17.3 dB from the plain jet at a Mach number of 1.5 as shown in Table VII.A-3 and Figure VII.A-16D. For longer rod lengths of 1/2 and 3/4 in. the overall sound power level reductions were 13.9 and 10.5 dB respectively. Thus, for a convergent nozzle operated at a Mach number of 1.5 with six 1/4 in. diameter rods placed downstream of the nozzle exit, Figure VII.A-14A, the overall sound power level reduction from the plain jet with shroud and induced flow decreased from 17.3 to 10.5 dB by increasing the rod lengths from 1/4 to 3/4 in.

Comparison of Acoustic Properties of M = 1.5 Parallel Flow and Convergent Nozzles with Suppressors

The acoustic results for parallel flow and convergent nozzles with a throat diameter of 2 in. and operated with the same pressure ratio of 3.7 to produce a Mach number of 1.5 are summarized in Table VII.A-3 and Figures VII.A-17A through 17C. For both of these nozzles the same shroud with an inside diameter of 4 in. and a length of 58 in. was placed at the nozzle exit as indicated in

Figures VII.A-14A and 15A with and without the gap between the shroud and the nozzle. Six 1/4 in. diameter rods of various lengths were placed at the nozzle exits.

The primary objective of the investigation of the two types of supersonic nozzles was to determine the type of nozzle which is more suitable for decreasing the overall sound power level with a shroud and induced flow.

For the plain jets at a Mach number of 1.5 the overall sound power levels were 153.1 and 156.2 dB for parallel flow and convergent nozzles respectively as presented in Table VII.A-3. The shock bottles, Figure VII.A-1, present with the convergent nozzle increased the acoustic power level by only 3.1 dB compared to the parallel flow nozzle without the shock waves. Over the initial angular positons of 19.1° to 50° from the jet axis, the sound pressure levels for the parallel flow nozzle were slightly higher than the convergent nozzle as indicated in Figure VII.A-17A. But for higher angular positions the sound pressure level decreased for the contoured nozzle and was lower than for the convergent nozzle. With the parallel flow nozzle the greatest overall sound power level reduction of 12.1 dB was obtained with the shroud, six rods of 3/4 in. length, and induced flow as indicated in Table VII.A-3. And the overall sound power level for this configuration was 141 dB. While with the convergent nozzle the greatest noise reduction of 17.3 dB was achieved with the shroud, six rods of 1/4 in. length, and induced flow. And the overall sound power level was 138.9 dB for this suppressor arrangement. In Figure VII.A-17A the sound pressure levels for these configurations are presented as a function of the angular position from the jet axis. At all angular positions the sound pressure level for the parallel nozzle flow with shroud, rods, and induced flow was a few dB higher than for the same shroud configuration with the convergent nozzle. For both nozzles the reduction in the sound pressure level with the suppressor was approximately 20 dB at the 19.1° angular position and the smallest reduction from the plain nozzle occurred at the 60° location. There was a large reduction in the sound pressure level at the higher angular positions for both types of nozzles with suppressor as shown in Figure VII.A-17A.

The comparison of the sound power level spectra for parallel flow and convergent nozzles at a Mach number of 1.5 are presented in Figure VII.A-17B with

and without the suppressors. Over the frequency range of 100 to approximately 4000 Hz the sound power level for the convergent nozzle was lower than that for the parallel flow nozzle. But at higher frequencies the sound power level increased monotonically from 4000 Hz for the convergent nozzle while the power spectra reached a plateau for the parallel flow nozzle and began to decrease for frequencies greater than 9000 Hz. This higher power level spectra for the convergent nozzle at higher frequencies is due mainly to the shock noise from the shock bottles in the supersonic region of the jet. With the addition of the 58 in. long shroud and six rods to the two types of nozzle, the sound power level spectra were decreased appreciably from the plain jets. The sound power level spectra for the parallel nozzle flow with the shroud and rods of 3/4 in. length was higher by nearly a constant amount over the frequency range from 100 to 4000 Hz than that for the convergent nozzle with the shroud and rod length of 1/4 in. The greatest difference between the two configurations occurred in the range of 1000 Hz and the power spectras at 14,000 Hz were about equal. With this type of suppressor the overall sound power level reductions from contoured and convergent nozzles at a Mach number of 1.5 were 12.1 and 17.3 dB respectively. For the same reservoir condition and throat diameter the sound power level for the convergent nozzle was 3.1 dB greater than the parallel flow nozzle but with the shroud, six rods, and induced flow the overall sound power level was 2.1 dB lower for the convergent nozzle. These results indicate that for a room temperature jet at supersonic Mach numbers it is possible to achieve greater noise reduction with the convergent nozzle than a parallel flow nozzle. Further investigations should be conducted to obtain additional flow and acoustic information at supersonic Mach numbers with suppressors.

The summary of the variation of the overall sound power level with rods, shroud, and induced flow for parallel flow and convergent nozzles at a jet Mach number of 1.5 is presented in Figure VII.A-17C. With the parallel flow nozzle two shrouds of 4 and 6 in. inside diameter and respective lengths of 58 and 36 in. were used in series with gaps at the entrance of both shrouds to permit ambient air to enter the shrouds, as shown in Figure VII.A-15A. By the use of the second larger diameter shroud it was possible to induce mass flow slightly larger than the primary jet flow. Without the six rods for the parallel flow

nozzle the overall sound power level reduction was 5.9 dB with the single shroud at an induced mass flow ratio of 0.66 and with the addition of the second shroud the overall sound power level reduction was increased to 9.4 dB with corresponding mass flow ratio of 1.07. When six rods of 1/4 in. length were inserted into the flow from the parallel nozzle exit, the overall sound power level was increased 1.5 dB from that of the plain jet as indicated in Table VII.A-3 and Figure VII.A-17C. But with the addition of these rods to the 58 in. long shroud with induced flow, the overall power level reduction was 12.1 which was 6.2 dB greater than for the case of the shroud without the rods as shown in Figure VII.A-17C, at approximately the same induced mass flow. As discussed earlier, the main difference in flow characteristics for these two cases is the velocity distribution at the shroud exit. Thus, these results indicate the necessity of having uniform velocity distribution across the shroud exit to utilize the induced flow in the suppressor for maximum noise reduction of the plain subsonic and supersonic jets.

With the addition of six rods of 1/4 in. length to the convergent nozzle Figure VII.A-14A, the overall sound power level was decreased 5.7 dB from the plain jet at a Mach number of 1.5 as shown in Table VII.A-3 and Figure VII.A-17C, while with the parallel flow nozzle the rods increased the sound power level. With the 58 in. long shroud and gap for induced flow, and no rods, the ratio of the induced mass flow to the primary jet flow was 0.36 and the corresponding overall power level reduction from the plain jet was 11.2 dB as indicated in Table VII.A-3 and Figure VII.A-17C. When the six rods of 1/4 in. length were added to this suppressor configuration, the induced mass flow ratio was increased to 0.44 and the overall power level reduction was increased to 17.3 dB. The difference in the sound power level reduction between the configuration without and with the rods is 6.1 dB, which is about the difference observed with the parallel flow nozzle with the 58 in. long shroud. Thus, for both types of primary nozzles the non-uniform velocity distribution at the shroud exit with induced flow will cause appreciable acoustic production over that of the uniform velocity distribution for the same average velocity.

VII.A.5 REVERSE SLOTTED CONE SUPPRESSORS

Reverse Slotted Cones and Shroud

The primary objectives of the reverse slotted cone suppressor concept[10,11] were to decrease the length of the supersonic region for a suppressor configuration which is simpler than the multitubes and multishrouds suppressor, Refs. 33 and 34. Since the acoustic radiation from the supersonic region is nearly 75 percent of the total radiation as observed experimentally in Refs. 1, 14, 28 and shown by the supersonic jet noise theory of Nagamatsu and Horvay[4], it was anticipated that by making the supersonic region extremely short with multiple slots the total acoustic power from the supersonic jets should be decreased.

It was shown in Refs. 4 and 5 from the available experimental data that the supersonic length was a function of jet Mach number and the jet diameter, Eq. (VII.A-2). Thus, for a given pressure ratio of 3.2, which corresponds to a jet Mach number of 1.4, the length of the supersonic region downstream of the slot is a function of the slot width to the first approximation. With this in mind the slot widths for the 60° and 75° cones with 28 and 58 slots respectively were selected so that sonic velocity was attained at the cone apex in Refs. 10 and 11. The photograph of the 60° reverse slotted cone with 28 slots is presented in Figure VII.A-18A and a sketch of the cone with a shroud is presented in Figure VII.A-18B. For these cones the ratio of the solid surface to the slot area was equal to 3 in order to permit mixing of the ambient air with the primary flow emerging from the slots. The area of the slots was equivalent to the area of a 2 in. diameter convergent nozzle. Two shrouds of 4.2 and 12 in. lengths with inside diameter of 4 in. were used with the reverse slotted cones as shown in Figure VII.A-18B.

Flow Characteristics

Both impact pressure and total temperature surveys were conducted across the jet downstream of the reverse slotted cones with and without the shroud and along the axis of the jet. From these measurements the Mach number, velocity, density, and temperature were determined and are presented in Ref. 11. The Mach number profiles across the jet at one in. downstream of the apex of

the 60° and 75° reverse slotted cones are presented in Figure VII.A-18A. At this axial location from the apex there is a relatively large region in the vicinity of the jet axis where the velocity is very low. For the 60° cone with 28 slots and 75° cone with 58 slots, where both of these cones were designed to achieve sonic velocity in the plane of the cone apex, the radial velocity distributions are similar with a slightly higher velocity and narrower jet for the 75° cone. When the number of slots was doubled for the same total slot area with the 60° reverse slotted cone the velocity downstream of the cone was higher and the jet was smaller than for the 28 slots configuration. Also, for the 56 slots configuration the region of the low velocity in the central portion of the cone was much greater than for the 28 slots.

The axial Mach number distributions for the convergent jet at a Mach number of 1.4 and for the 60° and 75° reverse cones with slots are presented in Figure VII.A-18D. For the plain jet with a throat diameter of 2 in. the sonic velocity was attained on the axis at approximately 28 in. form the nozzle exit. But with the slotted reverse cones the sonic velocity was located close to the cone apex and consequently, the jet velocity downstream of the cone was subsonic as indicated in this figure. Also, for these cones the wake regions were appreciable over the central portion of the cone; thus, the axial velocity downstream of the cone apex was very low over the initial distance and increased as the mixing progressed downstream. After this initial mixing portion of the core region the axial velocity remained nearly constant for a short distance before decaying like a fully developed subsonic turbulent jet as shown in Refs. 1, 2, 24 and 25. The highest axial flow Mach number of approximately 0.63 downstream of the reverse slotted cone occurred with the 75° cone with 58 slots and the lowest flow Mach number with the 60° cone with 28 slots. These results with the reverse slotted cone indicate that it is possible to drastically shorten the supersonic region and decrease the jet velocity by rapid mixing with the ambient air because of the large jet surface exposed for the mixing to occur.

By the use of the piezoelectric impact pressure probe. the distributions of the axial impact pressure fluctuations were determined for the 60° and 75° reverse slotted cones and the results are presented in Figure VII.A-18E. The

highest rms piezoelectric pressure fluctuations was approximately 1 mv for the 75° cone and was located at approximately 30 in. from the cone apex. For the 60° cone with 56 slots the peak piezoelelectric pressure fluctuations was slightly lower than for the 75° cone but the axial location of the peak was about the same. The lowest rms peak pressure fluctuations was for the 60° cone with 28 slots but this peak was located close to 40 in. from the cone apex. It is interesting to note that the piezoelectric impact pressure fluctuations downstream of the peak value decreased with distance similarly for these reverse slotted cones. This type of decrease has been observed for the fully developed turbulent subsonic jet decay in Refs. 1 and 2.

The base pressures on the central part of the solid portion were determined for the 60° and 75° reverse slotted cones as shown in Figure VII.A-18F for a nozzle pressure ratio of 3.2. For these cones the lowest base pressures existed close to the outer region of the cone. With the 60° cone with 56 slots the ratio of the base pressure to the ambient pressure was approximately 0.54 at a radial position of 0.18 in. from the outer edge. After the minimum pressures for these cones the base pressure increases towards the axis and at the cone apex the base pressure ratio was approximately 0.9 for these cones. Since the velocities over the central region of these reverse slotted cones were very low, the pressure in this wake region approached the ambient pressure. The base pressures for the reverse slotted cones can be increased by increasing the ratio of the solid conical area to the total slot area from 3 to a higher value, and thus, there will be more solid surface over which the ambient air can reach the interior of the reverse slotted cone surface.

Acoustic Characteristics

From the microphone measurements at eight angular positions on a 10-ft. radius from the jet axis, the overall sound pressure levels were determined in Ref. 11 and are presented in Figure VII.A-18G for the reverse slotted cone with and without the shrouds. Without the shroud the 60° reverse slotted cone with 28 slots had the highest overall sound pressure levels with approximately 15 dB reduction from the plain Mach 1.4 jet at the 19.1° position. The reduction was approximately 3 dB at the 60° position with a greater reduction at larger angular positions. The variations of the overall sound pressure level with the

angular position were quite similar for the three reverse slotted cones. For the 60° cone with 56 slots and 75° cone with 58 slots the overall sound pressure levels were quite close as indicated in this figure. The addition of the short shroud, $S_{4.2}$, to the reverse slotted cones increased slightly the overall sound pressure levels from the case without the shroud. But the addition of the longer shroud, S_{12}, to the 75° cone decreased the sound pressure levels for all angular positions from that existing with the cone alone. Even with the shrouds the highest sound pressure levels occurred at the 60° position from the jet axis.

The overall sound power levels for the convergent nozzle at a Mach number of 1.4 and for reverse slotted cones with and without the shrouds[11] are presented in Table VII.A-4. The corresponding power spectra are shown in Figure VII.A-18H together with the spectra for a plain jet at a Mach number of 0.85 for comparison purposes. For the 60° cone with 28 slots the overall sound power level reduction from a plain jet at a Mach number of 1.4 was 6.7 dB, and with 56 slots the sound power level reduction was increased to 12.4 dB as shown in Table VII.A-4 and Figure VII.A-18H. The power levels for this latter configuration were lower at all frequencies than that existing for the plain jet with the largest reduction of approximately 14 dB occurring at about 5000 Hz. The addition of the short shroud, $S_{4.2}$, to this 60° cone with 56 slots increased the power spectra slightly over most of the frequency range compared to the case without the shroud and the overall sound power level reduction from the plain jet was decreased to 10.2 dB.

For the 75° reverse slotted cone with 58 slots the sound power level spectra was very close to that for the 60° cone with 56 slots over the lower frequency range to 500 Hz and from this frequency to 10,000 Hz the power spectra was slightly lower with the greatest difference occurring at approximately 3500 Hz. For frequencies higher than 10,000 Hz the sound power levels for the 75° cone with 58 slots was 12.5 dB and the reductions were 12.0 and 14.3 dB with the short $S_{4.4}$ and longer shroud S_{12} respectively as presented in Table VII.A-4 and Figure VII.A-18H. The addition of the longer shroud to the 75° cone decreased the power levels from the case without the shroud at the higher frequencies and increased the overall power level reduction by 1.8 dB.

For both the 60° and 75° reverse slotted cones the sound power level spectra are higher than that for the plain jet at a Mach number of 0.85 as shown in Figure VII.A-18H. At a frequency of about 1000 Hz the difference is only about 4 dB but at higher frequencies the differences are much greater, becoming nearly 15 dB at 10 KHz. Since the velocities downstream of the reverse slotted cones are low as indicated in Figure VII.A-18D, the sound power levels being higher than the Mach 0.85 plain jet for frequencies higher than 1 KHz would indicate that the noise from the supersonic regions from the slot exits is contributing to this difference. Further investigations will be conducted to resolve the noise generation from reverse slotted cone suppressors and to achieve greater noise level reduction from supersonic jets.

VII.A.6 MULTITUBES AND MULTISHROUDS SUPPRESSORS

191 Tubes, 191 Shroud, and Single Shroud

Since the investigation of a single long shroud with supersonic jets indicated a large reduction of 17 dB in the overall sound power level from a Mach 1.4 jet, Refs. 6, 8, 13, it was decided to study similar phenomena with multitubes and multishrouds[33,34]. With the multitubes in place of a single nozzle, the length of the supersonic region is decreased for a given supersonic pressure ratio across the nozzle as shown by Equation (VII.A-2) and Refs. 4 and 5. As a first approximation the reduction in the supersonic region is related directly to the diameter of the tube; thus, by decreasing the single equivalent nozzle diameter of 1-9/16 in. to 191 tubes of 0.115 in. inside diameter, the length of the supersonic region should decrease by a factor of approximately 15. The supersonic region where most of the acoustic radiation is generated, as shown in Refs. 1 and 28, and by the supersonic jet noise theory of Nagamatsu and Horvay[4], is drastically decreased by the use of the multitubes. Also, the multitube configuration exposes greater surface area for the ambient air to be induced and mixed with the primary jet than with the single nozzle and shroud.

The second objective of the multitube suppressor concept was to determine the effectiveness of the multishrouds placed at the exits of each individual tube for reducing the overall sound power level from supersonic and subsonic

jets The shroud bundle consisted of 191 hexagonal passages with a maximum dimension across the hexagonal of 0.31 in. For this initial investigation the shroud length was 6 in. and the 191 tubes were located so that each tube was centered within each hexagonal passage of the 191 shroud bundle, as shown in Figures VII.A-19A and B. The length of the 191 tubes was selected to be 2 in. so as to permit adequate space for the ambient air to mix with the jets and to enter the multishrouds and single shroud as shown in Figure VII.A-19B. A detailed discussion of the model, flow, and acoustic results with the 191 tube suppressor is presented in Ref. 33 and some of the main results will be summarized in this report.

o Flow Characteristics

From the impact pressure and total temperature probe measurements, the local flow Mach number, velocity, temperature, and density were determined at various radial and axial locations from the jet or shroud exits. For these investigations the pressure ratio across the nozzle and tubes was 3.2, which corresponds to a nominal Mach number of 1.4. Radial Mach number distributions across the exits of the multitubes, multishrouds, and single shroud are presented in Figure VII.A-19C. At an axial distance of 1 in. from the 191 tube exits, the Mach number is not constant but varies across the tube bundle with the nighest Mach number existing downstream of the tube axis, and the velocity is lower towards the outer edge of the tube bundle. For the 191 shrouds of 1.667 and 3.335 in. lengths, the velocity at the shroud exits were subsonic with greater variations in the Mach number for the shorter shrouds. The addition of single shrouds of lengths 3.8 in., $S_{3.8}$, and 12 in., S_{12}, to the multitubes made the Mach number across the shroud exit quite uniform at Mach numbers of approximately 0.7 and 0.67 respectively, and these Mach numbers are slightly higher than for the 191 shrouds.

In Figure VII.A-19D the axial Mach number distributions for the plain convergent nozzle and multitubes with and without shrouds are presented for a jet Mach number of 1.4. For the equivalent single convergent nozzle of 1-9/16 in. diameter, the supersonic region extends to approximately 19 in. from the nozzle exit. With the 191 tubes of 0.115 in. inside diameter, the flow became sonic at approximately 1 in. downstream of the tube exit. This

is the distance expected because of the small tube diameter compared to the equivalent single nozzle diameter of 1-9/16in. Once the jets from the 191 tubes had merged the velocity on the axis was nearly constant at a Mach number of 0.72 for a distance of approximately 17 in. from the tube exits before decreasing like a subsonic jet. Thus, the merged jet flow behaves like a subsonic jet with a larger diameter.

With the single shroud of short length, $S_{3.8}$, Figure VII.A-19D, the Mach number on the axis was approximately 0.7 and remained nearly constant for a distance of approximately 12 in. before decreasing like a subsonic fully developed turbulent jet. For the 191 multishrouds of 1.667 in. length located with the entrance to the shrouds 3/16 in. upstream of the 191 tube exits, the velocity at the shroud exits decreased rapidly over the initial distance of 2 in. Downstream of this location the flow Mach number on the axis was approximately 0.6 for a distance of 12 in. before decreasing with distance. For the multishroud lengths of 3.335 and 6.0 in. the nearly constant flow Mach numbers on the axis were close to that for the shrouds of 1.667 in. length. But the decay of the flow velocity on the axis with distance was greatest with the 3.335 in. shroud length and the velocity decay for the 6 in. shroud length was less than for the 3.335 in. long shroud but greater than the shortest shroud length. This more rapid decay with the 3.335 and 6.0 in. multishroud length could be due to the viscous effects along the inside surfaces of the multishrouds.

Besides the impact pressure and total temperature measurements along the jet axis, piezoelectric impact pressure fluctuations were determined along the axis for various suppressor configurations and the results are presented in Figure VII.A-19E. The peak rms pressure fluctuation of approximately 4 mv occurred at a distance of 18 in. from the plain convergent nozzle exit for a jet Mach number of 1.4. This location was slightly ahead of the sonic location as indicated in Figure VII.A-19D. With the 191 tubes the peak piezoelectric pressure fluctuations occurred at approximately 26 in. from the tube exit and the peak value was close to 1.0 mv, which is much less than for the equivalent single convergent nozzle.

When the single shroud, $S_{3.8}$, was placed with the entrance of the shroud at the multitube exits, the location of the peak piezoelectric pressure fluctuations was slightly upstream of the 191 tube location but the magnitude of the peak rms value was close to that of the multitubes as indicated in Figure VII.A-19E. Since the velocity began to decrease closer to the shroud exit than for the multitubes, Figure VII.A-19D, the location of the peak pressure fluctuations was also closer to the shroud exit. The location of the peak pressure fluctuations and the magnitude for the multishroud of 1.667 in. was close to that of the multitubes and with single shroud. For the multishroud lengths of 3.335 and 6.0 in. the peak piezoelectric pressure fluctuations were approximately 0.6 mv but the peak for the 3.335 in. length was located slightly ahead of the 6.0 in. length. For all of the suppressor configurations and the plain convergent nozzle, the decay in the piezoelectric pressure fluctuations with distance downstream of the peak values had nearly the same slope as indicated in Figure VII.A-19E. This type of decay of the piezoelectric impact pressure fluctuations was observed for both subsonic and supersonic jets in Refs. 1, 2, and 8.

The base pressure distributions for the 191 tubes with multishrouds of various lengths and single shroud are presented in Figure VII.A-19F. With the 191 tubes alone the base pressure at the jet axis was 0.991 of the ambient pressure and the pressure increased towards the outer edge of the base plate. For this 191 tube configuration the ratio of the base area of the tube bundle to the total inside area of the tubes was 4.72. And also, the ratio of the ventilation area of the tube bundle to the tube total area was 11.86. Thus, there was a large area over which the outside air could enter the tube bundle so that the base pressure remained close to the ambient pressure.

The lowest base pressure of approximately 0.971 of the ambient pressure was obtained with the shortest multishroud length of 1.667 in. and the base pressure distribution increased with the multishroud length. These results indicate that the amount of induced air decreased with the multishroud length because of the boundary layer growth inside each shroud passage. By the addition of the single shroud, $S_{3.8}$, to the 191 tubes, the base pressure distribution was close to that of the multishroud of 3.335 in. length. Because

of the large area ratios for the base plate and the ventilation area to that of the total tube area, the base pressures for all of the configurations with the 191 tubes were very close to the ambient pressure.

o Acoustic Characteristics and Thrust Loss

From the microphone measurements at eight angular locations on a 10-ft. radius from the exit of the jet, the overall sound pressure level distributions for various configurations were determined in Ref. 33 and the results are presented in Figure VII.A-19G. In this figure the sound pressure level distribution for the plain convergent jet at a Mach number of 1.4 is presented for comparison purposes with the 191 tubes with and without shrouds. At the 19.1° angular position the sound pressure level with the multitubes was decreased approximately 18 dB from that existing for the plain jet. The smallest reduction of 12 dB occurred at the 43.8° location and at the largest angular position of 146.4° the reduction was approximately 20 dB.

The addition of 1.667 in. long multishrouds to the exit of the 191 tubes lowered the overall sound pressure level from that of the 191 tubes over the initial angular locations from 19.1° to 60° and for higher angular locations the sound pressure levels were about the same as shown in Figure VII.A-19G. The lowest overall sound pressure level distribution was obtained with the 6 in. long multishroud and at the 19.1° location the pressure level was nearly 26 dB lower than that for the plain jet. The reduction decreased to 17 dB at the 43.8° location and the reduction increased to 24 dB at the 146.4° location. With the 3.335 in. long multishroud the overall sound pressure levels were slightly higher than for the 6 in. long multishroud except at the 43.8° location. With the single shroud, $S_{3.8}$, the overall sound pressure levels were very close to that for the multitubes with slightly higher pressure levels over the angular positions of 80° to 146.4°. This may be due primarily to the noise radiated from the single shroud entrance region.

Sound power level spectra for multitubes with and without shrouds and for a 1-9/16 in. diameter convergent nozzle at a Mach number of 1.4 are presented in Figure VII.A-19H, for a pressure ratio of 3.2. With the 191 tubes of 2 in. length the overall sound power level was decreased 15.2 dB from that of the

plain jet. In Table VII.A-5 the overall sound power levels are presented for the various suppressor configurations and the plain jet obtained at different outside air temperature conditions. The overall sound power levels for the plain jet at a Mach number of 1.4 increased with the decrease in the ambient air temperature as discussed in Reference 8, but the reductions in the overall sound power levels from the plain jet with the various suppressor configurations were about the same to within the experimental accuracy as indicated in Table VII.A-5. Over the frequency range that was investigated the sound power levels for the multitubes were lower than that for the plain jet and the greatest reduction of approximately 25 dB occurred at about 4000 Hz.

When the 1.667 in. multishroud was placed with the entrance of the shroud located 3/16 in. upstream of the tube exits, the sound power levels were lower than the multitubes over the frequency range up to about 3500 Hz and for higher frequencies the power levels were greater than the multitubes as shown in Figure VII.A-19H. and the overall sound power level reduction from the plain convergent jet was 15.5 dB as indicated in Table VII.A-5, which is only slightly greater than for the multitubes alone. By increasing the multishroud length to 3.335 in. the overall sound power level reduction from the plain jet was increased to 19.0 dB, which is 3.5 dB greater reduction than the 1.667 in. multishroud, and the sound power levels were lower over the entire frequency range. With the multishroud length increased to 6 in. the overall sound power level reduction from the plain jet increased to 20.4 dB as presented in Table VII.A-5, which is an increase of 5.2 dB from that observed with the multitubes alone. For this longest multishroud the overall sound power level at 3500 Hz was approximately 30 dB less than that for the plain jet. Even at 16,000 Hz the sound power level was nearly 20 dB lower than for the plain jet.

With the single shroud located at the exit of the multitubes the sound power levels were slightly higher than the multitubes for the frequency range of 1000 to 5000 Hz and at higher frequencies the power levels were slightly lower as indicated in Figure VII.A-19H. The overall sound power level reduction was 13.7 dB from that of the plain jet, which is less reduction than the multitubes alone. These results with the multishroud and single shroud indicate

the importance of the types of shroud to be used in conjunction with the multitubes in order to obtain large noise reduction from supersonic jets. In a later section the acoustic analysis of the multitube suppressor will be presented to indicate the suppression phenomena of supersonic jets.

The variation of the overall sound power level reduction and the percentage thrust loss for 191 tubes with 191 shrouds of different lengths are presented in Figure VII.A-191. A thrust measuring device to determine the change in the thrust with various suppressor configurations was developed as discussed in Ref. 33. In this reference the base drag was calculated from the measured base pressure and the thrust loss due to the friction drag in the multitubes and multishrouds was calculated for the various shroud lengths. The calculated thrust losses for the various shroud configurations were correlated with the measured thrust losses and the agreement was reasonably good. For the multitubes the calculated thrust loss due to the base drag of 2.0 percent and the frictional drag inside the 191 tubes of 7.2 percent was 9.2 percent while the measured thrust loss was 10.2 percent. The corresponding overall sound power level reduction was 15.2 dB, as presented in Table VII.A-5 and Figure VII.A-191, which corresponds to 1.49 dB noise reduction per one percent measured thrust loss. The large frictional thrust loss for the 191 tubes of 2 in. length is due mainly to the large wetted surface for this number of tubes and by using a smaller number of tubes this thrust loss can be decreased as observed with 50 tubes[34], which will be discussed in the next part of this report.

With the addition of the 1.667 in. multishrouds to the multitubes, the thrust loss due to base drag was increased to 5.0 percent while the tube drag loss remained at 7.2 percent and the thrust loss of the multishrouds was 5.9 percent making the total calculated thrust loss 18.1 percent while the measured thrust loss was 16.8 percent. For this multishroud length the overall sound power level reduction was 15.5 dB, Table VII.A-5, which is only a 0.3 dB greater reduction with a 6.6 percent higher thrust loss than for the multitubes. For longer multishroud lengths of 3.335 and 6.0 in. the shroud frictional drag increased so that the thrust losses due to friction were 8.6 and 11.5 percent respectively. But with the 6.0 in. multishrouds the base drag thrust loss was only 2.11 percent while that for the 3.335 in.

multishroud was 4.41 percent and the total calculated thrust losses for these two shrouds were 20.8 and 20.2 percent respectively while the measured thrust loss was 26.7 percent for both lengths. The overall sound power level reductions and thrust losses for these multishrouds are presented in Table VII.A-5 and Figure VII.A-191. Because of the large wetted area for the longer multshroud losses, the frictional drag contributes to most of the thrust loss for these configurations. If the thrust loss is not too critical the multitubes with multishrouds are very effective in reducing a Mach 1.4 jet by 20.4 dB.

50 Tubes, 50 Shrouds, and Single Shroud

Since the single long shroud and 191 tubes and 191 shrouds were effective in decreasing the overall sound power levels for a Mach 1.4 jet by 15 and 21 dB respectively as discussed in Ref. 33, an investigation was conducted to determine whether 50 tubes of various lengths and with 50 shrouds are as effective as the 191 tube suppresser in reducing the noise from a Mach 1.4 jet. With the smaller number of tubes the multitube and multishroud suppressor concept is more practical to be used as a supersonic jet exhaust noise silencer. In Refs. 18 and 21 a greater number of tubes were investigated as a jet exhaust noise suppressor.

Also, it was desired to obtain information regarding the effect of the length of the 50 tubes, cf. Figures VII.A-20A and B, on the reduction of the noise level. The inside diameter of the tubes was 0.230 in. and the total area of the tubes was equal to a convergent nozzle with an exit diameter of 1-9/16 in., like the 191 tube suppressor. It was also desired to obtain information regarding the effect of the ratio of the base area to the total tube area so this ratio was decreased to 3.0, which again is more practical than the 191 tube configuration. The tube length was varied from 0 to 4 in. as shown in Figure VII.A-20A. For the 50 shrouds of 6 in. length the cross section was hexagonal and each tube exit was placed 3/8 in. inside the entrance to the shroud. Besides the multishrouds a single shroud, $S_{3.16}$, with an inside diameter of 3.16 in. and a length of 3.16 in. was used with the multitubes.

o Flow Characteristics

Impact pressure and total temperature surveys were conducted in the radial direction in the vicinity of the tube and shroud exits and along the center line in the axial direction and some of the representative results obtained in Ref. 34 are presented in Figures VII.A-20C through 20E. Immediately downstream of the tube exits for tube lengths of 0 to 4 in. the Mach number distributions in the radial direction were determined and are presented in Figure VII.A-20C. At the center of each tube exit the flow Mach number for all tube lengths was about the same with a slightly lower Mach number for the 4 in. long tube because of the greater viscous effects. Between the tube locations the flow Mach number was close to zero except for the 4 in. long tubes. Similar Mach number profiles across the exits of the 6 in. long multishroud and single shroud are presented in Figure VII.A-20D for a tube length of 2 in. At the shroud exits the Mach number varied from approximately 0.8 to 1.05 at the axis of the shroud. With the single shroud, $S_{3.16}$, the velocity at the shroud exit was higher than with the multishrouds. The radial Mach number distributions for other tube lengths were similar to that observed for the 2 in. length as discussed in Ref. 34.

In Figure VII.A-20E the axial Mach number distributions for 50 tubes with and without shrouds are presented for a tube length of 2 in. Because of the spacing between the tubes and the ratio of the base area to the tube area of 3.0, the Mach number of the merged jets was close to sonic for a pressure ratio of 3.2. And the axial velocity remained nearly constant to the 13 in. location before decreasing which is characteristic of a subsonic jet as observed in Refs. 1 and 2. Thus, the merged jet behaves like a uniform subsonic jet of larger diameter than the equivalent 1-9/16 in. diameter convergent jet, so the mixing of the multiple jets with the ambient air is very effective for both 191 and 50 tube configurations.

With the 6 in. long 50 shrouds, the axial flow Mach number was approximately 0.84, and the velocity remained nearly constant for approximately 15 in. downstream of the shroud exits before decreasing. The mixing of the ambient air with the supersonic jets within the 6 in. long multishrouds was effective

in decreasing the supersonic jet Mach number of 1.4 to 0.84. Besides permitting the momentum exchange within the shrouds, the multishrouds prevented the direct acoustic radiation from the supersonic region of the jet to the outside[4,5]. With the single shroud of 3.16 in. inside diameter, Figure VII.A-20B, the axial velocity downstream of the shroud exit was approximately 0.97 and remained nearly constant for about 10 in. before decreasing. As shown in the previous figure the radial Mach number distribution was not as uniform as observed with the 50 tube and 50 shroud configurations.

The axial variations of the piezoelectric impact pressure fluctuations were determined in Ref. 34 for the various tube lengths with and without shrouds and the results for the 2 in. long tubes are presented in Figure VII.A-20F. In this figure the impact pressure fluctuations for a 1-9/16 in. convergent nozzle at a Mach number of 1.4 are presented for comparison purposes. With this nozzle the rms peak value for the pressure fluctuations was approximately 4 mv and was located just ahead of the sonic point. With the 50 tubes the peak pressure fluctuation was slightly less than 2 mv and the location of the peak was farther downstream than for the plain jet. With the addition of the 6 in. long multishrouds to the 50 tubes, the peak rms value of the pressure fluctuations was decreased to approximately 1.6 mv. But with the use of the single shroud with the tubes the peak pressure fluctuation was approximately 2 mv. For all of these tube and shroud configurations and including the plain jet, the variations of the piezoelectric impact pressure fluctuations downstream of the location for the peak pressure fluctuation were similar and decreased approximately as $x^{-1.75}$ as observed in Refs. 1 and 2 for the decay of fully developed subsonic turbulent jets.

The base pressure distributions for various 50 tube lengths and shroud arrangements were determined in Ref. 34 for a pressure ratio of 3.2 and the results are presented in Figure VII.A-20G. For the tubes alone the lowest base pressure existed for the 1/4 in. tube length. The single shroud with tube length of 0, which corresponds to a base plate with holes as shown in Figure VII.A-20A, produced the lowest base pressures. As the tube lengths were increased the base pressure increased and was close to the ambient value for the 4 in. long tubes. The addition of the multishrouds to the tubes decreased the base pressure

compared to the tubes alone, but again for the longer tubes the base pressure approached the ambient pressure because of the large area for the ambient air to enter the multishrouds.

o Acoustic Characteristics and Thrust Loss

The overall sound pressure levels as a function of angular position from the jet axis for the 50 tubes with and without shrouds and for a convergent nozzle were determined in Ref. 34 and the results for a tube length of 2 in. are presented for a Mach 1.4 flow condition in Figure VII.A-20H. For the plain jet the overall sound pressure level was highest at the 19.1° position and decreased to the 60° location and for higher angles from the jet axis the sound pressure level remained nearly constant because of the shock bottles. When the plain jet was replaced by 50 tubes with the same total area as for the convergent nozzle, the overall sound pressure level decreased approximately 11 dB at the 19.1° location, and the pressure level decreased to the 100° location before increasing at higher angles. With the addition of 50 shrouds to the 50 tubes, the overall sound pressure level decreased approximately 16 dB at the 19.1° location from the plain jet. For this configuration the overall sound pressure level decreased monotonically with the angular position and at the 146° location the pressure level reduction was approximately 25 dB. With the single shroud and the 50 tubes of 2 in. length, the overall sound pressure level distribution was slightly higher than for the 50 tubes over the initial 115° and was lower for higher angles as indicated in Figure VII.A-20H. Similar overall sound pressure level distributions were obtained with other tube lengths with and without shrouds in Ref. 34.

From the eight microphone measurements on a 10-ft. radius, the overall sound power spectra were determined for various tube lengths both with and without the shrouds for a jet Mach number of 1.4 and representative power spectra are presented in Figure VII.A-20I a tube length of 2 in. In this figure the power spectra for a convergent jet at a Mach number of 1.4 is also presented. With the 50 tubes of 2 in. length the sound power level at all frequencies was lower than for the plain jet with the greatest reduction occurring at frequencies higher than 1000 Hz. The power level reduction at 4500 Hz was approximately

18 dB from that of the plain jet and the overall sound power level reduction was 11.5 dB as presented in Table VII.A-6 and Figure VII.A-20I.

With the single shroud the power spectra at all frequencies was slightly higher than that for the 50 tubes and the overall sound power level reduction was 10.3 dB. Thus, this type of shroud with the 50 tubes is not effective in increasing the overall sound power level reduction with the multitubes. Similar results were observed with the 191 tubes in Ref. 33. The addition of 6 in. long multishrouds to the 50 tubes reduced the sound power level from that of the multitubes at all frequencies. At lower frequencies the reduction in the power level from that of the plain jet was approximately 5 dB up to 500 Hz and at higher frequencies the reduction was even greater with a reduction of approximately 24 dB at 4500 Hz as indicated in Figure VII.A-20I. And the overall sound power level reduction was 18.1 dB from a plain Mach 1.4 jet as presented in Table VII.A-6. This level of power reduction was also achieved with 191 tubes with 191 shrouds in Ref. 33. Thus, the 50 tubes with 50 shrouds suppressor configuration is just as effective as the case with the larger number of tubes and shrouds.

From the measured base pressure distributions for the 50 tubes of various lengths with and without the shrouds, and from the calculated skin friction drag, the total thrust loss due to the base drag and the skin friction drags for the tubes and shrouds was calculated and correlated with the measured thrust loss. In the calculation of the skin friction drag the boundary layer was assumed to be laminar for the tubes because of the low Reynolds number and the boundary layer was assumed to be turbulent for the shrouds. Correlation of the calculated and measured thrust losses are presented in Ref. 34, for a jet Mach number of 1.4, and the measured thrust losses and the overall sound power level reductions are presented in Figure VII.A-20J as functions of the 50 tube lengths.

For a 50 tube length of 0 in., which corresponds to the base plate with holes, cf. Figure VII.A-20A, the calculated thrust loss was 15.3 percent while the experimental loss was 16.7 percent, and the overall sound power level reduction from a convergent Mach 1.4 jet was 15.0 dB as presented in Table VII.A-6 and Figure VII.A-20J. Nearly all of the thrust loss was due to the

low base pressure, Figure VII.A-20G. As the 50 tube length was increased the base pressure increased so that the thrust loss decreased. For 1 in. long tubes the thrust loss was only 3.34 percent while the overall sound power level reduction was 11.2 dB. For longer tubes the overall sound power level reduction was about the same and the thrust loss was also about the same as for the 1 in. tube length because the base drag decreased and the friction drag increased with the tube length.

The 6 in. long multishrouds were used only with tube lengths of 1 in. and greater as shown in Figure VII.A-20J. With the 1 in. tubes the thrust loss due to the base drag was 10.2 percent and the friction drag in the tubes and shrouds were 0.97 and 11.7 percent respectively with the resultant calculated thrust loss of 22.8 percent. For this configuration the measured thrust loss was 26.7 percent and the observed overall sound power level reduction from a Mach 1.4 jet was 14.5 dB. For the 2 in. tubes with multishrouds, the measured thrust loss was 20 percent and the overall sound power level reduction was 18.1 dB, Table VII.A-6. Because of the long length of 6 in. for the multishrouds, the thrust loss due to the frictional force on the surfaces of the shrouds was quite large. Further investigations are being conducted to decrease the length of the multishrouds for minimizing the thrust loss and still retain the large noise suppression feature of the multishroud.

VII.A.7 SUPERSONIC JET NOISE SUPPRESSOR ANALYSIS

Single Shroud, Multitubes and Multishrouds

The initial investigation of the single long shroud with both parallel flow and convergent nozzles at a Mach number of 1.5 indicated that a large reduction of 17 dB in the overall sound power level from that of the plain jet was possible[1,8]. Since the long shroud was not practical even though it did yield information regarding the required velocity reduction for supersonic jets and the corresponding noise reduction, the multitube and multishroud suppressor concepts were investigated with supersonic and subsonic jet exhaust velocities in Refs. 18, 33 and 34. Both 191 and 30 tubes and shrouds were effective in decreasing the overall sound power level of a Mach 1.4 jet from a convergent nozzle by approximately 20 dB as discussed in the previous section.

The flow and acoustic results from these suppressors will be analyzed and equations, based upon the experimental data, for estimating the overall sound power level reduction from supersonic jets will be derived.

From the axial impact pressure and total temperature probe surveys, the flow parameters were determined[33,34] for the various multitube and multishroud configurations for a pressure ratio of 3.2, which corresponds to a jet Mach number of 1.4. The flow Mach number after the multijets coalesced and remained constant before decreasing and is defined as the coalesced Mach number. The distance at which the uniform Mach number is attained is defined as the coalesced distance.

In Figure VII.A-21 the coalesced Mach number and the distance are presented as a function of the ratio of the tube spacing for a constant pressure ratio of 3.2 for 50 and 191 tubes and 50 and 313 holes in the base plate, which is referred to as the boiler plate configuration. The area ratios of the base plate area to the total tube area were 3.0 and 4.72 for the 50 and 191 tubes respectively. The ratios of the tube spacing to the tube diameter were .36 for the 50 tubes and .88 for the 191 tubes, and the coalesced Mach numbers were 1.0 and 0.73 respectively. The equation relating the coalesced Mach number to the tube spacing ratio for a pressure ratio of 3.2 across the tubes, which corresponds to a jet Mach number of 1.4 is given by

$$M_c = 1.4 - .71(s/d)^{.55} \qquad \text{(VII.A-6)}$$

In deriving this equation it was assumed that zero tube spacing ratio corresponded to a single convergent jet. This equation must be taken as a first approximation for estimating the coalesced Mach number as a function of the tube spacing because the area ratio of the base plate to the total tube area was not the same for the 50 and 191 tube configurations. The decrease in the coalesced Mach number from the plain single jet with the tube spacing is very large. As the spacing between the tubes becomes larger the amount of air induced before the jets become coalesced is increased with a corresponding decrease in the coalesced Mach number because of the greater mixing and momentum exchange between the primary jets and the ambient gas.

With the base plate with 50 holes, the coalesced Mach number was close to that observed with the 50 tubes of various lengths as shown in Figure VII.A-21. It was observed in Ref. 34 that the supersonic jet flow region was shorter with the 50 holes than with the 50 tubes of various lengths. For the 313 holes with the ratio of the base plate area to the hole area of 2.5, the coalesced Mach number was much less than that observed with the tubes for the hole spacing ratio as indicated in Figure VII.A-21. Evidently the coalesced Mach number is controlled by the hole spacing as well as the ratio of the base plate to the hole area[18]. Further investigation with various numbers of holes but keeping the base plate area ratio constant should be conducted to determine the variation of the coalesced Mach number with the ratio of the hole spacing.

For a pressure ratio of 3.2 for the multitubes and holes in the base plate, the distance in terms of diameter for the jets to coalesce and attain the coalesced Mach number was about the same as indicated in Figure VII.A-21. The coalesced distance was about 12 diameters of the tubes or holes for the nominal supersonic jet Mach number of 1.4. For this Mach number the sonic point on the jet axis was approximately 12.5 diameters downstream from the convergent nozzle exit in Reference VII.A-1. Thus, the distance for the multiple jets to coalesce for a supersonic Mach number of 1.4 is not sensitive to the tube or hole spacings or the base plate area ratio. This is not the case for the coalseced Mach number.

The overall sound power level reductions for multitubes, multiholes, and multishrouds are presented in Figure VII.A-22 as a function of the coalesced Mach number, similar to the summary for the power level reductions for a single long shroud in Figure VII.A-17C. In this figure the overall sound power level differences between the convergent nozzle with an exit diameter of 2 in. at a Mach number of 1.4 and that for the same nozzle operated at lower Mach numbers[1], taken as the coalesced Mach number, are presented. Since the mass flows at the lower Mach numbers with an exit diameter of 2 in. are less than for the Mach 1.4 jet, the effects of the mass flow upon the overall sound power level for a given jet velocity were corrected by the equation

$$\Delta dB = 10 \log_{10} \frac{m_1}{m_2}, \qquad \text{(VII.A-7)}$$

where m_1 is the mass flow for the Mach 1.4 jet and m_2 is the mass flow at the lower Mach numbers presented in Ref. 1. For both the subsonic jet noise theory of Lighthill[31] and the supersonic theory of Nagamatsu and Horvay[4], the overall acoustic power is related directly to the mass flow for constant jet properties. The decrease in the overall sound power level from that of a 2 in. diameter convergent nozzle at a Mach number of 1.4 for a pressure ratio of 3.2 can be approximated in Figure VII.A-22 by

$$\Delta dB = 56.4 - 66.2\, M_c + 37.8\, M_c^2 - 13.8\, M_c^3 \qquad \text{(VII.A-8)}$$

where the mass flow at lower jet Mach numbers is the same as for the Mach 1.4 jet.

With 50 tubes and tube spacing ratio of 0.36 and base plate area ratio of 3.0, the coalesced Mach number was approximately 1.0, Figure VII.A-20E, for a pressure ratio of 3.2. For 50 tube lengths of 1/4 to 4 in. the overall sound power level reductions varied from 11.5 dB to 13 dB as discussed in Ref. 34 so that in Figure VII.A-22 a value of 11.5 dB reduction was used for the 50 tubes of 2 in. length. For the 191 tube configuration[33] with the tube length of 2 in., the tube spacing ratio of 0.88, and base plate area ratio of 4.72, the coalesced Mach number was approximately 0.73, Figure VII.A-19D, for a pressure ratio of 3.2. The overall sound power level reduction from a convergent Mach 1.4 jet was approximately 15.6 dB as shown in Figure VII.A-22. It is interesting to note in this figure that the reductions of the sound power level from a convergent Mach 1.4 jet by the 50 and 191 tubes fair into a curve as a function of the coalesced Mach number. This curve for the reduction of the overall sound power level with multitubes from a convergent nozzle at a Mach number of 1.4 can be expressed as a function of the coalesced Mach number by

$$\Delta dB = 19.2 - 8.95\, M_c + 12.9\, M_c^2 - 11.7\, M_c^3. \qquad \text{(VII.A-9)}$$

At a coalesced Mach number of 1.0 the difference in the reduction in the sound power level by the 50 tubes and that due to a plain jet operated at Mach 1.0 with the same mass flow as the Mach 1.4 jet is not great as indicated in Figure VII.A-22.

By placing the 6 in. long multishrouds, Figure VII.A-20A, at the exits of 50 tubes of 2 in. length, the coalesced Mach number was 0.85, Figure VII.A-20E, and the corresponding overall sound power level reduction from a Mach 1.4 jet was 18.1 dB as shown in Figure VII.A-22. For 50 tubes of 4 in. length and multishrouds the coalesced Mach number was 0.82 and the corresponding sound power level reduction was 20.3 dB as observed in Ref. 34. With this suppressor configuration the overall sound power level was close to that observed for a plain jet at a Mach number of 0.82 and with the same mass flow as the 2 in. diameter Mach 1.4 jet. With the 191 tubes and 191 shrouds of 6 in. length[33], the coalesced Mach number downstream of the shroud was 0.60, Figure VII.A-19D, and the corresponding overall sound power level reduction was 21.9 dB as shown in Figure VII.A-22. For this configuration the overall sound power level reduction was less than that for a Mach 0.6 jet with the mass flow of the 2 in. diameter Mach 1.4 jet. The viscous losses due to the large wetted surface in the 191 shrouds were large and caused a more rapid decay in the velocity than a uniform jet as indicated in Figure VII.A-19D. This increased viscous phenomenon could cause greater noise than for a uniform jet. Further investigations will be conducted to investigate this viscous phenomenon. The equation for the overall sound power level reduction with multishrouds from a Mach 1.4 jet can be expressed as a function of the coalesced Mach number by

$$\Delta dB = 23.1 + 13.9\ M_c - 23.7\ M_c^2 + 2.87\ M_c^3. \qquad \text{(VII.A-10)}$$

The overall sound power level reductions achieved with 50 and 313 holes in the base plate are presented in Figure VII.A-22 as a function of the coalesced Mach number. For the 50 holes the hole diameter was 0.230 in. in the same base plate as for the 50 tubes of various lengths as discussed in Ref. 34. In place of 191 tubes, 313 holes of 0.125 in. diameter were used in the base plate. And the ratios of the hole spacing to the diameter were 0.375 and 0.50 for the 50 and 313 holes respectively. Because of the interaction of the jets from the holes, the coalesced Mach numbers were lower with the

multiholes than for the multitubes as shown in Figures VII.A-21. Due to the lower coalesced Mach numbers the overall sound power level reductions from the convergent nozzle at a Mach number of 1.4 were greater than for the multitubes as shown in Figure VII.A-22. With the 50 hole configuration the coalesced Mach number was 0.90 and the overall sound power level reduction was 15 dB, which was greater than for 50 tubes. For 313 holes the coalesced Mach number was 0.62 with corresponding sound power level reduction of 18.6 dB. And the equation for the overall sound power level reduction with multiholes from a convergent nozzle at a Mach number of 1.4 can be expressed as

$$\Delta dB = 14.9 + 18.4\ M_c - 19.7\ M_c^2 - 0.80\ M_c^3. \qquad \text{(VII.A-11)}$$

These results with the multihole configurations indicate a rather large reduction in the overall sound power level from a Mach 1.4 jet but the disadvantage is the relatively large thrust loss because of the low base pressure as discussed in Refs. 33 and 34. This thrust loss may be increased by the proper hole spacing to the base plate area for a given pressure ratio across the nozzle.

Acoustic Shielding of Supersonic Jets

The multitubes and multishrouds suppressors were very effective in decreasing the overall sound power level of a convergent nozzle at a Mach number of 1.4. An analysis was made by considering the flow and acoustic results for the 191 and 50 tubes to determine the acoustic radiation from the supersonic and subsonic regions of the jets. For 50 tubes the coalesced Mach number was 1.0 and the overall sound power level reduction from a Mach 1.4 jet was 11.5 dB and for 191 tubes the coalesced Mach number was 0.72 with overall sound power level reduction of 15.2 dB. In this section these results will be analyzed by using Lighthill's theory[31] for the subsonic portion of the jet and Nagamatsu and Horvay theory[4] for the supersonic region.

In Section VII.A-3 of this report the Lighthill's equation, Equation (VII.A-5), was presented for the subsonic jets, which have flow and acoustic characteristics that are reasonably close to the assumptions used in the derivation of the theory. But for supersonic jets the observed flow and

acoustic characteristics are quite different than for subsonic jets as observed in Refs. 1, 14 and 28. For supersonic jets the peak acoustic radiation occurs in the vicinity of the sonic location and the acoustic radiation per unit jet length is not constant but increases from the jet exit to the peak at the sonic location. And over the subsonic portion of the jet the acoustic radiation decreases as x^{-6}. Nagamatsu and Horvay[4] in developing the supersonic jet noise theory used these observed supersonic jet phenomena. The overall sound power radiation from supersonic jets was considered to consist of the contribution from the supersonic region given by

$$0 \leq x/D \leq L_s : W_A = \int_0^{L_s} w_d \, d(x/D) = \frac{10^{-4}}{9.6} m \frac{\rho_j}{\rho_a} \left(\frac{c_j}{c_a}\right)^5 c_j^2 M_j^{7-\alpha} (5M_j^2 + 0.8) \left[\frac{1 + M_j^{\alpha-\beta}}{2}\right] \quad \text{(VII.A-12)}$$

and for the subsonic region by

$$L_s \leq x/D \leq \infty : W_B = \int_{L_s}^{\infty} w_d \, d(x/D) = \frac{10^{-4}}{9.6} m \frac{\rho_j}{\rho_a} \left(\frac{c_j}{c_a}\right)^5 c_j^2 M_j^{7-\beta} \left(\frac{5M_j^2 + 0.8}{5}\right) \quad \text{(VII.A-13)}$$

And the equation for the total acoustic power output from supersonic jets is the sum of these equations

$$W = W_A + W_B = \frac{10^{-4}}{9.6} m \frac{\rho_j}{\rho_a} \left(\frac{c_j}{c_a}\right)^5 (c_j^2 M_j^7) (5M_j^2 + 0.8) \frac{M_j^{-\alpha} + M_j^{-\beta}}{2} + \frac{M_j^{-\beta}}{5} \quad \text{(VII.A-14)}$$

A detailed discussion of the derivation of these equations are presented in Ref. 4. Thus, the total acoustic power output from a supersonic jet is a function of the jet Mach number, density and velocity of sound for both

the jet and ambient gas and the parameters α and β which depend upon the type of nozzle as determined in Ref. 1.

For a convergent nozzle with an exit diameter of 1-9/16 in. and a pressure ratio of 3.2, which corresponds to a jet Mach number of 1.4, the values of α and β were 0.4 and -1.3 respectively as determined from the experimental acoustic overall sound power level in Ref. 1. The mass flow through the 191 tubes of 0.125 in. diameter at a pressure ratio of 3.2 was equivalent to that for the 1-9/16 in. convergent nozzle as observed in Ref. 33. Slightly downstream of the tube exits, the Mach number was 1.37 and decreased to a Mach number of 0.72 at 1 in. from the tube exit and remained at this Mach number until the 15 in. location on the axis before decaying as a fully developed subsonic jet as shown in Figure VII.A-19D.

With the 191 tubes at a pressure ratio of 3.2 the overall sound power level was 135.5 dB, while the plain 1-9/16 in. diameter nozzle at the same pressure ratio was 150.7 dB as presented in Table VII.A-5, which corresponds to an overall sound power level reduction of 15.2 dB. By assuming that the 191 tubes are radiating acoustically without interference from each other, the supersonic jet noise from each tube can be determined by the use of Equation (VII.A-12). Thus, the total acoustic power output from the supersonic region of 191 individual jets is 93.6 watts for the multitube mass flow of 0.0586 slugs/sec., and the acoustic power level is 149.7 dB. Using the experimental mass flow rate at the coalesced Mach number of 0.72 at 1 in. location downstream of multitubes, the acoustic power from this subsonic jet by Lighthill's Equation (VII.A-5) is 0.808 watts, which corresponds to a power level of 129.1 dB. For the 191 tubes the observed overall sound power level was 135.5 dB which corresponds to 3.55 watts. Hence, the difference in the acoustic power between this value and the acoustic power for the subsonic portion is 2.74 watts. And this can be considered as the acoustic power radiation from the supersonic region of the multijets. For each tube the acoustic power output from the supersonic region is 0.491 watts as given by Equation (VII.A-12). Hence, it requires only an equivalent of 5.68 tubes to produce sound power radiation of 2.74 watts, or approximately 39° from each of the outer ring of 52 tubes.

It is evident from this analysis of the acoustic data in Ref. 33 that the shielding effects of the supersonic region form 191 tubes are extremely large. Because of the large number of tubes of 0.125 in. diameter, the supersonic region extended to approximately 1 in. from the tube exits as shown in Figure VII.A-19D, as compared to an equivalent convergent nozzle of 1-9/16 in. diameter with a supersonic length of approximately 18 in. Only about 2.97 percent of the 191 tubes are radiating acoustic power from the supersonic region to the surrounding air. These results indicate that the acoustic radiations from the supersonic regions of the tubes located inside the outer row of 52 tubes are attenuated by the adjacent supersonic jets. Even for the outer ring of tubes the acoustic radiations are attenuated by the interference of the sound waves from adjacent tubes.

In Ref. 34 the flow and acoustic characteristics for 50 tubes of various lengths were investigated at supersonic flow conditions. At a pressure ratio of 3.2 the supersonic coalesced Mach numbers were close to 1.0. By assuming that 50 tubes are radiating acoustically without interference from each other with a total mass flow of 0.0651 slugs/sec., the total acoustic power output from the supersonic region of 50 individual jets was calculated from Equation (VII.A-12) and the value was 91.5 watts, or 1.83 watts per tube. The experimental overall sound power level for 50 tubes of 2 in. length was 140.3 dB, which corresponds to 10.72 watts. From the radial and axial surveys with impact pressure and total temperature probes the jet coalesced at approximately 3 in. downstream from the tube exits at a Mach number of approximately 1.0 as shown in Figure VII.A-20E. At an axial distance of 3 in. from the tube exits, the mass flow and the mean flow quantities of velocity, density, and temperature were determined from the radial surveys. Using these values for the properties of the merged jet, the acoustic power output from the sonic jet was calculated by Equation (VII.A-5) and the total power was found to be 5.26 watts.

The overall sound power level for 50 tubes of 2 in. length at a pressure ratio of 3.2 was found to be 140.3 dB, which corresponds to 10.72 watts, in Ref. 34 and presented in Table VII.A-6. By taking the difference in the overall sound power between this value and the calculated acoustic power of 5.26 watts

from the sonic jet, the sound power from the supersonic portion of the jet is 5.46 watts. Since the acoustic power from the supersonic region of each tube was calculated to be 1.83 watts, it would require only 2.99 tubes to obtain the acoustic power from the supersonic regions of the 50 tube bundle, or in supersonic region, only approximately 49° from each of the outer row of 22 tubes is radiating to the surroundings.

From the flow and acoustic results for 191 and 50 tubes presented in Refs. 33 and 34, the multitube concept is effective as a supersonic jet exhaust noise suppressor because of the following effects: (1) Since the supersonic region is proportional to the diameter of the nozzle and the supersonic jet Mach number or pressure ratio, the supersonic length is drastically decreased by using the smaller diameter tubes. (2) With the multitubes with spacing between the tubes, the primary jet is exposing a much larger surface area to the ambient air, and consequently the primary jet velocity is drastically decreased in a short distance and the coalesced jet behaves like a uniform jet at lower Mach numbers. (3) Finally, the most effective contribution to the noise reduction is the large attenuation of the acoustic waves through the supersonic region, only a small fraction of the acoustic radiation from the supersonic region is propagated to the surroundings.

VII.A.8 CONCLUSIONS

For subsonic Mach numbers, including sonic Mach number, the velocity on the axis remained constant over a distance of approximately 5 diameters before decreasing in the turbulent decay region as x^{-1}. The length of the supersonic region was proportional to M_j^2 and downstream of the sonic point the velocity decay was similar to that observed for subsonic jets.

The peak piezoelectric impact pressure fluctuations occurred for subsonic jets on the axis at approximately 9 diameters and decayed downstream in the fully developed subsonic turbulent jet as $x^{-1.75}$. For supersonic jet Mach numbers the peak impact pressure fluctuations occurred just ahead of the sonic point, and in the subsonic region the pressure fluctuations decreased like the subsonic jets.

The highest overall sound pressure levels occurred at an angular position of 19.1° from the jet axis for both subsonic and supersonic jets. Power spectra for subsonic jets were similar with the peak occurring for a 2 in. diameter convergent nozzle at approximately 4 KHz for Mach numbers of 0.6 to 1.0. At a Mach number of 1.4 the peak power occurred at a frequency of 5 KHz which corresponds to a Strouhal number of 0.64.

Overall sound power levels for Mach numbers of 0.6 to 1.5 were determined and compared with the subsonic theory of Lighthill and supersonic theory of Nagamatsu and Horvay. The exponents α and β in the supersonic theory were evaluated for convergent and parallel flow nozzles as functions of the jet Mach number.

At a jet Mach number of 1.5 the overall sound power level for a contoured nozzle with parallel flow was 3 dB less than for the convergent nozzle with shock bottles. The insertion of six small rods at the periphery of the jet increased the noise level for the contoured nozzle but the convergent nozzle noise level was decreased 6 dB. With the six rods and a long shroud to the jet exhaust for inducing and mixing the ambient air with the primary jet flow the overall sound power level was decreased 17 dB for the convergent nozzle.

With the reverse slotted cones the supersonic region was decreased to the apex of the cone by adjusting the opening of the slots, and the overall sound power level was reduced 14 dB for a Mach 1.4 jet with 58 slots for a 75° cone angle. Because of the low base pressure existing on the conical surface the thrust loss was appreciable with the reverse slotted cones.

For the 191 tubes with inside tube diameter of 0.115 in. the Mach 1.4 jet was decreased to a coalesced Mach number of 0.73 at approximately 1-1/2 in. from the tube exit. The overall sound power level reduction was 15.2 dB from the plain jet at a Mach number of 1.4 and the thrust loss was 10 percent. By adding 191 hexagonal shrouds to the tubes, the overall sound power level reduction was increased to 21 dB with a thrust loss of 27 percent. The large wetted area of 191 shrouds contributed 11.5 percent to the total thrust loss.

The 50 tube bundle with inside tube diameter of 0.23 in. decreased the Mach 1.4 jet to sonic velocity at approximately 2 in. from the tube exit and

the overall sound power level was reduced 11.5 dB from the plain jet with a thrust loss of 3.34 percent for tube lengths of 1 to 4 in. For shorter tube lengths the overall sound power level reduction was about the same as the longer tubes but the thrust loss was appreciable because of the low base pressure. The addition of 50 hexagonal shrouds to the tubes increased the overall sound power level reduction to 20 dB with a thrust loss of approximately 27 percent.

With the multiple tubes the acoustic radiation from the supersonic region of the inner tubes is attentuated drastically, and only the acoustic radiation from the supersonic region of the tubes located in the outer ring is transmitted to the surroundings. Even for these outer tubes there is attenuation of the sound waves by phase cancellation between adjacent tubes.

Based upon the flow characteristics for multiple tubes and holes with different ratios of spacing to the tube or hole diameter, an equation was derived for the coalesced Mach number as a function of the tube spacing ratio for a pressure ratio of 3.2, which corresponds to a jet Mach number of 1.4. Equations for predicting the overall sound power level reductions with multiple tubes, holes, and shrouds were derived as a function of the coalesced Mach number for a convergent nozzle at a Mach number of 1.4.

REFERENCES

1. H.T. Nagamatsu, R.E. Sheer, Jr., and M.S. Gill, "Flow and Acoustic Characteristics of Subsonic and Supersonic Jets from Convergent Nozzle," Report prepared under NASA-1784 Contract, AIAA Paper No. 70-802, June 1970.

2. H.T. Nagamatsu, R.E. Sheer, Jr., and E.C. Bigelow, "Mean and Fluctuating Velocity Contours and Acoustic Characteristics of Subsonic and Supersonic Jets," Report prepared under NASA-1784 Contract, AIAA Paper No. 72-157, January 1972.

3. H.T. Nagamatsu, R.E. Sheer, Jr., and E.C. Bigelow, "Subsonic and Supersonic Jet Flow and Acoustic Characteristics and Supersonic Suppressors," G.E. Research and Development Center Rept. (in process).

4. H.T. Nagamatsu and G. Horvay, "Supersonic Jet Noise," AIAA Preprint No. 70-237, January 1970.

5. H.T. Nagamatsu, R.E. Sheer, Jr., and G. Horvay, "Supersonic Jet Noise Theory and Experiments," NASA Proceedings of Basic Noise Research Conference, NASA SP-207, July 1969.

6. H.T. Nagamatsu, R.E. Sheer, Jr., and R.J. Wells, "Supersonic Jet Exhaust Noise Reduction with Rods, Shroud, and Induced Flow," Proceedings of AFOSR-UTIAS Symposium on Aerodynamic Noise, Toronto, 20-21 May 1968.

7. H.T. Nagamatsu, R.E. Sheer, Jr., and W.T. Pettit, "Slotted Cone Diffuser, Rods, Shroud, and Induced Flow for Decreasing Noise from a Supersonic Jet," G.E. Research and Development Center Rept. No. 67-C-427, November 1967.

8. H.T. Nagamatsu, W.T. Pettit, and R.E. Sheer, Jr., "Flow and Acoustic Measurements on a Convergent Nozzle Supersonic Jet Ejector," G.E. Research and Development Center Rept. No. 69-C-156, April 1969.

9. H.T. Nagamatsu, R.E. Sheer, Jr., and W.T. Pettit, "Effects of Solid Cone and Slotted Cup Diffusers, Rods, Shroud and Induced Flow on

Supersonic Jet Noise," G.E. Research and Development Center Rept. No. 68-C-014, January 1968.

10. H.T. Nagamatsu, W.T. Pettit, and R.E. Sheer, Jr., "Effects of Slotted Cone Diffusers, Daisy, Rods, Shrouds, and Induced Flow on Supersonic Jet Noise," G.E. Research and Development Center Rept. No. 68-C-173, May 1968.

11. R.E. Sheer, Jr., M.S. Gill, and H.T. Nagamatsu, "Acoustic and Flow Measurements of Supersonic Flow for 60° and 75° Reverse Slotted Cone Noise Suppressor," G.E. Research and Development Center Rept. No. 69-C-360, October 1969.

12. H.T. Nagamatsu, M.S. Gill, and R.E. Sheer, Jr., "Effect of Tabs, Rods, and TSEN Shroud on Supersonic Jet Exhaust Noise," G.E. Research and Development Center Rept. No. 69-C-011, December 1968.

13. H.T. Nagamatsu, R.E. Sheer, Jr., and M.S. Gill, "Effects of Rods, Shroud, Transversely Impinging Jets, and Reverse Slotted Cone on Supersonic Jet Exhaust Noise," G.E. Research and Development Center Report. No. 69-C-169, April 1969.

14. L.W. Lassiter and H.H. Hubbard, "The Near Noise Field of Static Jets and Some Model Studies of Devices for Noise Reduction," NACA Rept. 1261 (1954).

15. E.M.A. Mercer, "The Effect of 'Teeth' on the Noise from a Jet Engine," USAF, WADC TR 54-224, September 1954.

16. W.D. Coles and E.E. Callaghan, "Full-Scale Investigation of Several Jet-Engine Noise-Reduction Nozzles," NACA TN 3974, April 1957.

17. F.B. Greatrex and R. Bridge, "The Evolution of the Engine Noise Problem," Int'l. Noise Conf., November 1966.

18. G.S. Schairer, J.V. O'Keefe, and P.E. Johnson, "Perspective of SST Aircraft Noise Problem," AIAA Paper No. 68-1023, October 1968.

19. V.G. Harris, "Model/Full Scale GE4 Block I Jet Noise Testing," G.E. Flight Prop. Div. TM No. 68-15, January 1968.

20. P. Heck, "Jet Plume Characteristics of 72-Tube and 72-Hole Primary Suppressor Nozzles," G.E. Flight Prop. Div. TM No. 69-457, July 1969.

21. E.J. Stringas, "Review of Current Multi-Element Aerodynamic Characteristics," G.E. Flight Prop. Div. TN-70007, October 1970.

22. D.S. Dosanjh and F.J. Montegani, "Reduction of Noise from Under-expanded Axisymmetric Jet Flow Using Radial Jet Flow Impingement," Am. Inst. of Aero. and Astro. Paper No. 68-81 (1968).

23. E.S. Love, C.E. Grigsby, L.P. Lee, and M. Woodling, "Experimental and Theoretical Studies of Axisymmetric Free Jets," NASA Rept. TR-6 (1959).

24. W.R. Warren, "An Analytical and Experimental Study of Compressible Free Jets," Doctoral Dissertation Princeton University (1957).

25. J.M. Eggers, "Velocity Profiles and Eddy Viscosity Distribution Downstream of a Mach 2.22 Nozzle Exhausting into Quiescent Air," NASA TN D-3601 (1966).

26. J.C. Laurence, "Intensity, Scale, and Spectra of Turbulence in Mixing Region of Free Subsonic Jet," NACA Rept. 1292 (1956).

27. P.O.A.L. Davies, M.J. Fisher, and M.J. Barratt, "The Characteristics of the Turbulence in the Mixing Region of a Round Jet," J. Fluid Mech., Vol. 15, Part 2, 337-366, July 1963.

28. R.C. Potter and J.H. Jones, "An Experiment to Locate the Acoustic Sources in a High Speed Jet Exhaust Stream," Wyle Laboratories Rept. (1967).

29. J.H. Gerrard, "An Investigation of the Noise Produced by Subsonic Air Jet," J. Aero. Sci., 23, 855-866 (1956).

30. E. Mollo-Christensen and R. Narashimha, "Sound Emission from Jets at High Subsonic Velocity," J. Fluid Mech., 8, 49-60 (1960).

31. M.J. Lighthill, "Jet Noise," AIAA Jour., Vol. 1, No. 7, 1507-1517 (1963).

32. H.S. Ribner, The Generation of Sound by Turbulent Jets, Adv. Appl. Mech., Vol. 8, Academic Press, Inc., N.Y. (1964).

33. H.T. Nagamatsu, R.E. Sheer, Jr., and M.S. Gill, "Flow and Acoustic Characteristics of 191 Tubes and 191 Shrouds Supersonic Jet Noise Suppressor," AIAA Paper No. 71-153, January 1971.

34. H.T. Nagamatsu and R.E. Sheer, Jr., "Flow, Thrust, and Acoustic Characteristics of 50 Tubes with 50 Shrouds Supersonic Jet Noise Suppressor," G.E. Research and Development Center Rept. No. 71-C-258, September 1971.

TABLE VII.A-1

FLOW AND ACOUSTIC CONDITIONS FOR PARALLEL FLOW NOZZLE WITH SHROUDS, $P_r = 3.7$, $M_j = 1.5$

Configuration	Total Mass Flow (slug/sec)	Induced Mass Flow (slug/sec)	Momentum Flux (lb)	Energy Flux (ft-lb/sec)	Average Velocity (ft/sec)	L_w Measured (dB)	L_w Lighthill (dB)
Plain Jet	0.124	0.0	171.	118,821	1387	153.1	148.9
S1 (0)	0.125	0.0	71.2	20,488	560	148.0	120.0
S1 (1)	0.207	0.082	182.2	81,949	848	147.2	135.2
S1 (1), S2	0.259	0.132	153.6	46,933	565	143.7	123.2

TABLE VII.A-2

FLOW AND ACOUSTIC CONDITIONS FOR CONVERGENT NOZZLE WITH SHROUD AND RODS, $P_r = 3.7$, $M_j = 1.5$

Configuration	Total Mass Flow (slug/sec)	Induced Mass Flow (slug/sec)	Momentum Flux (lb)	Energy Flux (ft-lb/sec)	Average Velocity (ft/sec)	L_w Measured (dB)	L_w Lighthill (dB)	Difference (dB)
Plain Jet	0.123	0.0	≈170	------	≈1400	156.2	149.1	7.1
SI (0)	0.123	0.0	67.8	19,536	555	146.8	118.9	27.9
SI (OPEN)	0.167	0.044	139.1	51,975	736	145.0	129.4	15.6
SI (OPEN) 8 Rods (% L_c)	0.177	0.054	137.5	53,481	771	138.9	130.9	8.0

TABLE VII.A-3

COMPARISON OF ACOUSTIC PROPERTIES OF A $M_j = 1.5$ CONVERGENT AND PARALLEL FLOW NOZZLE WITH AND WITHOUT SUPPRESSORS

Configuration	Parallel Flow Nozzle L_w* (dB)	Parallel Flow Nozzle ΔdB from plain jet	Convergent Nozzle L_w* (dB)	Convergent Nozzle ΔdB from plain jet
Plain Jet	153.1	0	156.2	0
½ Rods (3/4 Lg)	157.0	+ 3.9	150.2	- 6.0
S1 (0)	148.0	- 5.2	146.8	- 9.4
S1 (0), ½ Rods (3/4 Lg)	-----	------	147.2	- 9.0
S1 (OPEN)	147.2	- 5.9	145.0	- 11.2
SL (OPEN), ½ Rods (½ Lg)	142.0	- 11.1	138.9	- 17.3
S1 (OPEN), ½ Rods (3/4 Lg)	141.1	- 12.1	145.7	- 10.5

*re 10^{-13} watts

TABLE VII.A-4

ACOUSTIC POWER LEVELS FOR CONVERGENT NOZZLE, $M_j = 1.4$, WITH REVERSE SLOTTED CONES AND SHROUDS

Configuration	L_W (dB re 10^{-13} watts) Measured	Suppression (dB from plain jet)
Plain Jet	154.4	0
60° Rev. Slot. Cone (28 slots)	147.7	- 6.7
60° Rev. Slot. Cone (28 slots), $S_{4.2}$	149.4	- 6.0
60° Rev. Slot. Cone (28 slots), S'_{12}	146.1	- 8.3
60° Rev. Slot. Cone (56 slots)	142.0	- 12.4
60° Rev. Slot. Cone (56 slots), $S_{4.2}$	144.2	- 10.2
75° Rev. Slot. Cone (58 slots)	141.9	- 12.5
75° Rev. Slot. Cone (58 slots), $S_{4.4}$	142.4	- 12.0
75° Rev. Slot. Cone (58 slots), S'_{12}	140.1	- 14.3

TABLE VII.A-5

ACOUSTIC POWER LEVELS FOR CONVERGENT NOZZLE, 191 TUBES, 191 SHROUDS, AND SINGLE SHROUD

A. Outside Air Temperature ~ 20°F

1. Pressure Ratio = 3.2, M_j = 1.4

Configuration	L_w (dB re 10^{-13} watts)	Suppression (dB from plain jet)
1-9/16" Dia. Convergent Nozzle	154.3	
191 Multitubes	138.3	- 16.0
191 Multitubes with 6" Long Multishroud (x_1 = 3/16")	132.4	- 21.9
191 Multitubes with 6" Long Multishroud (x_1 = 1")	136.7	- 17.6
191 Multitubes with 6" Long Multishroud (x_1 = 2", no induced flow)	135.5	- 18.8
191 Multitubes with Bellmouth Shrouds, S'_{12}	138.7	- 15.6

B. Outside Air Temperature ~ 68°F

1. Pressure Ratio = 3.2, M_j = 1.4

1-9/16" Dia. Convergent Nozzle	150.7	0
191 Multitubes	135.5	- 15.2
191 Multitubes with 6" Long Multishroud (x_1 = 3/16")	130.3	- 20.4
191 Multitubes with 3.335" Long Multishroud (x_1 = 3/16")	131.7	- 19.0
191 Multitubes with 1.667" Long Multishroud (x_1 = 3/16")	135.2	- 15.5
191 Multitubes with Short Shrouds, $S_{3.8}$	137.0	- 13.7

TABLE VII.A-6

ACOUSTIC POWER LEVELS FOR CONVERGENT NOZZLE AND 50 TUBES WITH SHROUDS, $M_j = 1.4$

Configuration	L_w (dB re 10^{-13} watts)	Suppression (dB from plain jet)
1-9/16" Jet, Pr = 3.2, T_a = 78°F	151.8	0
50 Tubes, L = ¼"	140.3	- 11.5
50 Tubes, L = ½" Single Shroud, $S_{3.16}$	143.6	- 8.2
50 Tubes, L = 1"	140.6	- 11.2
50 Tubes, L = 1" Single Shroud, $S_{3.16}$	142.4	- 9.4
50 Tubes, L = 1" 50 Shrouds	137.3	- 14.5
50 Tubes, L = 2"	140.3	- 11.5
50 Tubes, L = 2" Single Shroud, $S_{3.16}$	141.5	- 10.3
50 Tubes, L = 2" 50 Shrouds	133.7	- 18.1
1-9/16" Jet, Pr = 3.2, T_a = 81°F	152.5	0
50 Tubes, L = 4"	139.5	- 13.0
50 Tubes, L = 4" Single Shroud, $S_{3.16}$	140.5	- 12.0
50 Tubes, L = 4" 50 Shrouds	132.2	- 20.3
1-9/16" Jet, Pr = 3.2, T_a = 66°F	153.3	0
50 Tubes, L = 0"	138.3	- 15.0
50 Tubes, L = 0" Single Shroud, $S_{3.16}$	140.4	- 12.9

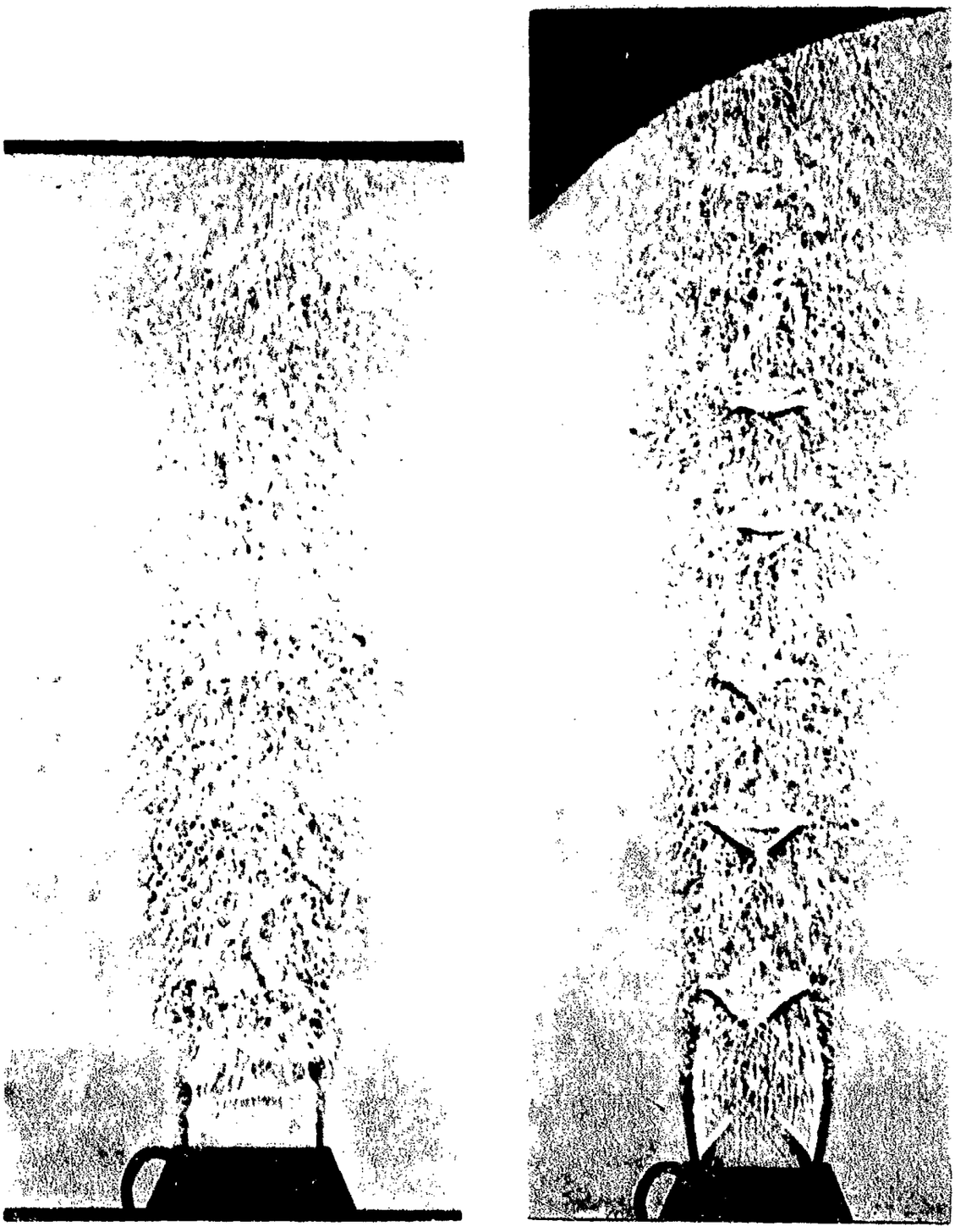


FIGURE VII.A-1 SHADOWGRAPH PHOTOGRAPHS OF FLOW FROM A CONVERGENT NOZZLE AT MACH NUMBERS OF 1.0 AND 1.4

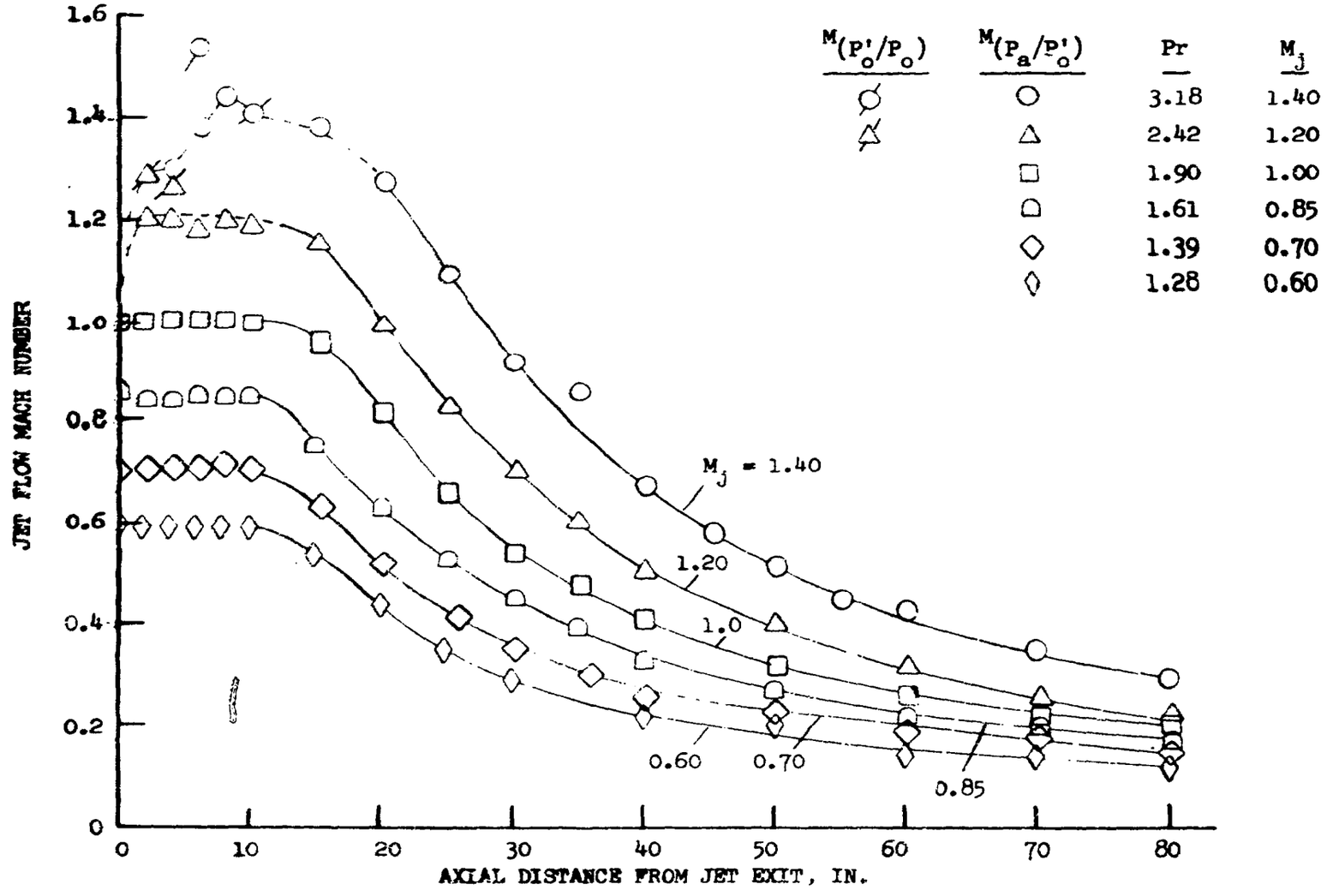


FIGURE VII.A-2A VARIATION OF FLOW MACH NUMBER ALONG THE JET AXIS WITH DISTANCE FOR CONVERGENT NOZZLE

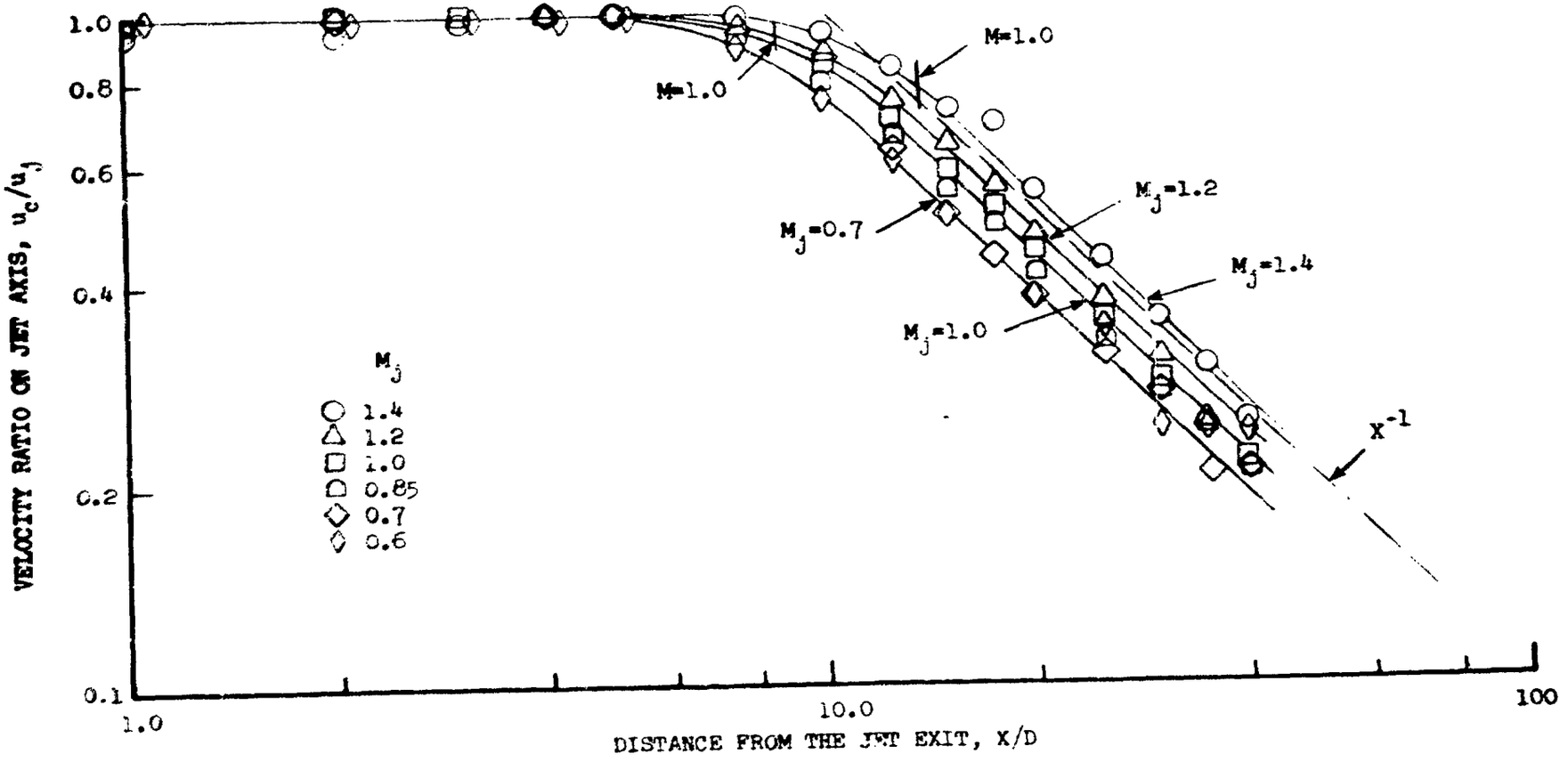


FIGURE VII.A-2B VELOCITY RATIO ON JET AXIS FOR TWO-INCH DIAMETER CONVERGENT NOZZLE

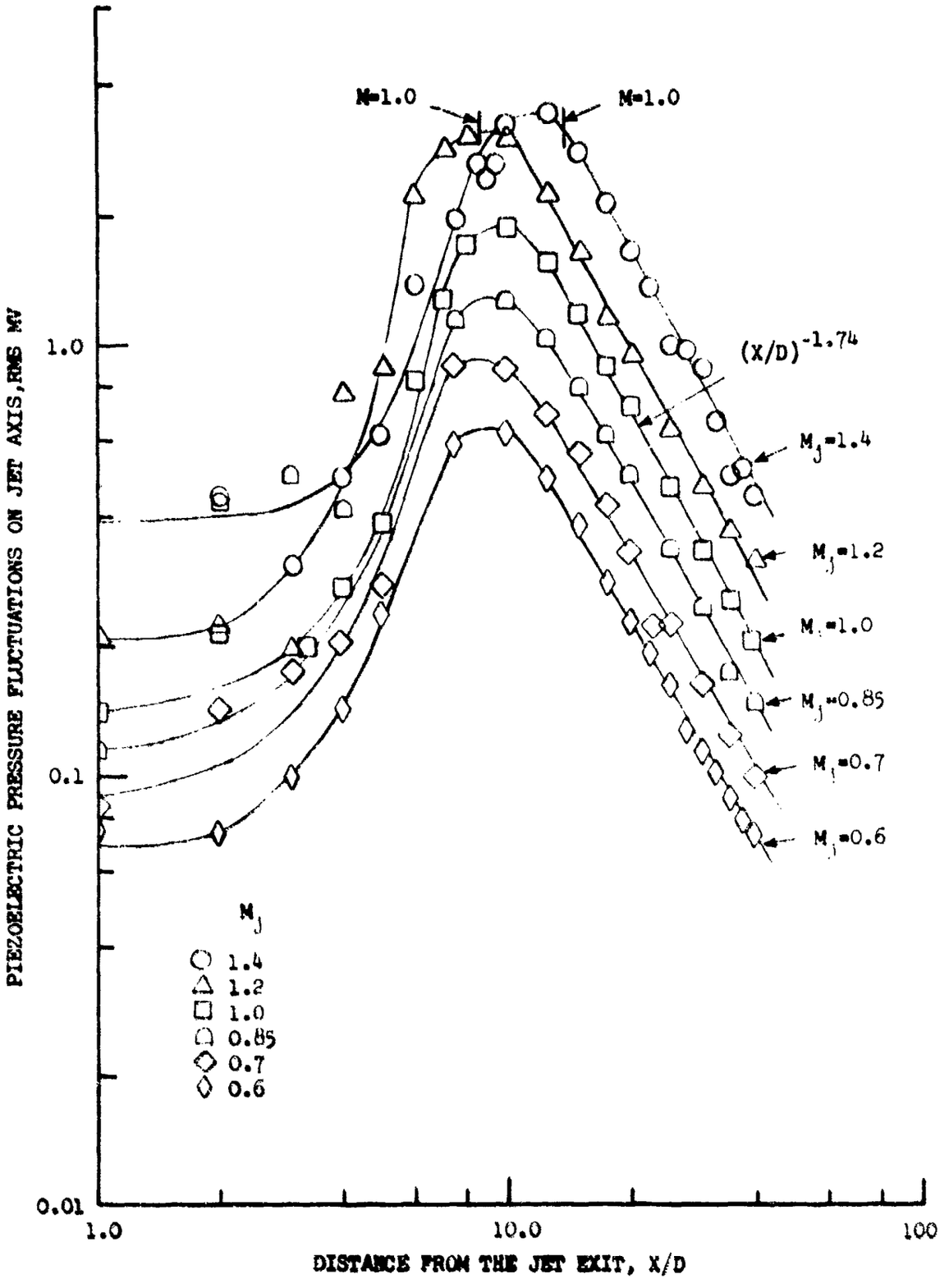


FIGURE VII.A-3 VARIATION OF IMPACT PRESSURE FLUCTUATIONS ON JET AXIS WITH DISTANCE FROM JET EXIT FOR TWO-INCH DIAMETER CONVERGENT NOZZLE

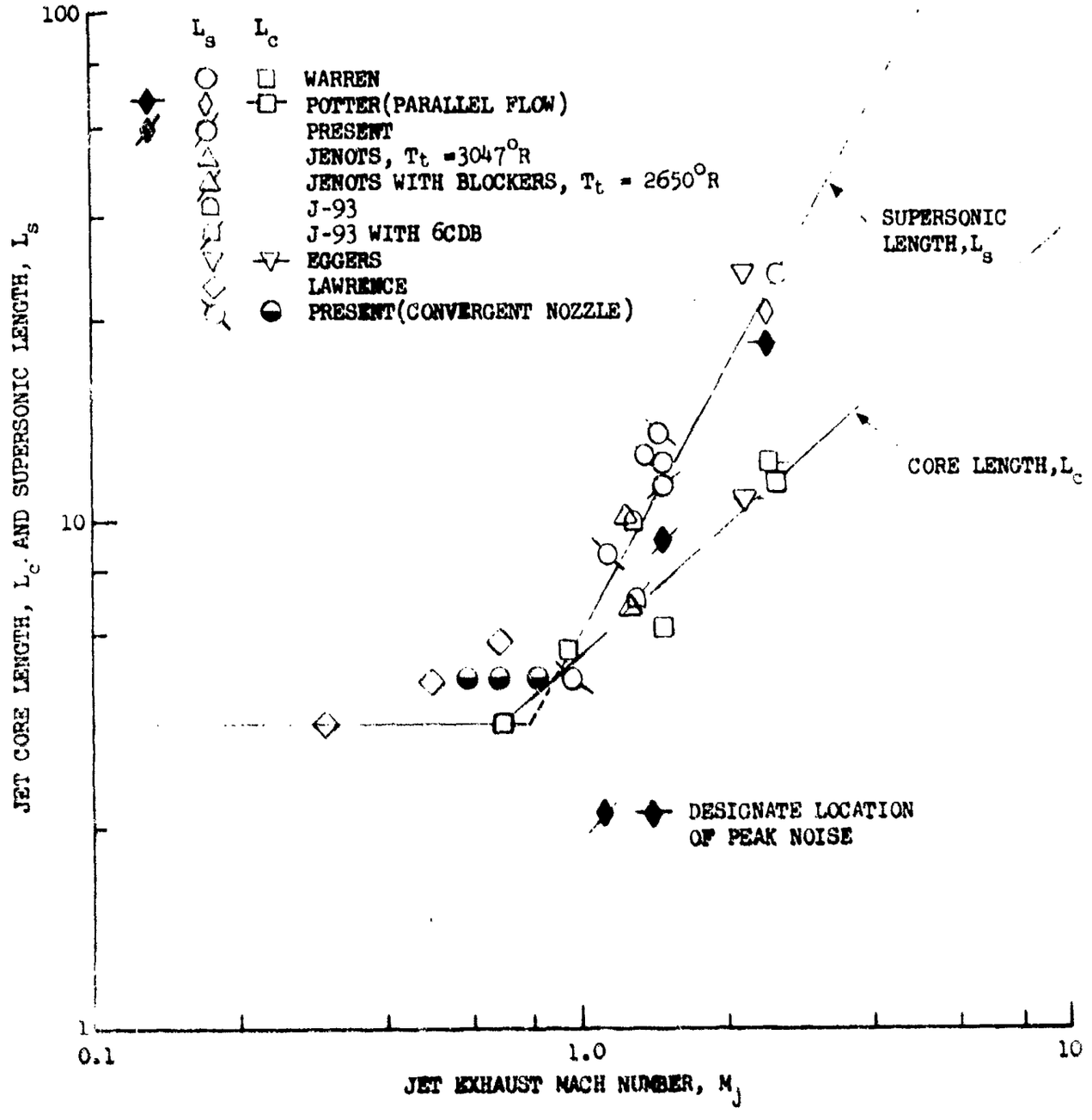


FIGURE VII.A-4 JET CORE LENGTH, AND SUPERSONIC LENGTH, AS A FUNCTION OF JET MACH NUMBER

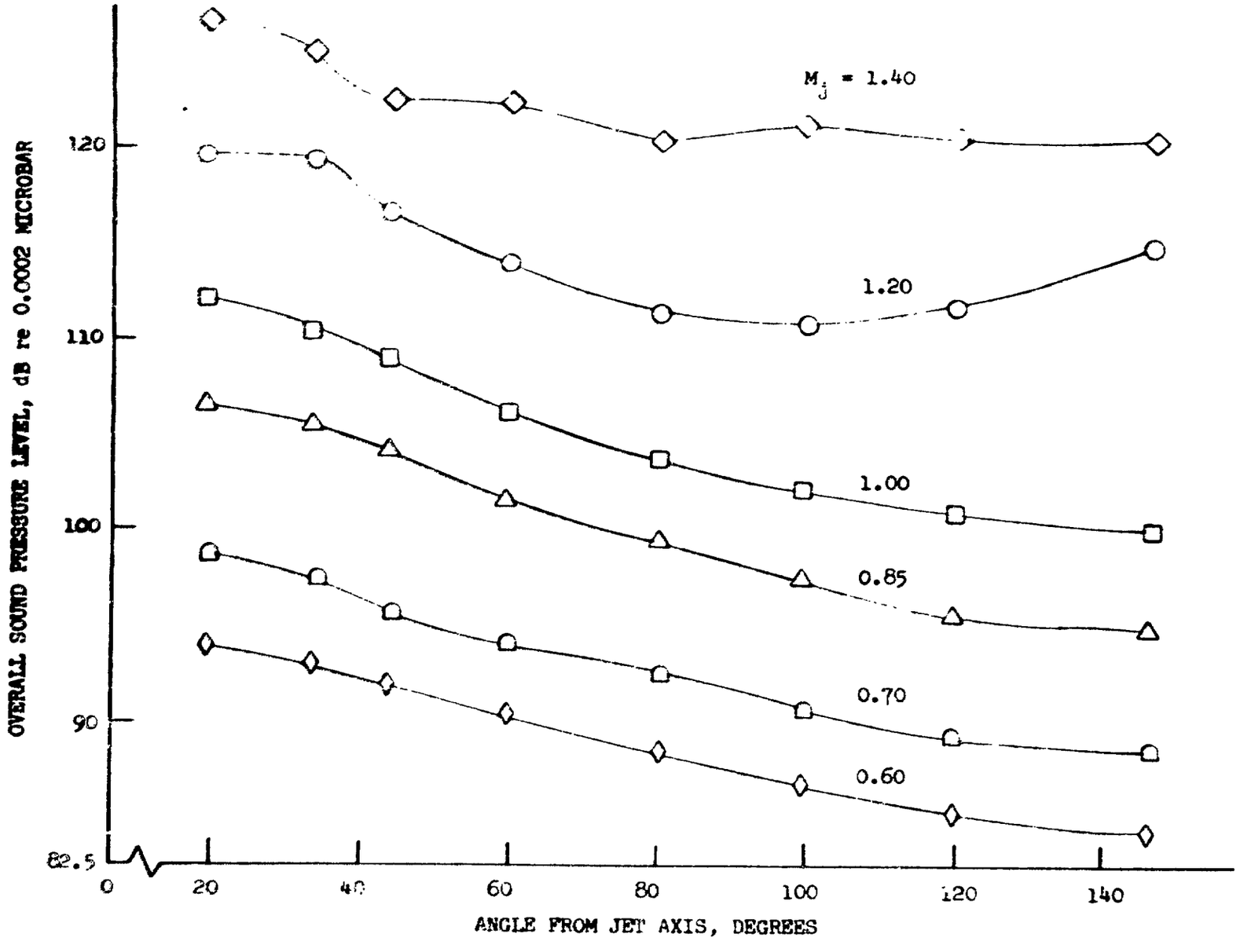


FIGURE VII.A-5 OVERALL SOUND PRESSURE LEVEL AS A FUNCTION OF ANGULAR POSITION FROM JET AXIS FOR DIFFERENT JET MACH NUMBERS

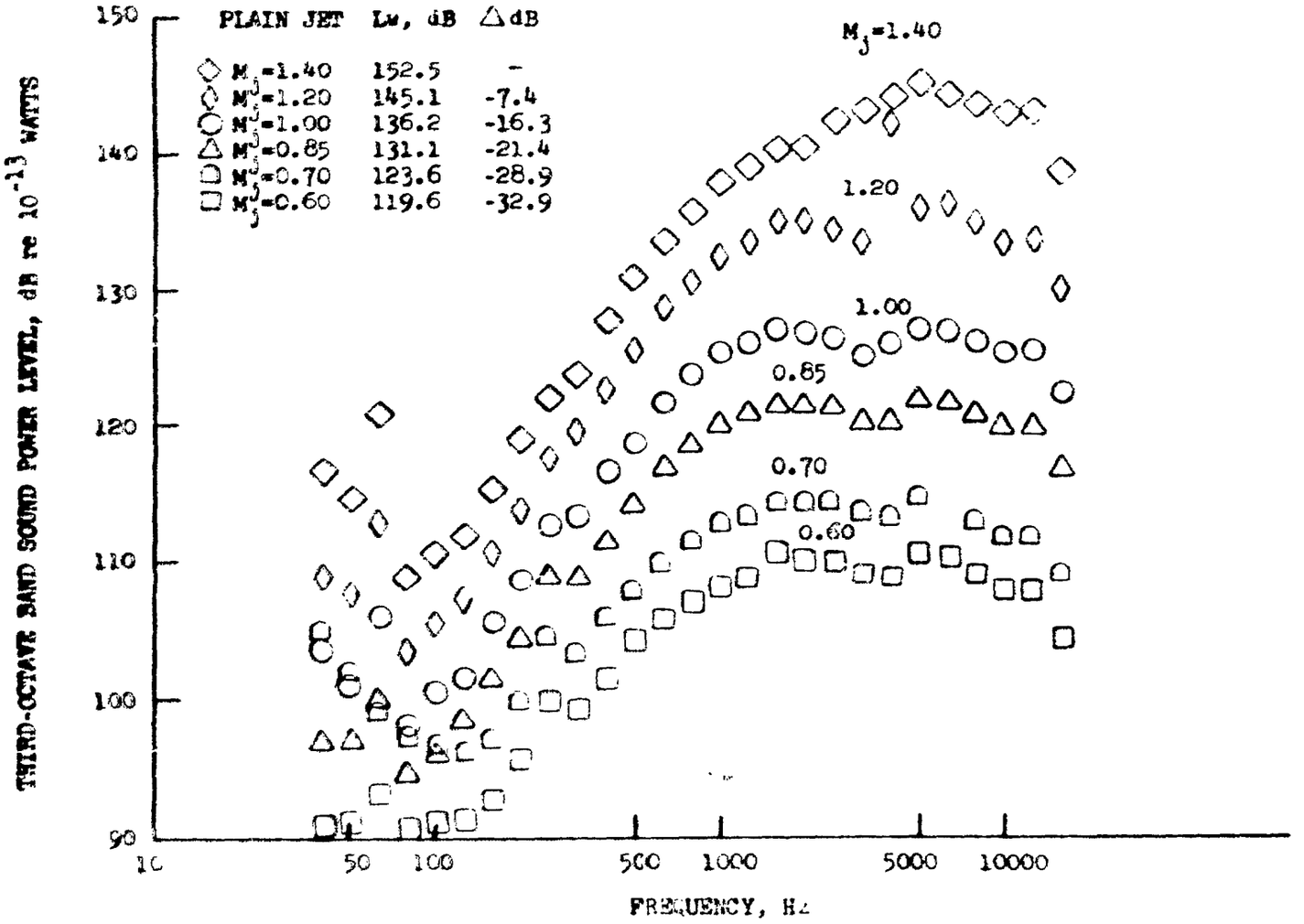


FIGURE VII.A-6 COMPARISON OF SOUND POWER SPECTRA FOR PLAIN CONVERGENT JET AT VARIOUS MACH NUMBERS

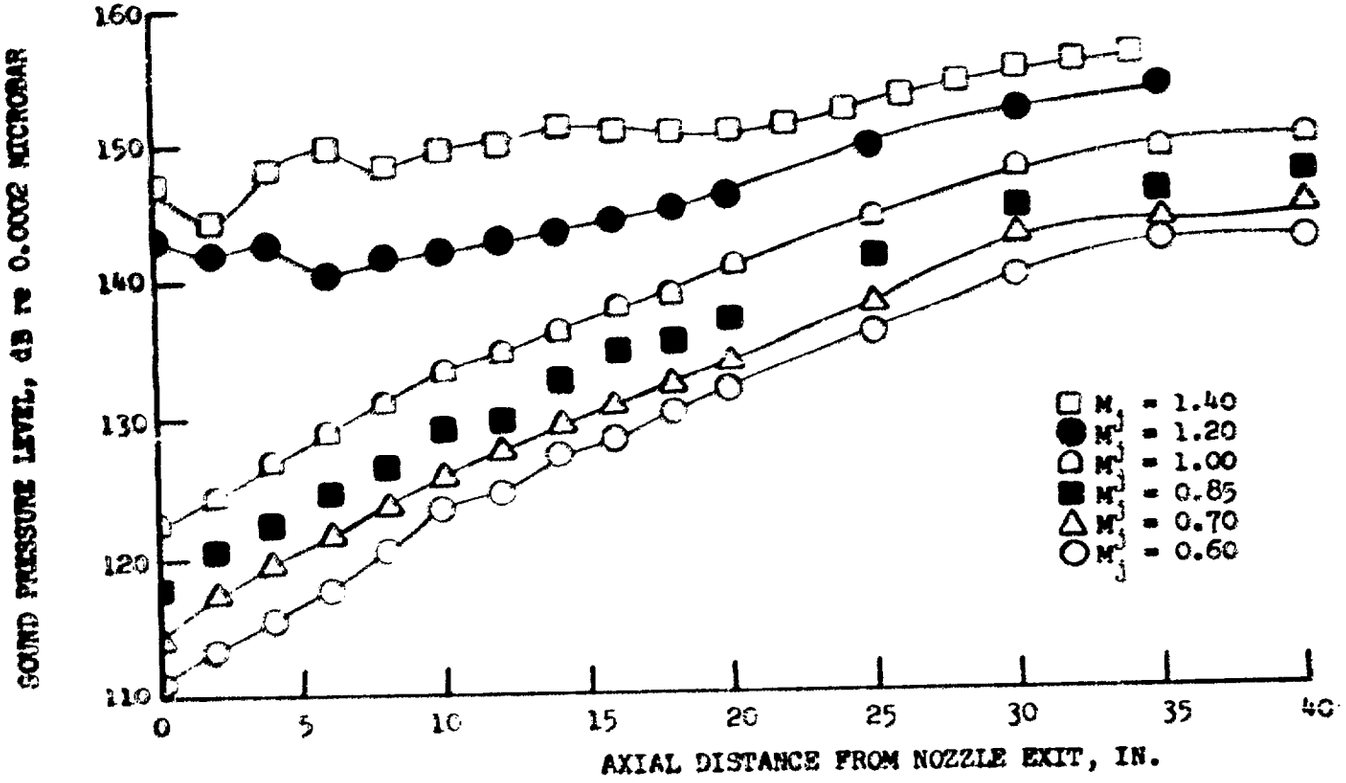


FIGURE VII.A-7 NEAR FIELD OVERALL SOUND PRESSURE LEVEL AS A FUNCTION OF JET MACH NUMBER AND AXIAL DISTANCE AT 2 DIAMETERS FROM NOZZLE EXIT

OVERALL ACOUSTIC POWER LEVEL	M_j =1.4	M_j =1.2
L_w - INTEGRATED OVER 2 NOZZLE DIA. CYLINDER	158 dB	149 dB
L_w - INTEGRATED OVER 10 FT. RADIUS SPHERE	156 dB	148 dB

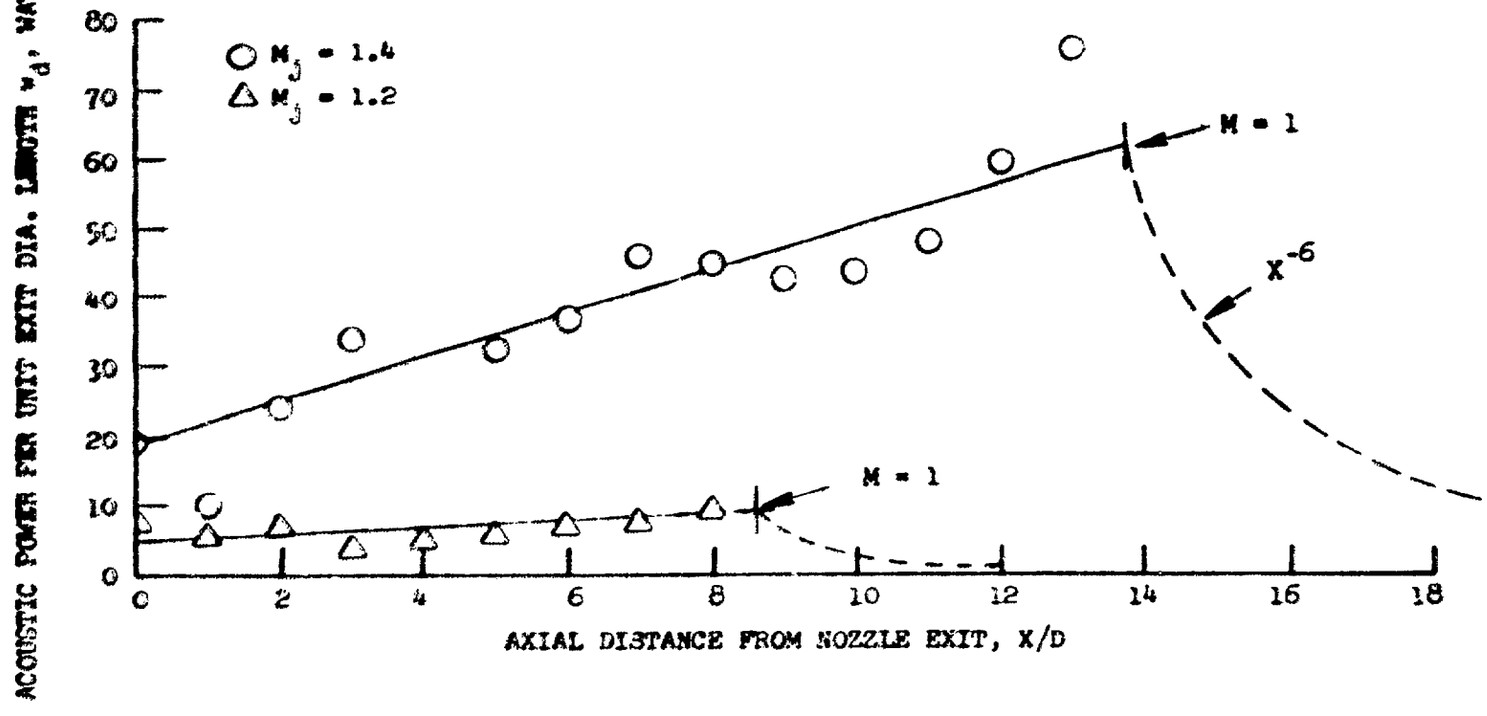


FIGURE VII.A-8 ACOUSTIC POWER PER UNIT LENGTH OF JET OBTAINED WITH MICROPHONE TRAVERSE PARALLEL TO JET AXIS AT TWO NOZZLE DIAMETERS FROM NOZZLE PERIPHERY

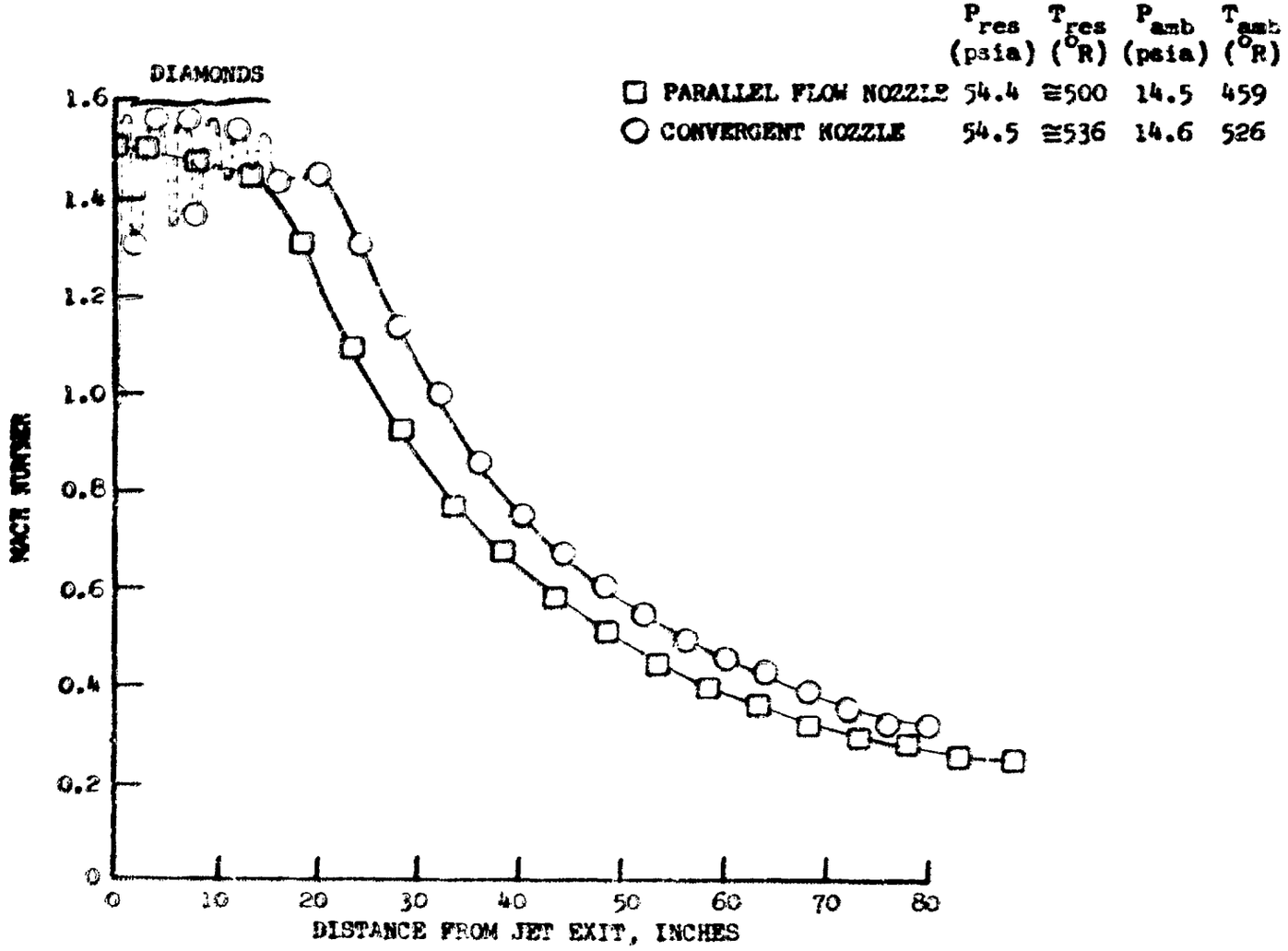


FIGURE VII.A-9 AXIAL MACH NUMBER PROFILE WITH PLAIN NOZZLE

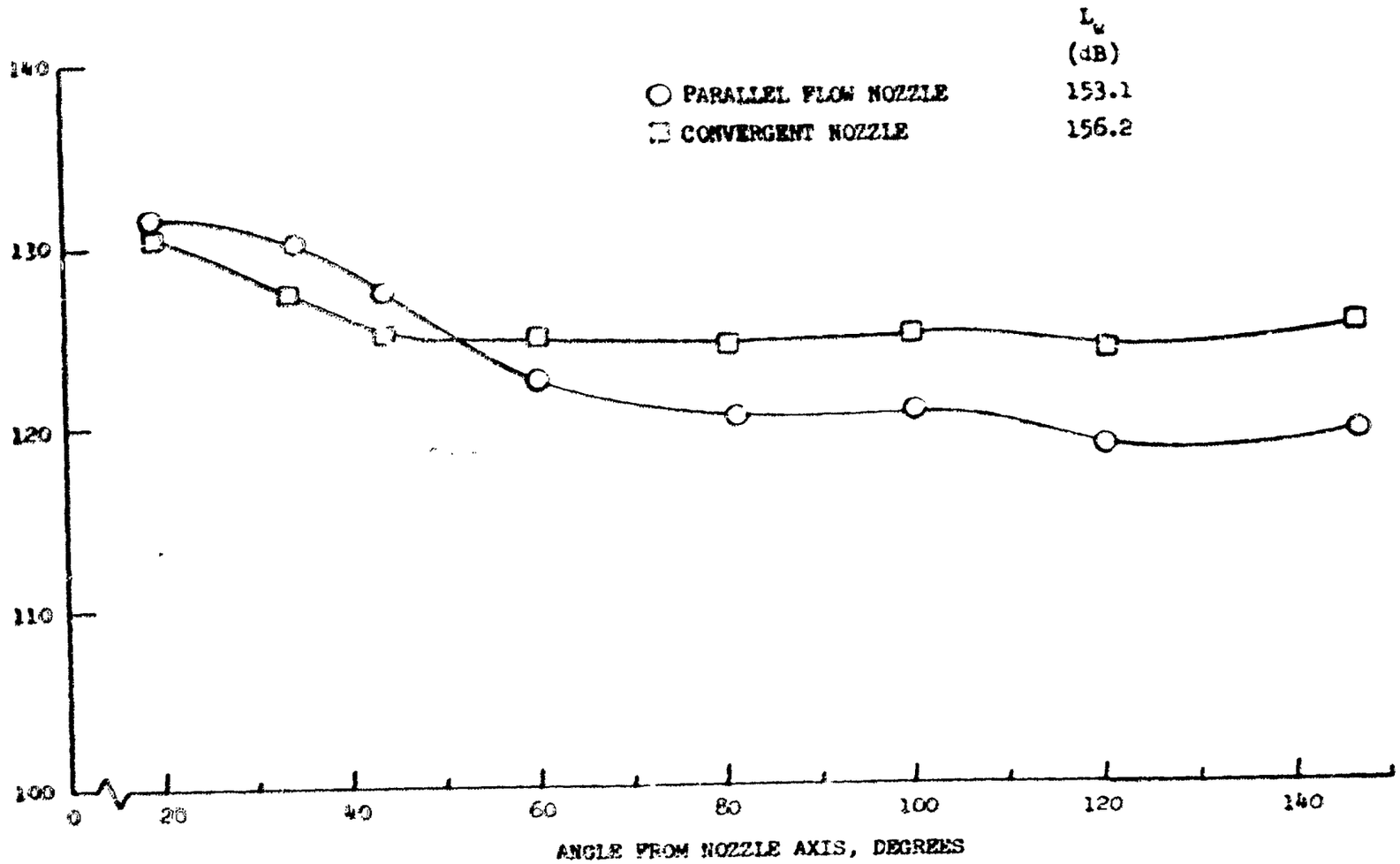


FIGURE VII.A-10 COMPARISON OF DIRECTIVITIES FOR M = 1.5 PARALLEL FLOW AND CONVERGENT NOZZLES

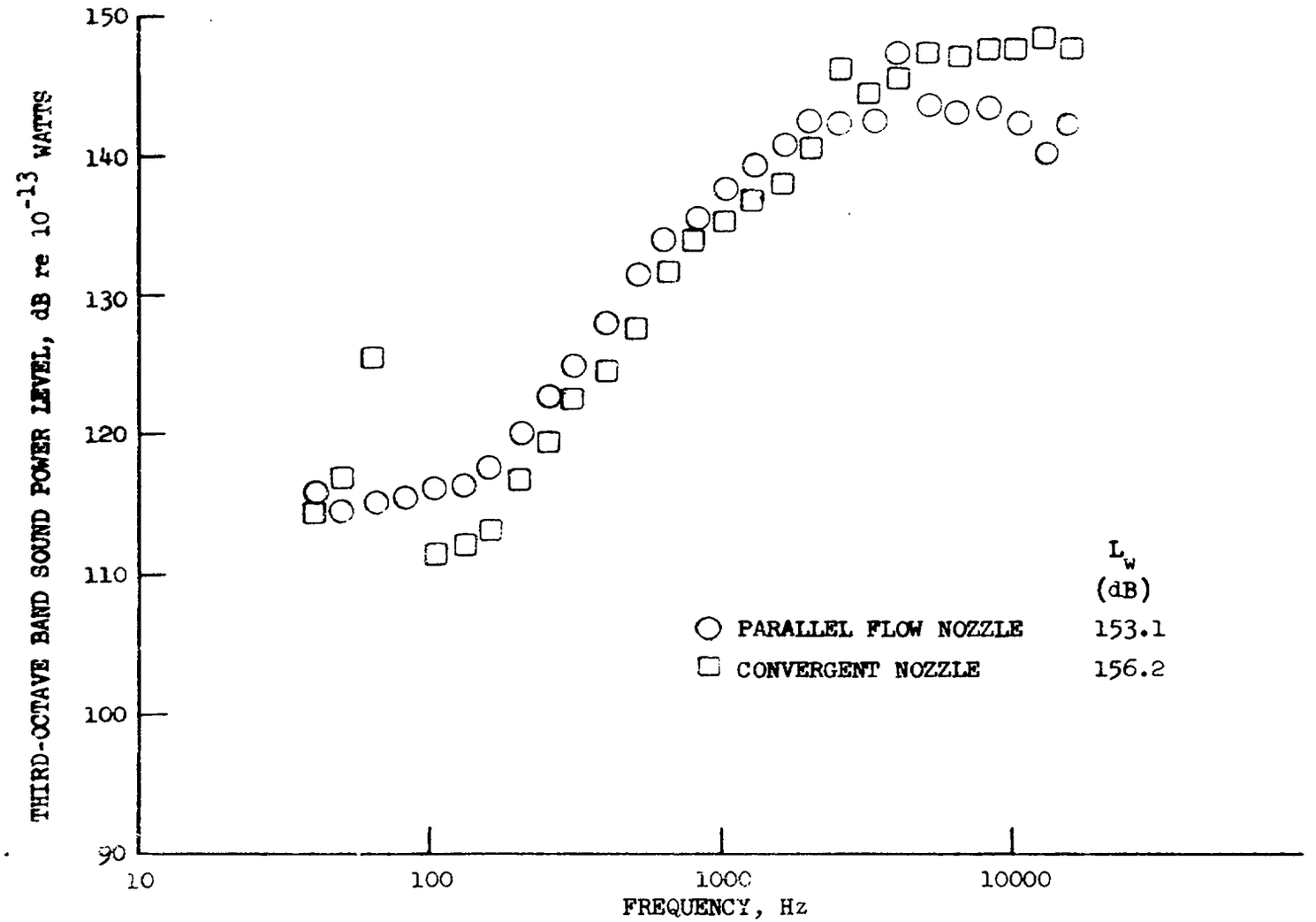


FIGURE VII.A-11 COMPARISON OF POWER LEVEL SPECTRA FOR M = 1.5 PARALLEL FLOW AND CONVERGENT NOZZLES

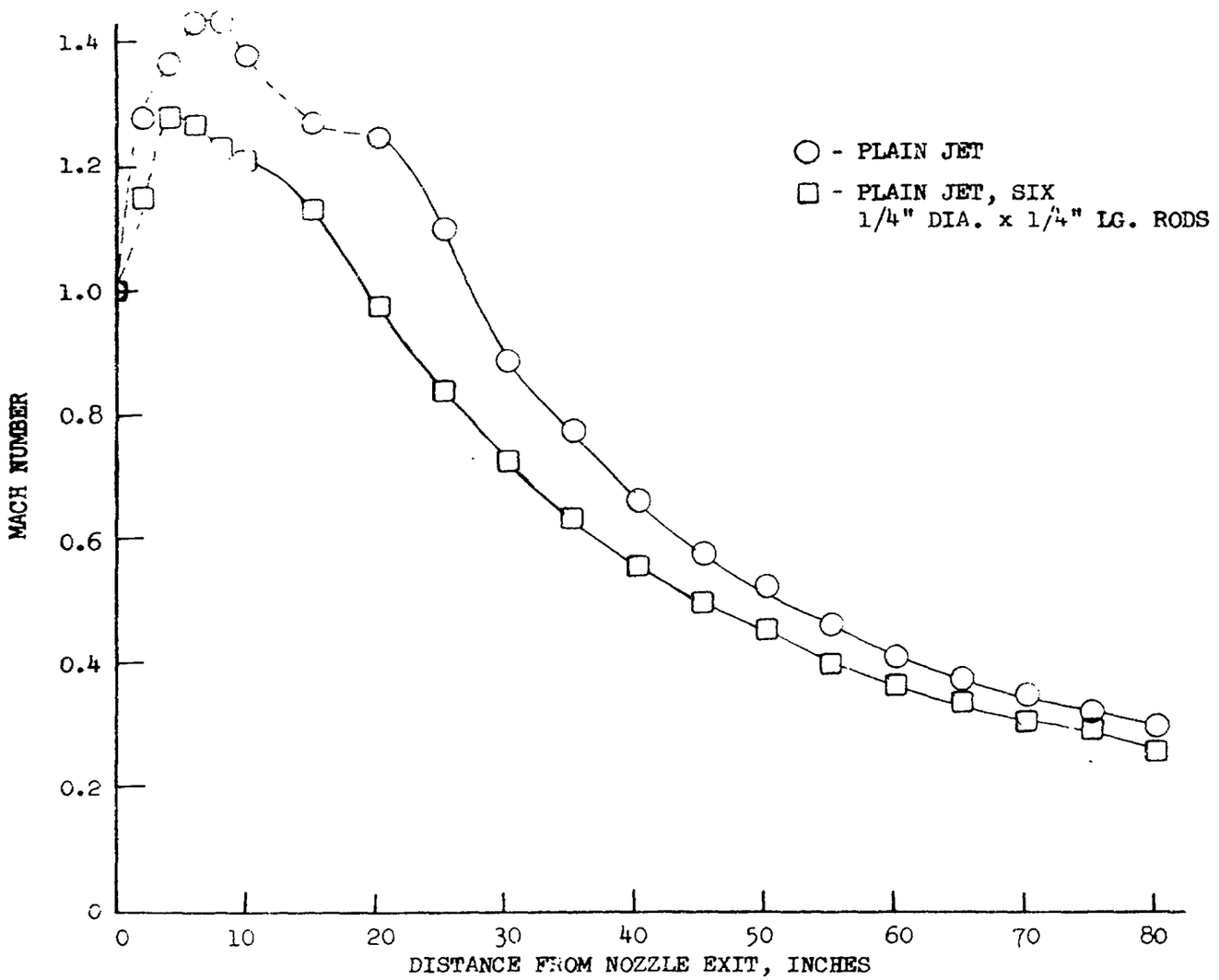


FIGURE VII.A-12A COMPARISON OF AXIAL MACH NUMBER VARIATION OF JET WITH AND WITHOUT RODS, CONVERGENT NOZZLE, Pr = 3.2, Mj = 1.4

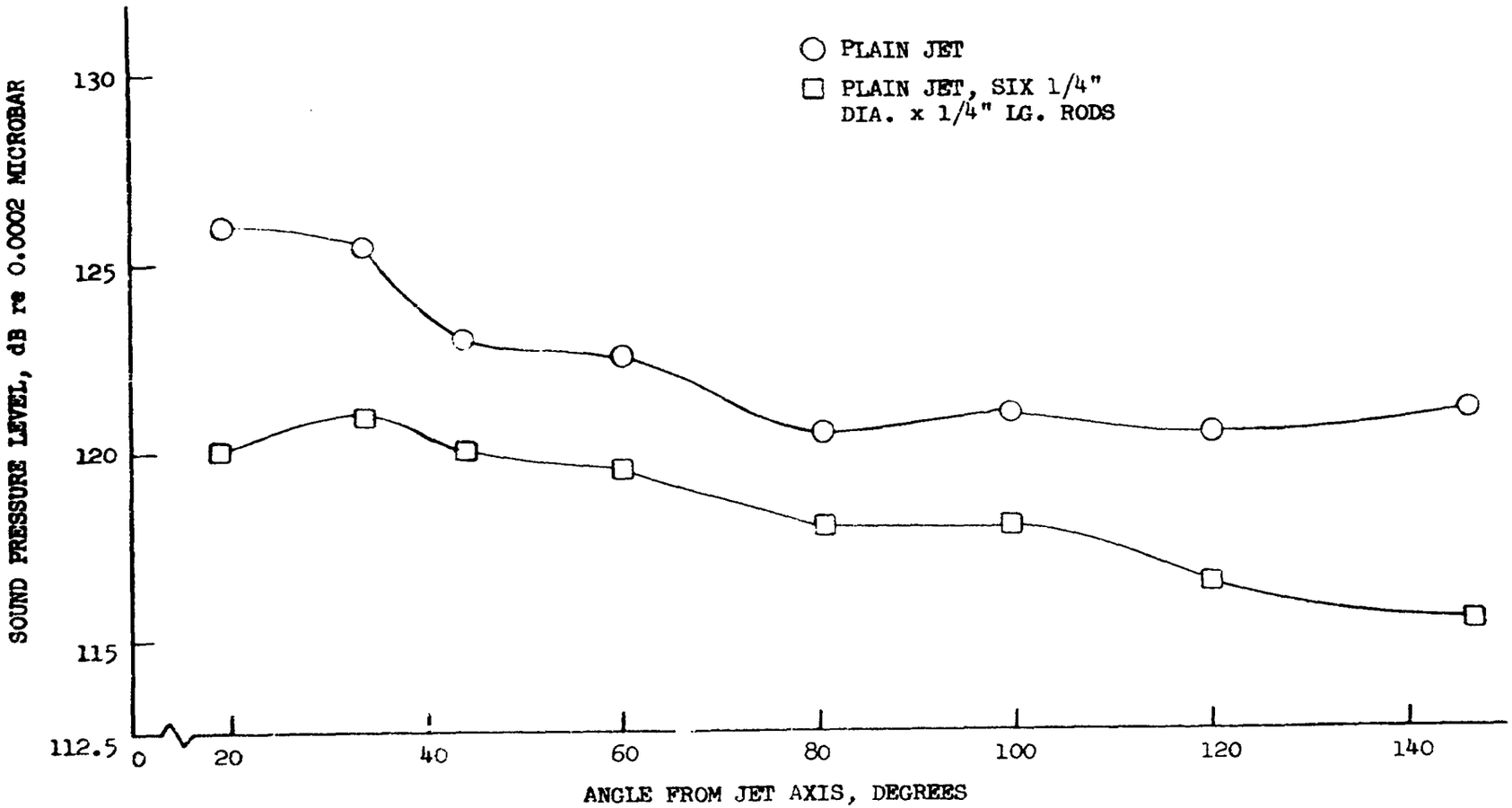


FIGURE VII.A-12B OVERALL SOUND PRESSURE LEVEL AS A FUNCTION OF ANGULAR POSITION FROM THE JET AXIS WITH AND WITHOUT RODS, CONVERGENT NOZZLE, Pr = 3.2, Mj = 1.4

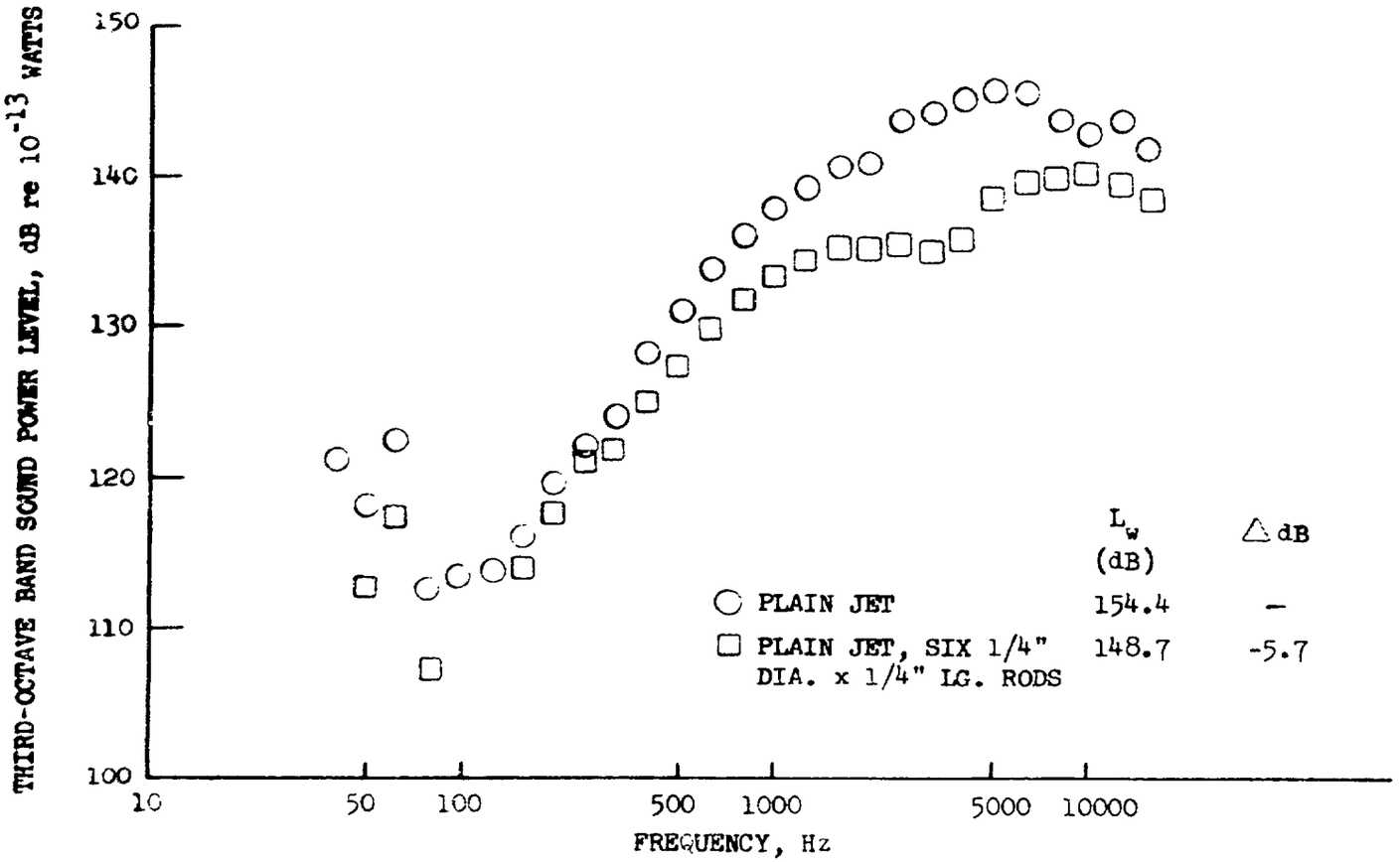


FIGURE VII.A-12C SOUND POWER LEVEL SPECTRA OF THE JET WITH AND WITHOUT RODS, CONVERGENT NOZZLE, Pr = 3.2, Mj = 1.4

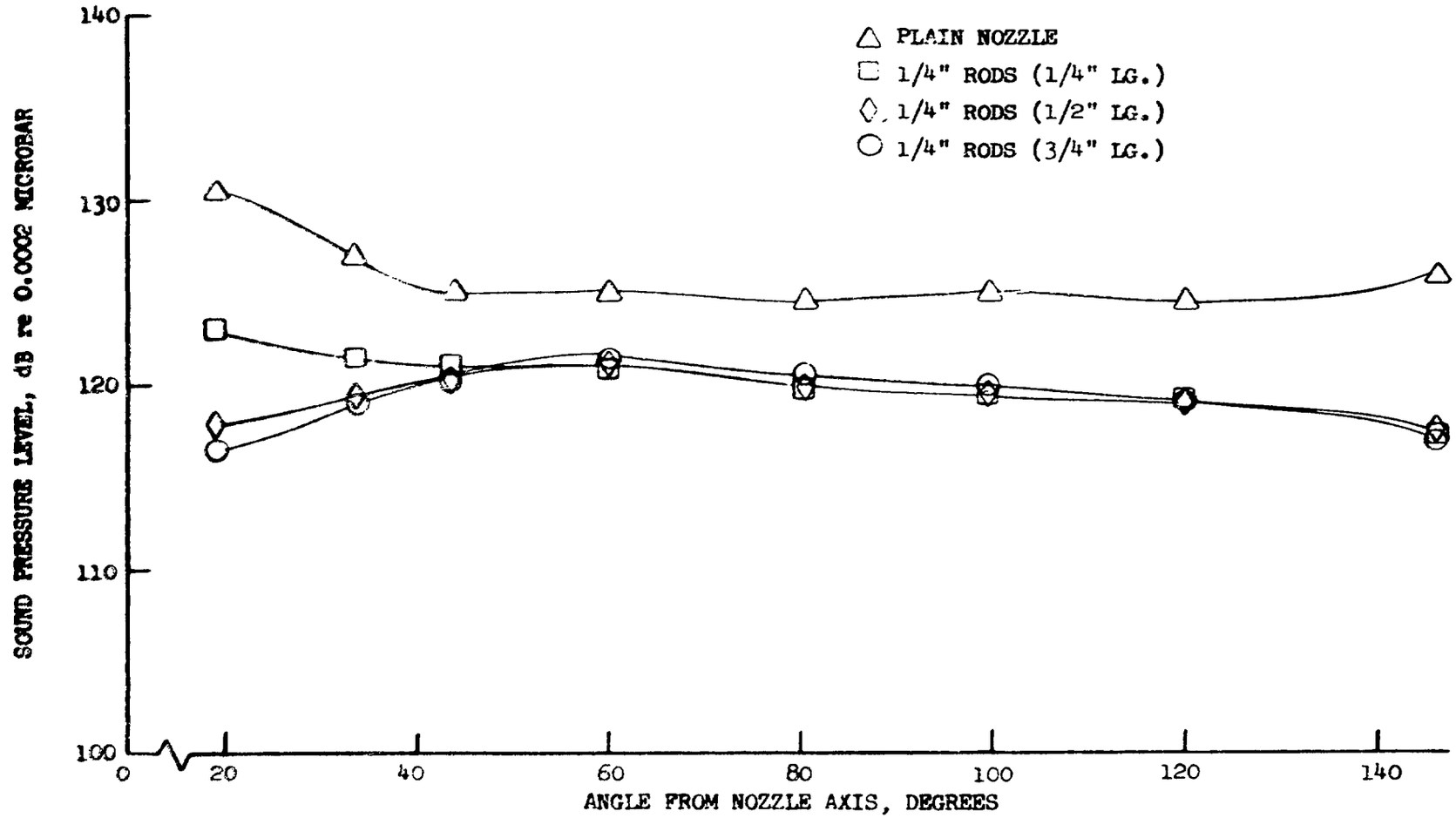


FIGURE VII.A-13A OVERALL SOUND PRESSURE LEVEL AS A FUNCTION OF ANGULAR POSITION FROM THE JET AXIS WITH RODS, CONVERGENT NOZZLE, Pr = 3.7, Mj = 1.5

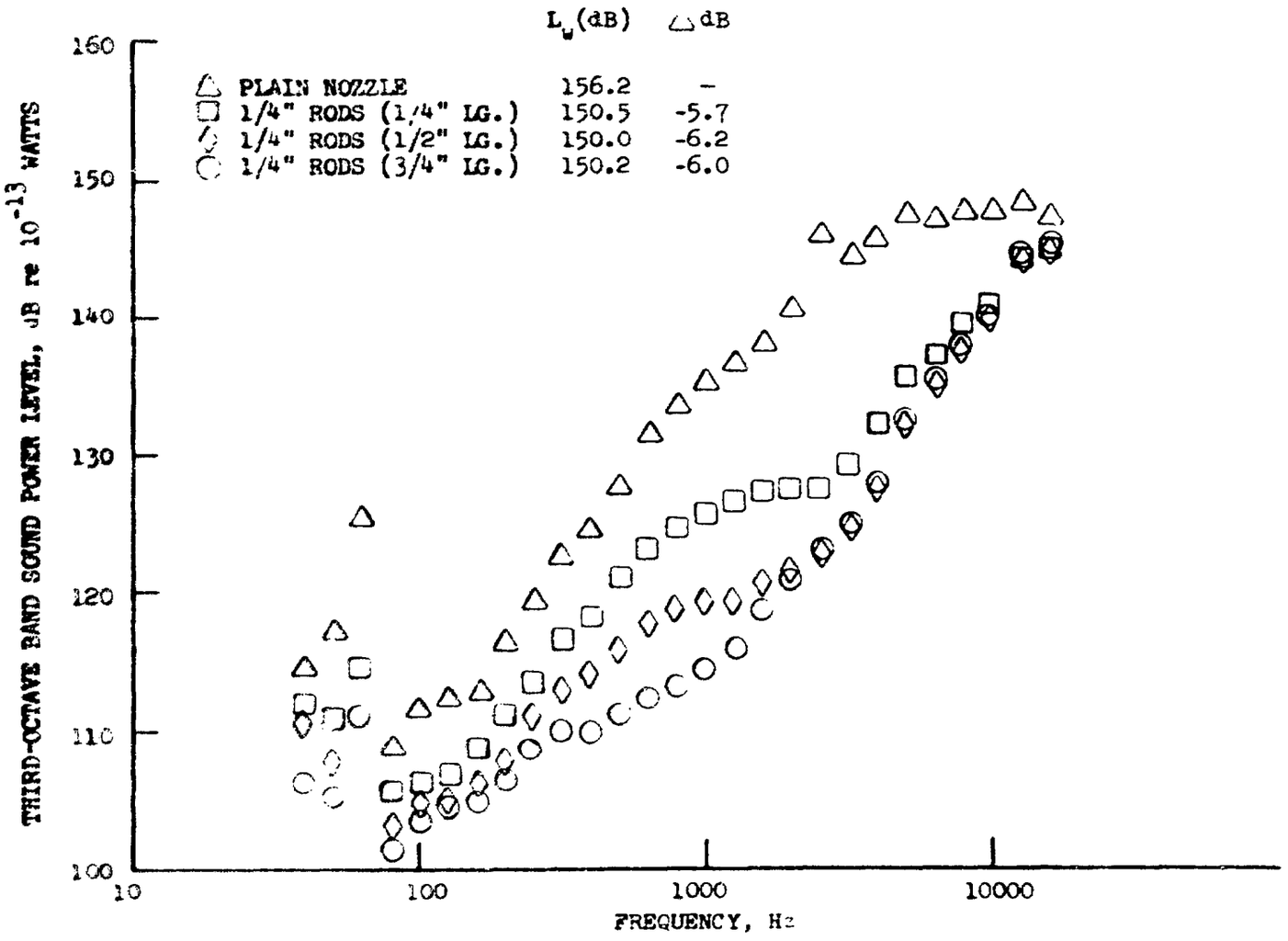


FIGURE VII.A-13B SOUND POWER LEVEL SPECTRA WITH RODS, CONVERGENT NOZZLE, Pr = 3.7, Mj = 1.5

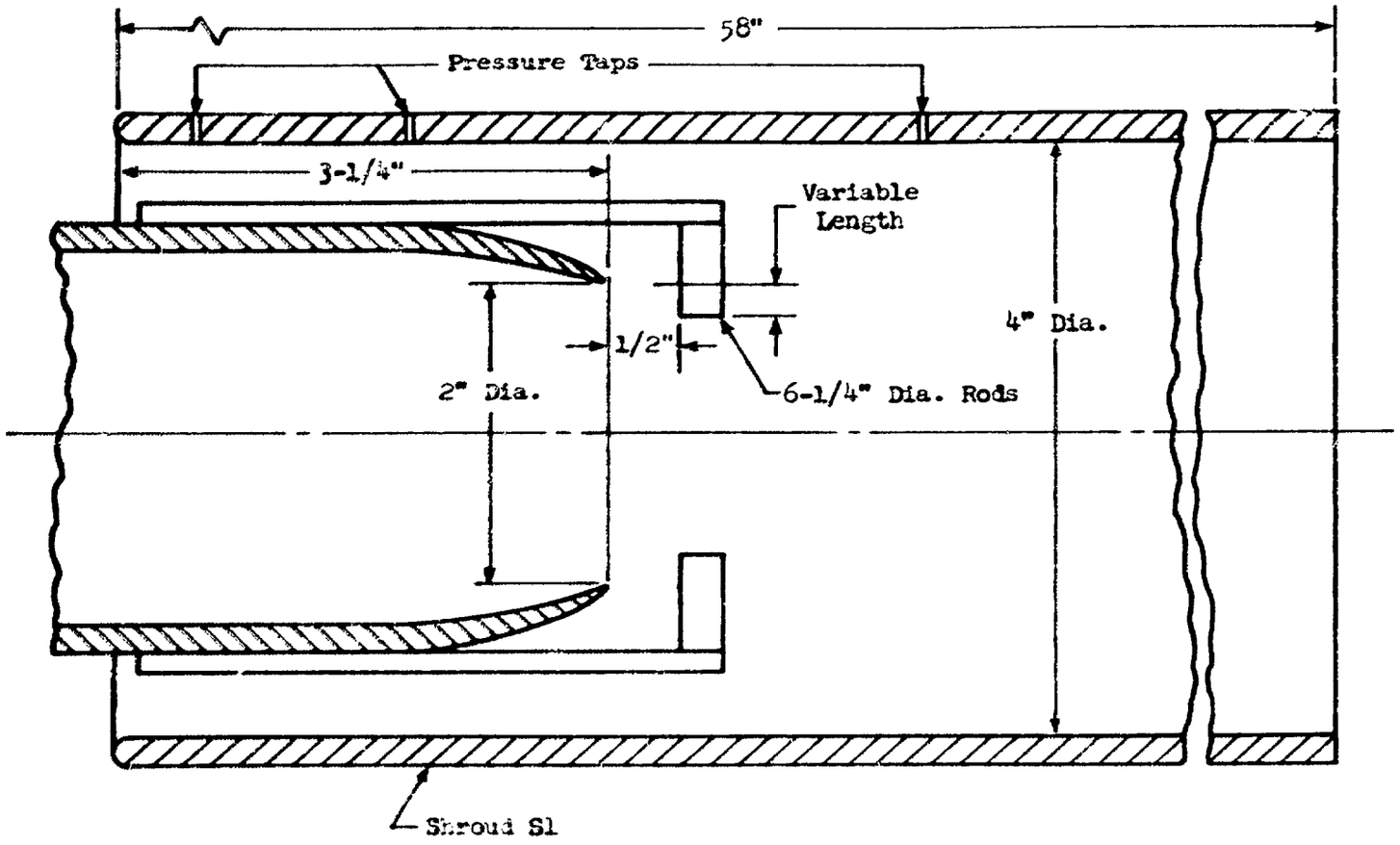


FIGURE VII.A-14A SKETCH OF CONVERGENT NOZZLE, SHROUD, AND RODS

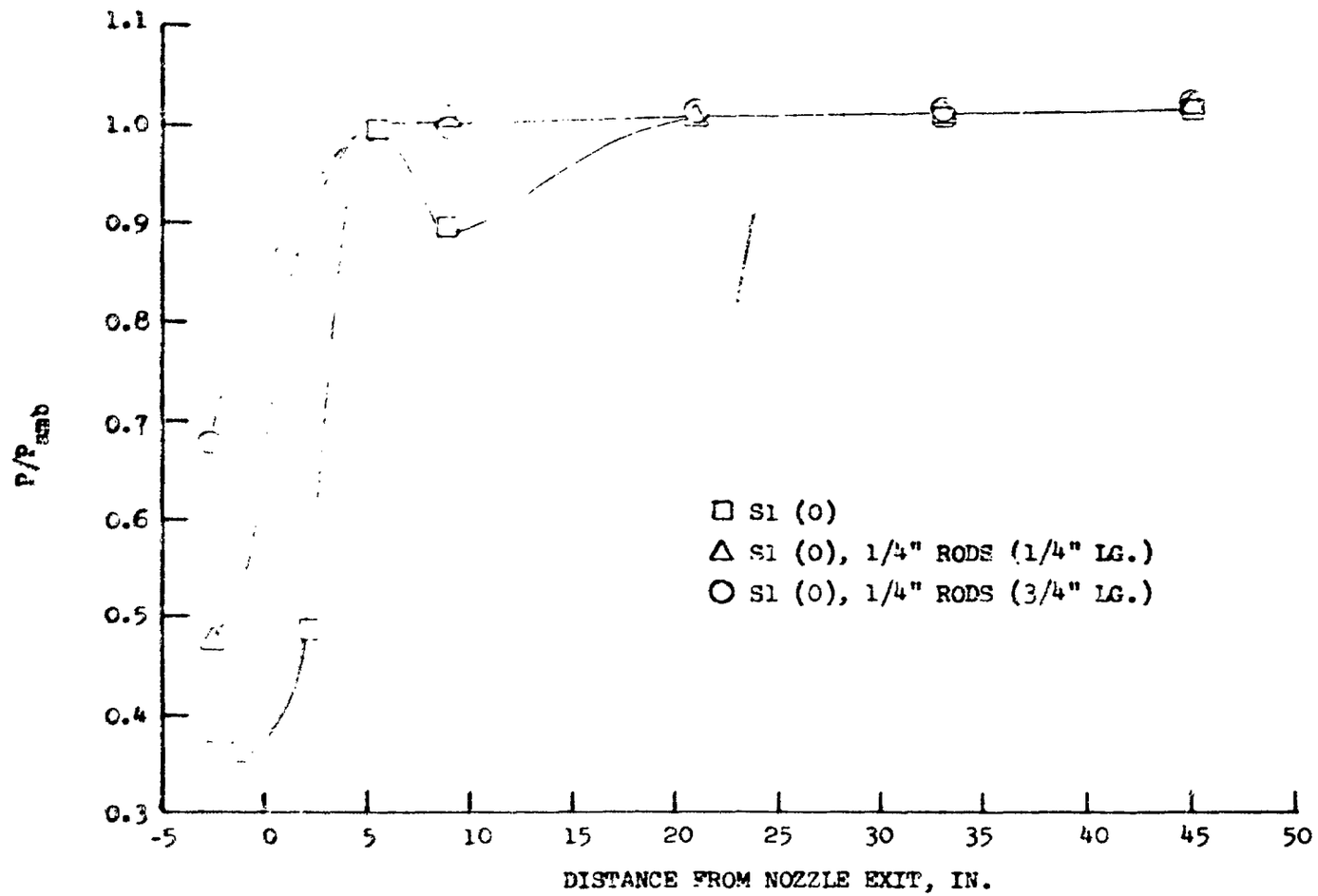


FIGURE VII.A-14B SHROUD PRESSURE DISTRIBUTION WITH RODS AND SHROUD CLOSED, CONVERGENT NOZZLE, Pr = 3.7, Mj = 1.5

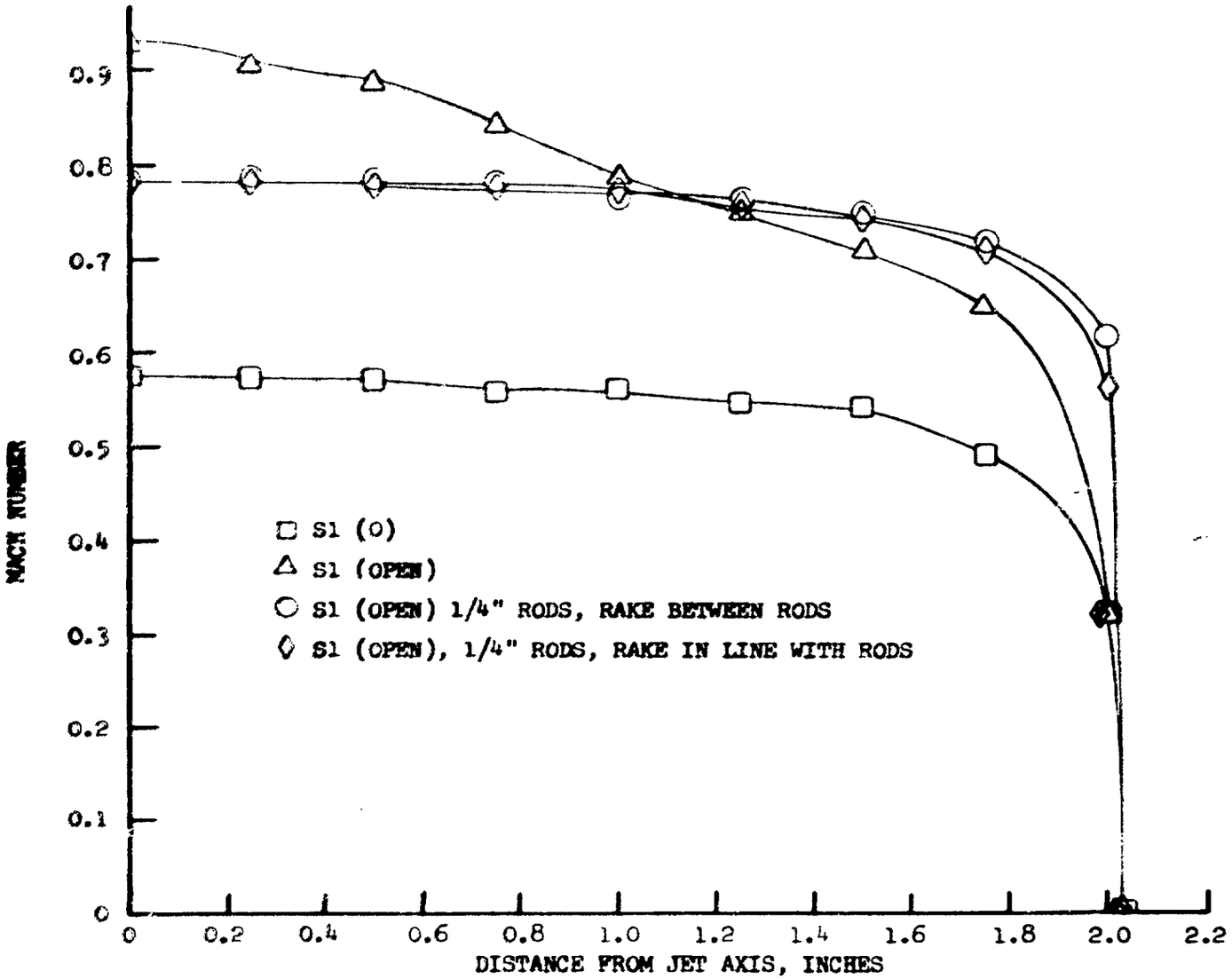


FIGURE VII.A-14C RADIAL MACH NUMBER PROFILE AT JET EXHAUST EXIT WITH RODS AND SHROUD, CONVERGENT NOZZLE, Pr = 3.7, Mj = 1.5

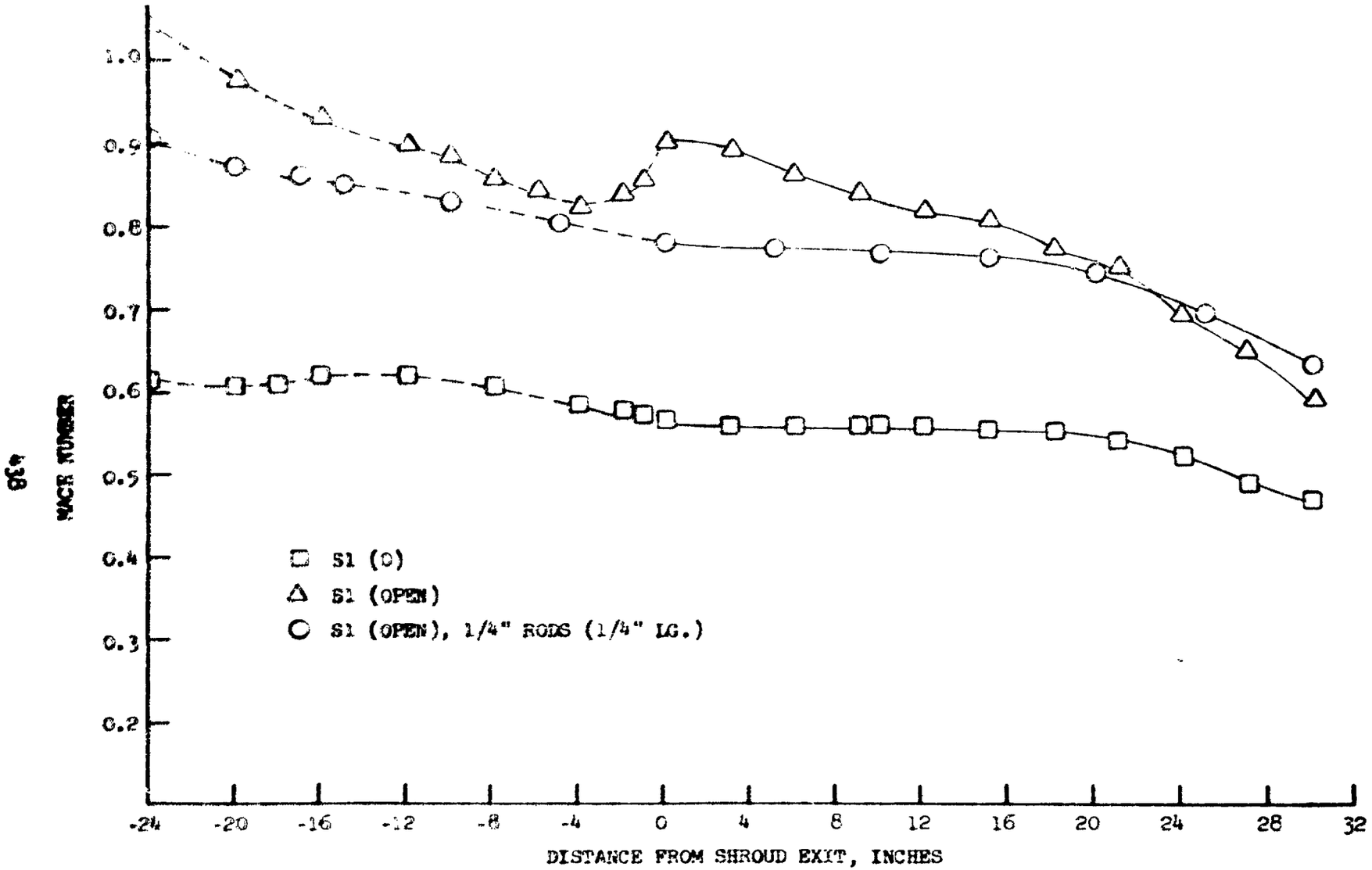


FIGURE VII.A-145 AXIAL MACH NUMBER PROFILE WITH RODS AND SHROUD, CONVERGENT NOZZLE, Pr = 3.7, Mj = 1.5

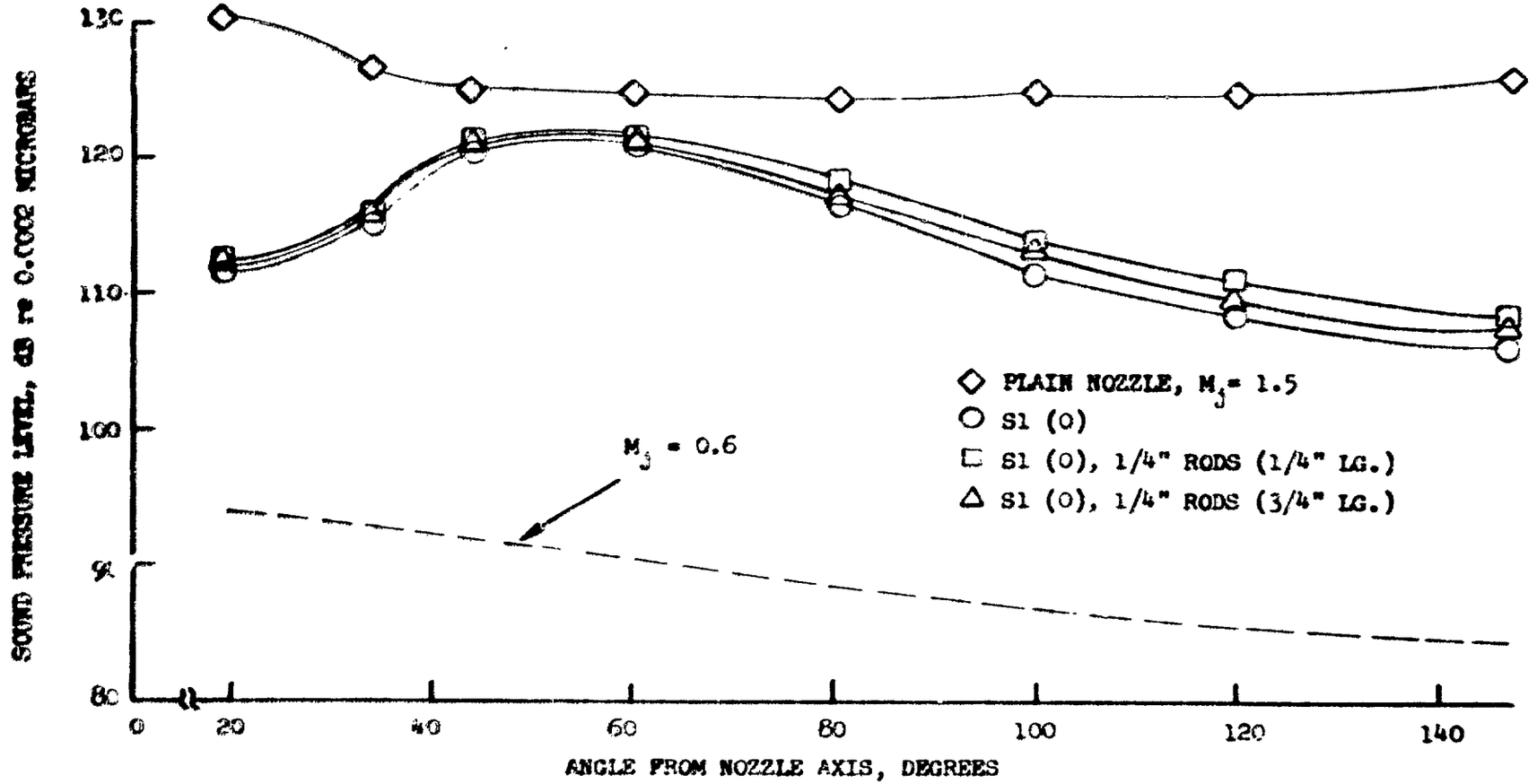


FIGURE VII.A-14E OVERALL SOUND PRESSURE LEVEL AS A FUNCTION OF ANGULAR POSITION FROM THE JET AXIS WITH RODS AND SHROUD CLOSED, CONVERGENT NOZZLE, Pr = 3.7, M_j = 1.5

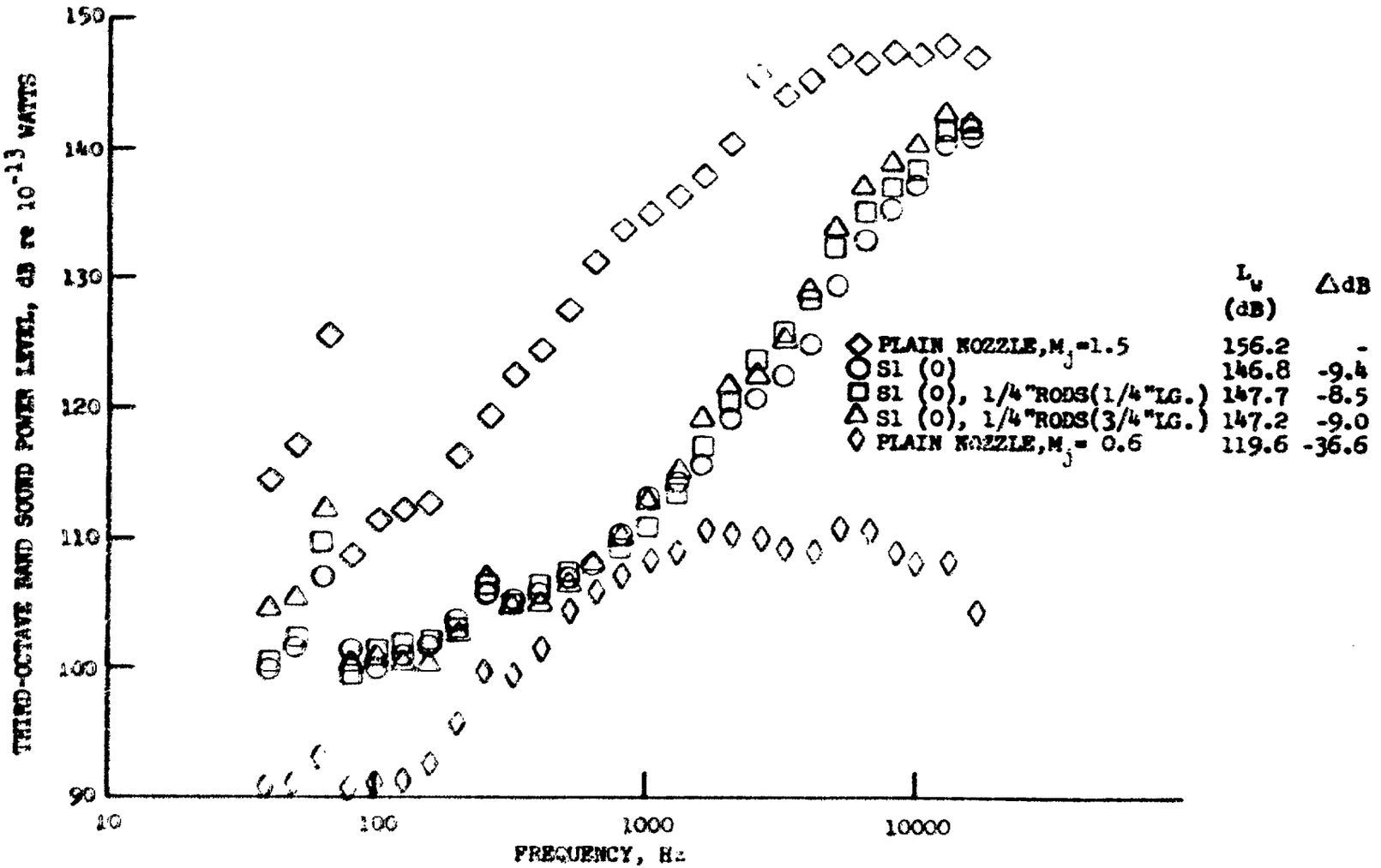


FIGURE VII.A-149 SOUND POWER LEVEL SPECTRA WITH RODS AND SHROUD CLOSED, CONVERGENT NOZZLE, Pr = 3.7, Mj = 1.5

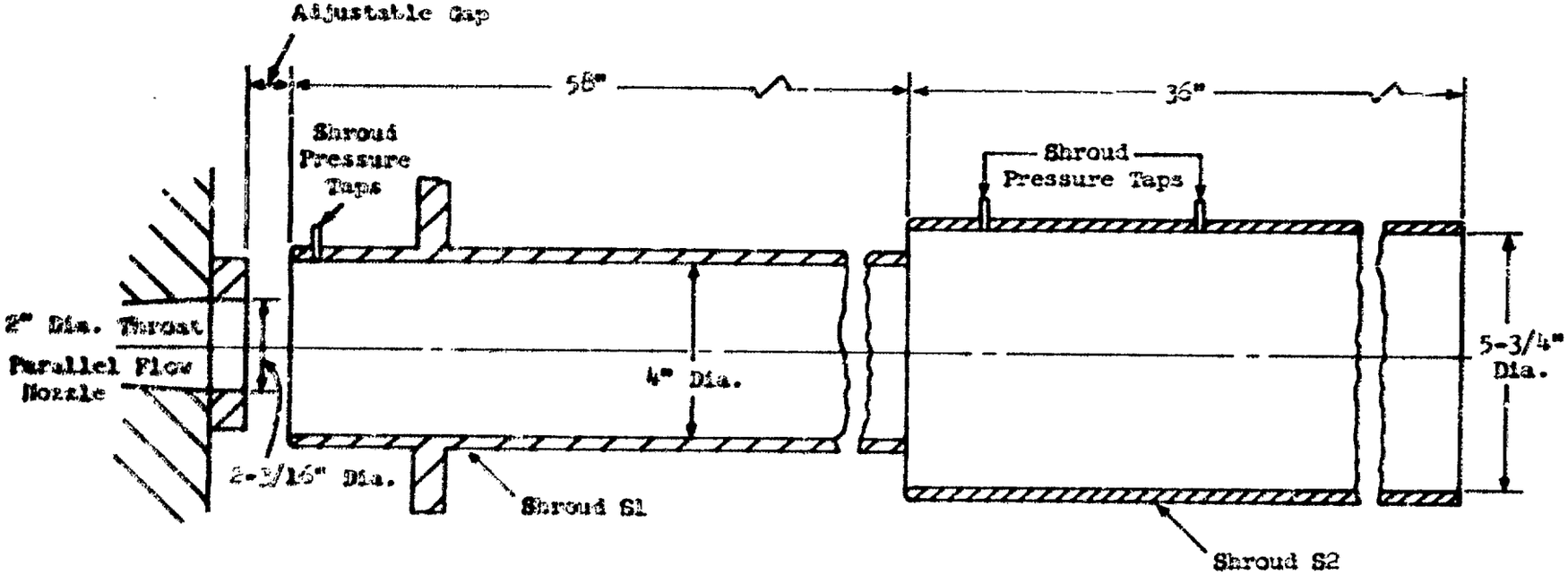


FIGURE VII.A-15A SKETCH OF NOZZLE AND SHROUDS

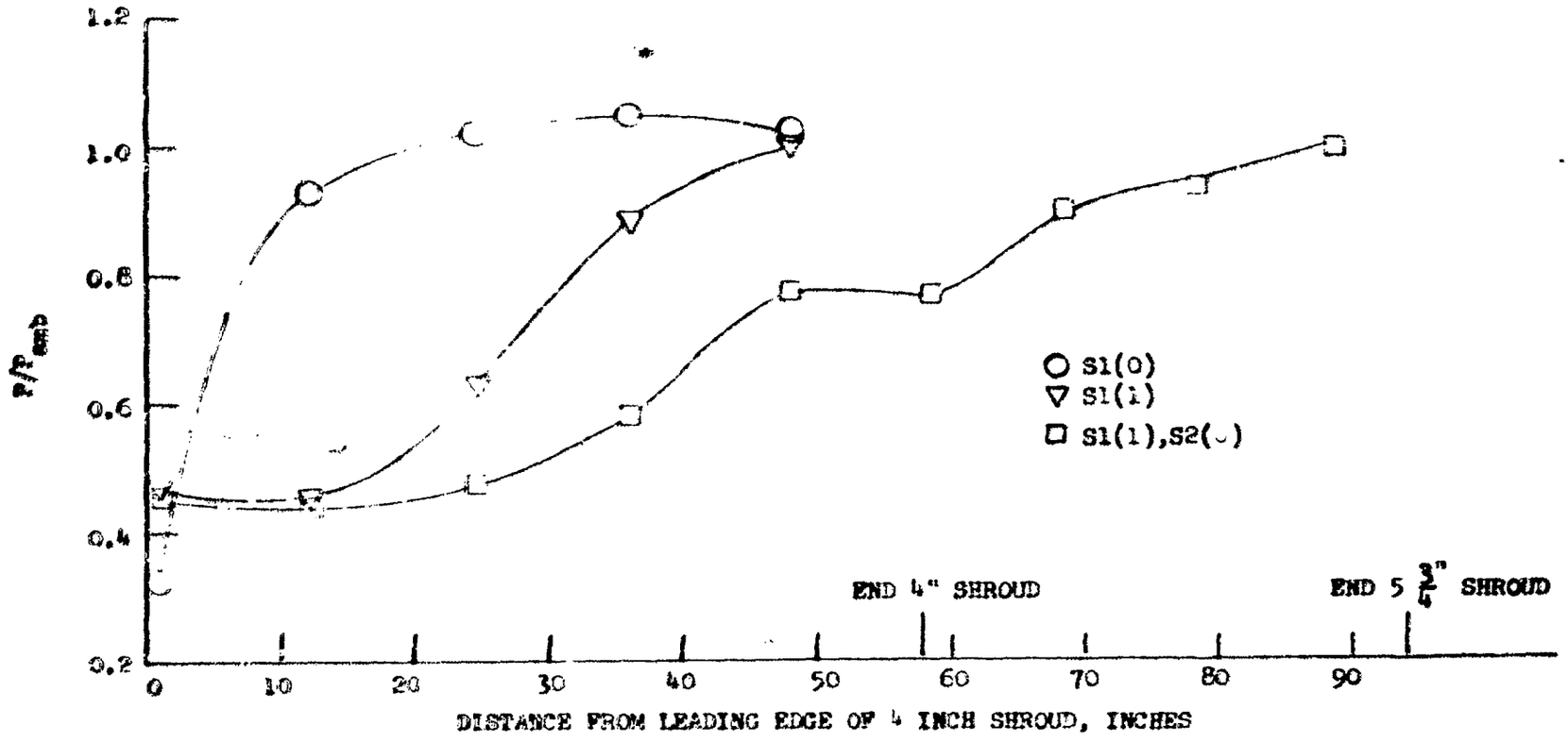


FIGURE VII.A-15B SHROUD PRESSURE DISTRIBUTION WITH 4 AND 6 INCH SHROUDS FOR PARALLEL FLOW NOZZLE, P_T = 3.7, M_∞ = 1.5

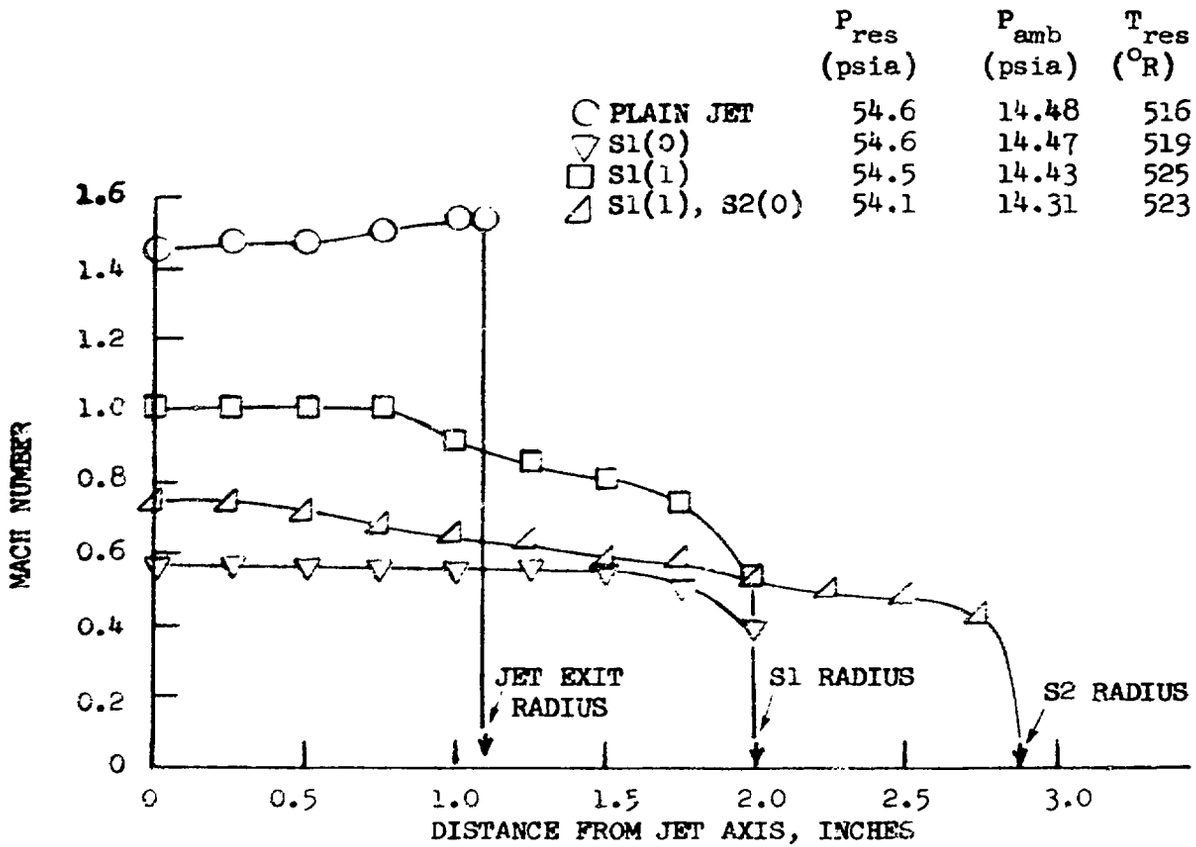


FIGURE VII.A-15C RADIAL MACH NUMBER PROFILE AT JET EXHAUST EXIT WITH SHROUDS FOR PARALLEL FLOW NOZZLE

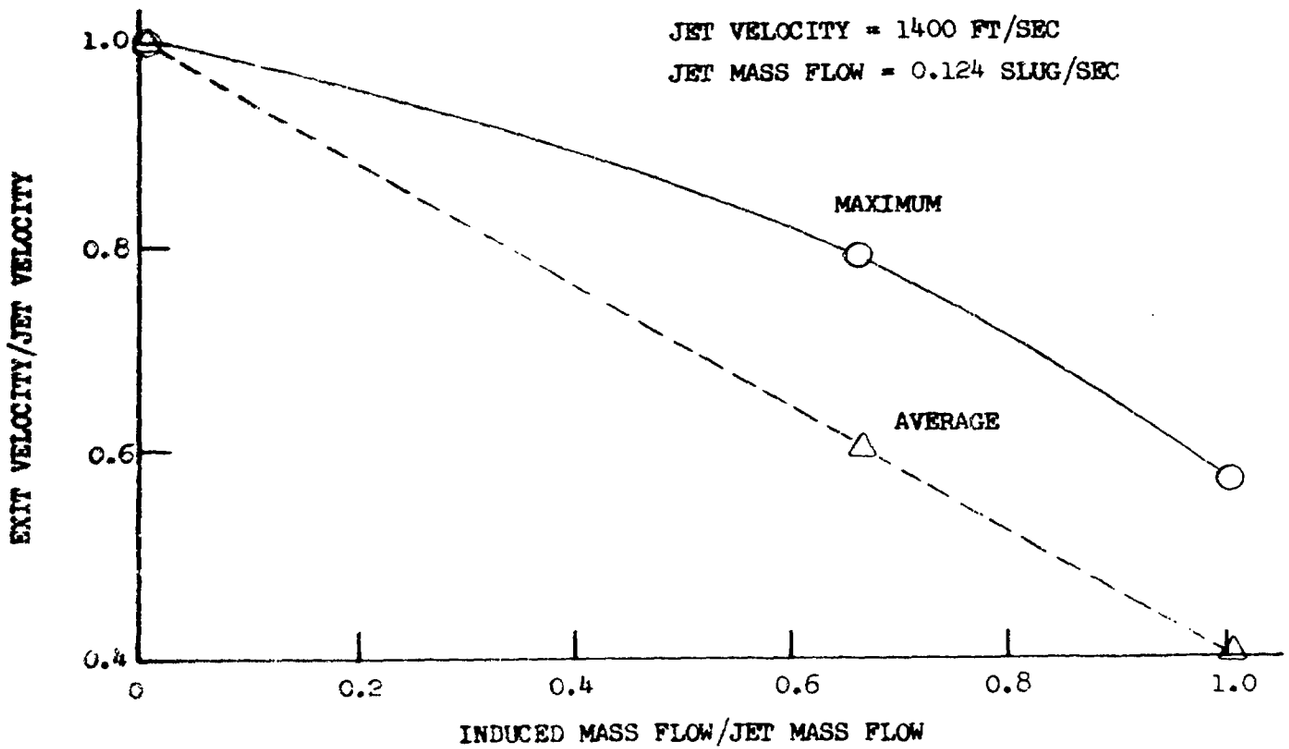


FIGURE VII.A-15D MIXED JET VELOCITY AS A FUNCTION OF INDUCED FLOW WITH SINGLE AND DOUBLE SHROUDS FOR PARALLEL FLOW NOZZLE

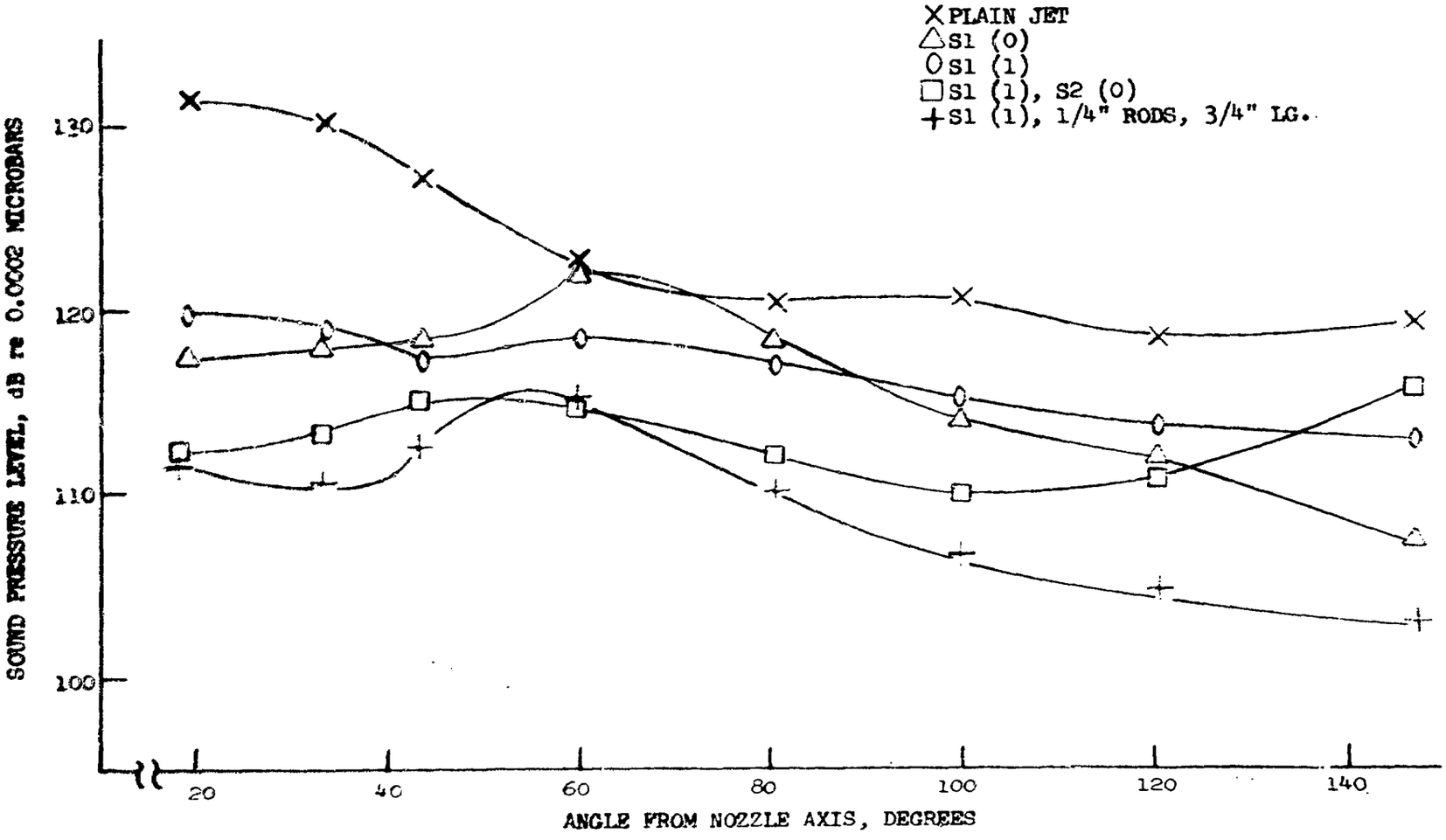
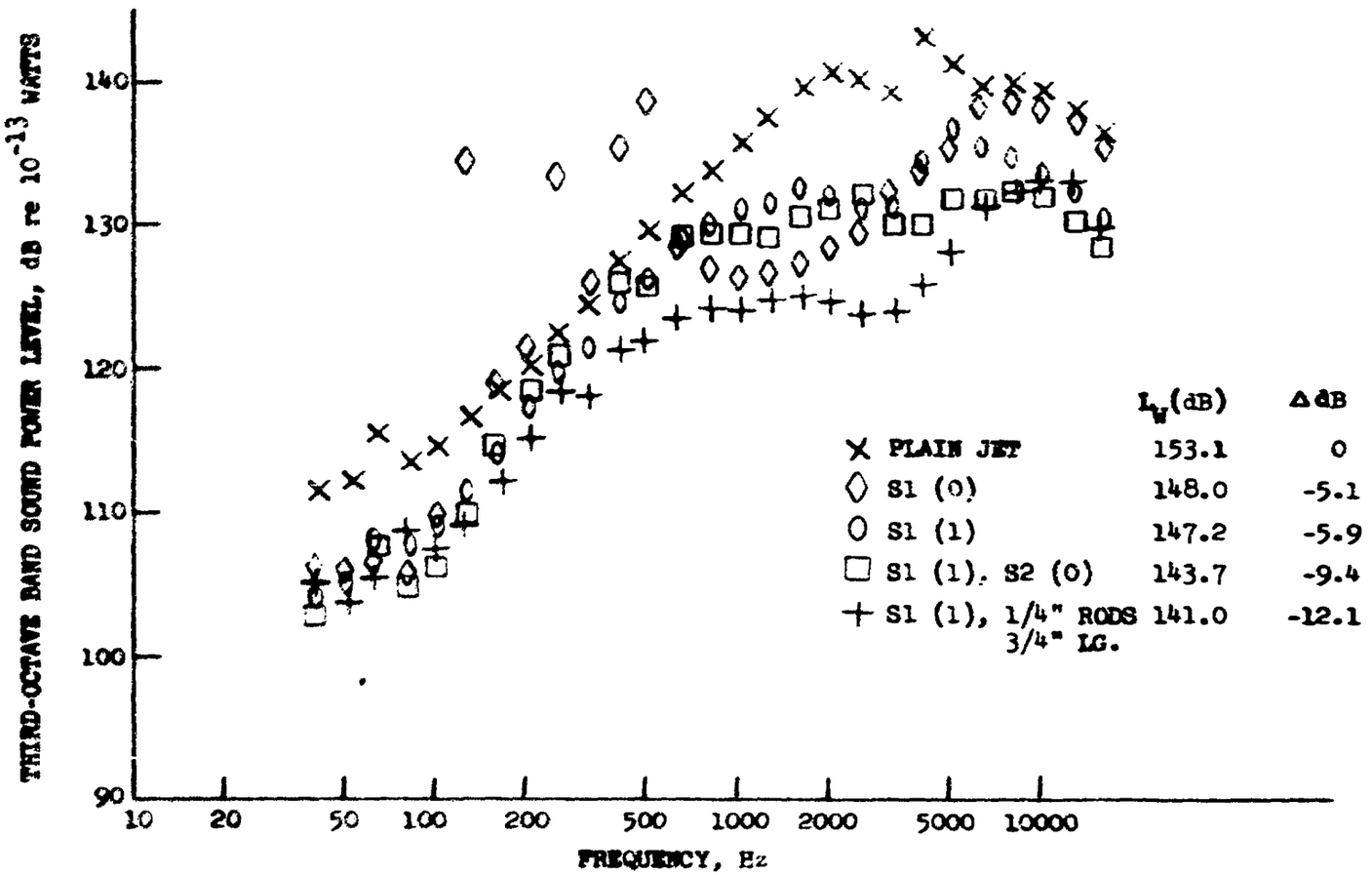


FIGURE VII.A-15E OVERALL SOUND PRESSURE LEVEL AS A FUNCTION OF ANGULAR POSITION FROM JET AXIS WITH 4 OR 6 INCH SHROUD FOR PARALLEL FLOW NOZZLE



FREQUENCY VII.A-15F SOUND POWER LEVEL SPECTRA WITH 4 OR 6 INCH SHROUDS FOR PARALLEL FLOW NOZZLE, Pr = 3.7, MJ = 1.5

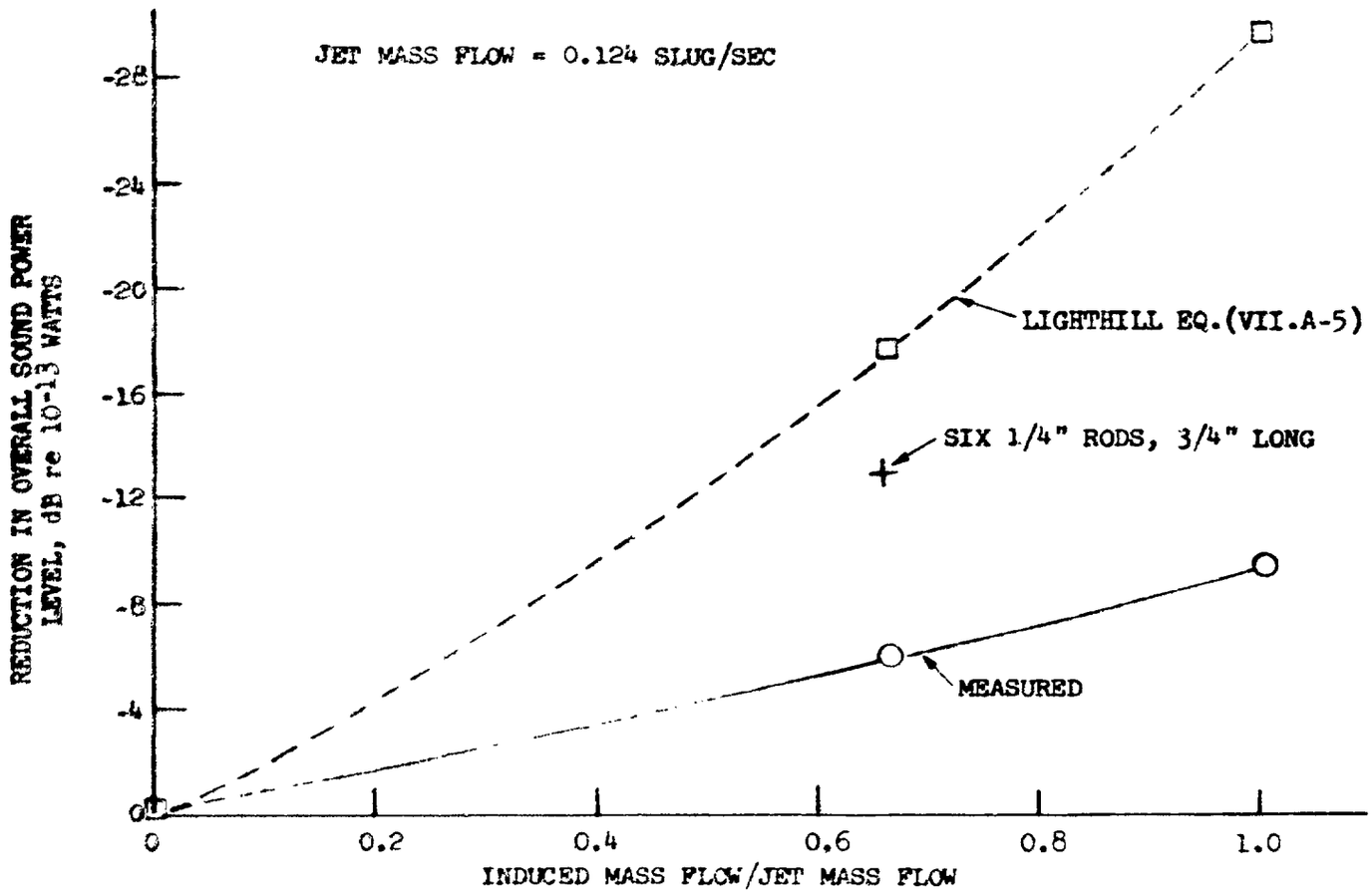


FIGURE VII.A-15 ACOUSTIC POWER REDUCTION AS A FUNCTION OF INDUCED FLOW FOR PARALLEL FLOW NOZZLE WITH 4 OR 6 INCH SHROUDS, Pr = 3.7, MJ = 1.5

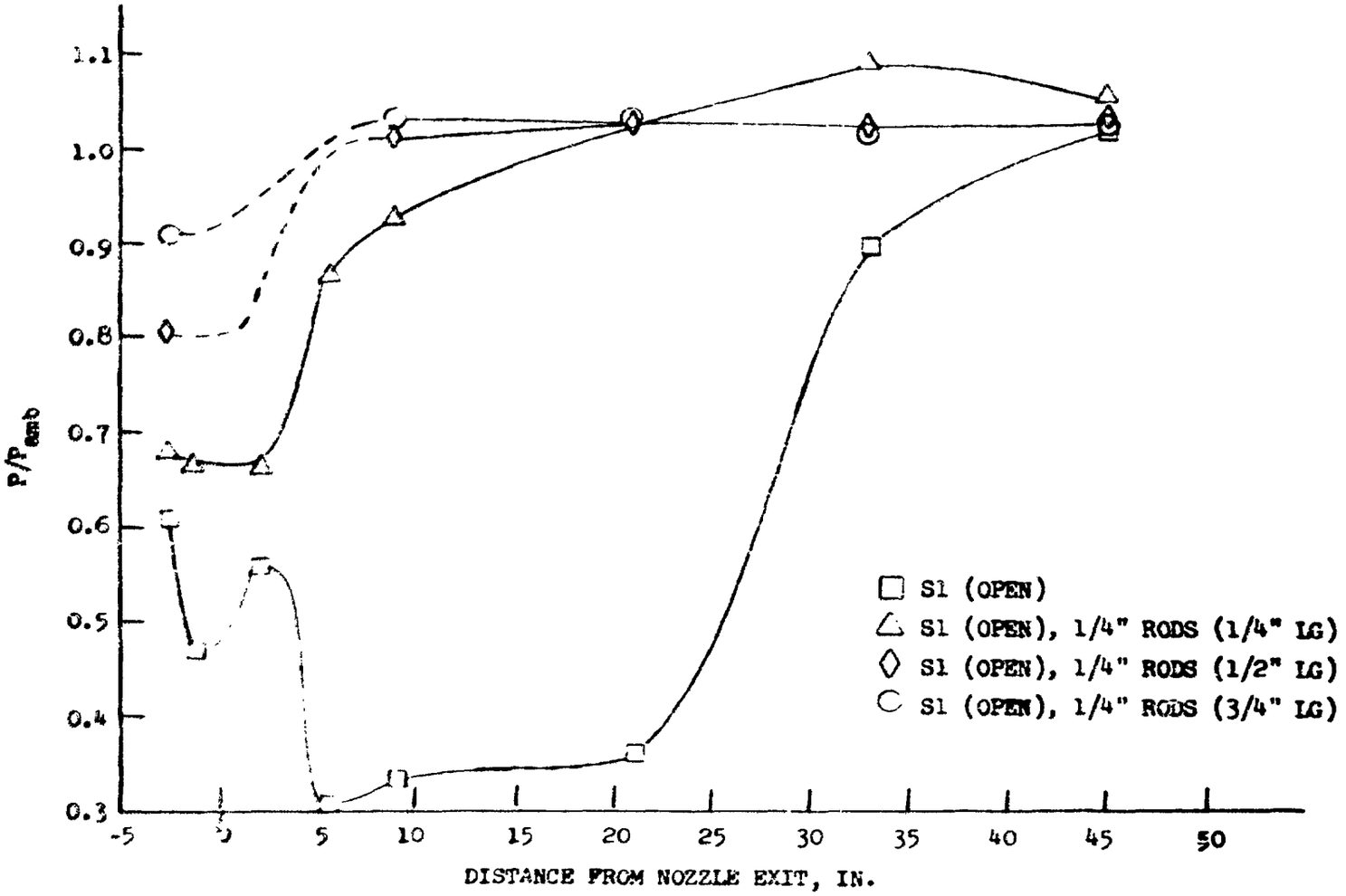


FIGURE VII.A-16A SHROUD PRESSURE DISTRIBUTION WITH RODS AND SHROUD OPEN, CONVERGENT NOZZLE, Pr = 3.7, Mj = 1.5

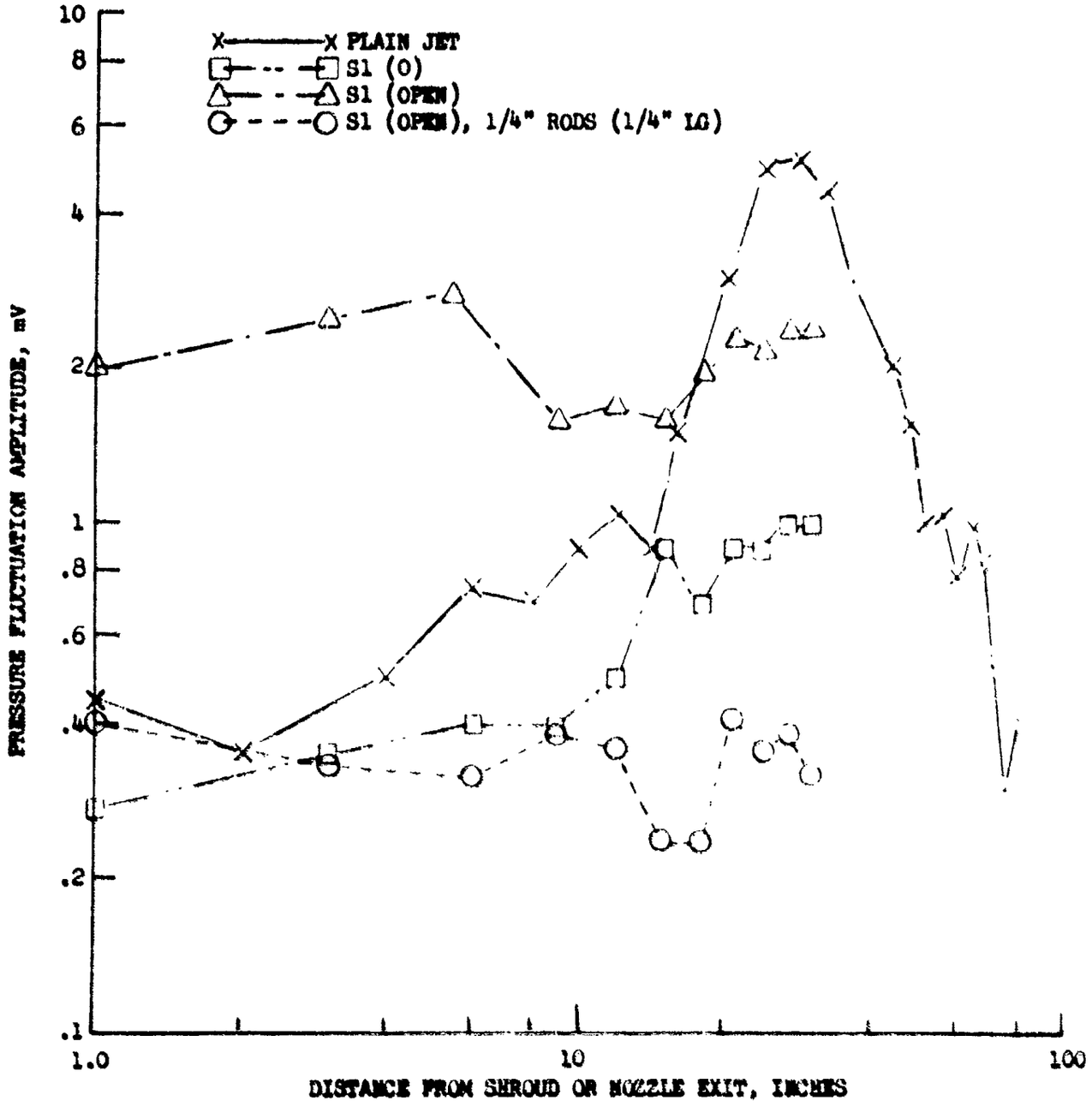


FIGURE VII.A-16B AXIAL PRESSURE FLUCTUATIONS FOR CONVERGENT NOZZLE AND SUPPRESSORS, Pr = 3.7, Mj = 1.5

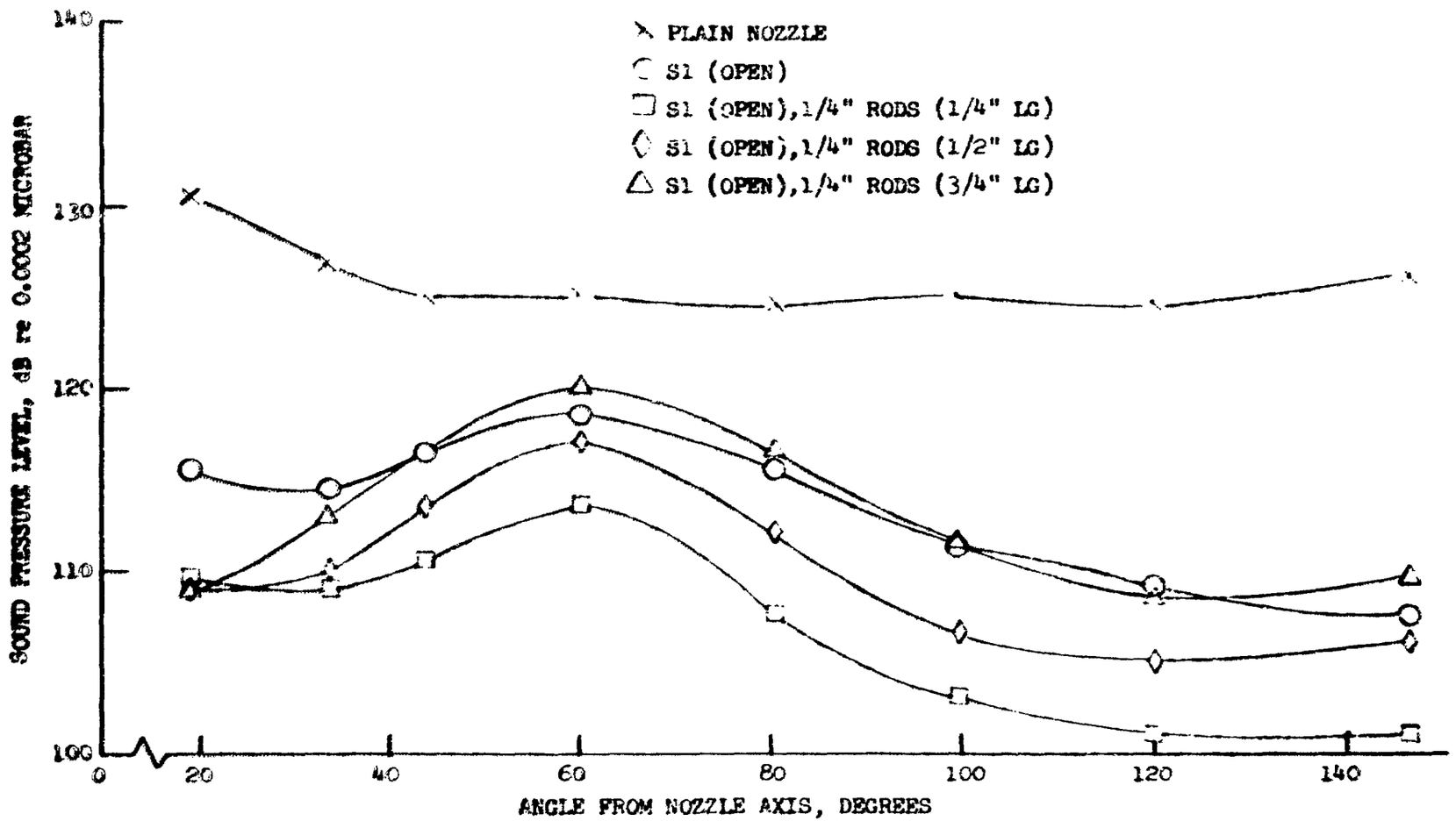


FIGURE VII.A-16C OVERALL SOUND PRESSURE LEVEL AS A FUNCTION OF ANGULAR POSITION FROM THE JET AXIS WITH RODS AND SHROUD OPEN FOR CONVERGENT NOZZLE, Pr = 3.7, Mj = 1.5

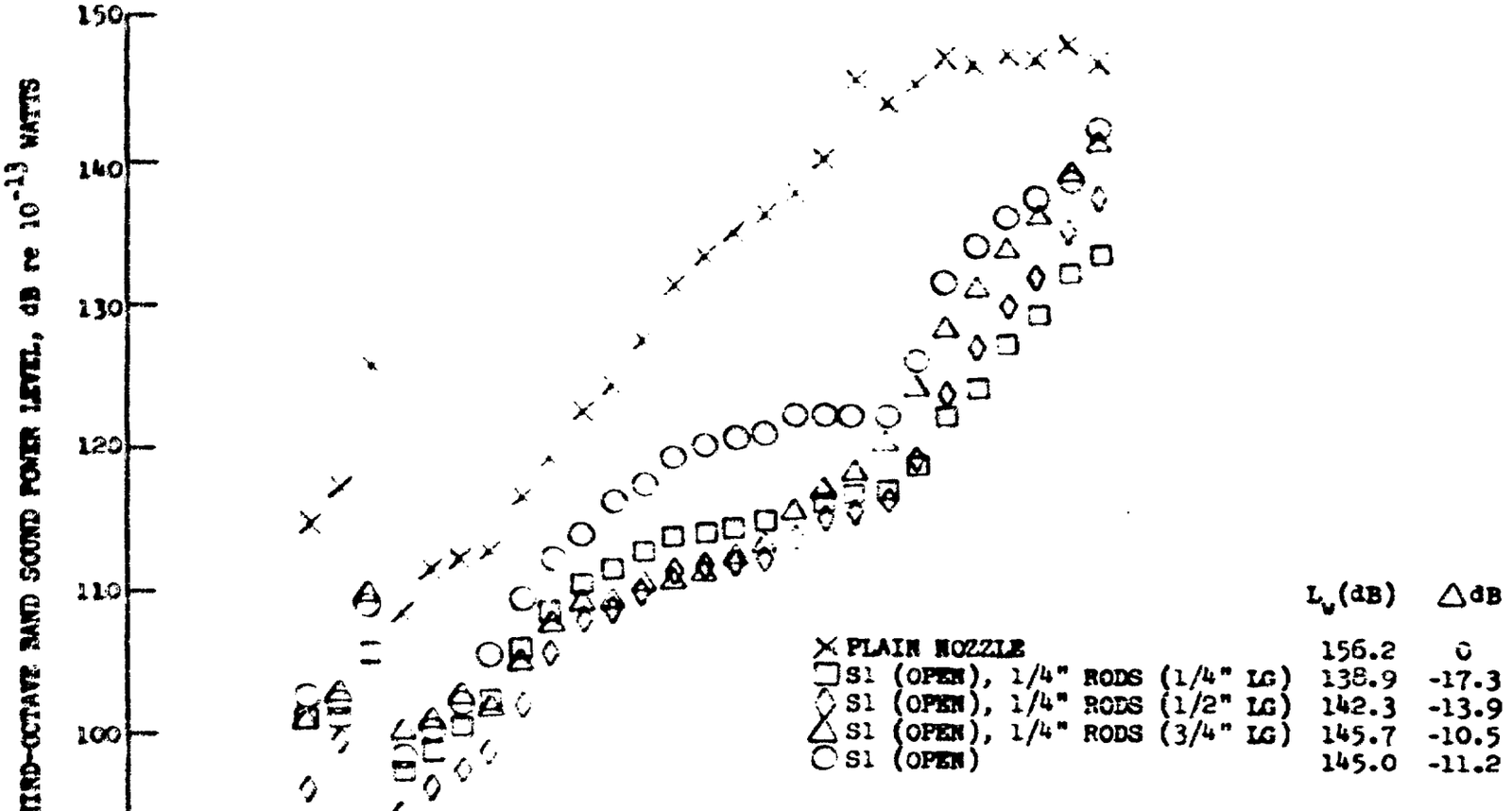


FIGURE VII.A-16D SOUND POWER LEVEL SPECTRA WITH RODS AND SHROUD OPEN FOR CONVERGENT NOZZLE, Pr = 3.7, Mj = 1.5

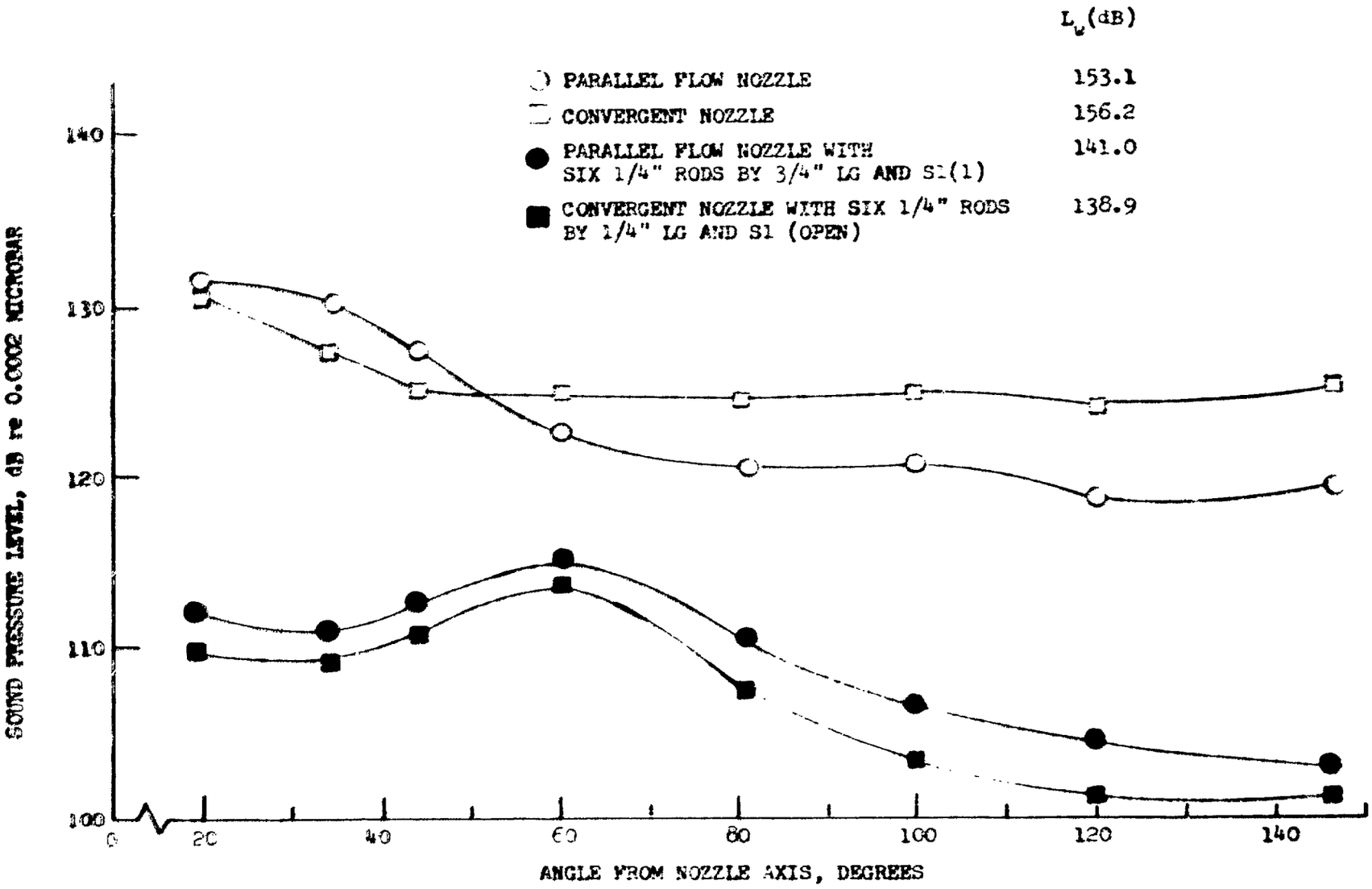


FIGURE VII.A-17A COMPARISON OF DIRECTIVITIES FOR M = 1.5 PARALLEL FLOW AND CONVERGENT NOZZLES WITH AND WITHOUT SUPPRESSORS

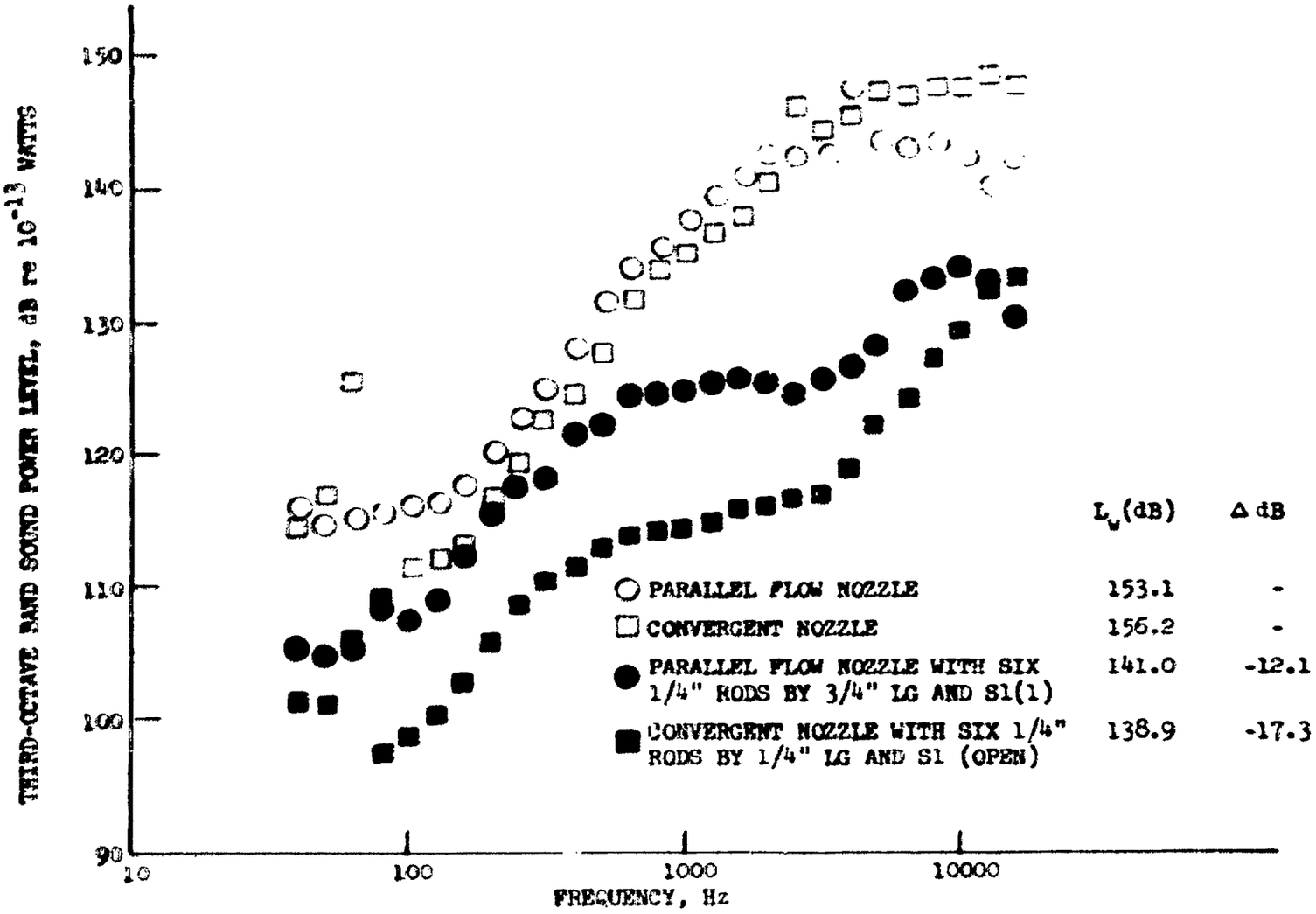


FIGURE VII.A-17B COMPARISON OF POWER LEVEL SPECTRA FOR M = 1.5 PARALLEL FLOW AND CONVERGENT NOZZLES WITH AND WITHOUT SUPPRESSORS

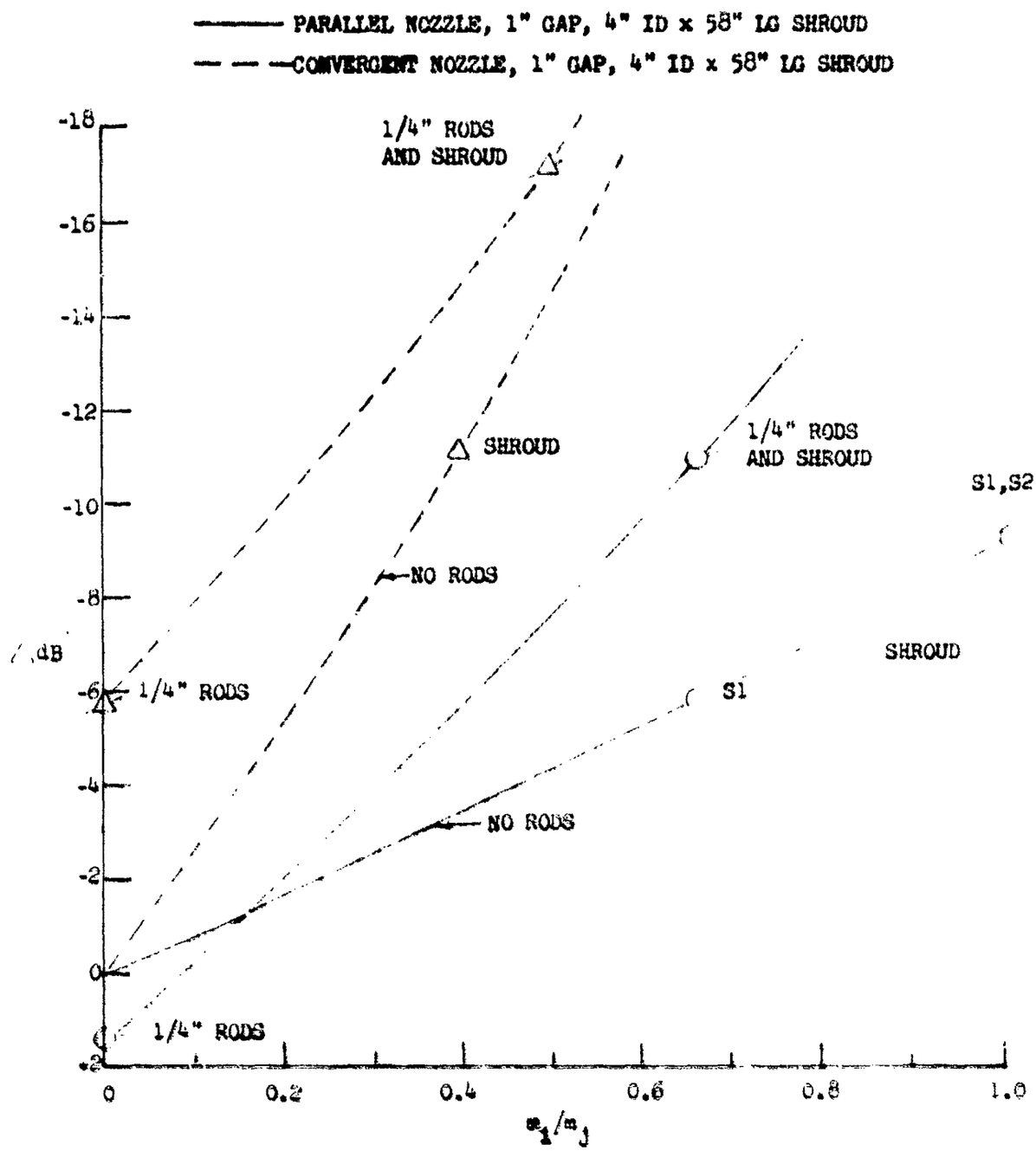


FIGURE VII.A-17C VARIATION IN OVERALL SOUND POWER LEVEL WITH RODS AND SHROUD AS A FUNCTION OF INDUCED MASS FLOW FOR M_j = 1.5

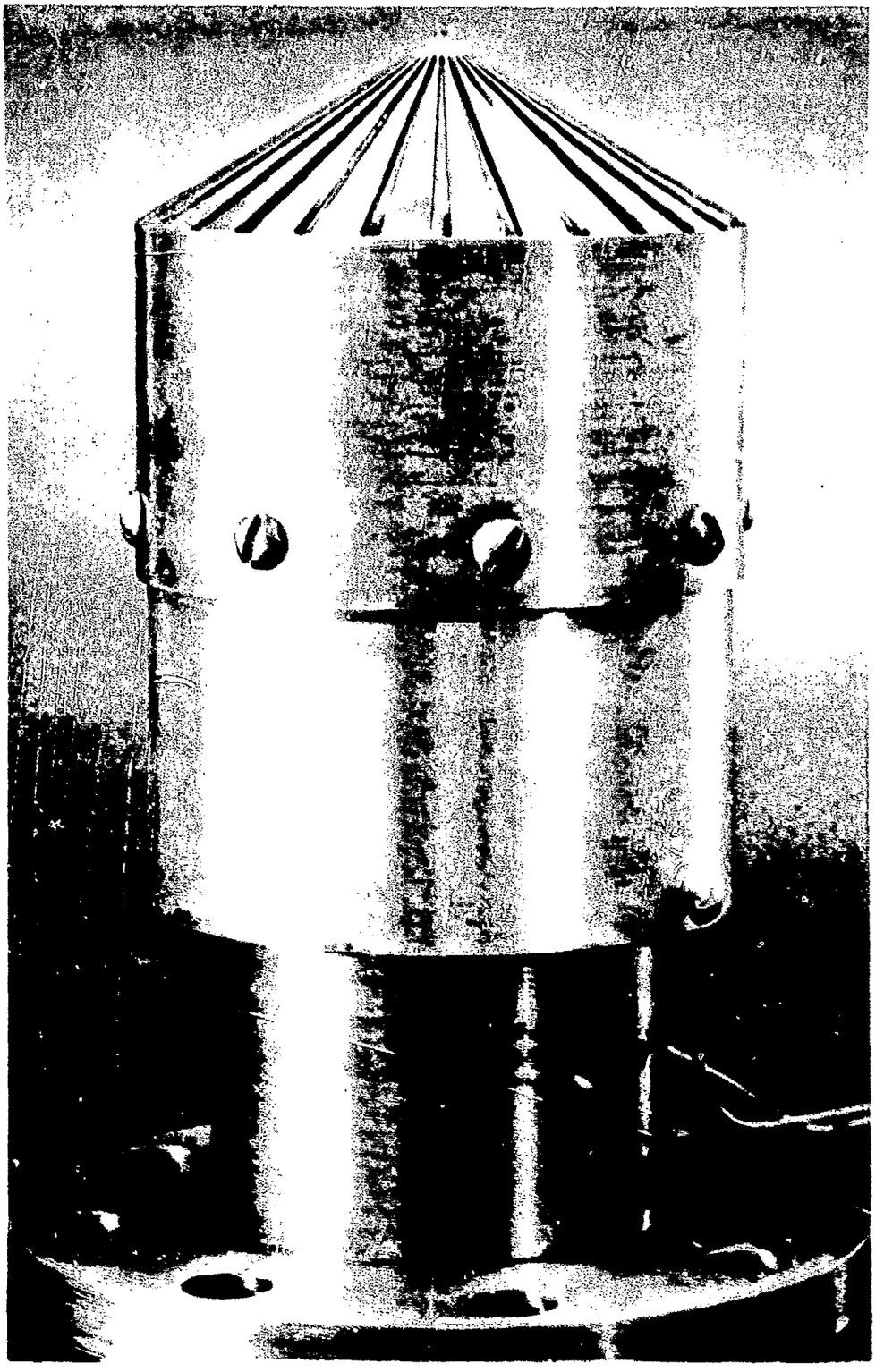


FIGURE VII.A-18A PHOTOGRAPH OF 60° REVERSE SLOTTED CONE WITH 28 SLOTS

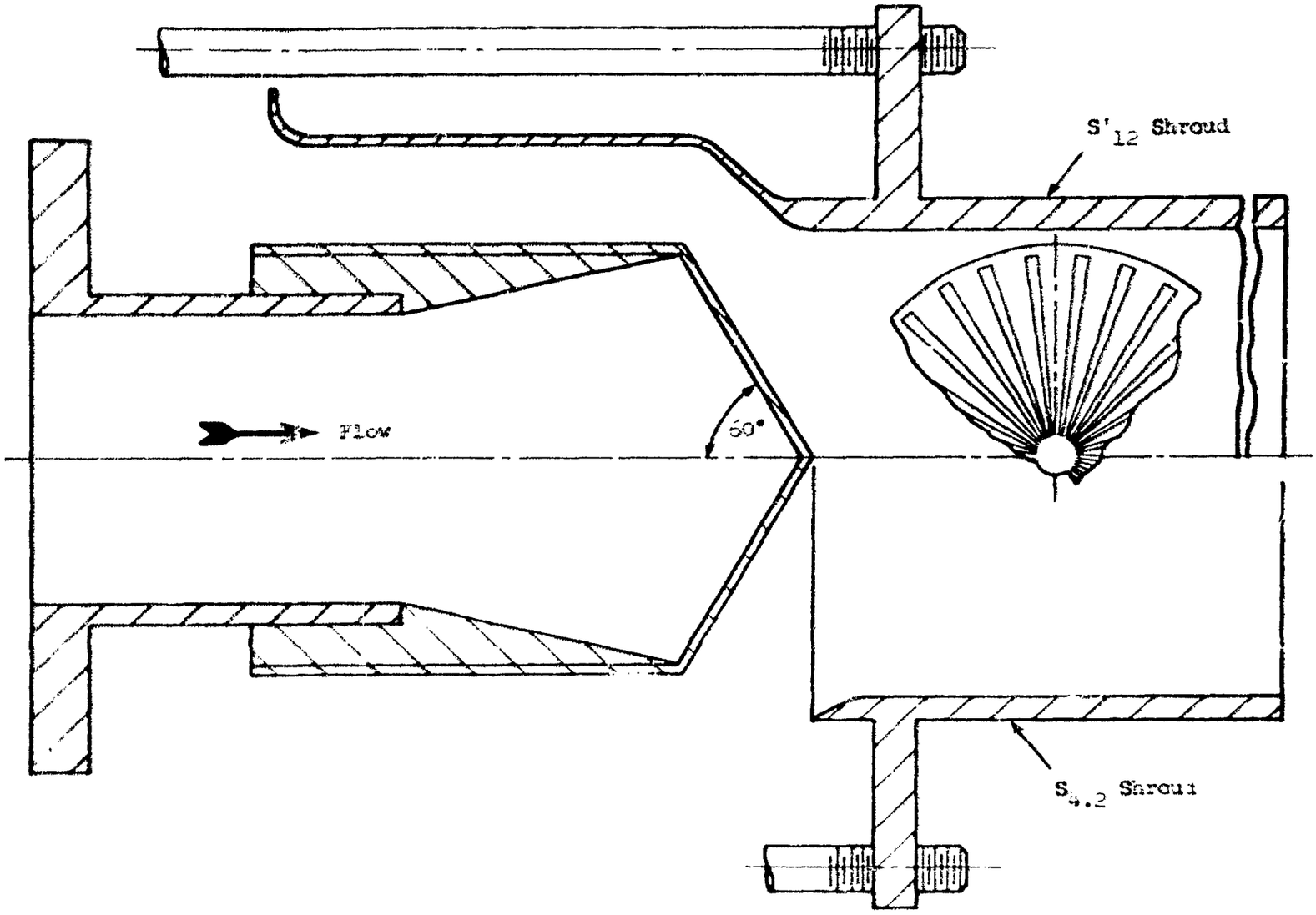


FIGURE VII.A-10B SKETCH OF 60° REVERSE SLOTTED CONE AND SHROUDS

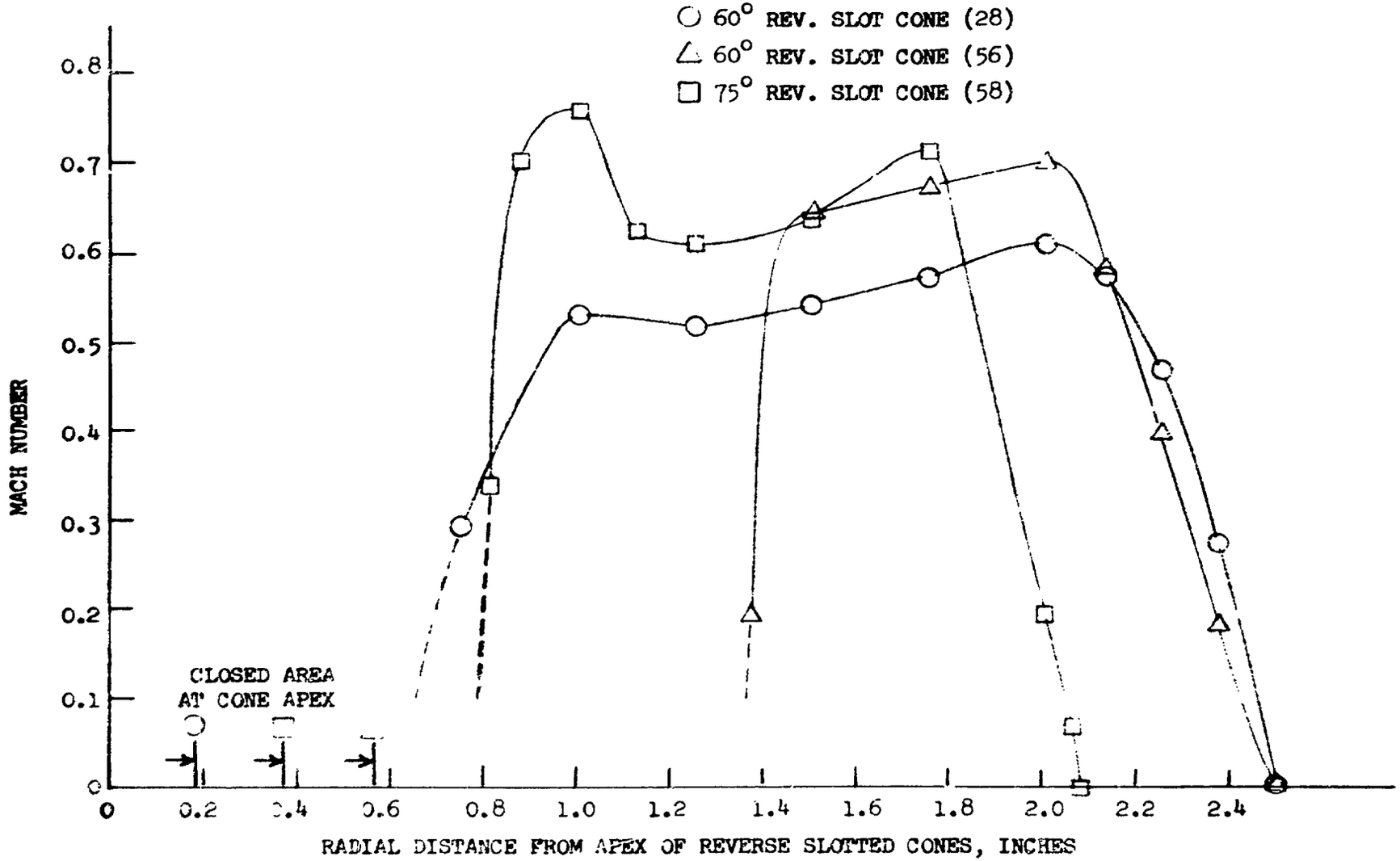


FIGURE VII.A-18C MACH NUMBER PROFILE ACROSS THE JET AT ONE INCH DOWNSTREAM OF APEX OF THE REVERSE SLOTTED CONES, Pr = 3.2, Mj = 1.4

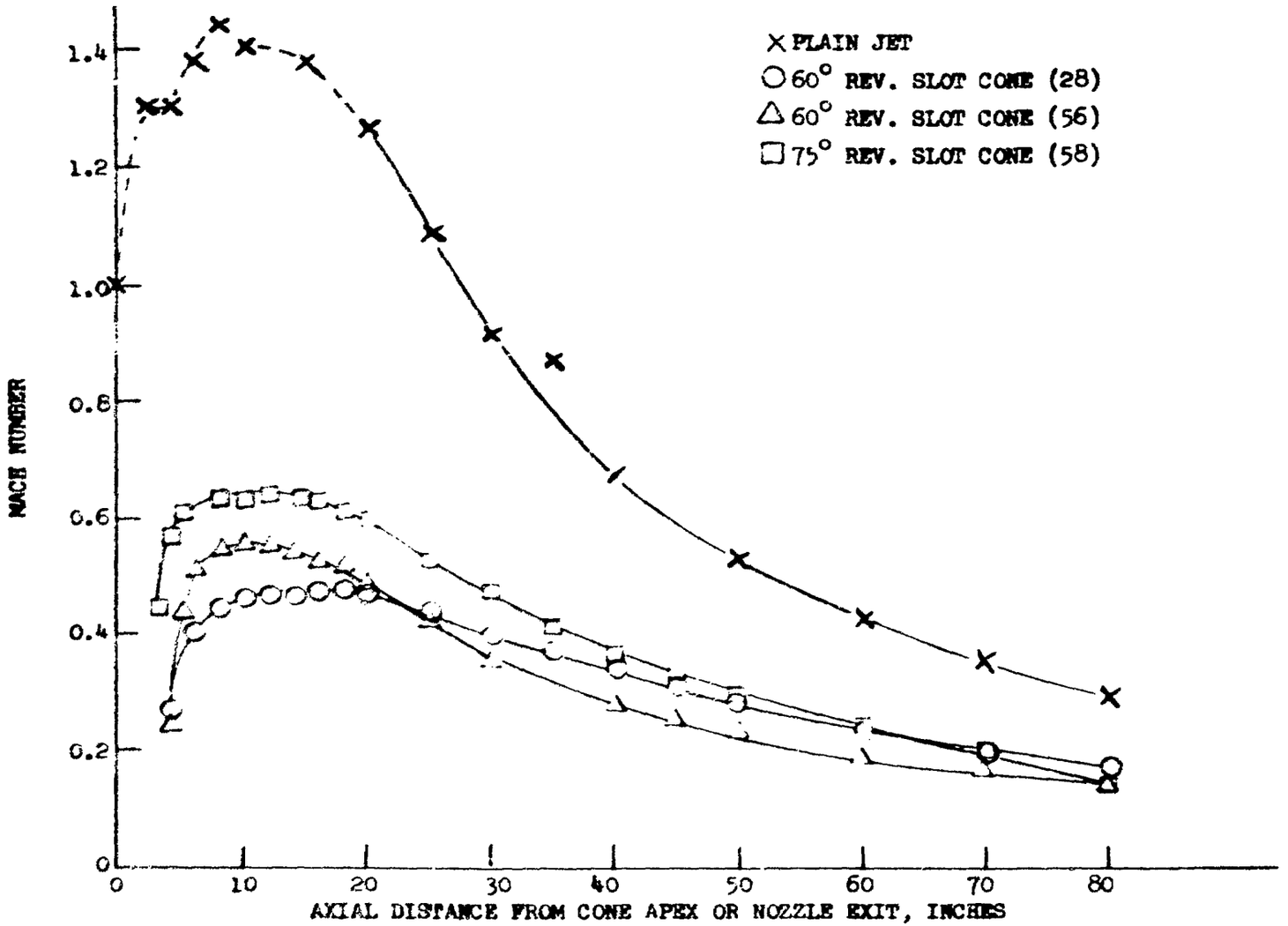


FIGURE VII.A-18D AXIAL MACH NUMBER VARIATION FOR REVERSE SLOTTED CONES AND PLAIN JET, Pr = 3.2, Mj = 1.4

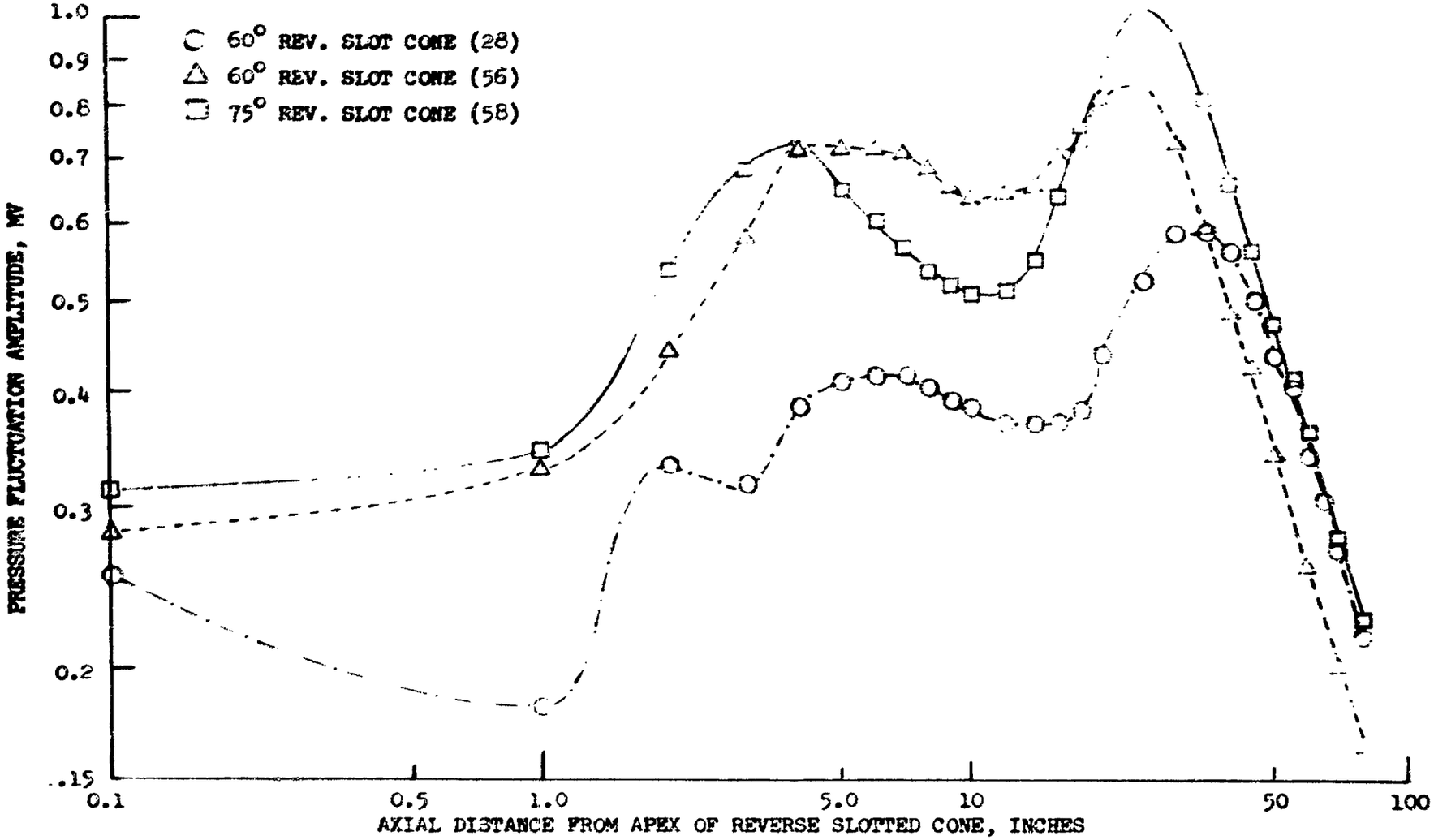


FIGURE VII.A-182 AXIAL DISTANCE FROM APEX OF REVERSE SLOTTED CONE - INCHES.
AXIAL IMPACT PRESSURE FLUCTUATIONS FOR REVERSE SLOTTED CONES, Pr = 3.2, Mj = 1.4

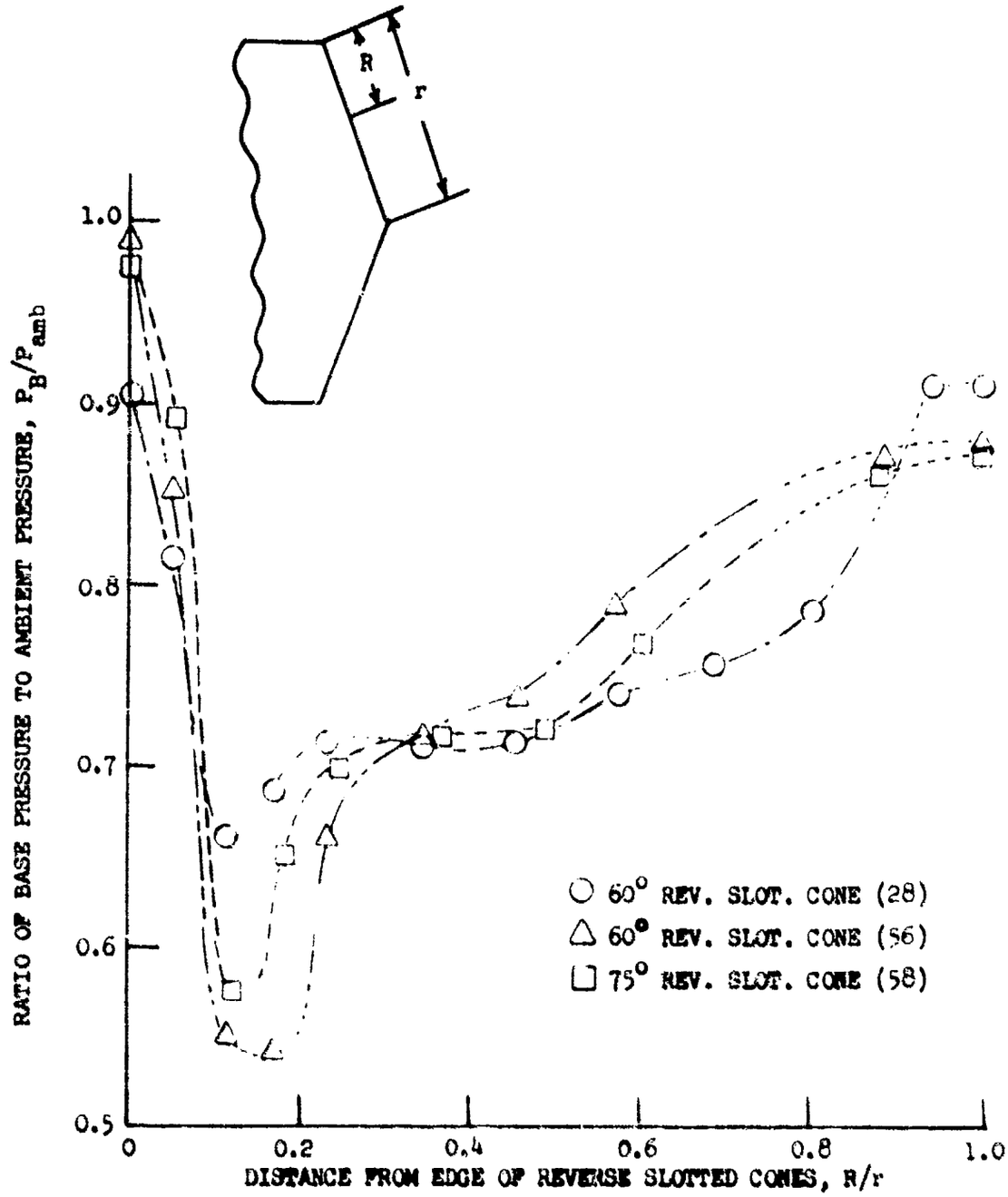


FIGURE VII.A-18P BASE PRESSURE ON THE SOLID PORTION OF THE REVERSE SLOTTED CONES, Pr = 3.2, MJ = 1.4

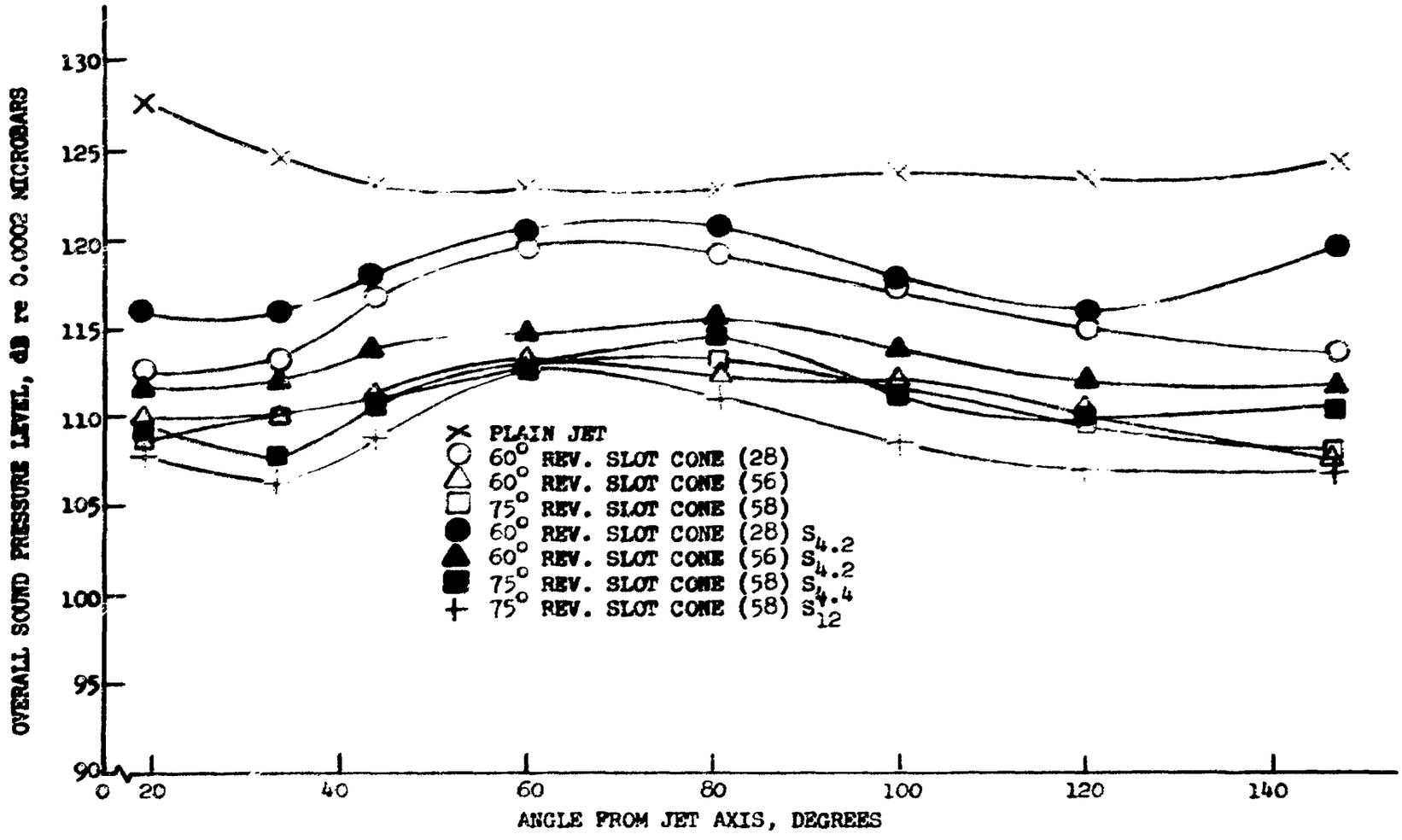


FIGURE VII.A-18G OVERALL SOUND PRESSURE LEVEL AS A FUNCTION OF ANGULAR POSITION FROM JET AXIS FOR REVERSE SLOTTED CONES WITH AND WITHOUT SHROUDS, Pr = 3.2, Mj = 1.4

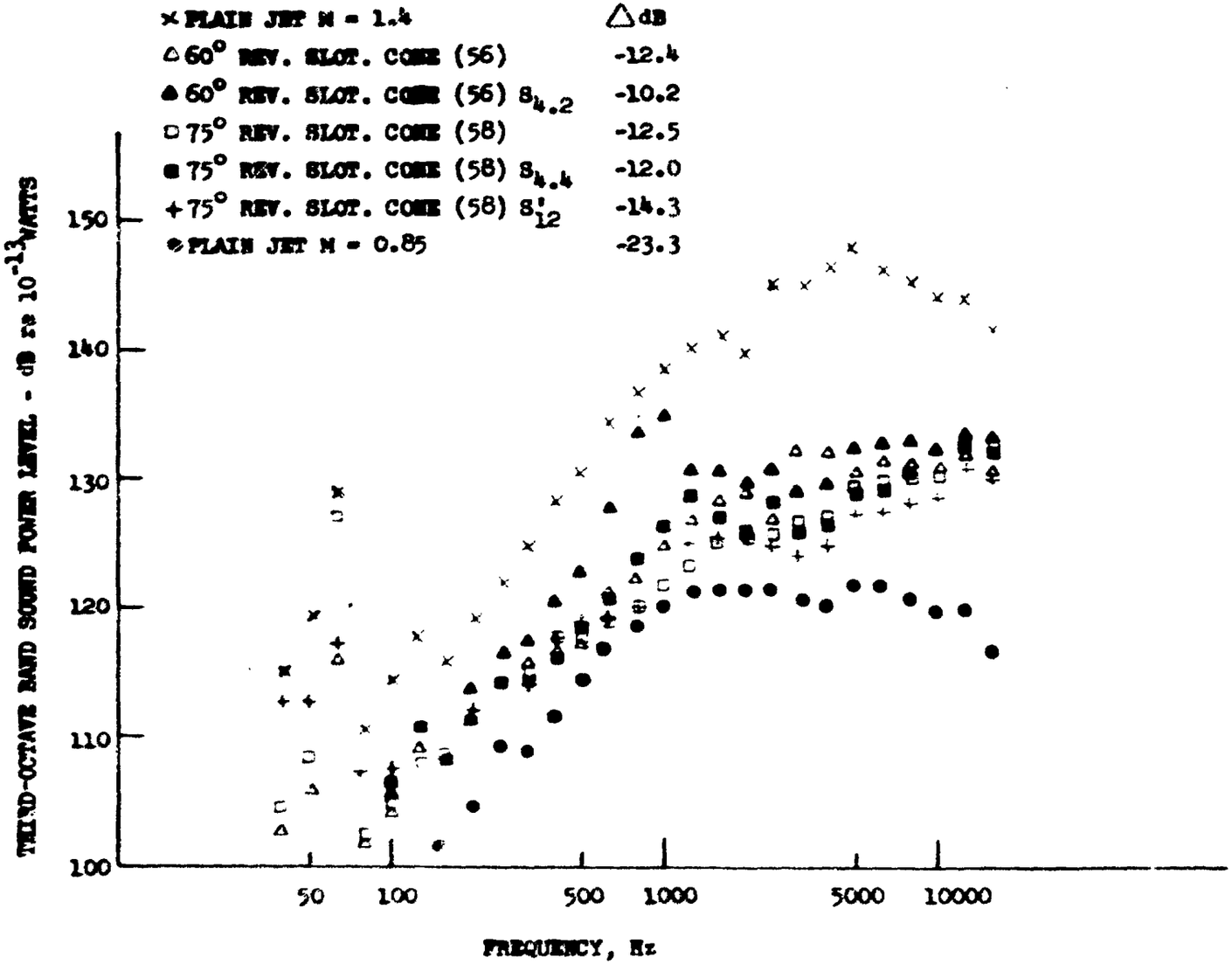


FIGURE VII.A 18: SOUND POWER LEVEL SPECTRA FOR REVERSE SLOTTED CONES WITH AND WITHOUT SHROUDS, Pr = 3.2, Mj = 1.4

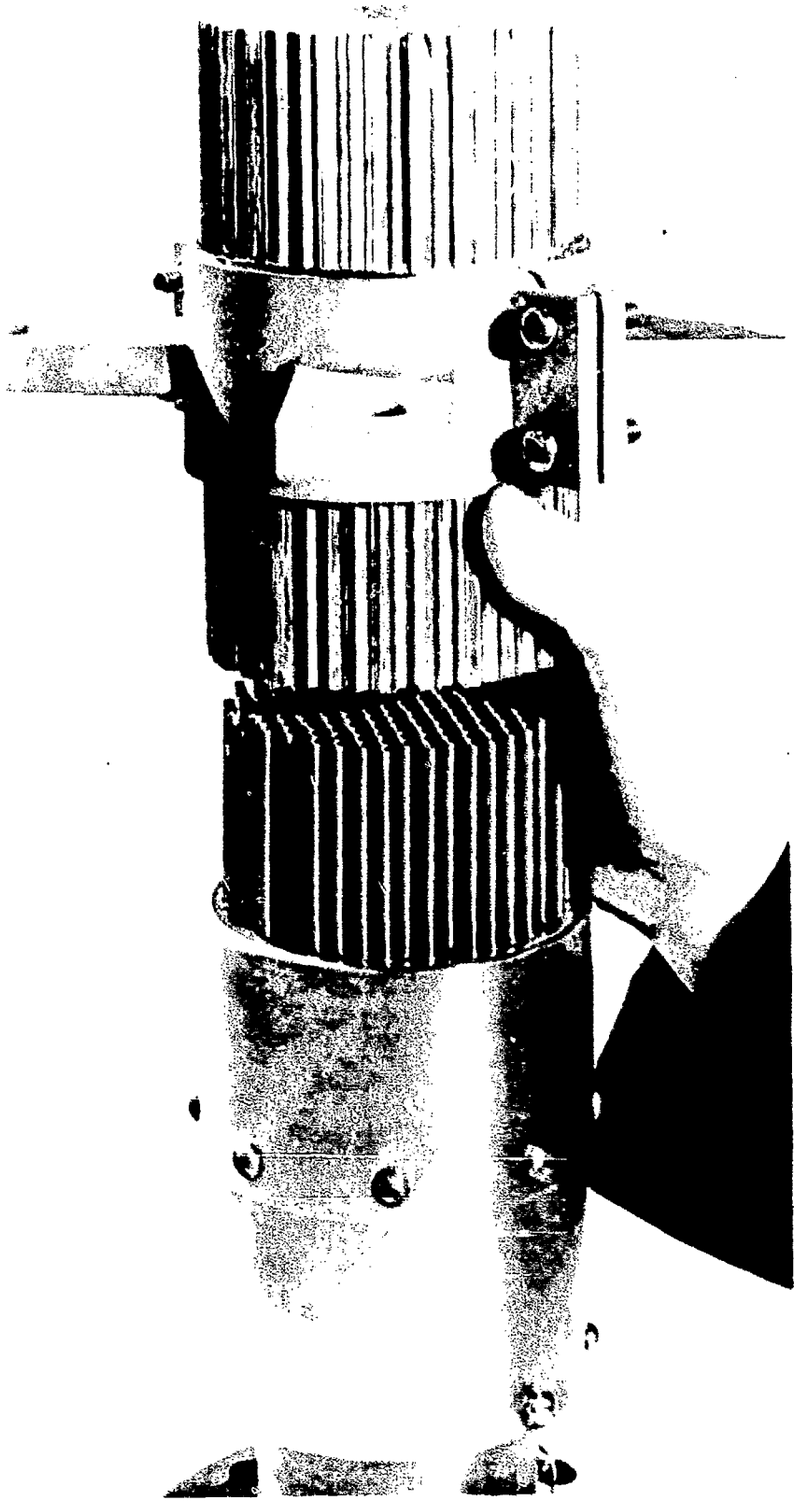


FIGURE VII.A-19A PHOTOGRAPH OF MULTITUBE AND MULTISHROUD SUPPRESSOR

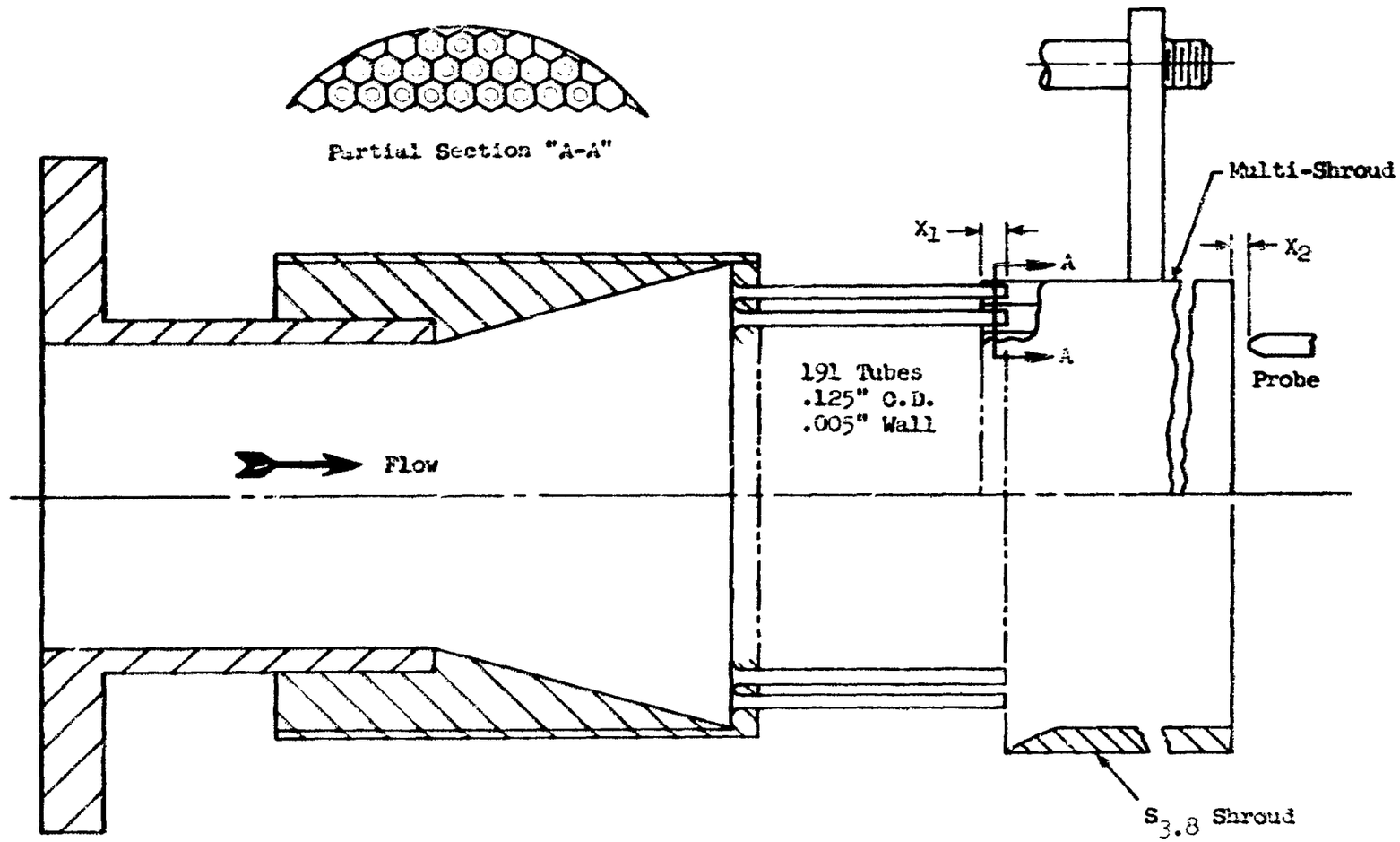


FIGURE VII.A-19B SKETCH OF MULTITUBE SUPPRESSOR AND SHROUDS

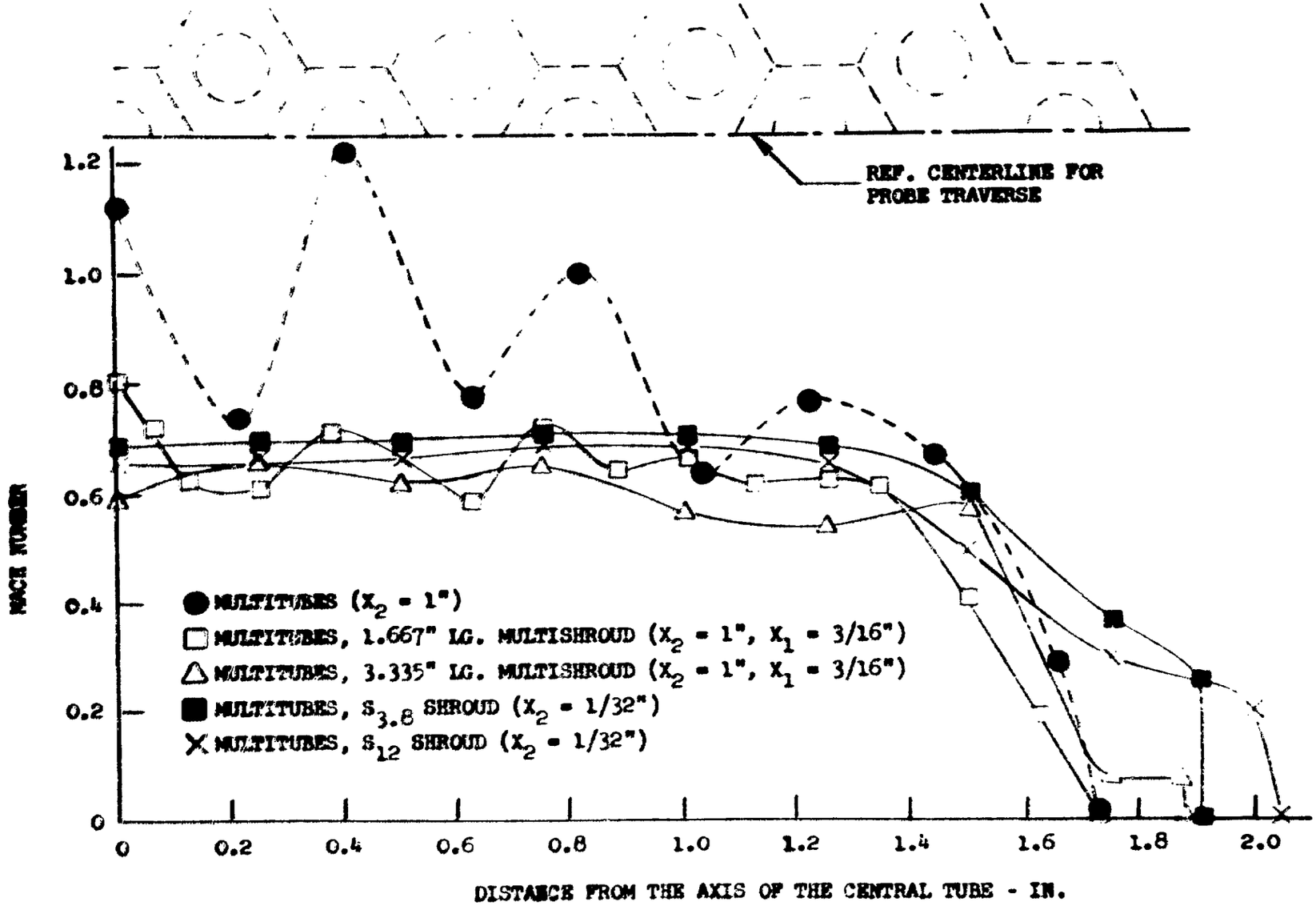


FIGURE VII.A-19C MACH NUMBER PROFILE ACROSS EXITS OF MULTITUBES AND MULTISHROUD

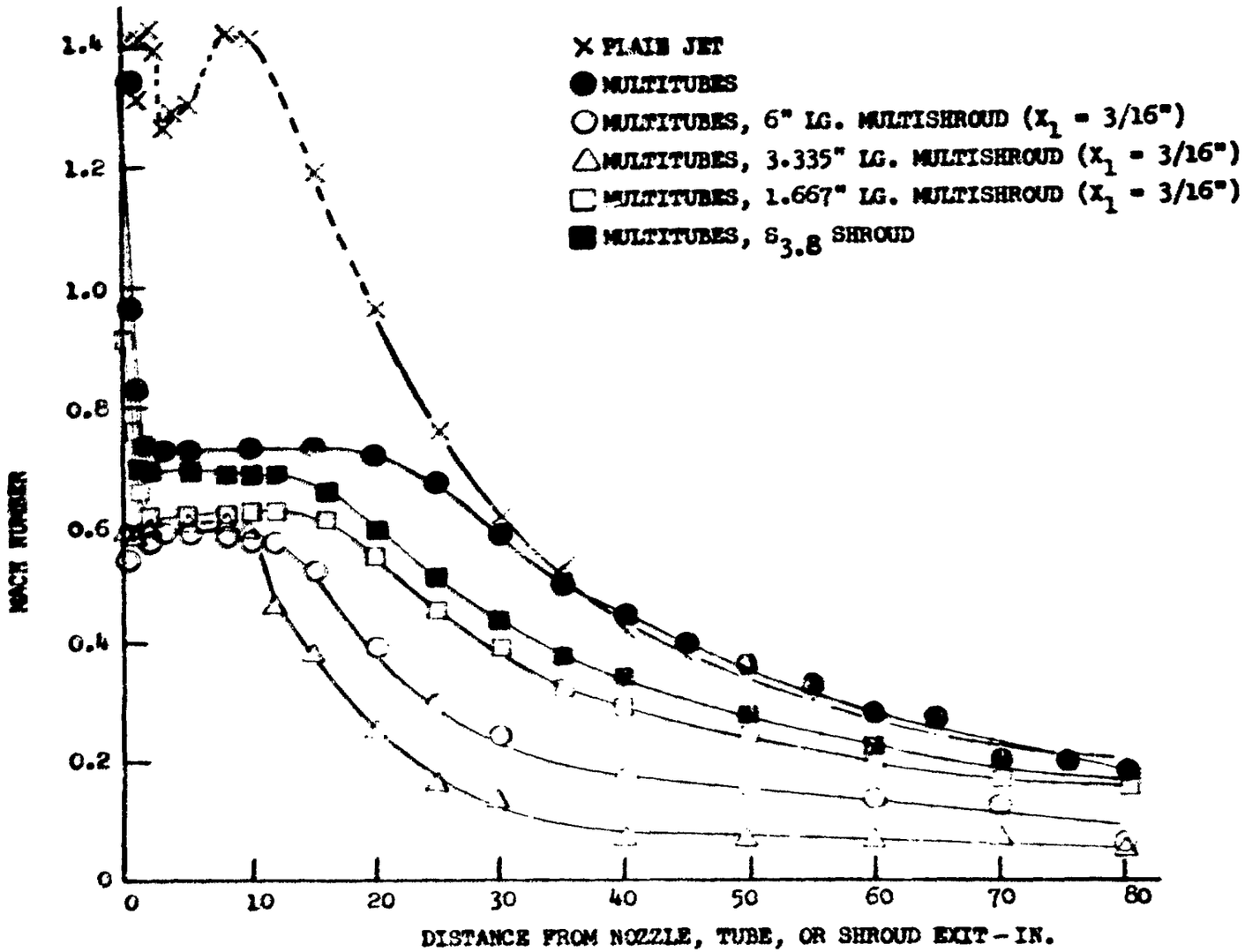


FIGURE VII.A-19D AXIAL MACH NUMBER VARIATION FOR MULTITUBES WITH AND WITHOUT SHROUDS

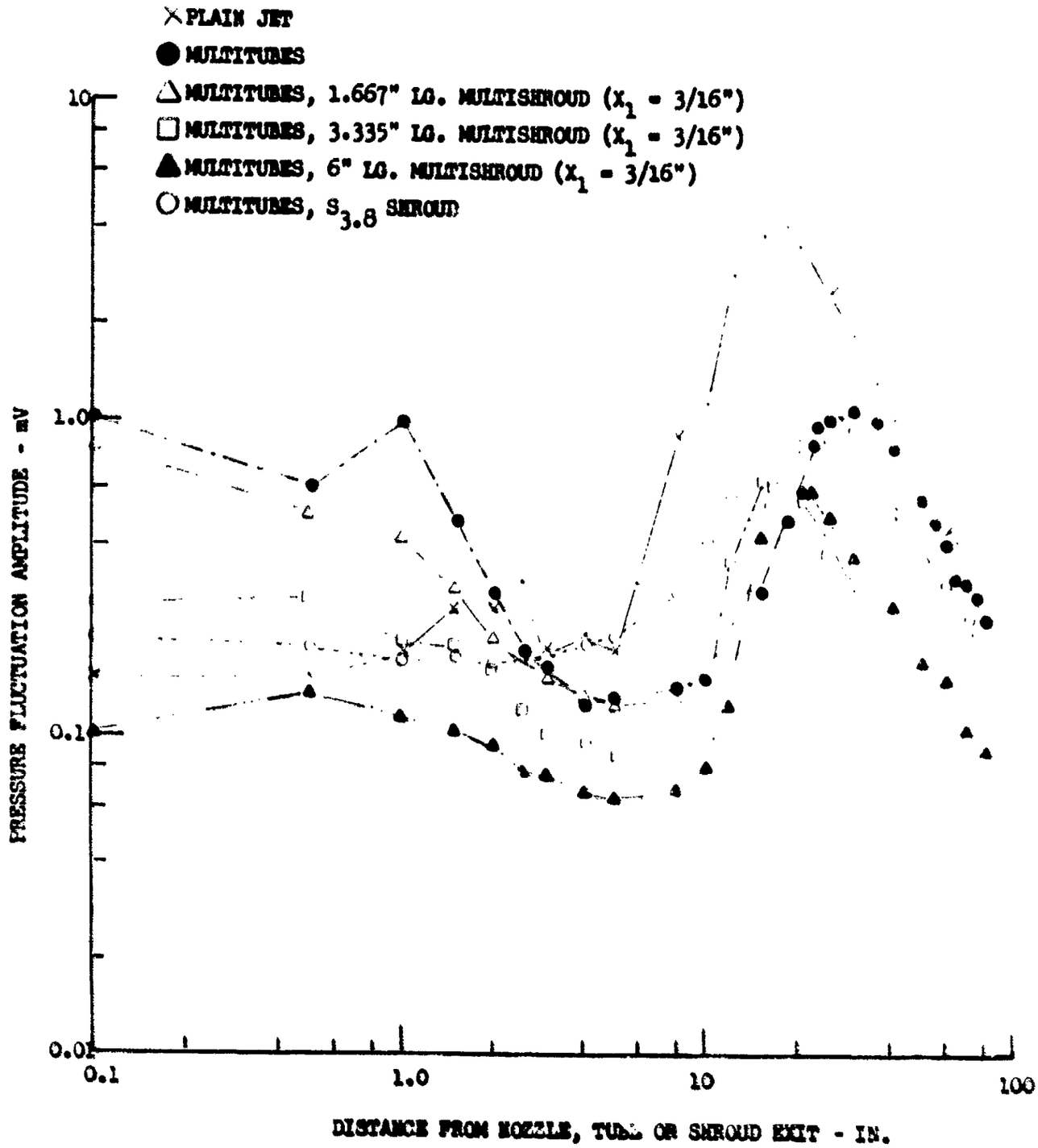
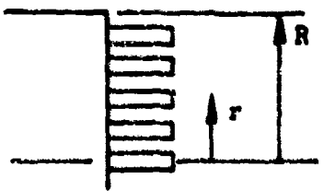


FIGURE VII.A-19S AXIAL IMPACT PRESSURE FLUCTUATIONS FOR MULTITUBES WITH AND WITHOUT SHROUDS



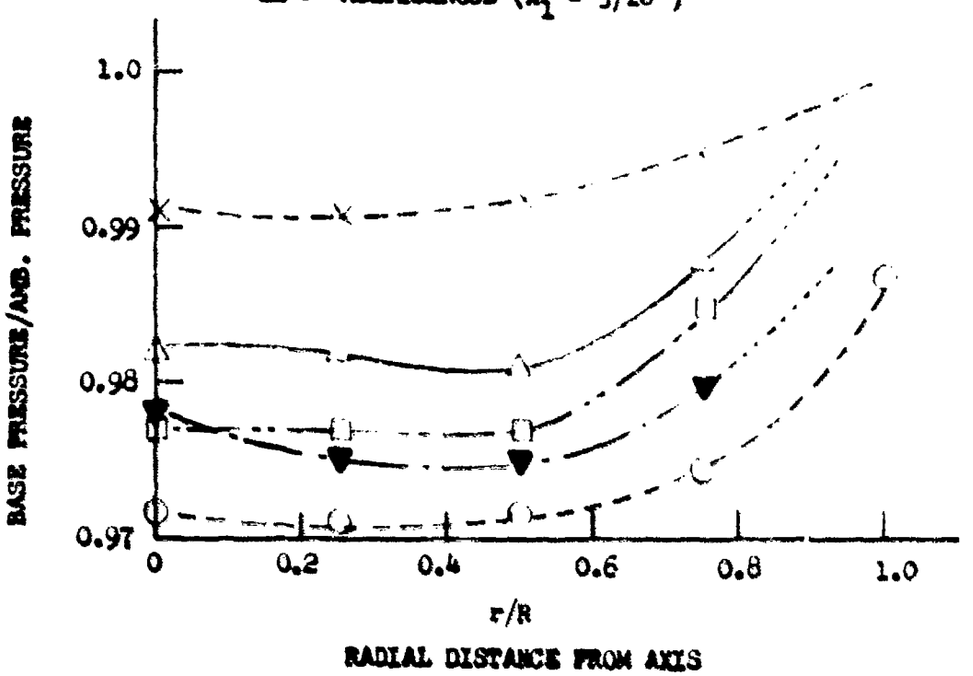


FIGURE VII.A-19P BASE PRESSURE DISTRIBUTION FOR VARIOUS MULTISHROUD CONFIGURATIONS

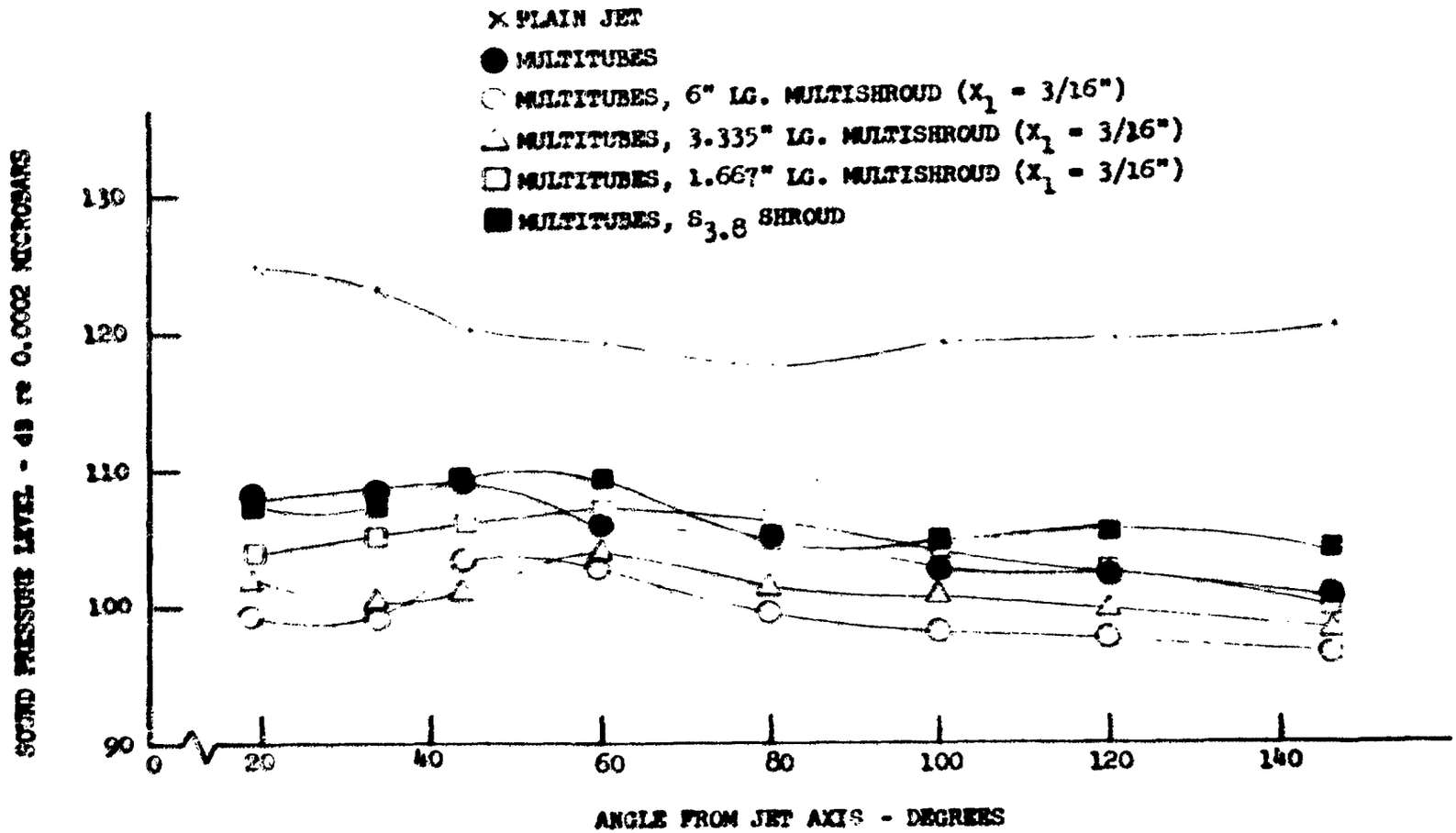


FIGURE VII.A-19G OVERALL SOUND PRESSURE LEVEL AS A FUNCTION OF ANGULAR POSITION FROM JET AXIS FOR MULTITUBES WITH AND WITHOUT SHROUDS

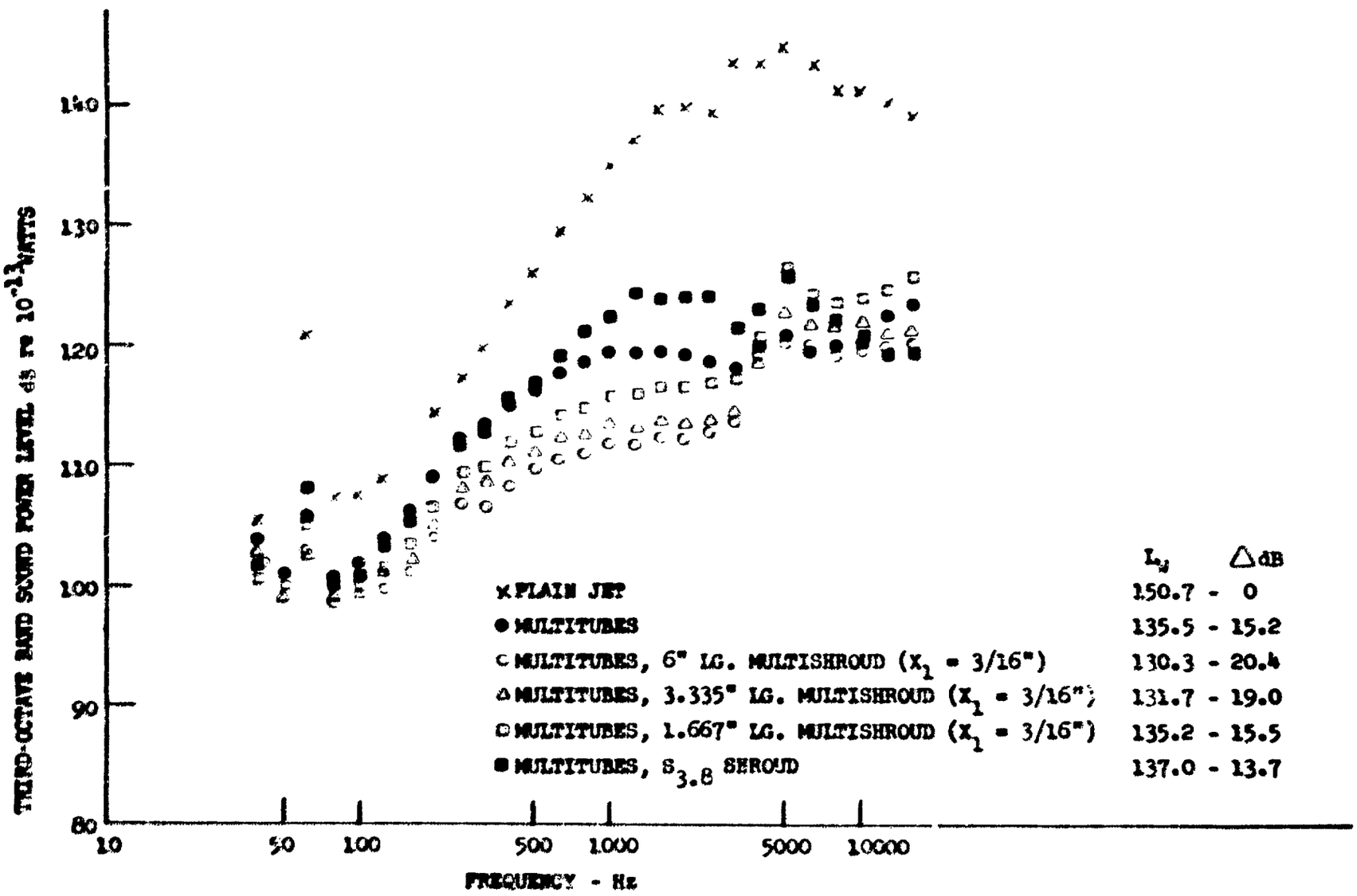


FIGURE VII.A-19: SOUND POWER LEVEL SPECTRA FOR MULTITUBES WITH AND WITHOUT SHROUDS

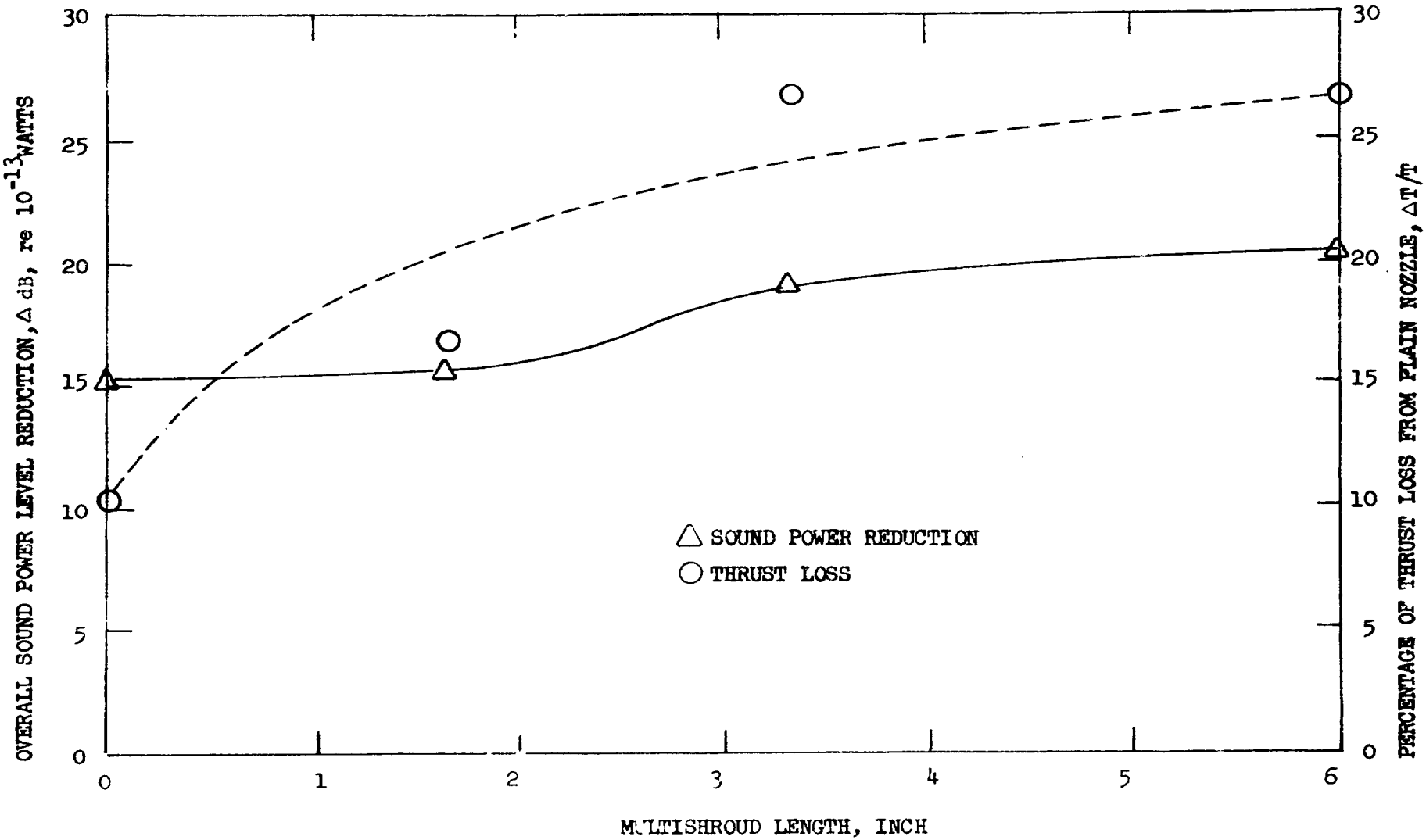


FIGURE VII.A-191 VARIATION OF OVERALL SOUND POWER LEVEL REDUCTION AND PERCENTAGE THRUST LOSS FOR 191 TUBES WITH 191 - SHROUD LENGTH

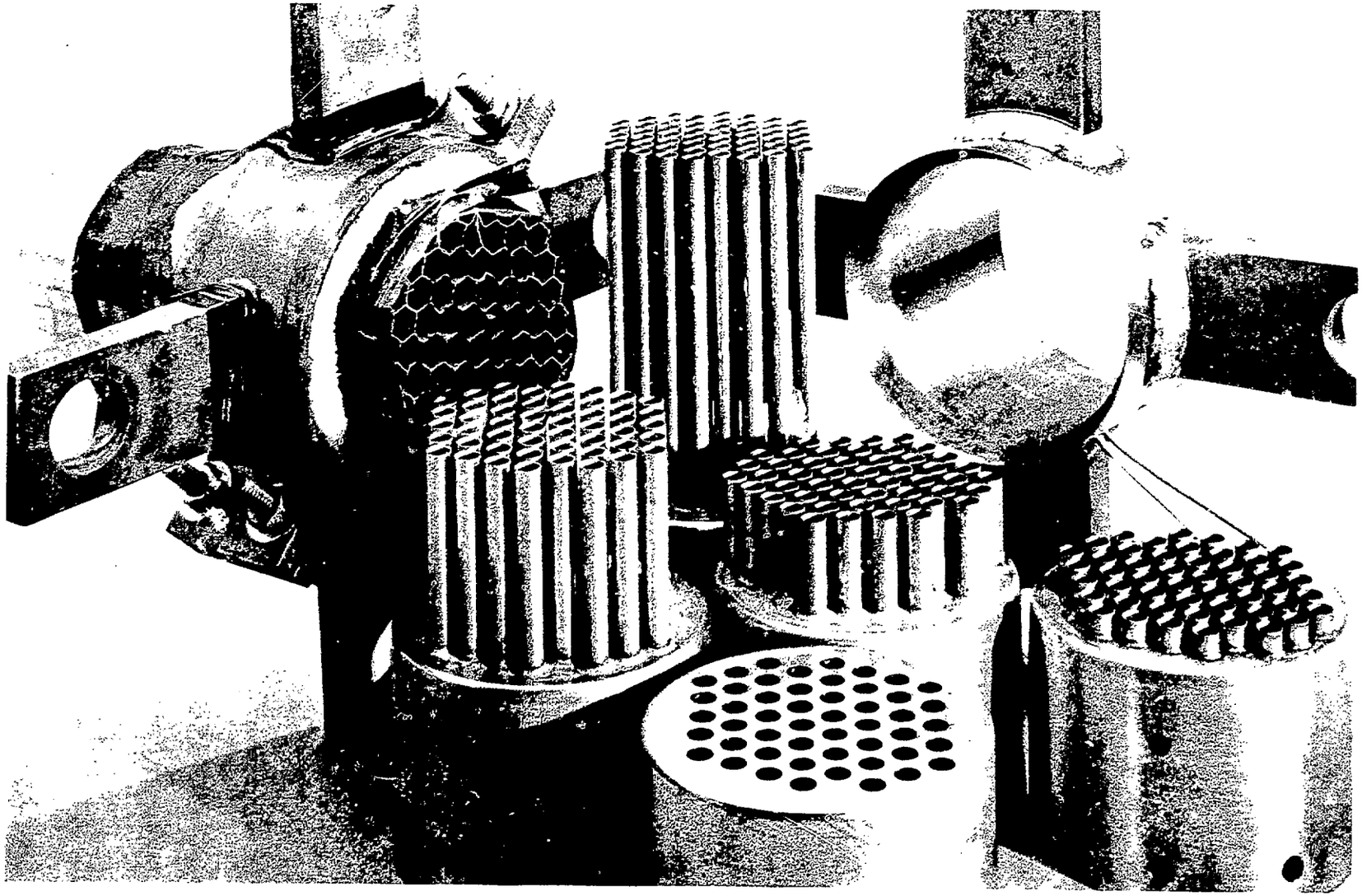


FIGURE VII.A-20A PHOTOGRAPH OF 50 TUBE SUPPRESSORS AND SHROUDS

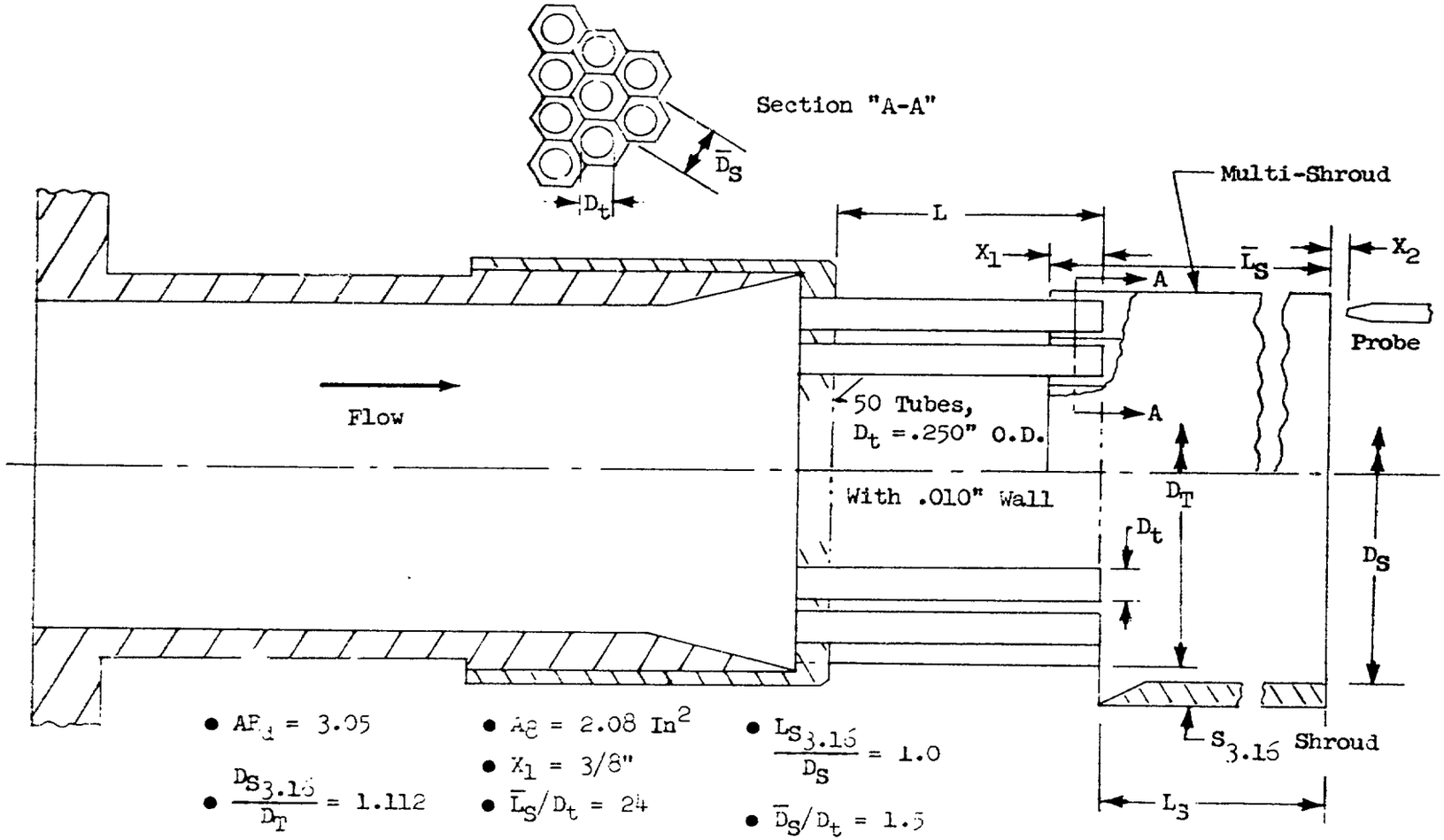


FIGURE VII.A-20B SKETCH OF 50 TUBE SUPPRESSOR AND SHROUDS

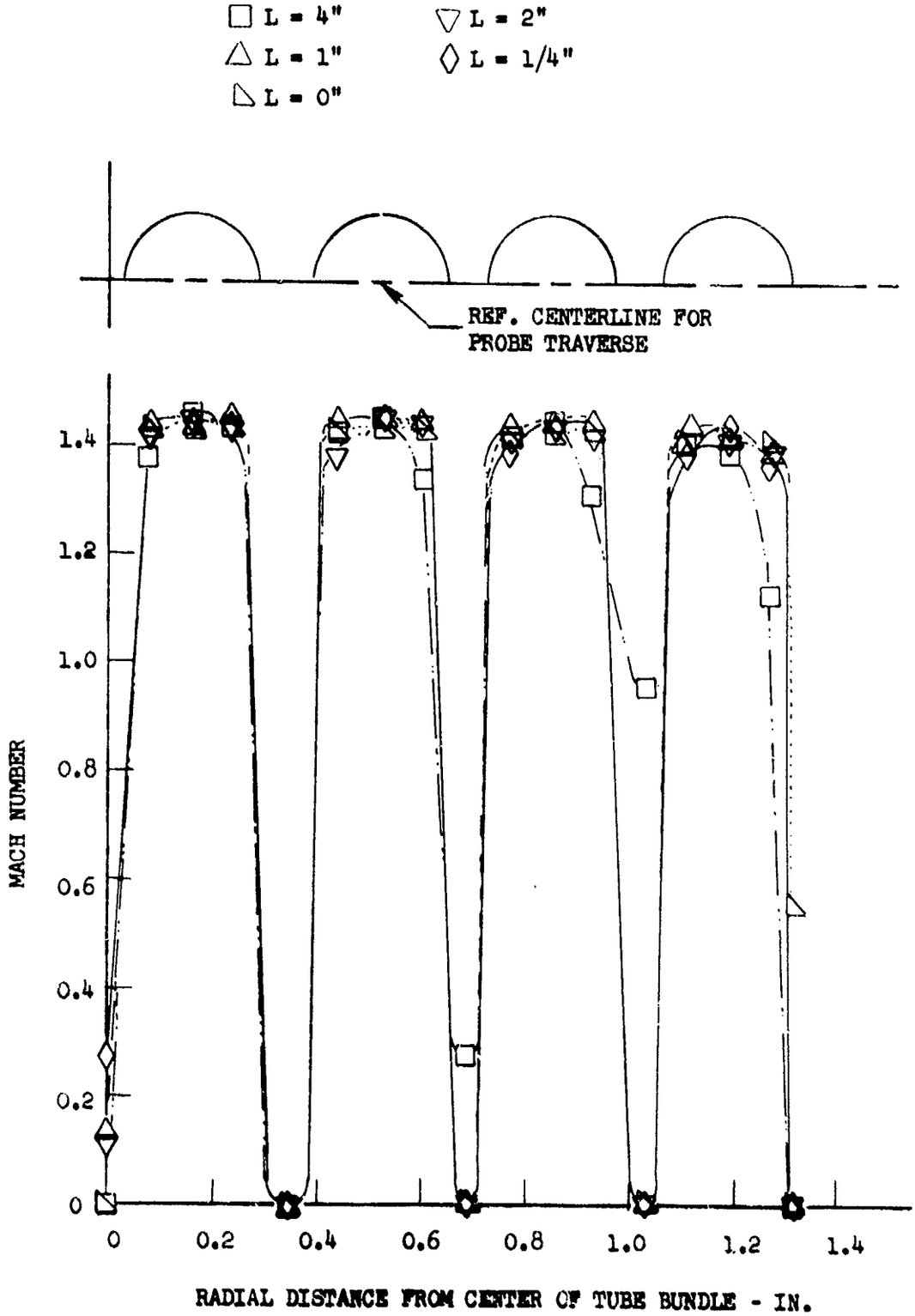


FIGURE VII.A-20C MACH NUMBER PROFILE ACROSS EXITS OF 50 TUBE NOZZLES 1/32" DOWNSTREAM OF TUBE EXIT, Pr = 3.2, Mj = 1.4

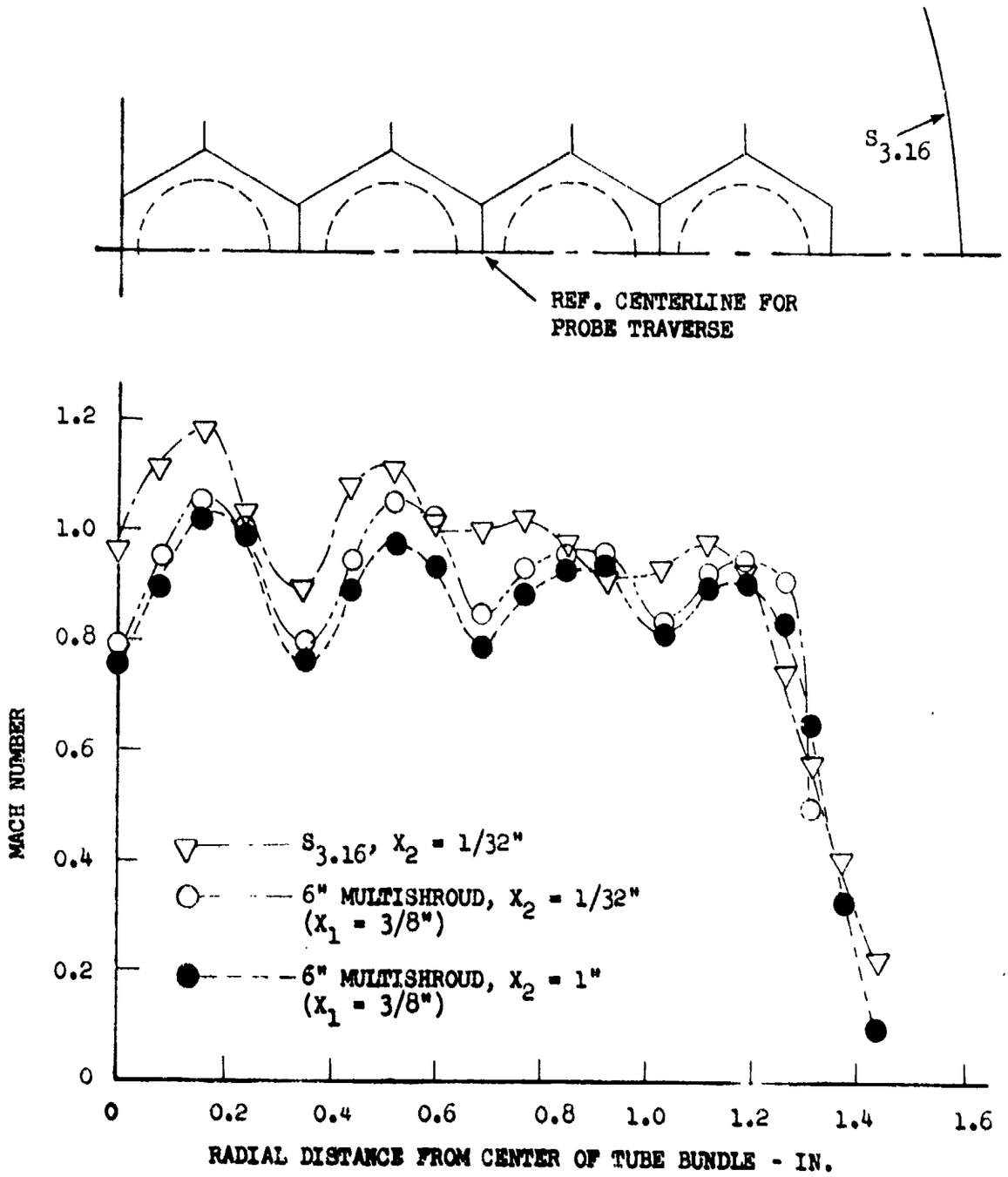


FIGURE VII.A-20D .MACH NUMBER PROFILE ACROSS EXITS OF SHROUDS, L = 2", L/D = 8

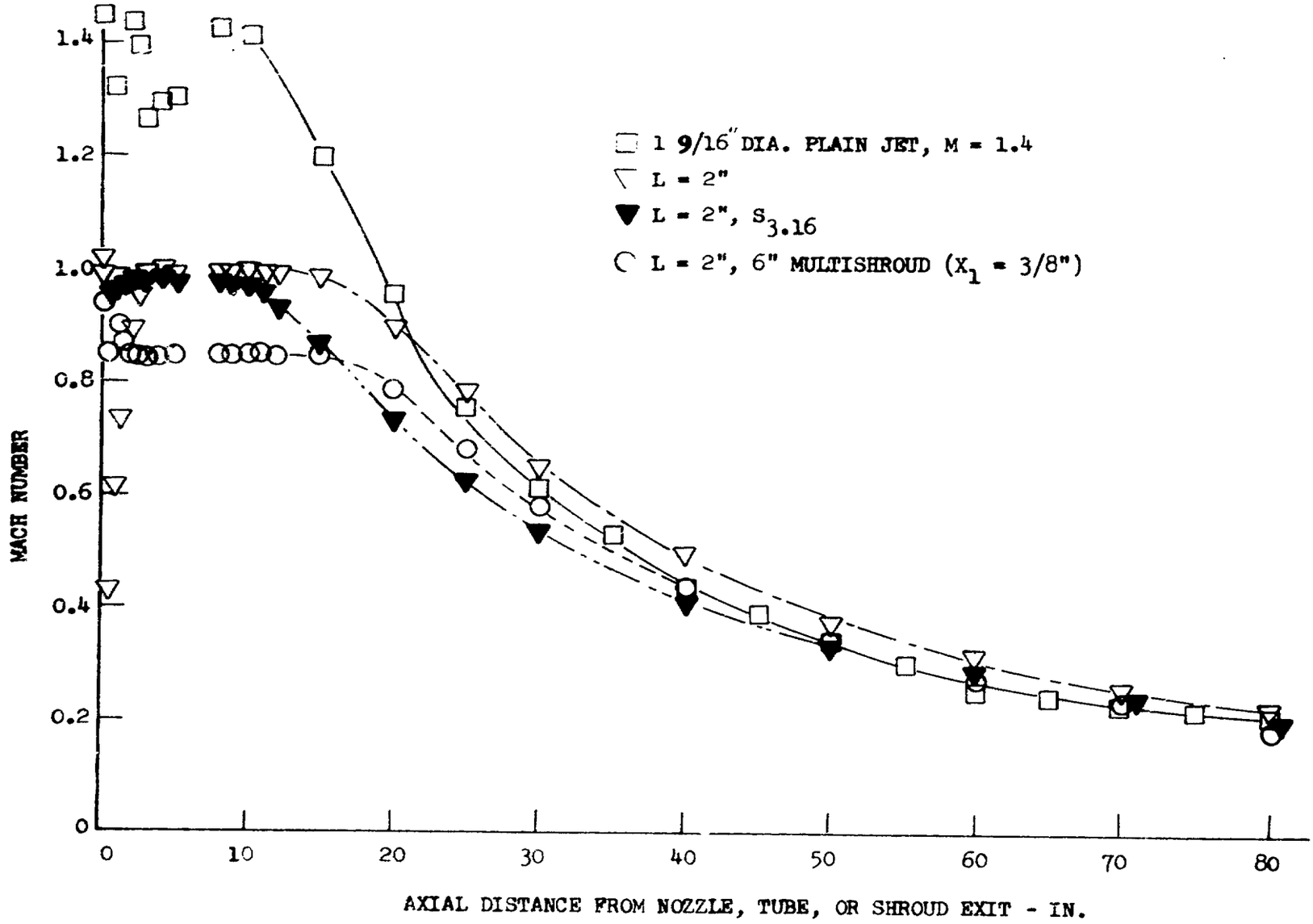


FIGURE VII.A-202 AXIAL MACH NUMBER DISTRIBUTION FOR 50 TUBE NOZZLE, WITH AND WITHOUT SHROUDS, L = 2", L/D = 8

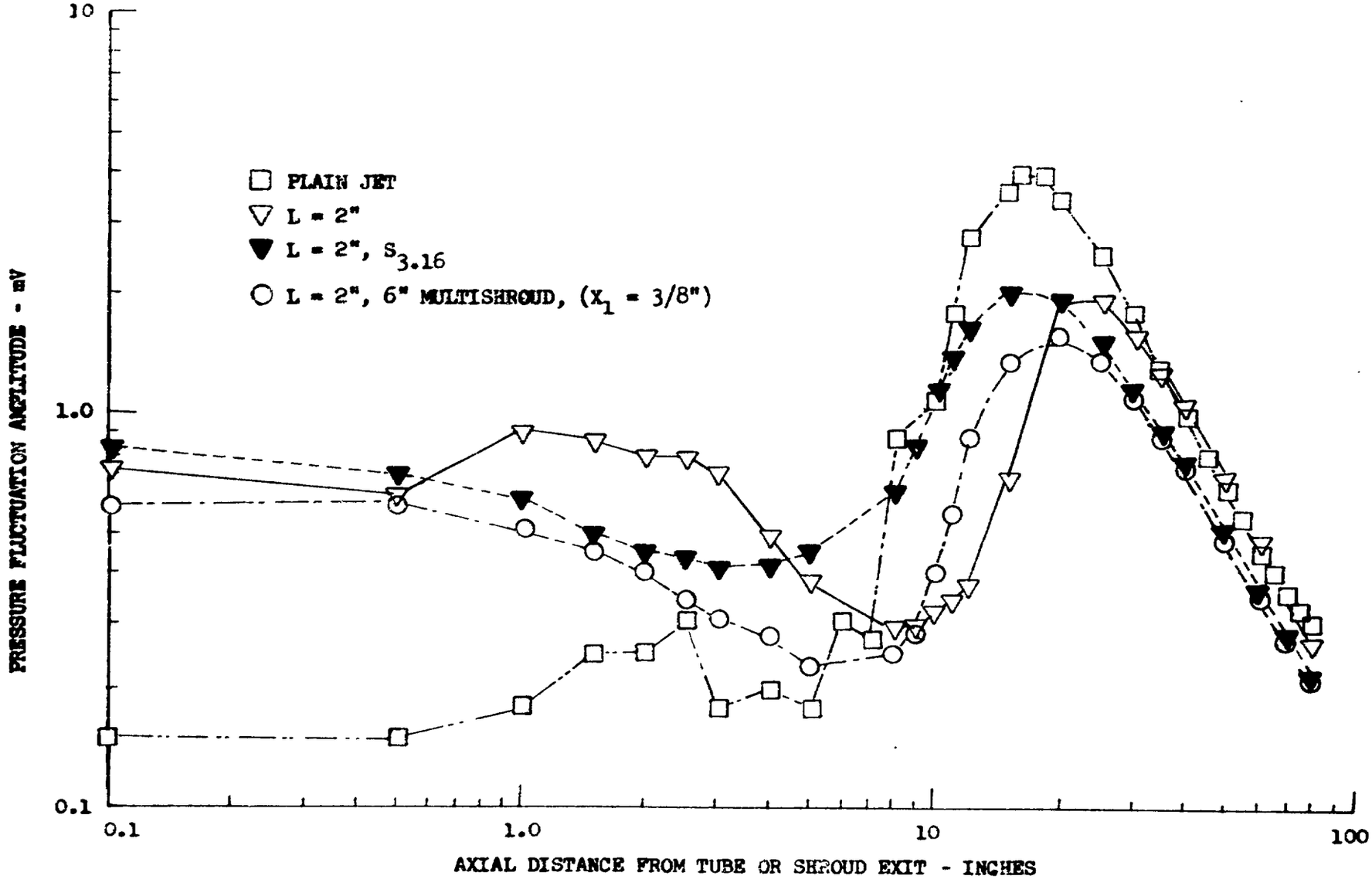


FIGURE VII.A-20F AXIAL IMPACT PRESSURE FLUCTUATIONS FOR 50 MULTITUBE NOZZLE WITH AND WITHOUT SHROUDS, L/D =8

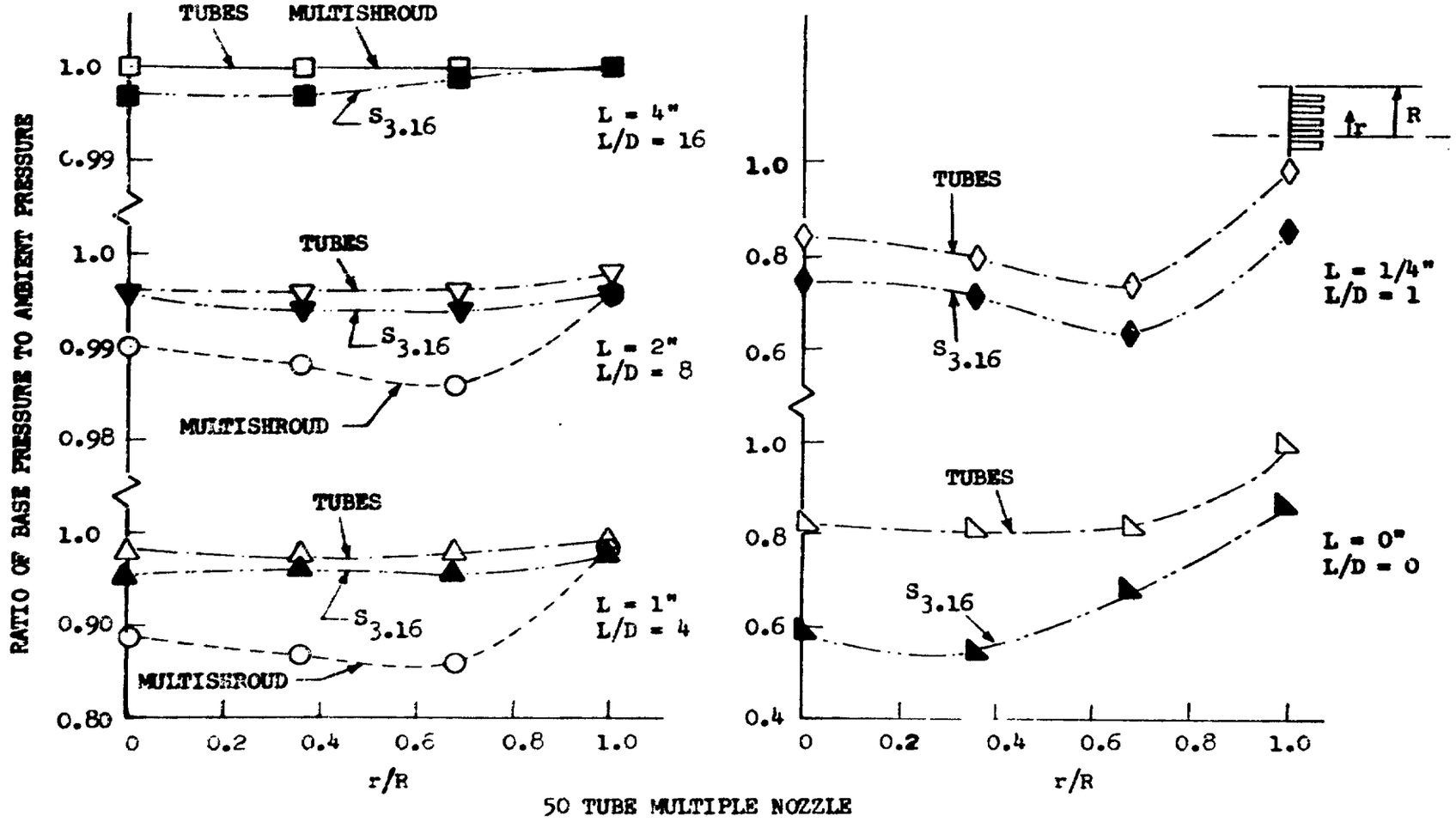


FIGURE VII.A-20G BASE PRESSURE DISTRIBUTION FOR VARIOUS MULTITUBE LENGTHS AND SHROUD ARRANGEMENTS

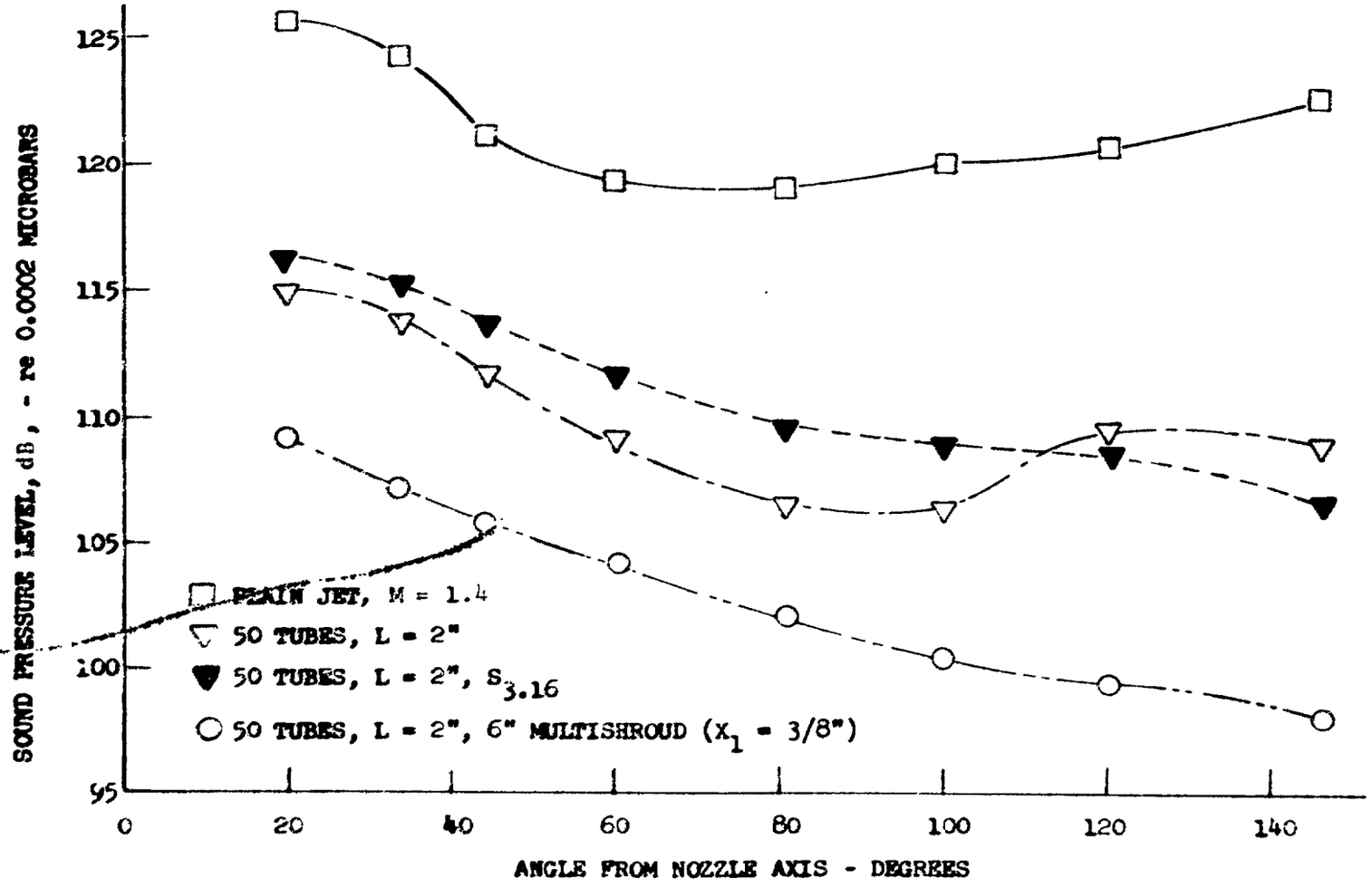


FIGURE VII.A-20H OVERALL SOUND PRESSURE LEVEL AS A FUNCTION OF ANGULAR POSITION FROM JET AXIS FOR 50 TUBE NOZZLE WITH AND WITHOUT SHROUDS, L/D = 8

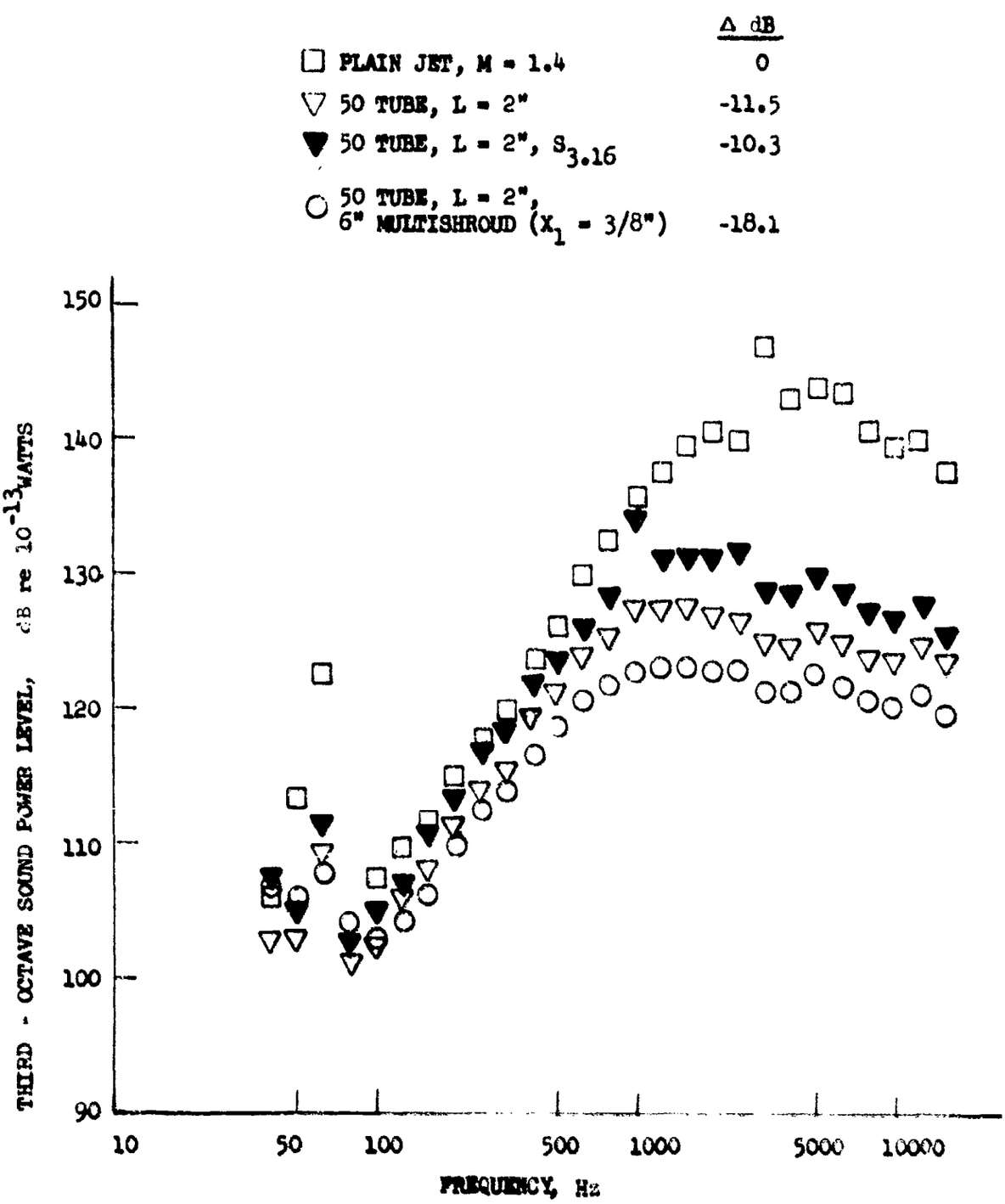


FIGURE VII.A-20I SOUND POWER SPECTRA FOR 50 TUBE NOZZLE WITH AND WITHOUT SHROUDS, L/D = 8

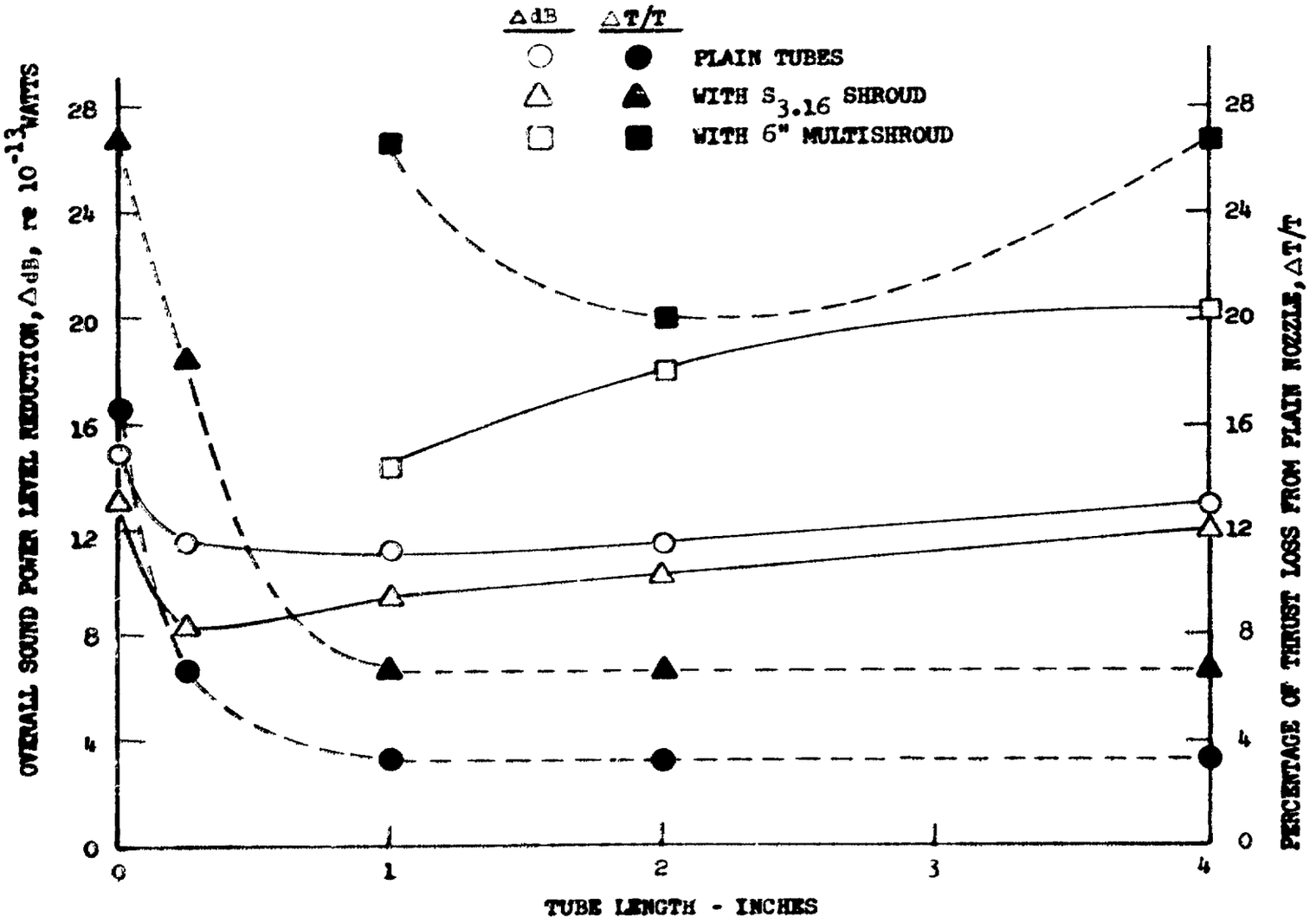


FIGURE VII.A-20J VARIATION OF OVERALL SOUND POWER LEVEL REDUCTION AND PERCENTAGE THRUST LOSS WITH TUBE LENGTH FOR 50 TUBE SUPPRESSORS WITH AND WITHOUT SHROUDS

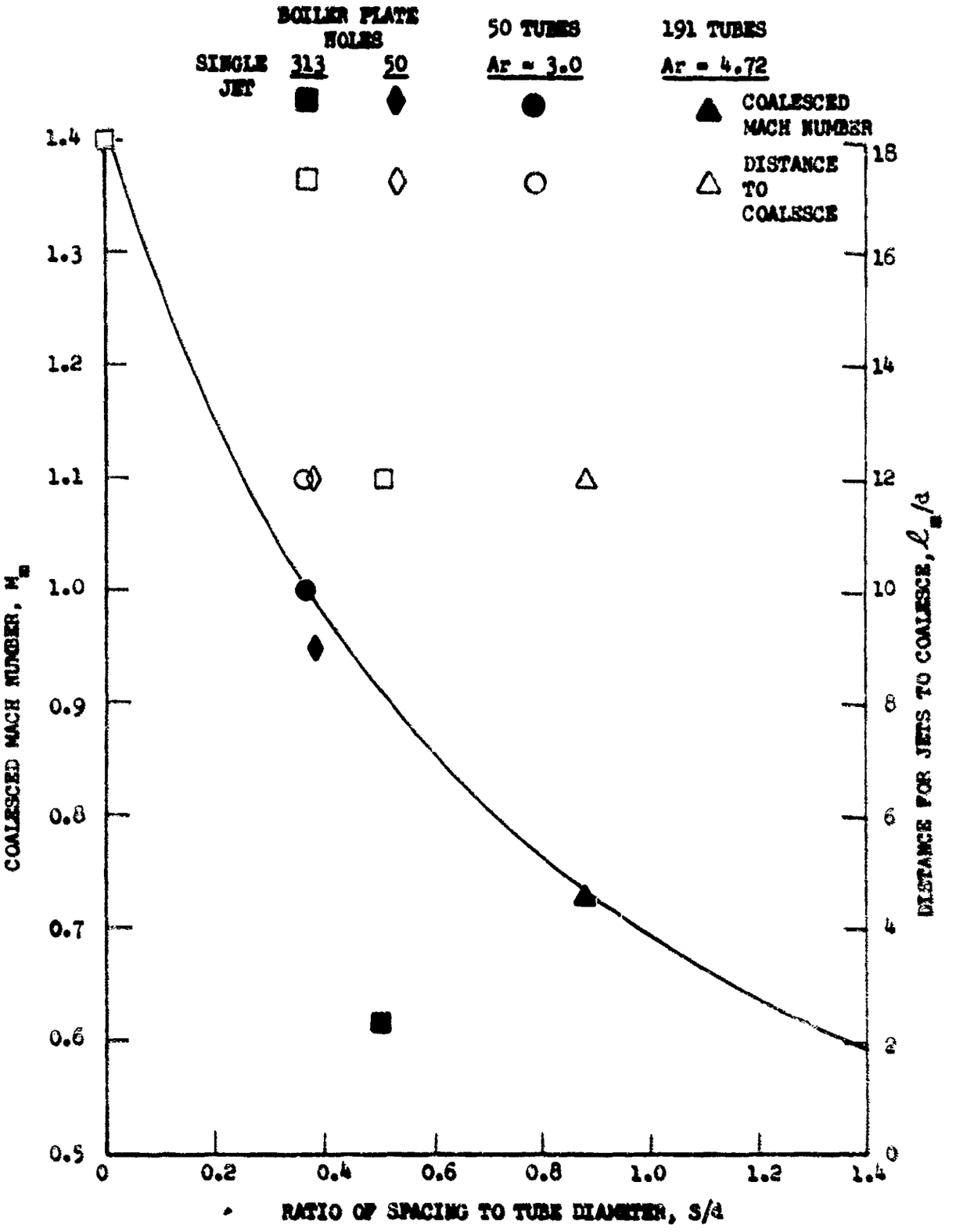


FIGURE VII.A-21 VARIATIONS OF COALESCED MACH NUMBER AND DISTANCE FOR JETS TO COALESCE AS A FUNCTION OF TUBE SPACING, Pr = 3.2

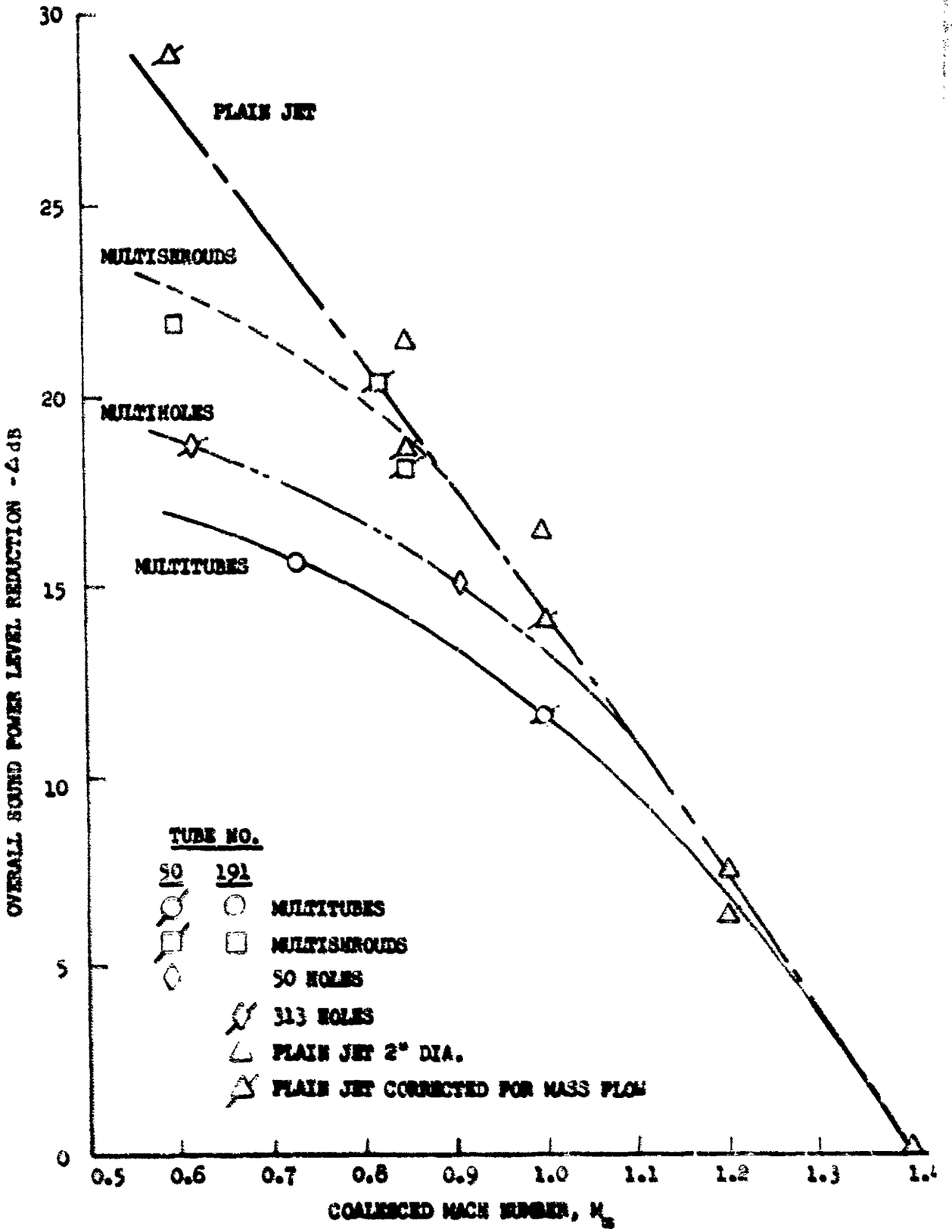


FIGURE VII.A-22 OVERALL SOUND POWER LEVEL REDUCTION AS A FUNCTION OF COALESCED MACH NUMBER FOR MULTIHOLES, MULTITUBES, AND MULTISHROUDS, Pr = 3.2 AND M_j = 1.4

APPENDIX A. NOMENCLATURE

Symbol		Units
A, A_8	Physical flow area at nozzle plane 8	(in^2),$(ft.^2)$
AR_d,A/R	Area Ratio: ratio of total circumscribed tube bunde area to physical flow area (tube nozzles)	
A/R	Area Ratio: ratio of total annulus area to physical flow area (annular plug nozzles)	
C/A	Chromel - Alumel wires used in thermocouples	
C_{D8}	Nozzle discharge coefficient: ratio of actual flow rate to ideal flow rate	
C_{fg}	Nozzle gross thrust coefficient, static and installed	
dB	Decible, re: 0.0002 dynes/cm^2	
D_s	a) Throat diameter of TSEN (Two stage ejector nozzle) b) Initial minimum internal diameter of cylindrical ejector (shroud)	(in)
D_t	Tube internal diameter	(in)
D_{Td}	Circumscribed tube bundle diameter	(in)
D_8	Internal diameter of conical primary nozzle at primary exit, plane 8	(in)
D_9	Internal diameter of secondary ejector at secondary exit, plane 9	(in)
EPNL	Effective perceived noise level	(EPNdB),(dB)
F_g	Measured gross thrust	(lb_f)
F_N	Net thrust	(lb_f)
$\frac{fD}{V}$	Strouhal number: a calculated function of frequency (f), nozzle diameter (D), and ideal jet velocity (V)	

APPENDIX A. NOMENCLATURE (Continued)

Symbol		Units
k	Ratio of specific heat	
L	Axial reference location of variable position inlet centerbody	(in)
L_S	Shroud internal length	(in)
L_t	Tube external length	(in)
L_{ti}	Tube internal length	(in)
M, M_o	Mach number	
% N_c	Percent corrected speed	(rpm)
OASPL	Overall sound pressure level; calculated by summation of sound pressure levels of each octave or 1/3 octave band	(dB)
OASPL-10 log ρA	Normalized OASPL	(dB)
PNL	Perceived noise level; a calculated annoyance weighted sound level	(PNdB),(dB)
PNdB	Contraction of PNL, dB	(PNdB),(dB)
PNdB-10 log ρ^2A	Normalized PNL	(PNdB)
PNdB-10 log ρA	Normalized PNL	(PNdB)
P_o	Ambient pressure	(psia)
$\bar{P}_{Base}$	Mean baseplate static pressure	(psia)
P_L	Local wall static pressure	(psia)
P_{T8}	Nozzle exhaust total pressure	(psia)
Peak PNL	Highest perceived noise level generated; usually referenced to a specific angle and distance from the source	(PNdB),(dB)
Peak OASPL	Highest overall sound pressure level generated; usually referenced to a specific angle and distance from the source	(dB)
% RH	Percent atmospheric relative humidity	

APPENDIX A. NOMENCLATURE (Concluded)

Symbol		Units
S	Distance between centerlines of tube/hole rows	(in)
SPL	Sound pressure level; a level of sound pressure that occurs in a specified frequency range at any specified interval of time.	(db)
T_{T8}	Nozzle exhaust total temperature	(°R), (°F)
V_j, V_J	Fully developed ideal jet velocity	(ft/sec)
W_B	Bleed weight flow (air or water)	(lb/sec)
W_8	Engine nozzle weight flow	(lb/sec)
W_T	Total primary and secondary flow	(lb/sec)
$\dot{W}$	Flow rate	(lb/sec)
X_S	Axial spacing from exit plane of primary nozzle to: a) throat (D_8) of TSEN (Two stage ejector nozzle) or b) initial minimum internal diameter of cylindrical ejector (shroud)	(in)
α	Tab angle	(deg)
β	Orifice coefficient	
θ	Angle between a straight line from source to microphone, and engine or nozzle centerline; referenced to inlet or exhaust	(deg)
ρ	Density of jet stream	(lb_m/ft^3)